University of Nevada – Reno

Geology of the Cove Mine, Lander County, Nevada, and a Genetic Model for the McCoy-Cove Magmatic-Hydrothermal System

A dissertation submitted in partial fulfillment of the
requirements for the degree of Doctor of Philosophy in Geology

by

Marcus K. Johnston

Dr. Tommy B. Thompson/Dissertation Advisor

May, 2003

UNIVERSITY OF NEVADA RENO **THE GRADUATE SCHOOL**

We recommend that the dissertation
prepared under our supervision by

MARCUS K. JOHNSTON

entitled

Geology of the Cove Mine, Lander County, Nevada, and a Genetic Model for The McCoy-Cove Magmatic-Hydrothermal System

be accepted in partial fulfillment of the
requirements for the degree of

DOCTOR OF PHILOSOPHY

_____
Tommy B. Thompson, Ph.D., Advisor

_____
Greg B. Arehart, Ph.D., Committee Member

_____
Richard A. Schweickert, Ph.D., Committee Member

_____
Maurice C. Fuerstenau, Ph.D., Committee Member

_____
Danny L. Taylor, Ph.D., Graduate School Representative

_____
Marsha H. Read, Ph.D., Associate Dean, Graduate School

May, 2003

ABSTRACT

The McCoy Au skarn and Cove Au-Ag deposits are located in the northern Fish Creek Mountains, Lander County, Nevada. Through 2001, large-scale open pit and associated underground mining at the two deposits produced 3.3 million ounces of Au and 108 million ounces of Ag. Most production was from Cove, making it the third largest Ag producer in the history of Nevada. This study focuses primarily on the geology and geochemistry of Cove, and secondarily on the relationships between Cove, McCoy, and other deposits in the Great Basin physiographic province of North America.

Cove is hosted by the middle to early late Triassic Augusta Mountain Formation, which consists of limestone with lesser dolostone and clastic units. Ore also is present locally in Eocene porphyritic granodiorite dikes and sills. The deposit comprises two distinct ore types: a central core of base metal vein-type (BMVT) ore and an outer aureole of relatively Ag-rich Carlin-style ore. BMVT ore consists of pyrite-sphalerite-galena-dominated, Au- and Ag-bearing veins, veinlets, stockworks, crustifications, and disseminations in clastic and carbonate strata, and locally in the intrusions. Carlin-style ore comprises disseminated Fe ± As sulfides with arsenian-argentiferous-auriferous components ± native Au-electrum in silty to sandy carbonate strata. BMVT ore has >50:1 Ag:Au ratios, and Carlin-style ore has Ag:Au ratios that decrease from ~50:1 near the feeder faults to ~1:1 in one of the more distal ore zones. Both types of ore are associated with decarbonatized, silicified, and sericitized/illitized rocks. New structural and age data for ~fresh and altered intrusive rocks indicate that mineralization at Cove occurred during active extension at ~39 Ma (^{40}Ar-^{39}Ar). Fluid inclusion and δD and δ^{18}O

data indicate that the mineralizing fluids were ~250 to 370°C and magmatic in origin, and that boiling did not occur.

Cove is located approximately 1.6 kilometers northeast of McCoy. Earlier studies indicate that early Tertiary igneous activity in the McCoy mining district occurred in two pulses. The first pulse consisted of a relatively oxidized magnetite-series magma, and formed the central stock at McCoy and related dikes that extend to the Cove deposit. This pulse occurred at ~41.5 Ma, and produced sub-economic skarn at McCoy. The second pulse consisted of a relatively reduced ilmenite-series magma, and produced economic skarn ore at McCoy. Adularia from a mineralized skarn assemblage at McCoy was dated at ~39 Ma (K-Ar). The age data indicate that McCoy and Cove formed contemporaneously. $\delta^{34}S$ data for ore-stage sulfides from skarn ore at McCoy and BMVT and Carlin-style ore at Cove indicate a common source for S for the three types of ore. Ostensibly, this source is the pulse of ilmenite-series magma.

Although the volume of the Carlin-style ore at Cove is substantially larger than that of the BMVT ore, the relatively high concentrations of base metals and clear associations with igneous activity have made Cove difficult to classify using traditional schemes. The new data indicate that Cove is a telescoped system consisting of BMVT (polymetallic vein) and porphyry-related, distal disseminated ores. The zonation for the McCoy-Cove system is nearly identical to zonations described by other workers for Au-enriched porphyry systems. In this case, the porphyry center and skarn ore at McCoy comprise the proximal component, and BMVT and Carlin-style ores at Cove are the intermediate and distal components, respectively. Economic concentrations of Au occur in all three zones, which are separated from one another by subeconomic concentrations of Au.

The Carlin-style orebodies at Cove share several important similarities with ores in classic Carlin-type deposits (CTDs), including ore characteristics, associated alteration styles, and host lithologies. The late Eocene age of the McCoy-Cove system is also a common age for CTDs in the Great Basin. Two criteria used to distinguish CTDs from porphyry-related, distal disseminated deposits are the paucity of base metals and lack of igneous associations for the CTDs. Recent studies, however, have suggested magmatic links for several classic CTDs, and indicate that at least some of these deposits should be reclassified as distal disseminated deposits. The genetic model for McCoy-Cove and the increased recognition of igneous associations for CTDs may be crucial to understanding the genesis and exploration potential of intrusion-related and Carlin-type deposits worldwide.

ACKNOWLEDGEMENTS

As with any other long-term, largely collaborative effort, there are many individuals and organizations that deserve appreciation and thanks for their help during this study. My first "thank you" goes to the Ralph J. Roberts Center for Research in Economic Geology (CREG), and its several industry sponsors, for providing me with this unique and challenging opportunity, and the funding and support to successfully complete the project. A special thanks goes to Echo Bay Minerals Company (now Kinross Gold Corporation) and Newmont Mining Corporation (NMC).

Several individuals provided technical training, insights, and friendly advice that not only contributed to the completion of this study, but also to my growth as a professional and as a person. Dr. Don Hudson (consultant) and soon-to-be Dr. Mike Ressel (UNR/NMC) assisted with the petrological studies, especially with the recognition and characterization of igneous components and alteration products. Dr. John McCormack (UNR) provided training and assistance with the SEM and EMP analyses. Mario Desilets (UNR) provided training and assistance with the XRD analyses. Discussions with Patrick Highsmith (ALS Chemex) helped in the selection of samples for ICP-MS and XRF analyses. Dr. Simon Poulson (UNR) spent many hours training and assisting me in the use of gas isolation lines for isotopic analyses.

Several former employees at the now closed McCoy-Cove operation also deserve recognition. Mike Schaffner provided discussion and detailed reports regarding the complicated metallurgy of the deposits. John Penton and Jay Fischer helped clarify my understanding of the general geology of the Cove deposit. A special thanks goes to Don Ryan, for helping me to understand the basic workings of a large-scale mining operation,

providing safety training, providing numerous data and figures, and freely sharing his opinions and observations regarding the system at Cove.

Many of the figures in the dissertation were digitized by employees of Echo Bay or NMC. Thanks to Jeanette Hunter and Randy Largent (both with NMC), and especially Marty Easter (formerly with Echo Bay Exploration Inc.) and Diana Neef (NMC/Blue Sky Digital Services). The dissertation is greatly enhanced by the quality of their work.

I would also like to thank the Geological Society of Nevada, and its members, for allowing me numerous opportunities to share my ideas through professional talks and a field trip to McCoy-Cove. Thanks also to the other CREG students, especially Gavan Heinrich, Carlos Altamirano, Alex Dewitt, Lori Clarke, Alexa Rayias, Shiela Hutcherson, and Tony Chakurian, for helping me figure out many of the concepts that did not sink in during lectures, and for general friendship and stress relief.

Many NMC geologists have helped me out over the last three years, whether it be through discussions of the various aspects of Carlin-type deposits, or allowing me the time to immerse myself in the geology of the Carlin trend. Thanks to all of the geology crew, especially Joe Sagar, Wayne Trudel, Leroy Schutz, and Dr. Steve Garwin.

Of ultimate importance to the successful completion of this endeavor are those persons directly tied to the project, whether they served in professionally or emotionally supportive roles. I would like to thank the members of my committee, Dr. Danny Taylor, Dr. Maury Fuerstenau, Dr. Rich Schweickert, and especially Dr. Greg Arehart and Dr. Tommy Thompson. Greg spent a great deal of time helping me to figure out some of the more esoteric aspects of this work, and significantly impacted the final quality through very thorough reviews and advice. Tommy has been the consummate educator, not only

in the many classes he taught, but also through his actions. He educates by example, and continues to set nearly impossible-to-achieve standards for professionalism, community service, and work ethic. Dave Emmons (Echo Bay Exploration Inc./Kinross Gold Corporation) served as a liason between me and Echo Bay throughout the duration of this study. Dave is credited with the discovery of Cove in 1987, and I greatly appreciate his willingness to trust me with his baby. I would also like to thank Dr. Jim Carr (UNR), Ingrid Ramos (UNR), and Shelley Harvey (CREG/UNR) for advice and invaluable assistance throughout this process.

Thanks to Dave Tretbar (CREG/Getchell Gold/Barrick Goldstrike Mines/etc.) for our many discussions, especially those pertaining to academics, the mining industry, and mineral collecting. Thanks to Don and Amy Duzenak for helping me to maintain some semblance of sanity, and some sense of connection with the larger world outside of geology and academics. My mom, dad, and sister were always willing to listen to my problems and to offer thoughtful advice. Floyd, Gonzo, and Raider Cat all provided timely moments of entertainment and companionship.

In saving the best for last, I want to thank my wife, Bonnie, for everything, including: leaving the ocean and forests of Wilmington, North Carolina, to come to desert of Nevada to pursue my goals; being the breadwinner for the most of the last eight years; tolerating my absence-complaints-exhaustion-(insert your own word(s)); offering unwavering love and emotional support; and most recently, for giving us Olivia. Now, it is my turn to repay these favors...

TABLE OF CONTENTS

LIST OF FIGURES

LIST OF TABLES

LIST OF PLATES

GEOLOGY OF THE COVE MINE, LANDER COUNTY, NEVADA, AND A GENETIC MODEL FOR THE McCOY-COVE HYDROTHERMAL SYSTEM

CHAPTER 1: INTRODUCTION AND METHODS

INTRODUCTION

Cove is a dominantly sedimentary rock-hosted Au-Ag deposit located in the McCoy mining district in the northern Fish Creek Mountains, 48 kilometers southwest of the town of Battle Mountain, Lander County, Nevada (Fig. 1). The Cove deposit is expressed by two separate but related hypogene systems with a supergene overprint. The most obvious hypogene system consists of Au- and Ag-bearing, base metal-dominated veins, veinlets, crustifications, stockworks, and disseminations that consist principally of pyrite, sphalerite, and galena. This type of ore is called "base metal vein-type" (BMVT) ore in the following text. The second hypogene system is dominated by Fe sulfides with Au- and Ag-bearing arsenian-rims that are similar, but not identical, to "Carlin-type" deposits in Nevada and elsewhere (terminology based on Berger and Bagby, 1993), and is referred to as "Carlin-style" ore in the ensuing text. The Cove system is located approximately 1.6 kilometers northeast of the McCoy Au (-Cu) skarn, and previous workers have suggested that the two deposits may be parts of a single zoned system related to a large buried intrusion.

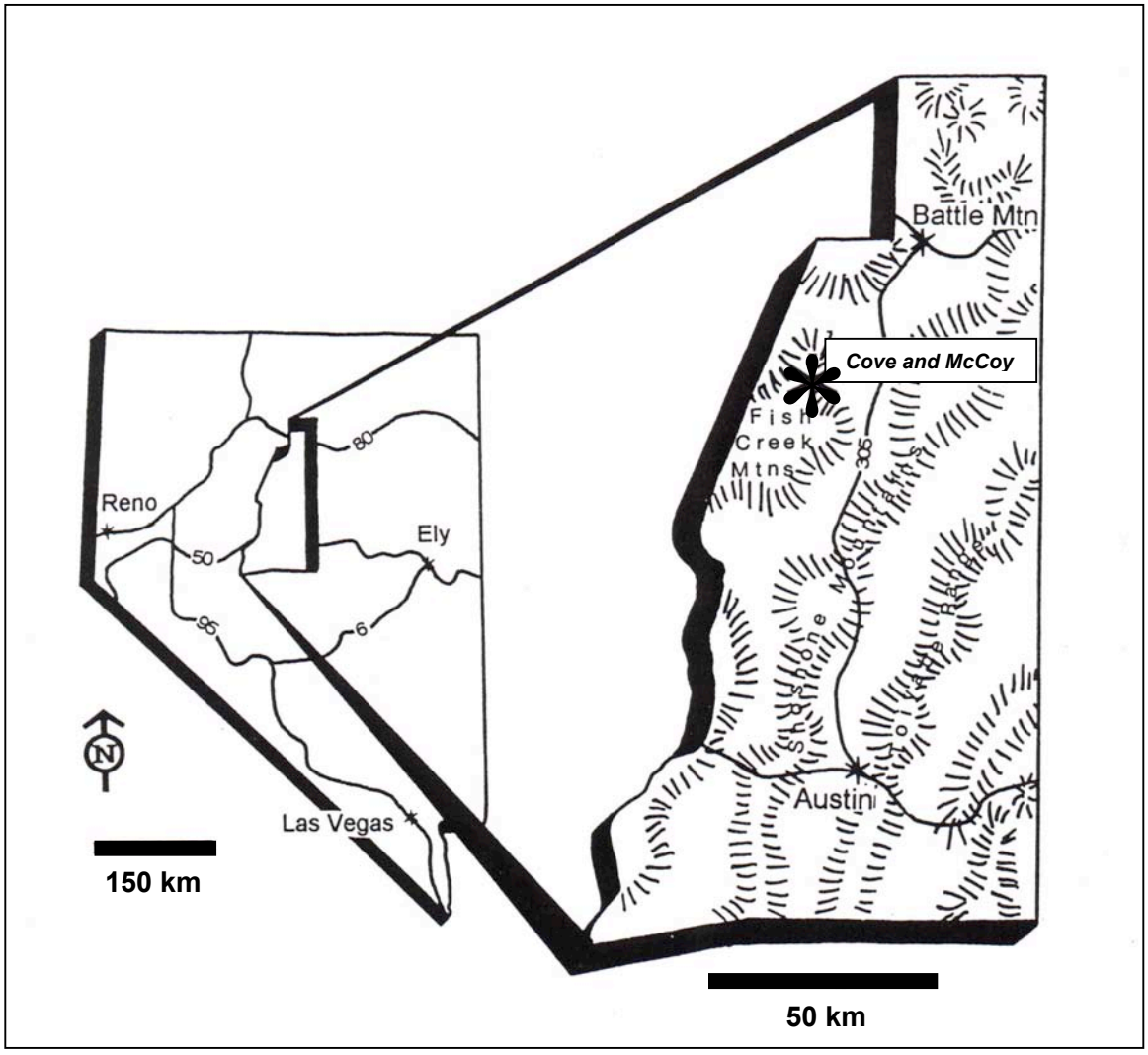

FIG. 1. Location of the Cove and McCoy Mines, Lander County, Nevada. The McCoy Mine is located approximately 1.5 kilometers southwest of Cove.

At Cove, the spatial relationships between orebodies and stratigraphy, structures, intrusions, and types of alteration have been studied (Kuyper et al., 1991; Emmons and Eng, 1995). Little conclusive work has been done, however, to assess the genesis of the seemingly unique deposit. The dual purposes of this study are: 1) construction of a genetic model for the Cove deposit based on mapping and petrological, microanalytical, geochemical, and isotopic studies, and radioisotopic dating; and 2) elucidation of the genetic relationships between the Cove and McCoy deposits. Implications for other deposits are also discussed.

Exploration and Mining History of the McCoy Mining District

Gold was first discovered in the McCoy mining district by Joseph H. McCoy in 1914 (Schrader, 1934). Early Au production was from Au-quartz veins that typically occupied northeast-striking faults and intersections between northeast- and northwest-striking faults (e.g. the Gold Dome mine), and from several placers. Most of the non-placer production was from argillized and oxidized skarn along the contact between the Eocene Brown stock and its host sedimentary units, the present-day site of McCoy open pit. Six mines operated in the district through 1969 (Stager, 1977): Gold Dome, Big Four, Gold Pirate, McCoy, Gold Pirate placer, and West Side placer. Much of the early production occurred in 1930 and 1931, with total Au production during this time estimated at 1000 ounces (Vanderburg, 1939). Total production from 1914 to 1977 was estimated at 10,000 ounces of Au, along with minor Ag, Pb, and Cu (Stager, 1977).

The district was explored for Cu and Au by several companies between 1969 and 1985. In chronological order, exploration efforts were initiated by Summa Corporation, Houston Oil and Minerals Corporation (subsequently Houston International Minerals Corporation and Tenneco Minerals Company), Gold Fields Mining Corporation, and Tenneco Minerals Company (Kuyper et al., 1991). Tenneco Minerals Company began development of the McCoy site in September, 1985 (Emmons and Eng, 1995). Modern production from the McCoy Au (-Cu) skarn began as an open pit heap leach operation in February, 1986, and the first Au was poured in April, 1986.

Systematic districtwide exploration was begun by Tenneco Minerals Company in 1985. Five hundred stream sediment samples were collected from an eight square mile (~21 square kilometers) area around the McCoy Mine (Emmons and Coyle, 1988). In early 1986, a cluster of seven samples having Au anomalies between 15 to 72 ppb and associated anomalous concentrations of Ag, As, Hg, Sb, and Tl were collected from the present location of the Cove Mine. Detailed geological mapping ensued, and mappers identified jasperoid, manganiferous limestone, and outcrops of altered felsic dikes in the anomalous area. Surface rock chip samples of these exposures all contained ore-grade Au (Emmons and Eng, 1995).

Subsequent soil sampling at the Cove site defined an 850-meter-long by 30- to 180-meter-wide Au anomaly ranging from 100 to 2600 ppb, and bulldozer trenching exposed ore-grade rock over the entire length of this anomaly. During the soil sampling campaign, Echo Bay Minerals Company acquired the precious metal holding of Tenneco Minerals Company in October, 1986. Exploration drilling was begun in January, 1987.

By March, 1987, 42 shallow exploration holes had been drilled, with development drilling ensuing in late March.

The majority of mining at Cove and McCoy was from large-scale open pits. Echo Bay Minerals Company started open pit mining at Cove in 1988. Supplemental underground mining was conducted at Cove and McCoy. The underground mining at McCoy was focused on high-grade Au skarn ore that occurred too deep for open pit mining. Three phases of underground mining were conducted at Cove. The earliest phase occurred from 1988 to 1993, and was implemented to recover high-grade BMVT ore. The second phase was initiated in 1999, and followed high-grade BMVT ore extending into the open pit wall near the bottom of the Cove pit. The final phase was focused on the Cove South Deep upper zone, which consisted of high-grade Carlin-style ore. The last two underground mining phases were completed on July 13, 2001.

Gold and Ag from both mines were recovered by milling of the higher-grade ore and heap leaching of the lower-grade ore. The McCoy deposit contained average grades of 0.034 ounces of Au and 0.14 ounces of Ag per short ton. The Cove deposit contained average grades of 0.041 ounces of Au and 1.84 ounces of Ag per short ton. Through 2001, a total of 3,331,481 ounces of Au and 108,495,855 ounces of Ag were produced from the two deposits, with the vast majority of both metals derived from Cove ore. The amount of Ag produced from Cove makes it one of the largest Ag producers in Nevada.

Geologic Setting and Previous Work

The regional stratigraphy at the Cove deposit is shown in Figure 2, and Figure 3 shows the generalized geology of the Cove/McCoy area. The oldest unit recognized in the region is the Mississippian-Permian Havallah sequence, which consists of altered calcareous sandstone and siltstone (Emmons and Eng, 1995). The Havallah sequence is unconformably overlain by strata of the Lower to middle-Upper Triassic Star Peak Group (nomenclature from Nichols and Silberling, 1977), a 1220-meter-thick section of marine platform limestone with lesser conglomerate, sandstone, siltstone, and dolostone. At McCoy, the Star Peak Group is conformably overlain by the Upper Triassic Cane Spring Formation, which consists of lower clastic and upper limestone members. At Cove, the Cane Spring Formation has been removed by erosion, and the Star Peak Group is unconformably overlain by the Oligocene Caetano Tuff, a crystal-rich quartz latite ashflow tuff (Gilluly and Masursky, 1965).

Cove Deposit

Ore at Cove occurs in the Augusta Mountain Formation of the Star Peak Group, which was first described by Muller et al. (1951). The Augusta Mountain Formation is subdivided into three members (see Emmons and Eng, 1995): 1) the lower Ladinian Home Station Member, which consists primarily of massively bedded limestone with diagenetic and/or hydrothermal dolostone, 2) the upper Ladinian Panther Canyon Member, which consists of a lower dolostone submember and an upper clastic submember, and 3) the late Ladinian to early Karnian Smelser Pass Member, which

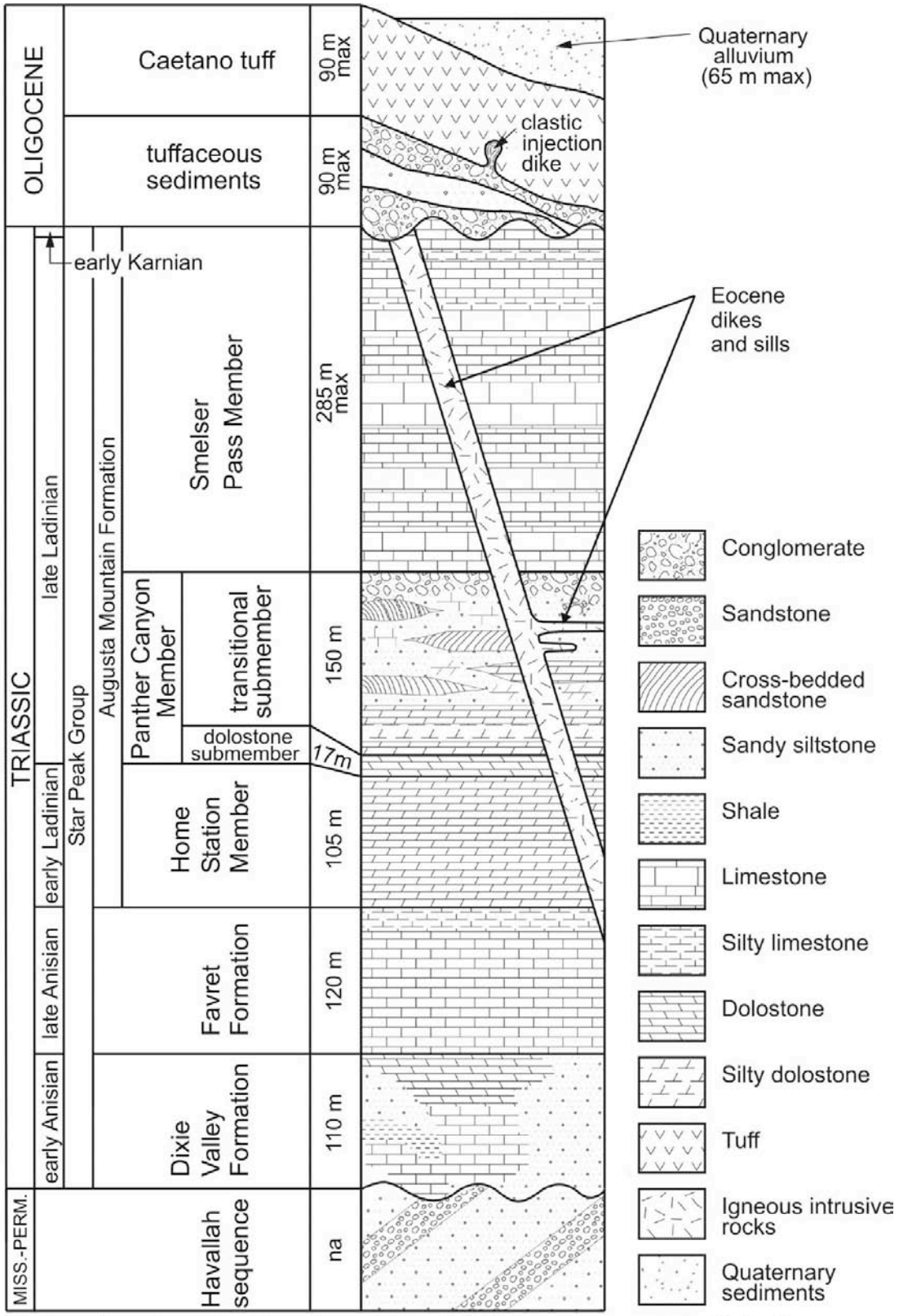

FIG. 2. Stratigraphy at the Cove deposit (modified from Kuyper et al., 1991; Emmons and Eng, 1995).

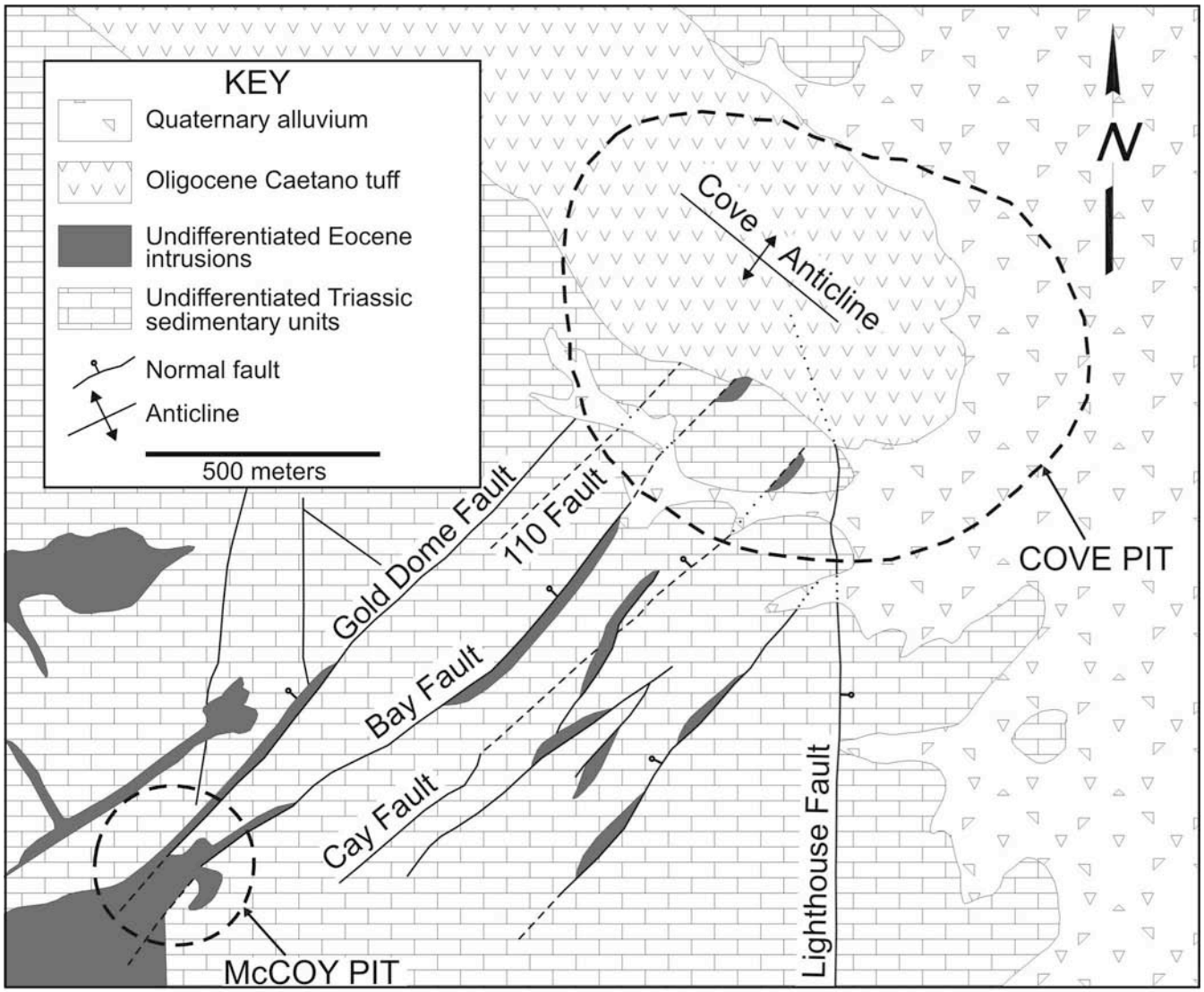

FIG. 3. Simplified geologic map of the Cove-McCoy area (modified from Emmons and Eng, 1995).

consists of medium-to thickly-bedded limestone. The clastic submember of the Panther Canyon Member is referred to as the "transitional submember" in the ensuing text, as it grades from carbonate-dominated strata in its lower half to clastic-dominated strata in its upper half.

Pre-mining in situ reserves at Cove consisted of 3.6 million ounces of Au, and 165 million ounces of Ag (Emmons and Eng, 1995). The deposit consisted of three principal economic orebodies: 1) an oxide orebody, 2) an upper high-grade sulfide orebody, and 3) a lower high-grade sulfide orebody. The oxide orebody was hosted mainly by the lower part of the Smelser Pass Member and consisted dominantly of a supergene overprint on hypogene sulfide assemblages. Higher-grade ore in the supergene system occurred in a central jasperoid zone, and commonly was associated with abundant Mn and Fe oxides. Geochemically, As, Sb, and Hg were highly anomalous, Pb and Zn were weakly anomalous, and Ag:Au ratios ranged from 5:1 to 10:1 in the supergene/oxide zone (Emmons and Eng, 1995).

The upper high-grade sulfide orebody was hosted mainly by the transitional submember of the Panther Canyon Member, and was localized in the footwall of a felsic sill (Kuyper et al., 1991). Typical grades in this zone were 0.25 ounces of Au and 10 ounces of Ag per short ton (Emmons and Eng, 1995). The lower high-grade sulfide orebody was hosted mainly by carbonate strata of the Panther Canyon and Home Station Members, and graded 0.045 ounces of Au and 2.5 ounces Ag per short ton. Silver:gold ratios in the sulfide orebody averaged approximately 50:1, and Pb, Zn, As, Sb, Hg, Cu, and Sn were also anomalous.

Hypogene BMVT ore was dominated by pyrite, sphalerite, and galena (Kuyper et al., 1991; Emmons and Eng, 1995), but the Carlin-style ore mineralogy and associations were poorly documented prior to this study. In general, the Carlin-style ore occurs peripheral to the BMVT ore. Carlin-style ore is found lateral to the BMVT ore in the Home Station and Panther Canyon Members, and is widespread in the Smelser Pass Member, both above and lateral to BMVT ore.

McCoy Deposit

Skarn ore at McCoy is genetically related to a comagmatic suite of Tertiary hypabyssal stocks and dikes of granodioritic composition and dikes and sills of monzonitic and lamprophyric compositions (Brooks, 1994). Gold was hosted principally by the Smelser Pass Member, with subordinate ore hosted by the Cane Spring Formation carbonates (Brooks et al., 1991). 17,200,000 short tons with an average grade of 0.04 ounces of Au per short ton were produced from proximal skarn in the McCoy open pit (Brooks et al., 1991). Pre-mining, in situ reserves at McCoy consisted of 880,000 ounces of Au and 2.3 million ounces of Ag (David L. Emmons, 2000, personal communication). Although the McCoy deposit was economical based solely on its Au content, rocks with significant subeconomic Cu (800 to 1000 ppm; Emmons and Eng, 1995) were present as well.

Ore-grade Au occurred up to 350 feet (~107 meters) laterally from the Eocene Brown Stock, with a vertical range of more than 1150 feet (~350 meters) from the pre-mining surface (Emmons and Eng, 1995). Gold occurred in its native state as grains ranging

from 20 to 100 micrometers in length, typically associated with fresh pyrite and the oxidized products of weathered pyrite (Emmons and Eng, 1995).

Although the host rocks at McCoy are dominantly limestones, localized dolostones also are present near the contact between the Panther Canyon and Smelser Pass Members. Microprobe analyses indicate the presence of up to several weight % each of MnO, MgO, and FeO in host carbonate rocks (Brooks et al., 1991). Host rocks with ore-grade Au are also anomalous in As, Bi, and Te, weakly anomalous in Se, and contain significant Pb and Zn (Brooks et al., 1991; Emmons and Eng, 1995). Although Brooks et al. (1991) believed that Au was not correlative with any elements except S, Emmons and Eng (1995) found Au to be correlative with Cu.

Possible Genetic Relationship between Cove and McCoy

Previous workers recognized that the McCoy Au (-Cu) skarn and the Cove deposit possibly represent district-scale metal zoning related to a single large intrusion (Kuyper et al., 1991; Brooks, 1994; Emmons and Eng, 1995). Such concentric metal zonations have been long recognized (Spurr, 1907; Emmons, 1933 and 1937). Modern discussions of the subject include those by Jerome (1966), cf. Roberts et al. (1971), Sillitoe (1983), Alvarez and Noble (1988), Sillitoe and Bonham (1990), Jones (1992), Hedenquist et al. (1998), and Lang et al. (2000). In the intrusion-related model, the McCoy Au (-Cu) skarn is the proximal component related to a porphyritic intrusion, and Cove, a hybrid BMVT and "Carlin-style" deposit, is the distal component. Five lines of evidence have been used to support the zonation model for McCoy and Cove (Kuyper et al., 1991; Brooks, 1994): 1)

the deposits are proximal to one another; 2) they are localized along the same northeast-striking fault zone; 3) they share identical host rocks; 4) they are associated with similar intrusive rock types; and 5) the associated intrusions for both are dated at about 40 Ma.

Kuyper et al. (1991) also suggested a possible affinity between the Cove sulfide system and the polymetallic vein deposits of the Bolivian Sn-Ag province, as described by Turneaure (1960 and 1971). However, Boyle (1979) noted that typical Sn deposits contain very low Au contents. Because of the high Au concentrations at Cove, the paucity of cassiterite, and relatively low base metal concentrations, Kuyper et al. (1991) strongly supported the metal zoning model instead.

METHODS

Field Methods

Rock types, structures, alteration, and ore characteristics of the Cove open pit were mapped during 73 field days between May, 1998, and August, 1999. The general pit map was completed at a 1:1200 scale, but geologically complex highwalls were mapped at 1:960 and 1:480 scales as necessary. All or part of 24 benches and 9 access/haulage roads were mapped via direct traverse for a total of 19,886 bench meters. Control points were either surveyed in or collected using a portable global positioning system (GPS) device to ensure map accuracy. Inaccessible benches were photographed during optimal lighting conditions to enhance the clarity of structures and lithologies. The photographs were assembled into montages for various portions of the open pit. Faults and lithologic

contacts were mapped onto the montages, field checked, and transferred to the final pit map (Plates 1 and 2). Four cross sections were constructed from the final pit map, using a Vulcan™ database that included cores and reverse-circulation drill holes.

During mapping, 60 attitudes of pervasive mineralized and unmineralized joint sets, 393 attitudes of bedding, and 299 attitudes of faults (APPENDIX I; see Plate 1 for locations) were measured to characterize structures and the structural paragenesis relative to the mineralizing event(s). These data were plotted graphically using Rockware™ software.

More than 340 rock samples were collected from the Cove open pit, underground operation, core, the McCoy open pit, and dike exposures between the McCoy and Cove open pits (APPENDIX II; see Plate 1 for locations). Some of these samples were donated or are on loan from the private collections of previous workers at Cove.

Laboratory Methods

Cross Sections

Cross sections for gold and silver were developed from a database of core and blasthole assays using Vulcan™ software. The individual blocks were contoured, and the contoured data were digitized onto geologic cross sections to determine spatial relations between structures, stratigraphic units, and precious metals.

Thin Sections, Polished Sections, and Doubly-Polished Plates

From the samples collected at the Cove mine, 82 thin and 65 polished sections were prepared by Spectrum Petrographics, Inc.™, 9 thin sections were prepared by San Diego Petrographics™, and 9 polished sections were prepared in the laboratory facilities at the University of Nevada, Reno. Fourteen extra-thick, doubly-polished plates were prepared by Spectrum Petrographics, Inc™ for fluid inclusion analyses. These 179 thin sections, polished sections, and doubly-polished plates were examined using standard reflected and transmitted light petrographic techniques for host rock, ore, and alteration mineralogy, textures, general characteristics, and relationships, and are described in detail in Chapters 4 and 5. Standard scanning electron microscopy, energy-dispersive X-ray, and electron microprobe analyses were performed on the polished sections as necessary to identify unknown minerals and to determine trace constituents and inclusions in known mineral phases. The doubly-polished plates were also used for fluid inclusion analyses described in Chapter 7.

Staining Techniques for Hand Samples

Thirty-one samples of carbonate host rocks from Cove were stained with a potassium ferricyanide and Alizarin red S mixture, following the procedure described by Dickson (1965) and Hitzman (1999), to clarify primary and secondary carbonate mineralogy and textures. Sixteen samples of Cove intrusive rocks were stained using sodium cobaltinitrite to determine K-feldspar and sericite-illite contents using the following procedure: 1) samples were immersed in concentrated HF (52 percent) for 1 minute; 2)

they were dipped in water, then quickly dipped twice in a 5 percent $BaCl_2$ solution; 3) samples were rinsed in water and immersed in a saturated sodium colbaltinitrite solution (10 grams sodium cobaltinitrite per 20 milliliters of water); and 4) the stained samples were rinsed in water to remove any excess cobaltinitrite and air dried. The results of these analyses were used to determine the primary and alteration mineralogies reported in Chapters 2 and 5.

X-Ray Diffraction

Standard X-ray diffraction (XRD) analyses using Jade™ analytical software were performed on more than 30 samples of Cove intrusive rocks (APPENDIX III). The samples were physically disaggregated using a hammer and stainless steel piston-like crusher. Small rock chips were then ground with acetone using an agate mortar and pestle, and slurried onto glass slides using acetone. In addition to the standard XRD runs, several of the samples were re-run to test for smectite-group clay content following the ethylene glycol solvation technique described by Moore and Reynolds (1989). The results were used to determine the hypogene alteration mineralogy discussed in Chapter 5.

X-Ray Fluorescence

Eight samples of Cove intrusive rocks that were also processed for geochemical analyses (see Chapter 6) were submitted to Chemex Labs, Inc.™ for X-ray fluorescence (XRF) analyses for Al_2O_3, CaO, Cr_2O_3, Fe_2O_3, MgO, MnO, P_2O_5, K_2O, SiO_2, Na_2O, and

TiO_2. All eight samples were altered to some degree, and are used primarily for classification purposes in Chapter 2.

Scanning Electron Microscopy

Standard scanning electron microscope (SEM) analyses using a JEOL JSM-840A™ machine coupled with a KEVEX™ energy dispersive X-ray (EDX) device, spectral analysis software, and X-ray mapping software were used as necessary to identify unknown mineral species, and to elucidate mineral zonations and submicroscopic mineral textures. Samples were processed and analyzed in the Electron Microbeam Laboratory of the Mackay School of Mines, University of Nevada, Reno. Because the analyses were principally dedicated to compositional work, all were coated with carbon using a sputter coating assembly. The results of these analyses are reported in Chapter 4.

Electron Microprobe

Electron microprobe (EMP) analyses performed for this project were conducted by Dr. John McCormack in the Electron Microbeam Laboratory of the Mackay School of Mines, University of Nevada, Reno. All samples were coated with C using a sputter coating assembly. Initial EMP analyses were run to determine the Fe content of sphalerite grains for potential use of the sphalerite geobarometer (Barton and Toulmin, 1966; Scott and Barnes, 1971; and Vaughan and Craig, 1997). Additional EMP analyses were done to identify an unknown mineral phase, and to examine chemical zonation in

tennantite-tetrahedrite crystals. The sphalerite data are contained in APPENDIX IV, and the results of all the EMP analyses are reported in Chapter 4.

Multi-Element Geochemistry

A database for multi-element geochemical studies of the Cove deposit was constructed for examination. The database consists of six sample suites, totaling 201 samples, that were analyzed for major, minor, and trace elements (APPENDIX V). Two sample suites were collected during this study. The first suite consists 22 grab samples mostly collected from intrusive rocks at Cove, and also from short transects along presumed conduits for mineralizing fluids. The second suite consists of 28 grab samples collected from a 120-foot (~37-meter) transect across a stratabound network of BMVT veins and pods exposed in the underground workings at Cove.

The 50 samples of the first two suites were submitted to Chemex Labs™ for processing and analyses by the inductively-coupled plasma mass spectrometry (ICP-MS) method for Al, Sb, Ba, Be, Bi, Cd, Ca, Ce, Cs, Cr, Co, Cu, Ga, Ge, Fe, La, Pb, Li, Mg, Mn, Mo, Ni, Nb, P, K, Rb, Na, Sr, Ta, Te, Tl, Th, Ti, W, U, V, Y, and Zn. Gold contents were determined by fire assay – atomic absorption spectrometry (FA-AAS) analyses. Silver and Sn contents were determined by AAS analyses. Arsenic concentrations were determined using an AAS–hydride/electrode discharge lamp method, and Hg concentrations were analyzed using an AAS-flameless method. The samples were also analyzed for trace level F using a specific ion method. Three heavily mineralized samples (HS-3, HS-4, and HS-5) were also analyzed for Pt and Pd using a FA-ICP-

atomic emission spectroscopy method, but the results were all below the detection limits for these elements. Samples with As, Cd, Fe, Pb, Mn, Hg, and/or Zn contents that exceeded the detection limits for the normal analytical methods were reanalyzed for these elements using the AAS method. Samples with Ag and/or Au contents that exceeded the detection limits for the normal analytical methods were reanalyzed for these elements using the FA-gravimetric method.

Geochemical data for sample suites 3 through 6 were collected from unpublished in-house reports for Echo Bay Mines. Sample suite 3 consists of 138 grab samples collected at 10-foot (~3-meter) intervals from 3 core holes. The samples were collected by on-site personnel, pulverized, and submitted to Chemex Labs Inc.™ for processing and ICP-atomic emission spectroscopy analyses for Al, Sb, As, Ba, Be, Bi, Cd, Ca, Cr, Co, Cu, Fe, Ga, La, Pb, Mn, Mg, Hg, Mo, Ni, P, K, Sc, Ag, Na, Sr, Tl, Ti, W, U, V, and Zn. Each sample was also analyzed for Sn using the AAS method. The report date for the Chemex™ results is 5/4/89. Concentrations of Au and Ag were determined by Monitor Geochemical Laboratory, Inc.™; the report dates for these results are 6/24/88, 7/14/88, 7/18/88, 2/10/89, and 2/15/89. No samples that exceeded the detection limits were reprocessed.

Sample suite 4 consists of 3 samples collected on 7/27/99 by David L. Emmons from Carlin-style ore exposed in the Cove underground workings. The samples were submitted to Cone Geochemical Inc.™ for processing ICP analyses for Sb, As, Ba, Be, Bi, B, Cd, Co, Cu, Pb, Li, Mn, Hg, Mo, Ni, P, Se, Ag, Sr, Te, Tl, Sn, Ti, W, V, and Zn.

Fire assay results for Au and Ag concentrations were also included in the report. No samples that exceeded the detection limits were reprocessed.

Sample suite 5 consists of 3 altered Home Station Member samples collected by David L. Emmons in March of 1999. The samples were submitted to Cone Geochemical Inc.™ for processing and ICP analyses for Sb, As, Ba, Be, Bi, B, Cd, Co, Cu, Pb, Li, Mn, Hg, Mo, Ni, P, Se, Ag, Sr, Te, Tl, Sn, Ti, W, V, and Zn. Fire assay results for Au and Ag concentrations were also included in the report. No samples that exceeded the detection limits were reprocessed.

Sample suite 6 consists of 7 samples collected by David L. Emmons on 6/18/99 from a core hole that penetrated the Carlin-style ore mined in the underground operation. The samples were processed analyzed using an ICP-AES method for Al, Sb, As, Ba, Be, Bi, B, Cd, Ca, Co, Cu, Pb, Li, Mn, Mg, Hg, Mo, Ni, P, K, Se, Ag, Na, Sr, S, Te, Tl, Sn, Ti, W, V, and Zn. No additional information regarding processing or analyses of this suite is available.

Two correlation matrices were constructed from the geochemical data (suites 1 through 6) using Microsoft Excel™ software. The first correlation matrix was constructed for the entire 201-sample geochemical database. After eliminating samples and dropping elements for which the geochemical data sets were incomplete, the matrix consists of correlations between 22 elements for 201 samples. The second correlation matrix was constructed from geochemical data for the 50 samples collected during this study.

Sample suites 2 and 6 represent transects across BMVT and Carlin-style ore zones, respectively. These transects are plotted graphically in Chapter 6 in order to identify elements that can be clearly assigned to either BMVT or Carlin-style ore, or both. Because the major components of the systems, such as Fe, Pb, and Zn for BMVT ore, and As and Sb for Carlin-style ore, tend to obscure the more cryptic components, multiple scales were used for the graphical plots of concentrations in order to normalize the magnitudes of peak concentrations.

Light stable isotopes

δD and $\delta^{18}O$ for Intrusive Rocks, and $\delta^{18}O$ for Jasperoid and BMVT Quartz: Eleven samples of altered intrusions were selected for O and H isotope analyses. These samples are from porphyritic intrusions that have been hydrothermally altered to a quartz-sericite-pyrite assemblage. Each sample was physically disaggregated using hammers, chisels, and/or Dremel™ rotary and etching tools, ground using a synthetic corundum mortar and pestle, and sieved using a #60 mesh screen to collect the -60 mesh fraction. The powdered samples were processed by the Stable Isotope Laboratory at Washington State University, Pullman, Washington.

Conventional fluorination techniques (Clayton and Mayeda, 1963) were used to extract O_2 from the powdered samples. ClF_3 was used as an oxidizing agent (Borthwick and Harmon, 1982). O_2 was converted to CO_2 on a resistance-heated carbon rod. The isotope ratio of this gas was measured on a gas source isotope ratio mass spectrometer in

the geochemical laboratories at WSU. Oxygen isotope ratios were reported in the standard δ notation, relative to V-SMOW. Raw data are corrected to an NBS-28 (African glass sand) value of 9.58 per mil, using the in-house standard MM-1 (Mica Mountain pegmatite quartz), which has a value of 12.9 per mil on the NBS-28 scale. Replicate analyses of MM-1 show a standard deviation of less than 0.2 per mil.

Splits from the eleven samples of intrusive rocks used for $\delta^{18}O$ analyses were analyzed for whole-rock silicate δD. All of the samples consisted of intrusions that have been altered to a quartz-sericite-pyrite assemblage. The samples were crushed using a synthetic corundum mortar and pestle, then sieved to a –60 mesh fraction. The sieved fractions were submersed in 10 percent HCl to dissolve calcite, which was present in each sample, then decanted twice in fresh water. After the samples were allowed to dry, the sericite was isolated using bromoform density separation. The sericite samples were sent to Oregon State University, Corvallis, OR, for δD analyses. Samples were analyzed for δD following the general procedure described by Bigeleisen et al. (1952). The H_2 yields were measured with a manometer (which allowed calculation of weight percent water), then sent to Washington State University, Pullman, WA, for mass spectrometry.

The δD values are reported relative to V-SMOW. One sample was analyzed in replicate, and gave values consistent with the accepted laboratory reproducibility of ±2 per mil. Four analyses of a laboratory standard sericite yielded –61.9, -61.3, -57.8, and –60.4 per mil. The accepted value of this standard is –60 ± 1 per mil. These results were within analytical error and accepted values.

Seven samples of BMVT quartz and three samples of jasperoid were also processed and analyzed for $\delta^{18}O$ following the same general procedure described above, except that no heavy liquid separation was necessary.

Carbonate $\delta^{13}C$ and $\delta^{18}O$: Forty-two samples were selected for C and O analyses of carbonate rocks. Nineteen samples were selected as a representative suite of carbonate host units, and consist of the following: five random samples of limestone from the Smelser Pass Member, four random samples of calcitic dolostone from the transitional submember of the Panther Canyon Member, four random samples of dolostone from the dolostone submember of the Panther Canyon Member, three random samples of limestone/dolostone from the Home Station Member, and three samples of dolostone from the Home Station Member from the 1999 Cove underground workings. Eleven samples of carbonate gangue associated with hypogene BMVT veins, eight samples of carbonate veins that cut the BMVT veins, and four samples of post-ore, probably supergene carbonate veins were selected to characterize the mineralizing fluids. All carbonate samples were processed at the stable isotope laboratory at the University of Nevada, Reno.

The 42 carbonate samples were dissagregated and sieved for the -60 mesh fraction following the procedure described for the silicates above. Duplicates were prepared for several samples, and an NBS19 standard was added to the batch. The 19 carbonate host samples were roasted to deactivate the residual organic carbon (McCrea, 1950). All samples were then reacted with concentrated phosphoric acid at 25ºC, and the CO_2

produced was collected in sealed glass tubes following the procedure described by McCrea (1950). Dolostone host samples were reacted with the acid at 25ºC for three hours, and the resultant gases were purged to eliminate interference from calcite. The remaining dolomite was reacted for 72 hours at 25ºC to completion. H_2S produced from acid-soluble sulfides during digestion can interfere with C and O isotopic analyses, and was removed during processing using an additional reaction with Ag_3PO_4 as described by Komor (1995).

The sealed glass tubes were sent to Argonne National Laboratory for mass spectrometric analyses. Carbon and oxygen isotopic results were reported in standard δ notation, relative to V-PDB and V-SMOW, respectively. Each sample was analyzed twice. In all cases, the two results were in close agreement and were averaged.

Sulfide $\delta^{34}S$: Fifteen samples of coarse sulfides were chosen for S isotope analyses. The samples consisted of four samples of pyrite from Cove BMVT ore, three samples of sphalerite from Cove BMVT ore, one sample of galena from Cove BMVT ore, three samples of realgar from Cove Carlin-style ore, one sample of stibnite from Cove Carlin-style ore, and three samples of pyrite from McCoy skarn ore. Because the sulfides were so coarse, simple dissaggregation and hand picking of sulfide grains were all that were required to isolate the samples.

The samples were shipped to Geochron Laboratories in Cambridge, MA, for analysis. For each sample, 10 to 15 milligrams of material were loaded into quartz tubing and secured with quartz wool plugs. The material was combusted at approximately 1100 °C

in a stream of pure O_2 (see Thode et al., 1961). The resulting SO_2 and other gases were passed through a series of cryogenic traps to condense the SO_2 and pump away the contaminants (excess O_2 and any other gases of combustion). The purified sample SO_2 was transferred to a sample flask for mass spectrometric analysis.

SO_2 samples were analyzed at Geochron Laboratories on a VG micromass 903 mass spectrometer. Samples were run in comparison to the in-house reference gas prepared from SR-0010 (Geochron sulfur flowers) that have been calibrated relative to the Cañon Diablo Troilite. Results were calibrated by analyzing a number of internationally accepted standards interspersed among the unknown samples. One duplicate was also run. The precision of this method of analysis is about ±0.3 per mil.

^{40}Ar-^{39}Ar Dating

Five samples were selected for ^{40}Ar-^{39}Ar analysis based on relative ages determined through mapping and petrographic study. Two of the samples contained macroscopic fresh and altered biotite grains, respectively. These samples were disaggregated using a hammer, and the fresh and altered biotites were hand-picked and cleaned using a Dremel™ etching tool. The other three samples contained significant amounts of microscopic illite/sericite that was intimately intergrown with quartz and sulfides. The illite/sericite-quartz-sulfide patches or coatings were pulverized and separated using the Dremel™ etching tool. All separates were placed in small glass vials and shipped to the Nevada Isotope Geochronology Laboratory at the University of Nevada, Las Vegas.

The samples were wrapped in Al foil and stacked inside a Pyrex™ tube. Individual packets averaged 3 millimeters in thickness. Neutron fluence monitors (ANU 92-176 and Fish Canyon Tuff sanidine) were placed every 5 to 10 millimeters along the tube. Synthetic K-glass and optical grade CaF_2 were included in the irradiation packages to monitor neutron-induced Ar interferences from K and Ca.

Loaded tubes were packed in an Al container for irradiation. Samples were irradiated for 14 hours in the D3 position on the core edge (fuel rods on three sides, moderator on the fourth side) of the 1MW TRIGA-type reactor at the Nuclear Science Center at Texas A&M University. Irradiations were performed in a dry tube device, shielded against thermal neutrons by a 5-millimeter-thick jacket of B_4C powder, which rotated about its axis at 0.7 revolutions per minute to mitigate horizontal flux gradients.

Correction factors for interfering neutron reactions on K and Ca were determined by repeated analyses of K-class and CaF_2 fragments. Measured $(^{40}Ar/^{39}Ar)_K$ values were 1.38 (±0.30) * 10^{-2}. Ca correction factors were $(^{40}Ar/^{39}Ar)Ca = 2.78$ (±0.02) * 10^{-4} and $(^{40}Ar/^{39}Ar)Ca = 6.82$ (±0.11) * 10^{-4}. J factors were determined by fusion of 4 to 5 individual crystals of neutron fluence monitors which gave reproducibilities of 0.05 percent to 0.27 percent at each standard position. An error in J of 0.5 percent was used in age calculations. Variation in neutron flux along the 100-millimeter length of the irradiation tubes was <4 percent. No significant neutron flux gradients were present within individual packets of crystals as indicated by the excellent reproducibility of the single crystal flux monitor fusions.

Irradiated crystals and CaF_2 and K-glass fragments were placed in a Cu sample tray in a high vacuum extraction line and were fused using a 20 watt CO_2 laser. Samples were viewed during laser fusion using a video camera system, and positioning was accomplished via a motorized sample stage. Samples analyzed by the furnace step heating method utilized a double vacuum resistance furnace similar to the Staudacher et al. (1978) design. Reactive gases were removed by a single MAP and two GP-50 SAES getters prior to being admitted to a MAP 215-50 mass spectrometer by expansion. The relative volumes of the extraction line and mass spectrometer allow 80 percent of the gas to be admitted to the mass spectrometer for laser fusion analyses and 76 percent for furnace heating analyses. Peak intensities were measured using the Balzers electron multiplier by peak hopping through 7 cycles; initial peak heights were determined by linear regression to the time of gas admission. Mass spectrometer discrimination and sensitivity was monitored by repeated analyses of atmospheric Ar aliquots from an on-line pipette system.

Measured $^{40}Ar/^{39}Ar$ ratios were 289.79 ± 0.35 percent during this work, thus a discrimination correction of 1.02972 (4AMU) was applied to measured isotope ratios. The sensitivity of the mass spectrometer was ~$2 * 10^{-17}$ mol mV^{-1} with the multiplier operated at a gain of 100 over the Faraday. Line blanks averaged $1.8 * 10^{-16}$ mol for mass 40 and $8.0 * 10^{-19}$ mol for mass 36 for laser fusion analyses and $7.0 * 10^{-16}$ mol for mass 40 and $8.0 * 10^{-18}$ mol for mass 36 for furnace heating analyses. Discrimination, sensitivity, and blanks were relatively constant over the period of data collection.

Computer-automated operation of the sample stage, laser, extraction line, and mass spectrometer, as well as final data reduction and age calculations, were performed using labVIEW software written by B. Idleman (Lehigh University). An age of 27.9 Ma (Steven et al., 1967; Cebula et al., 1986) was used for the Fish Canyon Tuff sanidine flux monitor in calculating ages for unknown samples.

For ^{40}Ar-^{39}Ar analyses, a plateau segment is defined as consisting of contiguous gas fractions having analytically indistinguishable ages (i.e. all plateau steps overlap at $\pm 2\sigma$ analytical error) and comprising a significant portion of the total gas released (typically >50 percent). Total gas (integrated) ages were calculated by weighting the amount of ^{39}Ar released, whereas plateau ages were weighted by the inverse of the variance. For each sample, inverse isochron diagrams were examined to check for the effects of excess Ar. Reliable isochrons are based on the criteria of Wendt and Carl (1991) and, as for plateaus, must comprise contiguous steps and a significant fraction of the total gas released. All analytical data are reported at the confidence level of 1σ (standard deviation).

The age data are used to constrain the timing of intrusion and alteration, discussed in Chapters 2 and 5, respectively. Three of the samples produced unreliable results; these results are included as APPENDIX VI.

Fluid Inclusions

Two groups of samples were selected for fluid inclusion analyses. The first group consisted of twelve BMVT ore samples in which macroscopic hydrothermal quartz was

observed. The second group consisted of three samples collected from a deep core. A doubly-polished plate was prepared from each sample by Spectrum Petrographics, Inc.™ An acetone-soluble epoxy was used to prepare the plates. Standard reflected-light petrographic analyses and identifications of ore stage minerals were performed on the samples to fit them into a paragenetic scheme. Standard transmitted-light petrographic techniques were then used to map the hypogene quartz for suitable primary fluid inclusions based on criteria outlined by Roedder (1979). Four samples from the first group and all three samples from the second group contained fluid inclusions suitable for study.

Upon completion of the initial visual inspection, the doubly-polished plates were placed in an acetone bath to separate the sample from the glass plate, then broken into chips. Fluid inclusion analyses were performed for homogenization temperatures (T_H) and final melting temperatures (T_M) on a FLUID, Inc.™ heating/freezing stage. Fluid inclusions were analyzed for T_H on the calibrated equipment. Freezing point depressions were run at later dates. The resultant T_M measurements had to be modified because the thermocouple wire had to be replaced and recalibrated. Unfortunately, several of the quartz crystals from the first group were lost prior to the T_M runs due to disaggregation of the samples.

The T_M measurements were converted to equivalent salinities using conversions from Bodnar (1993). Resultant T_H and T_M/salinity data were plotted graphically using Microsoft Excel™ software to establish trends relative to the hydrothermal system. The

nature of the inclusions (e.g. primary versus secondary) and possibility of inclusion necking are discussed in detail in Chapter 7.

Additional Methods for Data Collected from Internal Reports for Echo Bay

Selected data from unpublished in-house metallurgical reports regarding the Cove deposit are used extensively in Chapter 4. Samples were collected from the Cove open pit, the mill flotation circuit, and leached concentrates. The general sample preparation consisted of assaying for Au and Ag, sieving into suitable size fractions, and concentrating "heavy" and "light" components using a superpanner or heavy liquid media. Polished grain mounts were prepared from the "heavy" fractions, and studied using standard petrographic techniques for mineral associations and characteristics, electron microprobe (EMP) analysis to determine the compositions of Au- and Ag-carriers and the average Au content of selected grains, and secondary ion mass spectrometry (SIMS) analysis to determine the sub-microscopic Au and Ag concentrations and distributions in selected grains. The "light" fractions were typically assayed to determine the amount of Au associated with gangue minerals, most commonly quartz.

Because most of the Cove deposit was mined out prior to commencement of the current study, data from unpublished in-house geological reports are also used to fill in gaps in the data and to produce a deposit-scale understanding of the Cove system. The data used here were produced through standard petrographic analyses of samples from the open pit and processing mill.

CHAPTER 2: STRATIGRAPHY, INTRUSIVE ROCKS, AND STRUCTURAL GEOLOGY OF THE COVE DEPOSIT

INTRODUCTION

Figure 4 is the simplified pit map for the Cove deposit (see Plate 2 for the more detailed Cove open pit geology), and Figure 5 shows a west-east geological cross section developed from the pit map combined with a Vulcan™ cross section built from historical drill hole data. The geologic framework will be used as a basis for descriptions of the distribution, controls, and characteristics of ore and alteration assemblages in the ensuing chapters.

STRATIGRAPHY AND INTRUSIVE ROCKS OF THE COVE DEPOSIT

The stratigraphy of the McCoy mining district is well-documented, and has been described in detail by Emmons and Eng (1995). The following descriptions for units in the Cove open pit and underground operations are based on accessible exposures, hand sample petrography, microscopic petrography, and carbonate staining (Table 1).

Triassic Augusta Mountain Formation

The units described below include the Home Station Member, Panther Canyon Member, and Smelser Pass Member of the Triassic Augusta Mountain Formation (see Fig. 2). The Augusta Mountain Formation belongs to the Triassic Star Peak Group (nomenclature from Nichols and Silberling, 1977), which was formerly called the

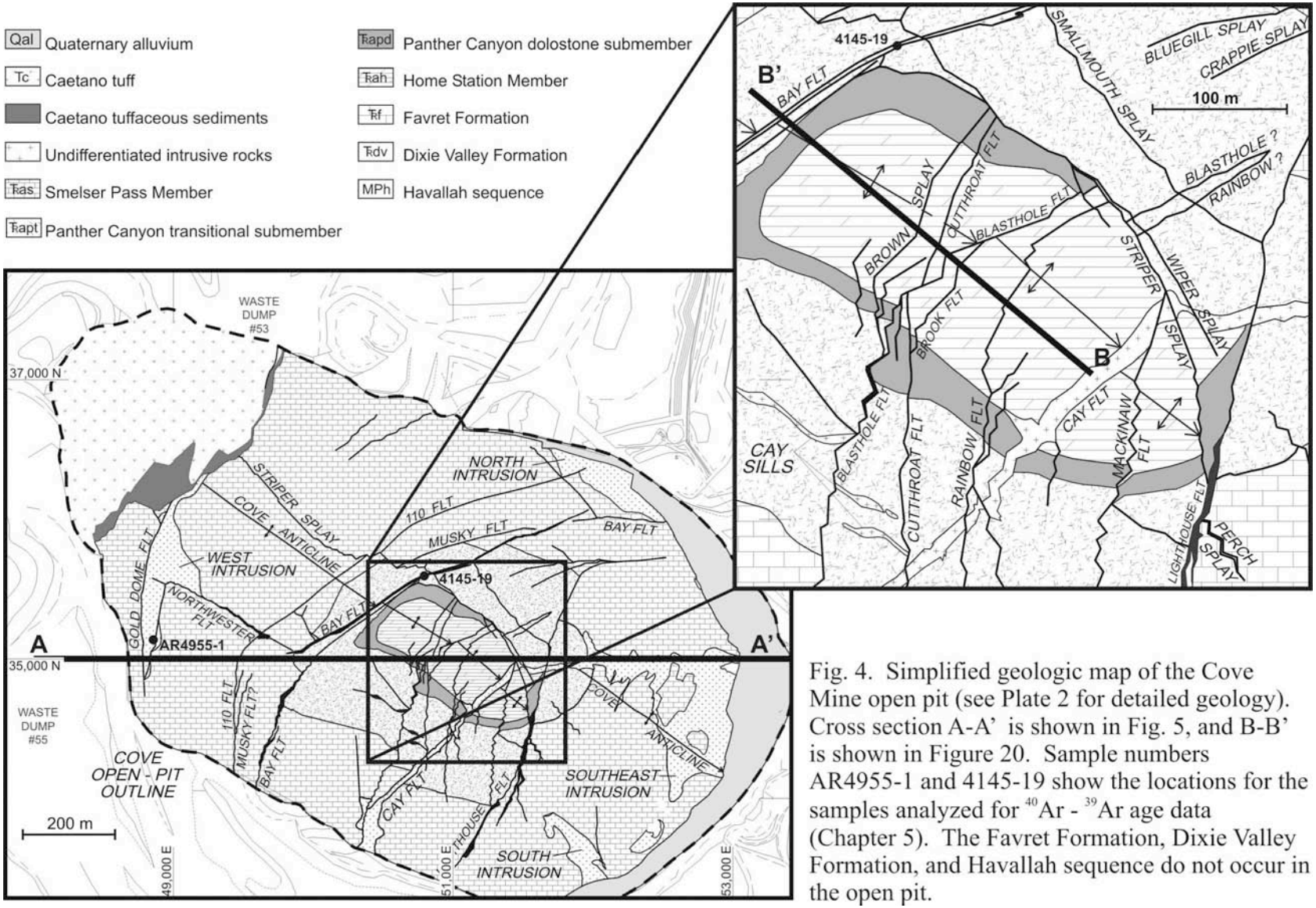

Fig. 4. Simplified geologic map of the Cove Mine open pit (see Plate 2 for detailed geology). Cross section A-A' is shown in Fig. 5, and B-B' is shown in Figure 20. Sample numbers AR4955-1 and 4145-19 show the locations for the samples analyzed for ^{40}Ar - ^{39}Ar age data (Chapter 5). The Favret Formation, Dixie Valley Formation, and Havallah sequence do not occur in the open pit.

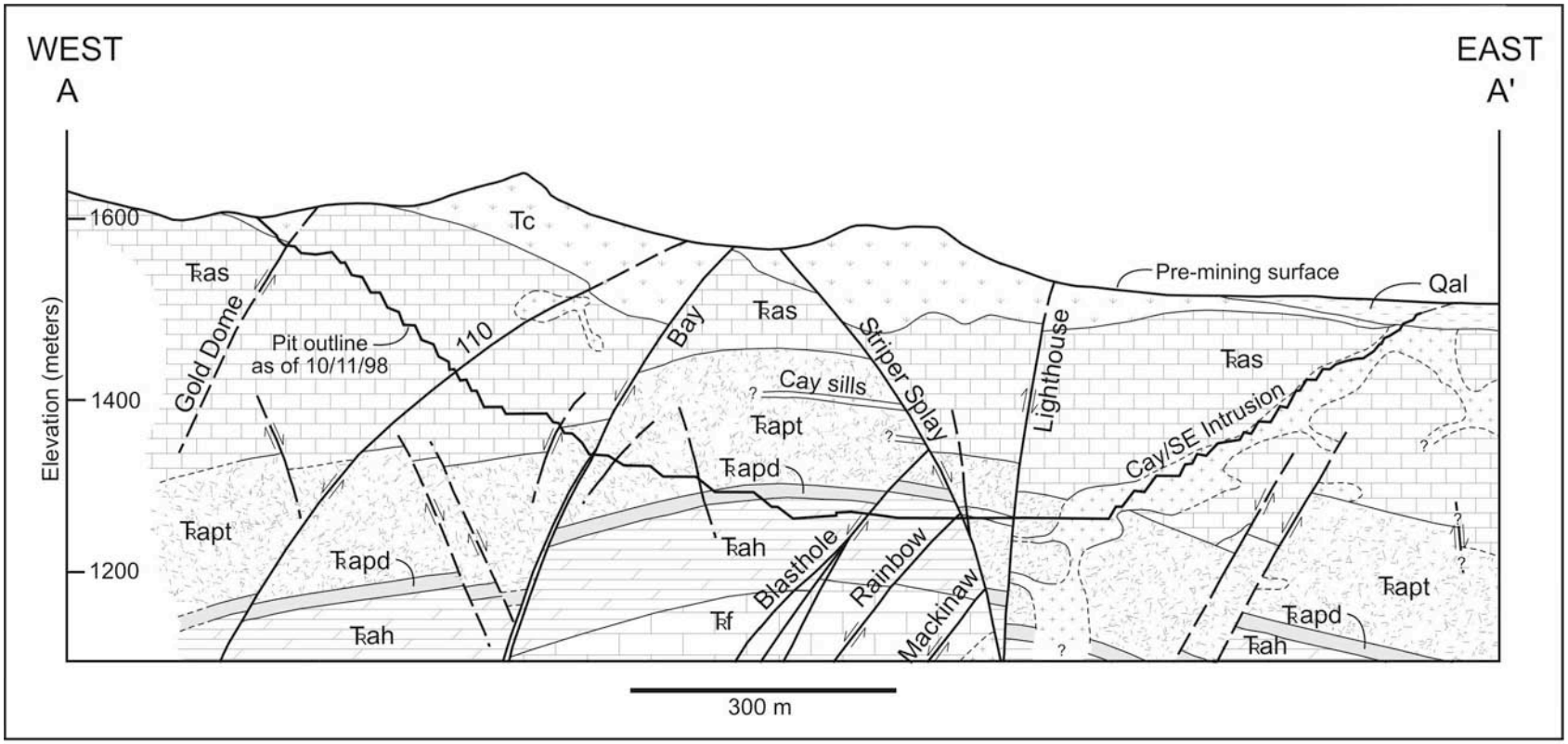

FIG. 5. W-E cross section across the Cove deposit. Refer to Figure 4 for location and lithologic key.

SAMPLE #	UNIT	STAIN RESULTS
4285E-5	Smelser Pass Member	calcite and ferroan calcite
AR4655E-2	Smelser Pass Member	calcite
4365E-4	Smelser Pass Member	calcite and ferroan calcite
25-50-4	Smelser Pass Member	calcite
4325E-3	Smelser Pass Member	ferroan calcite with lesser patches of ferroan dolomite
4525E-3	Smelser Pass Member	ferroan dolomite > ferroan calcite
4465E-8	Smelser Pass Member	calcite
4205E-11	PC transitional submember	weakly calcitic dolomite
4145E-23	PC transitional submember	calcitic dolomite
4205E-13	PC transitional submember	calcitic dolomite cut by ferroan calcite veinlet
4145E-17A	PC transitional submember	interlaminated ferroan dolomite > calcitic dolomite
4145E-38	PC transitional submember	weakly calcitic dolomite
4145E-24	PC dolostone submember	dolomite
CSD-3	PC dolostone submember	weakly calcitic dolomite
CSD-2	PC dolostone submember	very weakly calcitic dolomite
CSD-1	PC dolostone submember	ferroan dolomite
CVC4-1793	Home Station Member?	ferroan calcite = ferroan dolomite
CVC205A-1019.5	Home Station Member	calcite with lesser dolomite and ferroan calcite
CVC2?5A-10??.5	Home Station Member	weakly calcitic dolomite
CVC218-808	Home Station Member	dolomite, calcite vug with ferroan calcite center, recrystallized calcite patches
CVC218-813.5	Home Station Member	dolomite
CVC218-870.2	Home Station Member	dolomite
CVC218-877	Home Station Member	dolomite
CSD-7	Home Station Member	dolomite
CSD-5	Home Station Member	dolomite, very weakly calcitic?
CSD-6	Home Station Member	weakly calcitic dolomite

TABLE 1. Alizarin Red S and potassium ferricyanide stain results for Cove carbonate strata.

Augusta sequence (Silberling and Roberts, 1962; Stewart and McKee, 1977). In the McCoy mining district, the Star Peak Group comprises a 1220-meter-thick, conformable sequence of marine platform limestone with lesser conglomerate, sandstone, siltstone, and dolostone (Emmons and Eng, 1995).

Home Station Member

The Home Station Member is 90 to 120 meters thick (Emmons and Eng, 1995), and was previously described as consisting of massive calcareous and dolomitic limestone with lenses or beds of sandstone and conglomerate (Kuyper et al., 1991). At Cove, however, only the upper ~20 meters were exposed by mining. This portion of the unit is made up of medium- to dark-gray, very thick-bedded (beds greater than 1 meter in thickness) dolostone consisting 3 to 25 volume percent quartz grains (averaging 0.04 millimeters diameter) in a recrystallized dolomite matrix (Fig. 6). Therefore, this unit is classified as a silty dolostone. Scattered 1- to 3-centimeter-long patches of white recrystallized dolomite are typically kidney-shaped, suggesting that they originally may have been bioclasts. Although the contact between the Home Station Member and the overlying Panther Canyon Member was described as gradational by Kupyer et al. (1991), the contact mapped in the open pit at Cove is sharp.

Panther Canyon Member

The Panther Canyon Member at Cove is divided into two informal units, the lower dolostone submember and upper transitional submember.

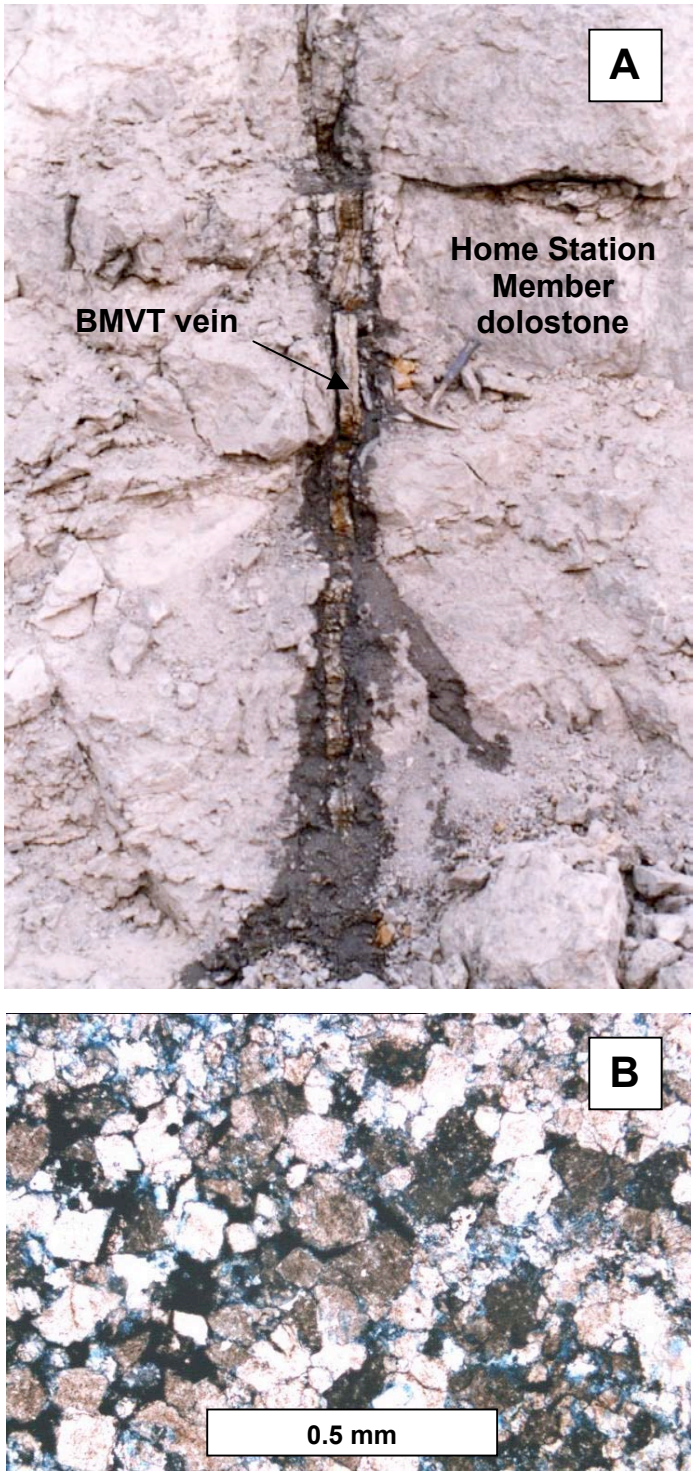

FIG. 6. Macroscopic and microscopic characteristics of the dolomitic Home Station Member. A shows a BMVT vein cutting the secondary dolostone. The unit is medium-bedded to massive. B is a transmitted light photomicrograph (crossed polars) for sample CSD-7, showing that the dolostone consists of recrystallized dolomite rhombs with significant intercrystalline porosity, indicated by the blue-dyed impregnating epoxy.

Dolostone Submember: This unit is uniformly ~17 meters thick, and consists of a well-bedded, medium-gray dolostone (Fig. 7). Individual beds are typically less than 1 meter in thickness. This unit is a primary dolostone, and commonly has stromatolitic algal textures (Emmons and Eng, 1995). Quartz grains (0.025 millimeters diameter) locally constitute up to 20 volume percent of the samples examined. No allochemical fragments were observed. Minor stylolites are present, and disseminated pyrite is widely distributed. The uppermost bed contains dissolution cavities averaging 1 to 3 centimeters in diameter. In samples from the hinge zone of the Cove anticline, these dissolution holes contain a recrystallized dolomite rind lined with cockscomb quartz and open-space growths of euhedral sulfides. The contact with the overlying transitional submember is very gradational over a distance of several meters.

Transitional Submember: This 150-meter-thick unit coarsens upward, from a basal primary dolostone, through middle silty and sandy dolostone and carbonate-cemented silt- and sandstone, to conglomerate near the top (Fig. 8 and Fig. 9). The general transition is not smooth, however, as contrasting lithologies are interspersed throughout the unit at all levels, typically as lensoid bodies. In order to simplify the following summary, the transitional submember is arbitrarily separated into a lower carbonate-rich and an upper clastic section.

Lithologies in the 50-meter-thick lower carbonate-rich section are highly variable. Although the strata are primarily made up of dolostone, lenses and beds of carbonate-cemented siltstone and very fine-grained sandstone, coarser sandstone, and conglomerate

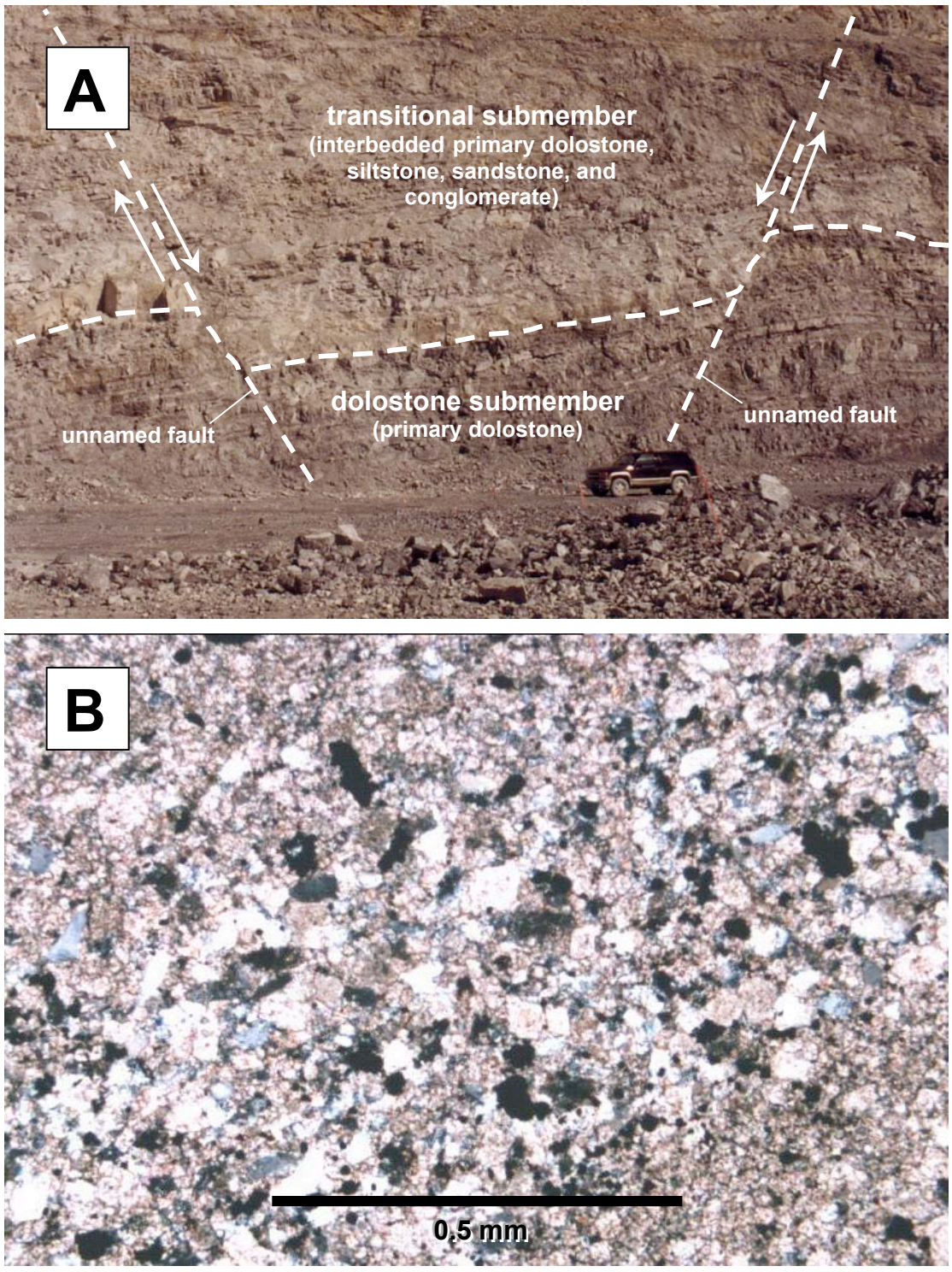

FIG. 7. Dolostone submember of the Panther Canyon Member. A shows the contact between the lower dolostone submember and the overlying transitional submember. B is a photomicrograph (crossed polars) of a sample from the dolostone submember (sample CSD-3), showing interlocking dolomite grains (white to pink) with lesser quartz grains (bluish-gray to black).

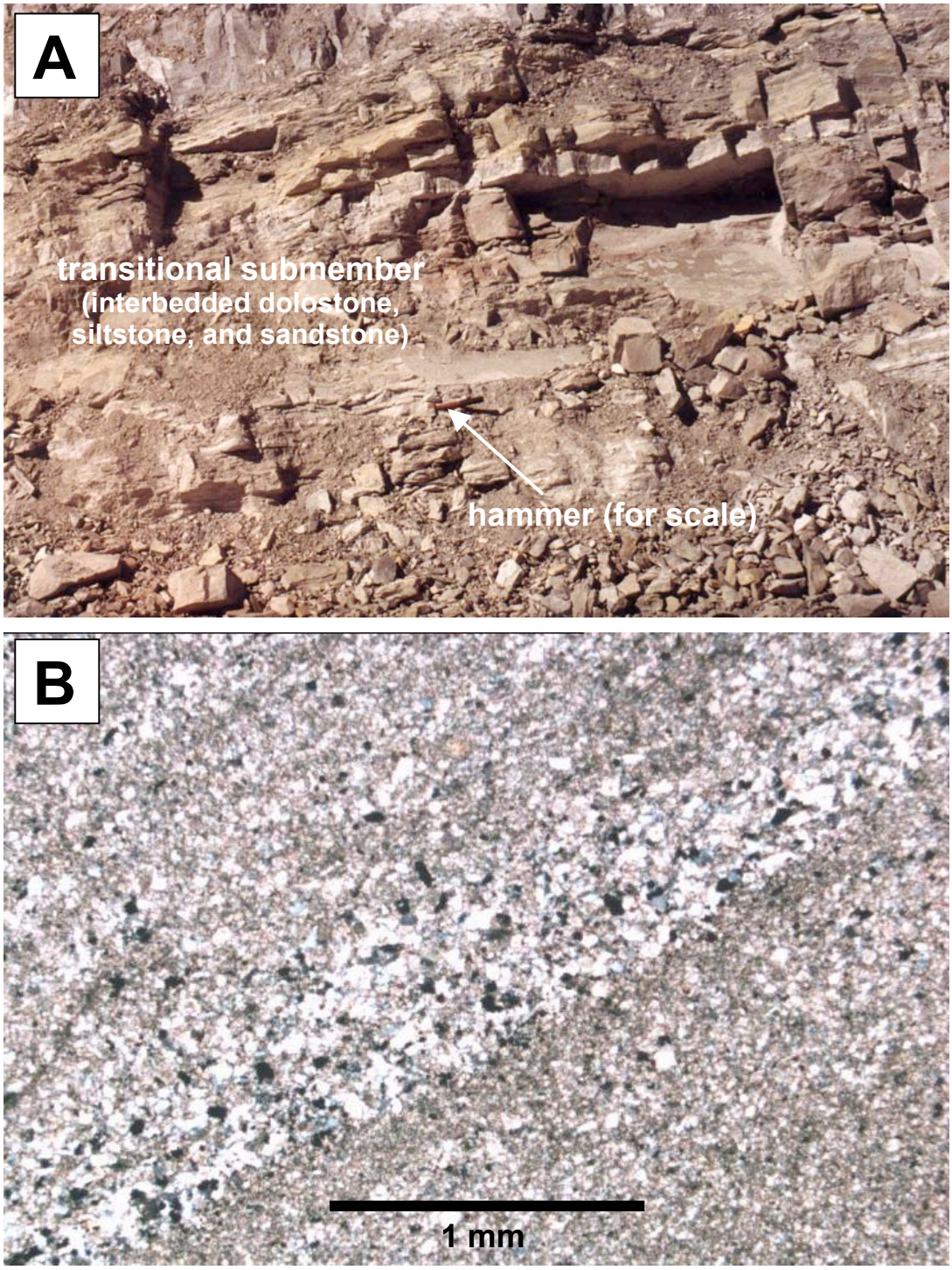

FIG. 8. Lower part of the transitional submember of the Panther Canyon Member. A is a photograph showing thin- to medium-bedded silty dolostone, siltstone, and sandstone. B is a transmitted light photomicrograph of sample 4205E-13 (crossed polars), showing general characteristics of the silty dolostone. As shown in Table 1, the carbonate component is interlocking grains of calcitic dolomite (white to pink coloration). Quartz grains are bluish-gray to black.

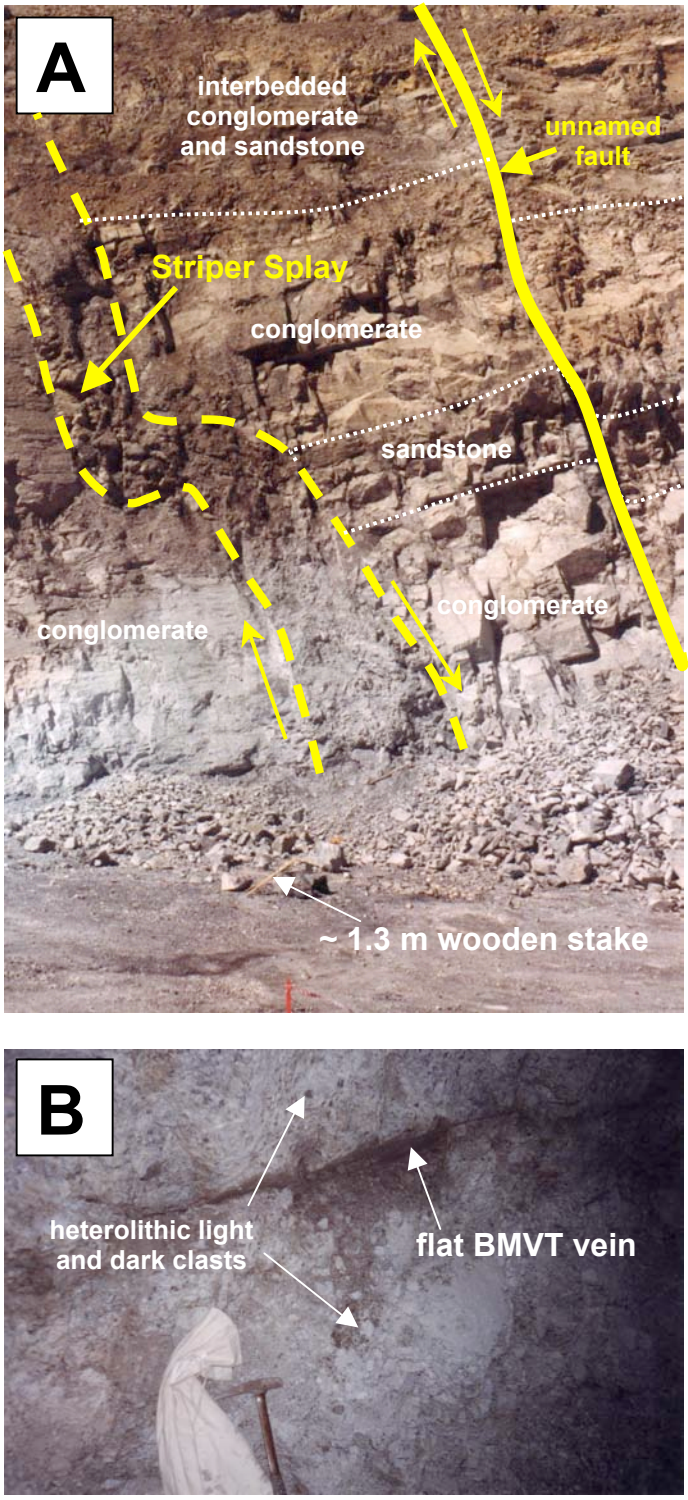

FIG. 9. Upper part of the transitional submember of the Panther Canyon Member. A is a photograph showing the generally medium-bedded to massive character of the sandy to conglomeratic strata. B is a 1999 photograph of a rib exposure of upper transitional submember conglomerate in the underground workings.

are abundant. The lower 25 meters of this section consist principally of massive dolostone. Typical strata in the upper 25 meters of this section consist of 0.025- to 0.08-millimeter-diameter, subrounded, moderately-sorted quartz grains. Individual beds are typically less than 1 meter in thickness. The diagenetic cement is calcite, but it has been dissolved and/or replaced by illite-sericite where hydrothermally altered.

The 100-meter-thick upper clastic section in the transitional submember generally consists of fine-grained sandstone to cobble conglomerate. The thickness of bedding is highly variable, but the conglomerate beds are generally thicker (up to 5 meters thick) than the sandstone beds (up to 1 meter thick). Cross-bedding is common, and conglomeratic strata typically grade upwards from relatively coarse- to relatively fine-grained sediments. Detrital grains and cobbles consist of chert, quartzite, and quartz. These grains are rounded to subrounded and moderately sorted. Primary porosity, which was originally high, has been greatly reduced in samples from the open pit by deposition of hypogene sulfides, illite-sericite, and silica. In one sample, sericite and subsequent calcite veins have obscured primary textures and reduced porosity to nearly zero volume percent. Current porosity in some samples, however, ranges up to 20 volume percent. The contact with the overlying Smelser Pass Member is gradational over several meters.

Smelser Pass Member

Having ~285 meters maximum thickness, this unit is volumetrically the largest at Cove. The unit is predominantly a microcrystalline limestone with abundant recrystallized bioclasts (Fig. 10), but the upper 150 meters contain very minor, 5- to 30-

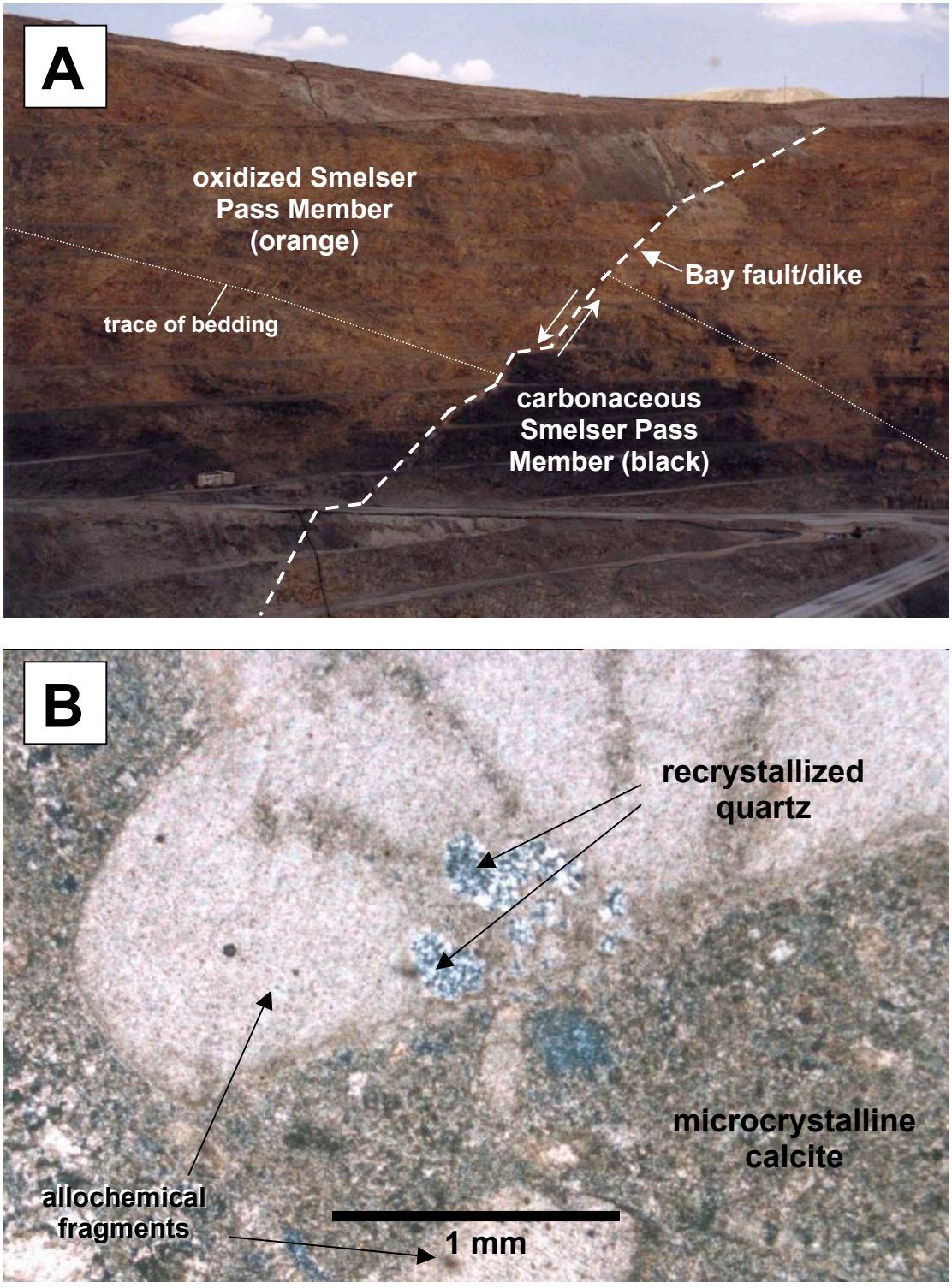

FIG. 10. Smelser Pass Member. A is a photograph of the north highwall of the Cove Mine showing oxidized and carbonaceous limestone. B is a transmitted light photomicrograph of sample 5015-3 (crossed polars) showing slightly silicified limestone consisting of bioclastic microcrystalline calcite.

centimeter-thick, interlaminated calcareous shale beds. The limestone is thick-bedded to massive, with individual beds ranging from 1 to 5 meters in thickness. Macro-allochemical remains consist of partial to complete brachiopods, pelecypods, gastropods, crinoids, corals, sponges (tentative identification), and ammonites, in decreasing order of abundance. The bioclasts typically are randomly packed, mostly partial fragments, indicating a thanatocoenosis ("death-assemblage"). However, several strata contain larger, complete, articulated brachiopods and/or corals in oriented positions, suggesting a biocoenosis or deposition resulting from a short-term, higher-energy event. The lowermost beds contain up to 15 volume percent 0.015-millimeter-diameter quartz grains.

The Smelser Pass Member is separated from the overlying Oligocene tuffaceous sediments and Caetano tuff by an angular unconformity. Kuyper et al. (1991) determined that the upper 175 meters of the Smelser Pass were removed by erosion prior to deposition of the Oligocene units. More than 650 meters of the Triassic Cane Spring and Osobb Formations, which overlie the Smelser Pass Member elsewhere in the McCoy mining district, are also missing at Cove. Much of the Smelser Pass Member has been subjected to supergene oxidation, giving the originally medium- gray limestone an orange to brown appearance.

Eocene Igneous Rocks

Discontinuous dikes and related sills are abundant at Cove. The dikes occupy the Lighthouse, Cay, Blasthole, Bay, 110, and Gold Dome faults (Fig. 4 and Plate 2), and occur as the large, irregularly-shaped West, Northeast, Southeast, and South intrusions

(Plate 2). All of the intrusions are nearly identical in composition and consist of 0.5- to 5.0-millimeter-long phenocrysts in a microcrystalline matrix (Fig. 11B). Phenocrysts average about 20 volume percent of the rock. In decreasing order of abundance, the phenocrysts are zoned plagioclase, biotite, hornblende, and resorbed quartz, with trace apatite, zircon, and monazite. The groundmass consists of aphanitic grains of phenocryst minerals with K-feldspar and trace zircon. Hydrothermal alteration is pervasive in these intrusive bodies, and is discussed in detail in Chapter 5.

Table 2 summarizes the XRF data produced for this report from selected samples of intrusive rocks, and is augmented by data from Emmons and Eng (1995) for the Brown stock at McCoy and feldspar porphyry dikes between the McCoy and Cove open pits. Although the primary mineralogy of the Cove intrusions is generally obscured by hydrothermal alteration, the petrological and geochemical data indicate that their original compositions were monzonitic to granodioritic. Emmons and Eng (1995) published five K-Ar dates for intrusive rocks at Cove (Table 3), indicating a late Eocene age of intrusion. New ^{40}Ar-^{39}Ar age data obtained in this study are discussed in detail in Chapters 5 and 7.

Oligocene Stratigraphic Units

Tuffaceous Sediments

A sequence of weakly consolidated sandstone and conglomerate underlies the Caetano tuff. These sediments are up to 90 meters thick (Kuyper et al., 1991), contain clasts of

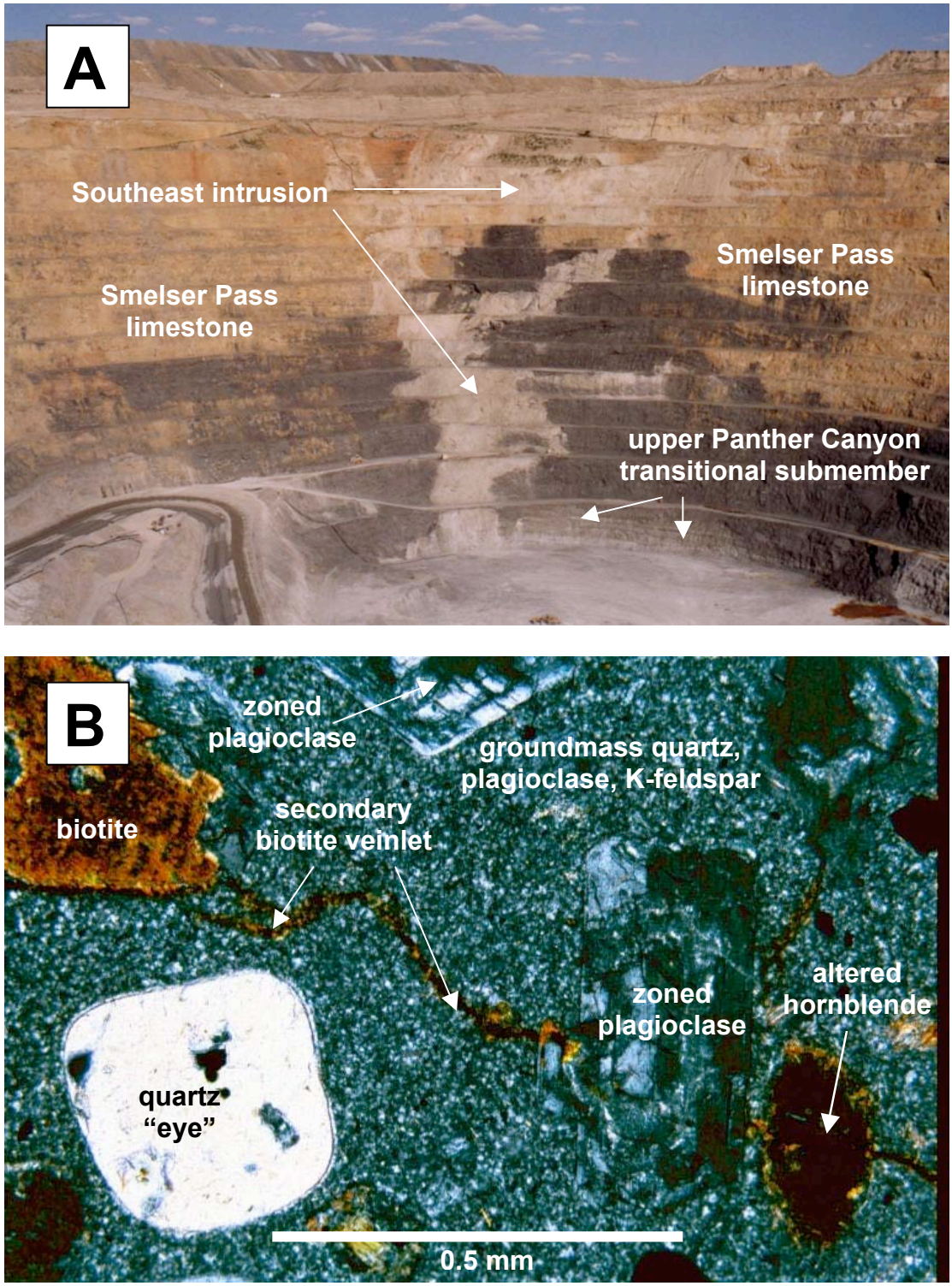

FIG. 11. Eocene porphyritic intrusions of the Cove deposit. A is a 1998 photograph of the Cove east highwall showing the general appearance of an altered intrusion. B is a transmitted light (crossed polars) photomicrograph of sample 4725E-4 showing the general mineralogy and textures of a slightly altered Cove intrusion.

SAMPLE	DESCRIPTION	ALTERATION INTENSITY
4725-4	From the east side of the Northeast Intrusion at Cove	*Weak*
4205-23	From the Southeast Intrusive at Cove	*Moderate*
4285-11	From the Cay sills at Cove	*Moderate-strong*
AR-8	From the Lighthouse fault and dike complex at Cove	*Moderate-strong*
4205-5	From the Bay fault and dike complex at Cove	*Strong*
4205-7	From the Bay fault and dike complex at Cove	*Total*
4405-2	From the 110 and Striper intersection at Cove	*Very strong*
HS-6	From the Cay dike at Cove	quartz-sericite-pyrite
143108	Feldspar porphyry dikes of Emmons and Eng (1995)	"some alteration"
143111	Feldspar porphyry dikes of Emmons and Eng (1995)	"some alteration"
143114	Feldspar porphyry dikes of Emmons and Eng (1995)	"some alteration"
320507	Brown stock at McCoy	no data
R85-85 625	Brown stock at McCoy	no data
R26-86 335	Brown stock at McCoy	no data
R28-86 225	Brown stock at McCoy	no data

SAMPLE	Al_2O_3	CaO	Cr_2O_3	Fe_2O_3	K_2O	MgO	MnO
4725-4	16.21	3.54	< 0.01	4.51	2.78	1.44	0.05
4205-23	14.64	2.91	< 0.01	2.73	3.03	2.04	0.06
4285-11	14.35	4.88	< 0.01	2.97	3.32	1.54	0.16
AR-8	16.25	4.94	< 0.01	3.55	2.62	1.69	0.05
4205-5	16.11	0.37	< 0.01	4.92	5.13	0.62	0.02
4205-7	17.33	0.42	< 0.01	8.10	4.37	0.58	0.01
4405-2	16.47	4.12	< 0.01	3.85	3.43	0.61	0.04
HS-6	16.48	0.32	< 0.01	2.87	2.61	0.50	< 0.01
143108	18.06	0.24	no data	0.70	1.24	0.28	< 0.01
143111	16.17	0.61	no data	0.78	2.25	0.24	< 0.01
143114	18.39	1.50	no data	0.99	3.34	0.40	< 0.01
320507	15.43	5.32	no data	1.45	0.76	1.89	< 0.01
R85-85 625	16.47	4.96	no data	5.30	2.82	2.53	< 0.01
R26-86 335	15.97	4.04	no data	4.19	3.30	1.67	< 0.01
R28-86 225	15.86	6.31	no data	2.23	5.60	1.52	< 0.01

SAMPLE	Na_2O	P_2O_5	SiO_2	TiO_2	LOI	TOTAL
4725-4	2.50	0.22	63.10	0.66	4.09	99.10
4205-23	1.81	0.12	64.34	0.38	6.70	98.76
4285-11	0.60	0.15	61.34	0.40	9.32	99.03
AR-8	0.99	0.25	57.71	0.63	10.51	99.19
4205-5	< 0.01	0.18	65.05	0.63	6.35	99.36
4205-7	0.12	0.20	59.25	0.79	7.87	99.04
4405-2	0.23	0.25	60.75	0.71	8.48	98.94
HS-6	< 0.01	0.16	69.81	0.48	6.40	99.63
143108	6.62	0.20	71.73	0.18	1.68	100.92
143111	7.50	0.06	72.09	0.20	1.34	101.23
143114	4.42	0.09	70.71	0.27	2.89	102.99
320507	4.48	0.16	68.50	0.41	1.57	99.96
R85-85 625	3.00	0.23	63.14	0.65	3.41	102.50
R26-86 335	3.16	0.20	64.49	0.50	2.06	99.57
R28-86 225	1.34	0.18	64.76	0.51	2.14	100.44

TABLE 2. Whole rock X-ray fluorescence (XRF) data for selected intrusions exposed in the Cove open pit, the Brown stock in the McCoy open pit, and from feldspar porphyry dikes exposed between the two mines. All data reported in percentages. Alteration types for samples 4725-4, 4205-23, 4285-11, AR-8, 4205-5, 4205-7, and 4405-2 are described in Chapter 3 of this volume. Brown stock and feldspar porphyry dike sample data from Emmons and Eng (1995).

Rock Unit	**Age Ma**	**Material**	**Comments**
Brown stock	40.0±1.5	sericite	biotite quartz monzonite
Brown stock	40.9±1.6	sericite	quartz monzonite
Brown stock	41.6±1.6	biotite	biotite quartz monzonite
Brown stock	42.9±1.9	sericite	altered quartz monzonite
"Mafic dike"	48.6±2.0	biotite	north of McCoy deposit
"Dike"	64.5±3.1	hornblende	dike near NW Brown zone
Feldspar porphyry	37.0±2.2	hornblende	McCoy decline
Feldspar porphyry	39.9±1.6	biotite	drill cuttings, pediment area
Bay dike	*40.3±1.2*	*biotite*	*Bay dike at Cove deposit*
Bay dike	*39.5±1.5*	*biotite*	*Bay dike at Cove deposit*
Cay dike	*39.4±1.2*	*biotite*	*Cay dike at Cove deposit*
Southeast Intrusion	*38.8±1.1*	*biotite*	*Southeast Intrusion at Cove*
Southeast Intrusion	*40.0±1.2*	*biotite*	*Southeast Intrusion at Cove*
Adularia vein	39.1±1.5	adularia	McCoy gold deposit
Adularia vein	38.7±1.1	adularia	McCoy gold deposit
Flow-dome complex	34.1±0.9	biotite	Pinnacle Mountain
Flow-dome complex	32.9±0.9	biotite	Pinnacle Mountain
McCoy pluton	140±6	whole rock	drill cuttings
McCoy pluton	139±7	whole rock	drill cuttings

TABLE 3. K-Ar age determinations in the McCoy mining district (from Emmons and Eng, 1995). The samples highlighted in italics were collected from the Cove deposit.

the Star Peak Formation units and Caetano tuff, and are asymmetrically concentrated on the south side of a paleo-valley that localized the Caetano tuff in this vicinity (Fig. 12A). The occurrence of clasts of Caetano tuff in these sediments indicates that the tuff may be the product of multiple eruptions.

Caetano Tuff

The Caetano tuff (Fig. 12A) is post-mineral and regarded as waste at Cove. The unit has a maximum thickness of ~90 meters, and contains 0.4- to 7-millimeter-long fragments of plagioclase, biotite, K-feldspar, and resorbed quartz phenocrysts in a glassy to devitrified matrix (Fig. 12B). Phenocrysts comprise 40 volume percent and matrix 60 volume percent of the rock. Stewart and McKee (1977) considered the unit to be Oligocene (33.5 Ma, by revised decay constants (Emmons and Eng, 1995; Table 4), on the basis of 12 radiometric ages (10 K-Ar and 2 fission track)). The oldest reported age for the Caetano tuff is 36.0 Ma (Emmons and Eng, 1995).

Figure 4 and Plate 2 show the presence of ejection sediments and clastic injection dikes that are related to the deposition of the Caetano tuff. The ejection sediments consist of tuffaceous sediments that were apparently squeezed out of the margins of the paleo-valley as it was filling with Caetano tuff. The clastic dikes consist of tuffaceous sediments that were injected into the base of the tuff as it was deposited, and prior to its lithification.

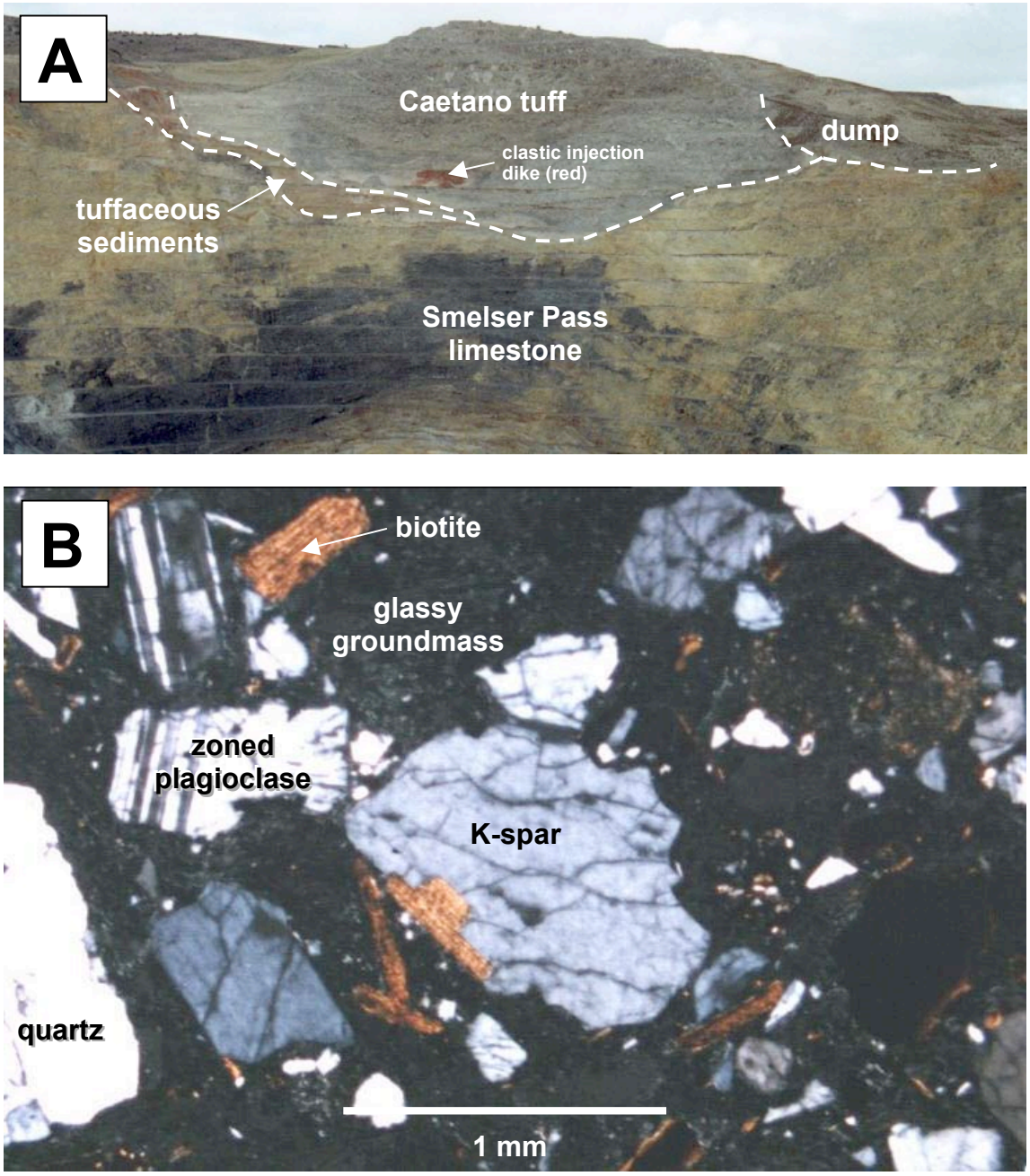

FIG. 12. Caetano tuff. A is a photograph taken in October, 2000, showing the Caetano tuff and underlying tuffaceous sediments occupying a paleo-valley in the Smelser Pass Member. B is a transmitted light (crossed polars) photomicrograph of sample 4955E-3, showing the mineralogy and texture of the Caetano tuff. Note that all of the phenocrysts are broken.

LOCATION	SOURCE OF DATA	MATERIAL DATED	AGE(S) (Ma)	AVERAGE AGE (Ma)
Cortez area, Eureka County	J.D. Obradovich, U.S. Geol. Survey, unpublished data	Biotite Sanidine	34.4±1.1 32.6±1.1	33.5
Northern Toiyabe Range	Armstrong, 1970	Biotite	30.6±0.6	30.6
Northern Toiyabe Range	Armstrong, 1970	RK (?)	31.2±1.0	31.2
Northern Toiyabe Range (?)	Gilluly and Masurky, 1965; G.H. Curtis, Univ. Calif. Berkeley, unpublished data	Biotite	31.5	31.5
East edge of Battle Mountain	McKee and Silberman, 1970	Biotite	33.6±1.3	33.6
Shoshone Range approximately 20 miles south of Mount Lewis	McKee and Silberman, 1970	Biotite Sanidine	31.3±1.3 31.0±1.0	31.2
Toiyabe Range approximately 25 miles south of Cortez	McKee and Silberman, 1970	Biotite	33.5±1.0	33.5
North end of Fish Creek Mountains	McKee and Silberman, 1970	Biotite Sanidine	33.4±1.4 31.3±1.3	32.3
Northwestern part of Fish Creek Mountains	E.H. McKee, unpublished data	Sanidine	32.7±1.1	32.7
North end of Fish Creek Mountains	Naeser and McKee, 1970	(Fission track)		33.3
North end of Carico Lake Valley	Naeser and McKee, 1970	(Fission track)	34.1 35.5 38.5	36.0
West edge, Carico Lake Valley	Naeser and McKee, 1970	Biotite		32.0
Average	_____	_____	_____	**32.6**

TABLE 4. Radiometric ages of Caetano tuff (from Stewart and McKee, 1977). Emmons and Eng (1995) used revised decay constants to recalculate the average age to 33.5 Ma.

Tertiary/Quaternary Karst Deposits

A few caverns in the upper portions of the Smelser Pass Member range in size from <1 to ~35 meters in width. These caverns are completely infilled with sand- to cobble-sized fragments of Caetano tuff, manganifereous jasperoid, and rocks with no obvious local source. In the largest cavern, the walls and bottom consisted of in-place intrusive rocks, indicating karstification of a dike related to the Southeast intrusion.

Quaternary Alluvium

Emmons and Eng (1995) divided the Quaternary surficial units in the McCoy mining district into alluvium, talus, and colluvium. Quaternary sediments exposed in the Cove open pit were not differentiated in this study. These sediments include unconsolidated sand and gravel, and are less than ~65 meters thick.

STRUCTURAL GEOLOGY OF THE COVE DEPOSIT

The Cove deposit is centered on a broad, gently southeast-plunging anticline that was modified by normal faults (Fig. 13). Folding probably occurred in the Mesozoic, and definitely predated the intrusion of Eocene dikes and sills (Emmons and Eng, 1995). Figure 13B is a stereonet of poles to bedding in the pit, showing a well-defined girdle of points. From the pole to the best-fit great circle for these points, it was determined that the Cove anticline hingeline trends S44°E and plunges 18°SE. The fold is slightly asymmetric, and its limbs dip approximately 25°SW and 40°NE, based on measured exposures in the open pit.

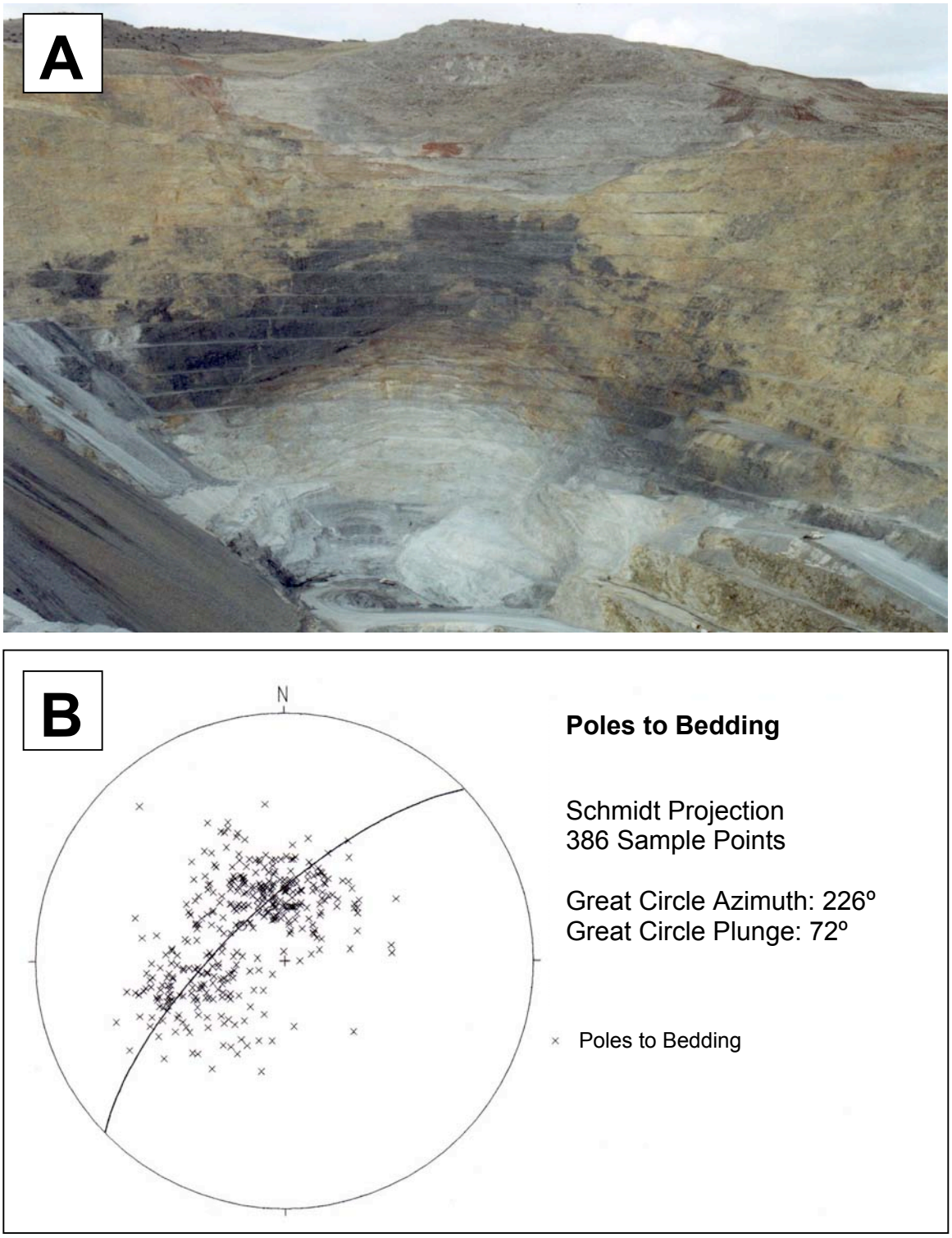

FIG. 13. Cove anticline. A is a photograph of the Cove pit northwest highwall (taken in October, 2000) showing the Cove anticline. B is a stereonet of poles to bedding in the pit.

Brittle deformation is expressed as joints and faults related to both the development of the Cove anticline and other episodes of faulting. Flexural slip during folding produced bedding-parallel reverse faults along bedding contacts and within less competent beds. These faults are now recognizable as continuous zones of fault gouge that parallel bedding, and commonly are mineralized in the vicinity of the hinge zone of the anticline.

The Cove anticline is cut by a series of steeply dipping (>60°) normal faults. Figure 14 is a stereoplot of poles to major (>1 meter offset and continuous) and minor (<1 meter offset or discontinuous) faults. The major faults are the Lighthouse, Cay, Bay, Musky, 110, Gold Dome, Mackinaw, Rainbow, Cutthroat, Blasthole, Brook, and Northwester faults, and the Perch, Pumpkinseed, Redear, Brown, Crappie, Bluegill, Striper, Wiper, and Smallmouth splays (Fig. 4 and Plate 2). The Crappie and Bluegill splays are probably extensions of the Cutthroat fault and Brown splay, respectively, in the Striper splay hanging wall, and will not be discussed separately. The major faults can be separated into three principal groups: ~N-striking faults, ~NE-striking faults, and ~NW-striking faults.

The N-striking fault group consists of the Lighthouse fault complex and the subordinate Perch, Pumpkinseed, and Redear splays. The general strikes for these faults range between N18°W and N20°E (APPENDIX IC). The Lighthouse fault complex is the most prominent visible feature in the Cove pit (Fig. 15). It strikes N10°E within the open pit, and N-S in areas south of the mine (Figs. 3 and 4). To the south-southwest of its intersection with the Striper splay, the Lighthouse is a complex of multiple normal fault planes that contain discontinuous dikes and minor BMVT veins. In many cases, the

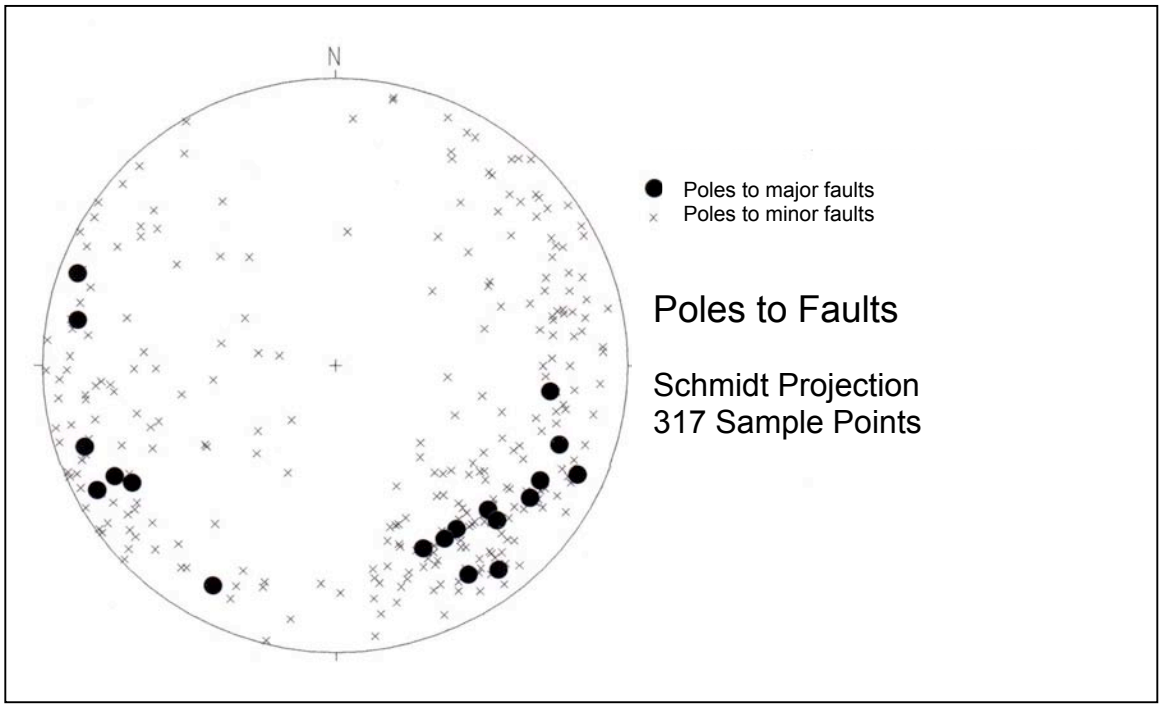

FIG. 14. Stereonet of poles to fault planes at the Cove pit (see text for definitions). The poles in the 90º to 180º quadrant belong to the generally NE-striking, NW-dipping faults, which are the most common faults in the pit.

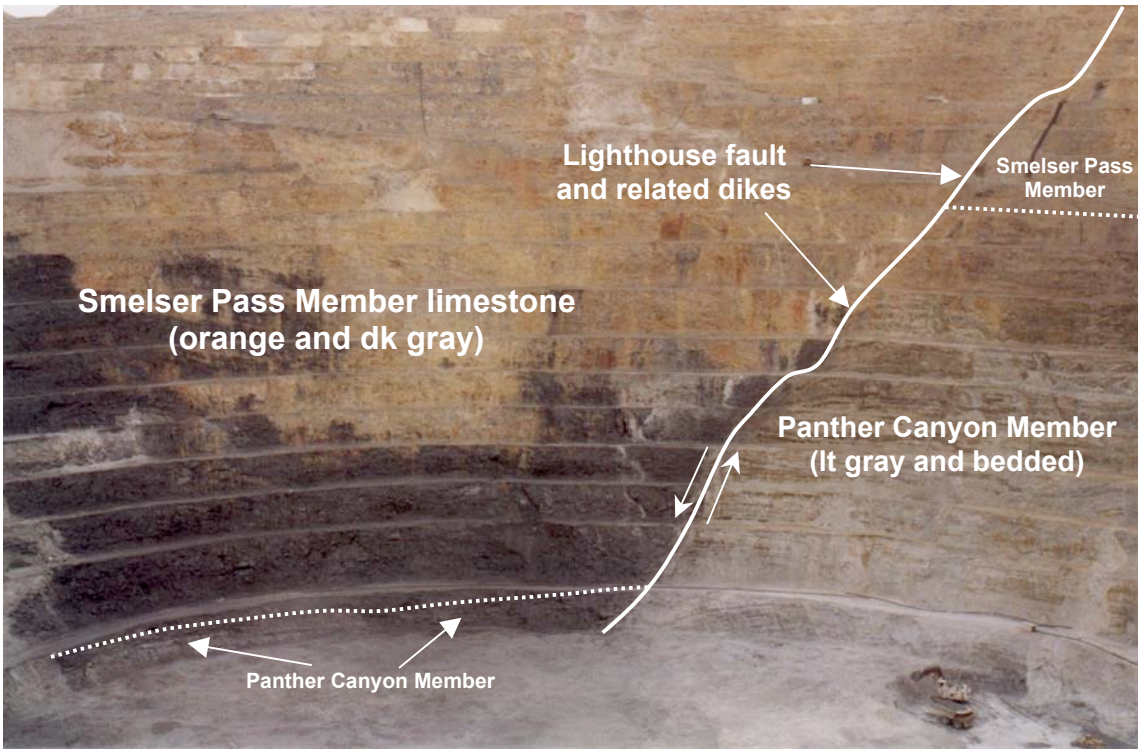

FIG. 15. 1998 photograph of the southeast highwall of the Cove Mine, showing the Lighthouse fault, its associated dikes, and offset of the Smelser Pass and Panther Canyon Members. A shovel and haul truck are present in the bottom right hand corner for scale.

veins and margins of the dikes have been brecciated by post-intrusion movement along the fault complex. The multiple fault planes form zones up to 30 meters in width. The general dip of the complex is 80°SE, and the maximum offset is about 150 meters.

To the north-northeast of its intersection with the Striper splay, however, the Lighthouse consists of a single fault plane with only about 40 meters of displacement. Here, the Lighthouse dips to the northwest, making it a reverse fault. Although the cause for the dip reversal is unclear, it may indicate that the initial development of the Lighthouse fault pre-dated the development of the Cove anticline. In this scenario, the original Lighthouse was rotated in the northeast limb of the anticline into an apparent reverse orientation during folding.

The ~NE-striking fault group consists of the Cay, Bay, Musky, 110, Gold Dome, Mackinaw, Rainbow, Cutthroat, Blasthole, and Brook faults, and the Brown splay. The NE-striking, NW-dipping normal faults are the most common faults in the Cove open pit (Fig. 14), and can be divided into two distinct subgroups. The major faults in subgroup I are the Cay, Bay, Musky, 110, and Gold Dome faults. These faults have strikes ranging from N52°E to N65°E, and dips ranging from 60°NW to 80°NW (APPENDIX IC). Within the open pit, the Cay, Bay, Musky, and 110 faults steepen with increasing depth from dips of less than 65º to dips greater than 80º. Measured displacements along these faults range from 10 meters or less (along the Cay fault) to as much as 80 meters (along the Bay fault).

Discontinuous dikes occupy the Cay, Bay, and Gold Dome faults. The widths of these faults ± dikes generally range between ~1 and 15 meters. However, the widths of the

dikes along these faults increase dramatically in the Southeast intrusion (related to the Cay fault) and the West intrusion (related to the Gold Dome fault). The reason(s) for these dilations is not known. The Northeast and South intrusions are also unusually large dikes, but they are not clearly associated with any of the faults of subgroup I. The Cay and Bay dikes commonly have BMVT ore localized in their footwalls, and base metal veins cut the Bay dike in the hinge zone of the Cove anticline. These relations indicate that these fault-dike complexes predate the BMVT mineralizing event(s).

The major faults in subgroup II are the Mackinaw, Rainbow, Cutthroat, Blasthole, and Brook faults, and the Brown splay. These faults have generally more northerly strikes than subgroup I, ranging from N25°E to N58°E, and dips ranging from 62°NW to 80°NW (APPENDIX IC). Unlike many of the faults in subgroup I, the faults in subgroup II do not clearly steepen with depth. Also, the faults in subgroup II are much thinner, with widths less than 1 meter. Only one of the faults in subgroup II has an associated dike; the Blasthole fault contains a discontinuous dike that is less than 0.5 meters wide where present. The Rainbow, Cutthroat, and Blasthole faults cut and offset the Cay fault-dike (Fig. 16). The faults of subgroup II are all the loci of intense quartz-sericite-pyrite alteration (including the Blasthole dike) and commonly contain veins of BMVT ore.

The major faults in the ~NW-striking fault group are the Northwester fault and the Striper, Wiper, and Smallmouth splays (Fig. 4 and Plate 2). The Northwester fault strikes N60ºW and dips 77ºNE (APPENDIX IC). It is up to 3 meters wide, and contains a discontinuous altered dike. The margins of the dike are brecciated and contain fragments of altered dike and BMVT veins.

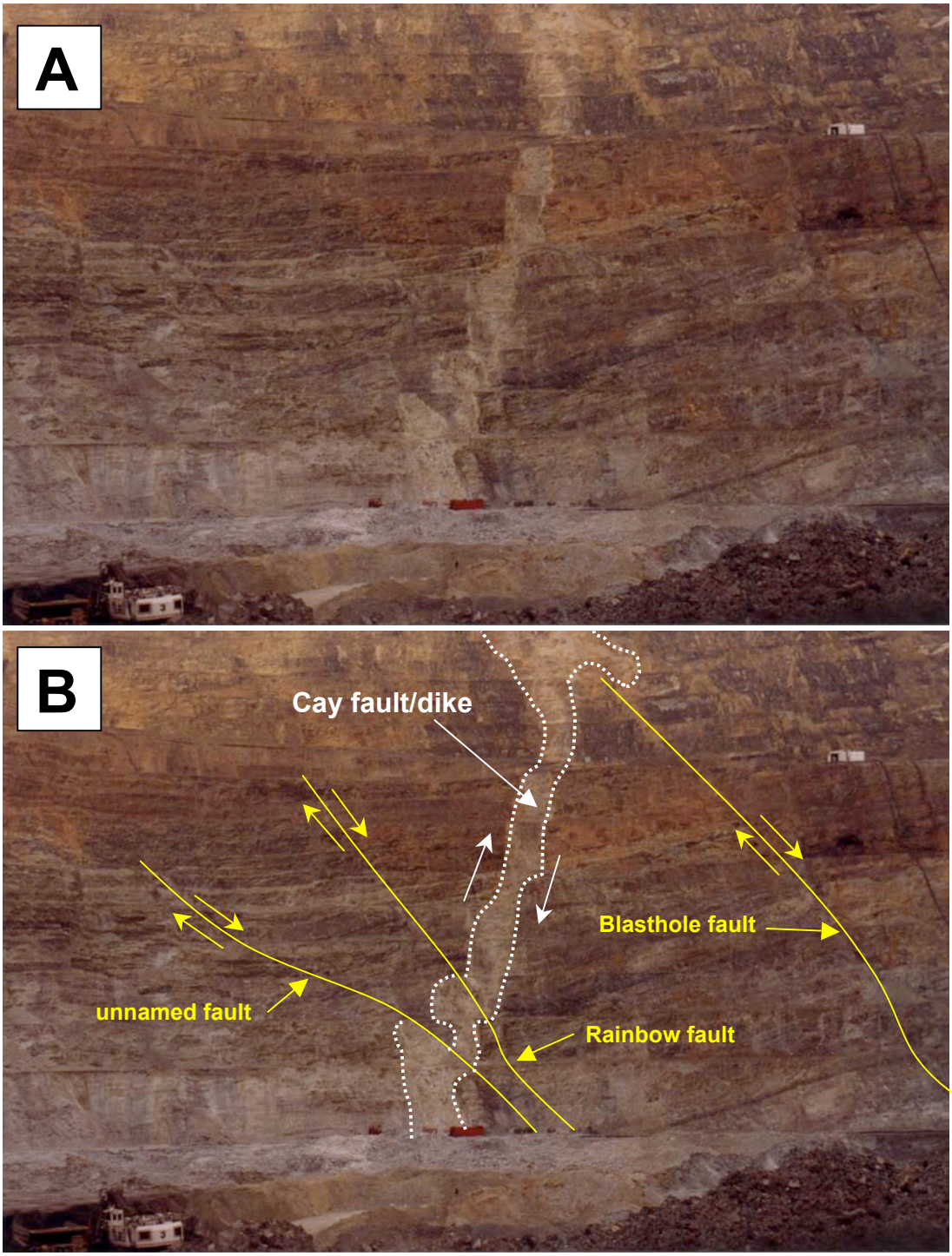

FIG. 16. 1998 photograph of the south highwall of the Cove Mine, showing two generations of NE-striking faults. A shows the actual appearance of the faults, and B shows the faults highlighted for emphasis (the earlier Cay fault is shown in white, and is offset by the later faults shown in yellow). A shovel is present in the bottom left corner for scale. Note that the apparently opposite dips are due to the steep dip of the Cay fault/dike (a normal fault) and the angle from which the photograph was taken.

The Striper, Wiper, and Smallmouth are apparently splays off of the Lighthouse fault complex. These three faults have general strikes of N27ºW to N30ºW, and general dips of 70ºNW to 83ºNW (APPENDIX IC). The widths of these faults are generally less than 1.5 meters, and none contain associated intrusive rocks. They do, however, contain brecciated fragments of BMVT ore that are apparently derived from the rocks they cut. Although the displacement along the Wiper and Smallmouth splays could not be determined, the displacement on the Striper splay is clearly variable. The displacement along the Striper splay is greatest near the Lighthouse fault, where the measured offset is ~110 meters. The offset diminishes toward the northwest, to less than 5 meters in the northwest highwall of the pit. It is also apparent that the Striper splay displaces hypogene orebodies (Chapter 3, Fig. 18).

Interpreted Structural Paragenesis

Based on cross cutting relationships observed in the Cove pit, four main stages of deformation are interpreted. In chronological order, these stages are: 1) early development of the Lighthouse fault, 2) development of the Cove anticline, 3) development of the two ~NE-striking fault subgroups, and 4) development of the Striper, Wiper, and Smallmouth splays. The four stages are discussed in relation to the late Eocene intrusive event(s) and subsequent mineralization, and account for all of the major structures in the pit except for the Northwester fault, which is discussed separately.

Stages I and II: Development of the Original Lighthouse Fault and the Cove Anticline

The Lighthouse fault complex appears to have originated prior to the development of the Cove anticline. In the northeast limb of the anticline, the Lighthouse has an apparent orientation of a reverse fault. One explanation for this orientation is that a part of the originally normal fault was rotated during the contractional deformation that produced the Cove anticline (Fig. 17A and B).

The Cove anticline developed in response to horizontal shortening oriented approximately N45ºE. Although the timing of the compressional event is poorly constrained, it post-dates the deposition of Triassic units, and pre-dates the late Eocene intrusions (and subsequent mineralization) at Cove. If the folding of the Triassic and older strata in the McCoy mining district occurred in the Mesozoic, as suggested by Emmons and Eng (1995), then the original Lighthouse is probably older. Normal faults of Mesozoic (and early Tertiary) age have been documented in various parts of the Great Basin by Allmendinger and Jordan (1984), Miller et al. (1989), and Vandervoort and Schmitt (1990).

Stage III: Development of the ~NE-Striking Faults

The major faults in subgroup I of the ~NE-striking fault group cut and displace the hingeline of the Cove anticline (Plate 2), and generally contain late Eocene dikes. These dikes and related sills are important controls on the distribution of gold and silver (discussed in Chapter 3), and the Bay fault-dike is cut by later BMVT veins. These relations indicate that the faults of subgroup I formed after the Mesozoic folding event,

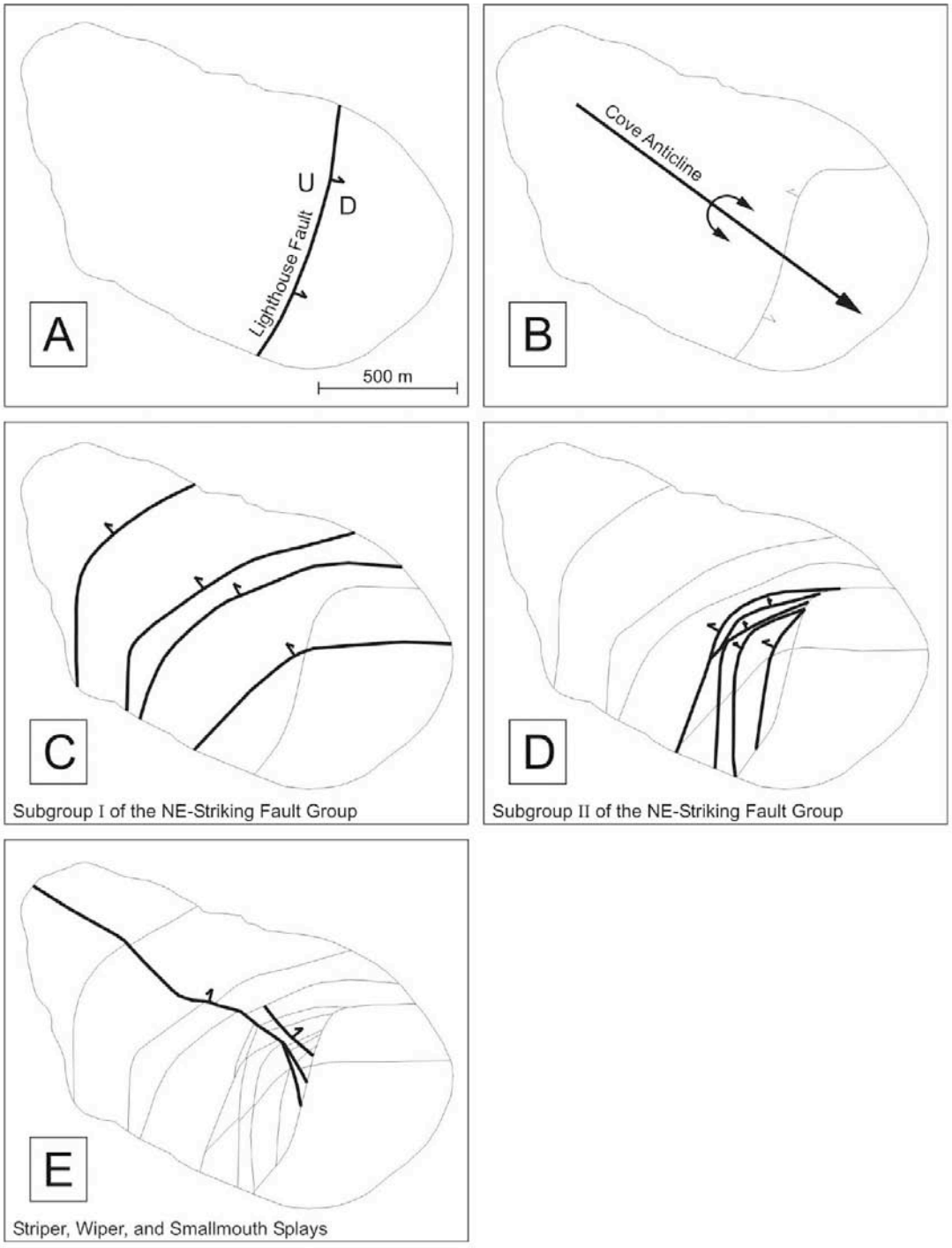

FIG. 17. Interpreted structural paragenesis at Cove. A and B show the development of the Lighthouse fault and the Cove anticline. As described in the text, there is some question regarding the temporal relationships between these two structures. C shows the development of the major faults belonging to subgroup I of th ~NE-striking fault group. D shows the development of the major faults belonging to subgroup II of the ~NE-striking fault group. E shows the later development of the Striper, Wiper, and Smallmouth splays.

and prior to the emplacement of late Eocene intrusions and subsequent mineralization (Fig. 17C).

The major faults in subgroup II of the ~NE-striking fault group cut and displace the fault-dikes of subgroup I (Fig. 16), and typically contain BMVT veins. Most of the BMVT veins are banded, indicating multiple episodes of deposition. In some cases, the BMVT veins are brecciated and cemented with subsequent BMVT sulfides. The discontinuous dike in the Blasthole fault may indicate that the faults in subgroup II formed before or during the intrusive event(s). The principal displacement along the faults in subgroup II occurred after the emplacement of the intrusions in subgroup I, and possibly during the mineralizing event that produced the BMVT ore (Fig. 17D).

The presence of discontinuous dikes and BMVT veins in the Lighthouse fault complex indicate that that the Lighthouse was reactivated during the deformation that produced the ~NE-striking fault group. As noted above, however, the dikes and BMVT veins are only present in the Lighthouse to the south-southwest of its intersection with the Striper splay.

Stage IV: Development of the Striper, Wiper, and Smallmouth Splays

The Striper, Wiper, and Smallmouth are all splays off of the Lighthouse fault complex. Because only the temporal relations between the Striper splay and the other major structures, the late Eocene intrusions, and the mineralizing event(s) are clear, the Wiper and Smallmouth splays are not discussed. The Striper splay is late in the structural paragenetic sequence: it cuts and offsets both the Bay dike (in the northwest corner of the pit) and the Cay-Southeast intrusion fault-dike (in the west-central pit bottom); it contains

fragments of BMVT ore derived from the rocks it cuts; and it offsets the Main Stratiform BMVT ore zone by ~110 meters (Chapter 3, Fig. 18).

The Striper splay apparently represents a late episode of faulting that reactivated a portion of the original Lighthouse fault and splayed near, and sub-parallel to, the hingeline of the Cove anticline (Fig. 17E). It is interesting to note that the displacement along the Lighthouse fault complex is approximately 150 meters to the south-southwest of the Striper splay, and only ~40- meters to the north-northeast of the splay. The ~110-meter difference is the same as the ~110-meter displacement along the Striper in the vicinity of the Lighthouse.

The relationships discussed above indicate that the Lighthouse fault complex is a long-lived structure that experienced at least three episodes of activation. The original Lighthouse fault (episode I) accounts for ~40 meters of displacement that pre-dated the development of the Cove anticline. At least a portion of the fault was reactivated during the deformational episode that produced the ~NE-striking fault group (episode II), as indicated by the presence of altered dikes and BMVT veins within the fault complex. The displacement along the Lighthouse during this second episode is unknown, but must have been relatively minor; the ~110 meters of additional displacement associated with the development of the Striper splay (episode III) account for the total measured Lighthouse displacement of ~150 meters. This third, post-mineral episode of deformation also explains the brecciation of BMVT veins within the Lighthouse fault complex.

The Northwester Fault

The origin of the Northwester fault and its relationships with the other structures remain enigmatic. The presence of a dike and fragments of BMVT veins within the Northwester indicate that it formed prior to the late Eocene intrusive event(s) and was reactivated during the mineralizing event(s), but the fault shares no cross cutting relations with the Lighthouse fault complex or the Cove anticline. Therefore, the only upper age constraint for the Northwester is the Triassic age of the Smelser Pass Member, which the fault cuts.

CHAPTER 3: THE DISTRIBUTION AND GENERAL CHARACTERISTICS OF HYPOGENE ORE AT THE COVE DEPOSIT

INTRODUCTION

In order to construct a genetic model for the Cove deposit, the relationships between BMVT and Carlin-style ore must be understood. This chapter takes steps toward this goal by presenting the general distribution and controls of Ag and Au, orebody descriptions and zonations, and general characteristics of the two ore types. These descriptions form a basis for the more detailed studies involving petrology and geochemistry presented in Chapters 4 through 6.

OREBODY DESCRIPTIONS AND CONTROLS

Figure 18 shows the distributions of Ag and Au relative to the stratigraphy and structures shown in the west-east cross section of the Cove deposit (Fig. 5). In Figure 18A, three principal zones of high Ag concentrations are present. The lower zone of Ag is stratabound in the Home Station Member, and is also weakly coincident with elevated Au concentrations shown in Figure 18B. Most of the lower zone is still present at Cove, but the middle and upper zones have been mined out. The middle zone of Ag occurred immediately beneath a sill related to the Cay dike, in the upper half of the transitional submember of the Panther Canyon Member. As shown in Figure 18B, this concentration of Ag corresponds spatially to the highest concentration of Au at Cove. The upper concentration of Ag and, to a lesser extent, Au, occurred at the contact between the

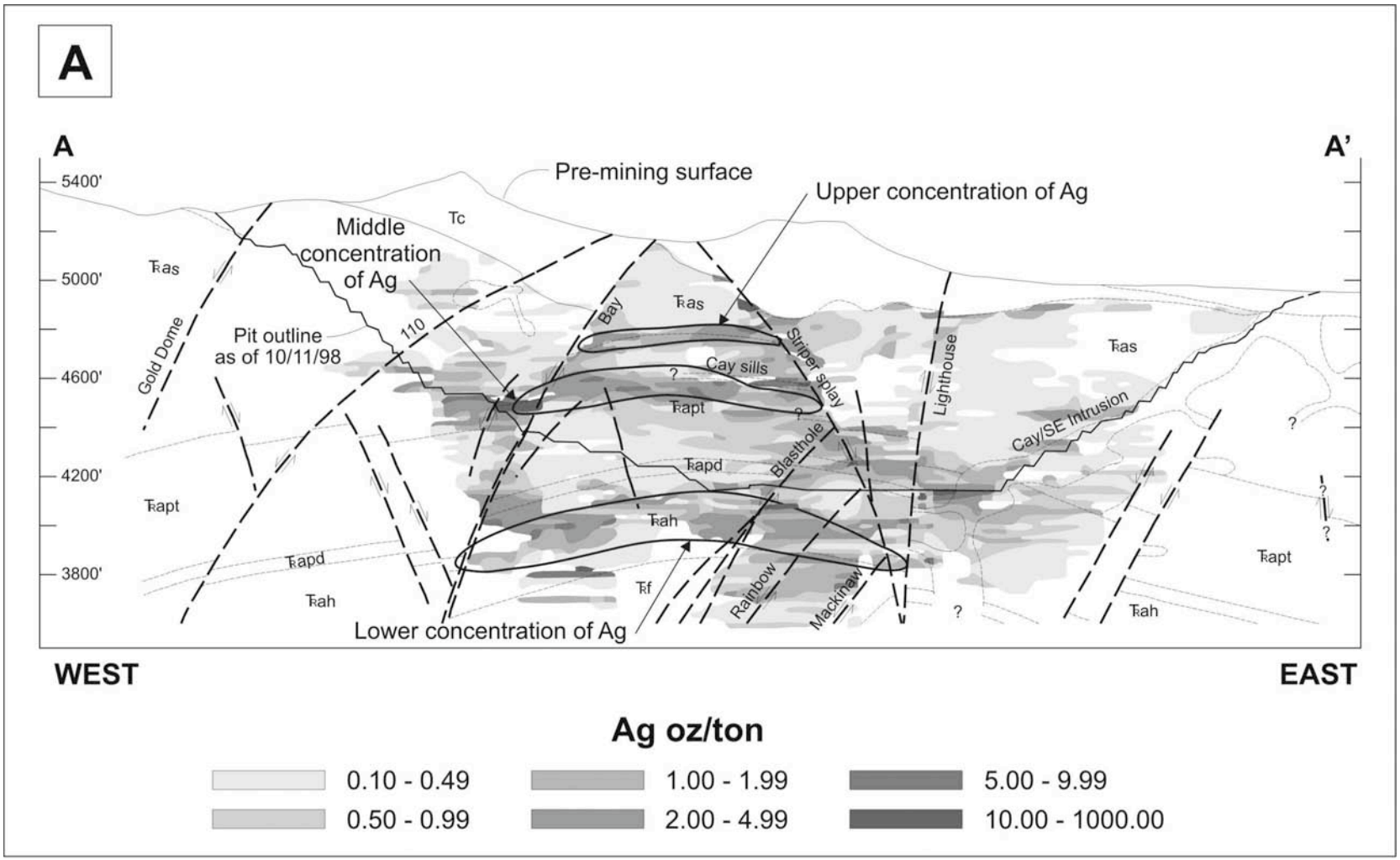

FIG. 18. Precious metals concentrations relative to structure and stratigraphy. A is a Ag distribution overlay, and B is a Au distribution overlay for the W-E cross section (refer to Figures 4 and 5 for orientation and geologic key).

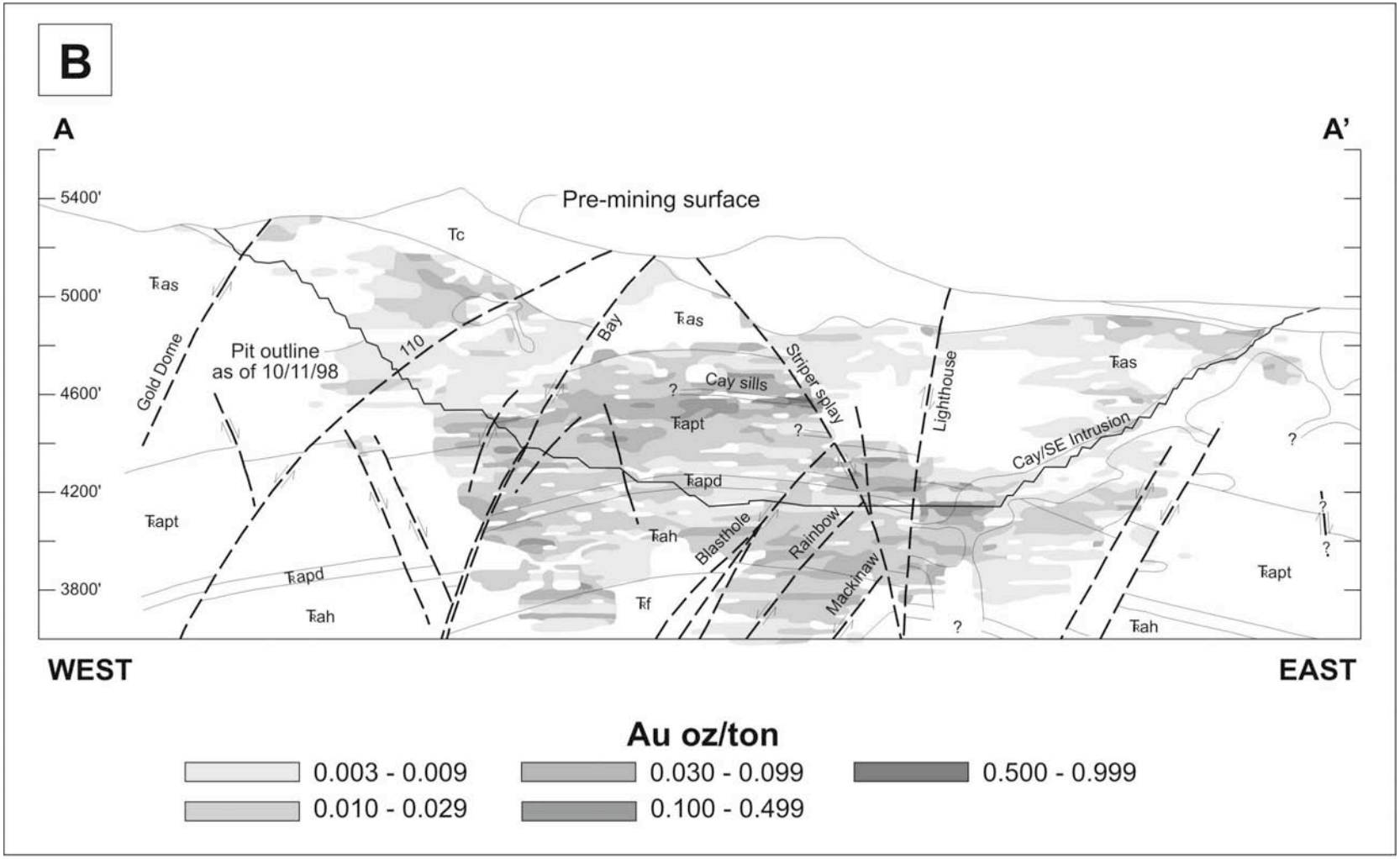

FIG. 18. Continued.

Panther Canyon and Smelser Pass Members. Subordinate zones of mined-out Ag and Au occurred in spatial association with the Cay sills in the hangingwall of the Striper splay and footwall of the Lighthouse fault. Another minor zone is still present at depth, in the vicinity of the Blasthole, Rainbow, and Mackinaw faults.

In order to simplify the following discussion, the zones of Ag and Au will be referred to by the orebody names they were given by previous workers at Cove (Fig. 19). The lower concentration of Ag and Au, in the Home Station Member, was arbitrarily separated into two orebodies: one is still present between the Blasthole fault and the Bay dike, and is called the "lower high-grade sulfide" (LHGS) orebody (Kuyper et al., 1991); and a second was partly mined out, occurs between the Blasthole and Lighthouse faults, and is called the "Cove South Deep" (CSD) orebody (David L. Emmons, 1998, personal communication). The middle concentration of Ag and Au is called the "upper high-grade sulfide" (UHGS) orebody (Kuyper et al., 1991), and the upper concentration of Ag with minor Au is called the "oxide" orebody (Kuyper et al., 1991). The subordinate concentration of Ag and Au in the footwall of the Lighthouse fault is called the "Cove East" orebody (David L. Emmons, 1998, personal communication). Orebody names have not been given to either the subordinate concentrations of Ag and Au in the hangingwall of the Striper splay, or to the concentrations at depth.

The Lower High-Grade Sulfide and Cove South Deep Orebodies

The LHGS and CSD orebodies are actually parts of a single, large, zoned orebody. This large orebody occurs in the Home Station Member, between the Lighthouse fault

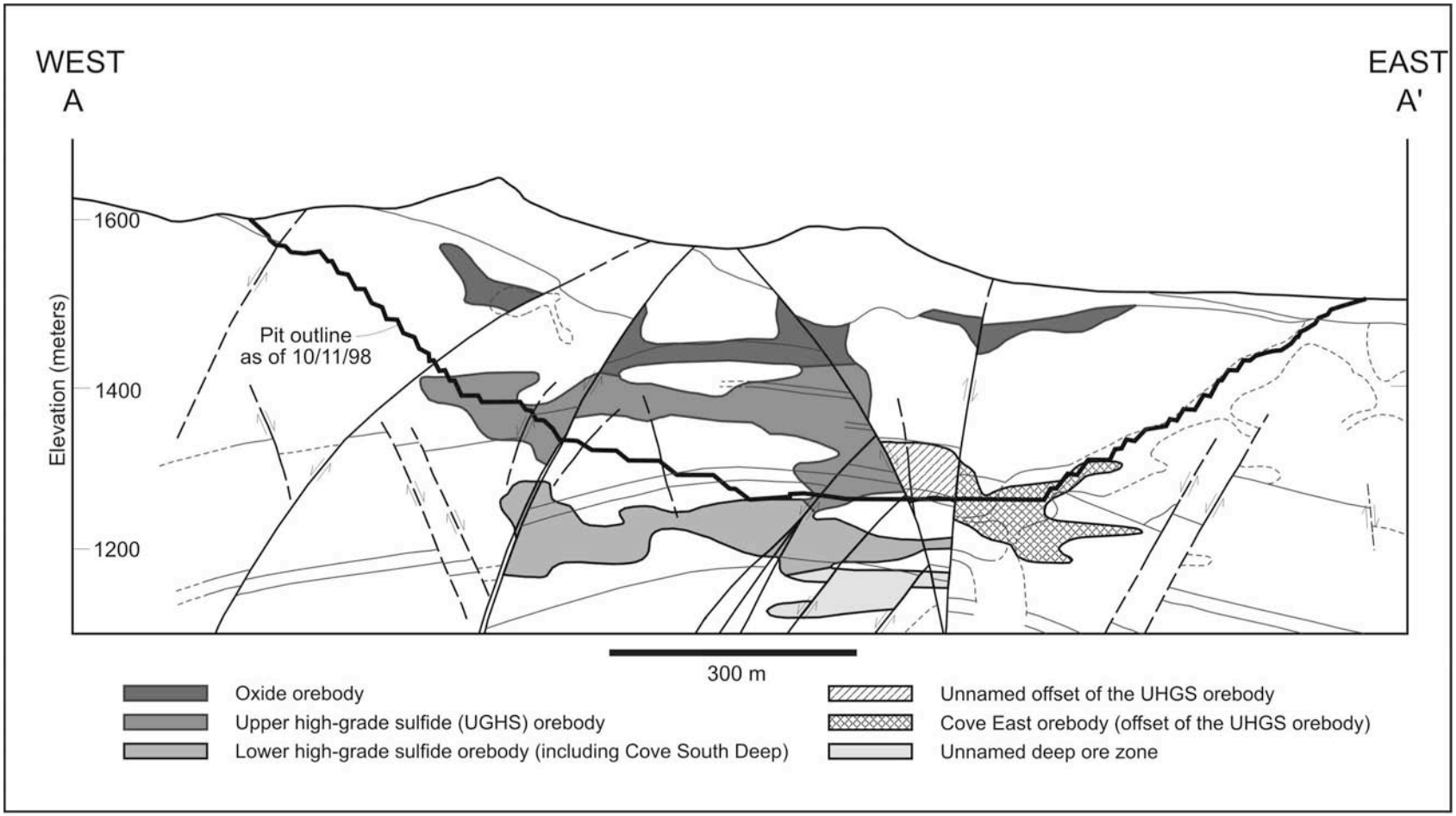

FIG. 19. Major orebodies at the Cove deposit, based on the distributions of Ag and Au shown in Figure 18 (refer to Fig. 4 and Fig. 5 for orientation and geologic framework).

and the Bay dike (Figs. 18 and 19). The zonation is expressed as BMVT ore that is spatially associated with the Blasthole, Rainbow, and Mackinaw faults, and as Carlin-style ore in the remainder of the LHGS orebody and in the CSD orebody. Based on assay results and observable sulfides in the underground workings, the BMVT and Carlin-style ores are separated by a pyrite halo with subeconomic concentrations of Ag and Au. The CSD orebody is further divided into two ore zones that show an additional zonation within the Carlin-style ore (David L. Emmons, 1998-2002, personal communications): 1) the lower ore zone is zoned from higher Ag:Au ratios in the northeast to lower Ag:Au ratios in the southwest; 2) and the upper ore zone has consistently low Ag:Au ratios. This zonation is discussed in greater detail later in this chapter.

The presence of multiple-episode BMVT veins in the Blasthole, Brook, Cutthroat, and Rainbow faults in the bottom of the pit and in the Cove South Deep underground workings suggests that these faults were principal feeders for the mineralizing fluid(s). The fluid(s) spread laterally from the feeders into the highly permeable, secondary dolostone of the Home Station Member, beneath the less permeable, primary dolostone of the Panther Canyon Member. To the northwest, the Bay dike impeded the lateral flow. To the southeast, the flow was contained in the footwall of the Lighthouse fault and hangingwall of the Omega dike (Fig. 28).

The Upper High-Grade Sulfide Orebody

Streiff (1994) referred to the bulk of the UHGS orebody as the "Main Stratiform ore zone" (Fig. 20). The Main Stratiform ore zone was hosted by the transitional submember

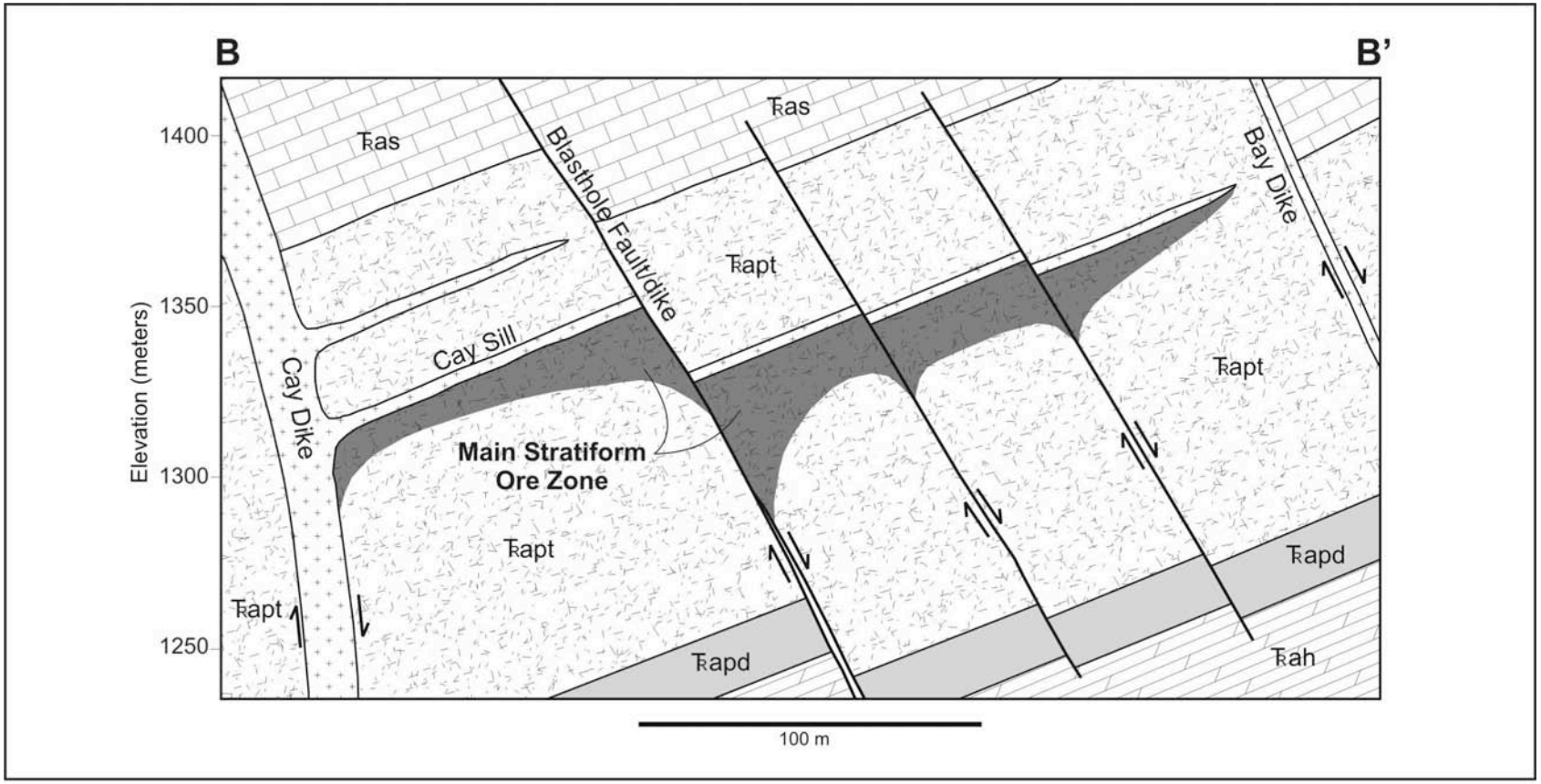

FIG. 20. Cross section of the Main Stratiform ore zone in the Upper High-Grade Sulfide orebody, showing intimate associations with a Cay sill (modified from Streiff, 1994). See Figure 4 for location and lithology.

of the Panther Canyon Member, and was localized beneath a sill related to the Cay dike (Kuyper et al., 1991; Figs. 18 and 19). This sill is one of two that extended northwest from the Cay dike. The sills were best developed in the hinge zone of the Cove anticline, and pinched out near the Bay dike. Their vestiges are still present in the south wall of the open pit (refer to Fig. 4 and Plate 2).

The Main Stratiform ore zone was 200 meters long, 90 meters wide, and 3 to 20 meters thick. Ore consisted principally of BMVT stockworks that locally graded into sulfide-cemented crackle breccias (Fig. 21). Streiff (1994) noted that a pyrite halo without significant amounts of ore-grade Au (and/or Ag) formed a 30- to 60-meter-wide envelope around the Main stratiform zone. This pyrite halo is similar to the one observed between the BMVT and Carlin-style ores in the LHGS-CSD orebody. The principal controls on the concentration of Au and Ag in this ore zone were the Cove anticline, Cay sill(s), and porous strata in the transitional submember of the Panther Canyon Member. The Cove anticline is a structural high, which helped to localize the ascent of the mineralizing fluid(s). The ascent was impeded by the presence of the less permeable sills, and changed to lateral flow in the underlying, sandy to conglomeratic strata of the Panther Canyon Member.

The Oxide Orebody

The oxide orebody consisted of disseminated Ag and Au hosted mainly in the lower Smelser Pass Member, and also in the upper Panther Canyon Member (Kuyper et al., 1991; Figs. 18 and 19). The oxide orebody was principally supergene in nature, and was

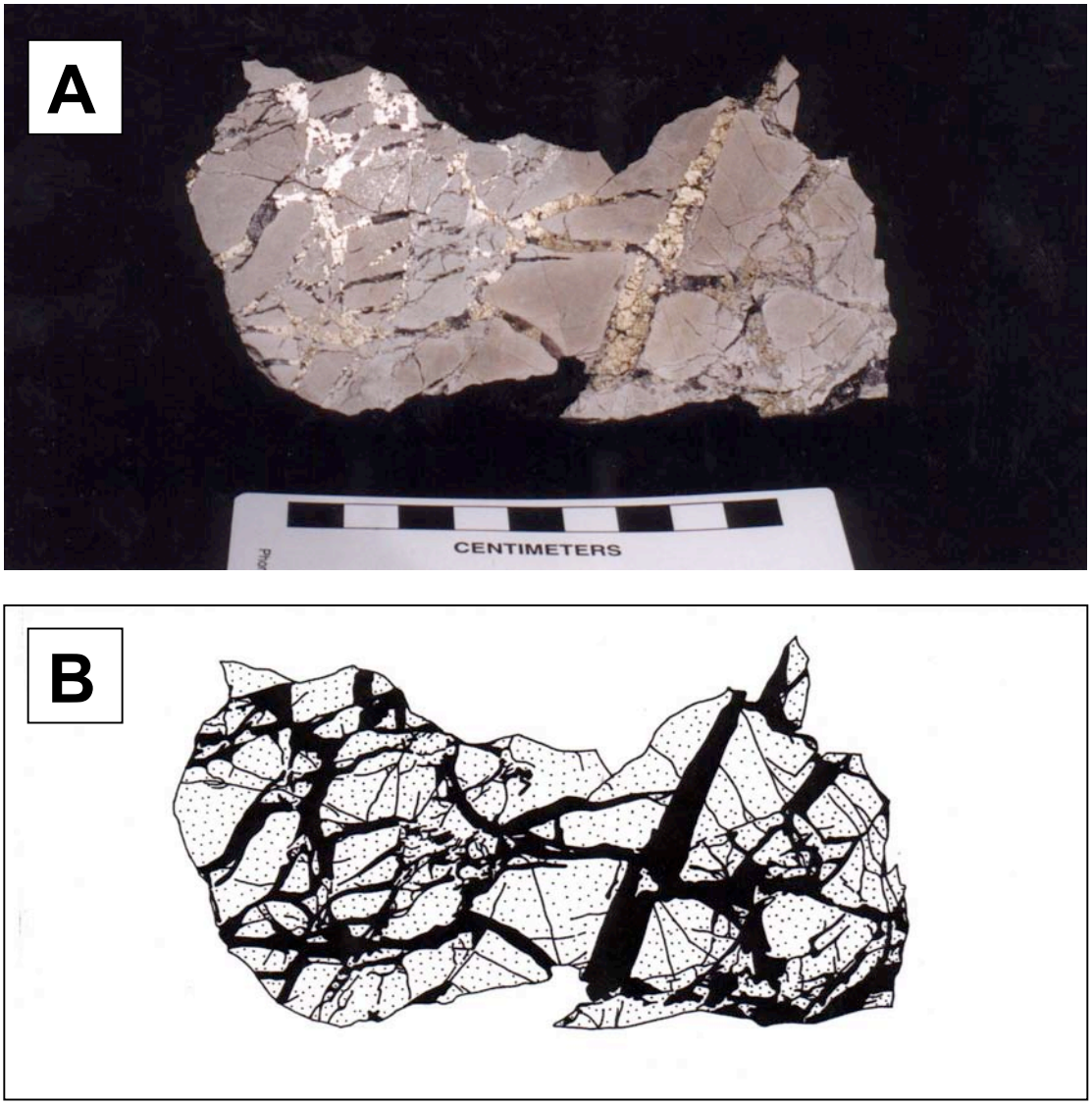

FIG. 21. Sulfide-cemented crackle breccia. A is a photograph of a specimen collected from the lower Panther Canyon transitional submember, in the immediate footwall of the Bay dike (sample location 4245E-17). B is a sketch of the same sample, using the same scale, showing sulfides in black.

associated with Mn flooding and jasperoid (Kuyper et al., 1991). Fresh, sulfidic analogs of the oxide orebody were observed in the North wall of the Cove open pit during mapping in 1998-99. Here, concentrations of sulfides occur at the contact between the Panther Canyon and Smelser Pass Members, in the vicinity of the Lighthouse fault and the Bluegill and Crappie splays (see Fig. 4 and Plate 2). The fresh sulfides consist of crustiform BMVT sulfides (pyrite with lesser sphalerite) in conglomerate at the top of the Panther Canyon Member, and abundant disseminated pyrite (Carlin-style) in the overlying Smelser Pass Member.

Based on the distribution of Ag and Au in Figure 18, and on the observations made during mapping, it is apparent that the principal control on the oxide orebody was the contact between the Panther Canyon and Home Station Members. The relatively low permeability of the microcrystalline limestone focused the flow of the mineralizing hydrothermal fluid(s) in the porous conglomerate at the top of the Panther Canyon Member. At least some permeability in the lower Smelser Pass Member is indicated by the presence of Carlin-style ore in the unit, and also by the presence of associated alteration (clay alteration, Mn flooding, and silicification; Kuyper et al., 1991; Emmons and Eng, 1995). It is not known, however, whether the permeability in the lower Smelser Pass Member was related to primary sedimentary characteristics, was generated by diagenetic or hydrothermal changes (especially dissolution), was produced by brittle deformation related to folding and/or faulting, or was related to some combination of these features.

Other Orebodies

The subordinate concentrations of Ag and Au in the hangingwall of the Striper splay (an unnamed orebody) and footwall of the Lighthouse fault (the Cove East orebody) occurred as BMVT ore. The orebodies were intimately associated with the Cay sills, and are apparently offset portions of the UHGS orebody. Post-mineral movement along these two faults downdropped the UHGS orebody in stair-step fashion to the east. The ore mined in the Cove East orebody was essentially identical to the BMVT ore in the UHGS orebody, based on descriptions by Kuyper et al. (1991), Streiff (1994), and Emmons and Eng (1995). The one notable exception to this similarity was the presence of very late wires of native Ag filling vugs in the UHGS orebody (see Chapter 4). These wires are interpreted to be supergene in origin and did not occur in the Cove East orebody, suggesting that the post-mineral offset occurred prior to the establishment of the supergene system at Cove.

The subordinate concentrations of Ag and Au at depth (an unnamed orebody) occur within the Favret Formation, which was not exposed in the Cove open pit or in any of the underground workings. The Favret Formation consists of limestone, with a 10- to 13-meter-thick calcareous shale marking its top (Kuyper et al., 1991). The Ag and Au concentrations occur in the vicinity of the Blasthole, Rainbow, and Mackinaw faults. This spatial association suggests that the ore may be restricted to the feeder faults, but the limited drilling at depth precludes making any conclusive interpretations. Most of the ore in the Favret is apparently Carlin-style (David L. Emmons, 2002, personal communication), but this ore has not been studied in detail.

GENERAL CHARACTERISTICS OF BMVT AND CARLIN-SYTLE ORE

The following description of macroscopic ore characteristics begins with the vertical zonation mapped in the Cove open pit for the BMVT ore in general. Although the Carlin-style ore is volumetrically the most abundant ore type (David L. Emmons, 1998-2001, personal communications; Mike Schaffner, 1999, personal communication), its distribution and characteristics were rarely mapped due to its very fine-grained nature. However, the Carlin-style features that were observed are also described here.

BMVT Ore

Figure 22 summarizes the characteristics of BMVT ore for each sedimentary host unit, and shows the mapped vertical zonation of ore styles. Figure 23 shows the lateral zonation of these ore styles in relation to one of the NE-striking feeder structures discussed in Chapter 2 and in the preceding sections. In many cases, BMVT ore veins are single episode veins, indicating their development during a single, discrete episode of fracturing and precipitation of ore and gangue minerals. Multiple-episode veins, large ore pods, and sulfide-cemented crackle breccias typically show episodic development with common overprinting relationships. In these cases, it appears that these ore types occur adjacent to or within the principal conduits related to BMVT fluid flow. The single vein structures, then, can be considered as relatively short-lived subordinate conduits.

Principal conduits include major NE-striking faults, such as the Blasthole fault. Subordinate conduits include the Lighthouse fault and dilational faults and joints occurring in the hinge zone of the Cove anticline in the Home Station Member, dolostone

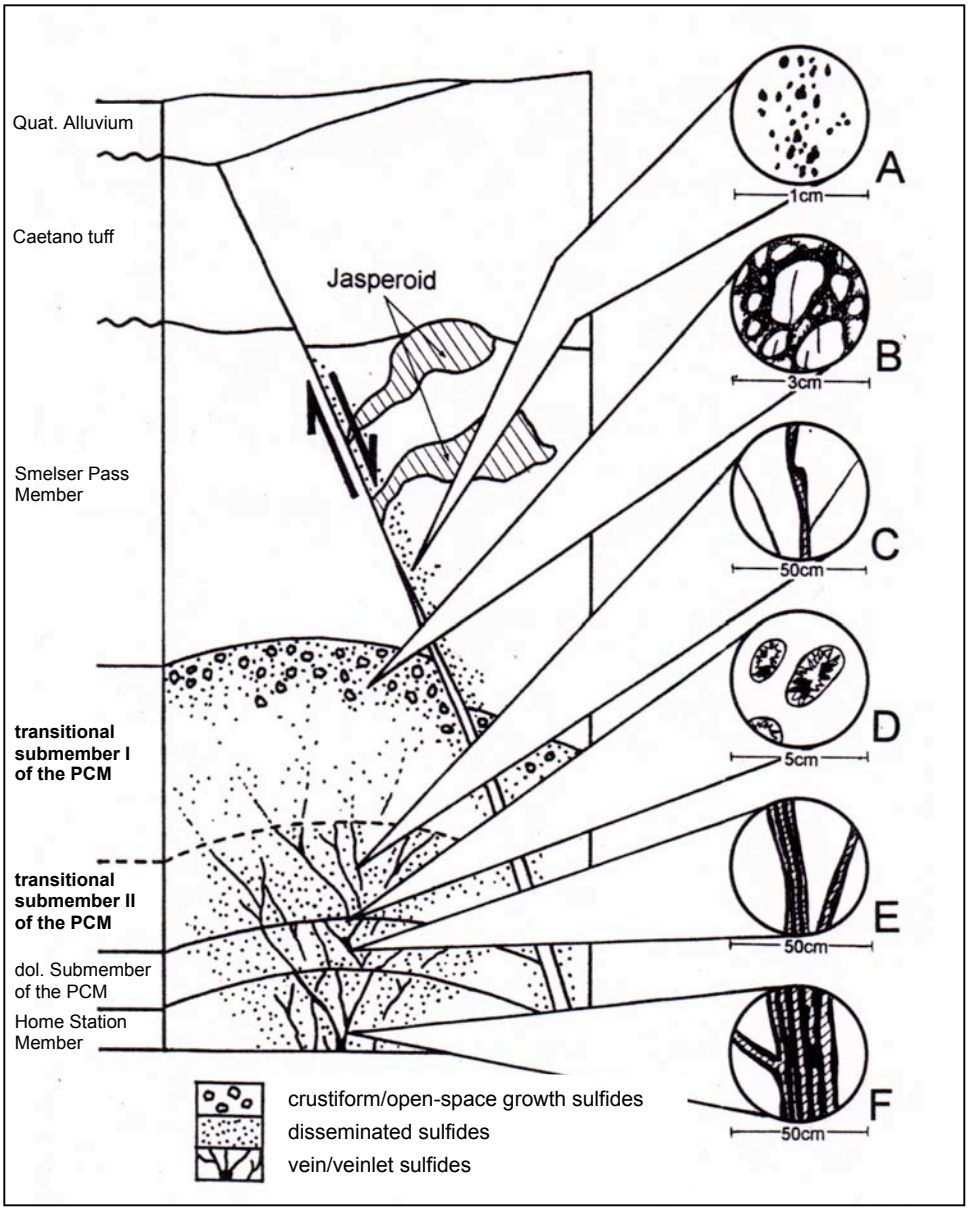

FIG. 22. Schematic diagram of macroscopic characteristics of BMVT ore. For A through F, sulfides are shown in black. A shows disseminated sulfides in the Smelser Pass Member. B shows crustiform sulfides in the clastic-dominated portion of the transitional submember of the Panther Canyon Member (transitional submember I of the PCM). C shows vein-veinlet sulfides in the carbonate-dominated portion of the transitional submember of the Panther Canyon Member (transitional submember II of the PCM). D shows open-space growth sulfides in dissolution holes in the uppermost bed of the dolostone submember of the Panther Canyon Member. E shows vein sulfides exhibiting multiple episodes of deposition in the dolostone submember of the Panther Canyon Member. F shows vein sulfides exhibiting multiple episodes of deposition in the Home Station Member. Note: the distribution of Carlin-style disseminated sulfide ore is not shown in the diagram.

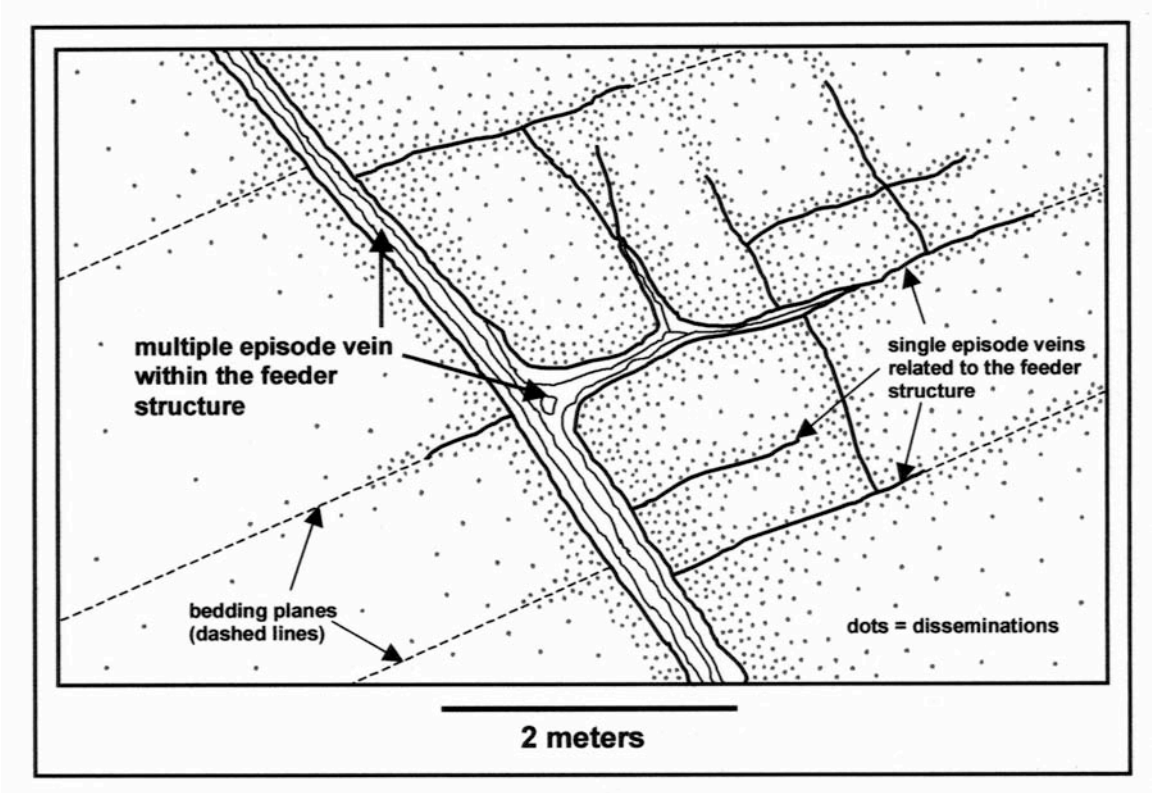

FIG. 23. Schematic lateral zonation of BMVT ore adjacent to a principal feeder structure (such as the Blasthole fault) in dolostones of the Home Station Member and Panther Canyon Member.

submember of the Panther Canyon Member, and the lower carbonate component of the transitional submember of the Panther Canyon Member. Several large veins (>10 centimeters width) having multiple episodes of dilation-precipitation were traced through all three of these host units (Fig. 24). The multiple-episode veins are generally restricted to the axis of the Cove anticline, between the Bay and Cay fault/dike complexes. They are most dense in the area of the Rainbow, Cutthroat, Blasthole, and Brook faults and the Brown splay, and continue across to the Bay dike.

In the Home Station Member, BMVT ore consists of: 1) 5- to 20-centimeter-wide veins radiating from the axis of the Cove anticline; 2) 0.5- to 5-centimeter-wide irregular veins in the anticline axis that are discordant to bedding; 3) 0.5- to 5-centimeter-wide veins that are concordant with bedding and thin and pinch out away from the anticline axis; and 4) pods associated with ~N- and ~NE-striking faults with or without associated dikes. The radial, irregular discordant, and concordant veins form a dense stockwork in the axis of the anticline, and typically show multiple vein episodes within single structures. Each episode is marked by irregular-banded base metal sulfides with calcite gangue, and is separated from successive vein bands by a thin layer of medium gray illite. The largest base metal pod seen in the Cove highwall was hosted by the Home Station Member in the footwall of the Cay dike, and consisted of a 4-meter-wide mass of sooty, friable base metal sulfides.

In the dolostone submember of the Panther Canyon Member, BMVT ore occurs as: 1) 3- to 10-centimeter-wide continuations of the radial veins seen in the Home Station Member; 2) 3- to 10-centimeter-wide veins that are discordant to bedding; 3) 1- to 5-

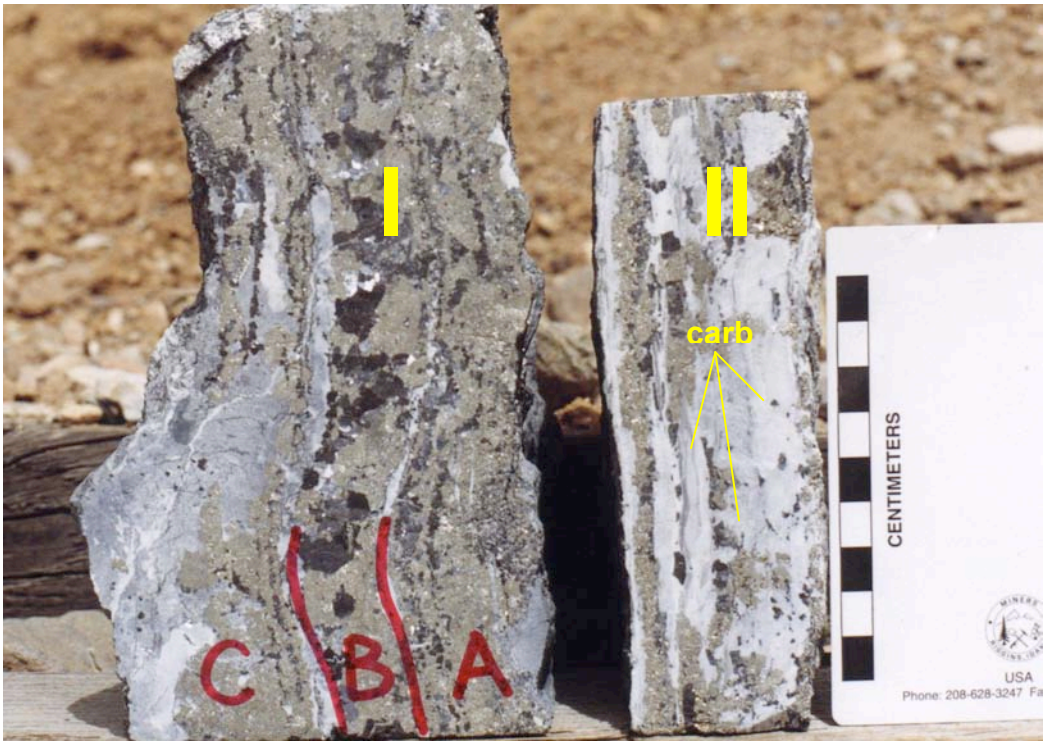

FIG. 24. Photographs of multiple-episode BMVT veins. **I** is a sample from the Home Station Member, with C, B, and A delineating 3 relatively large vein episodes. **II** is a sample from the dolostone submember of the Panther Canyon Member. Note that **II** has thinner individual vein episodes and a volumetrically larger carbonate gangue component than **I** (carbonates have white and gray coloration).

centimeter-wide veins that are concordant with bedding; 4) 20- to 30-centimeter-diameter pods; and 5) euhedral open-space growths in quartz-lined dissolution cavities in the 1-meter-thick uppermost dolostone bed (Fig. 25). The veins seen here also show multiple episodes of development, but differ from those in the Home Station Member in that they are thinner, more widely spaced, and contain a greater quantity of carbonate gangue (refer to Fig. 24). Pods consist of sooty, friable base-metal sulfides at intersections and splays of veins. The dissolution cavities in the uppermost bed range from 1 to 3 centimeters in diameter, and form an excellent marker horizon. Crustiform quartz linings and euhedral base metal sulfides, however, are only found in the general region of the anticline hinge zone.

BMVT ore characteristics in the clastic submember of the Panther Canyon Member vary based on principal lithology. In the lower microcrystalline dolostone and fine-grained sandstone units, ore occurs in veins similar to those in the dolostone submember, and also as thin Fe sulfide linings of joints radiating from the axis of the Cove anticline (Fig. 26). Vein density increases dramatically in the footwall of the Bay dike, locally coalescing into small pods of sulfide-cemented crackle breccia at the dike contact (refer to Fig. 21). In the upper sandstone and conglomerate units, ore is more variable and widely dispersed than in the lower units. In general, the veins in the lower units disappear into the sandstone and conglomerate. The ore style changes to crustiform linings in intergranular pore spaces (Fig. 27), disseminations, and thin (<1 millimeter wide) intragranular veinlets. The thin pyrite/marcasite linings of radial joints persist into

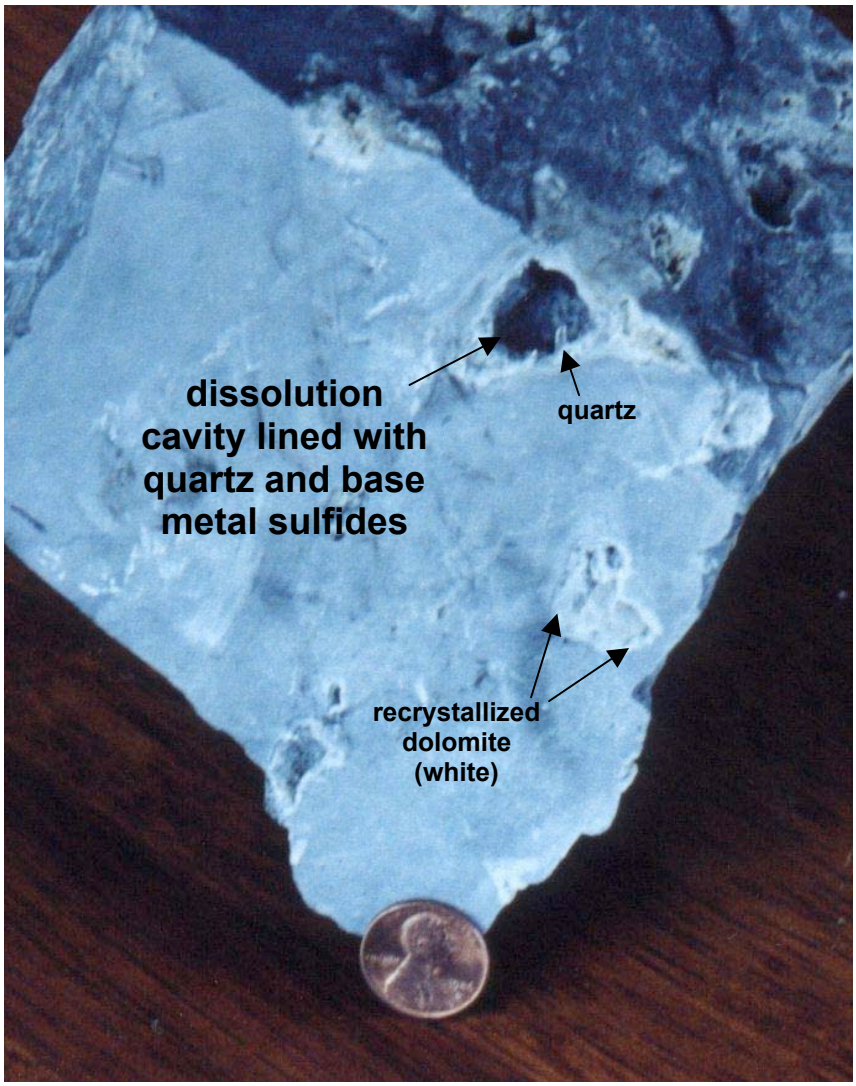

FIG. 25. Hand specimen showing quartz + sulfide-lined dissolution cavities from the uppermost bed in the dolostone submember of the Panther Canyon Member (bluish-gray). The white rind around the cavities is recrystallized dolomite. Quartz and sulfide linings were found only in the axis of the Cove anticline.

FIG. 26. Joint surface lined with pyrite ± marcasite. Such linings were commonly observed on radial joint sets in carbonate-dominated strata of the lower transitional submember of the Panther Canyon Member.

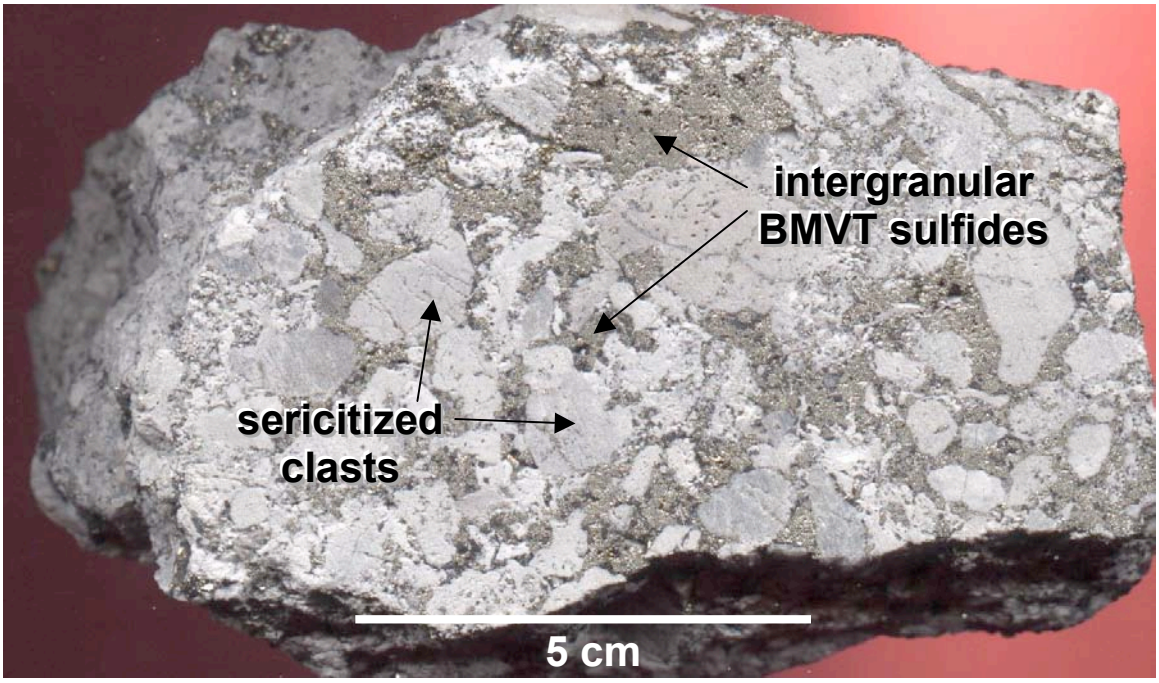

FIG. 27. BMVT sulfide crustifications in conglomerate of the transitional submember of the Panther Canyon Member. Pyrite and sphalerite occur in intergranular pore spaces, and the original quartz pebbles have been altered to sericite/illite (white).

the sandstone and conglomerate, but are not as well-developed as those in the lower dolostone and sandstone units.

BMVT ore in the Smelser Pass Member is strongly subordinate to Carlin-style disseminations and auriferous-manganiferous jasperoids. BMVT ore is generally restricted to the vicinity of large faults. Veins and veinlets up to 2 centimeters wide were observed, but disseminations are more common.

Carlin-Style Ore

The Carlin-style mineral assemblage consists principally of disseminated pyrite with lesser disseminated arsenopyrite, veins/veinlets of marcasite, and veins/veinlets and pods of realgar ± stibnite ± orpiment, typically with void-filling calcite that is paragenetically late (discussed in further detail in Chapter 4). Disseminated pyrite was observed during mapping of the open pit, and during tours of the underground workings in all of the reduced rocks in the Home Station Member, in the dolostone-dominated portions of the Panther Canyon Member, and in the Smelser Pass Member. Thin (3- to 10-centimeter-wide) veins lined by botryoidal marcasite and filled with calcite and disseminated arsenopyrite were observed in the Smelser Pass Member, principally in proximity to the Bay dike, Cay dike/Southeast intrusion, and Lighthouse fault. Several veins and pods of realgar with stibnite were also observed in the Smelser Pass Member. The largest of the pods occurs in the hangingwall of the Cay dike/Southeast intrusion, in the east wall of the open pit. Another pod was observed in the vicinity of the Northwester fault in the west

wall of the pit. Realgar was also found in exploration drill holes on the margins of the Cove system (Don Ryan, 1998, personal communication).

In all of these cases, the Carlin-style assemblage was observed peripheral to the central BMVT ore. Spatially coincident Carlin-style and BMVT ore assemblages were not observed during the mapping portion of this study, nor was this coincidence found in any of the thin or polished sections examined during the course of this study (Chapter 4), nor was this coincidence reported by earlier workers (Kuyper et al., 1991; Emmons and Eng, 1995).

THE SPATIAL RELATIONSHIP BETWEEN BMVT AND CARLIN-STYLE ORE

Based on the descriptions of orebodies in the preceding sections, the distribution of ore types at Cove is generalized as centralized BMVT ore with a wide halo of Carlin-style ore. This generalization is shown in Figure 28. Probably the best place to observe the spatial relationship between BMVT and Carlin-style ore is in the large, zoned orebody that comprises the LHGS and CSD orebodies. The following discussion is focused on the BMVT ore in the LHGS orebody, and the Carlin-style ore in the lower zone of the CSD orebody. The Ag and Au grades and Ag:Au ratios for these two areas are shown in Figure 29.

The distribution of Ag and Au in Figure 29 has three important implications. First, the elevated concentration of Ag between the LHGS feeders (the Mackinaw fault in Fig. 29) and the CSD orebody shows a southeasterly trend. This trend is inferred to indicate that the hydrothermal fluid flowed toward the southeast, and suggests that another control

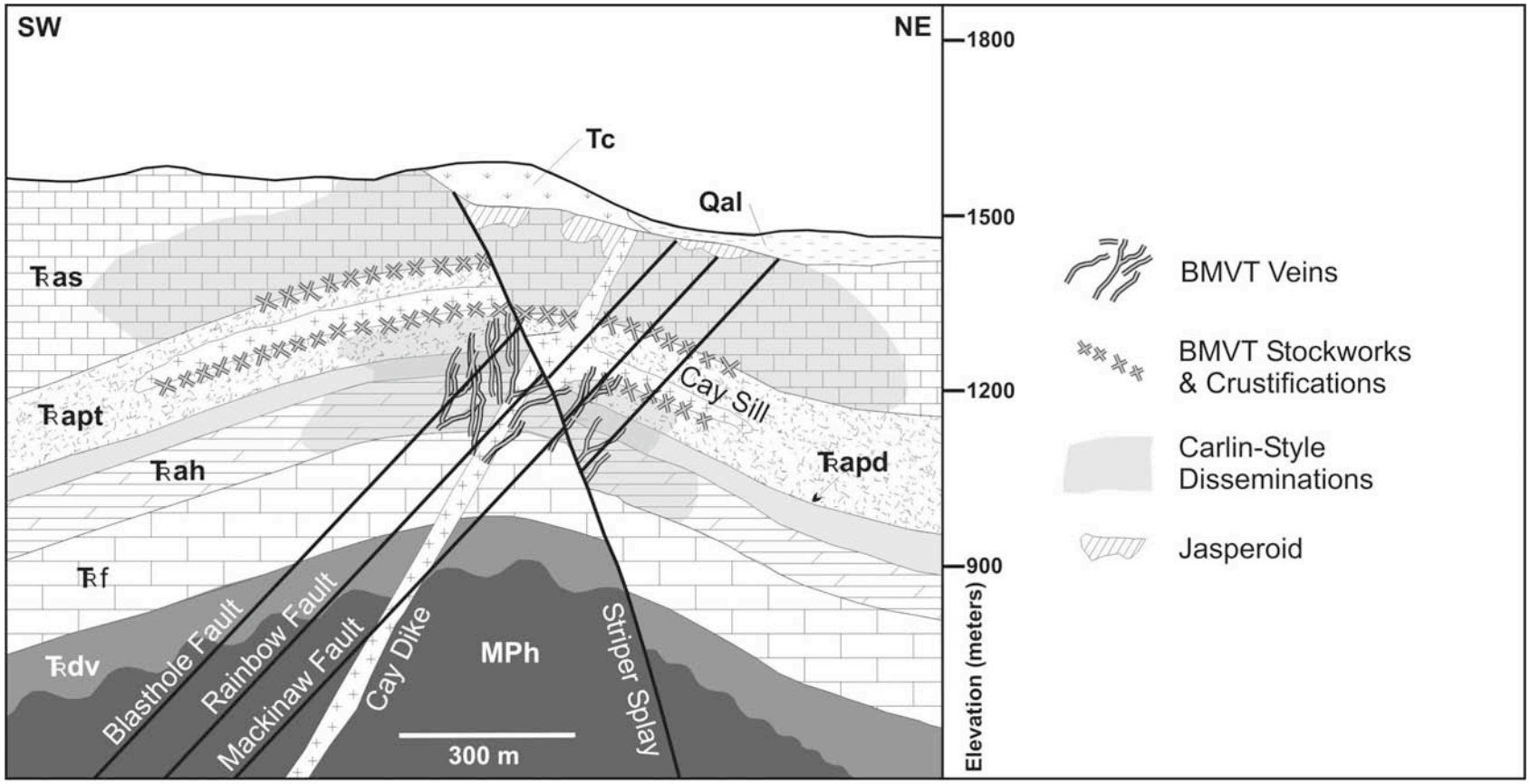

FIG. 28. Schematic cross section showing the generalized distribution of BVMT and Carlin-style ore at Cove. See Figure 4 for lithologic key.

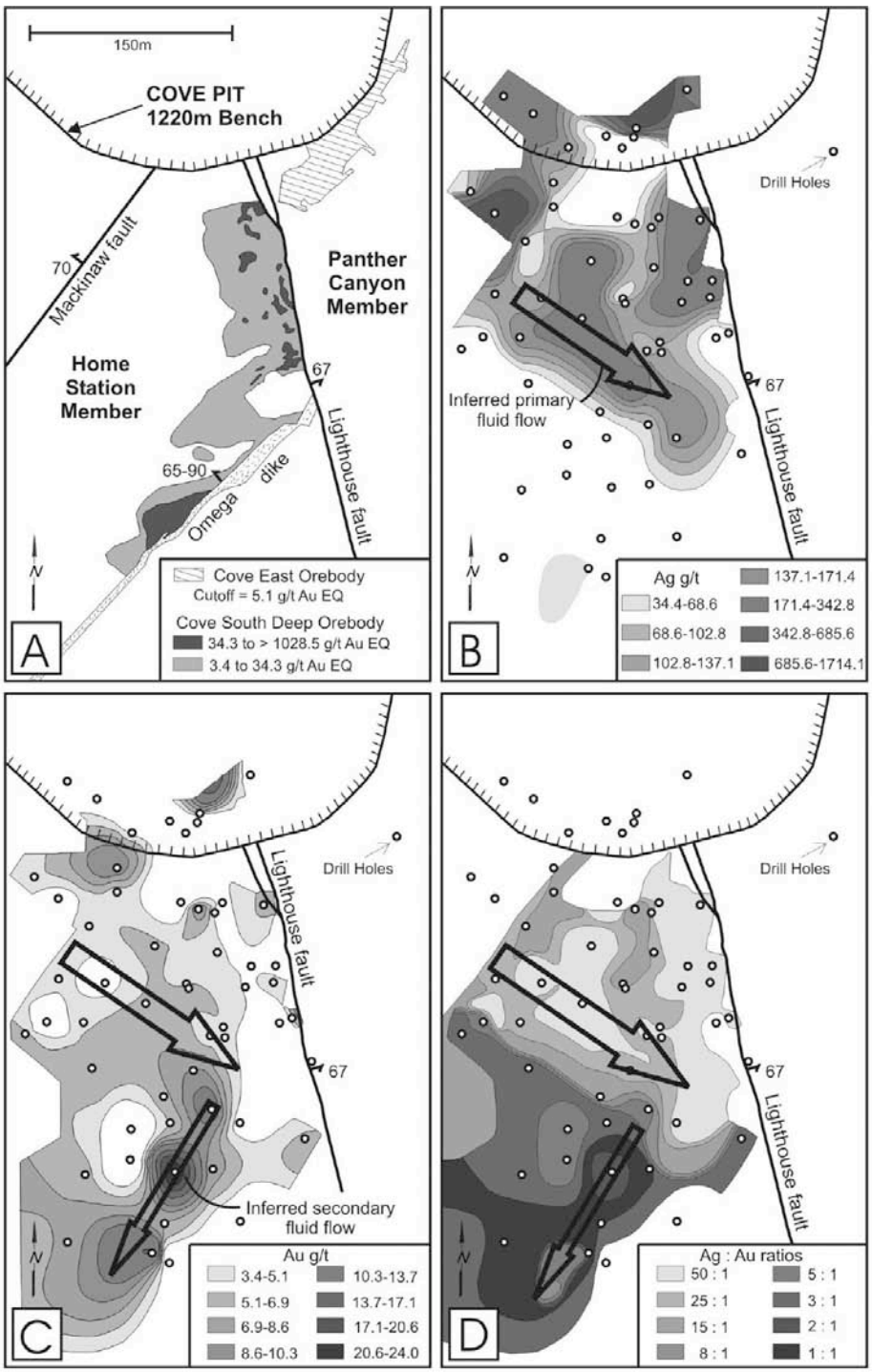

FIG. 29. Spatial relations and zonations between BMVT and Carlin-style ore. A shows the locations of the BMVT Cove East orebody and the Carlin-style upper zone of the CSD orebody. A large BMVT vein occurs along the Mackinaw fault (shown partially by the high Ag values in B). B and C show the average Ag and Au grades in the Carlin-style lower zone of the CSD orebody. D shows Ag:Au in the lower zone of the CSD orebody. B through D are based on assay data from the drill holes shown.

exists that was not observed during mapping of the open pit. This control may be structural, reflecting either folding or, perhaps more likely, the location of a NW-striking fault parallel to the Northwester fault mapped in the pit.

Second, the Carlin-style ore in the lower zone of the CSD orebody shows an increase in grade toward the southwest. The highest grades occur along the northwestern margin of the Omega dike. The grades gradually decrease toward the feeder faults to the northwest, but drop off dramatically to virtually zero Au and Ag in the hangingwall of the Lighthouse fault and footwall of the Omega dike. The zonation between the BMVT and Carlin-style ores, lack of grade in the hangingwall of the Lighthouse fault, and lack of grade in the footwall of the Omega dike indicate that neither the Lighthouse fault nor the Omega fault served as a principal feeder to this orebody. Instead, the increase in grade toward the southwest is inferred to indicate a secondary direction of fluid flow, where the fluids flowed laterally along the Omega dike.

The third, and perhaps most important implication is that the Carlin-style ore in the lower zone of the CSD orebody is clearly zoned from higher Ag:Au ratios in the northeast to lower Ag:Au ratios in the southwest. These ratios range systematically from >50:1 in the vicinity of the Mackinaw fault and in the non-ore grade zone separating the BMVT and Carlin-style ore, to <1:1 in the highest-grade portions of the Cove South Deep orebody. This relationship has important implications for classic "Carlin-type" deposits in Nevada and elsewhere, as they are dominated by Au, not Ag. These implications are discussed in Chapter 6.

CHAPTER 4: ORE MINERALOGY AND PARAGENESES

INTRODUCTION

The following descriptions are based primarily on data produced during this study, and are augmented by unpublished in-house reports prepared for Echo Bay Minerals Company by professional consultants. Table 5 summarizes the modes of the phases identified in polished sections. Of the 70 samples listed (including duplicates), 18 contained Carlin-style ore only, 51 contained BMVT ore ± disseminated pyrite, and one could not be definitely assigned to either category. The following quantitative modal descriptors are used: major = >5 percent of sample, minor = 1-5 percent of sample, trace = <1 percent of sample, and unique = only one grain observed in sample.

BMVT ORE MINERALOGY AND PARAGENESIS

Hypogene BMVT ore at Cove is a complicated assemblage of sulfides, sulfosalts, native metals, oxides, and carbonates. Although none of the polished sections examined contained all of the BMVT ore minerals, most showed wide variability in the phases and modal abundances observed, and all shared identical textures and relations between phases that could be fit into a deposit-scale paragenetic scheme (Fig. 30). The BMVT paragenesis can be summarized as an Fe sulfide pre-ore stage, an iterative vein stage equivalent to the main ore stage, and a supergene stage.

The iterative vein stage is responsible for all of the ore types described in the BMVT "ore distribution and characteristics" section except for the thin, pre-ore Fe sulfide linings

MINERALS \ SAMPLES	REALGARA	4365E-12	4145E-5B	4145E-52	4205E-11	4205E-23	4205E-13	7/26/98-1A	4145E-45	4205E-17	4145E-5	4145E-8B	4145E-1	4465E-8	CVC275A-107?.5
Acanthite															
Arsenopyrite															
Canfieldite															
Carbonates	67	8		1	1		tr								
Cassiterite															
Chalcopyrite															
Galena															
Native Gold-Electrum															
Kesterite															
Marcasite		2			1	1	1		1				tr		
Orpiment															
Pearceite															
Polybasite															
Proustite-Pyrargyrite															
Pyrite			tr	3	3	tr	2.5	4	6	2	2	2	2	tr	1
Pyrrhotite															
Quartz					tr										
Realgar	30														
Rutile															
Native Silver															
Sphalerite															
Stannite															
Stannite III															
Stibnite	3														
Stromeyerite															
Tennantite-Tetrahedrite															
Unknown I															

MINERALS \ SAMPLES	CVC205A-1019.5	CSD-2	CSD-A1	4325E-11	4145E-22	4145E-56	BOTTOMA-1	BOTTOMA-1 (dpp)	4205E-15	4145E-36	4205E-12	4205E-10	4245E-5	4245E-5 (dpp)	4145E-9
Acanthite							tr	tr					tr	tr	
Arsenopyrite		?		tr					tr			tr			2
Canfieldite						tr	tr	tr	tr		tr	tr	tr	tr	tr
Carbonates				74		15			35	2	10		95	95	
Cassiterite													tr	tr	
Chalcopyrite					tr	<tr	tr	tr	1	tr	tr	tr	tr	tr	tr
Galena						tr	tr	tr	1	tr	tr	tr	1	1	tr
Native Gold-Electrum															
Kesterite							tr	tr					tr	tr	
Marcasite				25					2	1					
Orpiment			3												
Pearceite															
Polybasite															
Proustite-Pyrargyrite															
Pyrite	1.5	3.5	2	tr	3	4	1	1	4	5	5	2	1.5	1.5	7
Pyrrhotite		?										tr			
Quartz							2	2	1	tr	tr				2
Realgar			70												
Rutile															
Native Silver													tr	tr	
Sphalerite					tr	tr	tr	tr	1	tr	tr	1	1.5	1.5	tr
Stannite						tr	tr	tr	tr		tr	tr	tr	tr	tr
Stannite III															
Stibnite															
Stromeyerite												tr			
Tennantite-Tetrahedrite															
Unknown I							tr	tr							

Carlin-style sample
Unclear affinity
BMVT sample

Table 5. Cove mineralogy and visually estimated modal abundances (percentages) from polished sections and doubly-polished plates. Pres = present, but abundance not available; tr = <1 percent of sample. See Plate 1 and APPENDIX II for sample locations and descriptions.

MINERALS \ SAMPLES	4145E-9 (dpp)	7/26/98-2A	7/26/98-2A (dpp)	7/26/98-2B	7/26/98-2B (dpp)	7/26/98-1B	4285E-15	4145E-21	7/26/98-1C	4245E-17	4285E-17A	4285E-17B	4145E-8	4145E-8 (dpp)	4365E-1
Acanthite				tr	tr		tr				tr	tr	tr	tr	tr
Arsenopyrite	2						tr	tr		tr	tr	tr	1	1	
Canfieldite	tr	tr	tr			pres		tr	tr	tr	tr	tr			tr
Carbonates				10	10			1							
Cassiterite				tr	tr					tr	tr	tr			
Chalcopyrite	tr	tr	tr	tr	tr	pres	tr	tr	tr	1	1	1	tr	tr	tr
Galena	tr	tr	tr	tr	tr	pres	2	1	3	5	5	5	tr	tr	tr
Native Gold-Electrum										tr					tr
Kesterite															
Marcasite							tr	3		20	20	20			
Orpiment															
Pearceite															
Polybasite															
Proustite-Pyrargyrite				tr	tr										
Pyrite	7	1	1	2.5	2.5	pres	10	20	60	30	30	30	4	4	25
Pyrrhotite						pres	tr	tr	tr	tr	tr	tr			
Quartz	2	tr	tr	tr	tr	pres	tr	1	1	1	1	1	tr	tr	tr
Realgar															
Rutile															
Native Silver															
Sphalerite	tr	tr	tr	2.5	2.5	pres	20	8	20	4	4	4	tr	tr	5
Stannite	tr	tr	tr	tr	tr	pres	tr	tr	1	tr	tr	tr	tr	tr	tr
Stannite III										tr					
Stibnite															
Stromeyerite															
Tennantite-Tetrahedrite				1	1					1	1	1	tr	tr	tr
Unknown I															

MINERALS \ SAMPLES	CVC4-1793	4245E-14	4245E-14 (dpp)	BOTTOMA-2	BOTTOMA-2 (dpp)	4145E-25	4285E-6	4285E-6 (dpp)	UK-1	TC8-A1	CSD-6	CVC218-808.5	ARPB-1	ARPB-1 (dpp)	TC8FS-150
Acanthite						tr			tr			tr			
Arsenopyrite	10								5			1.5	tr	tr	
Canfieldite		tr	tr	tr	tr	tr	tr	tr	tr						tr
Carbonates						tr	pres	pres							
Cassiterite										tr			tr	tr	
Chalcopyrite	1	tr	tr	tr	tr	tr	tr	tr	tr	tr		tr	tr	tr	tr
Galena	tr	2	2	tr	tr	2	2	2	2	tr	?		1	1	8
Native Gold-Electrum							tr	tr			tr				tr
Kesterite															
Marcasite	tr					tr			17		?		tr	tr	1
Orpiment															
Pearceite									tr						
Polybasite									tr						
Proustite-Pyrargyrite									tr		tr				
Pyrite	20	30	30	10	10	20	10	10	60	7	1	2	5	5	60
Pyrrhotite	1	tr	tr			tr			tr	tr			tr	tr	tr
Quartz		2	2	1	1		3	3	tr	1		15	30	30	6
Realgar															
Rutile	tr					tr									
Native Silver															
Sphalerite		4	4	2	2	3	3	3	5	tr		tr	2	2	20
Stannite				tr	tr	tr	tr	tr	tr			tr	tr	tr	tr
Stannite III															
Stibnite															
Stromeyerite		tr	tr			tr									
Tennantite-Tetrahedrite	tr					tr	tr	tr	tr	<tr			tr	tr	tr
Unknown I															

Carlin-style sample
Unclear affinity
BMVT sample

Table 5. Cont.

MINERALS \ SAMPLES	TC8FS-150 (dpp)	PB10/1-1: C-VEIN	PB10/1-1: B-VEIN	PB10/1-1: A-VEIN	ARPB-2	TC6FS-65	TC8-A2	CVC-8-1705 (dpp)	CVC-8-2180.5 (dpp)	CVC-8-2470.5 (dpp)
Acanthite										
Arsenopyrite		tr	1	1	tr				pres	
Canfieldite	tr					tr	tr			
Carbonates										
Cassiterite		tr	tr	tr	tr					
Chalcopyrite	tr	tr	tr	tr	tr	tr	tr		pres	pres
Galena	8	4	5	5	tr	2	2	pres	pres	pres
Native Gold-Electrum	tr					tr	tr			
Kesterite										
Marcasite	1				35					pres
Orpiment										
Pearceite										
Polybasite										
Proustite-Pyrargyrite										
Pyrite	60	50	75	75	30	75	15	pres	pres	pres
Pyrrhotite	tr	tr	tr	tr	tr				pres	
Quartz	6	tr			1	8	15	pres	pres	
Realgar										
Rutile										pres
Native Silver										
Sphalerite	20	10	10	10	20	5	5	pres	pres	pres
Stannite	tr	tr				tr				
Stannite III										
Stibnite										
Stromeyerite										
Tennantite-Tetrahedrite	tr	tr			tr		1	pres		
Unknown I										

Carlin-style sample
Unclear affinity
BMVT sample

Table 5. Cont.

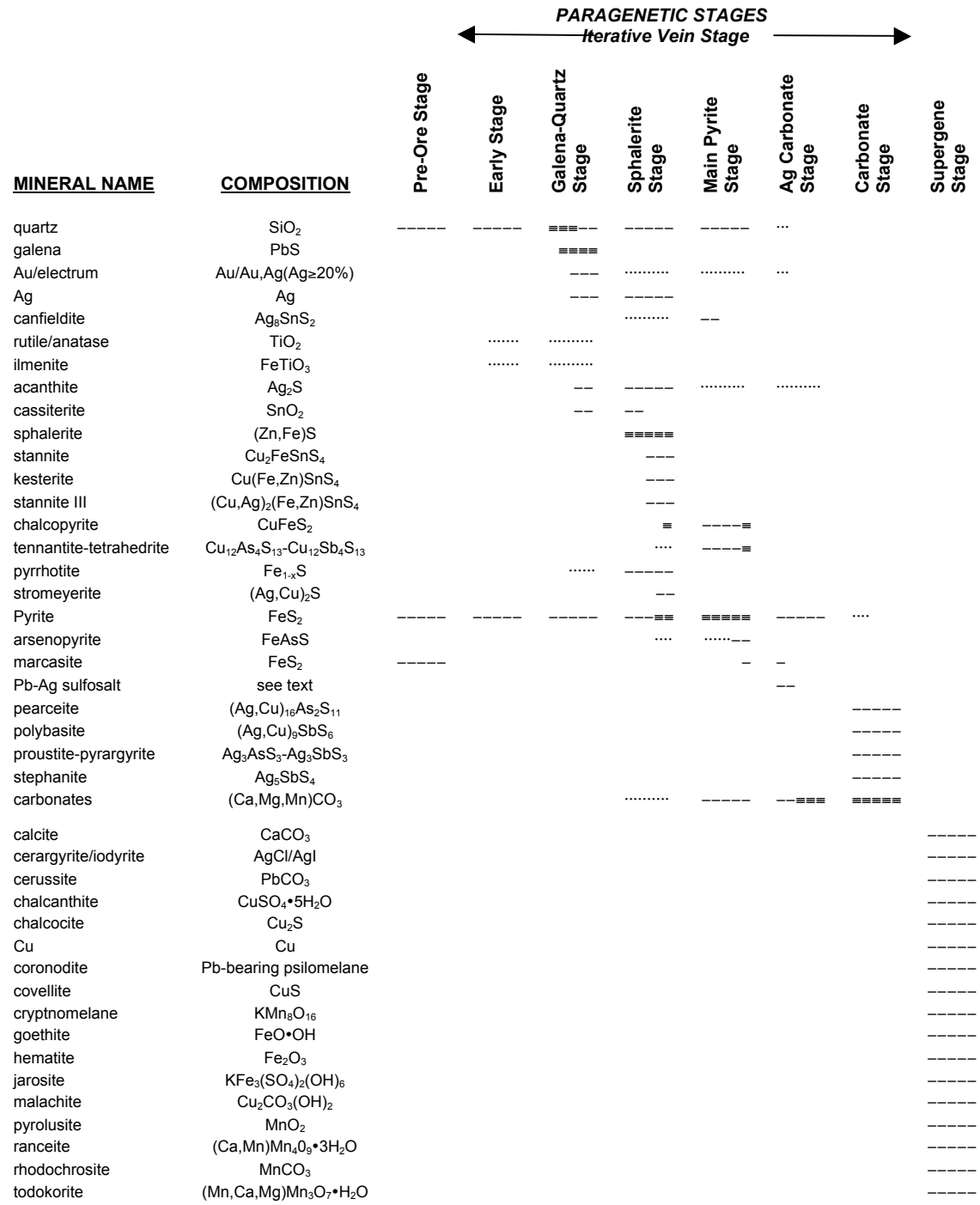

FIG. 30. Mineralogy and paragenesis for the hypogene BMVT ore system and supergene alteration (≡≡≡ = major component, ––– = ubiquitous minor component, ····· = sparse minor to trace component). Other minerals/phases identified in unpublished in-house reports, but lacking paragenetic information, are listed in the text. Note: the spatial gaps between stages do not indicate temporal gaps.

of anticline-related radial joints. This main BMVT ore stage is termed "iterative" becauses it developed in a dynamic environment of tectonic fracturing, dilation of preexisting fractures, and episodic hydrothermal fluid release and mineralization. The net results of these activities were the development of single veins, multiple vein structures related to episodic dilation and precipitation, vein breccias, sulfide-cemented crackle breccias, crustiform pore-lining sulfides, and widespread disseminations.

Disseminated Fe ± As sulfides, dominantly pyrite, are ubiquitous throughout the Cove system. They were deposited at all stages of alteration from pre-ore deuteric and throughout the hypogene Carlin-style and BMVT event(s), and possibly consist of diagenetic pyrite as well. The other BMVT ore styles were produced by pulses of mineralizing hydrothermal fluids during the BMVT main ore stage, and are associated with quartz-sericite alteration.

Each BMVT episode of fracturing, fluid transmission, and mineral precipitation is expressed in a clearly-defined paragenetic sequence based on mineral textures and associations. In Figure 30, this "iterative vein stage" is broken down into six substages: 1) an "early" stage consisting of cockscomb quartz, Fe ± Ti oxides, and iron sulfides; 2) a "galena-quartz" stage consisting dominantly of galena and quartz, with lesser Fe sulfides, and minor rutile, cassiterite, and Au/Ag-bearing phases; 3) a "sphalerite" stage consisting of sphalerite with lesser pyrite, and minor chalcopyrite, quartz, Au- and Ag-bearing phases, Sn-bearing phases (canfieldite, cassiterite, kesterite, stannite), tennantite-tetrahedrite, pyrrhotite, arsenopyrite, and carbonates; 4) a "main pyrite" stage consisting dominantly of pyrite with lesser chalcopyrite and tennantite-tetrahedrite, and minor

quartz, acanthite, canfieldite, arsenian pyrite, arsenopyrite, and carbonates; 5) a "Ag sulfosalt-carbonate" stage consisting of acanthite, pearceite-polybasite, proustite-pyrargyrite, stephanite, pyrite, a Pb-Ag sulfosalt, and carbonates; and 6) a "carbonate" stage consisting of essentially calcite and manganocalcite ± rhodochrosite.

The following mineral descriptions are based on petrographic and microchemical analyses (e.g. EMP, SEM-EDX) for the 51 hypogene BMVT ± Carlin-style ore polished sections examined during this study, and are arbitrarily listed in alphabetical order. Where applicable, these descriptions are supplemented by EMP and SIMS analyses detailed in unpublished in-house reports. Textural terminology is based on classifications and definitions from Schwartz (1951), Edwards (1954), Bastin (1957), and Craig and Vaughan (1994). A brief summary of additional probable BMVT phases identified by other workers, but not seen during the current study, is also included at the end of this section. Figure 31 shows the general mineralogy and textures of a single-iteration BMVT vein.

Acanthite (Ag_2S)

Acanthite was observed in 15 of the BMVT samples as anhedral trace constituents with the following associations: 1) ≤0.08-millimeter-long overgrowths on earlier galena, with well-developed galena cusps and acanthite caries; 2) ≤0.04-millimeter-long grains in association with irregular stannite as inclusions in sphalerite; 3) ≤0.09-millimeter-long inclusions in tennantite-tetrahedrite (var. freibergite) grains; and 4) late BMVT stage acanthite-pearceite-polybasite-proustite veinlets cutting earlier sphalerite (Fig. 32),

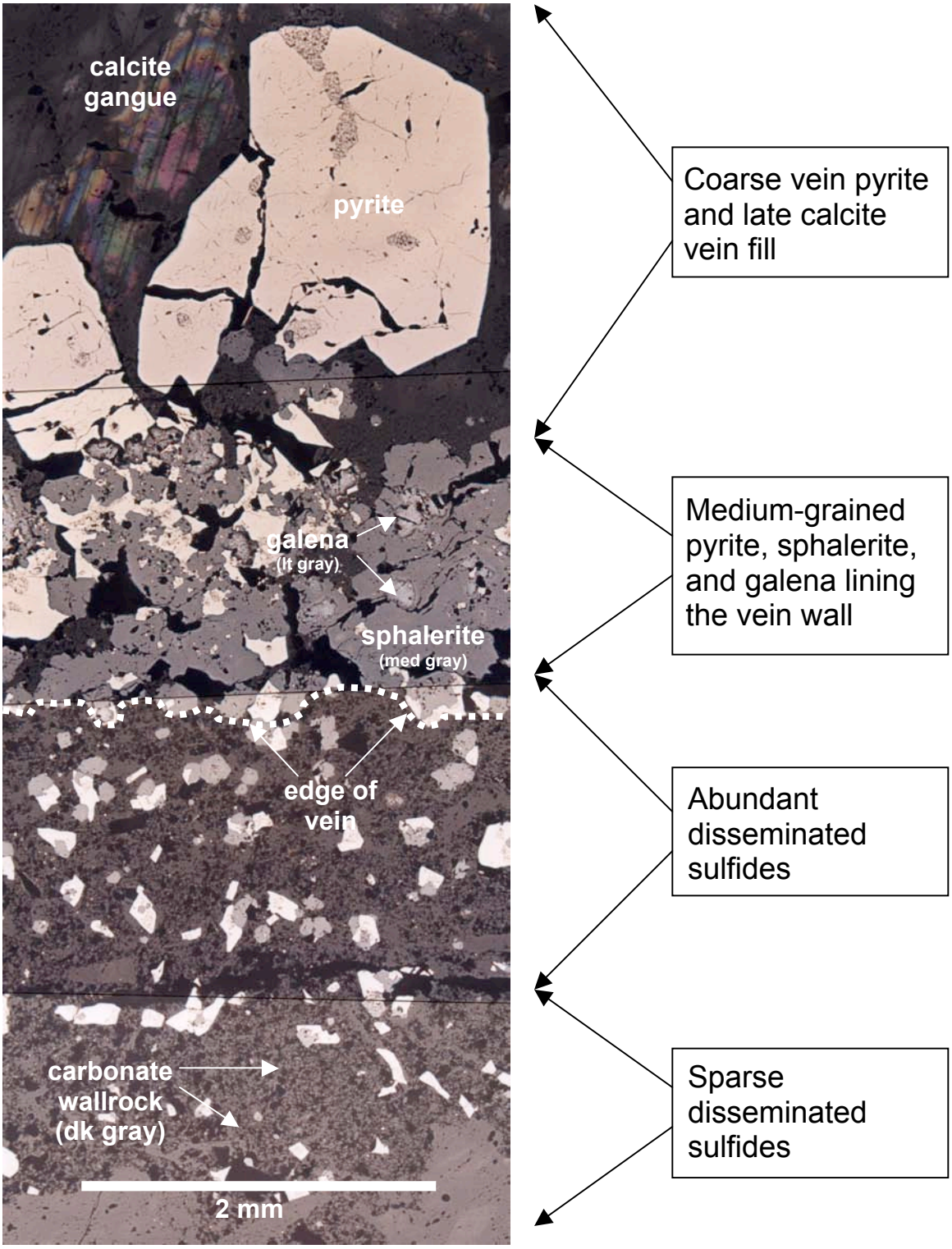

FIG. 31. Reflected light photomicrograph montage for sample 4285E-6 showing general characteristics of a single generation BMVT vein.

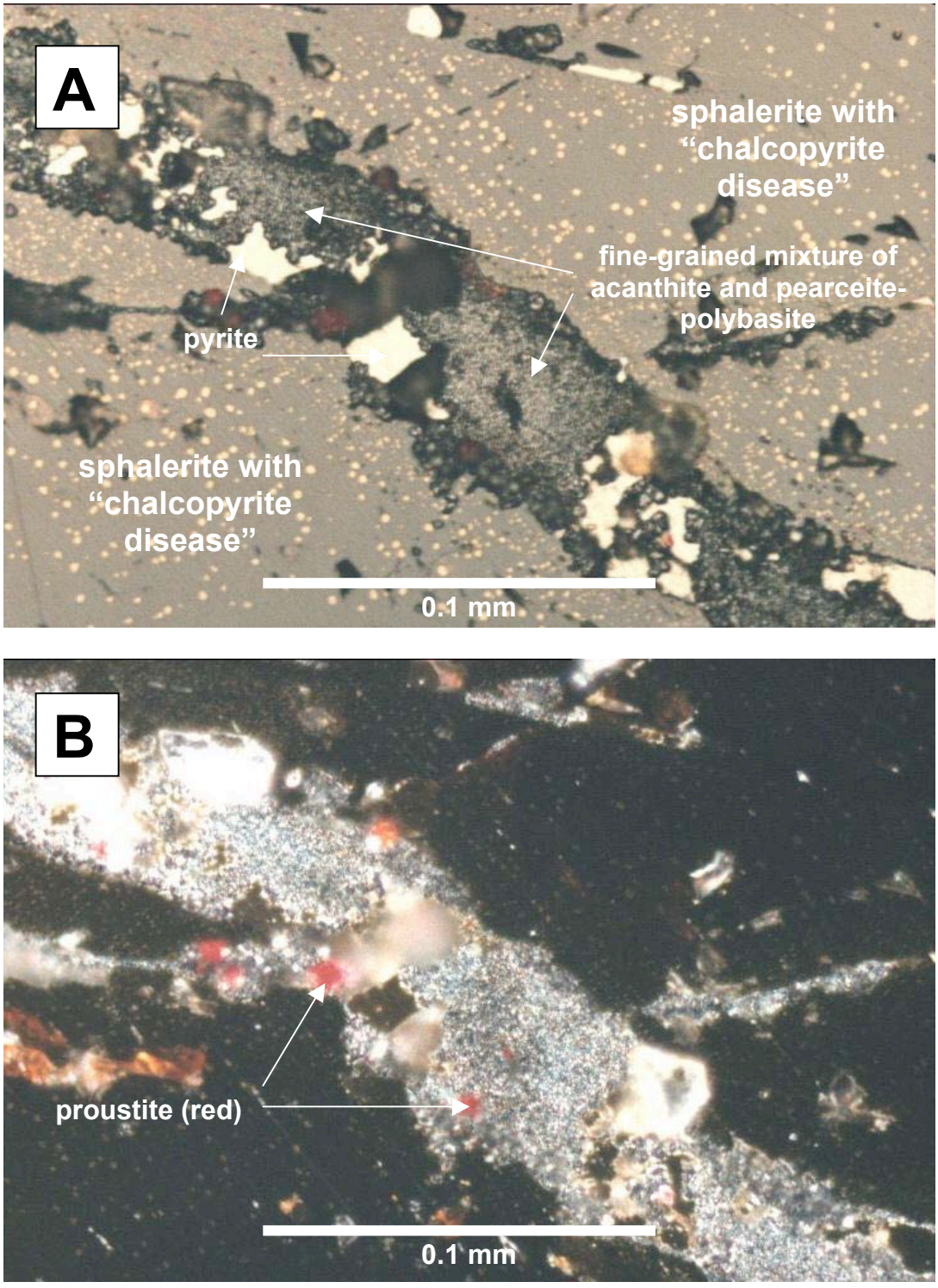

FIG. 32. General associations of acanthite. A shows a reflected light photomicrograph of sample UK-1, with a veinlet of fine-grained acanthite, pearceite-polybasite, and proustite (all Ag sulfosalt-carbonate stage) overprinting an earlier pyrite veinlet (main pyrite stage) that cuts a sphalerite grain (sphalerite stage). B is the same as A, under crossed polars.

acanthite rims on pyrargyrite, and spongy-looking acanthite "ice flowers" in carbonate gangue.

Arsenopyrite (FeAsS)

Arsenopyrite occurs as a trace to major component in 21 BMVT samples, typically as sub- to euhedral grains with pseudo-rhombic shapes. Some disseminated arsenopyrite was observed, which may be related to Carlin-style ore, but most occurs within or associated with BMVT veins and crustifications. In the case of the latter, ≤1.20-millimeter-long arsenopyrite typically forms intergrowths with and inclusions in pyrite grains (Fig 33B), and occurs in pyrite veinlets cutting earlier sphalerite. BMVT arsenopyrite also occurs as ≤0.25-millimeter-long inclusions in sphalerite, 0.15-millimeter-long inclusions with pyrite in euhdral quartz, ≤0.05-millimeter-long corroded grains in a tennantite-tetrahedrite (var. freibergite) matrix, ≤0.40-millimeter-long inclusions in elongate marcasite grains (Fig. 33A), and as disseminated grains immediately adjacent to base metal veins (Fig. 33C). These disseminated grains are up to 0.30-millimeters-long, and are cut by later marcasite veinlets in several samples.

Canfieldite (Ag_8SnS_2)

Canfieldite is most common as ≤0.08 millimeter blebs associated with shredded galena in pyrite (Fig. 34), and was observed as a trace component in 31 BMVT samples. Canfieldite also occurs as rims on the edges of galena grains, as blebby inclusions in

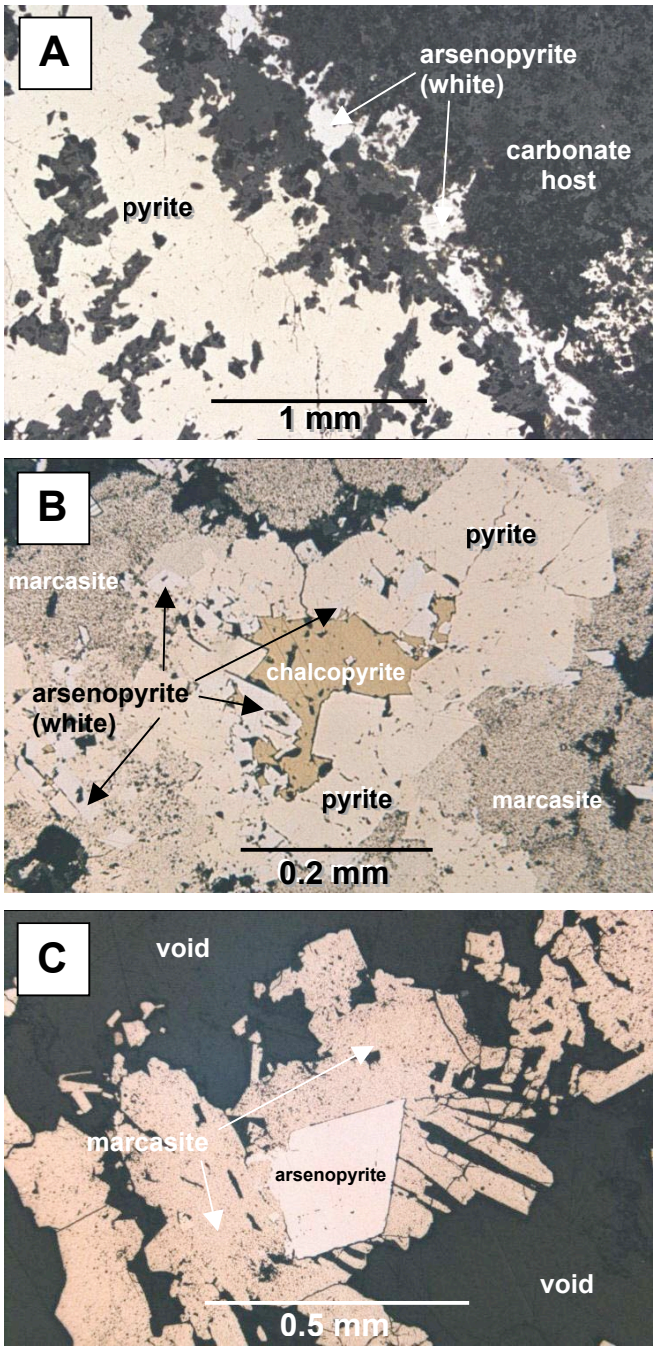

FIG. 33. Arsenopyrite associations and characteristics. A is a reflected light photomicrograph showing a thin arsenopyrite veinlet just outside of and parallel to a BMVT pyrite vein (both main pyrite stage) (sample CVC4-1793). B is a reflected light photomicrograph showing intergrown main pyrite stage pyrite and arsenopyrite, with slightly later chalcopyrite vug fill (all main pyrite stage), and latest main pyrite stage porous colloform marcasite linings (sample ARPB-2). C is a reflected light photomicrograph showing a main pyrite stage arsenopyrite crystal overgrown and partially replaced by late main pyrite stage bladed marcasite (sample ARPB-2).

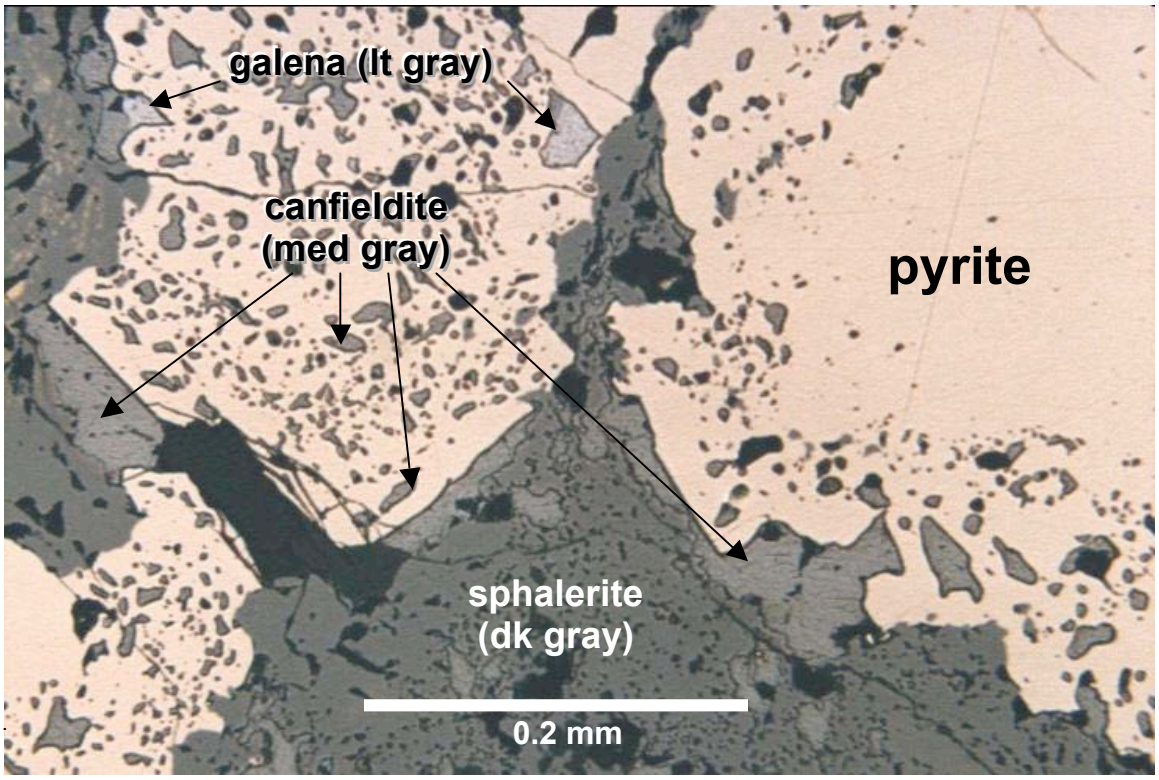

FIG. 34. Reflected light photomicrograph of sample TC6FS-65 showing canfieldite (sphalerite stage to early main pyrite stage) as blebs in main pyrite stage pyrite, and also as residual concentrations along the main pyrite stage front where the pyrite replaces sphalerite (sphalerite stage). Note that the canfieldite is also associated with shredded galena-quartz stage galena.

sphalerite, and as rare ≤0.17-millimeter-long irregular rims on pyrite grains containing shredded galena and blebby canfieldite inclusions.

Carbonates ($(Ca,Mg,Mn)(CO_3)$)

Carbonates were observed in only 12 BMVT polished sections, but are typically abundant macroscopic constituents of BMVT assemblages observed in hand samples and pit highwalls. Calcite occurs as late, pore-filling, interlocking sparry crystals and crustiform banded and/or radiating forms in base metal veins (Fig. 35A), crustifications, and breccia cements. The largest crystals observed have tabular habits and are typically up to 1 centimeter in diameter. SEM-EDX analyses indicate that BMVT calcite has typically low yet highly variable Mn contents, but none were pure rhodochrosite. Streiff (1994), however, did report the presence of rhodochrosite in the vicinity of feeder structures in the original Cove underground operations. Pure rhodochrosite was found during the current study as residual grains in the supergene system. Dolomite also was observed during the current study, cutting BMVT pyrite in one sample from deep drill core (CVC4-1793) (Fig. 35B).

Cassiterite (SnO_2)

Cassiterite is a trace component in 14 of the BMVT samples as small (≤0.14-millimeter-diameter) anhedral grains. They typically occur as inclusions in pyrite. One 0.04-millimeter-diameter grain occurs in an island-atoll feature as an inclusion in sphalerite and acanthite (Fig. 36A), and another grain is associated with stannite,

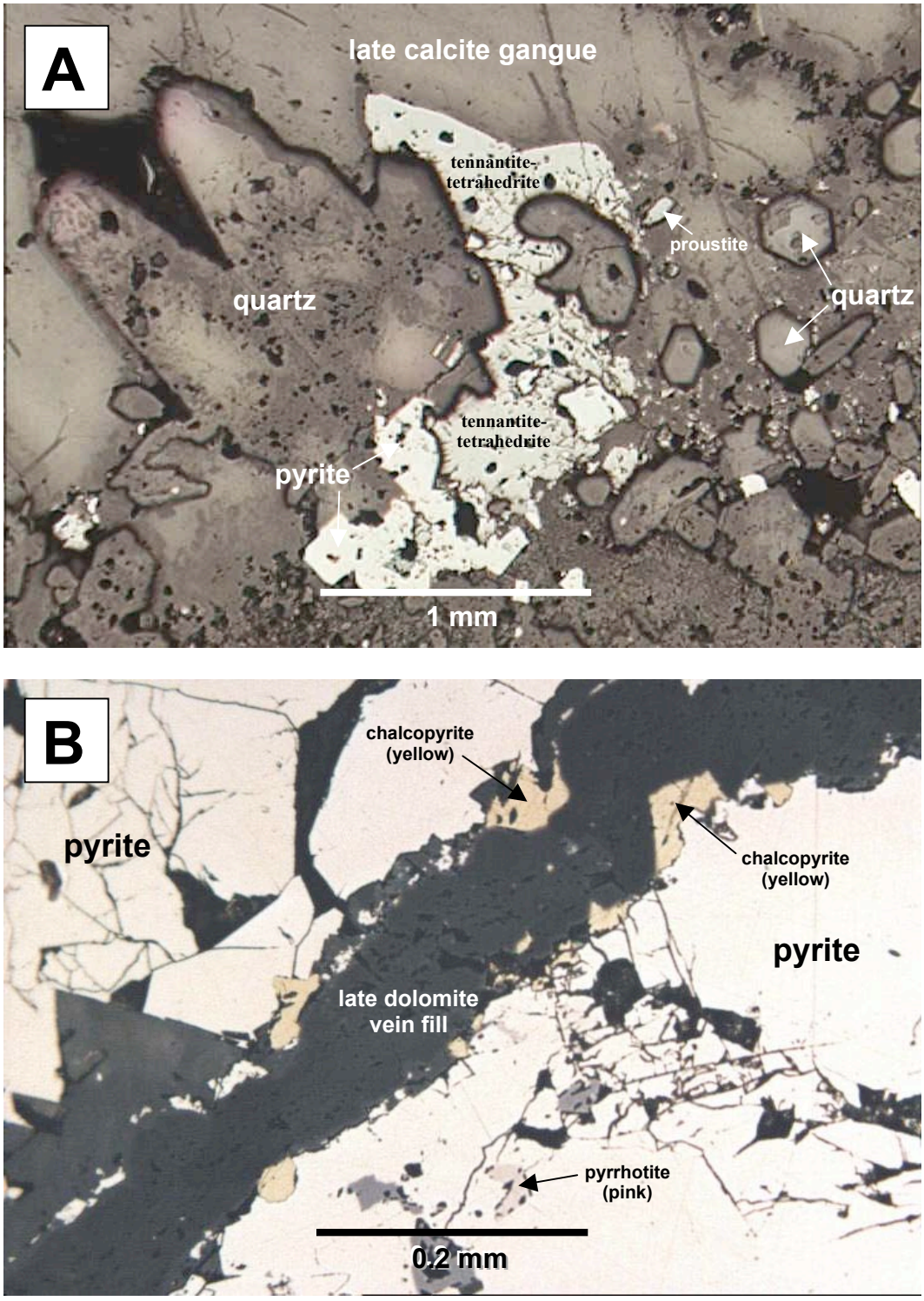

FIG. 35. BMVT carbonate associations. A is a reflected light photomicrograph showing latest calcite void fill (sample 7/26/98-2B). B is a reflected light photomicrograph showing a latest dolomite veinlet filling a fracture in a main pyrite stage BMVT vein (sample CVC4-1793).

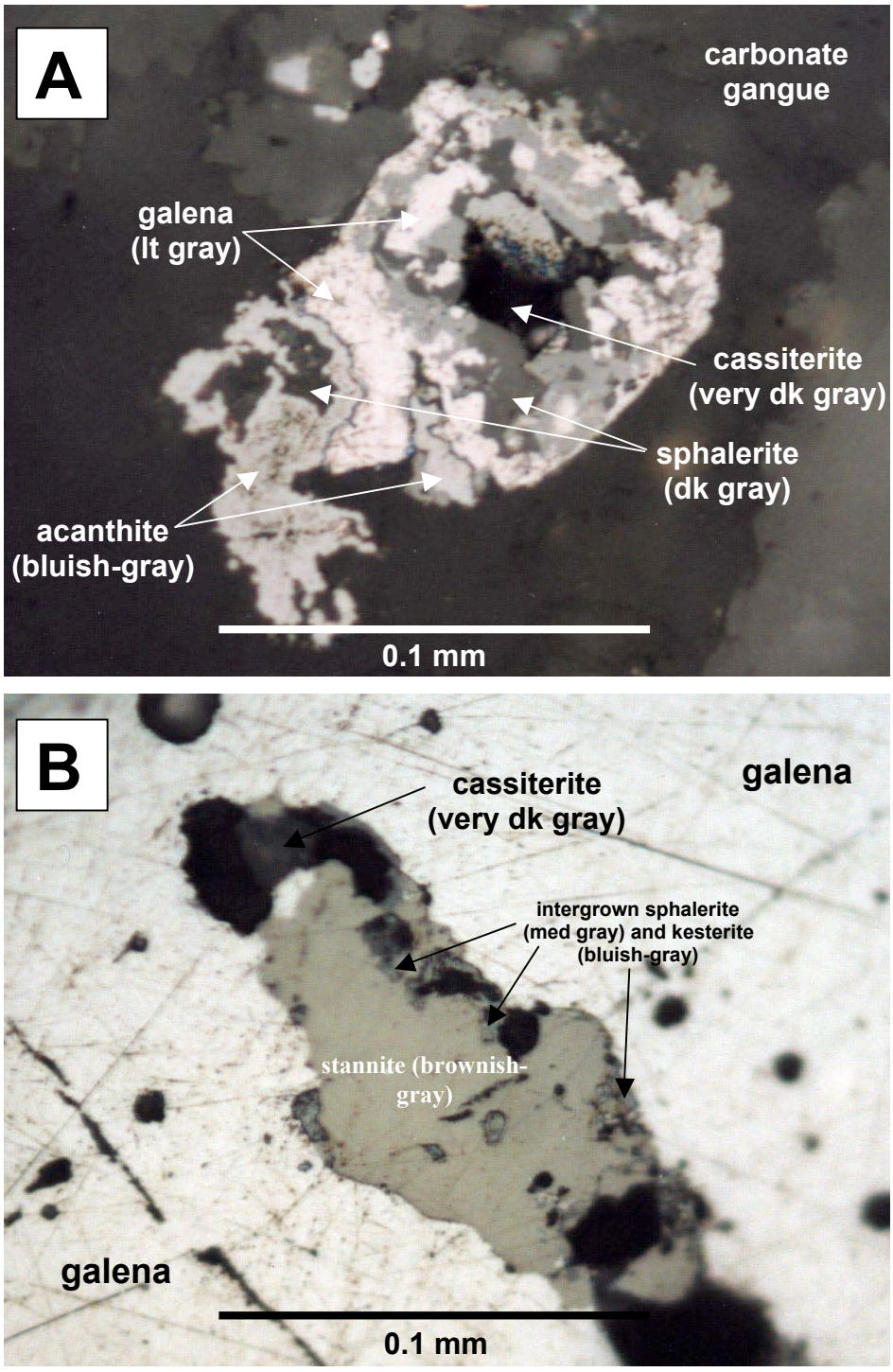

FIG. 36. Cassiterite associations. A is a reflected light photomicrograph showing an island-atoll feature consisting of multiple episodes of galena-quartz stage galena (with a cassiterite grain), sphalerite stage sphalerite, and sphalerite to Ag sulfosalt-carbonate stage acanthite (sample 4245E-5). B is a reflected light photomicrograph showing a cassiterite grain associated with sphalerite stage stannite, kesterite, and sphalerite replacing galena (sample 4245E-5).

kesterite, and sphalerite replacing galena (Fig. 36B). Because of their small size and similarity to other phases such as sphalerite, cassiterite grains were typically identified only through SEM-EDX scans.

Chalcopyrite ($CuFeS_2$)

Chalcopyrite was observed as a trace constituent in all BMVT samples but two, and has six modes of occurrence. The most widespread occurrence is as ≤0.0025-millimeter-long blebby inclusions in sphalerite (mode 1). This "chalcopyrite disease" is typically associated with pyrrhotite inclusions, and also rims stannite inclusions in sphalerite. The second mode is in ≤0.75-millimeter-wide patches cutting earlier sphalerite (Fig. 37A and 37B). These patches consist of pyrite euhedra or atoll features with tennantite-tetrahedrite cores, with matrix chalcopyrite intergrown with and/or rimmed by tennantite-tetrahedrite. The third mode consists of thin chalcopyrite ± pyrite ± marcasite ± tennantite-tetrahedrite veinlets cutting earlier sphalerite grains and galena along cleavage planes.

In samples with both patches and veinlets containing chalcopyrite, some of the veinlets occur as splays from the patches, indicating that modes 2 and 3 are contemporaneous. Increased density of chalcopyrite disease is associated with the veinlets cutting sphalerite, and grades outward into less dense chalcopyrite disease (Fig. 37C). The fourth mode consists of chalcopyrite patches with euhedral arsenopyrite ± anhedral sphalerite just outside of associated base metal veins. The fifth mode consists of

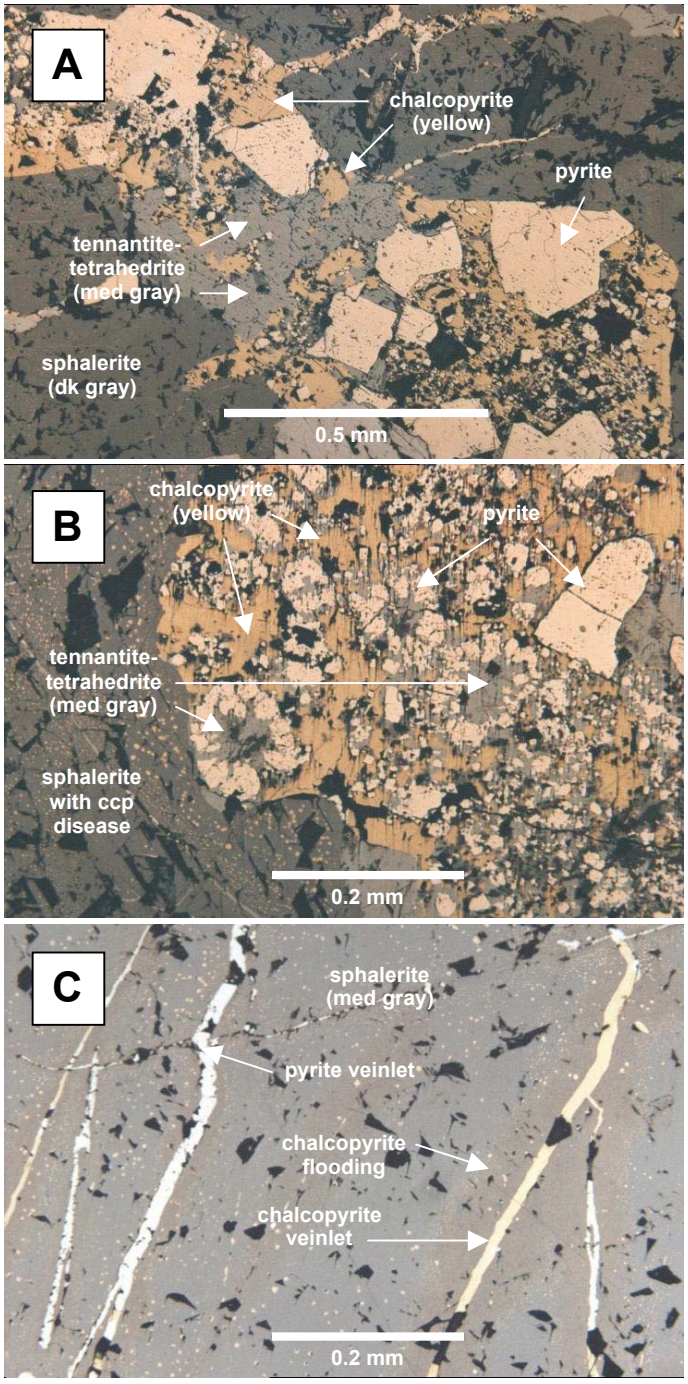

FIG. 37. General chalcopyrite textures and associations. A is a reflected light photomicrograph of sample UK-1 showing a late main pyrite stage pyrite euhedra + chalcopyrite + tennantite-tetrahdedrite patch/vein cutting earlier sphalerite stage sphalerite. B is a reflected light photomicrograph of sample UK-1 showing part of another late main pyrite stage pyrite + chalcopyrite + tennantite-tetrahdedrite patch cutting earlier sphalerite stage sphalerite. C is a reflected light photomicrograph of sample 4245E-17 showing late main pyrite stage chalcopyrite + pyrite veinlets cutting earlier sphalerite stage sphalerite, with chalcopyrite flooding away from the veinlets.

small inclusions of chalcopyrite-pyrrhotite ± sphalerite ± stromeyerite in vein pyrite. The sixth mode is a single chalcopyrite inclusion in vein quartz.

Galena (PbS)

Galena is a common trace to minor BMVT component observed in all the BMVT samples but three as anhedral grains up to 8 millimeters in diameter. Galena is an early BMVT phase, and in all samples is corroded by, replaced by, and/or included in all subsequent phases. The most obvious paragenetic relationships between galena and later sulfides are visible in common base metal island-atoll features, in which the early galena cores are enclosed by later sphalerite that is rimmed by latest pyrite (Fig. 38A). Some individual galena grains are embayed by sphalerite and/or pyrite caries textures, and others are veined along cleavage planes by pyrite-marcasite ± chalcopyrite ± tennantite-tetrahedrite. Where galena is replaced by pyrite, the outline of the original galena grain is commonly defined by the occurrence of shredded galena inclusions with associated canfieldite (Fig. 38B). Galena was also observed as small inclusions in vein quartz.

Gold-Electrum (Au-(Au,Ag (Ag≥20 percent)))

Gold-electrum occurs as a trace component in nine of the 51 BMVT samples, but its paragenetic relationships with the other BMVT phases is not entirely clear. The most abundant Au-electrum grains occurred in a very high grade (>4.0 ounces Au and >300 ounces Ag per short ton) BMVT vein sample (TC8FS-150) from the Cove underground workings. Gold-electrum is ubiquitous throughout this sample, occuring as ≤0.11-

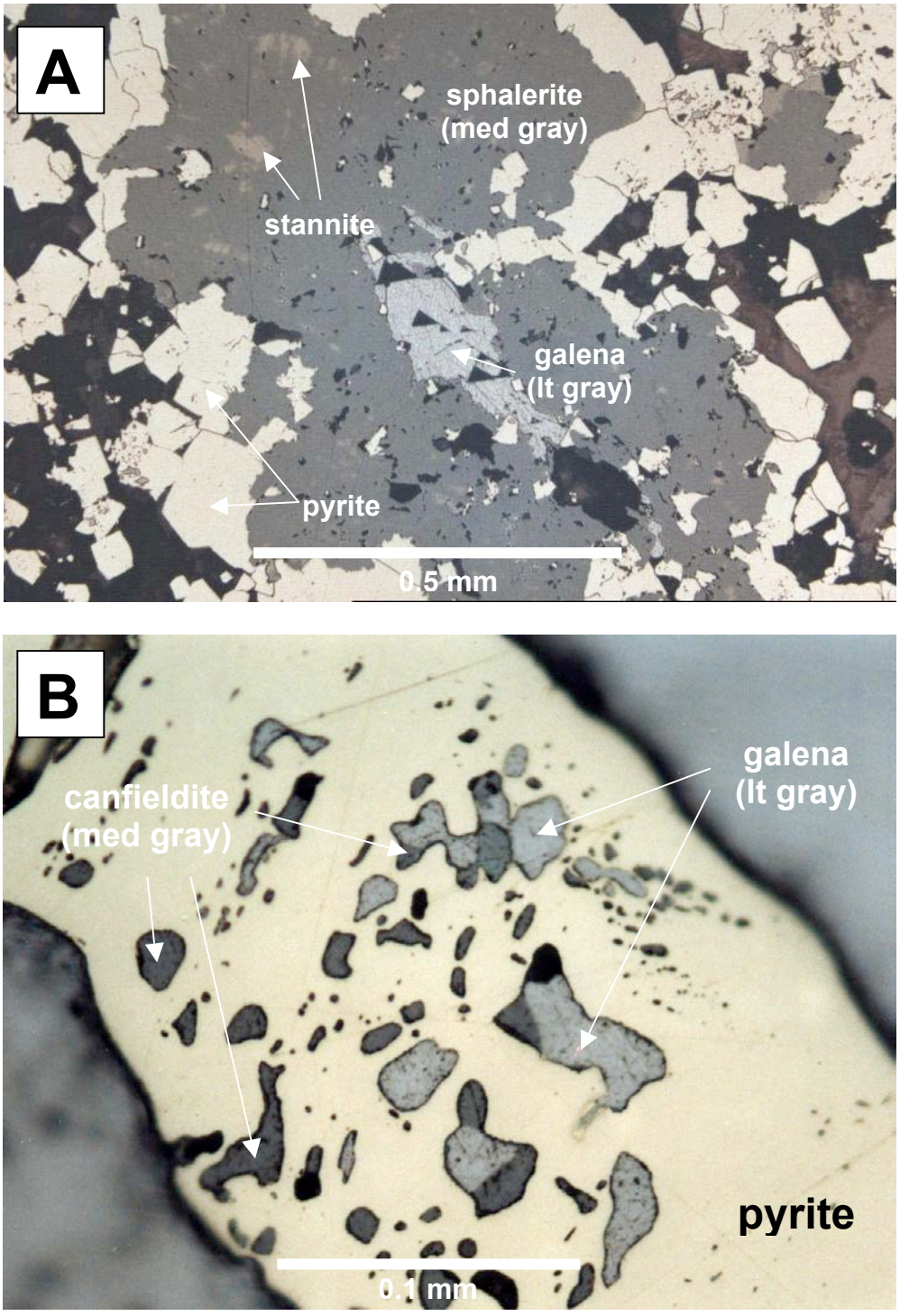

FIG. 38. General associations for galena. A shows an island-atoll structure with a galena-quartz stage galena core, surrounded by sphalerite stage sphalerite + stannite, with a relatively late main pyrite stage pyrite rim (sample 7/26/98-1C). B shows shredded galena (galena-quartz stage) in close spatial association with canfieldite (sphalerite to early main pyrite stage) in pyrite (main pyrite stage) (sample 4245E-5).

millimeter-diameter inclusions in galena, sphalerite, and pyrite (see similar modes of occurrence for sample TC6FS-65 in Fig. 39A). Other associations observed are as follows: 1) inclusions in pyrite associated with shredded galena and canfieldite; 2) inclusions in pyrite with no other apparent associations; 3) a 0.0125-millimeter-long inclusion associated with canfieldite and pyrite in carbonate vein gangue; 4) a discrete 0.05- millimeter-long grain in carbonate vein gangue; and 5) an irregular 0.0125-millimeter-long grain associated with Carlin-style microcrystalline pyrite immediately adjacent to a thin BMVT veinlet. EMP backscatter images of electrum in an unpublished in-house metallurgical report show distinct zonations (Fig. 39B).

Kesterite ($Cu(Fe,Zn)SnS_4$)

Kesterite was found in only four BMVT samples using SEM-EDX scans, and may occur in other samples. The kesterite in one sample occurs as inclusions in stannite with associated cassiterite in a patch replacing earlier galena.

Marcasite (FeS_2)

Marcasite was observed in 16 BMVT samples as a relatively late trace to major phase typically associated with pyrite. Marcasite occurs as ≤0.015-millimeter-diameter cores in disseminated BMVT pyrite, with pyrite ± chalcopyrite ± tennantite-tetrahedrite in thin veinlets cutting galena and sphalerite, in ≤0.11-millimeter-wide aggregates and zones intergrown with typically vuggy pyrite, as ≤0.15-millimeter-wide rims and porous overgrowths on pyrite (Fig. 40A), and as veinlets cutting pyrite. Marcasite also occurs as

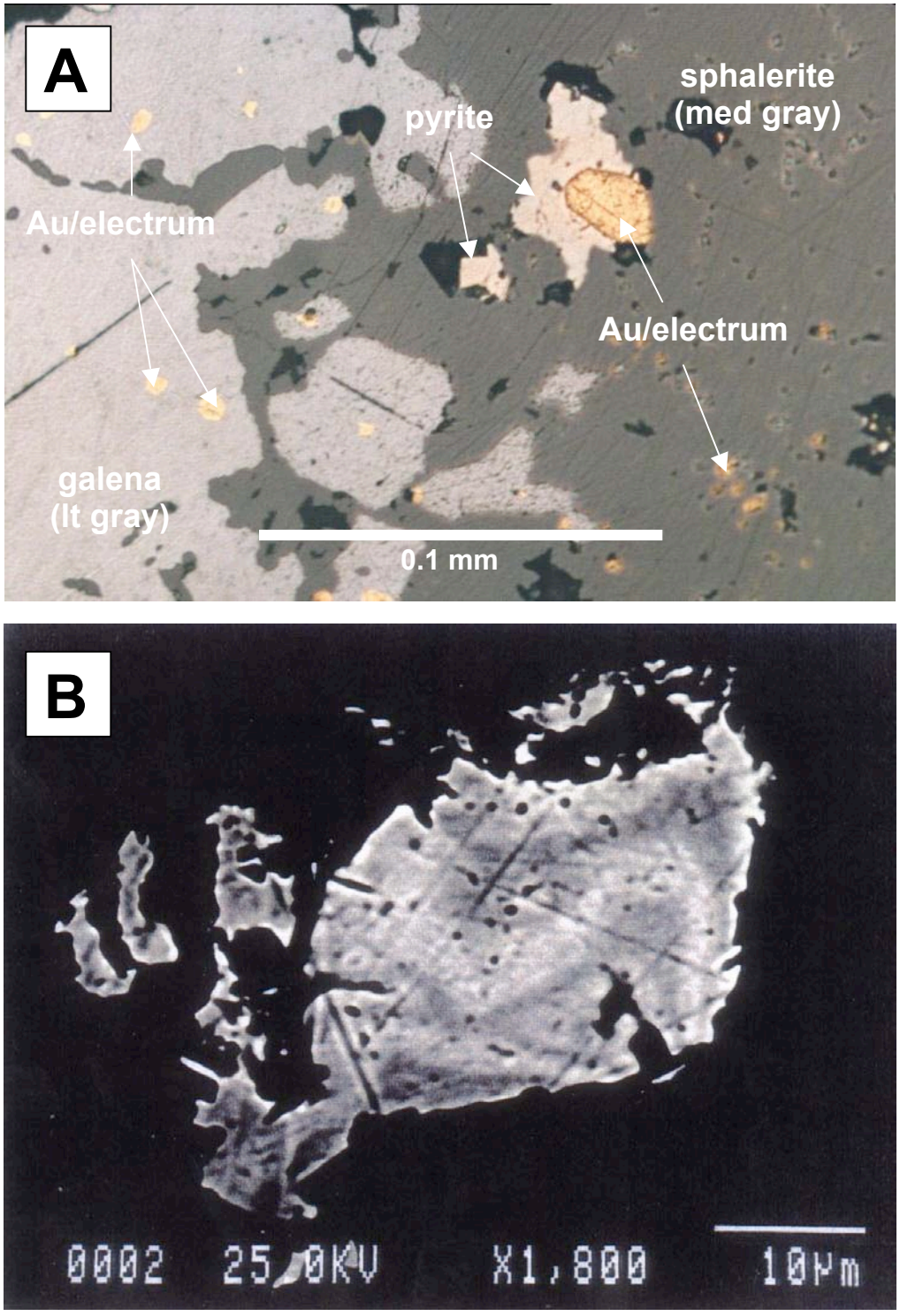

FIG. 39. Au/electrum general associations and characteristics. A shows Au/electrum inclusions (probably all early galena-quartz stage) in galena-quartz stage galena, sphalerite stage sphalerite, and main pyrite stage pyrite (sample TC6FS-65). B is an SEM backscatter image showing a zoned electrum grain; lighter areas have relatively higher Au contents (from Kingston et al., 1997).

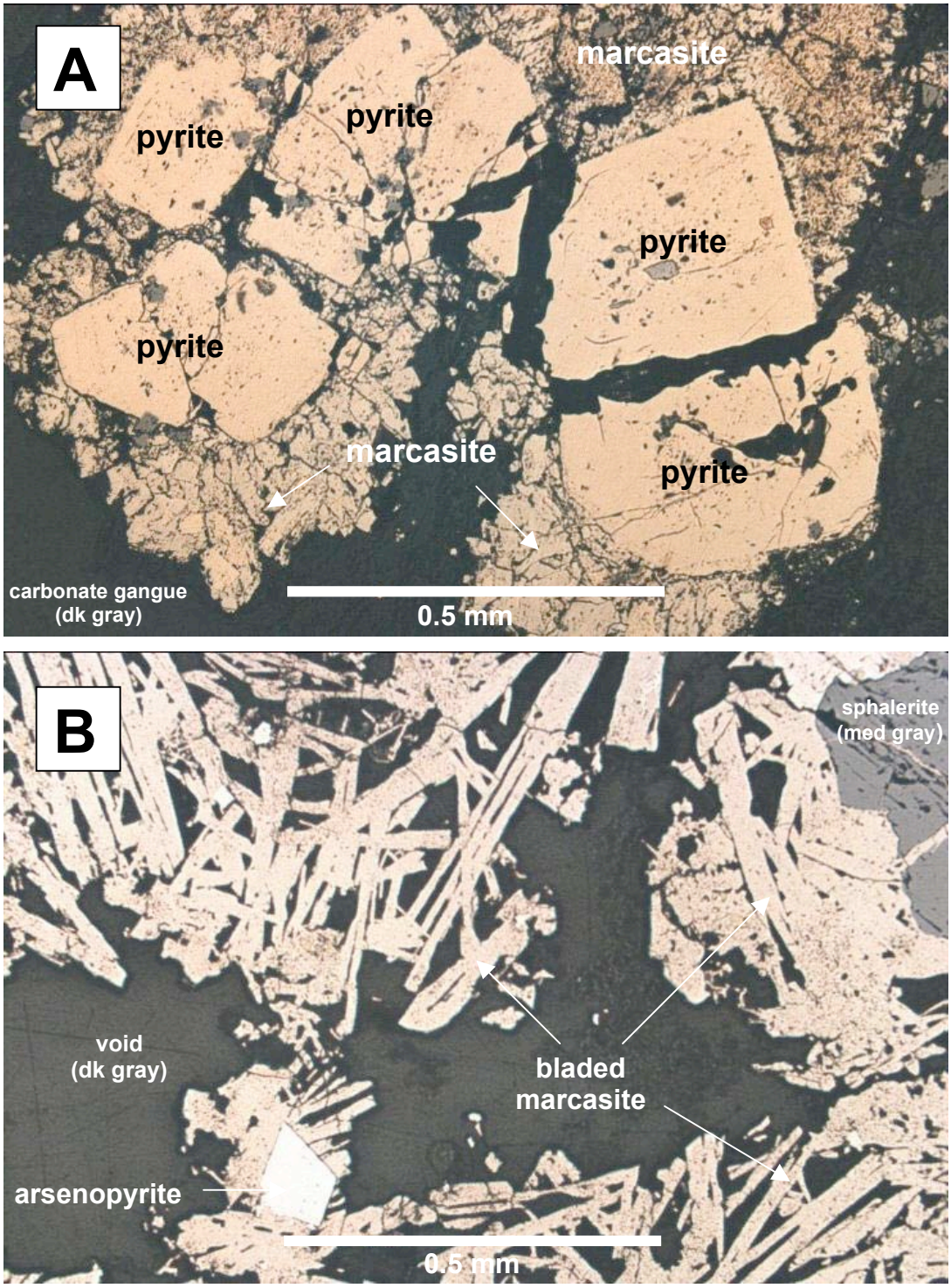

FIG. 40. Associations and habits for marcasite. A is a reflected light photomicrograph for sample 4145E-21 showing late main pyrite stage marcasite rims on earlier main pyrite stage euhedral pyrite. B is a reflected light photomicrograph of sample ARPB-2 showing relatively late main pyrite stage bladed marcasite (see Fig. 33C for a close-up view and description of lower left arsenopyrite rimmed and partially replaced by the marcasite).

arsenopyrite pseudomorphs, as ≤0.70-millimeter-wide patches of marcasite-only aggregates, as large (≤4.5-millimeter-long) bladed crystals (Fig. 40B) and porous botryoidal-colloform bands on earlier vein phases, and in thin irregular veinlets sub-parallel to BMVT veins cutting all other veinlet and disseminated BMVT phases.

Pearceite-Polybasite ($(Ag,Cu)_{16}As_2S_{11}$-$(Ag,Cu)_9SbS_6$)

Pearceite-polybasite was found in only one sample through the use of SEM-EDX scans on small unknown veinlet phases, and probably occurs as small grains in other samples. The veinlet examined cuts earlier sphalerite, and consists of earlier pyrite and arsenopyrite euhedra that are corroded and replaced by later acanthite, proustite, and pearceite-polybasite (Fig. 32).

Proustite-Pyrargyrite (Ag_3AsS_3-Ag_3SbS_3)

Proustite-pyrargyrite grains are trace constituents in four BMVT samples. Their compositions were determined through SEM-EDX and EMP analyses. In one sample, a 0.10-millimeter-long pyrargyrite crystal rimmed by acanthite occurs in carbonate gangue adjacent to an earlier tennantite-tetrahedrite crystal (Fig. 35 and Fig. 41). Proustite is associated with acanthite and pearceite-polybasite in a thin veinlet cutting earlier sphalerite (Fig. 32). Intermediate proustite-pyrargyrite occurs as ≤0.10-millimeter-wide overgrowths rimming earlier pyrite on the edge of a BMVT veinlet cutting Carlin-style ore. This relationship is interpreted to be the product of multiple pulses of mineralizing hydrothermal fluids that produced overprinting relationships between ore styles.

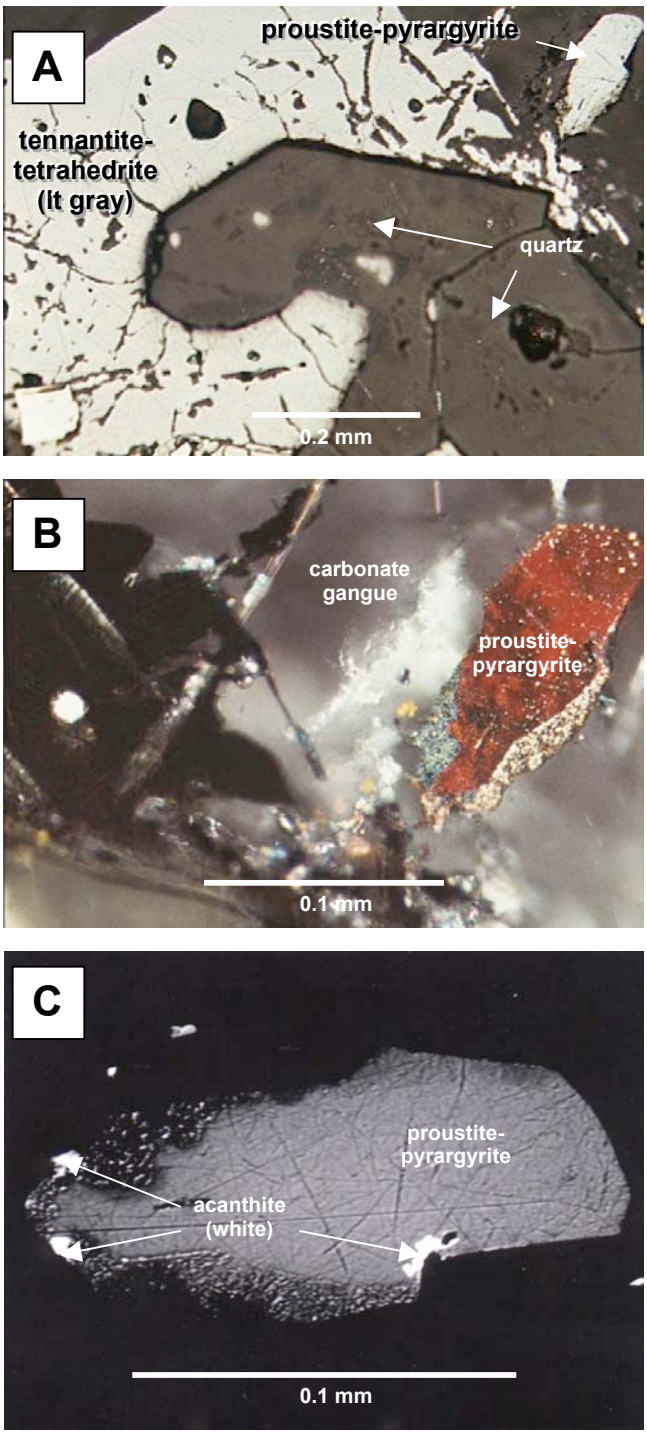

FIG. 41. Representative proustite-pyrargyrite grain. A is a reflected light photomicrograph of sample 7/26/98-2B, showing a large tennantite-tetrahedrite crystal (late main pyrite stage) with a late, outer grain of Ag sulfosalt-carbonate stage proustite-pyrargyrite (refer also to Fig. 35A). B shows a close up of the same proustite-pyrargyrite grain, under crossed polars. C is an EMP backscatter image of the same grain, showing cryptic associations with later Ag sulfosalt-carbonate stage acanthite.

Pyrite (FeS_2)

Pyrite is typically a major component in all 51 BMVT samples examined, constituting up to 75 volume percent of individual vein samples. Disseminated pyrite is common in many of the samples as coarse, blastic, fine, and microcrystalline disseminations outside of BMVT veins and veinlets in all of the host rock lithologies. BMVT pyrite has 8 modes of occurrence, and was precipitated throughout the duration of the BMVT mineralizing event(s). The first, second, and third modes are as small inclusions in vein quartz, ≤0.18-millimeter-diameter euhedral inclusions in galena, and 0.03-millimeter-average-diameter inclusions in sphalerite (Fig. 42A).

The fourth mode is volumetrically the most important in the BMVT system(s), and consists of generally coarse-grained (≤8.0-millimeter-diameter), sub- to euhedral vein pyrite overgrowths on and corrosions/replacements of earlier galena and sphalerite grains (Fig. 42B). This coarse pyrite typically contains inclusions of earlier phases, including quartz, galena, canfieldite, sphalerite, stannite, chalcopyrite, stromeyerite, and cassiterite, and is also commonly intergrown with arsenopyrite and marcasite. The fifth mode of occurrence is as ≤0.28-millimeter-diameter sub- to euhedral earlier grains in ≤0.75-millimeter-wide patches of quartz, chalcopyrite, and tennantite-tetrahedrite typically cutting earlier sphalerite (Fig. 37A and B). Related veinlets cutting sphalerite and galena grains is the sixth mode (Fig. 42C).

The final two modes do not have clear paragenetic relationships with the other BMVT phases, and consists of: mode 7) disseminated pyrite flooding away from BMVT veins into the host rocks, showing transitions from veinlet euhedra to coarse grains to small

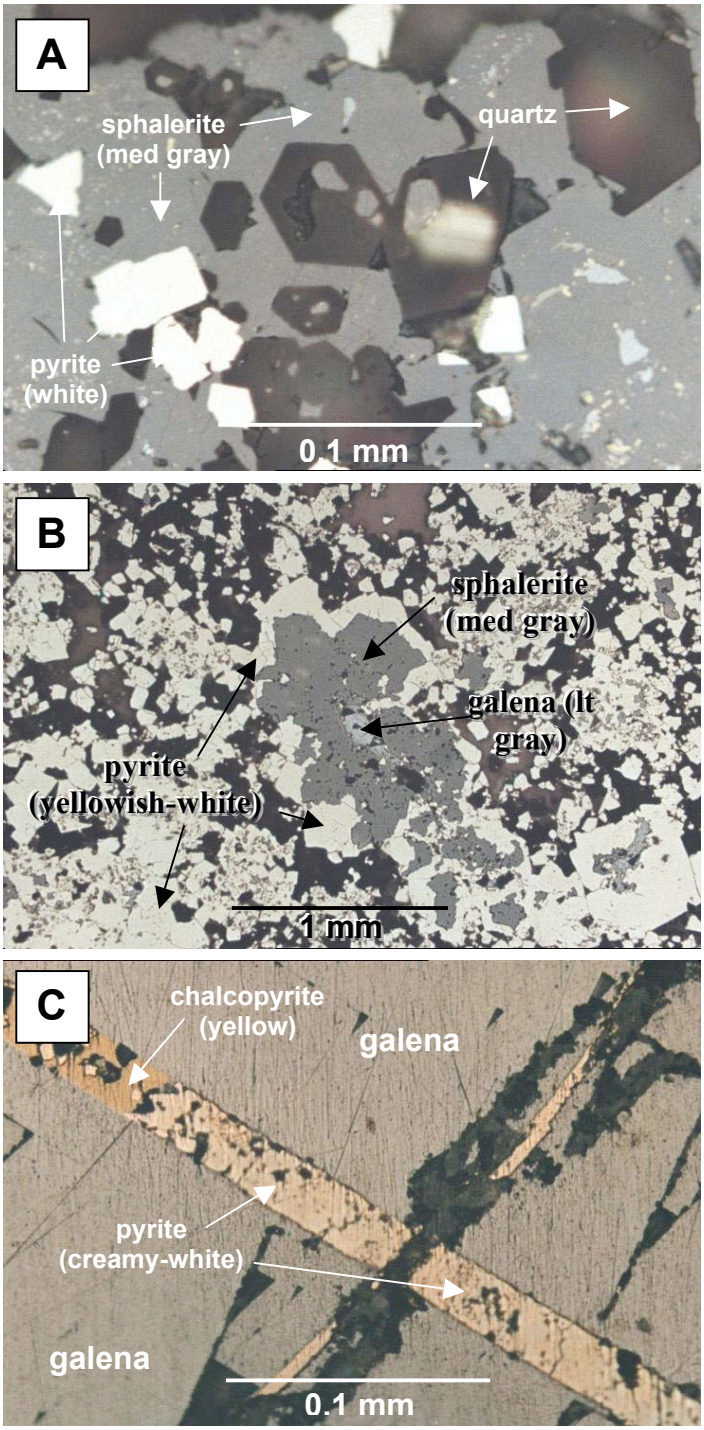

FIG. 42. BMVT pyrite associations and characteristics. A is a reflected light photomicrograph showing pyrite inclusions in sphalerite (both sphalerite stage) (sample 4145E-8). B is a reflected light photomicrograph showing the area around the island-atoll feature shown in Figure 38A, with abundant, euhedral main pyrite stage pyrite (sample 7/26/98-1C). C is a reflected light photomicrograph of a late main pyrite stage pyrite and chalcopyrite veinlet cutting galena along a cleavage plane (sample UK-1).

disseminations (Fig. 31); and mode 8) irregular pyrite ± marcasite veinlets cutting the host rocks. An important feature for all of these modes is the lack of arsenian-auriferous-argentiferous rims, as determined by petrographic, SEM backscatter image, and SEM-EDX X-ray mapping analyses.

Pyrrhotite ($Fe_{1-x}S$)

Pyrrhotite is typically a trace component observed in 23 BMVT samples and has three modes of occurrence: 1) as small (≤0.10-millimeter-diameter) blebby inclusions associated with chalcopyrite disease in sphalerite (Fig. 43A); 2) as ≤0.30-millimeter-diameter inclusions in pyrite (Fig. 43B), with or without intergrown chalcopyrite ± sphalerite ± stromeyerite (see also Fig. 49); and 3) as a single inclusion in vein quartz.

Quartz (SiO_2)

Quartz occurs in 40 BMVT samples as a minor to major component associated with BMVT veins and crustifications (Fig. 44A). The hypogene quartz euhedra contain abundant fluid inclusions that are discussed in Chapter 5 of this volume (Fig. 44B). The most common mode of occurrence is as early vein- and pore-lining cockscomb quartz that is typically free of sulfide inclusions, with crystals up to 1.8 millimeters long. In highly porous host lithologies, hypogene quartz also occurs within pore spaces immediately adjacent to the BMVT veins and crustifications.

In one sample from the Panther Canyon transitional submember, the pore-lining quartz was observed as syntaxial overgrowths on clastic quartz grains. Quartz euhedra

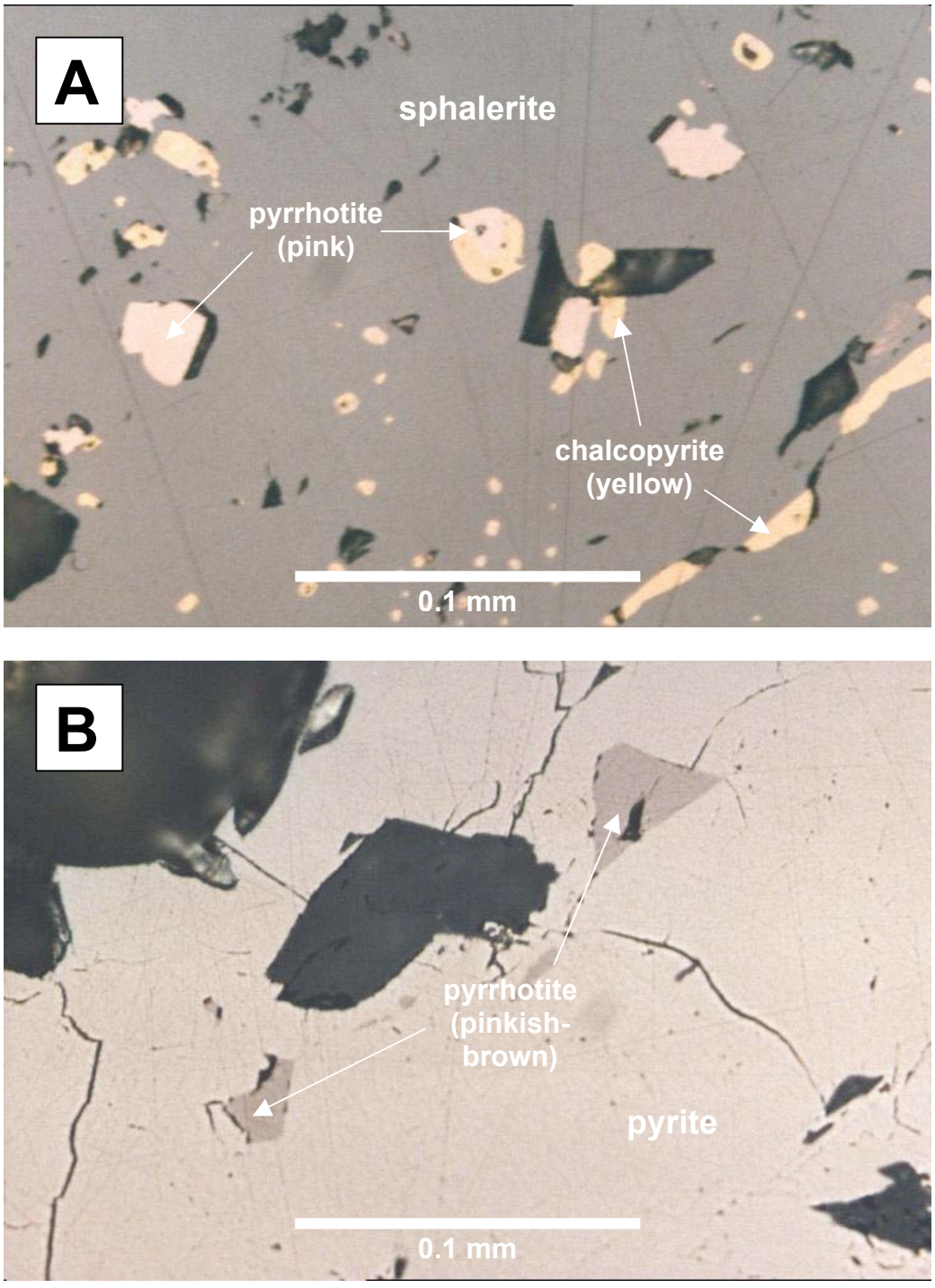

FIG. 43. Typical associations for pyrrhotite. A is a reflected light photomicrograph of sample ARPB-2 showing pyrrhotite blebs associated with chalcopyrite "disease" in sphalerite (all sphalerite stage). B is a reflected light photomicrograph of sample CVC4-1793 showing pyrrhotite blebs (sphalerite stage) in pyrite (sphalerite to main pyrite stage).

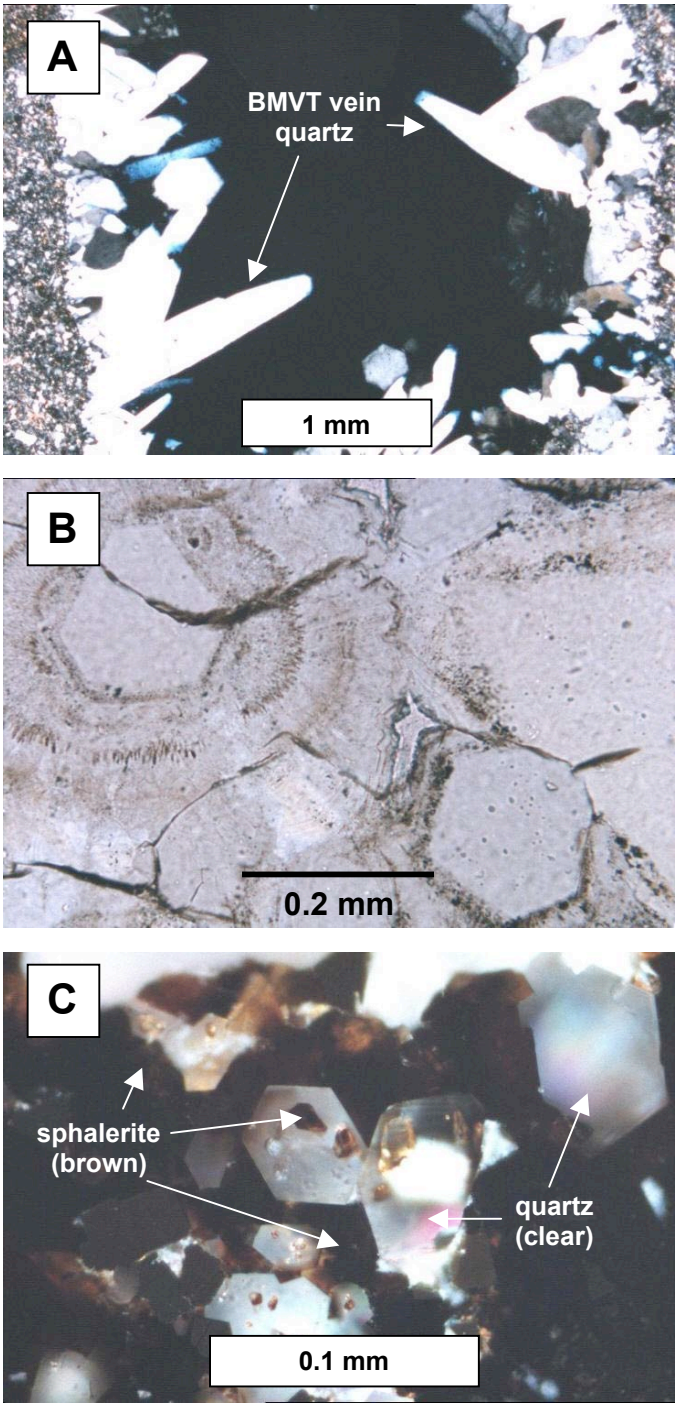

FIG. 44. Transmitted light photomicrographs showing general BMVT quartz associations and characteristics. A shows cockscomb quartz lining a vein (crossed polars; sample TC8-A2). B shows multiple growth zones in vein quartz, delineated by the presence of fluid, opaque, and translucent inclusions (uncrossed polars; sample TC8-A2). C shows sphalerite as inclusions in sphalerite stage vein quartz, and also overgrowing the same quartz (uncrossed polars; sample 4145E-8, refer to Figure 42A for the reflected light counterpart to this photomicrograph).

also were observed as ≤0.80-millimeter-long intergrowths with and overgrowths on BMVT vein and crustification sulfides. These quartz crystals commonly contain abundant tranluscent to transparent mineral inclusions, and less common inclusions of galena, sphalerite, chalcopyrite, pyrrhotite, arsenopyrite, and pyrite (Fig. 44B and C). This quartz is typically overgrown by sphalerite, pyrite, chalcopyrite, and/or tennantite-tetrahedrite. Vug-lining quartz-only euhedra up to 2.0-millimeters-long were observed in four BMVT samples, and are clearly earlier than the carbonate vein-filling gangue.

Rutile (TiO_2)

Rutile was observed as a trace constituent in three BMVT samples. In two cases, rutile occurs as small (≤0.025-millimeter-long) euhedra. In one sample, rutile occurs as an inclusion in sphalerite with chalcopyrite disease, which is rimmed by later stannite (Fig. 45).

Silver (Ag)

Silver was found by SEM-EDX analyses in only two hypogene BMVT samples, as single grains at junctions between galena, sphalerite, and cassiterite. One unpublished in-house metallurgical report identified a zoned native Ag grain with an acanthite rim (Fig. 46), but it is unclear whether this grain came from hypogene or supergene ore. Unpublished in-house metallurgical data for galena and sphalerite Ag contents are discussed fully in the "Ag distributions" section of this chapter, and indicate that native Ag occurs as microinclusions in these two sulfides (Fig. 58).

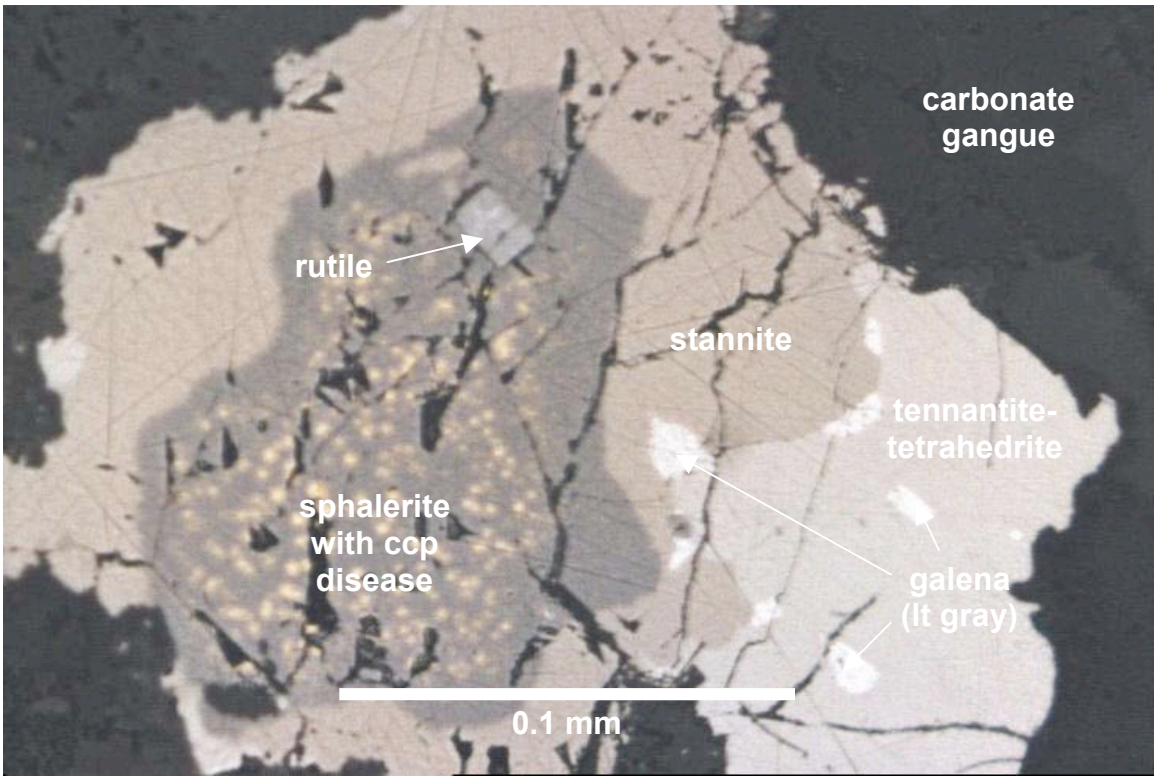

FIG. 45. Reflected light photomicrograph of sample 4145E-25 showing multiple paragenetic relationships. An early to galena-quartz stage rutile crystal is surrounded by sphalerite stage sphalerite with chalcopyrite "disease," which is rimmed by later sphalerite stage stannite. A late main pyrite stage tennantite-tetrahedrite grain borders the stannite, and both contain inclusions of galena-quartz stage galena. Carbonate stage gangue surrounds the island-atoll.

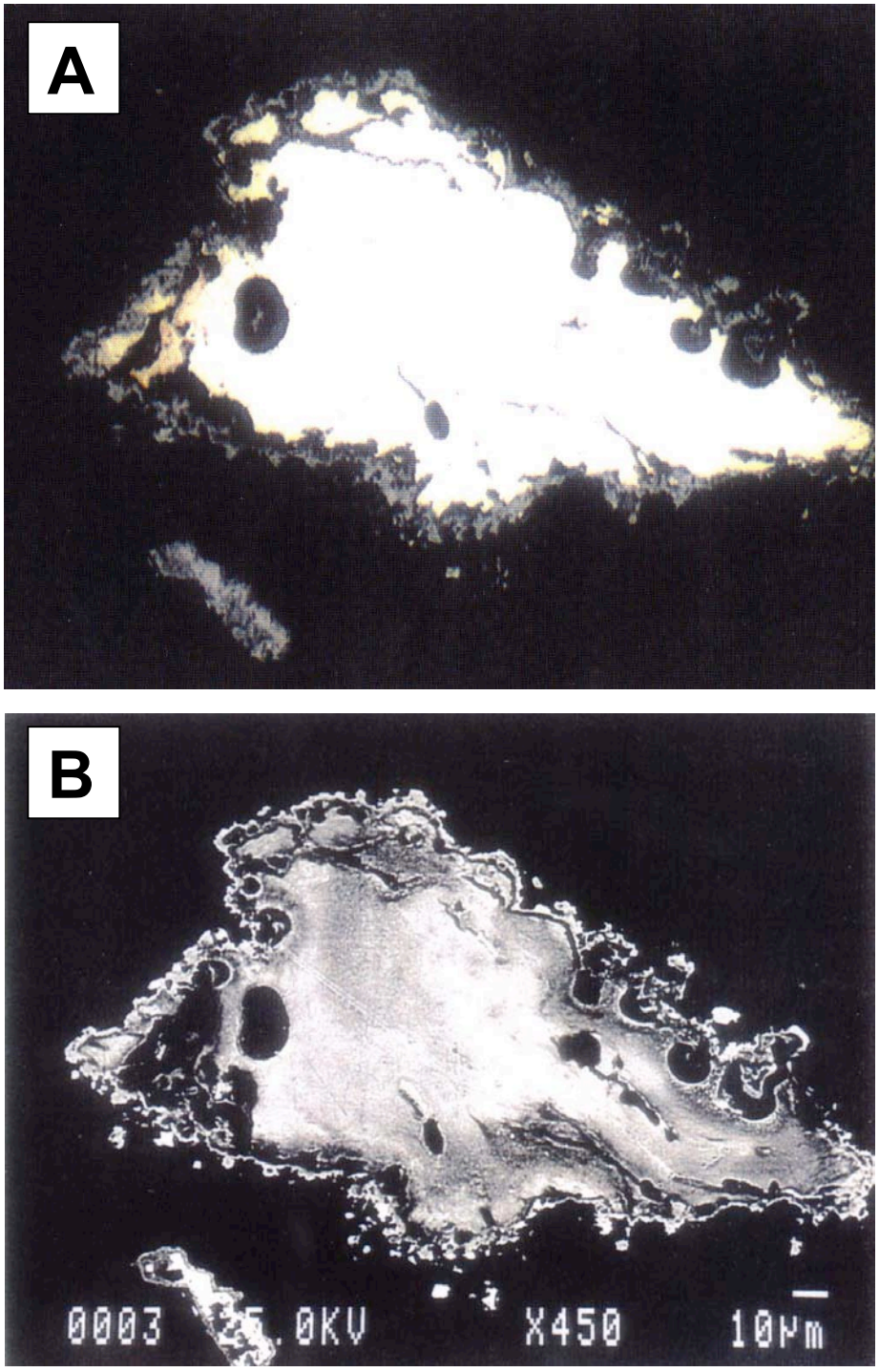

FIG. 46. Native Ag characteristics. A and B are reflected light and SEM backscatter photomicrographs, respectively, of a native Ag grain (white in A) with an acanthite (dark gray in A) rim (both images from Kingston et al., 1997). The rim also contains Cu and Au, accounting for the brighter spots in the rim in B (Kingston et al., 1997). Note: it is unclear whether this grain is a hypogene or supergene phase. Use the scale in B for both images.

Sphalerite ((Zn,Fe)S)

Sphalerite occurs in 49 of the 51 BMVT samples, and is volumetrically the second most important BMVT phase behind only pyrite. In the 49 samples, sphalerite is a trace to major component, constituting up to 20 volume percent of the hypogene vein and crustiform assemblages. Individual grains are up to 1.8 centimeters in diameter, and commonly contain inclusions of earlier galena, pyrite, and rarely, arsenopyrite. Sphalerite in all samples but one contains abundant inclusions of chalcopyrite (chalcopyrite disease) ± pyrrhotite (Fig. 43A). Irregular inclusions and/or intergrowths of stannite (Figs. 38A and 48) and microinclusions of native Ag (see the "silver-bearing minerals" section of this chapter, Fig. 58) are also common.

Because sphalerite in several samples is in apparent equilibrium with pyrite and pyrrhotite, it has been the subject about 100 EMP analyses for use as a geobarometer. The EMP data are tabulated in APPENDIX IV, and show a strong inverse correlation between Cu and Fe contents in the sphalerite. Sphalerite contains ~5.0 to ~10.5 weight percent Fe, and one sample sample contains sphalerite grains with optically distinct relatively high and low Fe zonations (Fig. 47B). In many samples, sphalerite is included in and/or rimmed by later pyrite (Fig. 47A), and is cut by chalcopyrite, pyrite, marcasite, and/or tennantite-tetrahedrite patches and/or associated veinlets.

Stannite (Cu_2FeSnS_4)

Stannite is a trace component in 37 BMVT samples, and has four principal modes of occurrence. Mode 1 is the most common, and consists of ≤0.16-millimeter-long

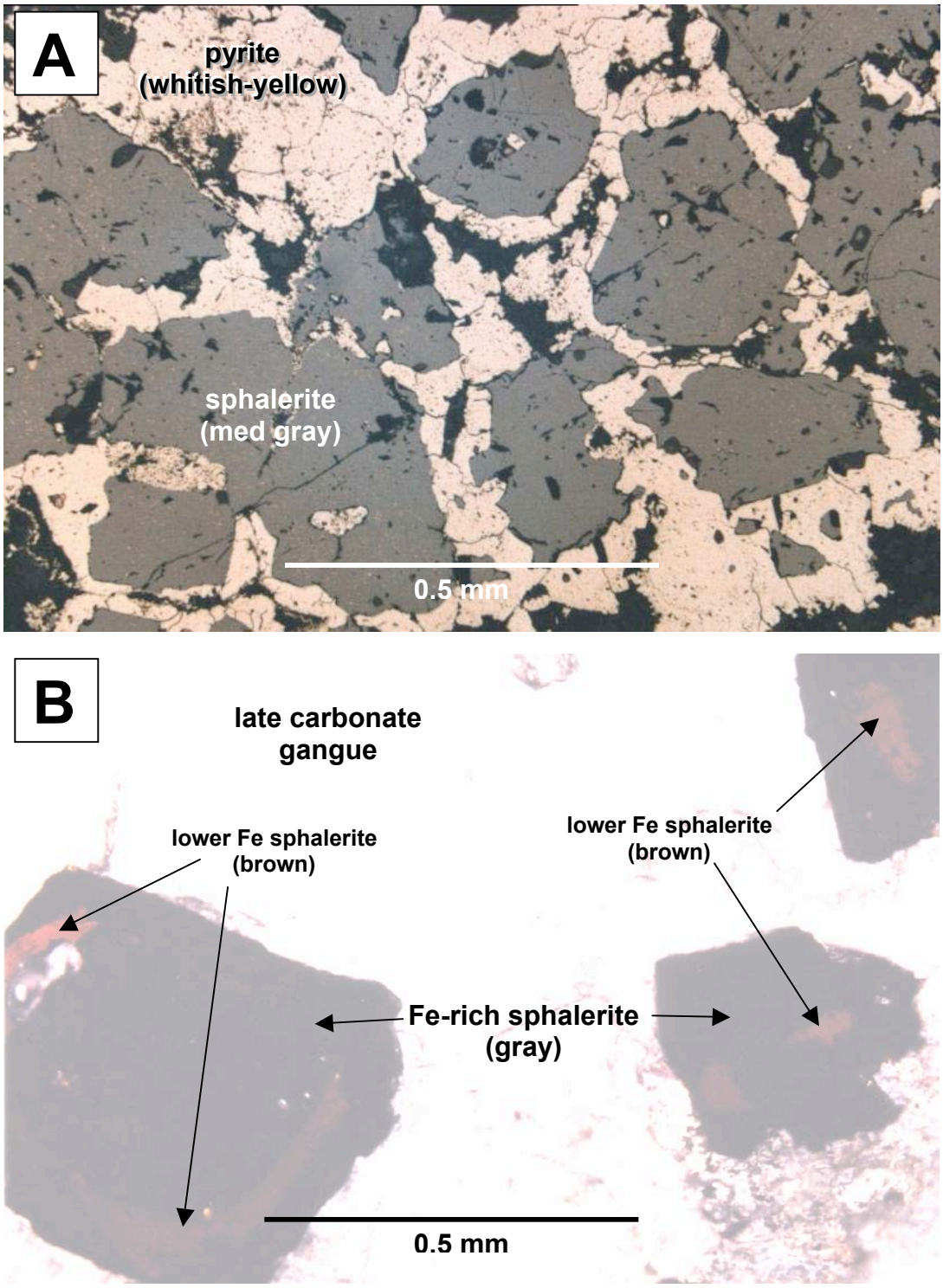

FIG. 47. Additional BMVT sphalerite associations and characteristics. A is a reflected light photomicrograph showing sphalerite stage grains rimmed by main pyrite stage pyrite (sample ARPB-1). B is a transmitted light photomicrograph showing zoned open-space growth sphalerite stage sphalerite crystals with later carbonate stage gangue (sample 7/26/98-2B) (true colors are lightened to accentuate the zonations).

inclusions and/or intergrowths in sphalerite (Fig. 48A). In several samples, these intergrowths-inclusions are associated with canfieldite, and are rimmed by later chalcopyrite associated with chalcopyrite disease in sphalerite. Stannite also occurs as ≤0.28-millimeter-long patches focused along fronts where pyrite replaced sphalerite (mode 2) (Fig. 48B). In one sample, stannite occurs as rims on discrete sphalerite grains, with associated tennantite-tetrahedrite (mode 3). Mode 4 is ≤0.23-millimeter-long inclusions in pyrite replacing earlier sphalerite.

Stromeyerite ($(Ag,Cu)_2S$)

Stromeyerite is a trace constituent in 4 BMVT samples, and occurs as ≤0.04 millimeter long irregular intergrowths with pyrrhotite ± chalcopyrite ± sphalerite as inclusions in coarse pyrite grains (Fig. 49).

Tennantite-Tetrahedrite ($Cu_{12}As_4S_{13}$-$Cu_{12}Sb_4S_{13}$) var. Freibergite

Tennantite-tetrahedrite var. freibergite occurs as a trace to minor component in 22 BMVT samples. Individual grains typically show As-Sb zonations in SEM and EMP backscatter images (Fig. 50B). Silver contents vary from grain to grain, and also show variations within individual grains. Tennantite-tetrahedrite has five modes of occurrence: 1) in ≤0.12-millimeter-wide pyrite, chalcopyrite, tennantite-tetrahedrite ± patches (Fig. 37A and B); 2) in veinlets associated with these patches, cutting earlier sphalerite and galena; 3) in association with stannite, as either thin tennantite-tetrahedrite and calcite veinlets cutting sphalerite, with stannite rimming all three phases, or as apparent

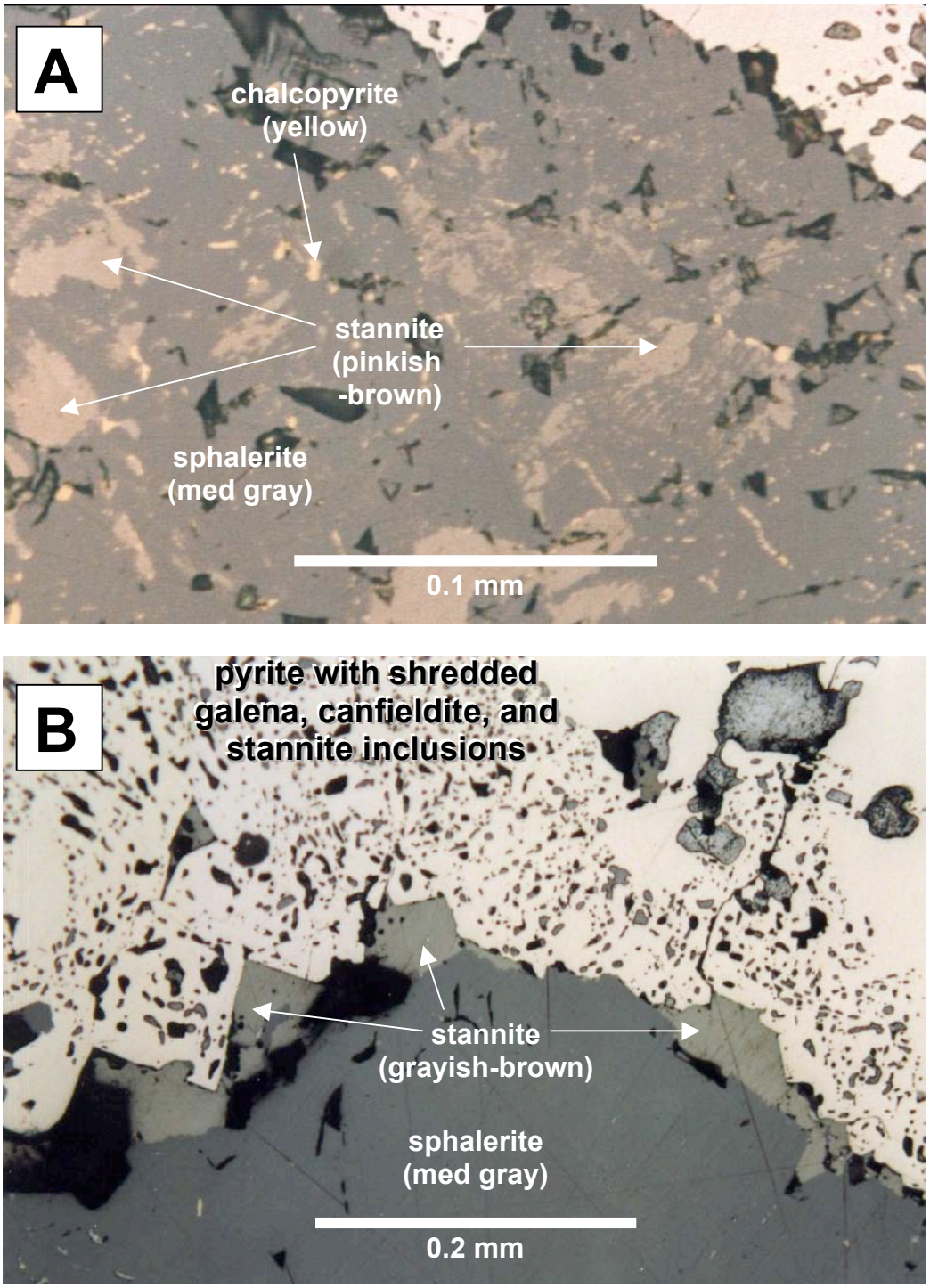

FIG. 48. Typical stannite associations. A is a reflected light photomicrograph of sample 4285E-6 showing blebs and oriented inclusions associated with chalcopyrite "disease" in sphalerite (all sphalerite stage). B is a reflected light photomicrograph of sample 4245E-5 showing an apparent residual concentration of stannite (sphalerite stage) at a front where later pyrite (main pyrite stage) replaces earlier sulfides.

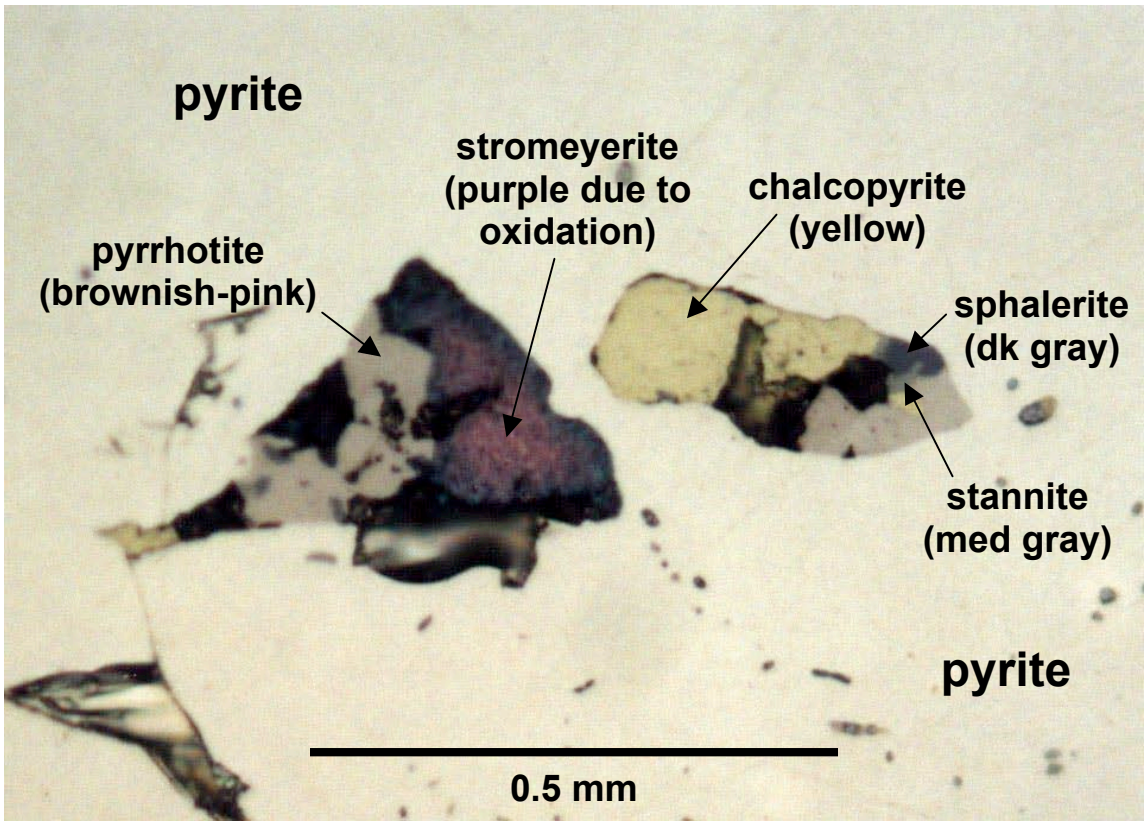

FIG. 49. Reflected light photomicrograph showing stromeyerite associated with sphalerite stage sphalerite, chalcopyrite, and pyrrhotite, and main pyrite stage pyrite (sample 4205E-10).

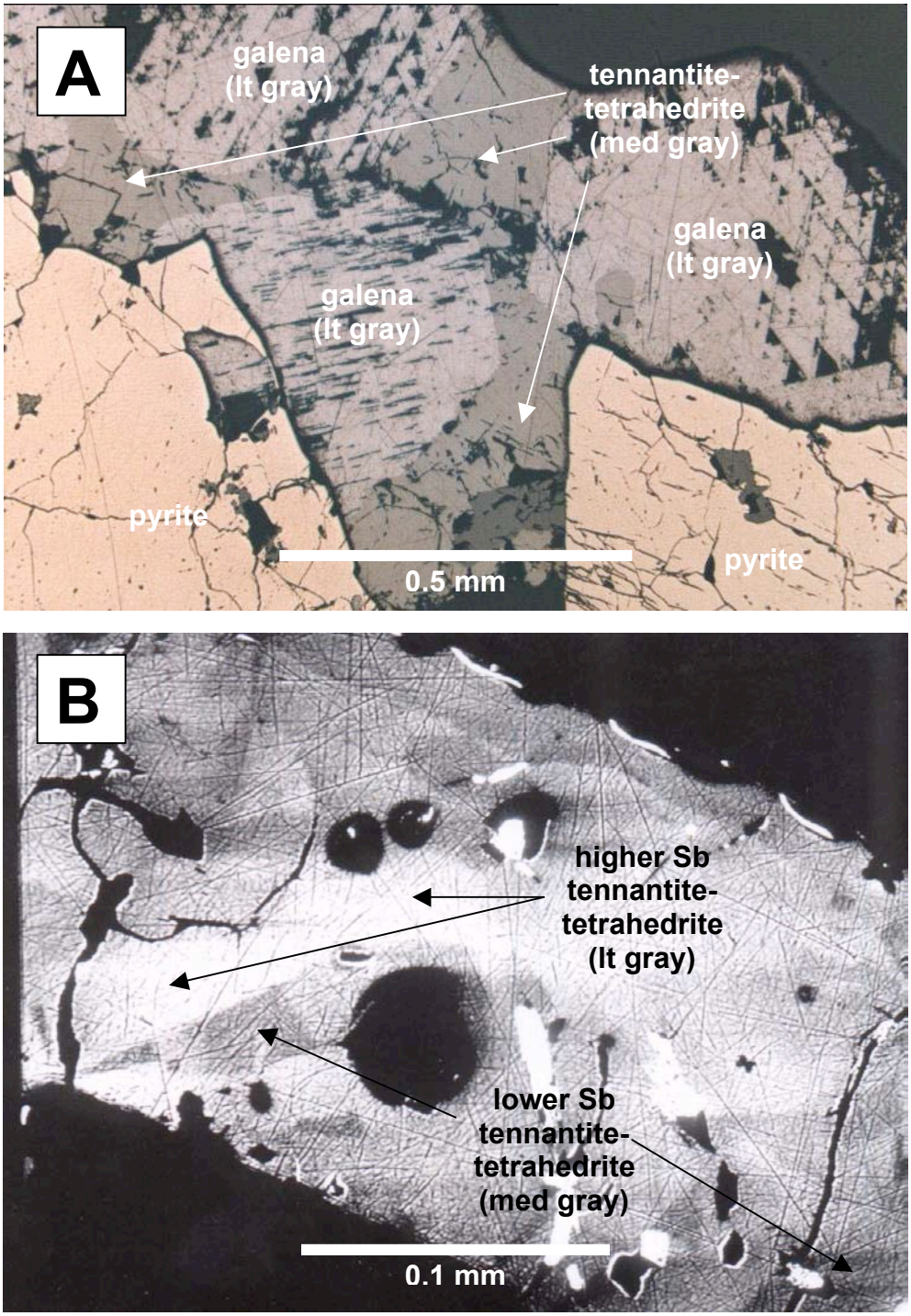

FIG. 50. Tennantite-tetrahedrite association and zonation. A is a reflected light photomicrograph of sample TC8FS-150 showing tennantite-tetrahedrite (late main pyrite stage) overgrowths on earlier galena grains (galena-quartz stage) and filling interstices between earlier pyrite (main pyrite stage). B is an EMP backscatter image of sample 7/26/98-2B (refer to Fig. 35A) showing zonations within a single grain of tennantite-tetrahedrite (lighter regions represent higher Sb concentrations).

overgrowths on stannite rims enclosing sphalerite; 4) as ≤1.0-millimeter-wide patches filling the interstices between corroded galena grains (Fig 50A); and 5) as ≤1.6-millimeter-long euhdral crystals with galena, acanthite, pyrite, and/or sphalerite inclusions (Fig. 35A).

Unidentified Pb-Ag Sulfosalt

An unidentified Pb-Ag sulfosalt occurs as acicular crystals associated with pyrargyrite in carbonate gangue in 1 BMVT sample (7/28/96-2B). The crystals are up to 0.8 millimeters long, and were initially mistaken for stibnite (Fig. 51). SEM-EDX analyses indicated that the crystals were not stibnite, leading to the EMP analyses in Table 6. Based on the atomic percentages shown in Table 6, a formula of $PbAg_4Sb_2S_6$ is tentatively assigned to the unidentified mineral, possibly with minor substitution of arsenic for antimony. Although this formula does not match any identified minerals, it is similar to diaphorite ($Pb_2Ag_3Sb_3S_8$).

Other BMVT Minerals

Other BMVT minerals identified by previous workers are bravoite ($(Ni,Fe)S_2$) (Kuyper et al., 1991), native bismuth/bismuthinite (Bi/Bi_2S_3) (Knipe et al., 1997), bournonite ($PbCuSbS_3$) (Knipe et al., 1997), chatkalite* ($Cu_6FeSn_2S_8$) (Kuyper et al., 1991), cinnabar (HgS) (Streiff, 1994; Kingston et al., 1997), digenite (Cu_9S_5) (Kuyper et al., 1991), enargite (Cu_3AsS_4) (Honea, 1991), gersdorffite ($(Ni,Fe)AsS$) (Kuyper et al., 1991), kesterite-stannite mix ($Cu_2(Fe,Zn)SnS_4$) (Kuyper et al., 1991), miargyrite*

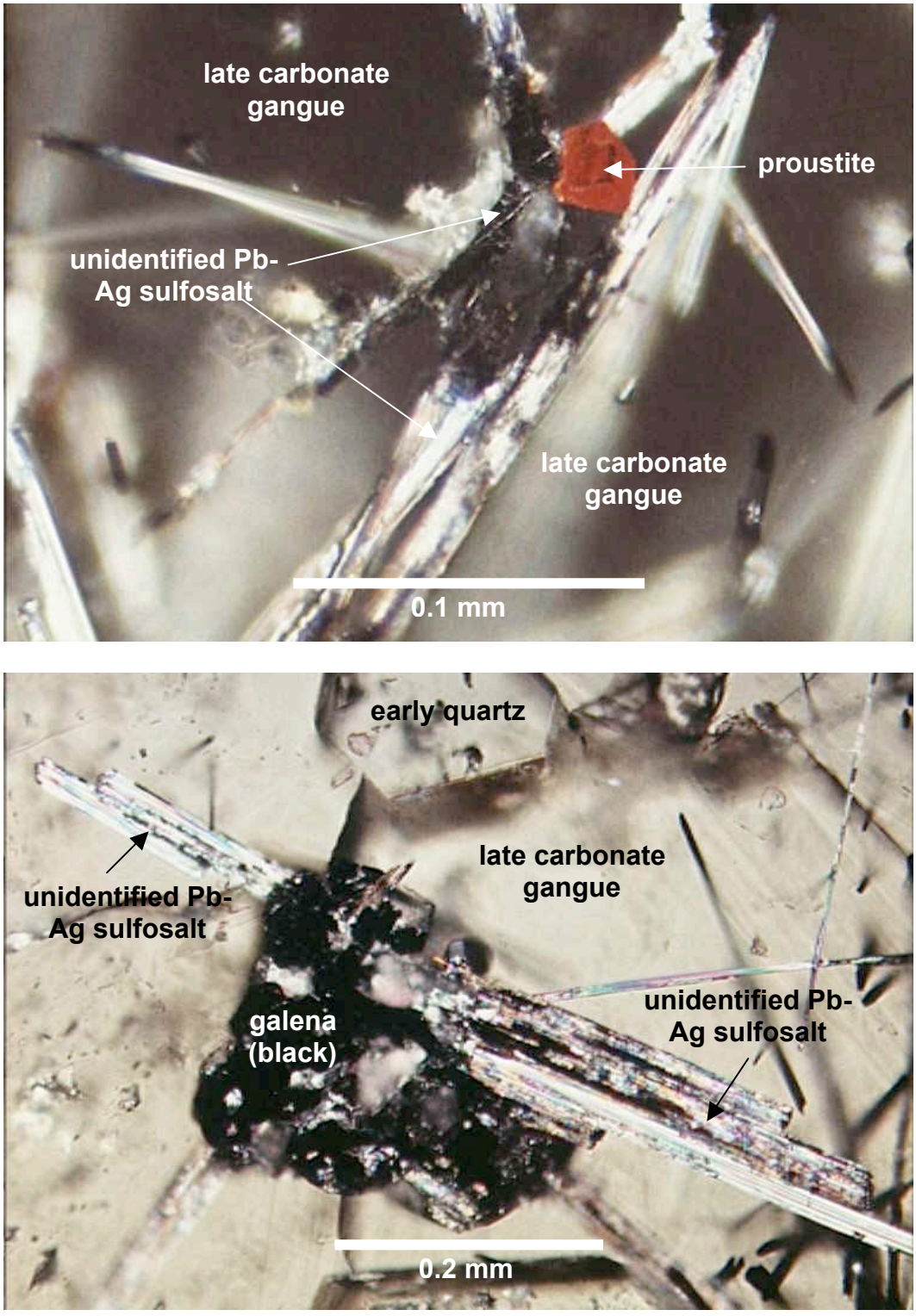

FIG. 51. Reflected light photomicrographs (crossed polars) of sample 7/26/98-2B showing general morphology and associations for BMVT mineral phase "unidentified Pb-Ag sulfosalt."

Pt #	Sb (wt%)	S (wt%)	Pb (wt%)	As (wt%)	Ag (wt%)	Tot
1	22.28	14.64	2.14	1.58	59.36	100.00
2	21.01	16.37	0.00	1.44	61.18	100.00
3	22.72	18.06	7.08	1.85	50.28	100.00
4	19.79	17.22	33.07	1.93	27.99	100.00
5	25.72	19.02	39.87	2.67	12.72	100.00
6	14.94	15.28	4.09	1.20	64.48	99.99
7	26.13	19.21	44.86	3.11	6.68	99.99
Ave	**21.80**	**17.11**	**18.73**	**1.64**	**40.38**	**100.00**
At%	**15.41**	**45.95**	**7.78**	**2.02**	**32.22**	**100.00**

TABLE 6. EMP results for BMVT unknown (results normalized to 100.00%).

($AgSbS_2$) (Honea, 1998), non-stoichiometric stannite (no chemical formula) (Kuyper et al., 1991), a non-stoichiometric Cu-Fe sulfide (no chemical formula) (Kuyper et al., 1991), shadlundite* ($(Pb,Cd)(Fe,Cu)_8S_8$) (Kuyper et al., 1991), and stannite III ($(Cu,Ag)_2(Fe,Zn)SnS_4$) (Kuyper et al., 1991). There are no conclusive paragenetic data for any of these mineral species.

* tentative identifications

CARLIN-STYLE ORE MINERALOGY AND PARAGENESIS

An erratically distributed assemblage consisting of realgar-stibnite-calcite was observed during mapping in the Smelser Pass Member. A more regularly-defined realgar ± orpiment assemblage was observed in the underground workings as realgar-dominated veins developed at the contact between the Home Station Member and overlying dolostone submember of the Panther Canyon. These assemblages are the only other obvious, mappable manifestations of the Carlin-style ore besides decarbonatization ± silicification.

The mineral paragenesis in the Smelser Pass Member is clear, with early stibnite, middle realgar, and late carbonate pore-filling (Fig. 52 and Fig. 53A). No stibnite has yet been observed in samples from the underground realgar occurrences (Fig. 53A is from an exposure in the open pit), in which a clearly defined sequence of early realgar coated with, or cut by, later orpiment has been observed (Fig. 53B). Barite was observed in two samples associated with thin pyrite veinlets, but its association with either the BMVT or Carlin-style assemblages is unclear. The paragenetic association of Au-bearing Carlin-

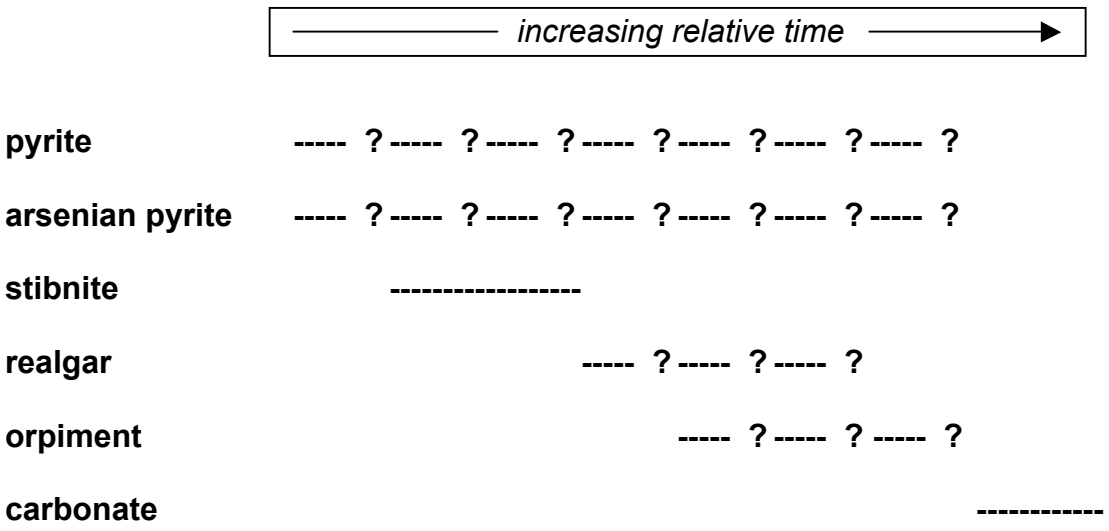

FIG. 52. General mineralogy and paragenesis for the hypogene Carlin-style ore system. Arsenopyrite and marcasite were also observed in Carlin-style ore, but no paragenetic information is available for these sulfides. Note that the Carlin-style arsenian pyrite ± pyrite is auriferous and argentiferous (see the "gold-bearing minerals" and "silver-bearing minerals" sections).

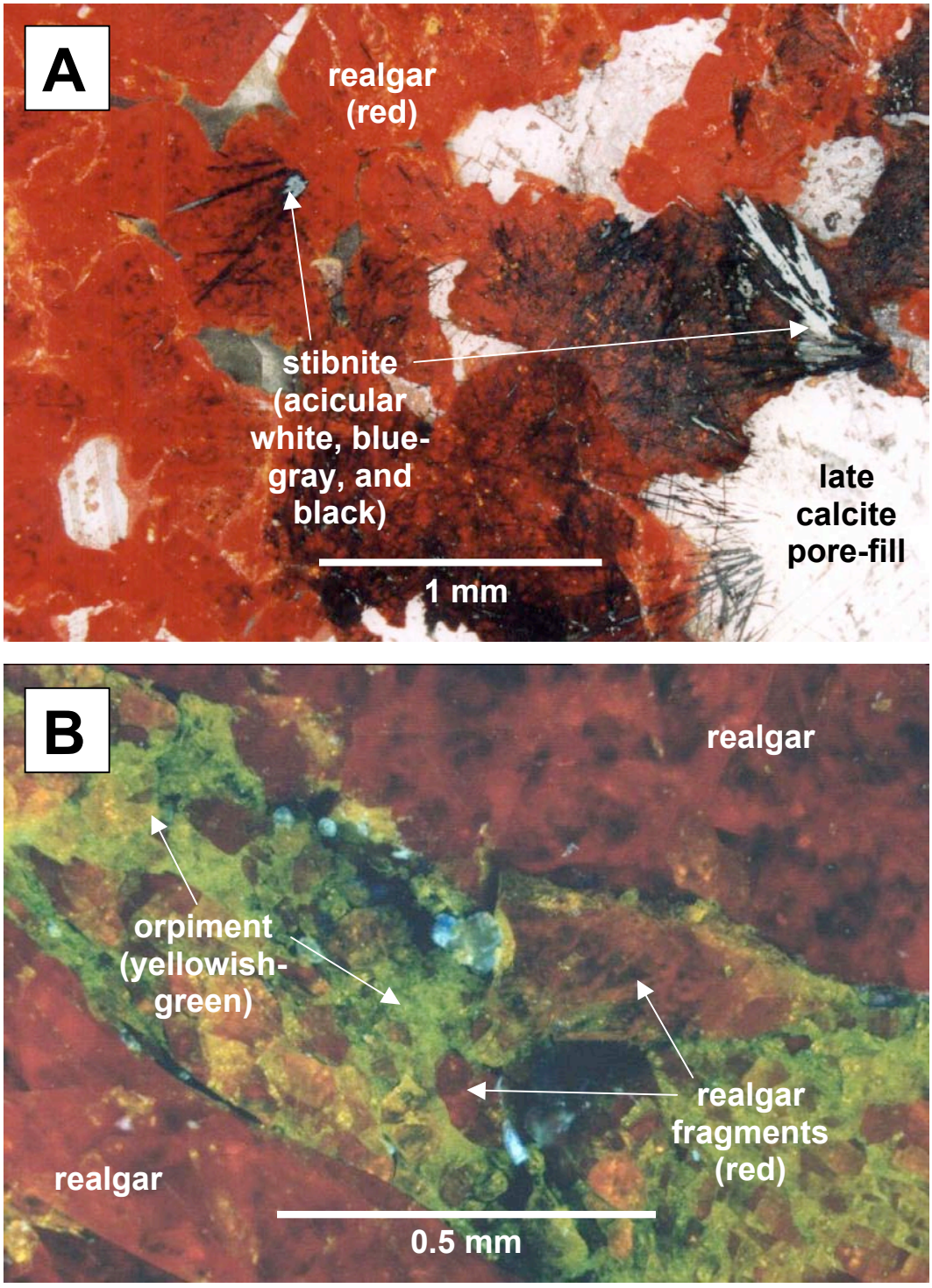

FIG. 53. General paragenetic relationships of Carlin-style ore. A is a reflected light photomicrograph (crossed polars) showing early stibnite with later realgar and latest calcite pore-fill (sample REALGARA). B is a transmitted light photomicrograph showing realgar cut by a later orpiment veinlet (sample U-6). Note that the blue color in B is due to a blue dye used during sample impregnation, and indicates porosity.

style Fe ± As sulfides (Fig. 54, see also Fig. 55) with the As and Sb sulfides is also unclear.

HYPOGENE PRECIOUS METALS ASSOCIATIONS

Gold-Bearing Minerals

The Au-bearing phases at Cove are electrum, native Au, arsenian pyrite, and arsenopyrite. Electrum and native Au (<2 weight percent Ag) share the same modes of occurrence as irregular inclusions in BMVT galena, sphalerite, pyrite, and gangue quartz, carbonates, and illite. This common association and the fact that some of the electrum grains are strongly zoned with regions of relatively high and low Ag content indicates that the electrum, native Au, and native Ag are probably intermediate and end members of a solid solution series precipitated simultaneously.

Paragenetically, the electrum/native Au (called electrum for simplicity in the ensuing text) are dominantly early "galena-quartz" to possibly the "main pyrite" BMVT ore stage phases that were coprecipitated with early quartz and galena ± middle sphalerite and pyrite. This inference is supported by: 1) the occurrence of electrum inclusions in early quartz and galena grains, and 2) the common associations of electrum with earlier-stage minerals such as galena and sphalerite that commonly form inclusions in later-stage pyrite. In the latter case, the earlier stage minerals appear as intergrowths with, and rims on, electrum grains. It is unclear, however, whether the electrum-only inclusions in sphalerite and pyrite are the results of middle- to late-main sulfide ore stage precipitation;

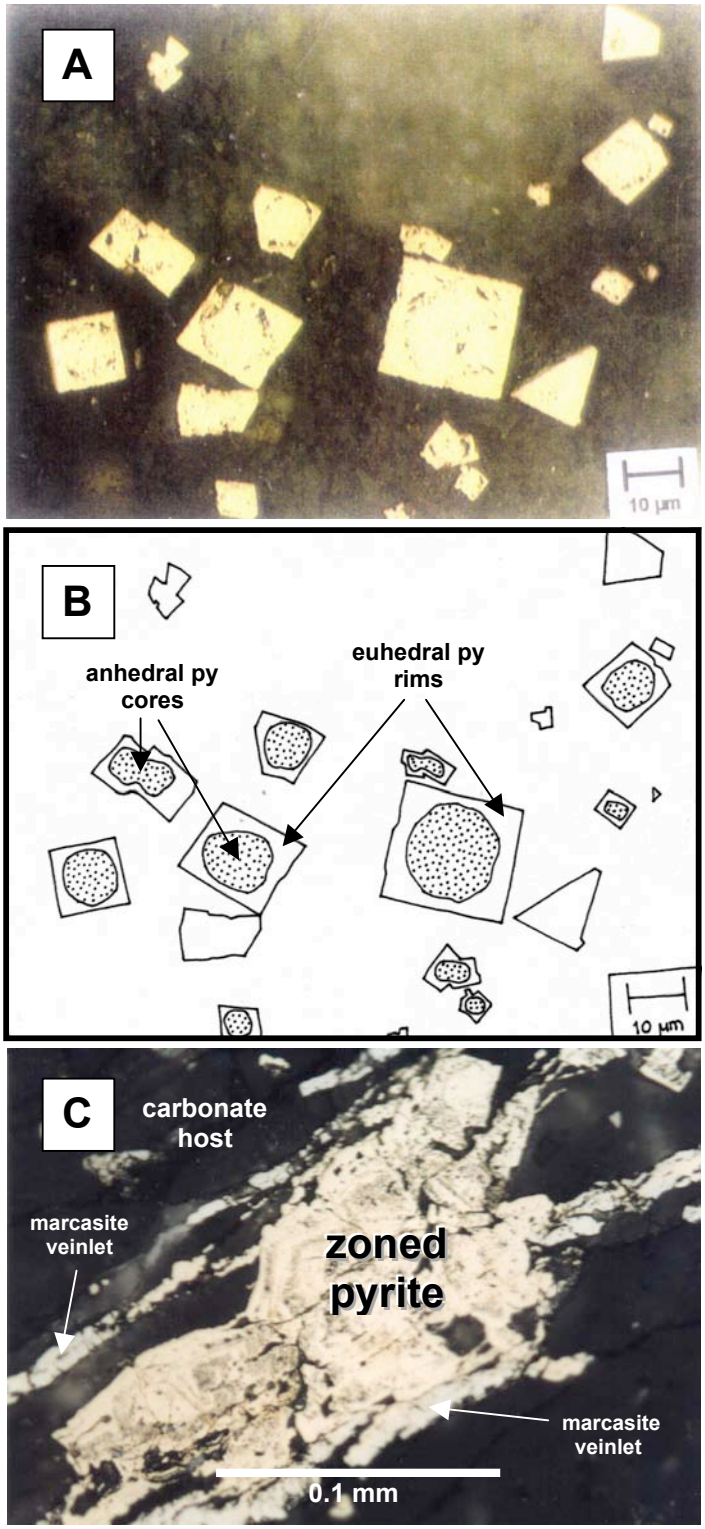

FIG. 54. Carlin-style ore disseminated pyrite. A is a reflected light photomicrograph showing early anhedral pyrite cores with euhedral rims (from Chryssoulis et al., 1997). B is a sketch of A that accentuates the pyrite cores and rims. C is a reflected light photomicrograph showing zoned pyrite with veinlets of marcasite (sample 4145E-1).

they may be the non-mobilized residual products of the corrosion and replacement of the early-stage galena with electrum inclusions.

Carlin-style arsenian pyrite and arsenopyrite contain Au and account for most of the refractory portion of the Cove ore (Fig. 55). Five morphological types of pyrite were recognized at Cove (see Fig. 56): 1) coarse; 2) zoned coarse; 3) blastic, with abundant pores and inclusions; 4) fine-grained (2 to 10 μm diameter); and 5) microcrystalline (<2 μm diameter). Because zonations are not always optically apparent, the "zoned coarse" pyrites are grouped here in the more general "coarse" pyrite category. All pyrite morphologies plus arsenopyrite may be present in any given sample.

Gold concentrations in the coarse, fine-grained, and microcrystalline pyrite and arsenopyrite grains are shown graphically in Figure 57. Gold concentrations are generally highest in the microcrystalline-grained pyrite and arsenopyrite, with decreasing values in the fine-grained and blastic pyrite, and lowest in the coarse-grained pyrite. Similar Carlin-style pyrite morphologies and refractory Au associations have been documented at the Twin Creeks Deposit, Nevada (Simon et al., 1999), and at the Getchell Deposit, Nevada (Weaver and Cline, 1999).

The different pyrite morphologies and Au contents are interpreted as temporally-controlled expressions of pyrite deposition beginning as early as diagenetic or deuteric pyrite and continuing through Carlin-style mineralization. The different external morphologies, then, are inferred to be the result of the relative timing of their initial nucleation and their continued or discontinued exposure to the Carlin-style ore fluid(s).

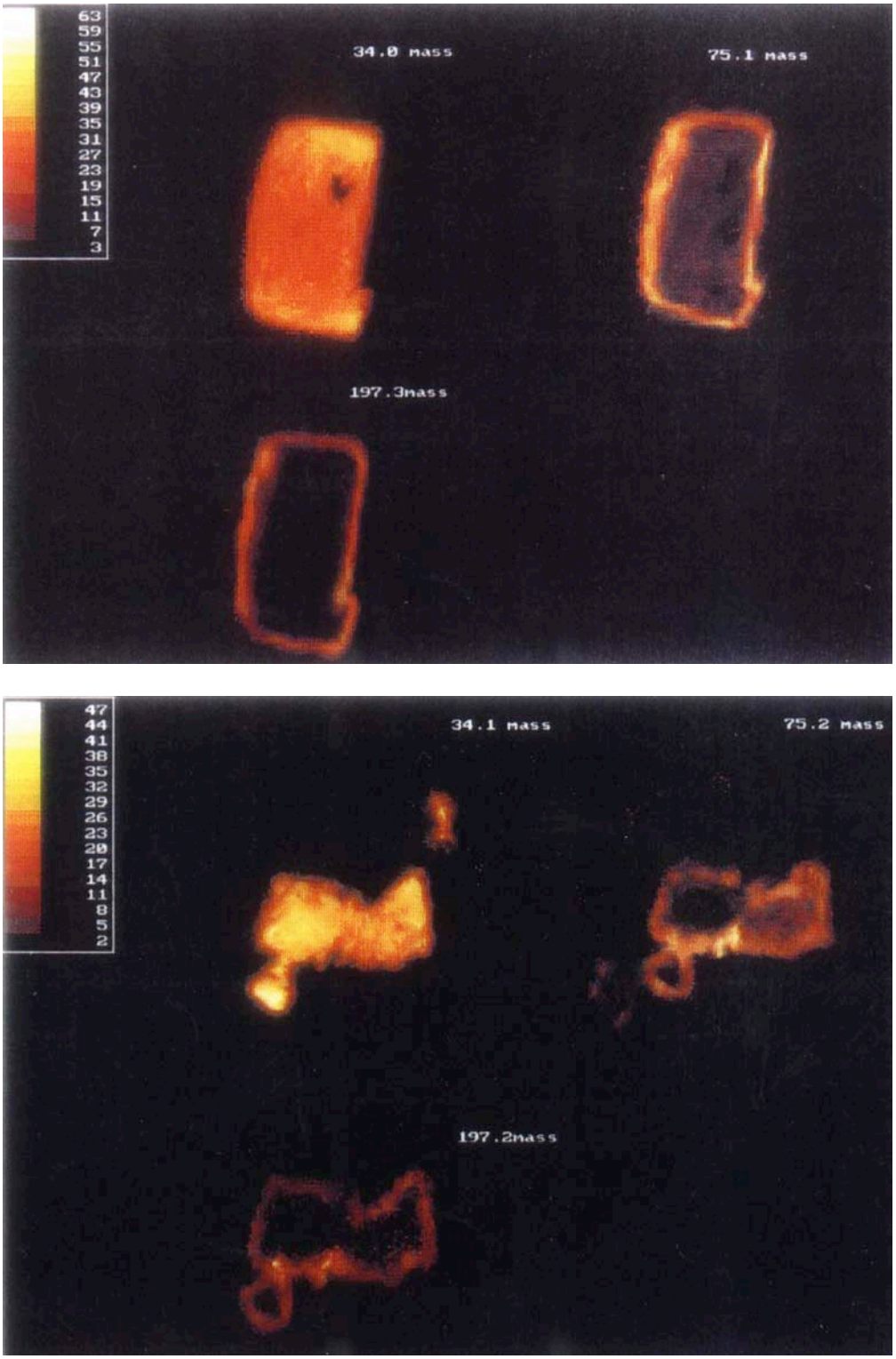

FIG. 55. SIMS ion maps of coarse pyrite grains from Carlin-style ore showing uniform distribution of S (34 mass), with As-rich (mass 75) and Au-rich (mass 197) rims. Both images from Chryssoulis et al. (1997).

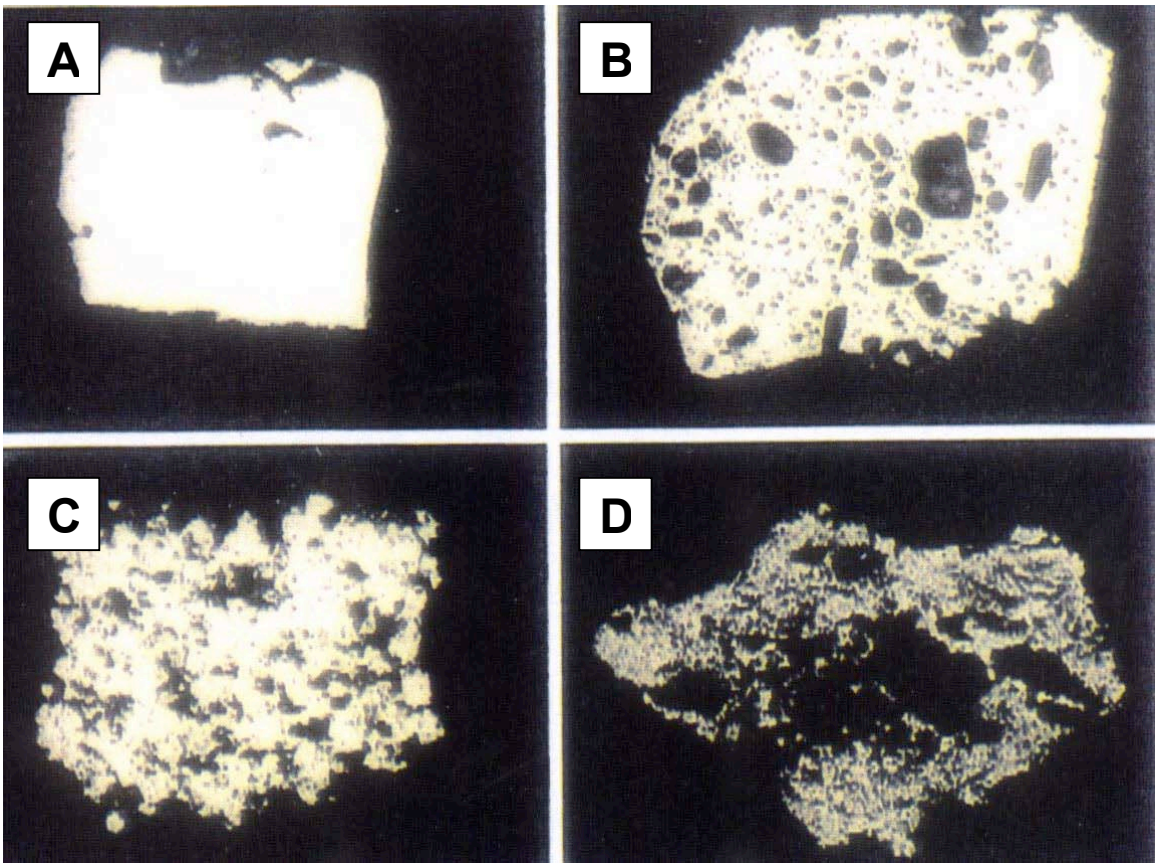

FIG. 56. Four of the five major morphological types of pyrite from Cove Carlin-style ore: A = coarse, B = blastic, C = fine-grained, and D = microcrystalline (from Kingston et al., 1997; no scales provided, but the images are reflected light).

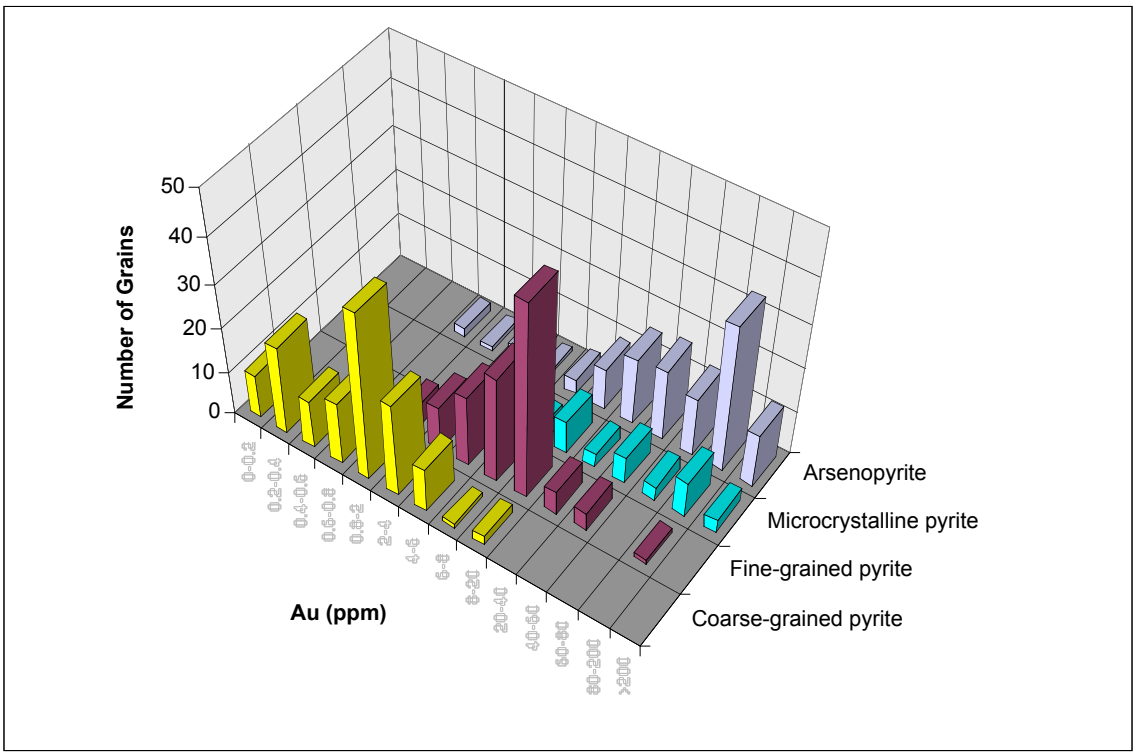

FIG. 57. Concentrations of "invisible" Au in Carlin-style ore coarse-grained pyrite (n = 127), fine-grained pyrite (n = 111), microcrystalline pyrite (n = 33), and arsenopyrite (n = 109) grains (SIMS data from Chryssoulis et al., 1997; see APPENDIX VII).

Silver-Bearing Minerals

The Ag-bearing phases at Cove are more diverse and typically more complex than those carrying Au. They were deposited during Carlin-style mineralization and in a clear paragenetic sequence during all stages of BMVT hypogene mineralization, and are common components of the supergene system (refer to Fig. 30). Although the BMVT Ag-bearing galena has relatively low Ag concentrations (0.26 weight percent Ag) compared to other phases such as tennantite-tetrahedrite var. freibergite (10.8 weight percent Ag), electrum (up to 42.10 weight percent Ag), and native Ag (~100 weight percent Ag), the relative abundance of galena makes it the most important Ag carrier in the BMVT system.

Figure 58 shows SIMS ion maps for BMVT galena and sphalerite grains. Silver occurs as microinclusions in both sulfides, and also in solid-solution with galena (Chryssoulis et al., 1997). This uneven distribution accounts for variable SEM EDX scan results for Ag in galena and sphalerite grains, which range from zero percent to nearly pure Ag. The BMVT Ag sulfosalt-carbonate ore stage owes its relatively high Ag content primarily to the presence of the Ag sulfosalt species proustite-pyrargyrite, stephanite, and pearceite-polybasite. In the samples where these phases were observed, the Ag sulfosalts are the latest main sulfide ore stage minerals precipitated. They occur as overgrowths on or in veinlets cutting all earlier phases, and are succeeded only by carbonate gangue.

In one unpublished in-house report (Chryssoulis et al., 1997), there is compelling evidence that Ag in the Carlin-style ore is directly related to Au content. In this case, the Ag content of pyrite was examined in the same context as for Au in coarse- versus fine-

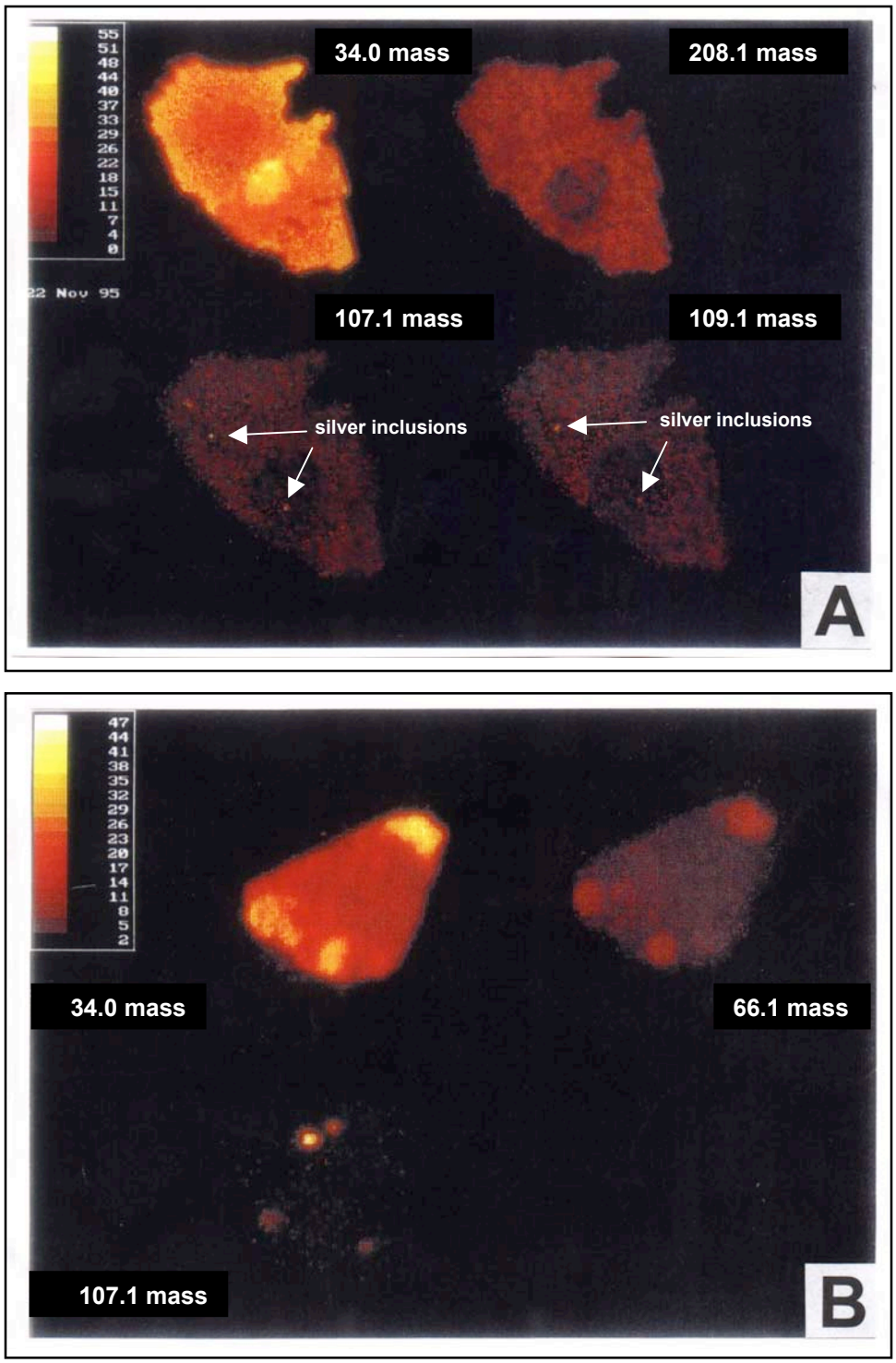

FIG. 58. SIMS ion maps for BMVT galena and sphalerite (images and interpretations from Chryssoulis et al., 1997). A shows a galena grain (mass 208.1 is Pb) with evenly distributed silver (107.1 and 109.1 masses) and tiny microinclusions of native silver. B shows a sphalerite grain (mass 66.1 is a Zn isotope) with silver as microinclusions.

versus microcrystalline-grained pyrite morphologies. For samples containing all three main pyrite morphologies, the Ag content appears to depend on the type of pyrite examined (Fig. 59) (Chryssoulis et al., 1997). There is a direct correlation between Ag and Au in these pyrite crystals (Fig. 60), which indicates that both Au and Ag are associated with arsenian pyrite in Carlin-style ore.

SUPERGENE ORE

The Cove oxide orebody described by Kuyper et al. (1991) and Emmons and Eng (1995) is a supergene overprint on the hypogene BMVT and Carlin-style ore, with attendant leaching, remobilization, and minor enrichment. The supergene oxidation is generally restricted to the Smelser Pass Member and upper portions of the transitional submember of the Panther Canyon Member, but penetrates deeper into the hypogene system along faults. The distribution of oxidation is readily visible in the Cove open pit as orange- and red-hued staining of the host sedimentary units and igneous intrusions (Fig. 61). Because the oxide orebody was entirely mined out by the time this study was begun, this section is based almost entirely on descriptions by previous workers.

The supergene oxide orebody was associated with strong hypogene silicification in the form of jasperoid and supergene Fe and Mn. Manganese alteration was characterized by the occurrence of psilomelane-group minerals and pyrolusite (Schurer and Fuchs, 1988; Honea, 1988; Kuyper et al., 1991). These minerals occurred with jasperoid in the high-grade core of the oxide orebody. The Mn alteration is interpreted in the current study to be a residual product of the dissolution and remobilization of rhodochrosite, manganoan

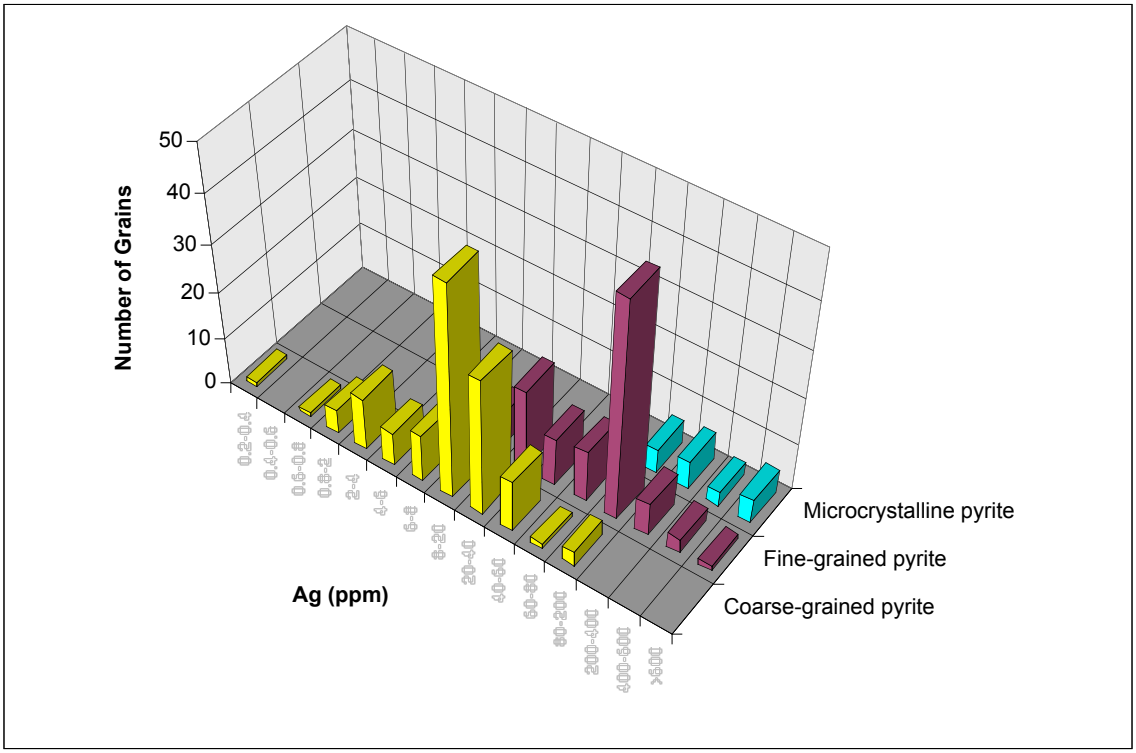

FIG. 59. Concentrations of "invisible" Ag in Carlin-style ore coarse-grained pyrite (n = 124), fine-grained pyrite (n = 103), and microcrystalline pyrite (n = 19) grains (SIMS data from Chryssoulis et al., 1997; see APPENDIX VII).

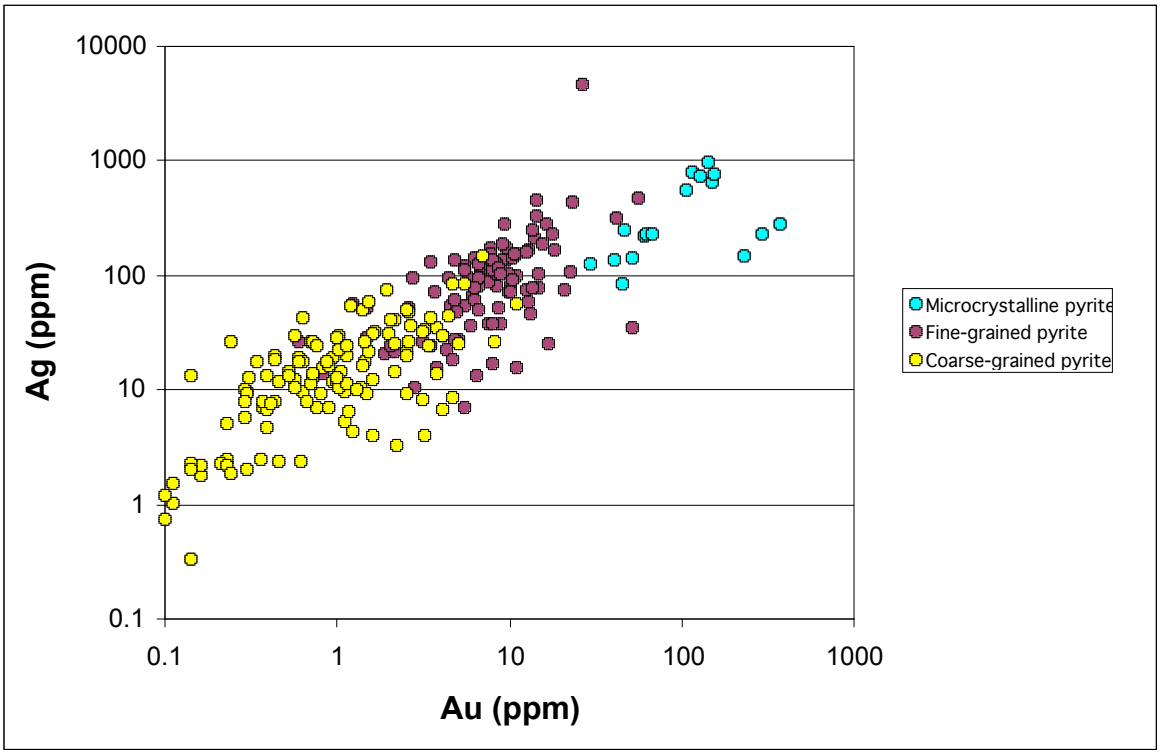

FIG. 60. Scatterplot of Ag versus Au for Carlin-style ore coarse-grained (n = 123), fine-grained (n = 101), and microcrystalline (n = 17) pyrite grains (SIMS data from Chryssoulis et al., 1997; see APPENDIX VII).

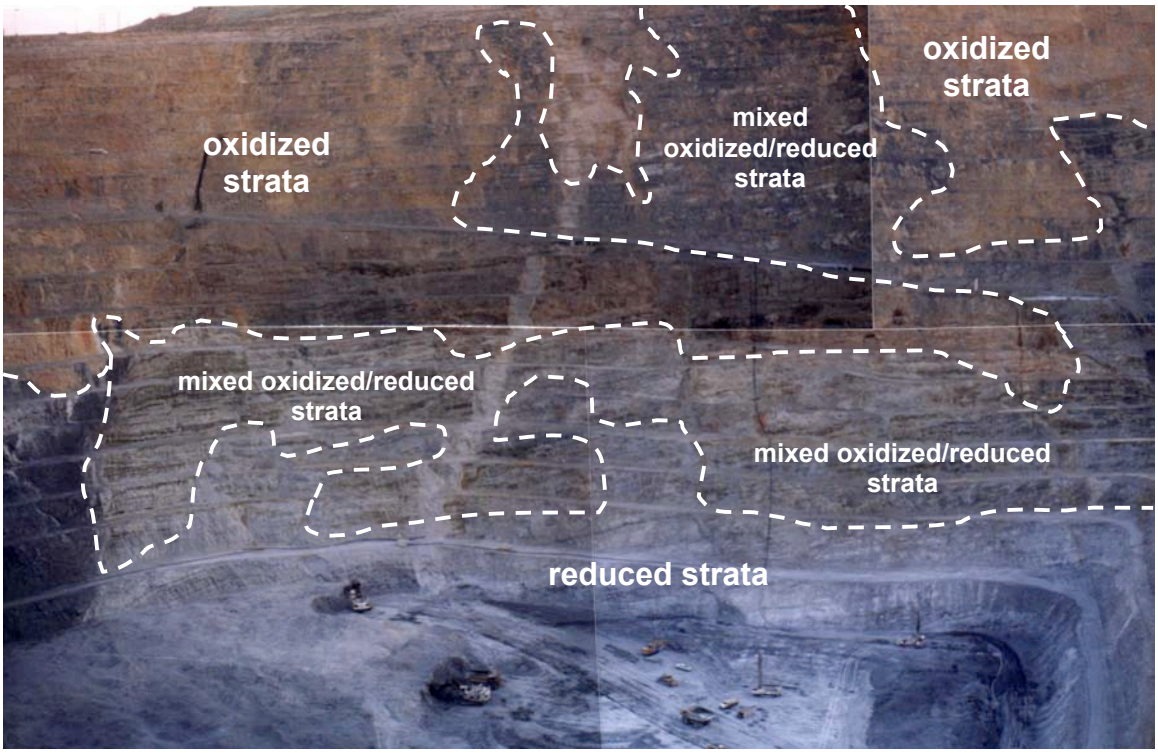

FIG. 61. Photograph montage of the south highwall of the Cove Mine (taken in 1998), showing generalized oxidized, mixed oxidized/reduced, and reduced zones.

calcite, and Mn-bearing hypogene sulfides, with either in-situ or exotic precipitation of Mn ± Fe oxides. SEM-EDX analyses of several highly corroded carbonate mineral grains from an oxidized BMVT vein in the Smelser Pass oxidized zone indicated that they were residual hypogene rhodochrosite crystals.

Kuyper et al. (1991) defined high-grade oxide ore as containing greater than 3.40 grams of Au per ton (0.100 ounces of Au per short ton) and 170.0 grams of Ag per ton (5.00 ounces of Ag per short ton). The high-grade ore coincided spatially with intensely Mn-altered host rocks. Gold occurred in electrum and in the native state. Silver also occurred in electrum, and as chlorargyrite (cerargyrite) and argentiferous psilomelane (Honea, 1988; Kuyper et al., 1991). Several BMVT phases, including sphalerite, galena, chalcopyrite, pyrrhotite, and tetrahedrite, were identified as sparse constituents during reflected light petrographic studies of gravity concentrates recovered from Mn-oxide ore (Honea, 1990; Kuyper et al., 1991). Pyrite and arsenopyrite were also identified, but it is unclear whether these minerals originated as BMVT phases, Carlin-style phases, or both.

Native Au/electrum was typically associated with Fe oxide minerals in the oxide orebody, suggesting to Honea (1988), Theodore and Jones (1990), and Kuyper et al. (1991) that primary Au was precipitated with hypogene pyrite, and was subsequently liberated as a residual component during supergene oxidation. Gold associations determined during the current study (refer to the "gold-bearing minerals" section) indicate that the residual Au is probably a product of the destruction of both BMVT and Carlin-style ore. Primary Au, then, could have occurred as inclusions in a number of sulfides, sulfosalts, and oxides in the original BMVT ore, and as submicroscopic

inclusions in arsenian-argentiferous-auriferous Fe ± As sulfides and/or rims on earlier Fe ± As sulfides in the original Carlin-style ore.

Enrichment at the redox boundary is a common component of supergene systems, and is best described for porphyry Cu deposits (e.g. Tunell, 1930; Tunell and Posnjak, 1931; Durek, 1964; Blanchard, 1968; Anderson, 1982; Titley, 1982; Titley and Marozas, 1995). Kuyper et al. (1991) observed wiry masses of native Ag in vugs and late fractures cutting sulfide veins in the upper high-grade sulfide orebody, and believed the Ag to be the result of supergene alteration. This conclusion is confirmed by the lack of native Ag in the original components of the upper high-grade sulfide orebody that were dropped by post-mineralization offset along the Striper splay. The lack of native Ag in these ore zones indicates that dip-slip movement along the Striper splay, with at least enough offset to drop the hanging wall ore zones below the redox boundary, occurred prior to the establishment of the supergene enrichment system.

CHAPTER 5: HYPOGENE ALTERATION AT THE COVE DEPOSIT, AND THE SPATIAL AND TEMPORAL RELATIONS BETWEEN INTRUSIONS, ALTERATION, AND MINERALIZATION

INTRODUCTION

The following descriptions of alteration at Cove are based on observations made during pit mapping, and on petrological and microanalytical data generated from more than 340 samples collected for this study. In both outcrops and thin sections, three generations of alteration are evident. The first of these generations predates mineralization, and consists of auto-deuteric alteration of the Eocene intrusions. The second generation accompanied the mineralizing event(s), and consists of pervasive and vein-controlled alteration of the Eocene intrusions and sedimentary host units. The third generation of alteration post-dates mineralization, and consists of supergene assemblages that overprint the earlier alteration assemblages in the upper portions of the Cove deposit. Because the primary goal of this study is to develop a genetic model for the deposit, attention is focused primarily on hypogene alteration.

Hypogene ore at Cove is principally associated with hypogene decarbonatization and quartz-sericite/illite-pyrite (QSP) alteration. Two reliable ^{40}Ar-^{39}Ar ages were produced for this study: 1) is from a QSP-altered sample of the Bay dike; and 2) is from a very weakly altered sample of the West intrusion. Together with the preexisting K-Ar ages presented in Chapter 2, these ages provide temporal constraints on the relationships between the Eocene intrusions, alteration, and mineralization of the Cove deposit. The

age of mineralization is one of the cornerstones of the genetic model, and together with ore and alteration characteristics, helps to form a basis for establishing relationships with other deposits in the Great Basin (see Chapter 6).

ALTERATION STYLES AT COVE

Figure 62 is a schematic alteration overlay for the W-E cross-section (refer to Fig. 5 for geologic base data), showing the distribution of alteration relative to structures and stratigraphic units. The characteristics of hypogene alteration are reported here in the context of the types of rocks they affect. Supergene alteration is discussed separately.

Alteration in Intrusions

Pre-ore to hypogene alteration of intrusive rocks is described first for three reasons: 1) the intrusions occur throughout the deposit; 2) they are essentially monolithologic, with only slight variations in their original mineralogy; and 3) they show consistent alteration patterns throughout the deposit. Ten alteration assemblages recognized in thin sections range from pre-ore deuteric to hypogene to supergene alteration (Table 7, Fig. 63). The eight hypogene assemblages are listed temporally from early weak biotitization, middle propylitization, later silicification-sericitization, and latest carbonatization. A supergene overprint consists principally of clay minerals, including kaolinite, with Mn and Fe oxides, and carbonates.

The relation of hypogene ore to alteration is examined in terms of primary mineral stabilities in the hypogene alteration environment. The major and minor primary

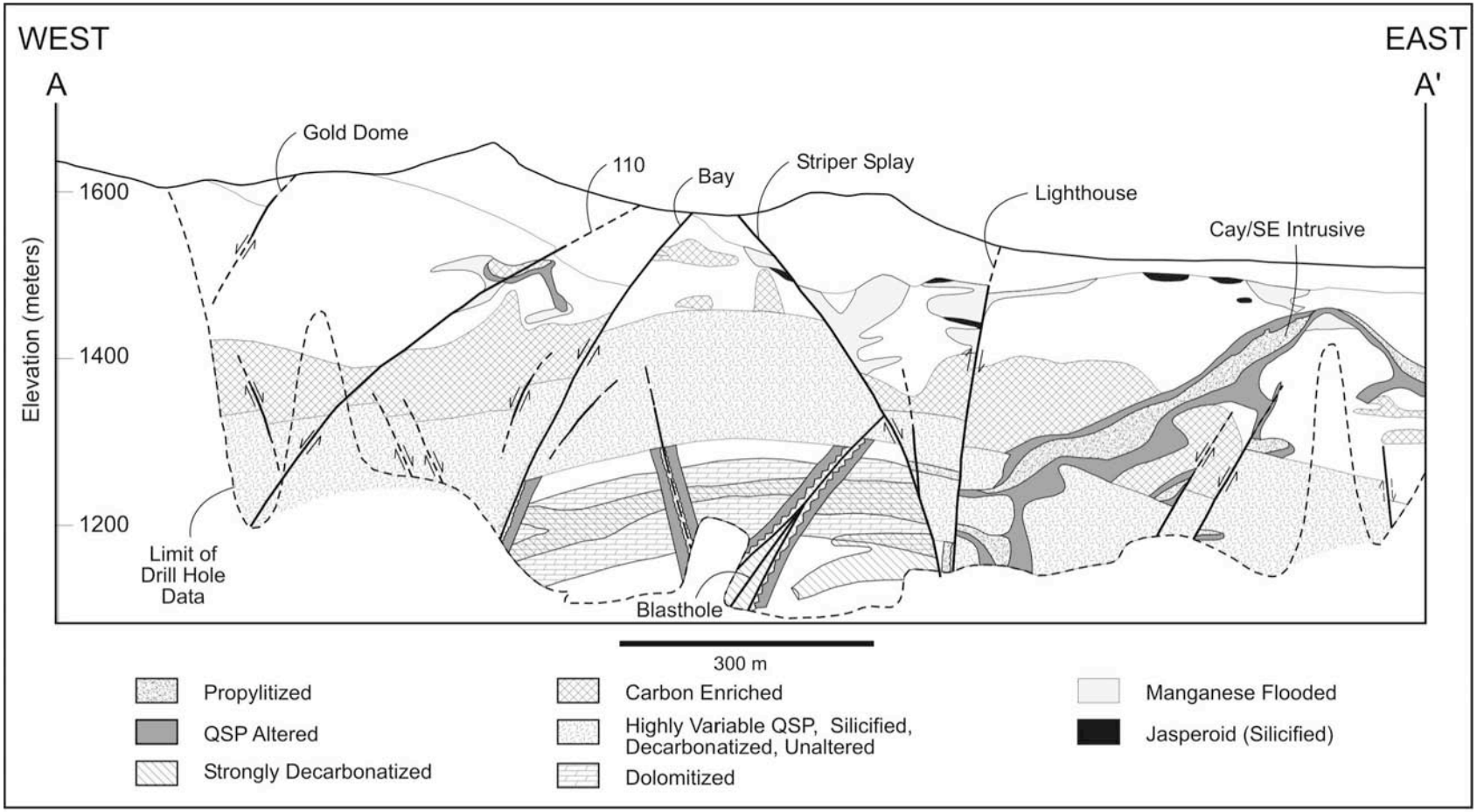

FIG. 62. Schematic alteration overlay for the W-E cross section (refer to Figures 4 and 5 for orientation and geologic framework).

TABLE 7. Alteration assemblages in Eocene porphyritic intrusions at Cove.

Alteration Assemblages:	**Notes:**
Pre-Ore Deuteric Alteration	
chlorite-zeolites-devitrification	observed only in samples with no ore-stage alteration effects
Ore-Stage Hydrothermal Alteration	
biotite-pyrite	secondary biotite veinlets and rims with associated pyrite
calcite-epidote ± quartz	in plagioclase sites
quartz-sericite	thin veinlets
quartz-sericite-pyrite (QSP)	pervasive
quartz-pyrite	veinlets seen only in outcrop
pyrite	veinlets cut QSP assemblage
sulfides-calcite ± sericite	veins and veinlets
calcite	late barren veins and veinlets cut all earlier assemblages
Post-Ore Supergene Alteration	
oxides-kaolinite-smectite	overprints all earlier assemblages

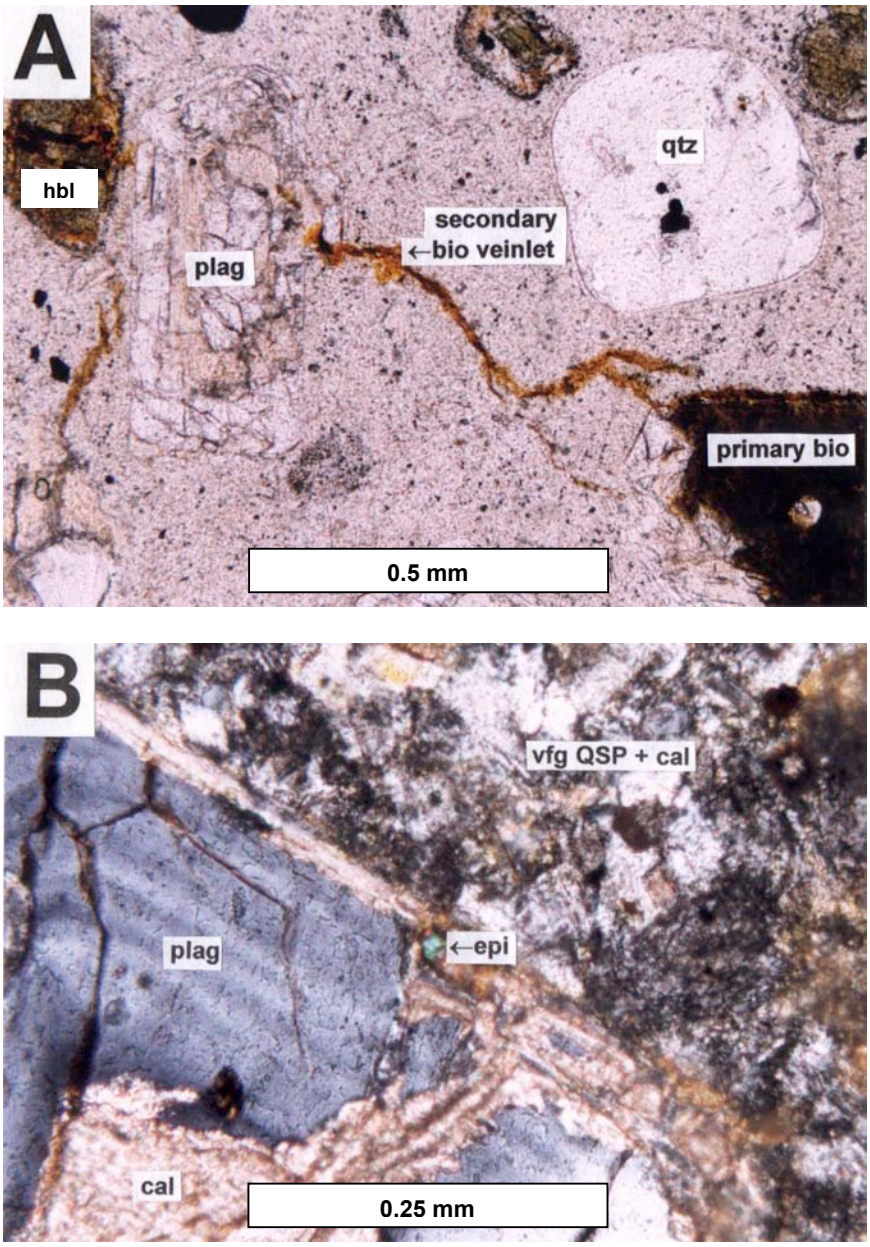

FIG. 63. Hypogene alteration assemblages in Eocene porphyritic intrusions. A shows early weak biotitization as a secondary biotite veinlet cutting a plagioclase (plag) phenocryst and groundmass, and also replacing an amphibole (hbl) crystal (transmitted light; sample 4725E-14). B shows propylitization in the form of calcite (cal) and epidote (epi) replacing a plagioclase (plag) phenocryst (crossed polars; sample 4205E-22).

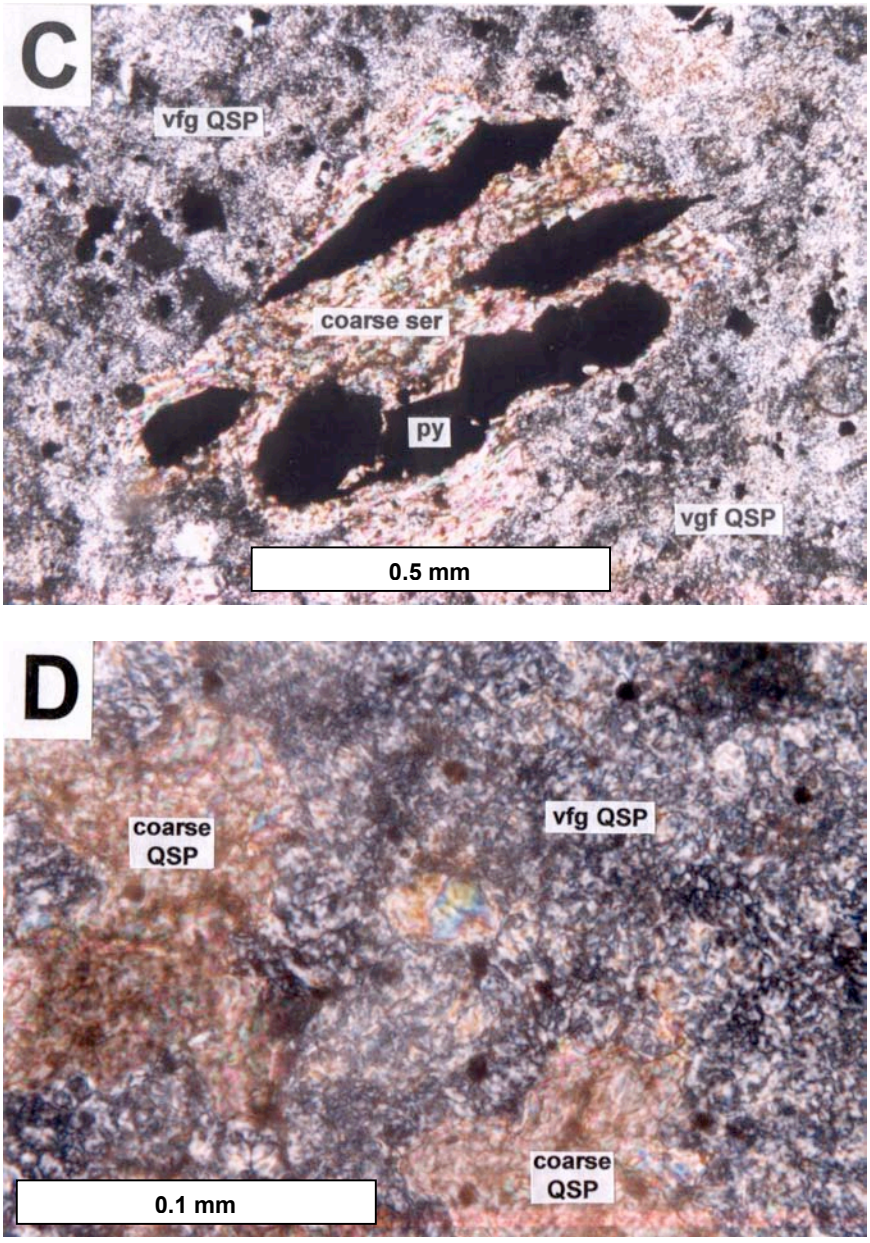

FIG. 63. Continued. C shows QSP alteration in which coarse sericite (ser) and pyrite (py) pseudomorph a biotite phenocryst, and fine-grained quartz-sericite-pyrite (vfg QSP) replace the groundmass (crossed polars; sample 4205E-5). D shows QSP alteration in a *totally* altered intrusion, with coarse quartz-sericite-pyrite (coarse QSP) in relict phenocryst sites, and fine-grained quartz-sericite-pyrite (vfg QSP) in the groundmass (crossed polars; sample 4405E-2).

minerals are ranked, based on their apparent susceptibility to alteration, from least to most stable as amphibole, biotite, plagioclase, K-feldspar, apatite, and quartz. The volume percentages of minerals and porosity reported in this section were determined by modal estimates from thin sections (Fig. 64). In *weakly* altered intrusions, all primary phases are present, but hornblende, biotite, plagioclase, and K-feldspar have all been slightly altered. In *moderately* altered intrusions, hornblende is essentially gone, and biotite, plagioclase, and K-feldspar are slightly altered. In *moderate-strongly* altered, the primary mineral stabilities are nearly the same, but the remaining phases are more altered. The *moderate-strongly* altered samples contain a propylitic alteration assemblage, with the highest average volume percentage of calcite and trace amounts of epidote. The calcite occurs in plagioclase sites, with associated quartz and epidote.

In *strongly* altered intrusions, only quartz and some of the apatite remain as stable phases. All other primary minerals were entirely replaced, but the relict outlines of phenocrysts are clear. The dominant alteration minerals are sericite/illite (averaging ~55 volume percent) and quartz (averaging ~25 volume percent). Biotite is pseudomorphed by coarse sericite/illite and pyrite, with finer-grained sericite/illite intimately intergrown with quartz and opaques (dominantly pyrite) in the plagioclase and hornblende phenocryst sites and groundmass. Because quartz, sericite/illite, and pyrite are also the dominant alteration minerals in the *very strongly* and *totally* altered samples, these samples are collectively considered as representatives of the QSP stage of alteration in the ensuing text. Porosity in these samples averages 8 volume percent, and consists of small vugs concentrated in the former phenocryst sites. Calcite is conspicuously absent,

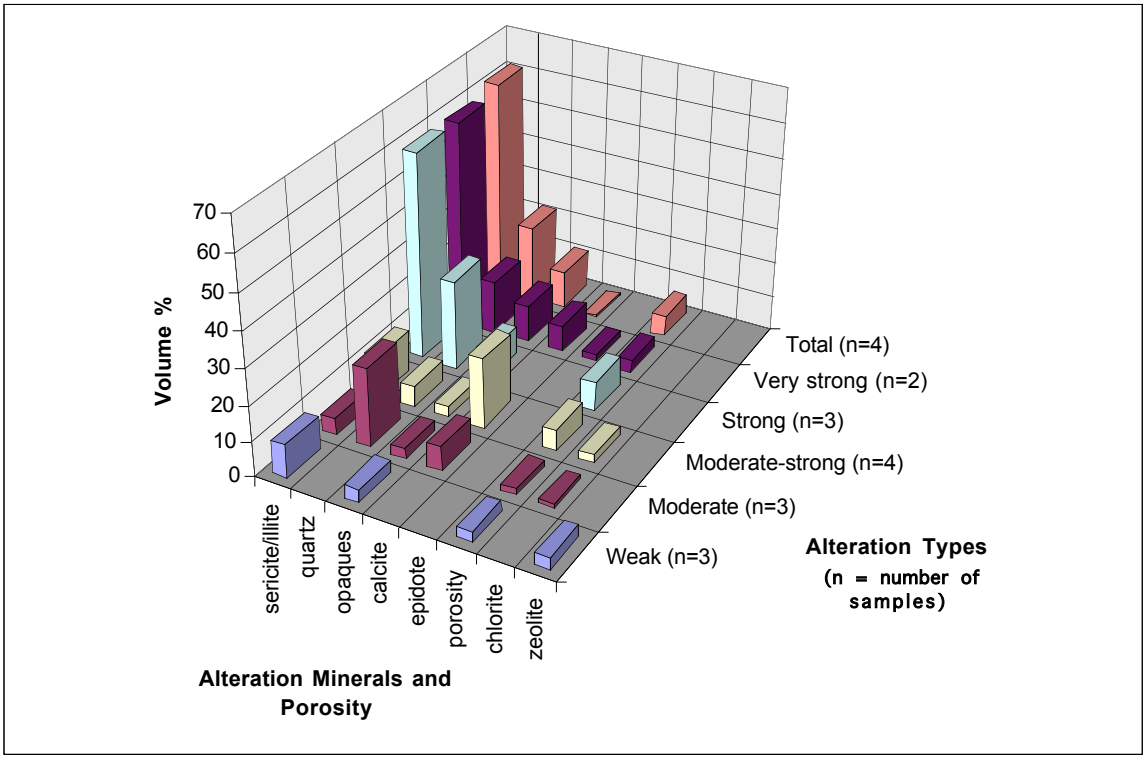

FIG. 64. Deuteric/hypogene alteration minerals and abundances in Eocene intrusions. Refer to text for descriptions of alteration types.

probably due to dissolution and/or replacement of earlier propylitic calcite with increasing a_{H+} during the QSP stage. Also, the volume percentage of opaques (pyrite and other ore minerals) increases from <6 volume percent in the *weakly* to *moderate-strongly* altered samples to 8 volume percent in the QSP stage.

In *very strongly* altered samples, the alteration is essentially the same as in the *strongly* altered samples, and sericite/illite again comprises ~55 volume percent of the intrusive rock samples. Very fine-grained sericite/illite is a minor component in the earlier alteration assemblages, and in all cases appears to replace primary minerals and earlier alteration minerals as irregular masses. Coarser sericite/illite also pseudomorphs biotite in the *very strongly* altered samples. Phenocryst sites are still discernable, typically due to the presence of coarser alteration minerals in these sites. The opaque (ore) mineral content in the *very strongly* altered samples increases to an average of 11 volume percent.

In *totally* altered intrusions, only quartz remains as a primary phase, and all primary textures have been obscured by the sericitic/illitic alteration. In decreasing order of abundance, the samples consist of sericite/illite (~60 volume percent), quartz (22 volume percent), and opaques (11 volume percent), and vuggy porosity (6 volume percent). Although the primary textures are destroyed, a few ghost phenocryst sites are inferred from somewhat polygonal patches of alteration minerals with slightly different textures and/or colors than the other alteration phases.

The latest stage of hypogene alteration of intrusive rocks involved late-main ore stage to post-ore calcite veining. In thin sections, polished sections, and hand samples, calcite typically occurs as late fill in main ore stage veins. Calcite veins cutting intrusions that

displayed all types of earlier alteration were commonly observed at hand-specimen and outcrop scales in the Cove open pit.

An important trend evident in Figure 64 is the increase in opaque (ore) mineral content with increasing intensity of alteration. The opaque content increases to a maximum of 11 volume percent associated with QSP alteration. These data corroborate field and hand-sample observations that the macroscopic BMVT veins and veinlets, crustiform sulfides, and sulfide pods are associated with intense QSP alteration, and that this intensity decreases with distance from the BMVT assemblages. For BMVT veins showing multiple stages of dilation and precipitation, the individual bands are typically separated by thin sericite/illite + sulfide selvages. Carlin-style mineralization is also spatially associated with QSP alteration, as inferred from the intimate associations between the Carlin-style ore and Omega dike in the Cove South Deep orebody (Fig. 29); the dike has been altered to a QSP assemblage, and contains Carlin-style stibnite crystals in vugs.

Alteration in Sedimentary Units

The sedimentary host units at Cove have each been altered to varying degrees of intensity. The hypogene alteration styles in the sedimentary units at Cove are dolomitization, decarbonatization, silicification, sericitization/illitization, bleaching, and carbon-enrichment.

Dolomitization

In drilling outside of the Cove deposit, the Home Station Member is a primary limestone (David L. Emmons, John Penton, and Don Ryan, personal communications, 1998-2000). Within the Cove open pit and underground workings, this unit is a secondary dolostone. It is not clear whether dolomitization occurred in response to the development of the Cove hydrothermal system, or if dolomitization occurred earlier. If earlier, dolomitization may be diagenetic or hydrothermal. For example, at least some diagenetic dolomitization may have occurred in the Home Station Member during the deposition of the primary dolostone of the overlying Panther Canyon Member. Dolomitization also may have occurred in response to an earlier hydrothermal system. Such a system occurs within a few kilometers of Cove, where the intrusion of a Jurassic pluton produced Fe skarns on its margins (Emmons and Eng, 1995), but no secondary dolostones have been observed in association with this pluton.

The isotopic signature ($\delta^{13}C$ and $\delta^{18}O$) of the secondary dolostone in the Home Station Member was compared to the signatures of the other carbonate host units and vein carbonates (see Chapter 6). While the secondary dolostone does not show a clear isotopic association with the vein carbonates, it cannot be dismissed as unrelated to the mineralizing event. Except for the samples from the Home Station Member, the carbonate host rock samples submitted for this isotopic study were selected because they occurred outside of mined orebodies, and appeared texturally and mineralogically unaltered. As discussed in Chapter 6, however, the isotopic signatures indicate that all of

these carbonates have been exposed to hydrothermal fluids. In this case, the most likely fluids are related to the system that mineralized Cove.

Regardless of the possible genetic association with the hypogene mineralizing system at Cove, the secondary dolostone in the Home Station spatially coincides with the distribution of hypogene Ag and Au in the lower high-grade and Cove South Deep orebodies (see Chapter 3 for full discussion). This coincidence is due to the high permeability of this unit relative to the primary dolostone in the overlying Panther Canyon Member. Calcite has larger unit cell dimensions than dolomite. Therefore, conversion of a primary limestone unit to dolomite reduces the overall volume of mineral within the unit. If, as in the case of the Home Station Member, the lithologic unit maintains its original volume, intercrystalline porosity is developed between the secondary dolomite crystals. The relatively high porosity/permeability allowed the mineralizing hydrothermal fluids to migrate laterally away from feeder faults. These fluids dissolved some of the dolomite (see the next section), and deposited sulfides, quartz, and illite/sericite in the intercrystalline pore spaces. Late calcite also occurs in some of these pores.

Decarbonatization

Decarbonatization was produced by reaction of the host carbonates with the mineralizing hydrothermal fluid(s), and occurs in all of the carbonate units at Cove. In general, decarbonatization is strongest to complete in proximity to presumed conduits for the hydrothermal fluids, and grades outward through weakly “sanded” carbonates into

essentially unaltered rocks (Fig. 65). From weakest to most intense, the products of decarbonatization at Cove are stylolites, micro- to macroscopic porosity, sanding, and complete dissolution and collapse.

Stylolites: Stylolites occur in thin sections from all of the carbonate units at Cove. In weakly altered to unaltered rock, the stylolites consist simply of irregular sutures. Residual concentrations of silt- to sand-sized quartz grains occur with the stylolites in some samples from the Home Station and Panther Canyon Members. In more strongly altered rock, and in samples in which abundant disseminated pyrite was observed, the stylolites are typically filled with thin, irregular veinlets of pyrite and/or marcasite, with or without observable sericite/illite (Fig. 66).

Micro- to Macroscopic Pores: Dissolution-related, intergranular and intercrystalline porosity occurs on a microscopic scale in many of the samples collected from the carbonate units at Cove. In general, this porosity increases in proximity to the orebodies described in Chapter 3. Decarbonatization also produced millimeter- to centimeter-scale dissolution holes throughout parts of the Home Station Member, and in the dolostone submember of the Panther Canyon Member. These dissolution holes are most abundant in the uppermost, 1-meter-thick bed of the dolostone submember of the Panther Canyon Member. In the axis of the Cove anticline, these dissolution holes are typically lined by white dolomite, and filled with cockscomb quartz and open-space growth sulfides (Fig. 27). The frequency of dissolution holes systematically decreases away from the axis of the anticline. Hypogene minerals were not observed in dissolution holes in the Panther

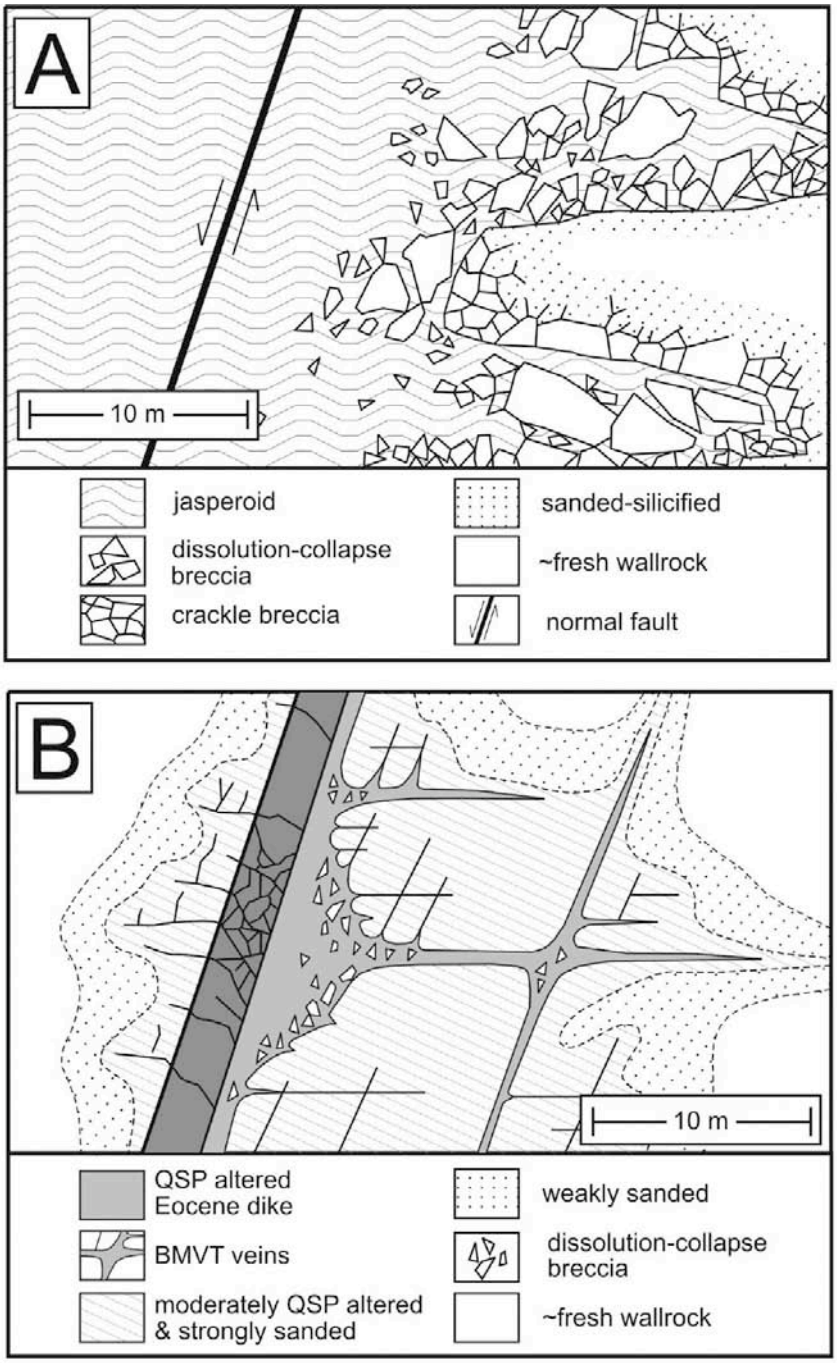

FIG. 65. Schematic effects and associations of strong decarbonatization. A shows complete replacement of limestone by jasperoid in the Smelser Pass Member, grading outward through crackle breccia and weakly sanded wallrock, into fresh wallrock. B shows a large BMVT pod localized in the footwall of a QSP altered dike. The pod occurs where carbonate has been completely removed. The effects of decarbonatization grade outward through strongly and weakly sanded wallrock, into fresh wallrock. QSP alteration is associated with the Eocene dike, the BMVT veins, and the strongly sanded wallrock. The zonation shown in B is based on observations in the Home Station and lower Panther Canyon Members.

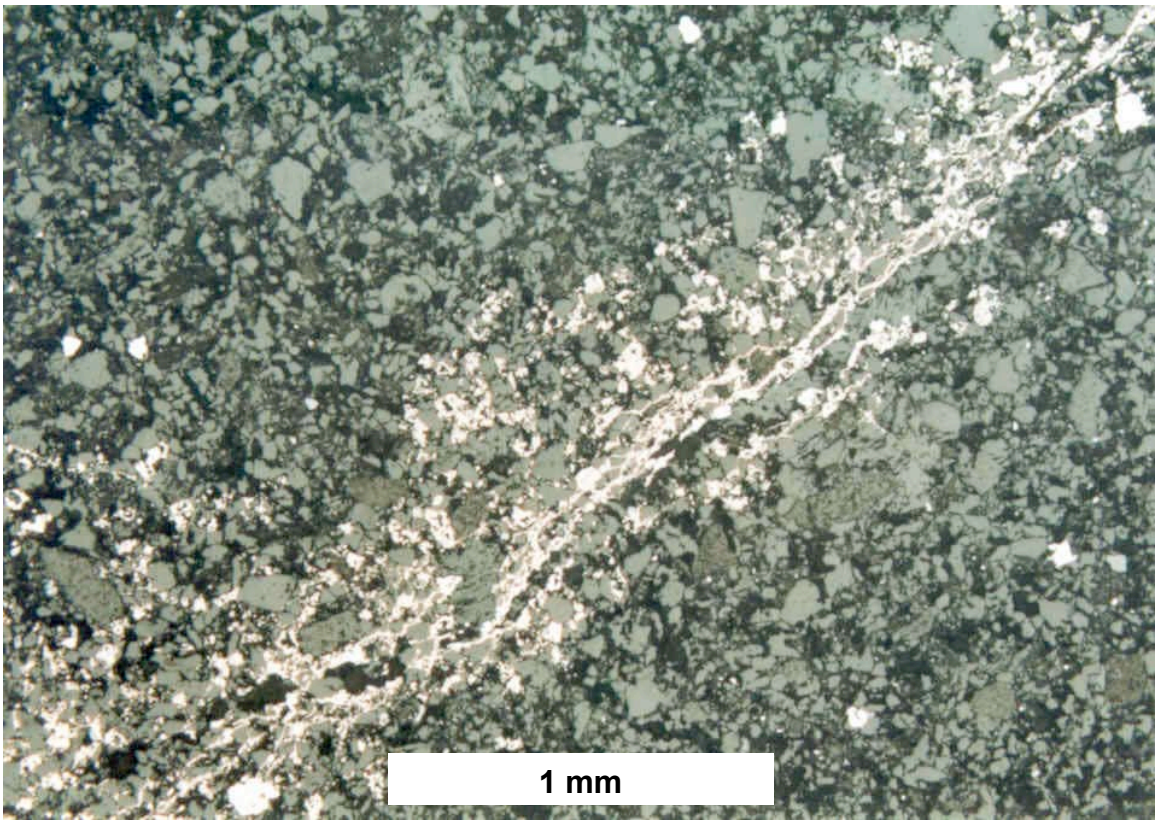

FIG. 66. An irregular pyrite veinlet (yellowish-white) along a stylolite in primary dolostone (medium to dark gray) of the Panther Canyon Member (reflected light photomicrograph, sample 4205E-15).

Canyon Member in the limbs of the anticline, nor were they observed in any of the relatively sparse dissolution holes in the Home Station Member.

Sanding: The term "sanding" is used to describe rocks in which decarbonatization has liberated silt- to sand-sized grains of residual carbonate or insoluble material (e.g. quartz) from their carbonate cement and/or matrix. The result is weakly friable to completely sanded rock, in which the sand-sized grains can literally flow like modern beach sand. Two sanding modes occur at Cove. In dolostone with moderate to high quartz sand and/or silt contents, such as parts of the Home Station Member and the lower dolostone part of the transitional submember of the Panther Canyon Member, sanding is manifest as a residual concentration of quartz grains that resulted from dissolution of the carbonate matrix. In dolomitic parts of the Home Station Member and the dolostone submember of the Panther Canyon Member, sanding occurred through dissolution along the intercrystalline boundaries of interlocking dolomite crystals. Sanding is commonly most intense (grading into complete decarbonatization) in the footwalls of semi-permeable intrusions in the Home Station Member and carbonate units in the Panther Canyon Member. BMVT pods and veins commonly are localized in these decarbonatized zones (Fig. 65).

Strong to Complete Decarbonatization: Strong decarbonatization is associated with both diagenetic and hydrothermal alteration. Diagenetic dissolution produced caverns and slump features in the Smelser Pass and Home Station Members, respectively. Caverns were mapped in several locations in the Smelser Pass. The larger caverns (up to

35 meters wide) typically contain fragments of Caetano tuff, requiring that karstification occurred after the Oligocene unit was deposited.

Slump features occur where overlying strata have collapsed into void spaces produced by diagenetic and/or hydrothermal dissolution. All of the slump features observed occur at the contact between the Home Station and Panther Canyon Members. The voids range from <1 to several meters in width, and occur in the Home Station Member, just below the contact. Most of the voids are channel-like, and have been filled with thinly bedded sediments (Fig. 67). Although some of these features may be local unconformity surfaces of primary sedimentary origin, most contain breccia clasts of the overlying dolostone submember of the Panther Canyon Member, indicating a diagenetic or hydrothermal origin.

Complete removal of carbonate also resulted from hydrothermal dissolution. The voids produced during the hypogene event(s) are filled by jasperoid in the Smelser Pass Member (Fig. 65A), and by BMVT sulfides, quartz, and sericite/illite in the Panther Canyon and Home Station Members (Fig. 65B). In all cases where they were mapped, the centralized voids occur in spatial association with major faults. The effects of decarbonatization grade outward from centralized voids (now filled), through middle dissolution-collapse breccias and outer crackle breccias, into fresh wallrock. The scale of this zonation is highly variable, from ~1 meter to >100 meters in width. Higher ore grades typically occur in centralized voids and/or dissolution-collapse breccia bodies. In many of the mined-out ore zones, no centralized voids were observed, but sanding and/or dissolution-collapse breccias were present.

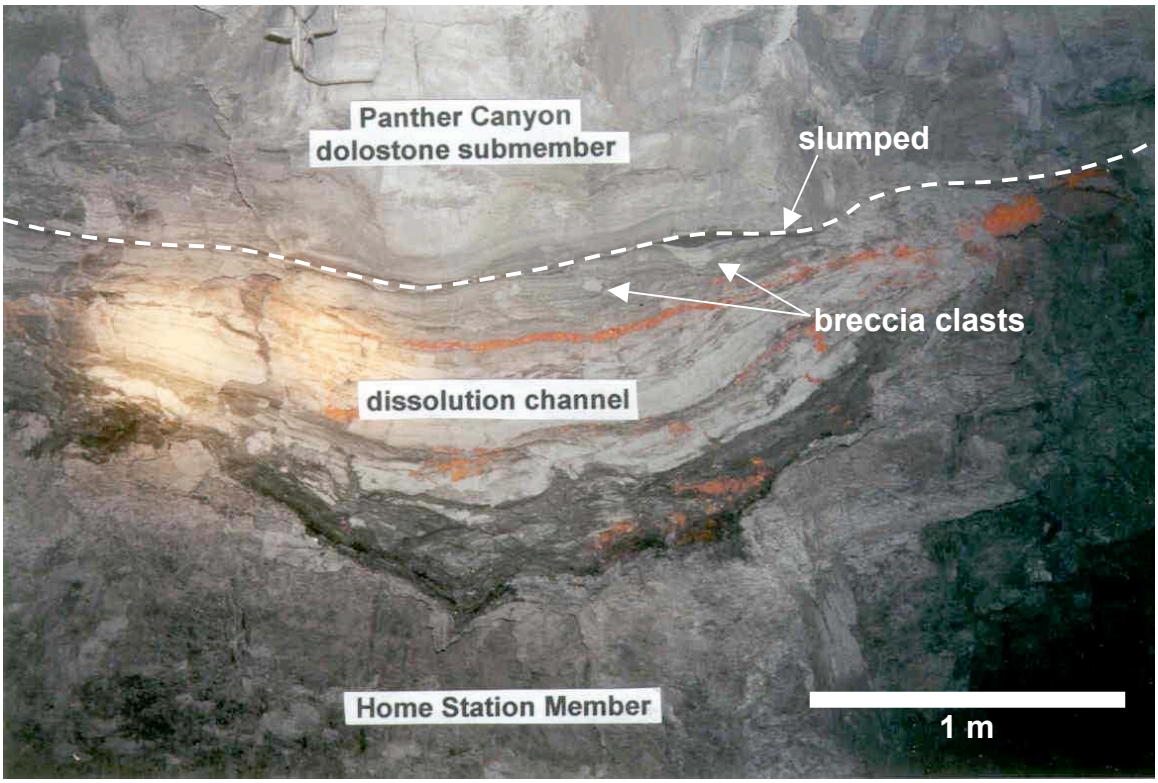

FIG. 67. Photograph of a slump feature in the CSD orebody (taken 7/27/99 by David L. Emmons). The slump feature occurs at the contact between the Home Station and Panther Canyon Members. Here, removal of carbonate by dissolution has caused the base of the Panther Canyon Member to slump into the void. The void has been filled with thin-bedded sediments and breccia clasts, and realgar (orange) has been introduced during the mineralizing event.

Silicification and Sericitization/Illitization

Silicification and sericitization are intimately associated with both BMVT and Carlin-style orebodies. In all of the sedimentary host units, silicification, with or without sericitization/illitization, is most pronounced near major faults. However, the relatively high permeabilities in the secondary dolostone of the Home Station Member and the porous clastic strata in the Panther Canyon Member allowed widespread fluid access and ubiquitous development of these alteration styles.

Silicification is most obviously expressed as jasperoid bodies in the Smelser Pass Member (Fig. 65A). These jasperoids are auriferous, commonly manganiferous, and generally associated with dissolution-collapse breccias. They occur along large faults, and are best developed in the hangingwall of the Lighthouse fault and adjacent to the Southeast intrusion.

In the Home Station Member and carbonate-dominated units in the Panther Canyon Member, silicification occurs as crustiform and cockscomb quartz along BMVT veins and in dissolution-related pore spaces (Fig. 44A). The walls of the veins contain disseminated sulfides and small anhedral masses of quartz that are commonly intergrown with sericite/illite and pyrite (QSP alteration) (Figs. 68B and 69). Further away from the veins, silicification occurs as irregular patches of recrystallized quartz (Fig. 68A).

In the clastic-dominated units in the Panther Canyon Member, silicification occurs as crustiform and cockscomb quartz along BMVT veins and in intergranular pore spaces. In the hinge zone of the Cove anticline, these pores are typically filled with intergrown quartz, sericite/illite, and sulfides (QSP alteration) (Fig. 69).

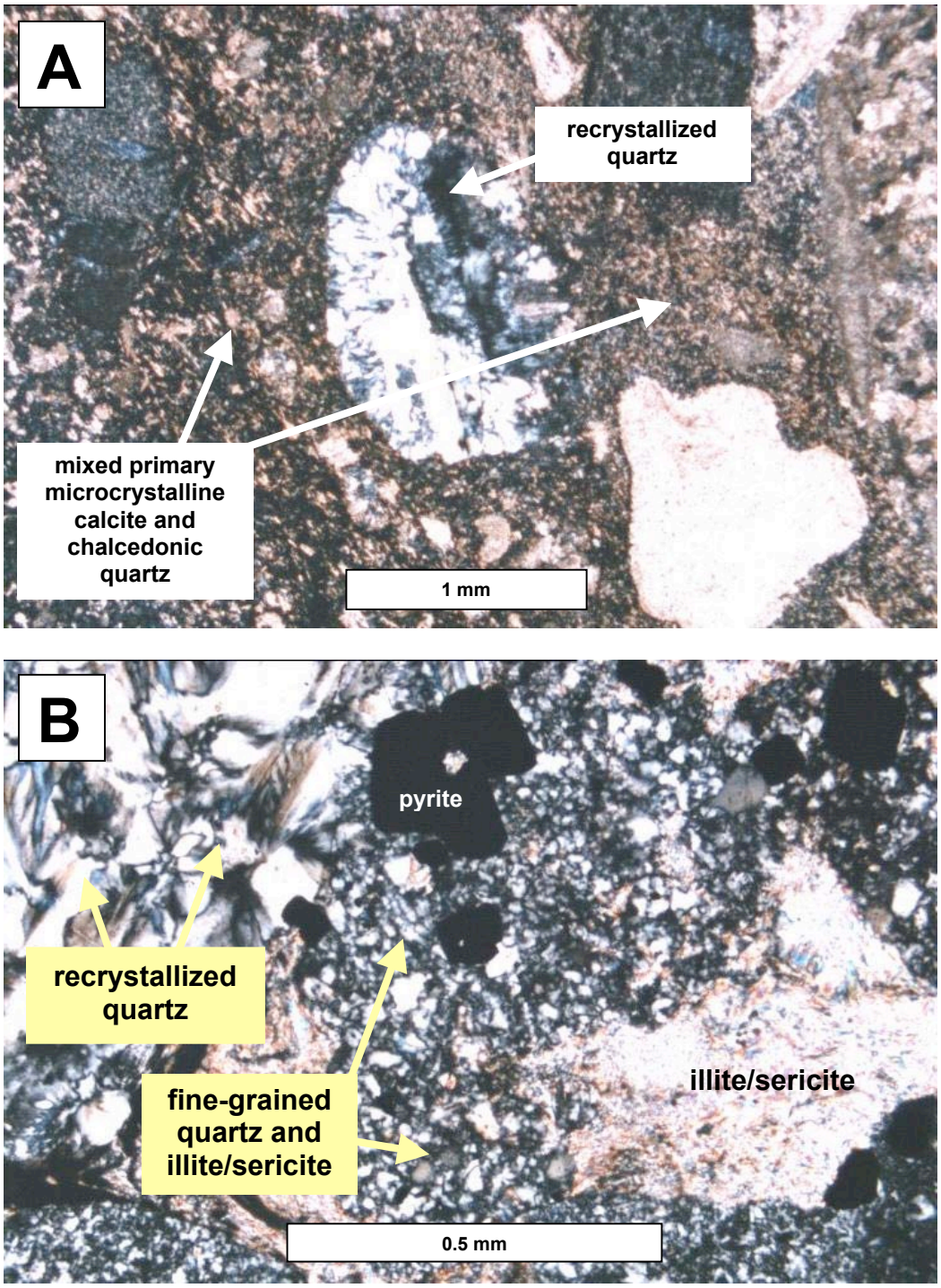

FIG. 68. Transmitted light photomicrographs showing various expressions of silicification in altered samples from the Cove deposit. A shows a patch of recrystallized quartz in limestone of the Smelser Pass Member (sample 5015-3). B shows fine-grained hydrothermal quartz associated with QSP alteration of the transitional submember of the Panther Canyon Member, and also recrystallized quartz (sample TC8-A1). See also Figure 44A.

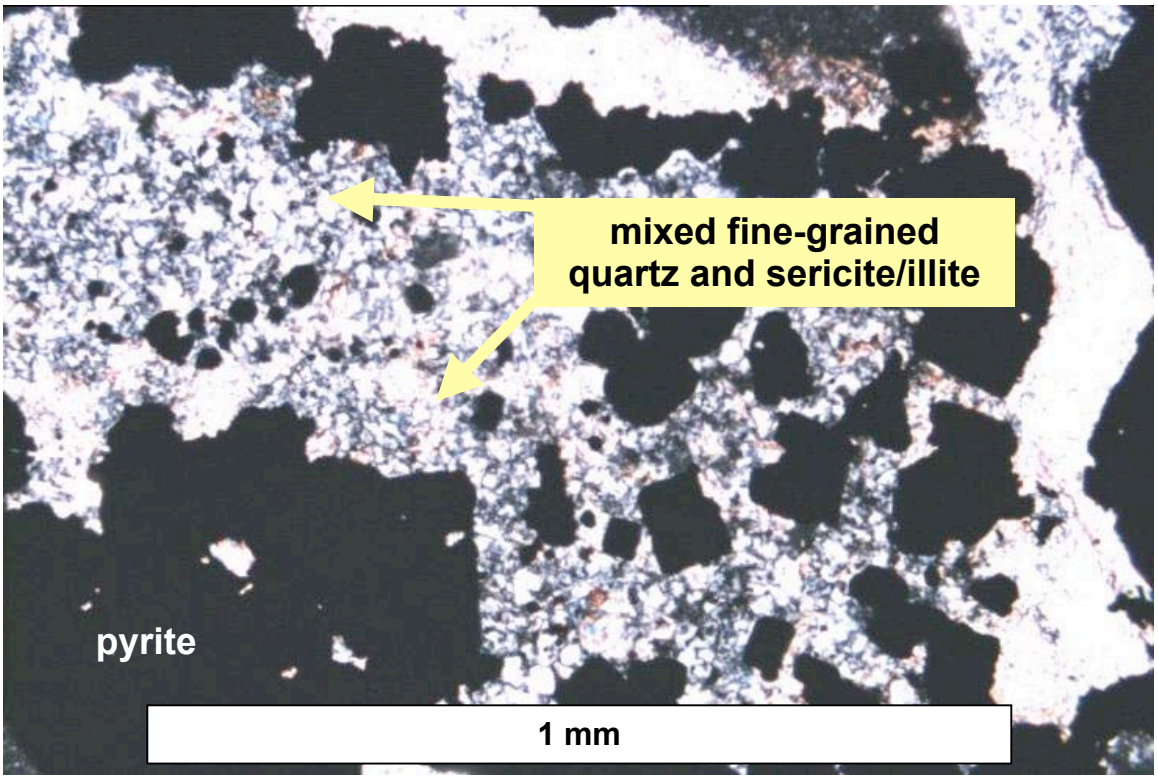

FIG. 69. Transmitted light photomicrograph of sample TC8-A1 (crosed polars) showing QSP alteration of conglomerate in the transitional submember of the Panther Canyon Member.

Bleaching and Carbon Enrichment

Bleaching (loss of organic components) and carbon enrichment are both hydrothermal effects. Bleaching occurs in limestone of the Smelser Pass Member, and is most pronounced adjacent to major faults. Between the Lighthouse fault and the Southeast intrusion, for example, bleaching is most intense closest to the faults, giving the originally dark gray limestone a purplish-gray hue. Because the widths of bleaching aureoles are variable and not consistently mappable, however, this alteration style is not shown in Figure 62.

In the Cove underground, carbon enrichment is pervasive in the strongly sanded dolostone of the Home Station Member, immediately below the contact with the overlying dolostone submember of the Panther Canyon Member. Carbon enrichment in the Smelser Pass Member commonly occurs as residual concentrations of insoluble carbon along stylolites, and was logged in core almost everywhere near the base of the unit. In the case of bleaching between the Lighthouse fault and Southeast intrusion, the bleaching decreases and gives way to carbon enrichment between the two faults, giving the limestone a sooty black appearance.

Supergene Alteration

Because this study is focused on the hypogene genesis of the Cove deposit, supergene alteration was not examined in detail. Exposed strata in the upper part of the Cove deposit have an orange to red coloration, due to the supergene oxidation of Fe sulfides. The principal products of supergene alteration are illite, smectite, and kaolinite clays, Fe

and Mn oxides, and late carbonates. Supergene alteration affects much of the Smelser Pass Member and the upper parts of the transitional submember of the Panther Canyon Member. The alteration mineralogy of the supergene zones is summarized in Chapter 4. The presence of Mn-bearing supergene phases is interpreted to reflect a residual concentration of manganese produced by the dissolution of Mn-bearing carbonates in the upper parts of the deposit. This association may indicate vertical zonation of hypogene carbonates, with more abundant Mn-bearing calcite and/or rhodochrosite at higher elevations.

THE AGE OF INTRUSION, ALTERATION, AND MINERALIZATION

The bases for interpretation of the age of alteration and mineralization at Cove are ^{40}Ar-^{39}Ar age data produced for this study, coupled with a preexisting K-Ar age database for Cove and McCoy (Table 3) and observed relationships between intrusions, ore, and alteration. The genetic model presented for the Cove/McCoy system in Chapter 6 is based on the geochronology discussed here.

Five samples from the Cove deposit were selected for ^{40}Ar-^{39}Ar analyses. Two of the samples submitted for analyses were individual mineral phases selected from 4145E-19 and AR44955E-2, and produced analytically and geologically acceptable ages. Three additional samples, CVC-218-857.5 and 4405E-1, 4145E-29, produced unreliable age data (see APPENDIX VI). The results presented here are based on interpretations generated for the age spectra by Terry Spell at the Nevada Isotope Geochronology Laboratory at the University of Nevada, Las Vegas.

^{40}Ar-^{39}Ar Dating Results for Sample 4145E-19

Sample 4145E-19 was collected from a *totally* altered part of the Bay dike (see Plate 1 for location). Coarse BMVT sulfides occurred in veins and as crustifications in intergranular pores immediately beneath the altered dike. The highwall from which this sample was collected has been subsequently mined out.

More than 98 volume percent of sample 4145E-19 consists of alteration products. In decreasing order of abundance, these products are sericite/illite, quartz, opaques (chiefly pyrite with lesser sphalerite and galena), pore space, and calcite. Coarser sericite/illite, quartz, and sulfides are intergrown in phenocryst sites, and finer sericite/illite, quartz, and sulfides are intergrown in the altered groundmass. A 1-millimeter-wide BMVT veinlet cuts this sample (Fig. 70A). This veinlet is filled with BMVT sulfides and later calcite. Relict biotite crystals are preserved as coarse intergrowths of sericite/illite, quartz, and pyrite (Fig 70B.). Many of these relict biotite grains are larger than 2 millimeters wide, and were physically plucked from the accompanying hand sample for radiometric dating.

The age spectrum produced for the sericitized/illitized biotite grains from sample 4145E-19 (Fig. 71) exhibits ages decreasing from an initial step of ~51 Ma to a plateau segment (steps 7 through 12) that yields an age of 39.37 ± 0.23 Ma and comprises 58 percent of the gas released. A valid isochron defined by steps 5-11 (comprising 69 percent of released gas) yields an age of 39.12 ± 0.30 Ma, which is indistinguishable from the plateau age. Because the sample is a sericite/illite replacement of primary igneous biotite, the age represents the timing of replacement of biotite by hypogene

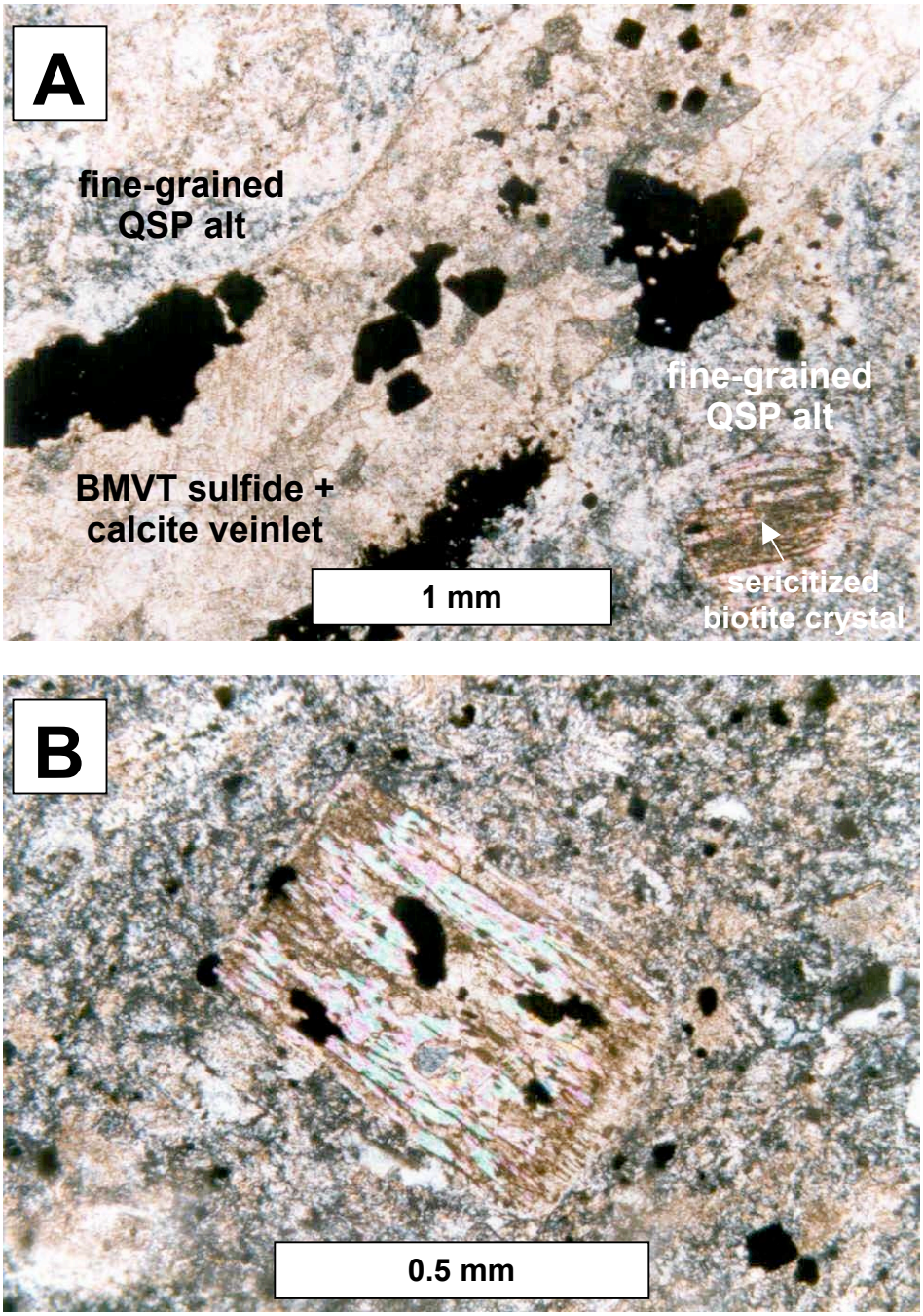

FIG. 70. Transmitted light photomicrographs of sample 4145E-19 (crossed polars). A shows a sulfide-lined, calcite-filled BMVT veinlet cutting the QSP altered rock. B is a close up of a relict biotite crystal that has been pseudomorphed by sericite/illite with pyrite. The groundmass in B consists of a fine-grained QSP assemblage.

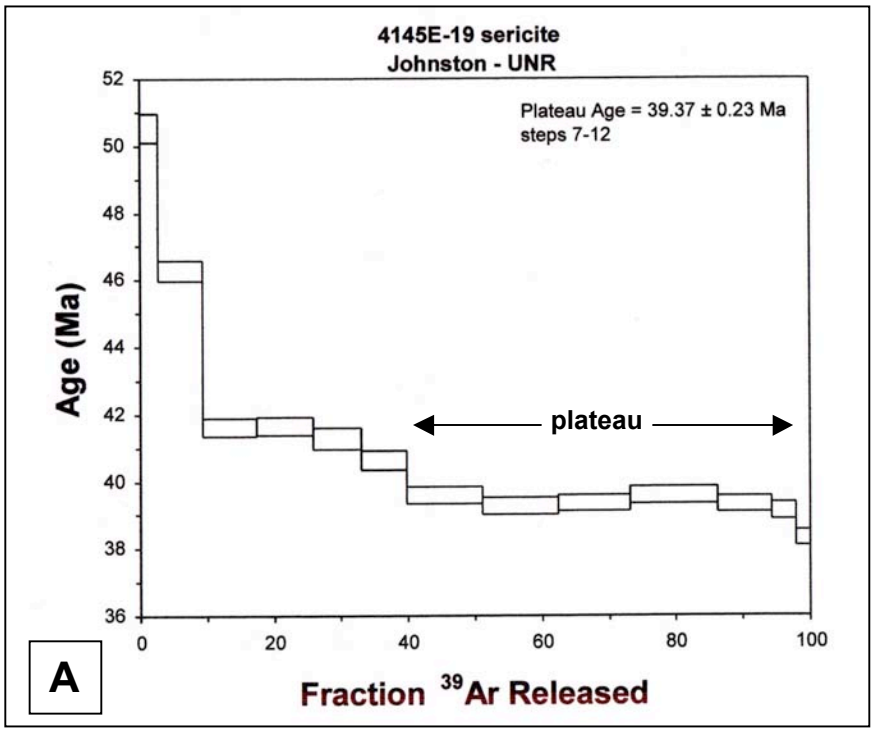

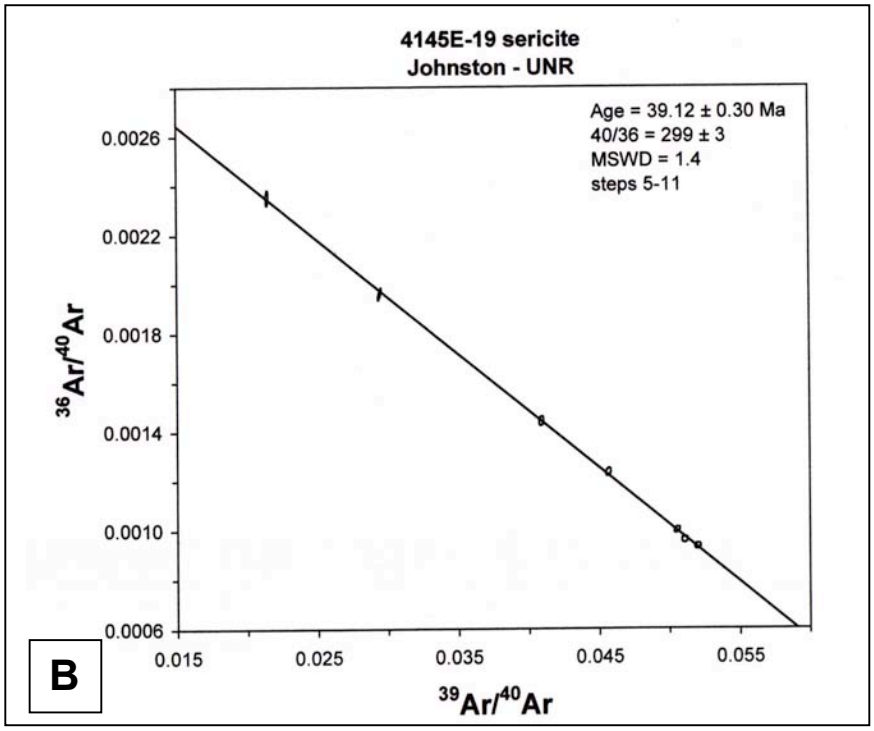

FIG. 71. Age data for sample 4145E-19. A. Incremental heating ^{40}Ar-^{39}Ar age spectrum. B. Isochron plot.

sericite/illite. The intimate association of the sericite/illite with BMVT sulfides in sample 4145E-19 indicates that this is also the age of BMVT mineralization.

^{40}Ar-^{39}Ar Dating Results for Sample AR44955E-2

Sample AR4955E-2 was collected from an apparently fresh exposure of the West intrusion (see Plate 1 for location). In thin section, however, it is apparent that the unit has been slightly propylitized. Hypogene calcite comprises about 10 volume percent of the sample, and occurs as a replacement phase on the margins of plagioclase grains and in the groundmass (Fig. 72). Minor secondary quartz is also present in the plagioclase sites and in the groundmass. The biotite crystals, however, generally appear fresh in both hand sample and thin section. The biotite contains no secondary sericite/illite, quartz, or calcite, but very minor (<1 volume percent) pyrite was observed along cleavage planes in a few of the biotite grains. The biotite crystals were up to 2 millimeters in diameter, allowing them to be physically separated and submitted for dating.

The age spectrum produced for the biotite grains yielded a nearly ideal, flat age spectrum, with steps 4-12 (comprising 97.5 percent of the gas released) defining a plateau age of 39.01 ± 0.22 Ma (Fig. 73). Steps 2-6 also define a valid isochron age of 38.68 ± 0.21 Ma, but account for only 22 percent of the gas released. Normally, an isochron age would be preferable, as it is not subject to assumptions regarding the isotopic composition of the trapped (non-radiogenic) Ar; ages for the age spectra are calculated assuming 295.5 for trapped Ar (air value), and are thus called “apparent” age spectra. For this sample, the isochron indicates trapped atmospheric Ar, for which the ^{40}Ar-^{39}Ar is

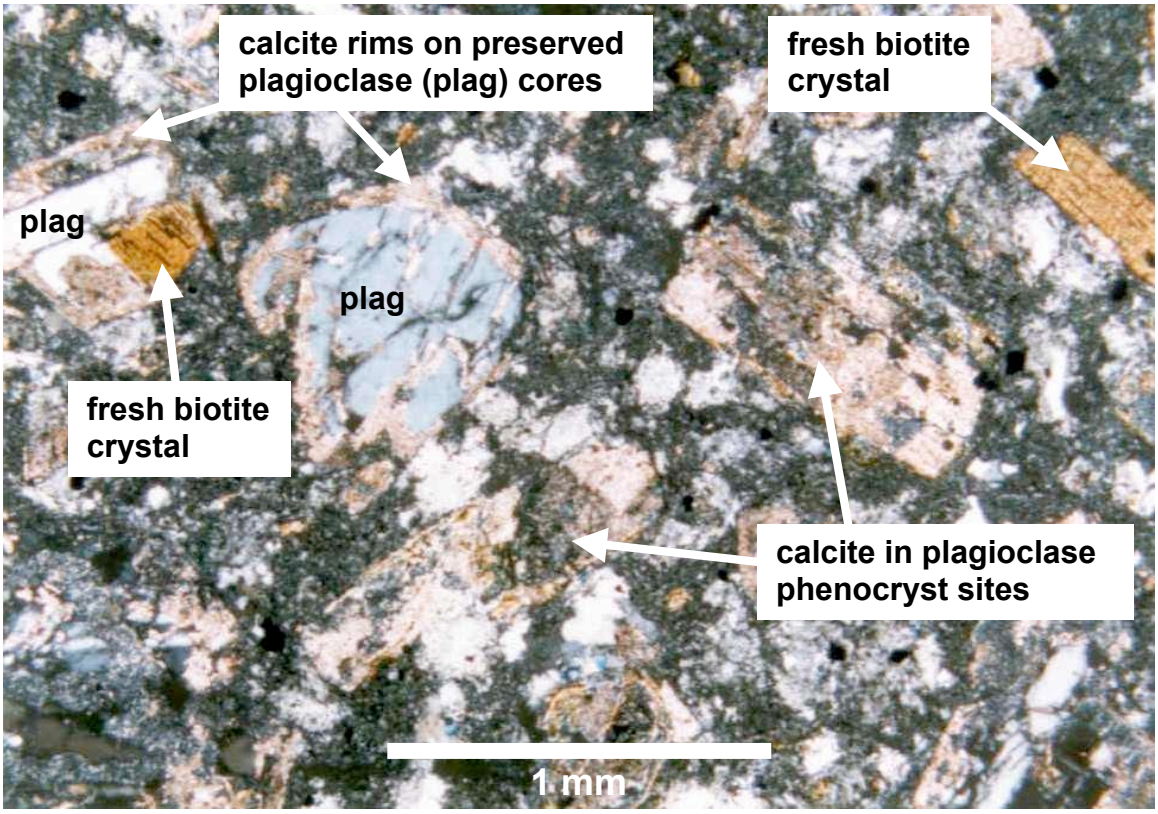

FIG. 72. Transmitted light photomicrograph of sample AR4955E-2 (crossed polars). Although the sample is moderately propylitized, as indicated by the alteration of much of the plagioclase to calcite, the biotite crystals are generally very fresh.

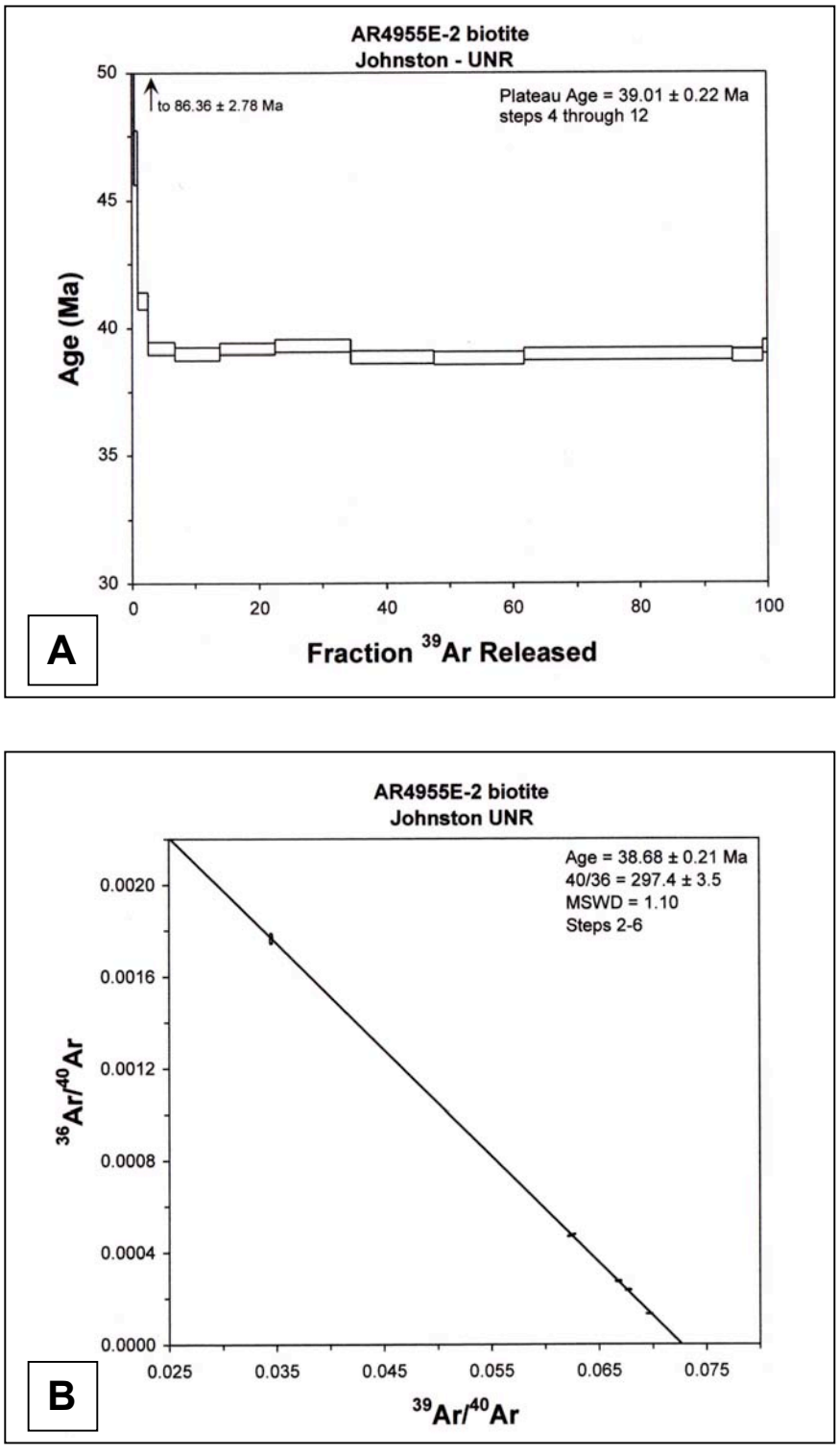

FIG. 73. Age data for sample AR4955E-2. A. Incremental heating ^{40}Ar-^{39}Ar age spectrum. B. Isochron plot.

indistinguishable from the air value of 295.5. Because the isochron is defined by a much smaller percentage of the gas than the plateau, the plateau age is preferred for the timing of deposition of the igneous biotite in this sample.

DISCUSSION

The data presented in Chapters 2 through 5 provide important information regarding the spatial associations and relative timing of intrusions, alteration, and mineralization at Cove. Preexisting K-Ar dates for biotite from the Bay dike, Cay dike, and Southeast intrusion range from 40.3 ± 1.2 Ma to 38.8 ± 1.1 Ma (Table 3). The ranges in uncertainty for these data bracket an age of 41.5 to 37.7 Ma for the Tertiary intrusions at Cove.

The Gold Dome, Bay, Cay, and Lighthouse faults contain Eocene dikes ± related sills. The Gold Dome, Bay, and Cay faults belong to subgroup I of the ~NE-striking fault group (refer to Chapter 2 for descriptions). Although it was only exposed in the underground workings in the Cove South Deep orebody, the Omega fault/dike (Fig. 23) also probably belongs to subgroup I. These intrusions helped to localize ore in the lower high-grade sulfide, Cove South Deep, Cove East, and upper high-grade sulfide orebodies, which are associated spatially with QSP alteration of the intrusions and various alteration styles (including dolomitization, decarbonatization, and QSP alteration) in the sedimentary units.

In the Cove open pit, the Bay and Cay dikes are cut and offset by the faults belonging to subgroup II of the ~NE-striking fault group (Chapter 2, Figs. 16 and 17). These later ~NE-striking faults include the Blasthole, Rainbow, and Mackinaw faults. BMVT veins

occur within the faults of subgroup II, and also cut dikes belonging to subgroup I. Larger and banded (multiple-episode) BMVT veins all have QSP altered selvages.

These data have three important implications. First, intrusion along the faults of subgroup I at least slightly pre-dated the mineralizing event. Second, the mineralizing fluid(s) produced associated QSP alteration in both igneous and sedimentary units. And third, the faults belonging to subgroup II were the principal feeder conduits for the ascending fluid(s). The ages of the fresh intrusion and the QSP alteration associated with mineralization are essentially identical within analytical uncertainty, supporting earlier conclusions that the Eocene magmatism and mineralization at Cove occurred simultaneously (Emmons and Eng, 1995).

CHAPTER 6: MICROANALYTICAL STUDIES, A DESCRIPTIVE GENETIC MODEL FOR THE McCOY-COVE SYSTEM, AND IMPLICATIONS FOR OTHER DEPOSITS

INTRODUCTION

The information presented in Chapters 1 through 5 provides a detailed account of the geologic framework of the Cove deposit, which has important implications for other deposits in the Great Basin physiographic province of western North America. The extent of these implications cannot be measured, however, without more detailed studies of the characteristics and source(s) of mineralizing fluids for the Cove deposit, and an assessment of the genetic relations between Cove and McCoy.

The microanalytical data presented here were generated from studies of fluid inclusions in BMVT quartz from Cove, multi-element geochemistry from various ore and host rock suites from Cove, and light stable isotopes from Cove and McCoy. These data are used together with information presented in preceding chapters, and with data from earlier studies by Brooks et al. (1991), Brooks (1994), and Emmons and Eng (1995) to construct a genetic model for the McCoy-Cove system. Implications for other deposits, including classic Carlin-type deposits, are also discussed.

FLUID INCLUSIONS IN BMVT QUARTZ FROM THE COVE DEPOSIT

During petrological analyses of BMVT ore samples, numerous fluid inclusions were observed in hypogene quartz. All of the BMVT samples studied contained clear, euhedral, cockscomb crystals of quartz that occurred as vein linings and/or crustifications

precipitated during the iterative vein stage of BMVT ore deposition. For a single precipitation event, quartz is an early- to middle-vein stage mineral (see Chapter 4; Fig. 30). Problems in assigning quartz to a specific stage of a specific precipitation event occur in samples where a later precipitation event(s) overprints an earlier one. Of the fourteen doubly-polished plates prepared for fluid inclusion analyses, only seven contained fluid inclusions that were large enough to study. Each sample comprises a single episode of precipitation, obviating the overprinting problem. Many of the quartz crystals analyzed contained sparse to minor inclusions of galena, sphalerite, pyrite and/or other mineral phases that could not be positively identified under the microscope.

Care was taken to try to avoid obvious secondary fluid inclusions based on the criteria described by Roedder (1979 and 1984), Shepherd et al. (1985), and Goldstein and Reynolds (1994). Although primary inclusions are best identified by their occurrence in growth zones that mimic the crystal morphology (Goldstein and Reynolds, 1994), the inclusions in growth zones of the Cove samples were generally too small to analyze. The inclusions analyzed were typically larger, isolated, and randomly distributed, and commonly displayed negative crystal shapes, which Goldstein and Reynolds (1994) cited as "inappropriate or ambiguous" lines of evidence for primary fluid inclusions. Nevertheless, the inclusions analyzed had no characteristics of secondary inclusions, which are typically fracture-controlled.

Consideration was also given to the possibility that the inclusions analyzed may have experienced necking down, which could lead to erroneous interpretations of hypogene fluid characteristics. The inclusions studied have fairly consistent liquid:vapor (L:V) ratios (see below), and closely spaced inclusions with variable temperatures of

homogenization (T_H) also have variable salinities. The regular L:V ratios suggest that none of the inclusions analyzed have experienced the degree of necking down that would interfere with interpretation of hypogene fluid data. Also, because multiple daughter inclusions should retain the salinity of the parent inclusion, the variability in the Cove fluid inclusion salinities indicates that each inclusion analyzed formed at a relatively different time under exposure to the hypogene fluid(s).

Table 8 summarizes the T_H, melting temperatures (T_M), and equivalent salinities for the fluid inclusions analyzed for this study. All of the fluid inclusions observed were liquid + vapor types with apparent L:V ratios ranging from 1:1 to 5:1 (Fig. 74). The variation in ratios, however, is due to the generally cylindrical shape of the inclusions and their orientations with respect to the plane of observation. In the planes of the doubly-polished plates, the fluid inclusions were typically elongate, and less commonly equant in apparent outline, and had long dimensions that ranged from ~2 to ~34 micrometers. The true L:V ratios probably have a tighter range of 4:1 to 5:1. No daughter products were observed in any of the inclusions. In all cases but one, the inclusions homogenized to liquid. For the exception, the vapor bubble expanded as it homogenized with the liquid until it filled the vacuole.

Figures 75 and 76 are graphical depictions of the empirical T_H and T_M (salinity) data. The 90 T_H measurements range between ~208°C and ~371°C, and average ~304°C (Table 8, Fig. 75). The range in T_H is variable for a given sample. Figure 76 is a graphical plot of T_H versus salinity. For the entire population of fluid inclusions, T_M ranged from –1.3°C to –4.8°C (-2.7°C average), and calculated salinities ranged from 2.2 to 7.6 (4.5 average) weight percent NaCl equivalent.

TABLE 8. All Cove project fluid inclusion data.

Number	Sample	T homogenization	T melting (actual)	Salinity (wt% NaCl eq)
1	BOTTOMA-1	327.7	-4.3	6.88
2	BOTTOMA-1	326.3	-3.4	5.56
3	BOTTOMA-1	321.6	-3.7	6.01
4	BOTTOMA-1	298.6	-4.0	6.45
5	BOTTOMA-1	329.1	-4.8	7.59
6	BOTTOMA-1	330.3	-3.5	5.71
7	BOTTOMA-1	330.4	-4.2	6.74
8	BOTTOMA-1	330.2	na	na
9	BOTTOMA-1	323.5	na	na
10	BOTTOMA-1	328.9	-3.8	6.16
11	BOTTOMA-1	323.3	-3.4	5.56
12	BOTTOMA-1	321.6	-3.8	6.16
13	BOTTOMA-1	301.4	-2.4	4.03
14	BOTTOMA-1	279.7	-3.7	6.01
15	BOTTOMA-1	302.7	-2.0	3.39
16	BOTTOMA-1	292.7	na	na
17	7/26/98-2B	290.5	-2.1	3.55
18	7/26/98-2B	277.6	-2.1	3.55
19	7/26/98-2B	280.8	-2.0	3.39
20	7/26/98-2B	301.2	na	na
21	7/26/98-2B	320.3	-1.7	2.90
22	7/26/98-2B	296.0	na	na
23	7/26/98-2B	284.9	na	na
24	7/26/98-2B	319.4	na	na
25	7/26/98-2B	304.7	na	na
26	7/26/98-2B	309.8	na	na
27	7/26/98-2B	305.0	na	na
28	7/26/98-2B	249.6	-3.0	4.96
29	7/26/98-2B	270.0	na	na
30	7/26/98-2B	327.0	na	na
31	7/26/98-2B	272.4	na	na
32	7/26/98-2B	278.0	na	na
33	4145E-9	310.5	na	na
34	4145E-9	282.7	na	na
35	4145E-9	290.4	na	na
36	4145E-9	300.9	na	na
37	4145E-9	333.3	na	na
38	4145E-9	299.5	na	na
39	4145E-9	312.3	-2.0	3.39
40	4145E-9	252.5	-1.9	3.23
41	4145E-9	303.3	-1.3	2.24
42	4145E-9	281.6	-1.5	2.57
43	4145E-9	255.5	-1.7	2.90
44	4145E-9	258.0	-2.2	3.71
45	4145E-9	293.9	-2.0	3.39
46	4145E-9	295.9	-2.3	3.87
47	4145E-9	342.7	-2.0	3.39
48	4145E-9	341.9	-1.8	3.06
49	4145E-9	286.6	-2.1	3.55
50	BOTTOMA-2	296.5	na	na
51	BOTTOMA-2	299.2	na	na
52	BOTTOMA-2	333.5	-2.7	4.49
53	BOTTOMA-2	315.9	-4.1	6.59
54	BOTTOMA-2	283.8	-2.1	3.55
55	BOTTOMA-2	281.3	-3.6	5.86
56	BOTTOMA-2	281.4	-3.6	5.86
57	BOTTOMA-2	306.0	-3.0	4.96
58	BOTTOMA-2	297.3	-2.2	3.71
59	BOTTOMA-2	298.2	-3.7	6.01
60	BOTTOMA-2	299.2	-4.1	6.59

TABLE 8. Continued.

Number	Sample	T homogenization	T melting (actual)	Salinity (wt% NaCl eq)
61	BOTTOMA-2	301.6	-1.3	2.24
62	BOTTOMA-2	300.2	-3.1	5.11
63	BOTTOMA-2	299.9	-3.3	5.41
64	BOTTOMA-2	297.1	-4.1	6.59
65	CVC-8-1705	339.4	na	na
66	CVC-8-1705	207.5	na	na
67	CVC-8-1705	273.8	na	na
68	CVC-8-1705	288.0	na	na
69	CVC-8-1705	287.4	na	na
70	CVC-8-2180.5	294.7	-2.8	4.65
71	CVC-8-2180.5	351.9	-2.6	4.34
72	CVC-8-2180.5	294.7	-1.4	2.41
73	CVC-8-2180.5	285.5	-2.9	4.80
74	CVC-8-2180.5	286.8	-2.6	4.34
75	CVC-8-2180.5	296.5	-4.4	7.02
76	CVC-8-2180.5	305.5	-2.3	3.87
77	CVC-8-2180.5	294.8	-1.6	2.74
78	CVC-8-2180.5	254.7	-2.3	3.87
79	CVC-8-2180.5	311.3	-2.0	3.39
80	CVC-8-2180.5	330.5	-2.1	3.55
81	CVC-8-2180.5	363.9	na	na
82	CVC-8-2470.5	327.1	-2.2	3.71
83	CVC-8-2470.5	325.7	-1.8	3.06
84	CVC-8-2470.5	357.0	na	na
85	CVC-8-2470.5	315.7	-1.4	2.41
86	CVC-8-2470.5	329.1	-2.2	3.71
87	CVC-8-2470.5	313.4	-3.2	5.26
88	CVC-8-2470.5	313.4	-1.4	2.41
89	CVC-8-2470.5	370.9	-3.8	6.16
90	CVC-8-2470.5	346.0	na	na
	AVERAGES	**303.9**	**-2.7**	**4.48**

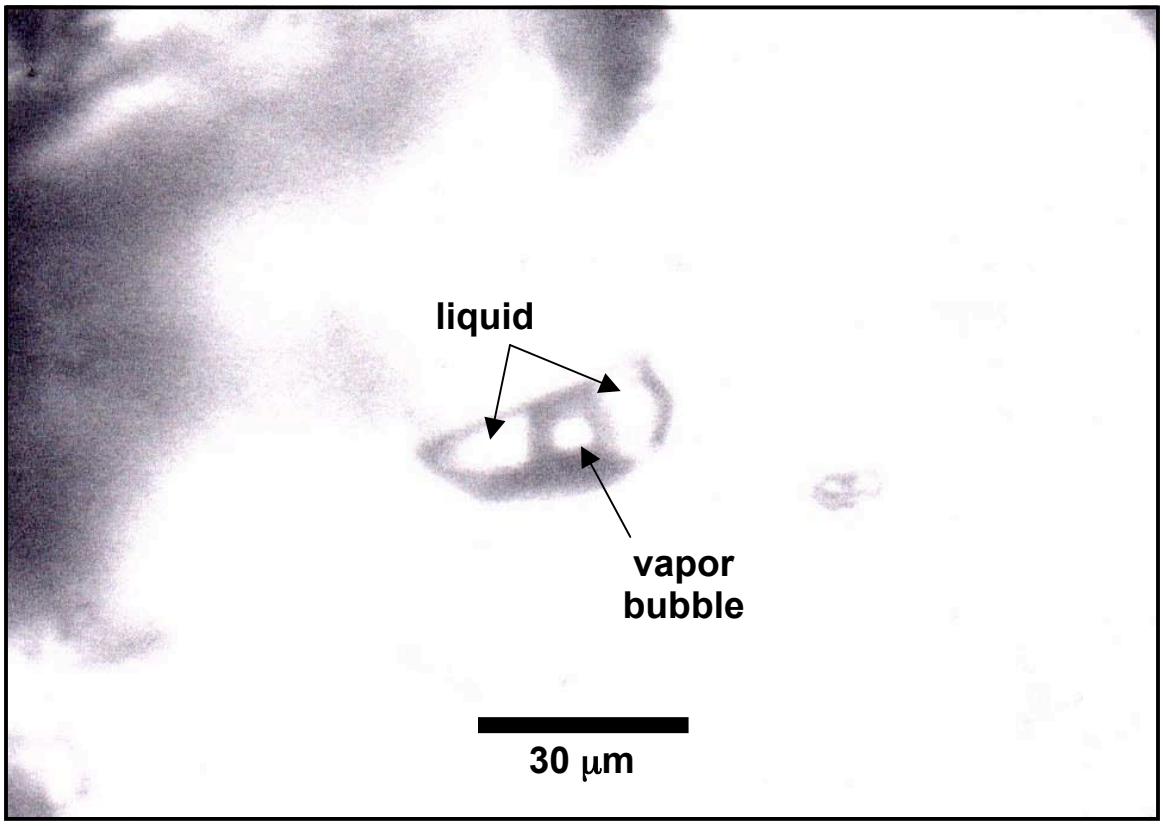

FIG. 74. Photomicrograph of liquid + vapor fluid inclusions in BMVT quartz (transmitted light).

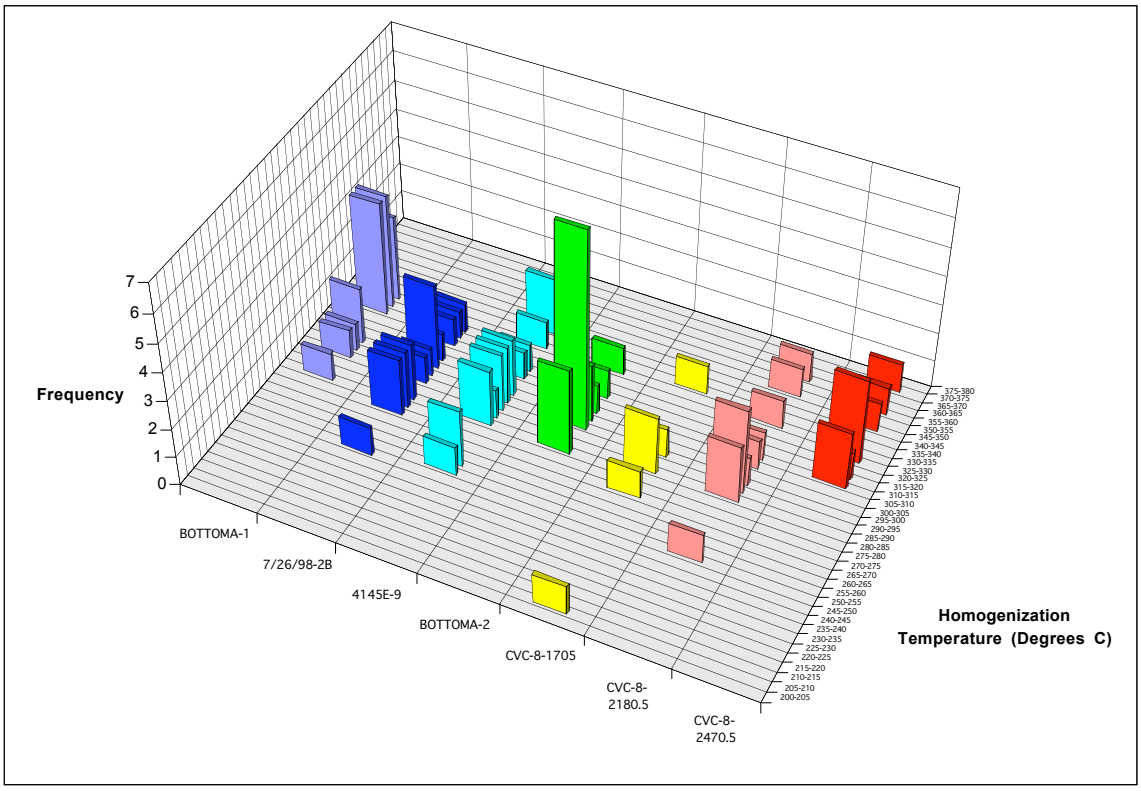

FIG. 75. Frequency distribution for Cove Mine BMVT quartz fluid inclusion T_H.

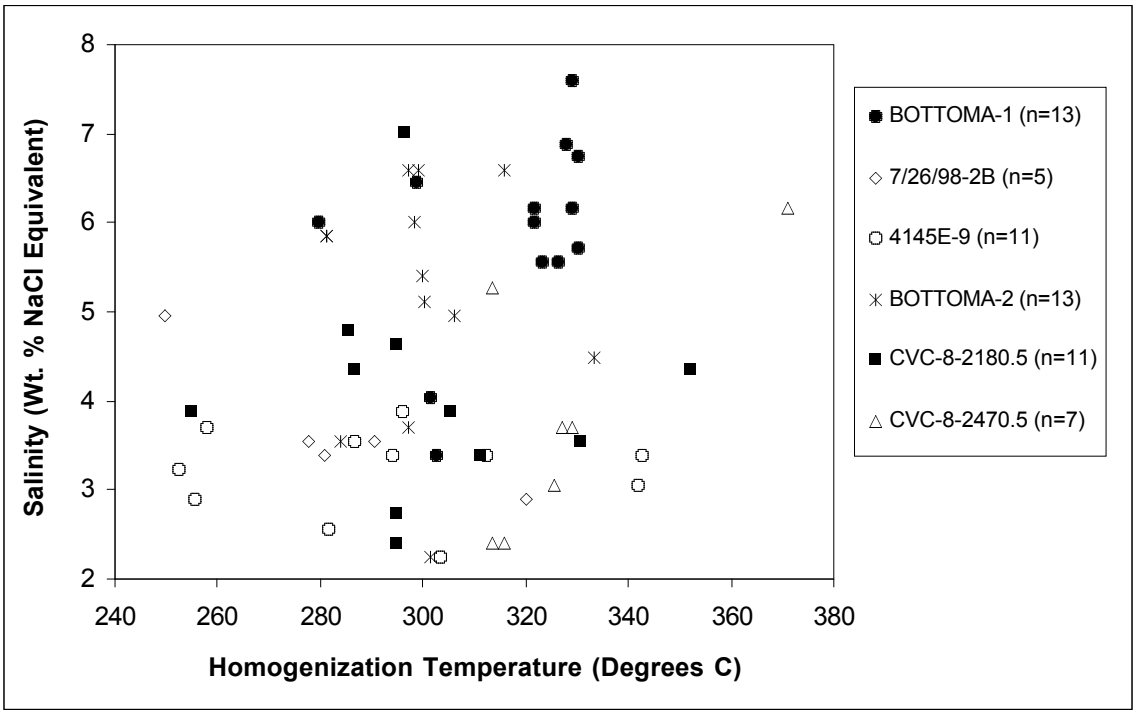

FIG. 76. T_H and salinity data for fluid inclusions from BMVT quartz.

Samples 4145E-9, 7/26/98-2B, BOTTOMA-1, and BOTTOMA-2 were all collected over an elevation range of only ~33 meters. In order of increasing depth, the following T_H averages were calculated: 293°C (4145E-9), 284°C (7/26/98-2B), and 308°C (collective average for BOTTOMA-1 and BOTTOMA-2). The mean of all these samples is 301°C. The samples from drill hole CVC-8 provide evidence for a vertical zonation in T_H. In order of increasing depth, the following T_H averages were calculated: 279°C (CVC-8-1705), 301°C (CVC-8-2180.5), and 328°C (CVC-8-2470.5) (Fig. 75).

No samples suitable for fluid inclusion analyses were found in the Carlin-style ore during the mapping and sampling phase of this study. Therefore, an indirect line of evidence must be used to propose possible temperatures of mineralization for the Carlin-style ore. The BMVT ore occupies the central part of the Cove deposit, and is strongly associated with the principal feeder faults (see Chapter 3). The general range of the minimum temperatures of mineralization for this part of the Cove system is between 250 and 350°C. The Carlin-style ore was precipitated on the margins of the BMVT ore as an outer aureole, in what was probably a relatively cooler environment. Therefore, the T_H measurements can be considered to indicate the maximum temperatures of deposition (uncorrected) for the Carlin-style ore.

Pressure Corrections for Fluid Inclusion Data

An attempt was made to use the "sphalerite geobarometer" as a means of estimating the depth (based on pressure) of the Cove deposit during mineralization (Chapter 4; APPENDIX IV). The geobarometer requires an equilibrium assemblage of sphalerite,

pyrite, and pyrrhotite, and is based on the concentration of Fe in the sphalerite (Barton and Toulmin, 1966; Scott and Barnes, 1971; Vaughan and Craig, 1997). Vaughan and Craig (1997) warn that sphalerite can reequilibrate to lower temperatures, with significant changes in the Fe content. Hutchison and Scott (1980) indicated that sphalerite in contact with pyrrhotite and chalcopyrite is particularly vulnerable to such reequilibration.

In the BMVT sphalerite at Cove, abundant chalcopyrite and less common pyrrhotite occur as blebby inclusions (see Chapter 4). Electron microprobe data indicate a strong inverse correlation between Cu and Fe contents in the BMVT sphalerite (APPENDIX IV). The lack of consistent Fe contents suggests that at least some reequilibration may have occurred, and precludes the use of the barometer to estimate the depth of formation at Cove. Although other data suggest that Cove may have formed at depths as shallow as one kilometer (based on stratigraphic reconstruction and current erosional levels; David L. Emmons, personal communications), they are inconclusive, and are not used here. Consequently, no pressure corrections are used for the T_H, and these should be considered as minimum temperatures for the mineralizing fluid(s).

MAJOR, MINOR, AND TRACE ELEMENT GEOCHEMICAL STUDIES OF THE COVE DEPOSIT

The host rock, ore, and gangue mineral assemblages described in Chapters 2, 4, and 5 can be separated into at least five categories. These categories are BMVT ore, Carlin-style ore, sedimentary host rocks, intrusive host rocks, and hydrothermal alteration assemblages. Each of these categories should have a distinct geochemical signature, based on mineralogy, but significant overlap and/or removal of elements can occur due to

similar mineralogy and/or the effects of alteration. For example, As and Sb occur in BMVT sulfosalts and in realgar, orpiment, and stibnite in Carlin-style ore. Silicon, K, and Al occur in quartz and feldspars in the intrusive rocks, and also in hydrothermal quartz and sericite/illite that is associated with both BMVT and Carlin-style ore. Calcium and Mg in the carbonate host units have commonly been removed by hydrothermal decarbonatization. Therefore, the mineralogy and geologic context are also considered when interpreting the geochemical data.

The five principal categories are used as an initial means of clarifying and interpreting the geochemical data by separating the results based on basic elemental "suites." The basic elemental suites consist of major elements for each of the five categories, and are based on mineralogy (see Chapters 2, 4, and 5). The basic elemental suite for BMVT ore consists of As, Sb, Cd, Cu, Fe, Au, Pb, Ag, Sn, and Zn. The basic elemental suite for Carlin-style ore consists of As, Sb, Fe, Au, and Ag. The basic elemental suite for the sedimentary host rocks is Ca and Mg. The basic elemental suite for the intrusive host rocks is the same as that for the BMVT and Carlin-style gangue, and consists of Al, K, and Si. The following sections add greater detail to the geochemical associations between major elements by analyzing the data for additional correlations with minor and trace elements, and by comparing two geochemical transects across BMVT and Carlin-style parts of the Cove South Deep orebody (see Chapter 3 for description).

Multi-Element Geochemical Correlations

Table 9 is a correlation matrix for the entire geochemical database, consisting of correlations between 22 elements (As, Sb, Ba, Be, Bi, Cd, Co, Cu, Au, Pb, Hg, Mo, Ni, P,

	As	Sb	Ba	Be	Bi	Cd	Co	Cu	Au	Pb	Hg	Mo	Ni	P	Ag	Sr	Tl	Sn	Ti	W	V	Zn
As	1.0000																					
Sb	0.8143	1.0000																				
Ba	-0.2987	-0.3962	1.0000																			
Be	-0.2097	-0.1689	0.2759	1.0000																		
Bi	0.2769	0.3410	-0.2983	0.2304	1.0000																	
Cd	0.5239	0.6441	-0.3575	-0.0427	0.5632	1.0000																
Co	0.1920	0.1221	0.3346	0.1972	0.3274	0.2590	1.0000															
Cu	0.4607	0.6257	-0.3113	-0.0972	0.5527	0.9196	0.3197	1.0000														
Au	0.7240	0.6642	-0.3346	-0.1900	0.1282	0.4243	0.0806	0.3677	1.0000													
Pb	0.4544	0.5808	-0.3707	-0.1583	0.3961	0.9197	0.1636	0.8929	0.4048	1.0000												
Hg	0.5408	0.6114	-0.3759	-0.2901	0.0216	0.3072	-0.1383	0.2690	0.4924	0.2989	1.0000											
Mo	0.2539	0.3526	-0.2938	-0.0226	0.1504	0.2518	-0.1689	0.1961	0.2383	0.2569	0.3783	1.0000										
Ni	0.1505	0.0212	0.2866	0.1014	0.1315	0.0654	0.5708	0.1078	0.0552	0.0028	-0.0730	0.0511	1.0000									
P	0.1018	0.2371	-0.2604	-0.1097	0.1239	0.1596	-0.0475	0.1553	0.1137	0.1634	0.3262	0.3854	-0.0236	1.0000								
Ag	0.6143	0.7956	-0.3067	-0.1352	0.3874	0.8141	0.2557	0.8172	0.5735	0.8111	0.4071	0.2625	0.1330	0.1592	1.0000							
Sr	-0.3965	-0.2296	0.1697	0.0364	-0.1016	-0.2185	-0.1270	-0.1602	-0.3350	-0.2055	-0.0473	0.0699	-0.3131	0.3969	-0.3064	1.0000						
Tl	0.5641	0.5269	-0.1469	0.0049	0.1309	0.1380	0.0119	0.0805	0.4737	0.0413	0.5981	0.2206	-0.0092	0.0777	0.2294	-0.2012	1.0000					
Sn	0.4038	0.4829	-0.3031	-0.1838	0.3402	0.8101	0.2397	0.8246	0.3340	0.8615	0.1326	0.1257	0.0739	0.0109	0.7439	-0.3835	-0.0324	1.0000				
Ti	0.1566	0.0773	0.3401	0.2565	-0.3705	-0.2675	0.0546	-0.3056	0.0909	-0.3082	0.0554	-0.0354	-0.0912	-0.1068	-0.1640	-0.0373	0.3435	-0.2559	1.0000			
W	0.2950	0.3972	-0.2036	0.1413	0.6661	0.6679	0.2756	0.6947	0.1386	0.5859	0.0707	0.1069	0.1310	0.1171	0.5001	-0.1341	0.0061	0.5635	-0.2263	1.0000		
V	0.0059	-0.0601	0.3075	0.2523	-0.2359	-0.1306	0.2017	-0.0835	-0.0411	-0.1096	-0.1192	0.0315	0.2281	0.1443	-0.0836	0.0100	0.0970	-0.0372	0.5493	-0.0116	1.0000	
Zn	0.4261	0.5625	-0.2955	-0.0049	0.5066	0.9629	0.2776	0.9213	0.3635	0.9364	0.2140	0.1849	0.0731	0.0979	0.7982	-0.2260	0.0438	0.8466	-0.2525	0.6643	-0.0724	1.0000

TABLE 9. Correlation matrix for all Cove mine geochemical data. Strong correlations are highlighted in yellow, good correlations are highlighted in green, and weak correlations are highlighted in blue (see text for descriptions of strong, good, and weak correlations).

Ag, Sr, Tl, Sn, Ti, W, V, and Zn) for 201 samples. Of these 201 samples, 50 were collected as a part of the current study, and 151 are composite samples collected from drill holes by site geologists and processed prior to the start of this study. Because the composite samples may produce artificial elemental associations by mixing mineral assemblages that were spatially separated, and also because a more complete data set was produced for the 50 samples analyzed during the current study, a second correlation matrix was constructed using these 50 samples (Table 10). The second matrix consists of correlations between 44 elements (Al, As, Sb, Ba, Be, Bi, Cd, Ca, Ce, Cs, Cr, Co, Cu, F, Ga, Ge, Au, Fe, La, Pb, Li, Mg, Mn, Hg, Mo, Ni, Nb, P, K, Rb, Ag, Na, Sr, Ta, Te, Tl, Th, Sn, Ti, W, U, V, Y, and Zn), and has an advantage over the first correlation matrix in that the associations with ore, gangue, and/or host rocks are known for each of these samples.

Based on the r^2 values in the two matrices, the following positive correlations are considered: 1) < 0.500 = no correlation, 2) 0.500 to 0.699 = weak correlation, 3) 0.700 to 0.799 = good correlation, and 4) 0.800 to 1 = strong correlation. According to these criteria, four principal sets of correlative elements are established. In each set of correlative elements, all element pairs have values of 0.500 or higher. Based on comparisons between the data in Table 10 and the mineral assemblages in the 50 hand sample counterparts, the four principal sets of correlative elements reflect four of the five basic elemental suites described above for BMVT ore, Carlin-style ore, sedimentary host rocks, and intrusive host rocks. The four sets of correlative elements expand the associations for these basic elemental suites, and will be called “elemental suites” in the ensuing text.

	Al	As	Sb	Ba	Be	Bi	Cd	Ca	Ce	Cs	Cr
Al	1.0000										
As	-0.0931	1.0000									
Sb	-0.0800	0.9280	1.0000								
Ba	0.7382	-0.5588	-0.5433	1.0000							
Be	0.8419	-0.3677	-0.3606	0.7690	1.0000						
Bi	0.3469	0.2868	0.3271	0.0965	0.2892	1.0000					
Cd	0.1249	0.7080	0.7946	-0.3518	-0.0966	0.5333	1.0000				
Ca	-0.5544	0.0968	0.0756	-0.5553	-0.5731	-0.6874	-0.1389	1.0000			
Ce	0.8497	-0.2878	-0.3040	0.6533	0.7832	0.2215	-0.0909	-0.4944	1.0000		
Cs	0.7372	0.0287	0.0813	0.6060	0.6188	0.4851	0.1755	-0.6690	0.5666	1.0000	
Cr	0.6843	0.2318	0.2476	0.4452	0.5392	0.7422	0.3612	-0.8149	0.5694	0.7273	1.0000
Co	0.7681	0.0309	0.0249	0.5650	0.6632	0.5095	0.1548	-0.6316	0.6467	0.7225	0.7272
Cu	0.1663	0.7383	0.8404	-0.3054	-0.1139	0.5797	0.8985	-0.2103	-0.0408	0.2525	0.4765
F	0.7080	0.3513	0.3358	0.2261	0.4312	0.2777	0.3595	-0.1941	0.6464	0.5455	0.5420
Ga	0.9520	0.0782	0.1205	0.6236	0.7738	0.5227	0.3608	-0.6175	0.7543	0.7924	0.7686
Ge	0.6854	-0.3110	-0.2580	0.6622	0.7416	0.5699	0.1053	-0.8109	0.5974	0.6539	0.6878
Au	-0.2203	0.7932	0.8311	-0.5903	-0.4973	0.0628	0.6443	0.2094	-0.3496	-0.1256	-0.0253
Fe	0.5976	0.4343	0.4654	0.1992	0.4137	0.8045	0.6805	-0.6388	0.3714	0.6064	0.7935
La	0.9404	-0.2136	-0.2107	0.8077	0.8467	0.2976	-0.0133	-0.6090	0.8931	0.7310	0.6865
Pb	-0.0006	0.7932	0.8697	-0.4816	-0.2261	0.4539	0.9411	0.0157	-0.2431	0.0395	0.2271
Li	0.6768	-0.0189	0.0071	0.3510	0.5076	-0.0937	0.0778	0.0066	0.5355	0.2396	0.1499
Mg	-0.6138	0.0398	0.0107	-0.5472	-0.5887	-0.7398	-0.2593	0.9530	-0.5094	-0.6637	-0.8269
Mn	-0.4698	0.4537	0.4517	-0.5920	-0.6185	-0.5209	0.2074	0.8325	-0.5575	-0.5395	-0.5741
Hg	-0.2887	0.7328	0.7480	-0.5853	-0.5254	0.0355	0.4854	0.2094	-0.4618	-0.1230	-0.0326
Mo	-0.3851	0.3600	0.3306	-0.5583	-0.4685	-0.1690	0.1557	0.5150	-0.4004	-0.4913	-0.3068
Ni	0.2590	0.1101	0.1094	0.2367	0.2643	0.2799	-0.0835	-0.3863	0.2303	0.4862	0.5245
Nb	0.9443	-0.0731	-0.1033	0.7047	0.8025	0.2884	0.0402	-0.5528	0.8448	0.6927	0.6714
P	0.1628	0.5594	0.5327	-0.2369	-0.1652	-0.1316	0.3746	0.3991	0.0789	-0.0108	-0.0072
K	0.6764	-0.4916	-0.4180	0.8052	0.6852	0.2257	-0.1720	-0.5760	0.6685	0.7832	0.4921
Rb	0.7051	-0.3983	-0.3219	0.7843	0.6774	0.2557	-0.1041	-0.5874	0.6624	0.8479	0.5382
Ag	-0.0359	0.8172	0.8879	-0.4785	-0.2655	0.4381	0.8466	-0.0325	-0.2133	0.0652	0.3069
Na	0.5763	-0.5718	-0.4792	0.5885	0.6134	0.2012	-0.1083	-0.3694	0.6495	0.2727	0.2377
Sr	0.2095	-0.4369	-0.4024	0.3679	0.1559	-0.3949	-0.2677	0.2905	0.2656	-0.0985	-0.1993
Ta	0.6702	-0.4412	-0.4143	0.6847	0.7880	0.5256	-0.0423	-0.7566	0.7115	0.6358	0.6180
Te	-0.1785	0.3426	0.3636	-0.2073	-0.0820	0.5745	0.4956	-0.3618	-0.3248	0.0511	0.2650
Tl	0.0818	0.4696	0.5131	-0.1535	-0.1304	0.3276	0.4406	-0.2209	-0.1515	0.2571	0.2537
Th	0.9208	-0.1296	-0.1474	0.7393	0.7837	0.2002	-0.0658	-0.4880	0.7856	0.6745	0.5684
Sn	0.0935	0.7764	0.8268	-0.3957	-0.1663	0.4510	0.8425	-0.0886	-0.0827	0.1149	0.3568
Ti	0.9629	-0.0498	-0.0672	0.6993	0.8432	0.3758	0.1383	-0.5903	0.8602	0.7172	0.7299
W	0.5507	0.5926	0.6066	0.0492	0.3456	0.5550	0.6876	-0.3691	0.3098	0.4094	0.6473
U	0.5298	0.5172	0.5036	0.0385	0.2681	0.2009	0.4512	-0.0393	0.3410	0.2748	0.3879
V	0.8608	0.0939	0.0236	0.5605	0.7404	0.3351	0.1838	-0.5105	0.8295	0.6292	0.6990
Y	0.8276	-0.0085	-0.0433	0.5464	0.6067	0.0557	-0.0066	-0.2236	0.8032	0.5784	0.4896
Zn	0.2612	0.6214	0.7159	-0.2259	0.0626	0.6054	0.9678	-0.2533	0.0549	0.2629	0.4725

TABLE 10. Correlation matrix for geochemical data produced exclusively for the current study (see Table 9 for color key).

	Co	Cu	F	Ga	Ge	Au	Fe	La	Pb	Li	Mg
Al											
As											
Sb											
Ba											
Be											
Bi											
Cd											
Ca											
Ce											
Cs											
Cr											
Co	1.0000										
Cu	0.2488	1.0000									
F	0.4435	0.4059	1.0000								
Ga	0.7599	0.3901	0.7223	1.0000							
Ge	0.5532	0.1393	0.2746	0.7236	1.0000						
Au	-0.1688	0.6459	0.1349	-0.0491	-0.3849	1.0000					
Fe	0.6993	0.7225	0.4629	0.7745	0.5677	0.2694	1.0000				
La	0.7437	0.0449	0.6646	0.8774	0.7172	-0.3416	0.5040	1.0000			
Pb	0.0384	0.8797	0.3014	0.2366	-0.0842	0.7432	0.6111	-0.1485	1.0000		
Li	0.2993	0.0701	0.6134	0.5843	0.2755	-0.0162	0.1799	0.5936	0.0673	1.0000	
Mg	-0.6769	-0.3305	-0.2422	-0.7071	-0.8145	0.1539	-0.7672	-0.6371	-0.1231	-0.0616	1.0000
Mn	-0.5157	0.1589	-0.0786	-0.4343	-0.7781	0.5545	-0.3164	-0.5679	0.3648	0.0413	0.7509
Hg	-0.2713	0.4989	0.0408	-0.1610	-0.3596	0.7664	0.1273	-0.3957	0.5760	-0.1363	0.2161
Mo	-0.6285	0.1212	0.0231	-0.3508	-0.4239	0.3636	-0.2313	-0.4603	0.3113	-0.0495	0.4664
Ni	0.2914	0.0043	0.3061	0.2376	0.2719	-0.1241	0.1389	0.3215	-0.1464	-0.0786	-0.2359
Nb	0.7819	0.1259	0.6737	0.8720	0.5921	-0.2514	0.5443	0.9041	-0.0773	0.6056	-0.5958
P	-0.1006	0.3743	0.6962	0.1938	-0.3298	0.4597	0.0658	0.0942	0.4548	0.4311	0.3109
K	0.6362	-0.1339	0.2764	0.6364	0.6831	-0.4621	0.3143	0.7305	-0.3567	0.1995	-0.5555
Rb	0.6635	-0.0630	0.3407	0.6827	0.6714	-0.3959	0.3657	0.7412	-0.2855	0.2135	-0.5704
Ag	0.1291	0.8945	0.2477	0.1799	-0.1182	0.7664	0.6068	-0.1671	0.8872	-0.1007	-0.1211
Na	0.3805	-0.1336	0.2053	0.5248	0.6147	-0.4206	0.2284	0.5920	-0.2163	0.4192	-0.4110
Sr	-0.0165	-0.2634	0.0276	0.0969	-0.0224	-0.2554	-0.2345	0.2326	-0.2704	0.2709	0.2118
Ta	0.6271	-0.0384	0.2518	0.6719	0.8910	-0.5119	0.4934	0.7245	-0.2378	0.1608	-0.7429
Te	-0.0254	0.4340	-0.2108	0.0619	0.2315	0.2861	0.4975	-0.1840	0.5023	-0.3637	-0.4384
Tl	0.0990	0.4840	0.0483	0.2220	0.1563	0.5479	0.4426	-0.0237	0.4477	-0.0158	-0.2487
Th	0.7060	0.0068	0.6057	0.8170	0.5241	-0.2849	0.4259	0.8540	-0.1589	0.6288	-0.5132
Sn	0.1758	0.8671	0.4005	0.3025	-0.0582	0.6740	0.6496	-0.0374	0.8714	0.0745	-0.2111
Ti	0.7894	0.1908	0.7140	0.9236	0.6801	-0.2382	0.6180	0.9378	0.0032	0.6064	-0.6418
W	0.3607	0.6987	0.6987	0.6978	0.3799	0.4088	0.7521	0.4463	0.6680	0.4537	-0.4625
U	0.2817	0.4521	0.7446	0.5805	0.0948	0.3857	0.4759	0.4209	0.5133	0.5825	-0.1217
V	0.6930	0.2320	0.7290	0.8404	0.6015	-0.0844	0.5896	0.8551	0.0600	0.5336	-0.5527
Y	0.5811	0.0515	0.8488	0.7237	0.3557	-0.1899	0.2912	0.8288	-0.1048	0.6758	-0.2483
Zn	0.2883	0.8787	0.4008	0.4866	0.2447	0.5594	0.7718	0.1255	0.8879	0.1410	-0.3819

TABLE 10. Continued.

	Mn	*Hg*	*Mo*	*Ni*	*Nb*	*P*	*K*	*Rb*	*Ag*	*Na*	*Sr*
Al											
As											
Sb											
Ba											
Be											
Bi											
Cd											
Ca											
Ce											
Cs											
Cr											
Co											
Cu											
F											
Ga											
Ge											
Au											
Fe											
La											
Pb											
Li											
Mg											
Mn	1.0000										
Hg	0.4430	1.0000									
Mo	0.4835	0.5354	1.0000								
Ni	-0.3904	0.0600	0.0022	1.0000							
Nb	-0.4542	-0.3265	-0.4367	0.2659	1.0000						
P	0.5105	0.3824	0.4945	0.0024	0.1130	1.0000					
K	-0.6324	-0.5504	-0.6972	0.2588	0.6162	-0.3014	1.0000				
Rb	-0.6103	-0.4718	-0.6717	0.3012	0.6433	-0.2223	0.9881	1.0000			
Ag	0.3418	0.6059	0.2277	-0.0051	-0.0509	0.3427	-0.3093	-0.2456	1.0000		
Na	-0.5458	-0.5536	-0.3820	-0.1210	0.4437	-0.1791	0.6095	0.5601	-0.3182	1.0000	
Sr	0.1140	-0.3110	0.0044	-0.2706	0.1409	0.1345	0.2395	0.2102	-0.3078	0.4661	1.0000
Ta	-0.8448	-0.5340	-0.5489	0.2776	0.6111	-0.4118	0.7894	0.7585	-0.2243	0.7141	0.0420
Te	-0.0574	0.2261	0.0085	-0.0964	-0.1985	-0.2401	-0.1528	-0.1447	0.4363	-0.1909	-0.5266
Tl	0.0076	0.7149	0.2376	0.1810	-0.0054	0.1087	-0.1070	-0.0425	0.4757	-0.1458	-0.2765
Th	-0.4193	-0.3168	-0.3860	0.2908	0.9516	0.1238	0.5893	0.6264	-0.1487	0.4061	0.1567
Sn	0.3188	0.4617	0.1670	-0.1360	0.0903	0.4451	-0.2639	-0.1966	0.8544	-0.2592	-0.3230
Ti	-0.4953	-0.3222	-0.4226	0.2859	0.9651	0.1299	0.6429	0.6674	-0.0067	0.4984	0.1528
W	-0.0008	0.3113	0.1255	0.2194	0.4886	0.4474	0.0121	0.0704	0.5834	0.0584	-0.2476
U	0.1619	0.2776	0.3255	0.2428	0.4616	0.6987	-0.0567	0.0169	0.4229	0.0484	0.0191
V	-0.3916	-0.1774	-0.2590	0.3093	0.8446	0.2363	0.5026	0.5363	0.1004	0.4033	0.1740
Y	-0.2347	-0.2208	-0.1855	0.3316	0.8271	0.4909	0.4842	0.5288	-0.1045	0.3504	0.2995
Zn	0.0773	0.3590	0.0475	-0.0299	0.1721	0.3028	-0.0361	0.0236	0.8010	0.0325	-0.2424

TABLE 10. Continued.

	Ta	Te	Tl	Th	Sn	Ti	W	U	V	Y	Zn
Al											
As											
Sb											
Ba											
Be											
Bi											
Cd											
Ca											
Ce											
Cs											
Cr											
Co											
Cu											
F											
Ga											
Ge											
Au											
Fe											
La											
Pb											
Li											
Mg											
Mn											
Hg											
Mo											
Ni											
Nb											
P											
K											
Rb											
Ag											
Na											
Sr											
Ta	1.0000										
Te	0.1042	1.0000									
Tl	0.0037	0.3438	1.0000								
Th	0.5260	-0.2791	0.0169	1.0000							
Sn	-0.1705	0.4579	0.3192	-0.0186	1.0000						
Ti	0.6895	-0.1265	0.0050	0.8878	0.1371	1.0000					
W	0.2050	0.3906	0.3828	0.3918	0.6926	0.5670	1.0000				
U	-0.0310	-0.0643	0.2341	0.4533	0.4949	0.5028	0.7360	1.0000			
V	0.5814	-0.1243	0.0714	0.7655	0.1604	0.9024	0.5944	0.5557	1.0000		
Y	0.3753	-0.4890	-0.0836	0.8053	0.0153	0.8256	0.3994	0.5701	0.8073	1.0000	
Zn	0.1201	0.4896	0.4180	0.0506	0.8142	0.2754	0.7224	0.4873	0.2797	0.0721	1.0000

TABLE 10. Continued.

The first and second elemental suites are (Cd-Cu-Fe-Pb-Ag-Sn-W-Zn ± As, Sb, Bi, Hg, Te, U, and Au), and (As-Sb-Au-Hg-Ag ± Tl), and represent BMVT ore and Carlin-style ore, respectively. The "±" designation is used for elements that have r^2 values of 0.500 or higher with at least some, but not all of the other elements in the suite. Elements that fall into the "±" designation commonly are associated with more than one elemental suite. For example, As, Sb, Au, and Hg are associated with both BMVT and Carlin-style ore, but As, Sb, Au, and Hg fall under the "±" designation for the BMVT ore. In general, the first two elemental suites were identified in both correlation matrices (Tables 9 and 10). These suites correspond well with the mineralogy of BMVT and Carlin-style ore discussed in Chapter 4.

The third elemental suite consists of (Ca-Mg-Mn), and was identified only in the second correlation matrix (Table 10). This elemental suite represents the carbonate host rocks at Cove. It is not clear whether the Mn is a primary component of the rocks, or if it is a product of Mn-alteration. The fourth elemental suite is weakly expressed in Table 9 as (Co-Ni) and (Ti-V) correlations. In Table 10, however, this elemental suite is greatly expanded to (Al-Ba-Be-Ce-Cs-Co-Ga-Ge-La-Nb-Rb-Ta-Th-Ti-V ± Bi, Cr, F, Fe, Li, K, Na, W, U, and Y). This elemental suite represents the intrusive rocks at Cove, but Al and K in non-intrusive rocks may be indicative of hydrothermal sericite/illite. It is important to note here that none of the samples used to generate Table 10 were analyzed for Si.

Geochemical Transects

Figure 77 shows the location of two geochemical transects collected across parts of the Cove South Deep (CSD) orebody. One transect was collected as drill core composites from the Carlin-style portion of the CSD orebody (hole CVC-218), and the other transect was collected as grab samples (CU-series) from a manto-like BMVT vein exposed in the south rib of a major access tunnel to the CSD orebody (Fig. 78).

Figure 79 shows geochemical data collected across 80 vertical feet (~24 meters) of an exploration drill core (CVC-218) that intersected the Carlin-style portion of the CSD orebody. The host rock is dolostone of the Home Station Member, which has been intruded by a dike and decarbonatized and brecciated to varying degrees in the vicinity of the orebody. The scales for the different elements are adjusted to normalize the actual concentrations for the different elements. The elemental suites identified in the correlation matrices (Tables 9 and 10) are the bases for the different transect plots shown in Figure 79.

Figure 79A shows the concentrations of the BMVT elemental suite (Cd-Cu-Fe-Pb-Ag-Sn-W-Zn ± As, Sb, Bi, Hg, Te, U, and Au). The samples collected from CVC-218 were not analyzed for Fe, Te, or U. Bi and W concentrations were below the detection limits. All of the Sn values except for one (61 ppm for the 246.9 to 247.4-meter interval) were also below the detection limit. Therefore, Bi, Fe, Te, Sn, W, and U are not plotted in Figure 79A. Also, Au and Hg are shown in Figure 79B to keep Figure 79A more legible. The peak concentrations for Sb, Cd, Cu, Pb, Sn (not shown), and Zn are all in the 246.9 to 247.4-meter interval (Fig. 79A).

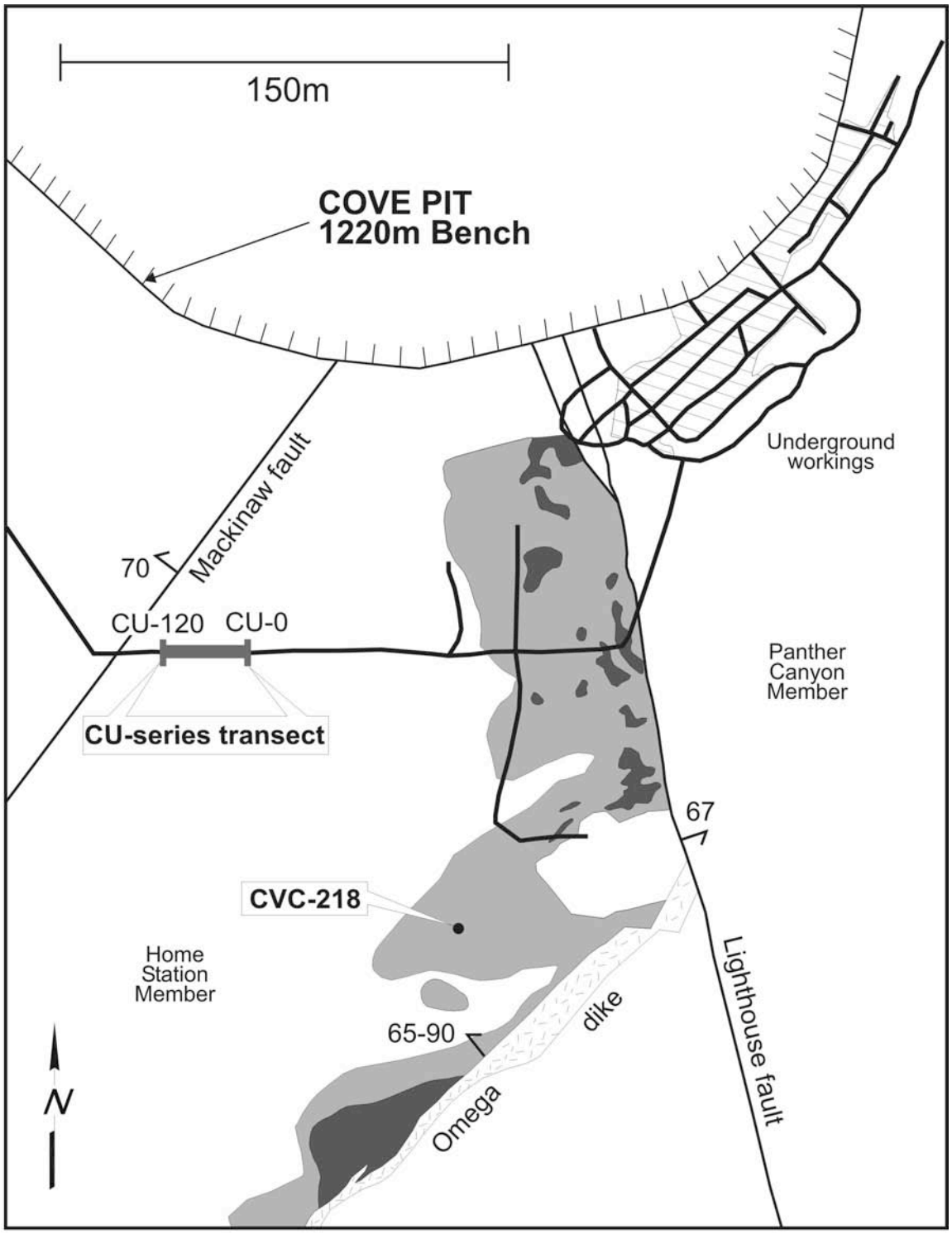

FIG. 77. Locations of the two geochemical transects (refer to Fig. 23 for key).

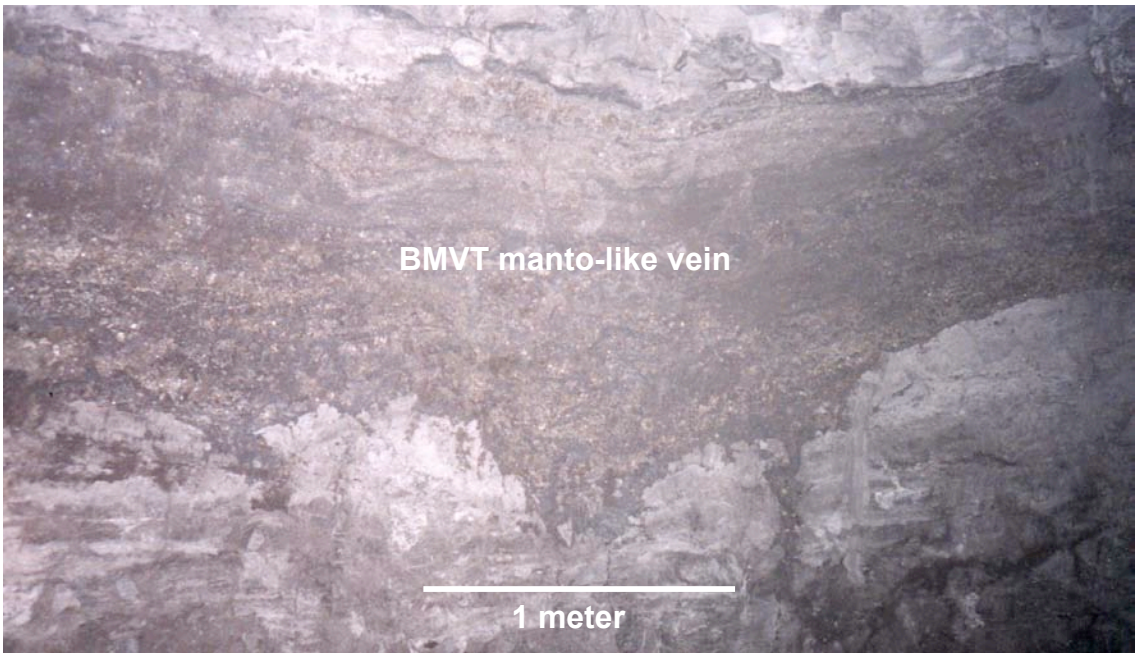

FIG. 78. Manto-like BMVT vein in the Cove South Deep orebody.

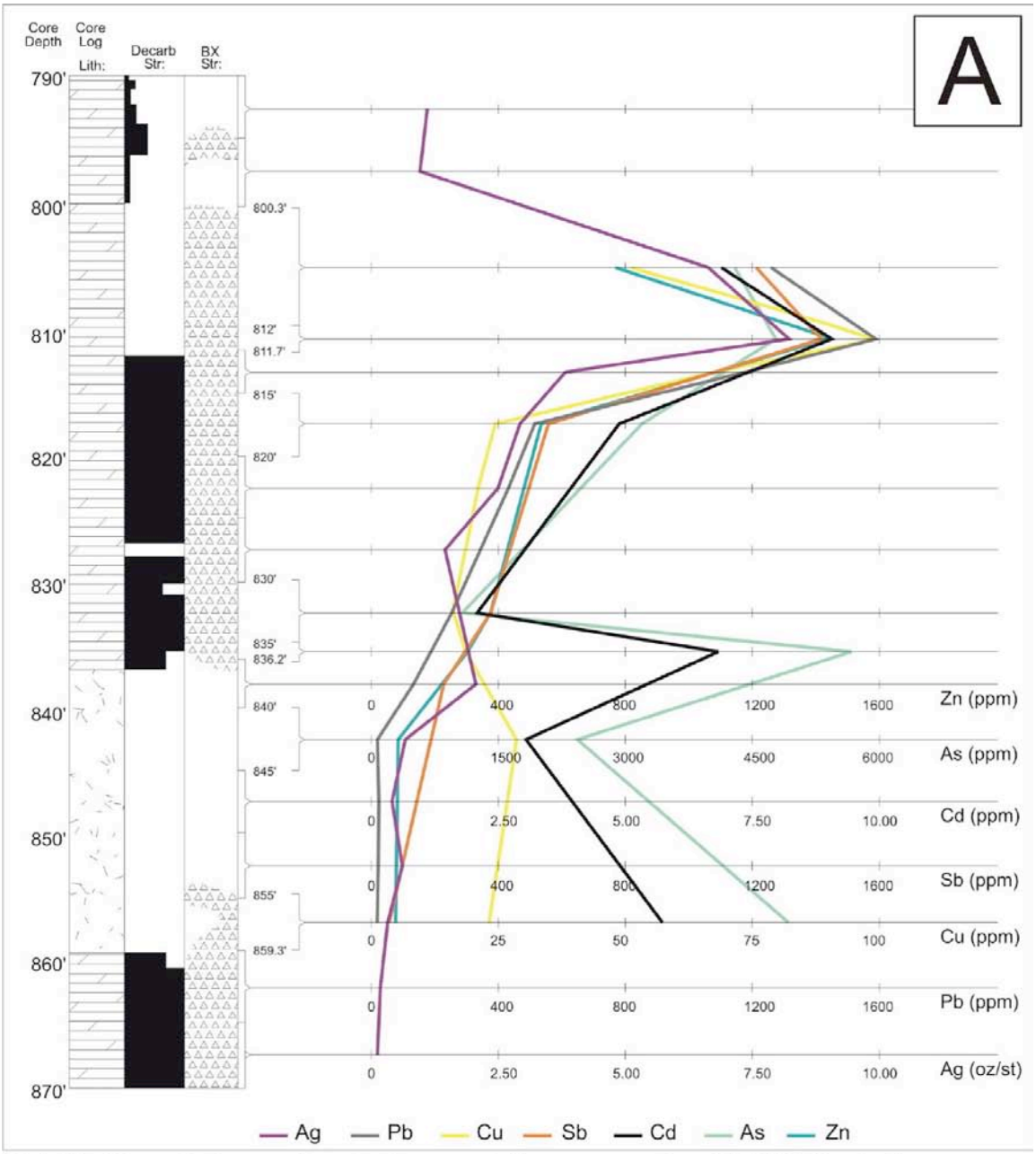

FIG. 79. Downhole geochemical transect for core number CVC-218. A shows concentrations of BMVT ore indicators (As, Sb, Cd, Cu, Pb, Ag, and Zn). B shows concentrations of Carlin-style ore indicators (As, Sb, Au, Hg, and Ag). C shows concentrations of alteration indicators (Al, Ca, Mg, K, and SiO_2). The three graphic logs shown on the left are digitized from the actual core logs, and show lithology (Core Log Lith) and the relative strengths of the effects of decarbonatization (Decarb Str) and brecciation (BX Str). The host unit is the Home Station Member, with dolostone shown as a diagonal brick pattern in the lithology column, and silty dolostone as the same with small dots. A dike occurs in the interval from 255 to 262 meters, and is shown as small random line segments.

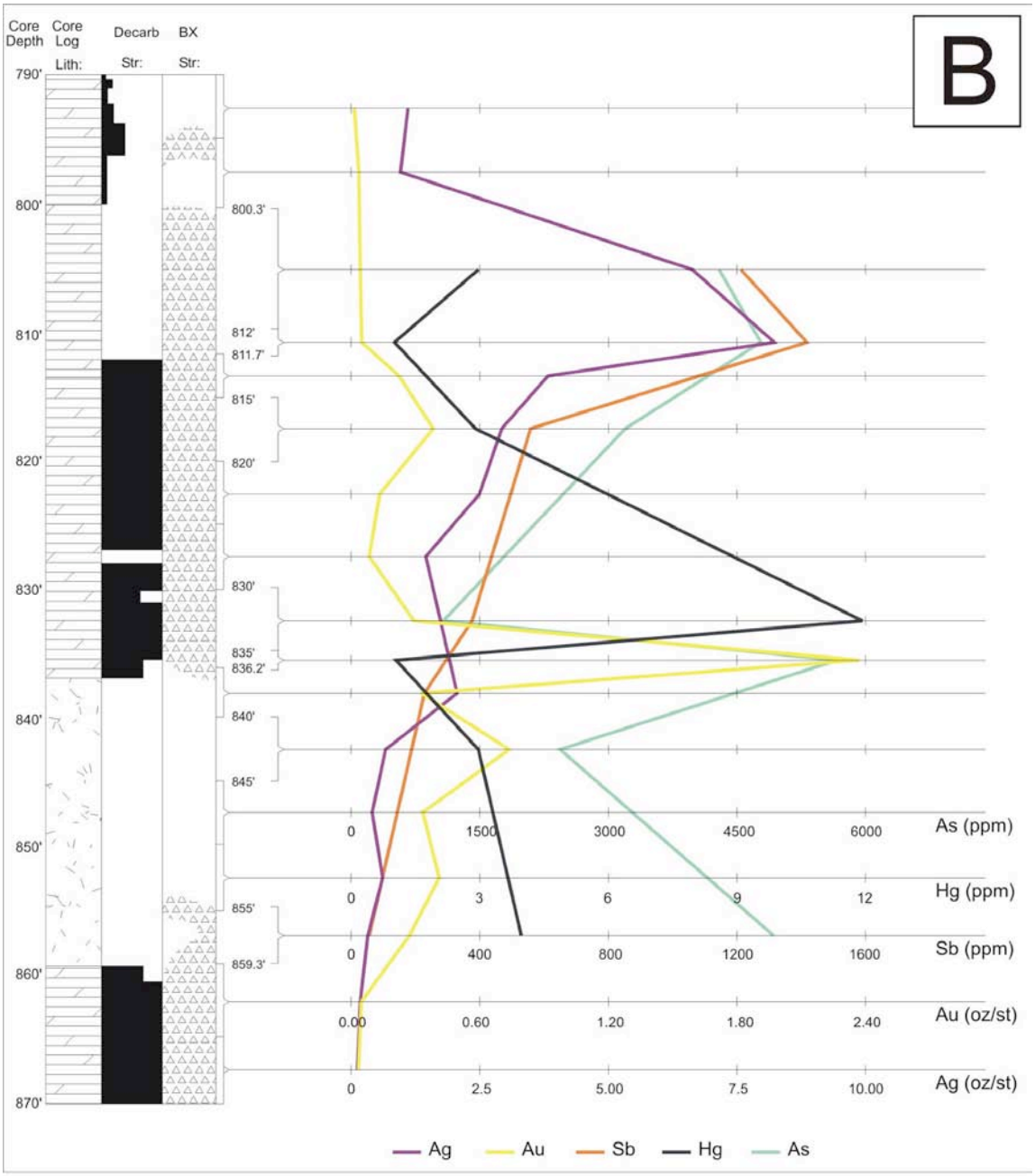

FIG. 79. Continued

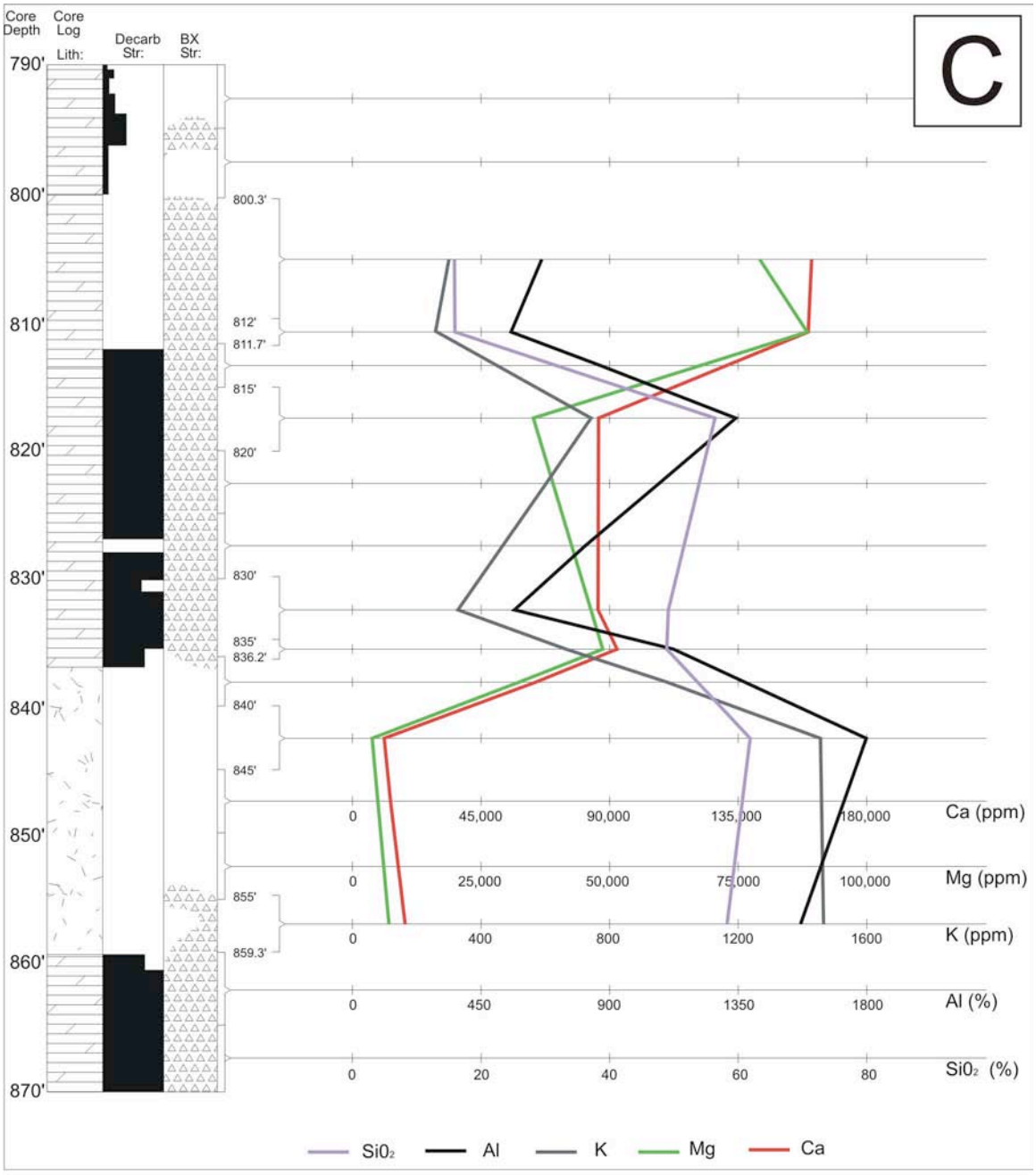

FIG. 79. Continued

Figure 79B shows the concentrations of the Carlin-style suite (As-Sb-Au-Hg-Ag ± Tl). All of the Tl values are below the detection limit for these samples, so it is not shown. The peak concentrations for As and Au occur in the 254.5 to 254.9-meter interval, and the peak concetration for Hg occurs in the 252.9 to 254.5-meter interval (Fig. 79B), and these elements correspond with Carlin-style ore in the CVC-218 transect (based on observations of the core).

Figure 79C shows the elemental suite for the carbonate host rocks (Ca-Mg), and part of the elemental suite for intrusive rocks that also corresponds to quartz-sericite/illite alteration (Al-K-Si). Ca and Mg have peak values in the 243.9 to 246.9-meter and 246.9 to 247.4-meter intervals, respectively. Their concentrations drop off significantly with depth, corresponding well with increased decarbonatization. It is interesting that the 243.9 to 247.4-meter interval has the highest Ca and Mg values and no apparent decarbonatization, considering that this interval also has the highest concentrations of BMVT suite elements. Al, K, and Si are plotted as indicators of the presence of intrusive rock and/or sericitic/illitic alteration. All three of these indicators have peak values in the Eocene dike.

Al, K, and Si also have subordinate peak alteration values in the 248.4 to 249.9-meter interval, possibly corresponding to sericite/illite associated with the overlying concentration of BMVT suite elements in the 243.9 to 247.4-meter interval. Si also has relatively high values in the 243.9 to 254.9-meter range, corresponding to the peak values for the Carlin-suite elements As, Au, and Hg. The drop in the Al and K values in the 243.9 to 254.5-meter range suggests that the Si peak in this range indicates silicification, and not sericitic/illitic alteration.

The second geochemical transect was collected across a large, manto-like body comprising BMVT sulfides (Fig. 80). The different sample numbers correspond to different footages along the 120-foot-long (~37 meter) transect. In general, Figure 80 shows the same geochemical associations observed in Figure 79. The principal difference between the two transects is the magnitudes of the concentrations of the BMVT and Carlin-style elemental suites.

Figure 80A shows the BMVT elemental suite. All of the values for Te but four were below the detection limit, so Te is not shown in Figure 80A. Hg and Tl are shown in the Carlin-style elemental suite (Fig. 80B). The highest peak concentrations for As, Sb, Bi, Cd, Cu, Fe, Pb, Ag, Sn, W, U, and Zn are in the general range of CU-60 to CU-95. Gold is more complicated; it shows peaks clearly associated with the other BMVT element peaks, but shows additional peaks (especially at CU-110) not obviously associated with the BMVT elements. The Au peak at CU-110 is associated with the peaks for Hg and Tl, possibly indicating a zone of Carlin-style ore.

Figure 80C shows the elemental suite for the carbonate host rocks (Ca-Mg), and part of the elemental suite for intrusive rocks that also corresponds to sericitic/illitic alteration (Al-K). The samples were not analyzed for Si, preventing the recognition of any silicification outboard of the ore zone. In general, there is an inverse relationship between carbonate-related elements (Ca-Mg) and elements associated with hydrothermal sericite/illite (Al-K), which indicates that decarbonatization and sericitic/illitic alteration are both associated with the BMVT manto-like body. This inference is corroborated by the observance of abundant sericite/illite during the collection of the CU-series samples in the manto-like zone.

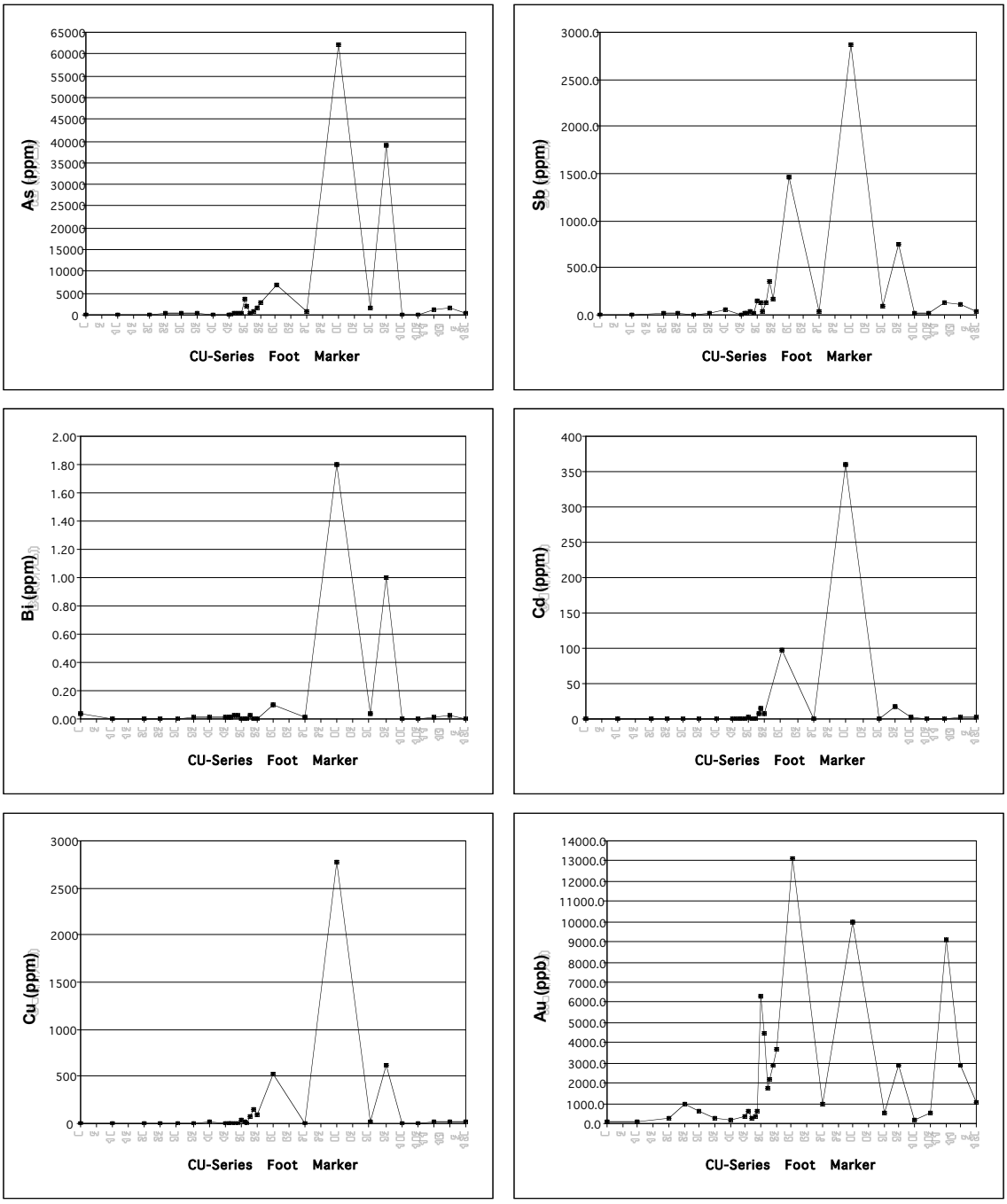

FIG. 80. Geochemical transect across a BMVT manto-like vein. A. BMVT ore indicators (As, Sb, Bi, Cd, Cu, Au, Fe, Pb, Ag, Sn, W, U, and Zn) from the underground geochemical transect. Note: because samples are labeled based on their footage along the transect, feet are used as the units for the x-axis.

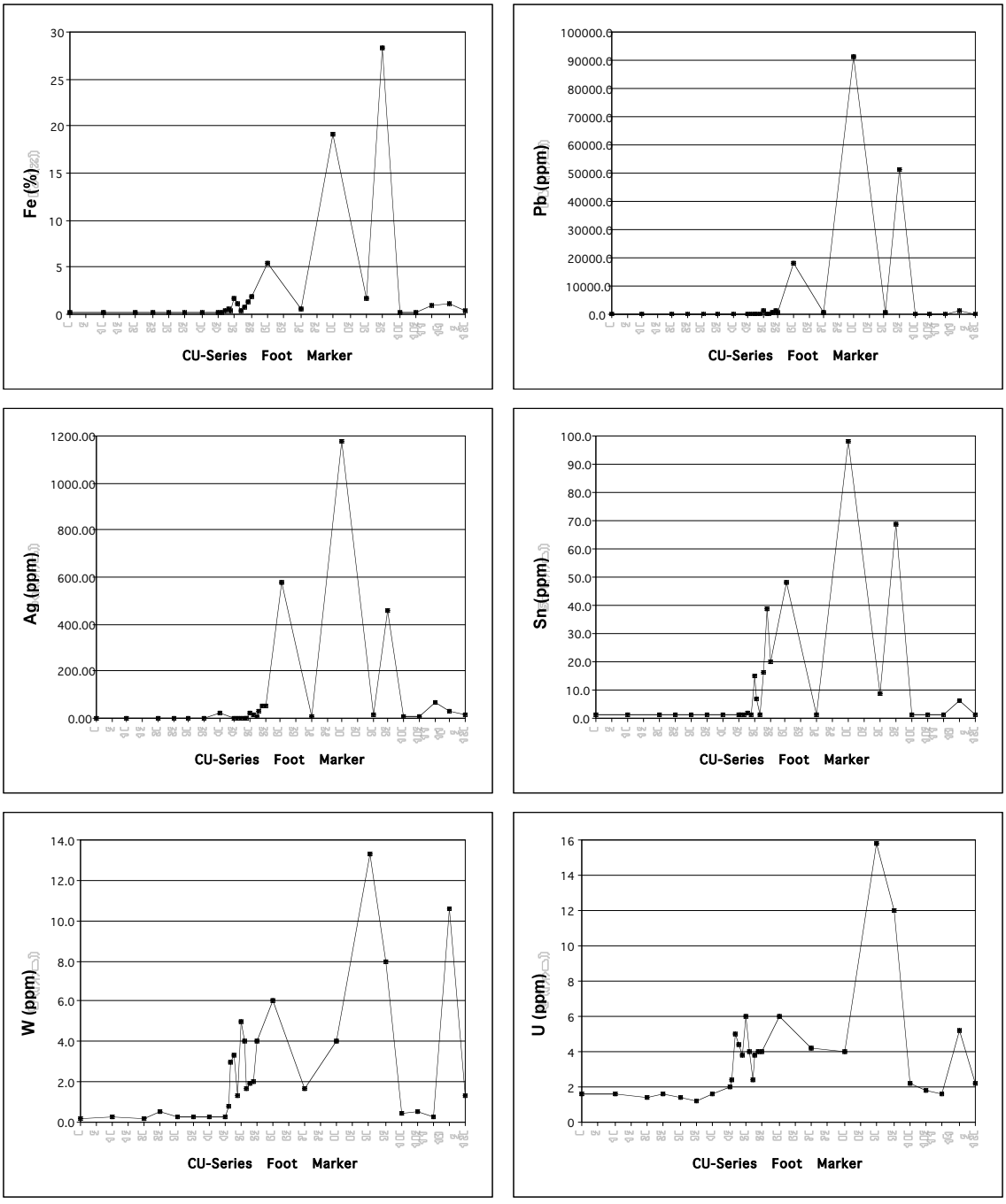

FIG. 80A. BMVT ore indicators (continued).

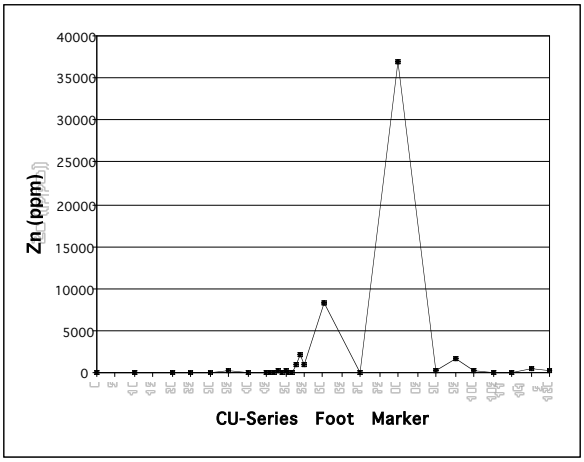

FIG. 80A. BMVT ore indicators (continued).

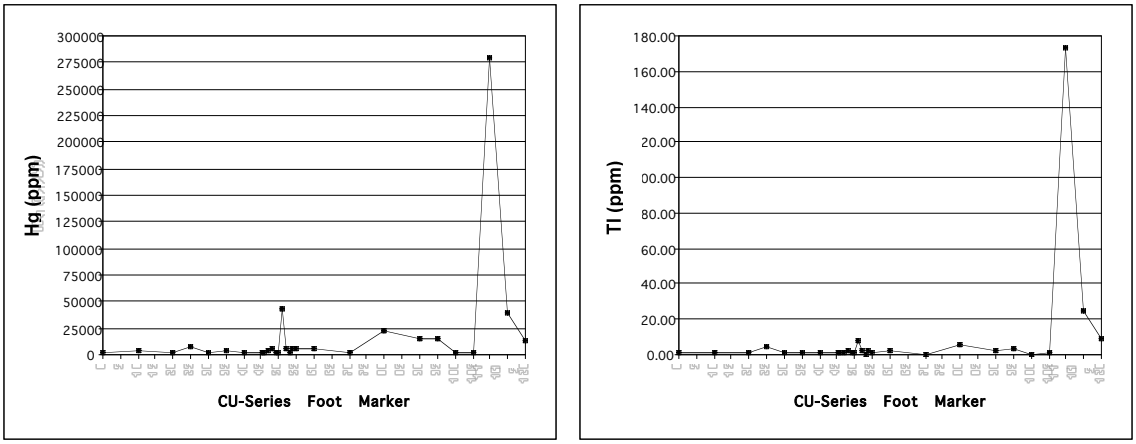

FIG. 80B. Carlin-style ore indicators (As, Sb, Au, Hg, Ag, and Tl) from the underground geochemical transect. Refer to Figure 80A for As, Sb, and Ag. Note: because samples are labeled based on their footage along the transect, feet are used as the units for the x-axis.

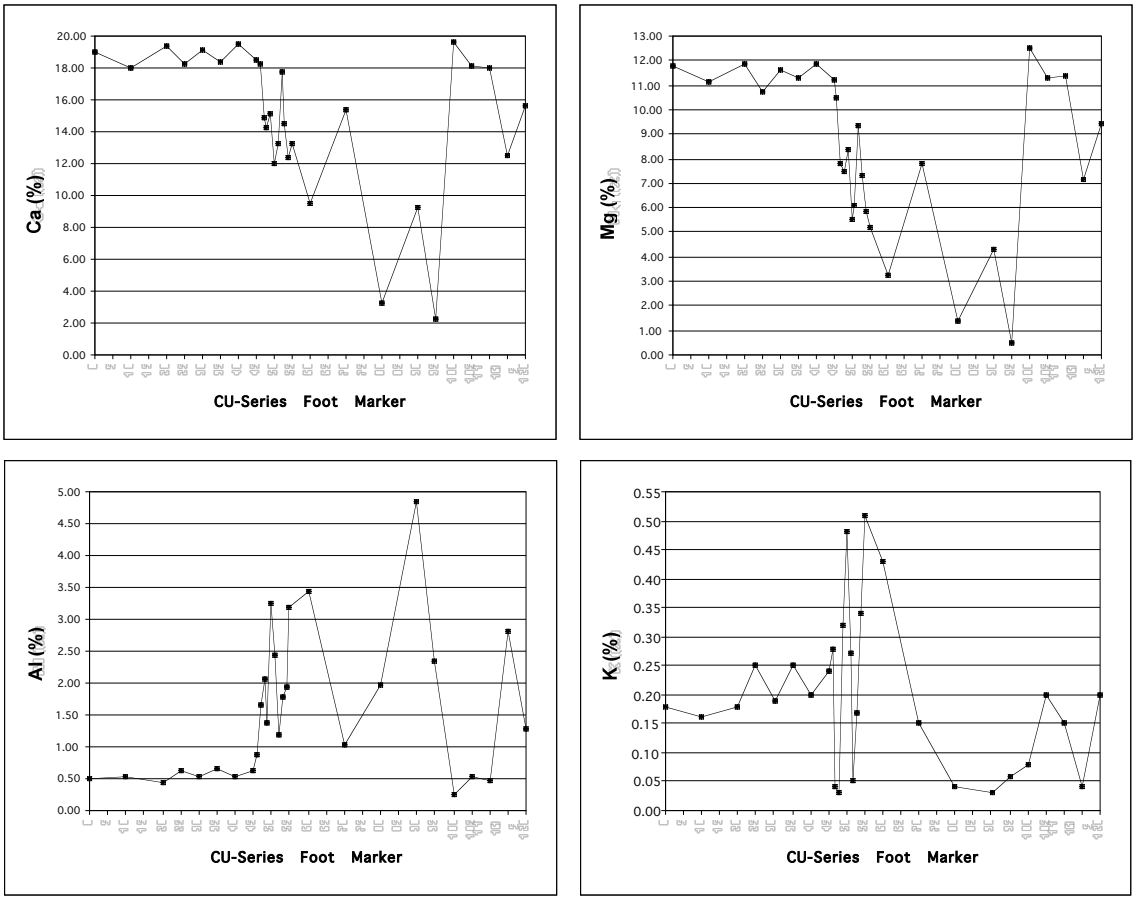

FIG. 80C. Alteration indicators (Ca, Mg, Al, and K) for the underground geochemical transect. Note that Si data were not produced for these samples. Note: because samples are labeled based on their footage along the transect, feet are used as the units for the x-axis.

LIGHT STABLE ISOTOPE STUDIES OF THE COVE AND McCOY DEPOSITS

This section presents the results of studies of light stable isotopes (δD, $\delta^{13}C$, $\delta^{18}O$, and $\delta^{34}S$) from a variety of assemblages from Cove and McCoy. Much of the meaning of isotopic data is interpretive, and is based on relationships observed in other systems/deposits. For each of the following sections, the empirical data are listed and discussed first, and are then interpreted within the contexts of other isotopic studies of similar deposits.

δD and $\delta^{18}O$ Values for QSP-Altered Intrusive Rocks from Cove, and $\delta^{18}O$ Values for Jasperoid and BMVT Quartz from Cove

Table 11 summarizes the δD and $\delta^{18}O$ results for studies of sericite/illite from QSP-altered intrusive rocks from the Cove deposit. The δD values range from -51 to -102 per mil, with a majority of the values between -72 and -51 per mil. The $\delta^{18}O$ values have a more restricted range of 10.0 to 18.5 per mil. Because the temperatures of homogenization for fluid inclusions in ore-stage quartz in BMVT veins generally range from around 250 to 350°C (not corrected for pressure), and these veins are clearly associated with QSP alteration of intrusive and sedimentary host rocks, the δD and $\delta^{18}O$ data were recalculated for fluids in equilibrium with the hydrothermal sericite/illite at 250, 300, and 350°C (Fig. 81).

For the nine samples analyzed, seven cluster fairly tightly and two are outliers. For the temperature range considered, the cluster lies within or just to the right of the magmatic water box (Fig. 81). Based on these results and the close temporal relationship

TABLE 11. δD and $\delta^{18}O$ results for QSP-altered intrusive rocks at Cove. Both are reported relative to VSMOW. The "samples lost" in the δD_{VSMOW} column (CVC218-857.5 and 4145E-19) were consumed during laboratory analyses, but no data were produced. Plate 1 shows the sample locations.

Sample Number	**δD permil**	**$\delta^{18}O$ permil**
4405E-2	-51.3	13.7
CVC218-857.5	sample lost	18.5
4145E-46	-63.4	15.7
4145E-19	sample lost	14.3
4205E-19	-93.0	10.0
4405E-1	-70.6	16.0, 16.1 (ave 16.0)
4145E-17C	-61.7	15.4
4205E-7	-72.2	15.3
25-50-1	-99.0, -104.8 (ave -102±4)	10.6
4205E-5	-68.4	13.5
4145E-29	-63.0	14.2
Misasa Ser*	-61.9	-
Misasa Ser*	-65.3	-
Misasa Ser*	-57.8	-
Misasa Ser*	-60.4	-

* Sample Misasa Ser is a laboratory standard with an accepted value of -60±1 permil.

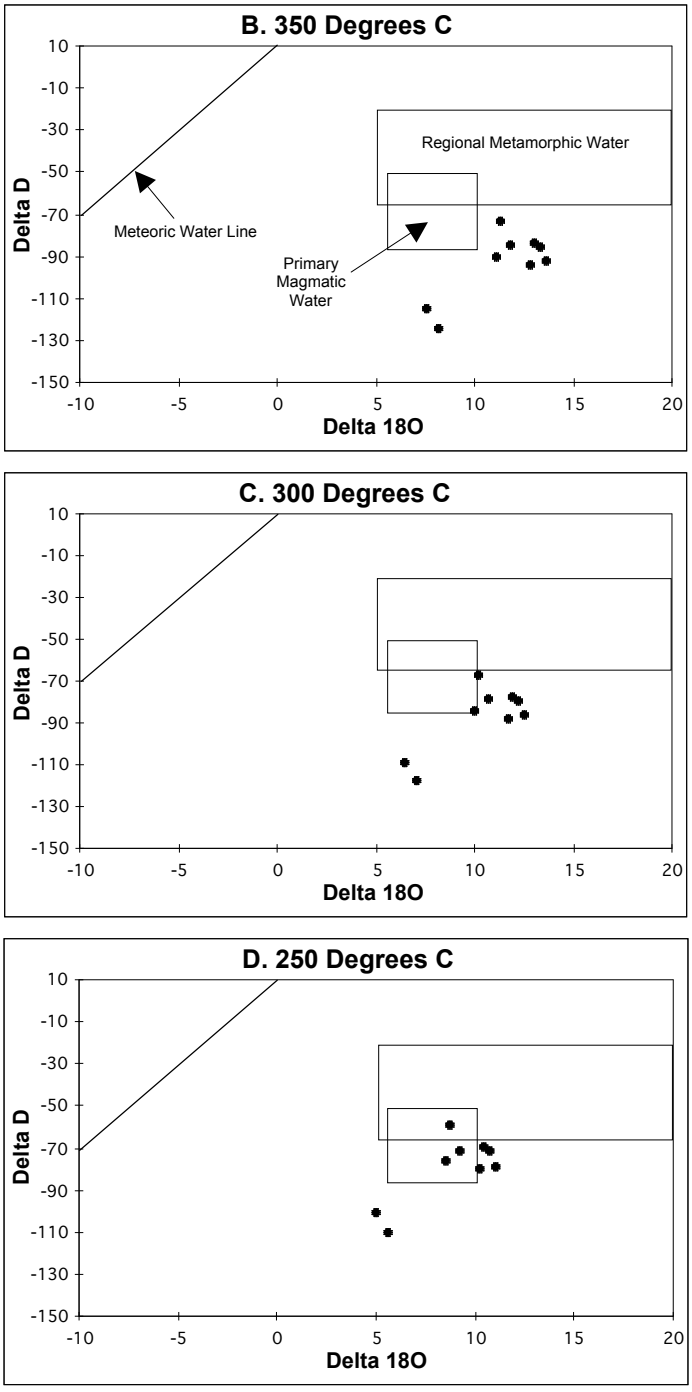

FIG. 81. $\delta^{18}O$ and δD data and calculated fluid compositions. A, B, and C show calculated fluid compositions for waters in equilibrium with the hydrothermal sericite/illite at 350°C, 300°C, and 250°C. The fractionation factor for $\delta^{18}O$ was determined from the fractionation equation of Sheppard and Gilg (1996). The fractionation factor for δD was determined from the fractionation equation of Capuano (1992) and Girard and Fouillac (1995). Primary magmatic, metamorphic, and meteoric water values from Taylor (1997).

between magmatism and mineralization at Cove (Chapter 5), the source for the mineralizing fluid(s) is interpreted to be magmatic. The shift toward slightly higher $\delta^{18}O$ values at 350 and 300°C (Fig. 81) may indicate contamination of the magma chamber by assimilation of country rocks during its ascent. The two outlier points have lower δD and $\delta^{18}O$ values than the cluster, and may indicate some dilution of the magmatic fluid(s) by meteoric or exchanged meteoric water, but the cause for this shift in isotopic values is unclear.

Table 12 shows the $\delta^{18}O$ results for studies of hydrothermal quartz from BMVT veins and jasperoid at Cove. The seven samples of BMVT quartz share a restricted range of $\delta^{18}O$ values from 17.0 to 18.2 per mil. The $\delta^{18}O$ values for the jasperoid samples range from 14.8 to 21.1 per mil. These values are similar to the raw $\delta^{18}O$ values from the sericite/illite from QSP-altered intrusive rocks (Table 11), which suggests a common source for oxygen in these various silicate/siliceous phases. In this case, the likely source is magmatic fluid(s).

The higher $\delta^{18}O$ values (15.5 to 21.1 per mil) for the samples from Cove are characteristic of pluton-related quartz veins throughout Nevada, including those associated with the Jurassic Goldstrike and Bald Mountain stocks (Emsbo et al., 2000; Nutt et al., 2000). The calculated $\delta^{18}O$ values for water in equilibrium with these Jurassic systems are typical of magmatic water (Nutt et al., 2000). The $\delta^{18}O$ values for water in equilibrium with quartz, jasperoid, and sericite/illite from Cove are also indicative of a magmatic source, and may include a weak signature of assimilated country rock or exchange at the higher end of the range. A similar conclusion was reached by Nutt et al.

TABLE 12. $\delta^{18}O$ results for jasperoid and BMVT quartz from the Cove deposit. The precision for the analyses is better than ±0.1 permil.

Sample Source	**Sample Number**	**$\delta^{18}O$ permil**
Hydrothermal jasperoid	4725E-3	15.5
	DW-12-1	14.8
	4835E-2	21.1
Hydrothermal BMVT quartz	4145E-24	18.2
	STOPE 5	17.3
	7/26/98-2	18.0
	ARPB-1	17.0
	TC4MID+66’	17.6
	UK-3	18.1
	AUK-1	17.7

(2000) for jasperoid and later drusy quartz in the Bald Mountain district. They concluded that the higher $\delta^{18}O$ values (up to 19.1 and 19.5 per mil, respectively) were likely produced from magmatic water that had traveled some distance from the progenitor stock, and had experienced cooling and exchange with carbonate wallrocks during this travel.

$\delta^{34}S$ Values for Sulfides from Skarn Ore from McCoy, and BMVT and Carlin-Style Ore from Cove

The $\delta^{34}S$ values for sulfides from McCoy and Cove are shown in Table 13. All of the values cluster tightly between 1.6 and 4.5 per mil. The BMVT sulfides from Cove and pyrite from skarn ore at McCoy share a particularly tight range of 2.2 to 3.3 per mil. These relationships indicate a common source for S in the various types of ore from the two deposits.

Sulfur components can be strong indicators of likely source rocks, as indicated for Carlin-type deposits by Arehart (1996). The most likely source for S in sulfide ore minerals from both McCoy and Cove is the Eocene magmatic system that comprises the Brown stock at McCoy and the related dikes and sills at McCoy and Cove. As discussed in previous chapters of this work, Brooks et al. (1991) and Brooks (1994) have substantiated the genetic association between skarn ore at McCoy and the progenitor Brown stock, and the mineralization at Cove is essentially coeval with this magmatism. The δD and $\delta^{18}O$ results for studies of hydrothermal sericite/illite, quartz, and jasperoid at Cove also indicate a magmatic fluid source.

TABLE 13. $\delta^{34}S$ results for BMVT and Carlin-style sulfides from Cove, and pyrite from McCoy.

Sample Number	**Source**	**Mineral Analyzed**	**$\delta^{34}S$ permil**
ARPB-2	Cove BMVT ore	sphalerite	2.4
ARPB-2	Cove BMVT ore	pyrite	2.6
CUBM-59	Cove BMVT ore	galena	2.4
CUBM-59	Cove BMVT ore	pyrite	2.2
CUBM-59	Cove BMVT ore	sphalerite	2.8
10/10-1B	Cove BMVT ore	sphalerite	2.8, 2.9 (ave 2.8)
10/10-1B	Cove BMVT ore	pyrite	2.8
10/10-1A	Cove BMVT ore	pyrite	3.3
CVC-218-808	Cove Carlin-style ore	stibnite	1.6
CSD-4	Cove Carlin-style ore	realgar	3.7
CSD-A1	Cove Carlin-style ore	realgar	4.0
REALGARC	Cove Carlin-style ore	realgar	4.5
CSD31	McCoy skarn ore	pyrite	3.1, 3.2 (ave 3.2)
P-1PY	McCoy skarn ore	pyrite	2.2
P-2PY	McCoy skarn ore	pyrite	2.8

The absence of sulfate minerals at McCoy and near absence of sulfate minerals at Cove suggests that the ratio of reduced S to oxidized S was high during mineralization at both deposits. Therefore, the $\delta^{34}S$ values for sulfides from the two deposits should approximate actual S values of the mineralizing fluids. Ostensibly, the $\delta^{34}S$ values that are most indicative of the magmatic fluids are from pyrite from the skarn ore at McCoy. Overlap of values from the McCoy skarn ore with values of both BMVT and Carlin-style sulfides from Cove further substantiates a magmatic source for the S components at Cove.

It has long been recognized that $\delta^{34}S$ values from sulfides in igneous rocks and porphyry Cu deposits of the western United States are usually near zero per mil (Ohmoto and Rye, 1979). More recent studies have shown that $\delta^{34}S$ components of igneous rocks can vary widely due to the amount and isotopic composition of S assimilated from country rocks (Ohmoto and Goldhaber, 1997). Such variation occurs especially in porphyry Mo, W, and Sn deposits, and a recent study of sulfides related to the Jurassic stock at Bald Mountain, Nevada, shows that magmatic S in this system ranged from 15.5 to 19.3 per mil (Ohmoto and Goldhaber, 1997; Nutt et al., 2000). These relationships indicate that the S values for McCoy-Cove may originally be entirely magmatic, but the possibility of at least some incorporation of S from country rocks cannot be ruled out.

$\delta^{13}C$ and $\delta^{18}O$ Values for Carbonate Wallrocks and Veins from Cove

The $\delta^{13}C$ and $\delta^{18}O$ values for carbonate wallrocks, late ore-stage and post-ore carbonate veins from Cove are shown in Table 14, and are also displayed graphically in

TABLE 14. $\delta^{13}C$ and $\delta^{18}O$ results for Cove deposit carbonate isotopic analyses. The $\delta^{13}C$ data are reported relative to VPDB, and the $\delta^{18}O$ data are reported relative to VSMOW. The reported $\delta^{18}O$ were converted to actual $\delta^{18}O$ values to account for isotopic fractionation during H_3PO_4 extraction (at 25°C; Friedman and O'Neil, 1977). The conversion used for calcite is: $\delta^{18}O_{VSMOW}$ = reported $\delta^{18}O_{VSMOW}$ – 10.20 permil. The coversion used for dolomite is: $\delta^{18}O_{VSMOW}$ = reported $\delta^{18}O_{VSMOW}$ – 11.03 permil. Plate 1 shows the sample locations.

Sample Source	Sample Number	$\delta^{13}C$ permil	$\delta^{18}O$ permil
Smelser Pass Member	AR4655E-2	1.8	11.7
	4285E-2	1.0	12.5
	4835E-4	1.4	13.3
	4365E-4	0.9	11.7
	4465E-8	0.9	9.9
transitional submember of the PCM	4145E-38	-3.5	11.4
	4145E-17A	-4.3	13.6
	4145E-23	-7.9	8.8
	4145E-47	-2.3	16.2
dolostone submember of the PCM	4145E-31	-0.0	16.4
	CSD-2	-0.5	16.9
	7/26/98-2	-2.4	16.0
	4145E-24	-1.8	16.7
Home Station Member	ARPB-4	-3.4	8.4
	4005E-A1	-1.9	8.4
	4005E-1	-4.3	9.7
	CSD-5	0.7	13.2
	CSD-6	0.1	12.9
	CSD-7	0.5	13.3
BMVT calcite	UK-1	-4.6	0.8
	4145E-53	-5.9	-8.1
	UK-8	-10.7	7.3
	ARPB-1	-8.4	3.9
	4205E-15	-10.4	4.9
	4145E-29	-4.6	1.6
	UK-4	-9.1	4.8
	4145E-56	-8.8	4.6
	4325E-11	-2.8	-2.1
	10/10-2	-4.3	1.5
	4005E-6A	-8.3	5.0
late calcite veins	4325E-8	-2.0	-2.0
	4005E-4	-4.1	1.0
	4205E-24	-5.7	6.2
	ARPB-3	-6.1	-2.6
	4005E-6B	-6.1	-3.1
	4285E-3	-1.9	-1.9
	4285E-8	-4.6	-2.9
	UK-7	-3.0	-4.1
latest hypogene to supergene calcite	4325E-A1	-5.0	1.1
	UK-6	-3.7	4.5
	4325E-5	-3.2	-0.7
	UK-5	-4.7	5.3

Figure 82. Despite the fact that the wallrock samples selected for analyses appeared texturally and mineralogically fresh, the relatively low $\delta^{18}O$ values indicate that these samples have all been at least slightly altered. The general trend from weakly to more strongly altered wallrocks to carbonate veins is toward lower $\delta^{13}C$ and $\delta^{18}O$ values.

Arehart (1996) notes a similar shift toward lower $\delta^{18}O$ values with increasing hydrothermal alteration associated with other sedimentary rock-hosted disseminated gold (Carlin-type) deposits in the Great Basin. With some exceptions, however, there is a shift toward higher $\delta^{13}C$ values for ore-related veins within individual ore systems (Arehart, 1996). Ilchik (1990) and Arehart (1996) also document a local increase in $\delta^{13}C$ values within the wallrocks as such veins were approached. Supergene veins in these systems have lower $\delta^{13}C$ values than the wallrocks, which Arehart (1996) suggested to be indicative of atmospheric CO_2 and input of meteoric water. It is not known whether the shift toward lower $\delta^{13}C$ and $\delta^{18}O$ values for altered rocks and veins from Cove also indicates atmospheric/meteoric input, are the result of reequilibration of the wallrock carbonates with pore fluids at higher temperatures, or indicate an unput of hydrothermally-sourced CO_2.

A DESCRIPTIVE GENETIC MODEL FOR THE McCOY-COVE SYSTEM

The descriptive model for the McCoy-Cove system is based on several permissive and/or absolute lines of evidence for a genetic link between the two deposits. Kuyper et al. (1991) and Brooks (1994) cited five lines of support for the genetic link: 1) the two deposits are proximal to one another (~1.5 kilometers apart); 2) they are localized by the

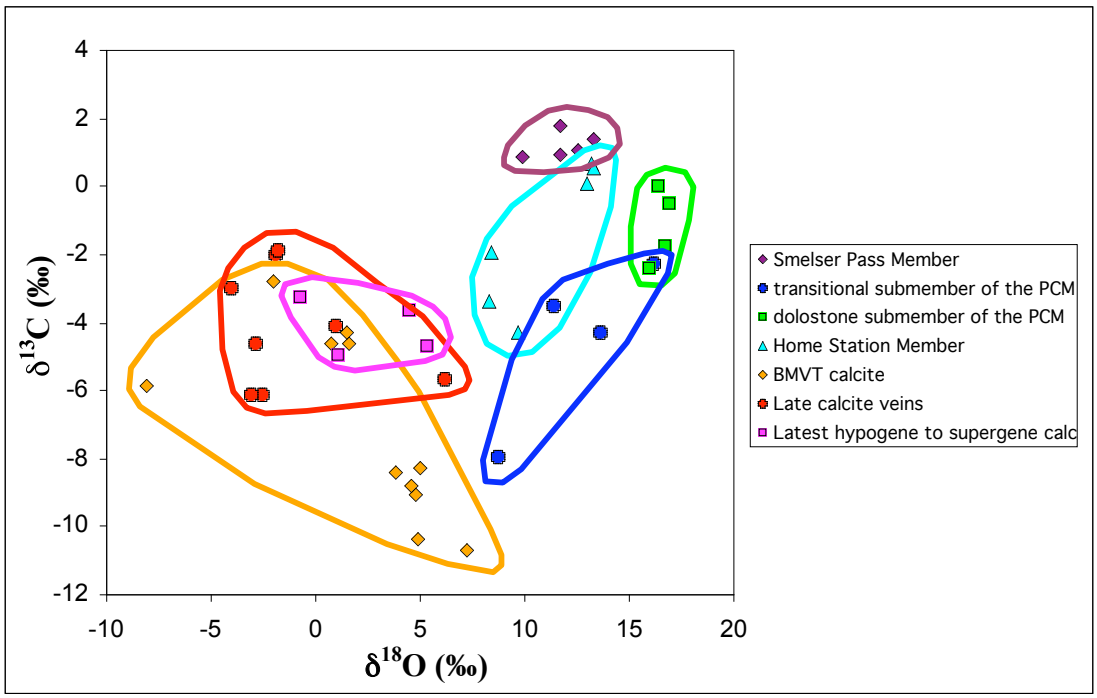

FIG. 82. $\delta^{13}C$ and $\delta^{18}O$ isotopic fields for carbonates from the Cove deposit.

same northeast-striking fault zone; 3) they share identical host rocks; 4) they are spatially associated with similar to identical intrusive rocks; and 5) the intrusive rocks at both deposits were dated at about 40 Ma (K-Ar). While the genetic association between the skarn ore at Cove and the Eocene Brown stock has been clarified in earlier studies (Brooks et al., 1991; Brooks, 1994), the relationships between the BMVT and Carlin-style ore at Cove and the magmatic center were ambiguous prior to the commencement of the current study.

More recent data from Emmons and Eng (1995) and the current study substantiate the magmatic connection for ore at Cove, refine the earlier lines of evidence for a genetic link between Cove and McCoy, and offer additional, more robust lines of support. The principal data used in the model and ensuing discussion are newer K-Ar and ^{40}Ar-^{39}Ar ages for magmatic and hydrothermal minerals, temperatures (T_H) and salinities for fluid inclusions in ore-stage BMVT quartz, δD and $\delta^{18}O$ values for hydrothermal sericite/illite at Cove, and $\delta^{34}S$ values for ore-stage sulfides from McCoy and Cove. The mineralogical (ore and gangue) and geochemical zonations presented in the preceding text are also important aspects of the system, and are discussed relative to other deposits in the ensuing text.

The descriptive model is separated into three principal stages: 1) late Eocene extension in the McCoy mining district, emplacement of an early stage of the Brown stock with associated dikes and sills, and the development of early sub-economic skarn at McCoy; 2) evolution of the Brown stock porphyry system concurrent with continued extensional faulting, and related economic mineralization at McCoy and Cove; and 3) post-ore tectonic and supergene/diagenetic effects on the two systems. For comparison,

Figure 83 shows the middle to late Eocene, pre-ore framework for McCoy and Cove, based on descriptions in Chapter 2.

The results of stage 1 are shown in Figure 84. Emplacement of a magnetite-bearing component of the Brown stock occurred around 41.5 Ma (Brooks, 1994; Emmons and Eng, 1995). The stock was localized by a series of northeast-striking faults belonging to subgroup I of the ~NE-striking fault group at Cove (described in Chapter 2). Related dikes and sills were also emplaced along these faults, and extended from the Brown stock at McCoy toward Cove in the northeast. At McCoy, hydrothermal activity related to the early stage of the Brown stock produced proximal hornfels and skarnoid in sedimentary rocks, and pyroxene- and amphibole-bearing assemblages in the intrusive rocks (Brooks, 1994). Sub-economic concentrations of Au were also deposited with these early assemblages (Brooks, 1994).

Figure 85 shows the results of stage 2 of the genetic model. Sometime around 39 Ma, a second pulse of magma ascended along the same paths as the earlier Brown stock and related dikes. This pulse of magma contained appreciable Ti, which Brooks (1994) attributed to magma mixing at a deeper level of the system. The Ti was precipitated as ilmenite, which distinguishes the second pulse of magma from the earlier, magnetite-bearing one (Brooks, 1994). Hydrothermal activity associated with the later stage of the Brown stock produced an economic Au (-Cu) skarn at McCoy, which overprinted the earlier sub-economic skarn (Brooks, 1994). At Cove, mineralizing fluids ascended along subgroup II of the ~NE-striking fault group, which developed after the emplacement of the ~41.5 Ma dikes and sills at Cove. The distribution of BMVT and Carlin-style ore was controlled in part by the earlier dikes and sills, and associated alteration overprinted the

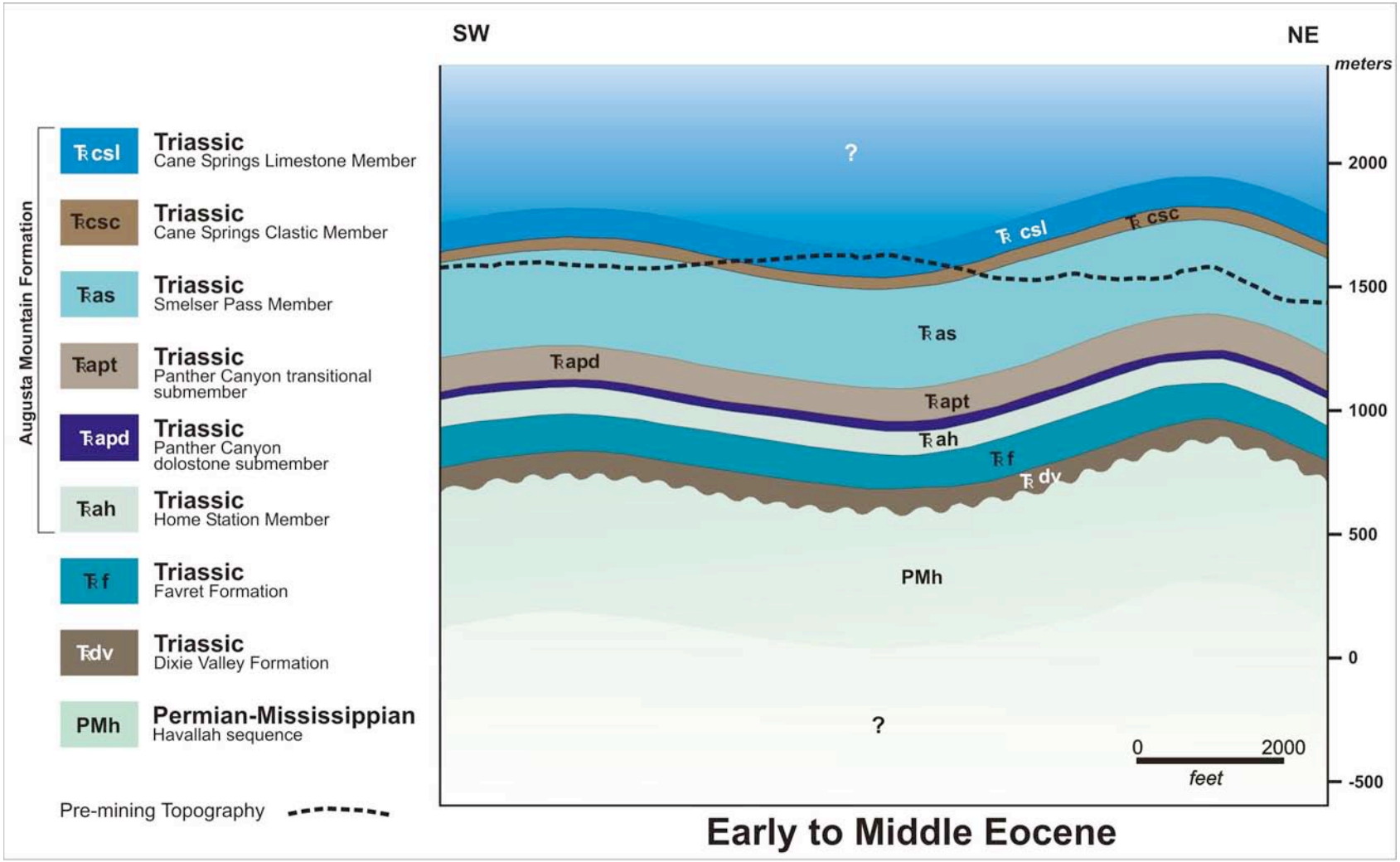

FIG. 83. Pre-late Eocene cross section for McCoy-Cove (early to middle Eocene).

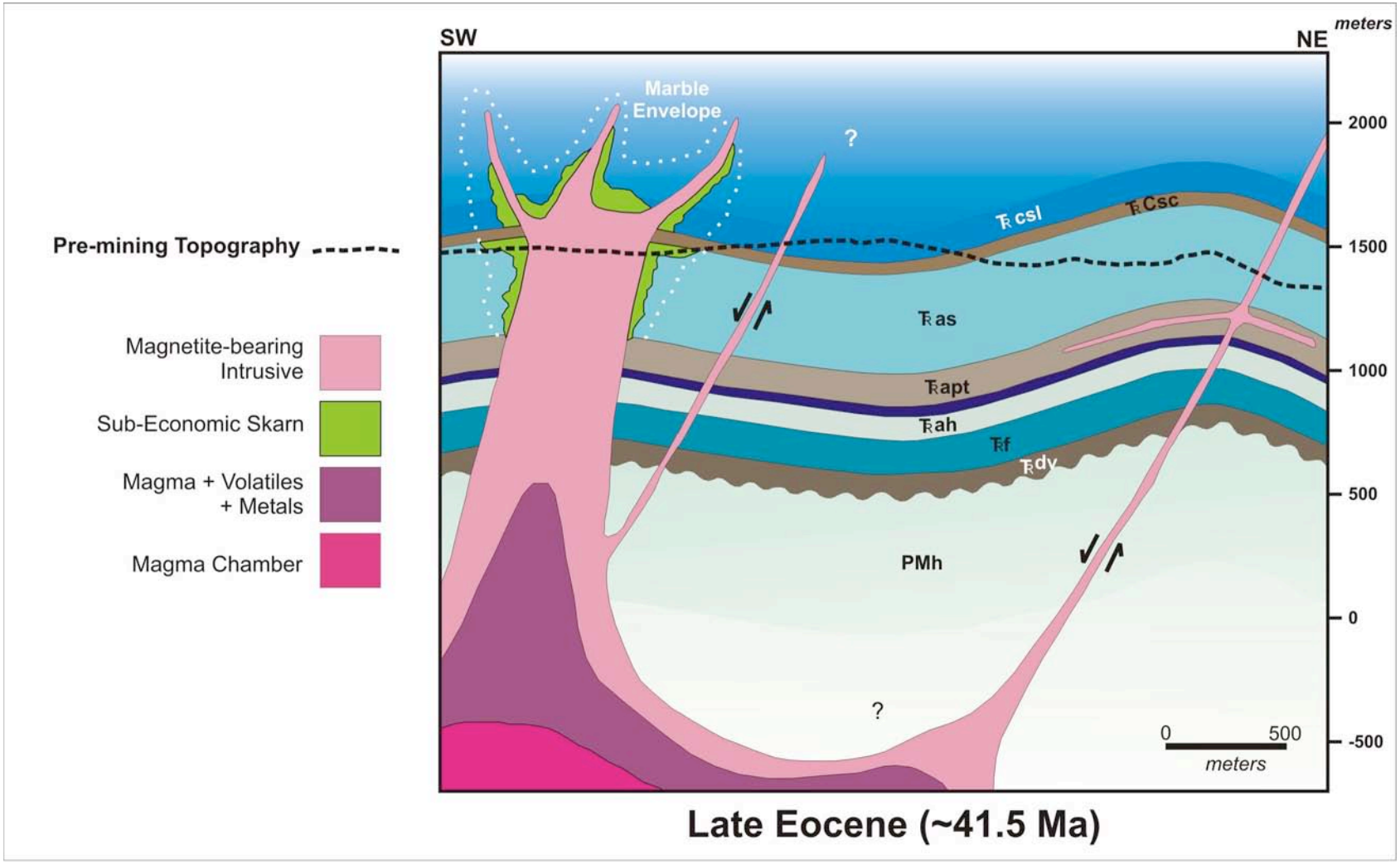

FIG. 84. Stage 1, magmatism, and sub-economic mineralization at McCoy-Cove (~41.5). See Figure 83 for rock unit symbols.

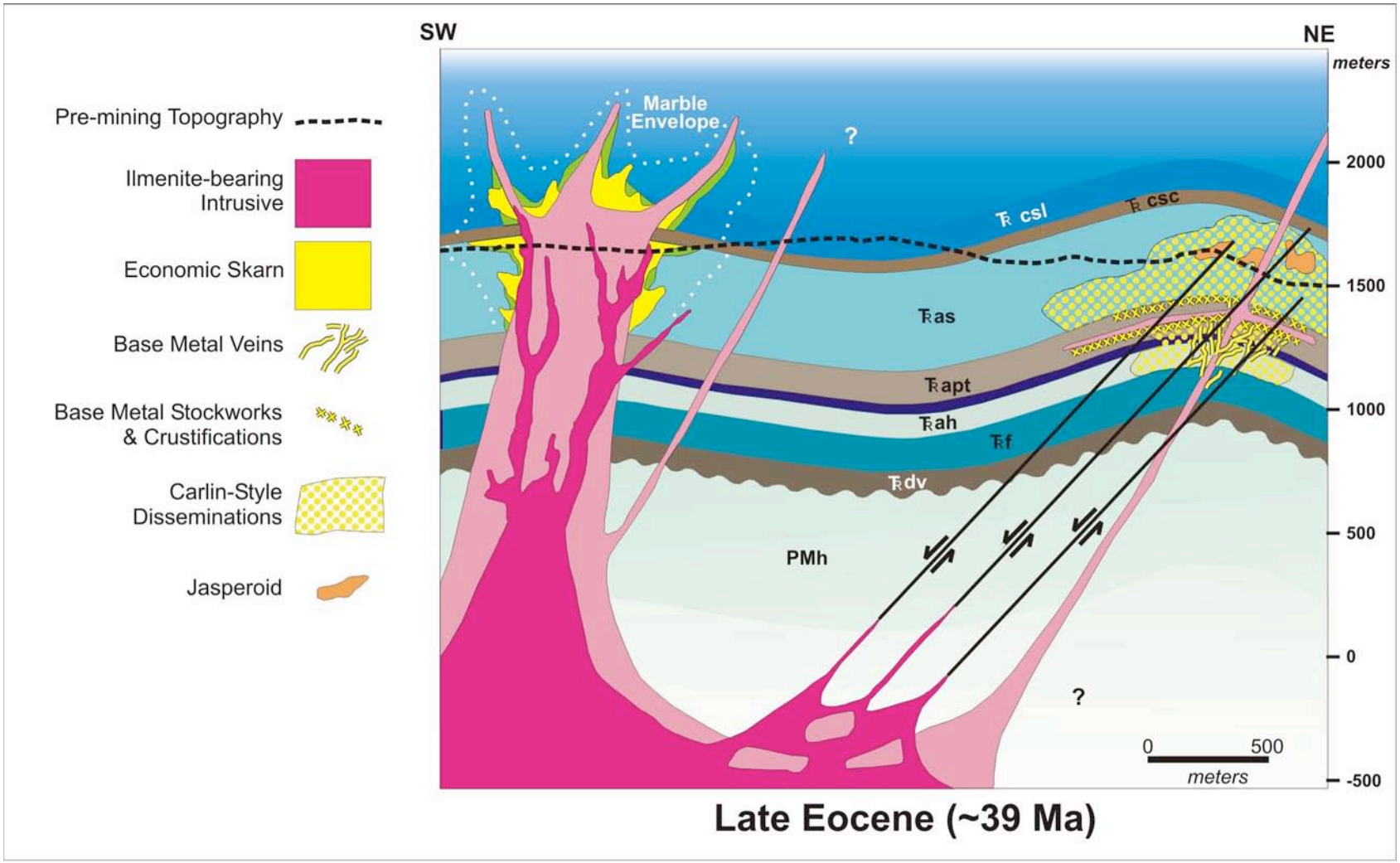

FIG. 85. Stage 2 magmatism and economic mineralization at McCoy-Cove (~39 Ma). See Figures 83 and 84 for symbol explanations.

primary igneous and sedimentary assemblages. Adularia from mineralized quartz-pyrite ± adularia assemblages at McCoy, sericite/illite from an ore-related QSP alteration assemblage at Cove, and fresh biotite from a weakly altered portion of the Gold Dome dike at Cove all yielded ages of 39 Ma (Emmons and Eng, 1995; Chapter 5 of this text).

Figure 86 shows the post-ore effects on the McCoy-Cove system. These effects were produced by volcanic, tectonic, sedimentary, and diagenetic/supergene processes. The deposition of the post-mineral Caetano tuff around 36 Ma provides the lowest constraint on the age of mineralization at Cove (Emmons and Eng, 1995). Post-ore development of the Striper splay segmented the highest-grade orebody at Cove (see Chapter 3). Weathering and erosion resulted in oxidation of much of the ore in the upper parts of Cove and McCoy, and exposed the Brown stock at McCoy and resistant jasperoids at Cove. At least some remobilization of components occurred at Cove, and Ag was redeposited as native Ag wires at the paleo-redox boundary (see Chapters 3 and 4).

DISCUSSION

The spatial associations and proposed genetic links for the late Eocene magmatic center and skarn ore at McCoy and BMVT and Carlin-style ore at Cove, the mineralogical and geochemical zonations for the entire McCoy-Cove system, the various locations of ore-grade Au within this system, and the local zonation from higher to Ag:Au ratios to higher Au:Ag ratios at Cove all have implications for other deposits. These implications are especially important for the late Eocene (to early Oligocene) porphyry-related (skarn and Carlin-like/distal disseminated) and Carlin-type deposits in the Great Basin. The mineralogical and geochemical zonations and positions of Au

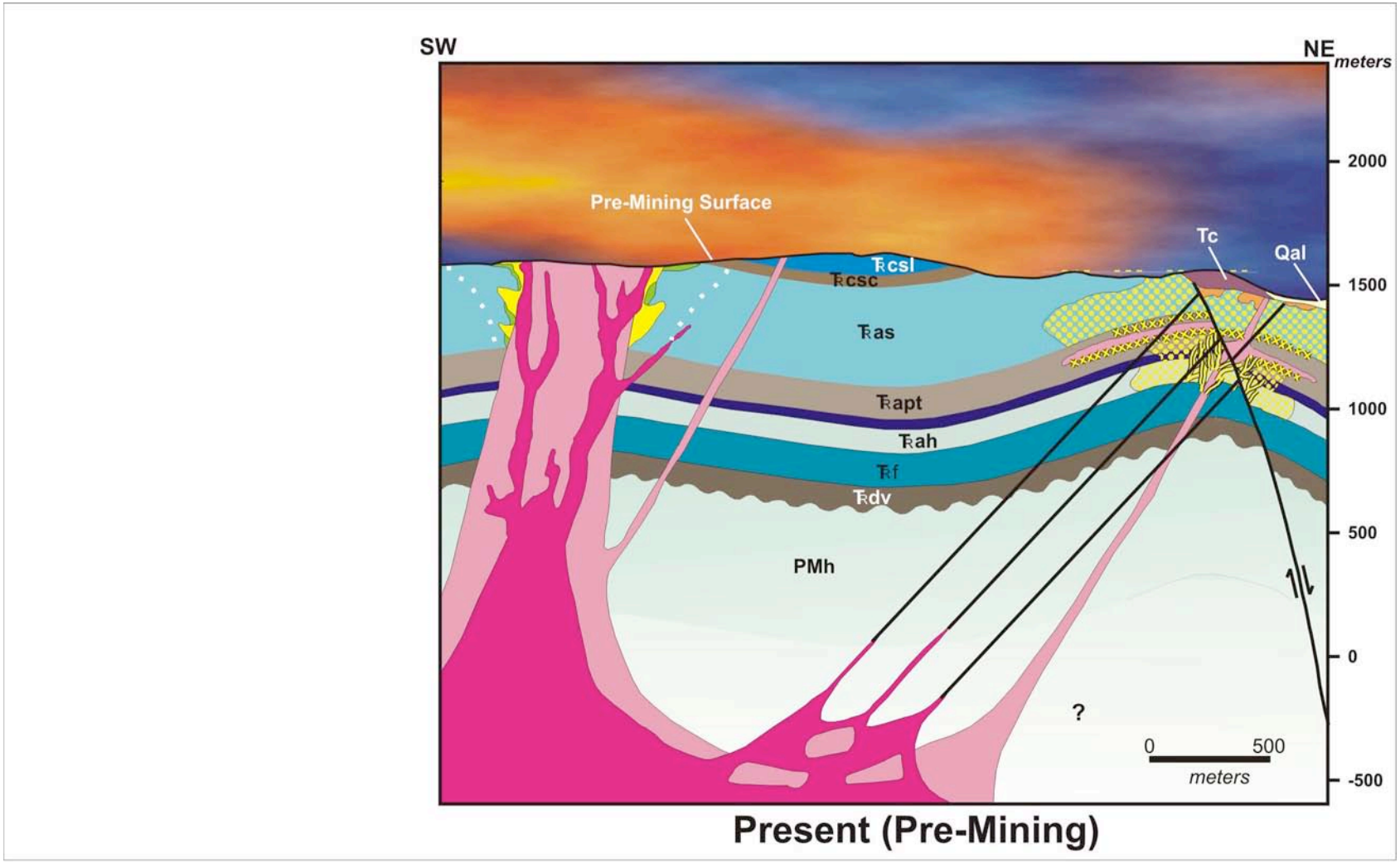

FIG. 86. Post-ore effects on the McCoy-Cove system. See Figures 83, 84, and 85 for symbol explanations.

within the McCoy-Cove system are similar to those observed in other magmatic systems, and are discussed first.

The mineralogical zonation for McCoy-Cove can be summarized as a proximal Au (-Cu) skarn centered on a porphyritic stock, with intermediate BMVT (polymetallic vein) ore, and more distal Carlin-style ore. The BMVT ore is considered to be intermediate because it occupies the center of the apparently telescoped Cove deposit, and is surrounded by a wide outer aureole of Carlin-style ore. Within the generalized zonation, economic grades of Au occur in association with three principal assemblages: 1) as native Au particles associated with skarn ore at McCoy, at least some of which are believed to have been originally encapsulated in pyrite (Brooks, 1994), 2) as blebs of native Au and electrum in BMVT veins at Cove (see Chapter 4), and 3) as submicroscopic concentrations of Au in arsenian pyrite and arsenopyrite in Carlin-style ore at Cove. The residence and associations of Au in the auriferous, manganiferous jasperoid bodies at Cove were not determined during this study.

The three principal concentrations of ore-grade Au in the McCoy-Cove system are similar to the principal positions of Au in other Au-enriched, porphyry-related systems. Emmons (1927) summarized classical studies of hypogene metal and mineral concentrations in Au-enriched porphyry Cu deposits, and recognized two principal Au-bearing zones: 1) occurs in the central Cu orebody, and 2) more or less overlaps with an outer Pb-Zn-Ag zone. A later review by Jerome (1966) described a Au-enriched porphyry Cu orebody, but did not describe any peripheral or distal Au mineralization in the surrounding pyrite halo or more distal Pb-Zn-Ag zone.

Jones (1992) presented a more recent description of the distribution of Au in Au-enriched porphyry Cu deposits. His idealized mineralogical zonation is, from the center outward, a barren (sub-economic) core, molybdenite, bornite-Au, chalcopyrite, a pyrite halo, Pb-Zn-Ag-bearing minerals, and distal epithermal Au. In this zonation, Au occurs in three principal zones. In many Au-enriched porphyry copper deposits (ex. Dos Pobres, Granisle, Bell, Dizon, Panguna, Sapo Alegre, and Ok Tedi, among others), Au is positively correlative with Cu in the proximal potassic alteration zone. Jones (1992) called this the "central" Au zone. In other similar deposits (ex. Fortitude, Star Pointer, San Manuel-Kalamazoo, Tanama, Helecho, and Mt. Milligan, among others), the Au-rich zone apparently falls outside of the more proximal Cu zone, and inside of the more distal Pb-Zn-Ag zone. Jones (1992) called this the "intermediate" Au zone, and noted that it is coincident with the pyrite halo in many porphyry Cu systems. Some sedimentary rock-hosted disseminated Au deposits (ex. Barneys Canyon, Melco, Mercur, La Plata, Bau, and Purisma-Concepcion, among others) are possible examples of the "distal" Au zone (Alvarez and Noble, 1988; Sillitoe and Bonham, 1990; Jones, 1992).

The three principal Au zones for the McCoy-Cove system can be considered as a slight variation on the scheme of Jones (1992). In this case, the central Au zone comprises the Au (-Cu) skarn at McCoy, where Au is positively correlative with Cu (Emmons and Eng, 1995). The intermediate and distal Au zones both occur at Cove. The intermediate Au zone is somewhat different from the idealized intermediate Au zone of Jones (1992) in that it occurs within the Pb-Zn-Ag (BMVT) part of the system at Cove. The distal Au zone is separated from the intermediate Au zone by a barren

(subeconomic) pyrite halo (Chapter 3), and occurs as disseminated Carlin-style ore in carbonate host rocks.

Jones (1992) discussed other Au-enriched porphyry copper systems that also have multiple Au zones, which he characterized as containing giant porphyry Cu deposits with exceptional endowments of Au. These systems include Lepanto and Bingham. The deposits at Bingham are particularly relevant to the discussion of the McCoy-Cove system in that both systems are located in the Great Basin, and both are genetically related to late Eocene magmatic-hydrothermal activity. From the center of the system outward, the metal zoning at Bingham comprises: 1) a barren (sub-economic) core, 2) a moybdenite zone, 3) a bornite zone, 4) a chalcopyrite zone, 5) a pyrite halo, 6) a Pb-Zn-Ag zone, and 7) Au-Ag viens (James et al., 1961; John, 1975 and 1978; Atkinson and Einaudi, 1978; and Jones, 1992). Gold occurs in all of these zones except the barren core and molybdenite zone (John, 1978; Jones, 1992). The Carlin-type deposits at Barneys Canyon and Melco may be more distal expressions of the Bingham system (Sillitoe and Bonham, 1990), which would add an eighth zone to this system.

Implications for Carlin-Type and Distal Disseminated Deposits

The zonations observed for McCoy-Cove and Bingham are applicable to many other deposits in the Great Basin. In order to simplify the following discussion, the focus will be on deposits that have been demonstrated or interpreted to be Eocene, to possibly early Oligocene, in age. These deposits include porphyry-related skarn, polymetallic vein, distal disseminated/Carlin-like, Carlin-type, and epithermal vein deposits. Although the "distal disseminated," "Carlin-like," and "Carlin-type" classification schemes have been

described by a variety of authors, their usage by industry personnel and in numerous papers is commonly colloquial. Furthermore, some workers believe that a continuum exists between these classifications, and that the use of these schemes may be somewhat misleading (Sillitoe and Bonham, 1990; Weiss et al., 2000). Regardless, the following terminology will be used in the following discussion: 1) the "distal disseminated" classification will be used for deposits that have established genetic links with Eocene (to early Oligocene) magmatism, and 2) the "Carlin-type" classification will be reserved for deposits that have been described as lacking such genetic links with igneous activity.

Many Au (and Ag) deposits in the Great Basin fall along the Getchell, Battle Mountain-Eureka, and Carlin Au trends/belts in Nevada, and at or near Bingham in Utah (Figure 87). While it has long been recognized that many of these deposits, including the porphyry-related deposits at Bingham, Copper Canyon, and McCoy, are late Eocene in age (Theodore, 1998a; Emmons and Eng, 1995; Henry and Ressel, 2000), the ages of Carlin-type deposits in the Great Basin have been debated for the last 40 years. Various interpretations range from syngenetic deposition of Au with Paleozoic sedimentary rocks, at least as a partial source for Au (Emsbo et al., 1999), to contemporaneous with Miocene extension (Joralemon, 1951; Radtke et al., 1980). The most favored interpretations have been Eocene (~40 Ma; Seedorff, 1991; Maher et al., 1993; Thorman et al., 1994 and 1996; Groff et al., 1997; Henry and Boden, 1998; Henry and Ressel, 2000) and Cretaceous (~80 to 120 Ma; Kuehn and Rose, 1992; Arehart, et al., 1993b; Wilson and Parry, 1995; Drews-Armitage et al., 1996; Groff et al., 1997; Henry and Ressel, 2000).

Recent studies indicate that most, and possibly all, Carlin-type deposits in the Great Basin are Eocene (Seedorff, 1991; Emsbo et al., 1996; Ballantyne et al., 1997; Groff et

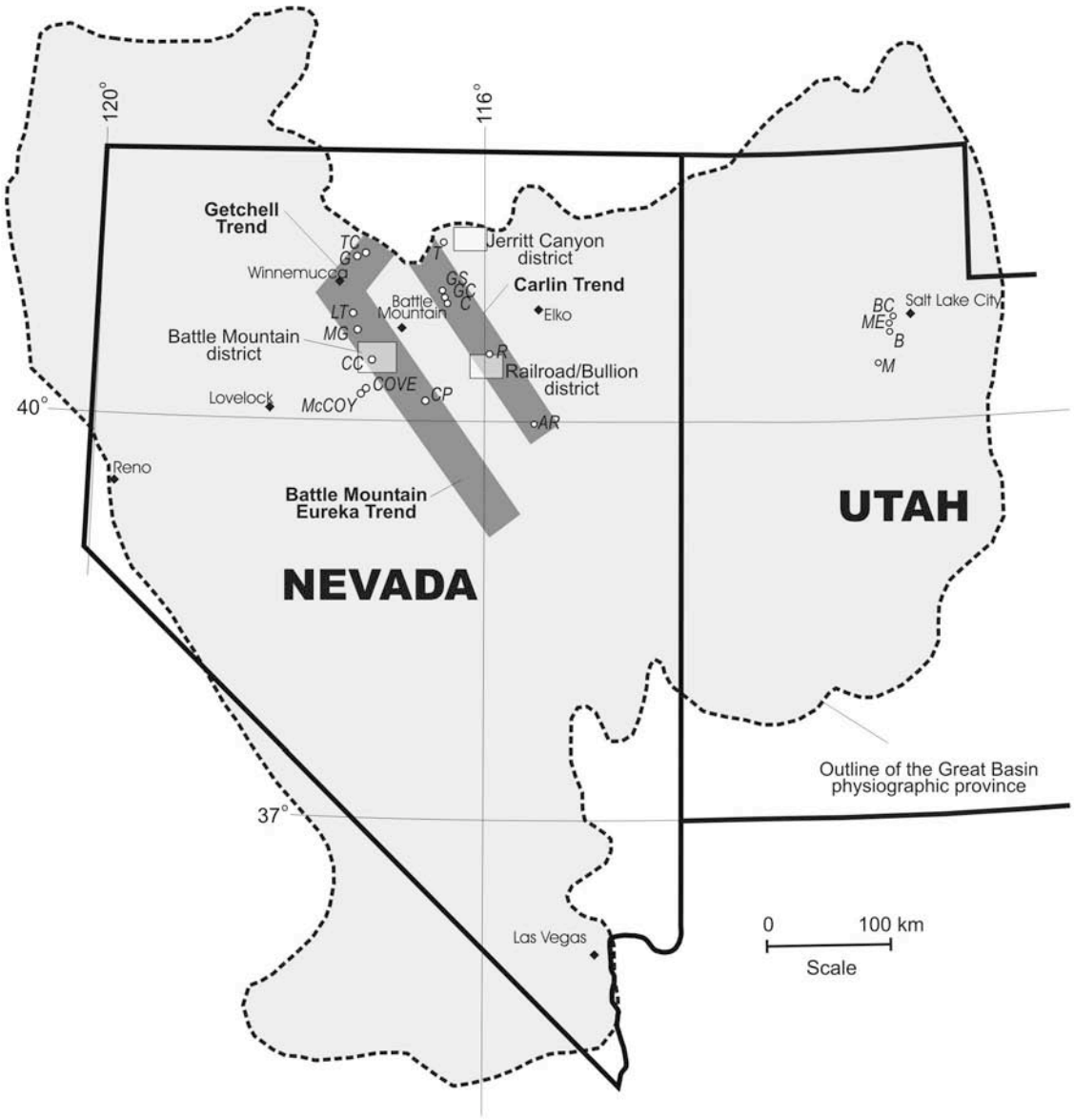

FIG. 87. Locations of gold trends and deposits discussed in the text (modified from Ressel et al., 2000b). AR = Alligator Ridge, B = Bingham, BC = Barneys Canyon, C = Carlin (includes Carlin East), CC = Copper Canyon, CP = Cortez/Pipeline, G = Getchell, GC = Genesis complex (includes Beast, Deep Star, and Genesis), GS = Goldstrike (includes Betze-Post, Griffin, Meikle, and Rodeo), LT = Lone Tree, M = Mercur, ME = Melco, MG = Marigold, R = Rain, T = Tuscarora, and TC = Twin Creeks.

al., 1997; Hall et al., 1997; Ressel et al., 1998, 1999, 2000a, 2000b; Hofstra et al., 1999; Henry and Ressel, 2000). Several examples occur along the Carlin trend, where the Betze-Post, Meikle, Griffin, Deep Star, Genesis, and Beast deposits are at least partly hosted by essentially coeval Eocene dikes (Emsbo et al., 1996; Leonardson and Rahn, 1996; Altamirano and Thompson, 1999; Ressel et al., 1999, 2000a, 2000b; Henry and Ressel, 2000). More examples occur at Jerritt Canyon, where Eocene dikes are mineralized, and light stable isotopic studies and cross-cutting relationships in the deposits indicate that the mineralization occurred during the Eocene (Hofstra, 1994; Phinisey et al., 1996; Hofstra et al., 1999; Henry and Ressel, 2000). Within the Getchell trend, dating of syn-ore adularia, sericite, and ore-stage galkhaite indicate that mineralization at the Getchell and Twin Creeks Carlin-type deposits occurred during the Eocene (Groff et al., 1997; Hall et al., 1997; Arehart et al., 2000). Ore-stage galkhaite has also recently been used on the Carlin trend to date the Rodeo deposit as late Eocene (Tretbar, 2001).

Several other deposits with mineralogies and alteration characteristics that are similar to classic Carlin-type deposits are considered as distal disseminated deposits based on close associations with Eocene magmatism. In the Battle Mountain district, the distal disseminated deposits at Lone Tree and Marigold have been interpreted to be coeval with porphyry Cu and Au skarns (e.g. those at Copper Canyon; Theodore, 1998b). Polymetallic vein and replacement bodies with lower concentrations of Au and/or Ag are also present in the district (Doebrich and Theodore, 1996; Theodore, 1998a). These occurrences support a proposed continuum between porphyry, skarn, and polymetallic

deposits (Carten et al., 1993; Titley, 1993; Pierce and Bolm, 1995), all of which are widespread in the Battle Mountain district (Theodore, 1998a).

In the Railroad (Bullion) district, distal disseminated deposits comprise the mineralized jasperoid bodies located as far as three kilometers from the late Eocene/early Oligocene Bullion stock (~36 Ma; Armstrong, 1970; Rayias, 1999). The Bullion stock is associated with proximal Cu and W skarn deposits, and Pb-Zn mantos occur between the proximal and distal disseminated deposits (Gillerman, 1982). In the Bingham area, Barneys Canyon and Melco lie just outside of the pyritic halo of the Eocene Bingham stock, and Eocene intrusions are also spatially associated with the Mercur deposit (Wilson and Parry, 1995; Presnell and Parry, 1996; Ballantyne et al., 1997; Mako, 1997).

Despite the strong temporal links between the various types of Eocene deposits in the Great Basin, and the fact that many of the porphyry-related (including distal disseminated) deposits display classic zonations in which Carlin-type deposits would occupy the most distal positions, the Carlin-type deposits have traditionally been considered as a separate and unrelated class of deposits. In regard to the Carlin-type deposits, the five principal reasons for this separation are: 1) $\delta^{34}S$ isotopes from several deposits implicate a sedimentary source for S, 2) δD and $\delta^{18}O$ isotopes from several deposits implicate meteoric water as the mineralizing fluid(s), 3) zonations for hypogene alteration assemblages, metal ratios, and fluid inclusion temperature data have not been demonstrated, 4) there is a lack of appreciable base metal concentrations within deposits, and 5) there is a lack of obvious associations with Eocene magmatism. Together, these reasons indicate a lack of genetic association with contemporaneous igneous activity for Carlin-type deposits, which has been used as the defining criterion to separate them as a

class from distal disseminated deposits (Weiss et al., 2000). Recent isotopic, multi-element geochemical, and mineralogical studies have provided new insights into many Carlin-type deposits, however, and implicate at least some genetic links with Eocene magmatism.

Pertinent Recent Studies of Carlin-Type Deposits

Isotopic data for S remain equivocal, as the relatively high $\delta^{34}S$ values suggest sedimentary sources for the S to many workers (Radtke et al., 1980; Ilchik, 1990; Arehart et al., 1993a; Hofstra, 1994; Arehart, 1996; Ilchik and Barton, 1997). The $\delta^{34}S$ values for orpiment, realgar, and stibnite from the Alligator Ridge Carlin-type deposit, however, span a broad range of –7.7 to 14.4 per mil (Nutt et al., 2000). These values overlap with the range for sulfides from Jurassic, porphyry-related deposits in the same area, which range from –5.7 to 11.3 per mil. The upper range for magmatic S here suggests that the interpretations for the higher $\delta^{34}S$ values in many Carlin-type deposits may not be conclusive evidence for purely sedimentary sources in all deposits.

Recent δD and $\delta^{18}O$ isotopic studies are more conclusive, and implicate the involvement of magmatic and/or metamorphic fluids in some Carlin-type deposits. For example, δD values for mineralizing fluids at the Getchell deposit suggest that they may be magmatic or metamorphic in origin (Folger et al., 2000), and that variably exchanged meteoric water was also present (Hofstra and Rye, 1998). A more detailed isotopic study of ore-stage kaolinite from the Deep Star deposit indicates the system is isotopically zoned (Heitt et al., in press). Calculated values for fluids that produced kaolinite in the center of the orebody are near the magmatic water field, with a mixing path toward

exchanged Mid-Tertiary meteoric water near the eastern orebody margin (Heitt et al., in press). The identification of a magmatic water component in ore-stage minerals at Deep Star has extremely important ramifications for deposits along the Carlin trend, as Deep Star is regarded by many workers to occur within one of the principal feeder zones for the trend (numerous personal communications with various geologists, 2000-2003).

The apparent lack of mineralogical zonations and paucity of base metals associated with Carlin-type deposits are discussed together here, as these observations may share common origins. The apparent lack of zonations for mineral occurrences and base metals may be due, at least in part, to extensive weathering effects. Other explanations are: 1) lack of consistent analyses for metals other than Au, and 2) lack of appreciation for the possible scales of the systems responsible for Carlin-type deposits. Along the Carlin trend, for example, a substantial expense is associated with processing and analyzing the huge number of samples from blasthole, production, and exploration drillholes. Consequently, the types (and therefore numbers) of standard analyses have been greatly reduced to those pertaining to day-to-day operations. Other than Au (± Ag) and elements of metallurgical concern (e.g. C and S), few to no other elements are routinely analyzed.

In the last few years, numerous geochemical studies have been conducted for deposits along the Carlin trend and elsewhere. Many of these studies do indicate common geochemical zonations on deposit- and district-scales (numerous confidential personal communications), but discussion of these zonations is largely precluded by the proprietary nature of the data. One notable exception to this general confidentiality is a recent paper by Heitt et al. (in press), in which they discuss mineral and geochemical zonations for the Deep Star deposit. Ore-stage clays at Deep Star are zoned outward

from a central zone of intense kaolinite, through weak to moderate kaolinite and kaolinite + smectite, to illite (Terry Leach, written communication in Heitt et al., in press). The authors also identify a suite of geochemical elements whose distribution is related to the mineralizing event. This suite includes Au, of course, and the elements that are routinely used as pathfinder elements for Carlin-type and other deposits (As, Sb, Hg, and Tl). Perhaps more noteworthy is the inclusion of anomalous elements that are more typically associated with igneous-related deposits, such as Bi, Cd, Cu, Pb, Ag, Te, W, and Zn. Clarke et al. (2000) found anomalous concentrations of similar elements related to the mineralizing system at the Rain Carlin-type deposit, including Mo, Ag, Te, W, and Zn. They also indicate that the recognition of anomalous concentrations of many of these elements, such as Bi, Te, and W, were at least partly due to recent dramatic improvements in the detection limits for these elements.

Within the suite of elements identified for Deep Star, those most closely associated with Au are As, Sb, Hg, Tl, Ag, and Zn (Heitt et al., in press). Silver is strongly associated with Au in the BMVT and Carlin-style ore at Cove, but the residence of Zn was recognized only in sphalerite in the BMVT ore. Ore-stage sphalerite and other base metal- ± Ag-bearing sulfides and/or sulfosalts have been identified in recent mineralogical studies for several Carlin-type deposits. Ferdock (1998) identified sphalerite as an ore-stage component of the Betze-Post deposit, along with other minerals that include base metal sulfides and Ag sulfides. Schilling et al. (1998) found sphalerite in the refractory ores at the Rain deposit, which were later included in the ore-stage paragenesis for Rain (Shallow and Thompson, 1999; Williams et al., 1999).

Tretbar (2000) identified an ore-stage assemblage at Getchell that includes base metal-bearing galena, sphalerite, jordanite ($Pb_{14}(As,Sb)_6S_{23}$), and galkhaite $(Cs,Tl)(Hg,Cu,Zn)_6(As,Sb)_4S_{12}$. In mineralized dacite from Meikle, Griffin, and Rodeo, ore-stage veinlets consisting of quartz-pyite ± sericite (and also rutile) are cut by possibly late ore-stage veinlets consisting of quartz and Ag sulfosalts (including pyrargyrite, miargyrite, and dyscrasite), with rare arsenian pyrite, arsenopyrite, and chalcopyrite (Ressel et al., 2000a). Silver-bearing minerals, including Ag-sulfosalts and tetrahedrite (var. freibergite) have been identified in ores from the Meikle deposit (Lauha and Bettles, 1993; Volk et al., 1996; Ressel et al., 2000a). Sphalerite occurs with barite in veins along what are thought to be feeder faults at the Carlin East deposit (Mike Robinson, personal communication, 2002).

For the Carlin-type deposits, the recognition of enrichments of elements other than those belonging to the classic "Carlin-suite" of elements (As, Sb, Au, Hg, and Tl), and the occurrence of numerous base metal (and other) sulfides in ore assemblages, have not been discussed in great detail. The lack of focus on such anomalies may be due to the relatively low concentrations of these elements and minerals, and may also be due to the fact that they are typically not analyzed. Data from the current study and earlier works suggest that rather than focusing on relative concentrations of elements and minerals in Carlin-type deposits, consideration should be given to their positions within a four-dimensional framework. Three-dimensions comprise the geologic framework of a given deposit, and the fourth comprises time. Time is included because future studies must be able to distinguish elements/minerals that are genetically, and therefore temporally, related to the mineralizing system from those produced or concentrated by unrelated

sedimentary, igneous, metamorphic, diagenetic or hydrothermal processes. Improvements in analytical techniques and detection limits should also continue to improve our understanding of the zonations and extents of geochemical anomalies associated with Carlin-type deposits. Understanding the distribution of ore-related elements has important implications, as recognition of such important geochemical, isotopic, and/or mineralogical indicators serve as guides for exploration, and may help to bridge the sub-economic gaps between the mineralized zones of complex systems.

CLOSING COMMENTS

^{40}Ar-^{39}Ar age data indicate that skarn ore at McCoy and BMVT (polymetallic vein) and Carlin-style ores at Cove formed contemporaneously, and that magmatism and mineralization at Cove are essentially coeval. Although the data are sparse, isotopic studies indicate a magmatic source for the mineralizing fluids at Cove, and also indicate a common source of S for the hypogene sulfides at McCoy and Cove. The S at Cove can be indirectly linked to the magmatic source based on the occurrence of sulfides with the same isotopic signatures at McCoy. The McCoy-Cove system exhibits mineralogical and geochemical zonations that are nearly identical to idealized zonations proposed for other porphyry-related systems (e.g. Sillitoe and Bonham, 1990; Jones, 1992). Based on these relations, and using conventional classification schemes, Cove is a telescoped deposit consisting of polymetallic vein and distal disseminated ore.

Mineralization at Cove produced telescoped BMVT and Carlin-style ores, and the deposit is located only 1.5 kilometers from the proximal McCoy Au (-Cu) skarn. The deposits at McCoy and Cove are genetically related to a larger magmatic system that

evolved during the late Eocene in a two-phase manner. The initial pulse produced relatively oxidized, magnetite-bearing intrusive rocks (e.g. Takahashi et al., 1980). The second pulse produced relatively reduced, ilmenite-bearing intrusive rocks (e.g. Takahashi et al., 1980). During both pulses, fluids were presumably released from a larger pluton at depth, and heat and fluid flow were focused at shallower levels by the apical Brown stock. It is important to note, however, that economic mineralization occurred with the second, relatively reduced pulse. Broadly similar models have been proposed for porphyry-related, polymetallic vein, and distal disseminated/Carlin-type deposits in the Battle Mountain district (Theodore, 1998b) and at Bingham (Sillitoe and Bonham, 1990; Jones, 1992), but these models do not include descriptions of magmatic systems evolving toward relatively reduced states. A recent descriptive model by Keith and Swan (2000), however, does implicate reduced magmas as the source for Carlin-type deposits.

The isotopic data from the Getchell and Deep Star deposits indicate potential igneous associations, and a strong association with Eocene magmatism has been identified for other deposits in the Goldstrike area and Genesis complex along the Carlin trend. These relationships suggest that at least several deposits that are widely regarded as Carlin-type deposits, including two of the largest deposits on the Carlin trend (Betze-Post and Genesis), should be reclassified as distal disseminated deposits. For these deposits, the magmatic center may be the northern Carlin trend-Emigrant Pass complex (Henry and Ressel, 2000). This igneous complex lies directly adjacent to the Carlin trend, and has been suggested to be the largest Eocene magmatic center in Nevada, which may help to explain the unusually large concentration of Au along the trend (Henry and Ressel,

2000). Other magmatic centers have been proposed for Carlin-type deposits elsewhere (Henry and Ressel, 2000).

Using McCoy-Cove as a model, the distal disseminated and Carlin-type deposits on the Carlin trend (and elsewhere) would occupy the most distal part of the system. Here, the Au:Ag ratios are highest. The best example of this position at Cove is the relatively Au-rich part of the Cove South Deep orebody (refer to Chapter 3; Fig. 22 and Fig. 23). Because this position is on the margin of the Cove deposit, it seems likely that it would be most susceptible to the influx of local waters circulated by the convective cell. Although no data were generated during the current study to substantiate such a theory, the influx of local meteoric, exchanged meteoric, or other waters may help to explain the non-magmatic isotopic signatures for many Carlin-type deposits.

The Carlin-style ore at Cove contains significantly more Ag than classic Carlin-type deposits, but this enrichment is not considered here to be intrinsically important to the proposed model for distal disseminated/Carlin-type deposits. The BMVT and Carlin-style orebodies at Cove are telescoped, and Cove is hosted by different units than most of the distal disseminated/Carlin-type deposits elsewhere in Nevada. At Cove, significant overlap of Ag may occur between the BMVT and the Carlin-style ores. Also, the basement rocks beneath the McCoy-Cove system and/or the Triassic host rocks may be enriched in Ag relative to the basement and Paleozoic host rocks along other parts of the Carlin, Getchell, Independence, and Battle Mountain-Eureka trends. In either scenario, abundant Ag may have been incorporated by the magma chamber during ascent, or may have been remobilized from country rocks by hydrothermal activity.

For Carlin-type deposits along the Carlin trend, pre-enrichments of Au in the Paleozoic rocks have been proposed to be factors during mineralization (Emsbo et al., 1999; Young-Mitchell and Titley, 2000), and may also help to account for higher concentrations of Au here than elsewhere in the Great Basin. Remobilization of at least some components during mineralization cannot be ruled out, and may be universal. Circulation of meteoric, connate, or other fluids, and associated remobilization of other components may account for non-magmatic signatures of mineralizing fluids and variable isotopic signatures for mineralizing components observed in many Carlin-type deposits.

Regardless of the ultimate source(s) of fluids and/or mineralizing components, Eocene magmatism is the heat source responsible for driving the convective hydrothermal cell at McCoy-Cove. Eocene magmatism has also been proposed to be the driving force for porphyry, skarn, polymetallic vein, distal disseminated, and most Carlin-type deposits along the various Au trends in Nevada and at Bingham (Sillitoe and Bonham, 1990; Theodore, 1998b; Henry and Ressel, 2000). In some cases, magmatic links have been already been established for the Carlin-type (distal disseminated) deposits. In other cases, such as Cortez/Pipeline and Alligator Ridge, no clear magmatic links have yet been recognized.

Establishing such genetic links to Eocene magmatism does not imply that continued exploration of Carlin-type systems will ultimately lead to the discovery of related Eocene polymetallic vein, skarn, or porphyry deposits. Magma chambers at depth can release mineralizing fluids capable of producing distal disseminated/Carlin-type deposits during many stages of their evolution (Keith and Swan, 2000). The contemporaneous emplacement of stocks capable of producing porphyry and/or skarn deposits at

appropriate levels in the crust may be entirely fortuitous. Nevertheless, the McCoy-Cove model in this study and/or the Bingham model of Jones (1992) should serve as bases of comparison for exploration in and around the occurrences of Carlin-type and porphyry-related deposits in the Great Basin.

As the hypogene components of Carlin-type deposits continue to be studied in greater detail, and with continued improvements in our analytical capabilities and sensitivities, a strong possibility exists that other links to Eocene magmatism will be identified for many, and possibly all, Carlin-type deposits in the Great Basin. Out of this possibility, at least one obvious question arises: what happens to the "Carlin-type" classification if the type locality is shown to be a distal disseminated deposit?

REFERENCES

Altamirano, C., and Thompson, T.B., 1999, Structural geology and hydrothermal alteration associated with the Deep Star orebody, northern Carlin trend, *in* Ralph J. Roberts Center for Research in Economic Geology Annual Meeting Program and Reports, January 7-8, 1999, University of Nevada, Reno, 19 p.

Allmendinger, R.W., and Jordan, T.E., 1984, Mesozoic structure of the Newfoundland Mountains, Utah: Horizontal shortening and subsequent extension in the hinterland of the Sevier belt: Geological Society of America Abstracts with Programs, v. 15, p. 513.

Alvarez, A.A., and Noble, D.C., 1988, Sedimentary rock-hosted disseminated precious metal mineralization at Purisma Concepcion, Yauricocha District, central Peru: Economic Geology, v. 83, p. 1368-1378.

Anderson, J.A., 1982, Characteristics of leached capping and techniques of appraisal, *in* Titley, S.R., ed., Advances in the geology of the porphyry copper deposits, southwestern North America: Tucson, Arizona, University of Arizona Press, p. 117-137.

Arehart, G.B., 1996, Characteristics and origin of sediment-hosted disseminated gold deposits: a review: Ore Geology Reviews, v. 11, p. 383-403.

Arehart, G.B., Eldridge, C.S., Chryssoulis, S.L., and Kesler, S.E., 1993a, Ion microprobe determination of sulfur isotope variations in iron sulfides from the Post-Betze sediment-hosted disseminated gold deposit, Nevada, USA: Geochimica et Cosmochimica Acta, v. 57, p. 1505-1519.

Arehart, G.B., Foland, K.A., Naeser, C.W., and Kesler, S.E., 1993b, $^{40}Ar/^{39}Ar$, K-Ar, and fission-track geochronology of sediment-hosted disseminated gold deposits at Post/Betze, Carlin trend, northeastern Nevada: Economic Geology, v. 88, p. 622-646.

Arehart, G.B., Tretbar, D., Chakurian, T., Christensen, J.N., Donelick, R., Zhang, X., and Foland, K.A., 2000, Review of the age of Carlin-type deposits in the Great Basin and implications for their formation, *in* Cluer, J.K., Price, J.G., Struhsacker, E.M., Hardyman, R.F., and Morris, C.L., eds., Geology and Ore Deposits 2000: The Great Basin and Beyond, May 15-18, 2000: Reno, Nevada, Geological Society of Nevada Symposium Proceedings, p. A1.

Armstrong, R.L., 1970, Geochronology of Tertiary igneous rocks, eastern Basin and Range province, western Utah, eastern Nevada, and vicinity, U.S.A.: Geochimica et Cosmochimica Acta, v. 34, p. 203-232.

Atkinson, W.W., Jr., and Einaudi, M.T., 1978, Skarn formation and mineralization in the contact aureole at Carr Fork, Bingham, Utah: Economic Geology, v. 73, p. 1326-1365.

Ballantyne, G., Smith, T.W., and Redmond, P.E., 1997, Distribution and mineralogy of gold and silver in the Bingham Canyon porphyry copper deposit, Utah: Society of Economic Geologists Guidebook Series, v. 29, p. 207-219.

Barton, P.B., Jr., and Toulmin, P., 1966, Phase relations involving sphalerite in the Fe-Zn-S system: Economic Geology, v. 61, p. 815-849.

Bastin, E.S., 1957, Interpretations of ore textures: Geological Society of America Memoir 45, 101 p.

Berger, B.R., and Bagby, W.C., 1993, The geology and origin of Carlin-type gold deposits, *in* Foster, R.P., Gold Metallogeny and Exploration: London, England, Chapman and Hall, p. 210-248.

Bigeleisen, J., Perlman, M.L., and Prosser, H.C., 1952, Conversion of hydrogenic minerals to hydrogen for isotopic analysis: Analytical Chemistry, v. 24, p. 1356-1357.

Blanchard, R., 1968, Interpretations of leached outcrops: Nevada Bureau of Mines Bulletin 66, 196 p.

Bodnar, R.J., 1993, Revised equation and table for determining the freezing point depression of H_2O-NaCl solutions: Geochimica et Cosmochimica Acta, v. 57, p. 683-684.

Borthwick, J., and Harmon, R.S., 1982, A note regarding ClF_3 as an alternative to BrF_5 for oxygen isotope analysis: Geochimica et Cosmochimica Acta, v. 46, p. 1665-1668.

Boyle, R.W., 1979, The geology of gold and its deposits: Canada Geological Survey Bulletin 280, p. 140.

Brooks, J.W., 1994, Petrology and geochemistry of the McCoy gold skarn, Lander County, Nevada: Pullman, Washington, Washington State University, Ph.D. dissertation, 607 p.

Brooks, J.W., Meinert, L.D., Kuyper, B.A., and Lane, M.L., 1991, Petrology and geochemistry of the McCoy gold skarn, Lander County, Nevada, *in* Raines, G.L., Lisle, R.E., Schafer, R.W., and Wilkinson, W.H., eds., Geology and ore deposits of the Great Basin, April 1-5, 1990: Reno, Nevada, Geological Society of Nevada Symposium Proceedings, p. 419-442.

Capuano, R.M., 1992, The temperature dependance of hydrogen isotope fractionation between clay minerals and water: Evidence from a geopressured system: Geochimica et Cosmochimica Acta, v. 56, p. 2547-2554.

Carten, R.B., White, W.H., and Stein, H.J., 1993, High-grade granite-related molybdenum systems: Classification and origin, *in* Kirkham, R.V., Sinclair, W.D., Thorpe, R.I., and Duke, J.M., eds., Mineral Deposit Modeling: Geological Association of Canada Special Paper 40, p. 521-554.

Cebula, G.T., Kunk, M.J., Mehnert, H.H., Naeser, C.W., Obradovich, J.D., and Sutter, J.F., 1986, The Fish Canyon Tuff, a potential standard for the ^{40}Ar-^{39}Ar and fission-track methods: Terra Cognita (6th Internation Congress on Geochronology, Cosmochronolgy and Isotope Geology), v. 6, p. 139.

Chryssoulis, S.L., Zhou, Y., Weisener, C., and Kingston, D., 1997, Deportment of gold and silver in testwork products of select McCoy ore zones: AMTEL report 97/55, unpublished report for Echo Bay Minerals Company, 59 p.

Clarke, L.J., Highsmith, R.P., and Thompson, T.B., Geochemical characteristics of the Rain orebody, Elko County, Nevada, *in* Cluer, J.K., Price, J.G., Struhsacker, E.M., Hardyman, R.F., and Morris, C.L., eds., Geology and Ore Deposits 2000: The Great Basin and Beyond, May 15-18, 2000: Reno, Nevada, Geological Society of Nevada Symposium Proceedings, p. B6.

Clayton, R.N., and Mayeda, T.K., 1963, The use of bromium pentafluoride in the extraction of oxygen from oxides and silicates for isotopic analyses: Geochimica et Cosmochimica Acta, v. 27, p. 43-52.

Craig, J.R., and Vaughan, D.J., 1994, Ore microscopy and ore petrography: New York, New York, John Wiley & Sons, Inc., p. 120-163.

Dickson, J.A.D., 1965, A modified staining technique for carbonates in thin section: Nature, v. 205, no. 4971, p. 587.

Doebrich, J.L., and Theodore, T.G., 1996, Geologic history of the Battle Mountain Mining District, Nevada, and regional controls on the distribution of mineral systems, *in* Coyner, A.R., and Fahey, P.L., eds., Geology and Ore Deposits of the American Cordillera: Reno, Nevada, Geological Society of Nevada Symposium Proceedings, p. 453-483.

Drews-Armitage, S.P., Romberger, S.B., and Whitney, C.G., 1996, Clay alteration and gold deposits in the Genesis and Blue Star deposits, Eureka County, Nevada: Economic Geology, v. 91, p. 1383-1393,

Durek, J.J., 1964, Some characteristics of weathered outcrops of disseminated copper deposits: New York, Columbia University, Ph.D. dissertation, 149 p.

Edwards, A.B., 1954, Textures of the ore minerals and their intergrowths: Australian Institute of Mining and Metallurgy, 242 p.

Emmons, W.H., 1926, Relations of metalliferous lode systems to igneous intrusives: Transactions of the American Institute of Mining and Metallurgical Engineers, v. 1571, no. 74, p. 42.

Emmons, W.H., 1933, On the mechanism of the deposition of certain metalliferous lode systems associated with granitic batholiths, *in* Lindgren, W., ed., Ore Deposits of the Western States: American Institute of Mining and Metallurgical Engineers, p. 327-349.

Emmons, W.H., 1937, Gold deposits of the world: McGraw-Hill Book Company, Incorporated, p. 32-35.

Emmons, D.L., and Coyle, R.D., 1988, Echo Bay details exploration activities at its Cove gold deposit in Nevada: Mining Engineering, v. 40, no. 8, p. 791-794.

Emmons, D.L., and Eng, T.L., 1995, Geology and mineral resources of the McCoy Mining District, Lander County, Nevada: text to accompany Nevada Bureau of Mines Map 103, 12 p.

Emsbo, P., Hofstra, A.H., Park, D., Zimmerman, J.M., and Snee, L., 1996, A mid-Tertiary age constraint on alteration and mineralization in igneous dikes on the Goldstrike property, Carlin trend, Nevada: Geological Society of America Abstracts with Programs, v. 28, no. 7, p. A-476.

Emsbo, P., Hutchinson, R.W., Hofstra, A.H., Volk, J.A., Bettles, K.H., Baschuk, G.J., and Johnson, C.A., 1999, Syngenetic Au on the Carlin trend: Implications for Carlin-type deposits: Geology, v. 27, no. 1, p. 59-62.

Emsbo, P., Hofstra, A.H., and Lauha, E.A., 2000, Jurassic auriferous polymetallic mineralization at the Goldstrike mine, Carlin trend, Nevada, *in* Cluer, J.K., Price, J.G., Struhsacker, E.M., Hardyman, R.F., and Morris, C.L., eds., Geology and Ore Deposits 2000: The Great Basin and Beyond, May 15-18, 2000: Reno, Nevada Geological Society of Nevada Symposium Proceedings, p. B2.

Ferdock, G., 1998, Mineralogy, alteration and geomechanic aspects of the Goldstrike mine in areas in and exterior to the Betze orebody, *in* Ralph J. Roberts Center for Research in Economic Geology Annual Meeting Program and Reports, January 8-9, 1998, University of Nevada, Reno, 19 p.

Folger, H.W., Hofstra, A.H., and Cline, J.S., 2000, Alteration and mass transfer in igneous dikes at the Getchell Carlin-type gold deposit, Nevada, *in* Cluer, J.K., Price, J.G.,Struhsacker, E.M., Hardyman, R.F., and Morris, C.L., eds., Geology and Ore Deposits 2000: The Great Basin and Beyond, May 15-18, 2000: Reno, Nevada Geological Society of Nevada Symposium Proceedings, p. A2.

Friedman, I., and O'Neal, J.R., 1977, Compilation of stable isotope fractionation factors of geochemical interest: United States Geological Survey Professional Paper 440-KK, p. 1-12.

Gillerman, V.S., 1982, Tungsten and copper skarns of the Railroad mining district, Nevada: Berkeley, California, University of California, Ph.D. dissertation, 195 p.

Gilluly, J., and Masurky, H., 1965, Geology of the Cortez quadrangle, Nevada: United States Geological Survey Bulletin 1175, 117 p.

Girard, J.P., and Fouillac A.M., 1995, Géochimie isotopique de l'oxygène et de l'hydrogène des argiles: Exemples d'application aux domaines diagénétique et géothermique, Bulletin des Centres de Recheches Exploration-Production Elf-Aquitaine 19, p. 167-195.

Goldstein, R.H., and Reynolds, T.J., 1994, Sytematics of fluid inclusions in diagenetic minerals: Society of Economic Paleontologists and Mineralogists Short Course 31, 199 p.

Groff, J.A., Heizler, M.T., McIntosh, W.C., and Norman, D.I., 1997, $^{40}Ar/^{39}Ar$ dating and mineral paragenesis for Carlin-type gold deposits along the Getchell trend, Nevada: Evidence for Cretaceous and Tertiary gold mineralization: Economic Geology, v. 92, p. 601-622.

Hall, C.M., Simon, G., and Kesler, S.E., 1997, Age of mineralization at the Twin Creeks SHMG Deposit, Nevada, *in* Vikre, P., Thompson, T.B., Bettles, K., Christensen, O., and Parratt, R., eds., Carlin-type Gold Deposits Field Conference: Society of Economic Geologists Guidebook Series, v. 28, p. 151-154.

Hedenquist, J.W., Arribas, A., Jr., and Reynolds, T.J., 1998, Evolution of an intrusion-centered hydrothermal system: Far Southeast-Lepanto Porphyry and epithermal Cu-Au deposits, Philippines: Economic Geology, v. 93, p. 373-404.

Heitt, D.G., Dunbar, W.W., Thompson, T.B., and Jackson, R, G., in press, Geology and geochemistry of the Deep Star Gold Deposit, Carlin trend, Nevada: Economic Geology.

Henry, C.D., and Boden, D.R., 1998, Eocene magmatism: The heat source for Carlin type deposits of northern Nevada: Geology, v. 26, p. 1067-1070.

Henry, C.D., and Ressel, M.W., 2000, Eocene magmatism of northeastern Nevada: The smoking gun for Carlin-type gold deposits, *in* Cluer, J.K., Price, J.G.,Struhsacker, E.M., Hardyman, R.F., and Morris, C.L., eds., Geology and Ore Deposits 2000: The Great Basin and Beyond, May 15-18, 2000: Reno, Nevada, Geological Society of Nevada Symposium Proceedings, p. 365-388.

Hitzman, M.W., 1999, Routine staining of drill core to determine carbonate mineralogy and distinguish carbonate alteration textures: Mineralium Deposita, v. 34, p. 794-798.

Hofstra, A.H., 1994, Geology and genesis of the Carlin-type gold deposits in the Jerritt Canyon district, Nevada: Boulder, Colorado, University of Colorado, Ph.D. dissertation, 719 p.

Hofstra, A.H., and Rye, R.O., 1998, δD and $\delta^{18}O$ data from Carlin-type gold deposits – implications for genetic models, *in* Tosdal, R.M., ed., Contributions to the Gold Metallogeny of Northern Nevada: United States Geological Survey Open-File Report 98-338, p. 202-210.

Hofstra, A.H., Snee, L.W., Rye, R.O., Folger, H.W., Phinisey, J.D., Loranger, R.J., Dahl, A.R., Naeser, C.W., Stein, H.J., and Lewchuk, M., 1999, Age constraints on Jerritt Canyon and other Carlin-type gold deposits in the western United States: Relationship to mid-Tertiary extension and magmatism: Economic Geology, v. 94, p. 769-802.

Honea, R.M., 1988, Upper Cove oxide sample: unpublished report for Echo Bay Minerals Company, 15 p.

Honea, R.M., 1990, Silver mineralogy of oxide ores: unpublished report for Echo Bay Minerals Company, 45 p.

Honea, R.M., 1991, Analysis of samples from the flotation concentrate, leached concentrate residue, and leached oxide tailings of the Cove deposit: unpublished report for Echo Bay Minerals Company, 35 p.

Honea, R.M., 1998, Polished section examination of 4105 bench, Cove samples 1 and 2: unpublished report for Echo Bay Minerals Company, 18 p.

Hutchison, M.N., and Scott, S.D., 1980, Sphalerite geobarometry applied to metamorphosed sulfide ores of the Swedish Caledonides and U.S. Appalachians: Norges Geologiske Undersoekelse Bulletin 360, p. 59-71.

Ilchik, R.P., 1990, Geology and geochemistry of the Vantage gold deposits, Alligator Ridge-Bald Mountain mining district, Nevada: Economic Geology, v. 85, p. 50-75.

Ilchik, R.P., and Barton, M.D., 1997, An amagmatic origin of Carlin-type gold deposits: Economic Geology, v. 92, no. 3, p. 269-288.

James, A.H., Smith, W.H., and Bray, R.E., 1961, Bingham district – a zoned porphyry ore deposit, *in* Cook, D.R., ed., Geology of the Bingham Mining District and Northern Oquirrh Mountains: Utah Geological Society Guidebook 16, p. 81-100.

Jerome, S.E., 1966, Some features pertinent in exploration of porphyry copper deposits, *in* Titley, S.R., and Hicks, C.L., eds., Geology of the Porphyry Copper Deposits, Southwestern North America: Tuscon, Arizona, University of Arizona Press, p. 75-83.

John, E.C., 1975, Mineral zones of the Bingham district, *in* Bray, R.E., and Wilson, J.C., eds., Guidebook to the Bingham Mining District: Bingham Canyon, Utah, Kennecott Copper Corporation, p. 59-72.

John, E.C., 1978, Mineral zones in the Utah copper orebody: Economic Geology, v. 73, p. 1250-1259.

Jones, B.K., 1992, Application of metal zoning to gold exploration in porphyry copper systems: Journal of Geochemical Exploration, v. 43, p. 127-155.

Joralemon, P., 1951, The occurrence of gold at the Getchell mine, Nevada: Economic Geology, v. 46, p. 267-310.

Keith, S.B., and Swan, M.M., 2000, The Carlin gold giants: Linkages to reduced, wet, calc-alkalic differentiation sequences, deep-seated strike-slip fault kinematics, and regional compressive/transpressive Andean arc dynamics, *in* Cluer, J.K., Price, J.G., Struhsacker, E.M., Hardyman, R.F., and Morris, C.L., eds., Geology and Ore Deposits 2000: The Great Basin and Beyond, May 15-18, 2000: Reno, Nevada, Geological Society of Nevada, Symposium Proceedings, p. A3.

Kingston, D., Chryssoulis, S., Semenyna, L., Weisener, C., Knipe, S., and Venter, D., 1997, Process mineralogy of McCoy's 'problem' ore of May 1997: AMTEL report 97/53, unpublished report for Echo Bay Minerals Company, 54 p.

Komor, S.C., 1995, Chemistry and petrography of calcite in the KTB pilot borehole, Bavarian Oberpfalz, Germany: Chemical Geology, v. 124, p. 199-215.

Knipe, S., Chryssoulis, S., Kingston, D., and Dimov, S., 1997, Deportment of gold in leached pyrite concentrate of McCoy's SE extension: AMTEL report 97/50, unpublished report for Echo Bay Minerals Company, 35 p.

Kuehn, C.A., and Rose, A.W., 1992, Geology and geochemistry of wall-rock alteration at the Carlin gold deposit, Nevada: Economic Geology, v. 87, p. 1697-1721.

Kuyper, B.A., Mach, L.E., Streiff, R.E., and Brown, W.A., 1991, Geology of the Cove gold-silver deposit: Society for Mining, Metallurgy, and Exploration, Inc., Preprint no. 91-125, 19 p.

Lang, J.R., Baker, T., Hart, C.J.R., and Mortensen, J.K., 2000, An exploration model for intrusion-related gold systems: Society of Economic Geologists Newsletter, n. 40, p. 1 and 6-15.

Lauha, E.A., and Bettles, K.H., 1993, A geologic comparison of the Post-Betze and Purple Vein deposits of the Goldstrike and Meikle mines, Nevada: Society for Mining, Metallurgy, and Exploration, Inc., Preprint no. 93-170, 20 p.

Leonardson, R.W., and Rahn, J.E., 1996, Geology of the Betze-Post gold deposits, Eureka County, Nevada, *in* Coyner, A.R., and Fahey, P.L., eds., Geology and Ore Deposits of the American Cordillera, April, 1995: Reno/Sparks, Nevada, Geological Society of Nevada Symposium Proceedings, p. 61-94.

Maher, B.J., Browne, Q.J., and McKee, E.H., 1993, Constraints on the age of gold mineralization and metallogenesis in the Battle Mountain-Eureka mineral belt, Nevada: Economic Geology, v. 88, p. 469-478.

Mako, D.A., 1997, Characterization and dating of argillic alteration in the Mercur gold district, Utah – A discussion: Economic Geology, v. 92, p. 633-634.

McCrea, J.M., 1950, The isotopic chemistry of carbonates and a paleotemperature scale: Journal of Chemical Physics, v. 18, p. 849-857.

Miller, D.M., Wooden, J.L., and Wright, J.E., 1989, Mantle-derived Late Jurassic plutons emplaced during possible regional extension of the crust, northwest Utah and northeast Nevada: Geological Society of America Abstracts with Programs, v. 21, no. 5, p. 117.

Moore, D.M, and Reynolds, R.C., Jr., 1989, X-ray diffraction and the identification and analysis of clay minerals: Oxford, New York, Oxford University Press, p. 199-200.

Muller, S.W., Ferguson, H.G., and Roberts, R.J., 1951, Geology of the Mount Tobin quadrangle, Nevada: United States Geological Survey Geologic Quadrangle Map GQ-7.

Nichols, K.M., and Silberling, N.J., 1977, Stratigraphy and depositional history of the Star Peak Group (Triassic), northwestern Nevada: Geological Society of America Special Paper 108, 73 p.

Nutt, C.J., Hofstra, A.H., Hart, K.S., and Mortensen, J.K., Structural setting and genesis of gold deposits in the Bald Mountain-Alligator Ridge area, east-central Nevada, *in* Cluer, J.K., Price, J.G., Struhsacker, E.M., Hardyman, R.F., and Morris, C.L., eds., Geology and Ore Deposits 2000: The Great Basin and Beyond, May 15-18, 2000: Reno, Nevada Geological Society of Nevada Symposium Proceedings, p. 513-537.

Ohmoto, H., and Goldhaber, M.G., 1997, Sulfur and carbon isotopes, *in* Barnes, H.L., ed., Geochemistry of Hydrothermal Ore Deposits, 3rd edition: New York, New York, John Wiley & Sons, Inc., p. 517-612.

Ohmoto, H., and Rye, R.O., 1979, Isotopes of sulfur and carbon, *in* Barnes, H.L., ed., Geochemistry of Hydrothermal Ore Deposits, 2nd edition: New York, New York, Wiley Interscience, p. 509-567.

Phinisey, J.D., Hofstra, A.H., Snee, L.W., Roberts, T.T., Dahl, A.R., and Loranger, R.J., 1996, Evidence for multiple episodes of igneous and hydrothermal activity and constraints on the timing of gold mineralization, Jerritt Canyon district, Elko County, Nevada, *in* Coyner, A.R., and Fahey, P.L., eds., Geology and Ore Deposits of the American Cordillera, April, 1995: Reno/Sparks, Nevada, Geological Society of Nevada Symposium Proceedings, p. 15-39.

Pierce, F.W., and Bolm, J.G., eds., 1995, Porphyry copper deposits of the American Cordillera: Tuscon, Arizona, Arizona Geological Society Digest, v. 20, 656 p.

Presnell, R.D., and Parry, W.T., 1996, Geology and geochemistry of the Barneys Canyon gold deposit, Utah: Economic Geology, v. 91, p. 273-288.

Radtke, A.S, Rye, R.O., and Dickson, F.W., 1980, Geology and stable isotope studies of the Carlin gold deposit, Nevada: Economic Geology, v. 75, p. 641-662.

Rayias, A.C., 1999, Stratigraphy, structural geology, alteration, and geochemistry of the northeastern Railroad district, Elko County, Nevada: Reno, Nevada, University of Nevada, M.S. thesis, 180 p.

Ressel, M.W., Noble, D.C., and Connors, K.A., 1998, Eocene dikes of the Carlin Trend, Nevada: Magmatic As, Sb, Cs, Tl, CO^2 & excess argon suggest a deep degassing model for gold mineralization: Geological Society of America Abstracts with Programs, v. 20, p. A118.

Ressel, M.W., Noble, D.C., Henry, C.D., and Trudel, W.S., 1999, Eocene magmatism and coeval episodic gold mineralization in the northern part of the Carlin trend, Nevada: Geological Society of America Abstracts with Programs, v. 31, no. 6, p. A-88.

Ressel, M.W., Noble, D.C., Heizler, M.T., Volk, J.A., Lamb, J.B., Park, D.E., Conrad, J.E., and Mortensen, J.K., 2000a, Gold-mineralized Eocene dikes at Griffin and Meikle: bearing on the age and origin of deposits of the Carlin Trend, Nevada, *in* Cluer, J.K., Price, J.G., Struhsacker, E.M., Hardyman, R.F., and Morris, C.L., eds., Geology and Ore Deposits 2000: The Great Basin and Beyond, May 15-18, 2000: Reno, Nevada, Geological Society of Nevada, Symposium Proceedings, p. 79-101.

Ressel, M.W., Noble, D.C., Henry, C.D., and Trudel, W.S., 2000b, Dike-hosted ores of the Beast deposit and the importance of Eocene magmatism in gold mineralization of the Carlin trend, Nevada: Economic Geology, v. 95, p. 1417-1444.

Roedder, E., 1979, Fluid inclusions as samples of ore fluids, *in* Barnes, H.L., Geochemistry of Hydrothermal Ore Deposits, 2nd edition: Wiley Interscience, p. 684-737.

Roedder, E., 1984, Fluid inclusions: Reviews in Mineralogy, v. 12, 634 p.

Roberts, R.J., Radtke, A.S., Coats, R.R., Silberman, M.L., and McKee, E.H., 1971, Gold bearing deposits in north-central Nevada and southwestern Idaho, with a section on periods of plutonism in north-central Nevada: Economic Geology, v. 66, p. 14-33.

Schrader, F.C., 1934, The McCoy mining district and gold veins in Horse Canyon, Lander County, Nevada: United States Geological Survey Circulation 10, 13 p.

Schurer, V., and Fuchs, W.A., 1988, Ore microscopy and electron microprobe analysis results for a selected suite of metallurgical samples from the Cove deposit, Nevada: unpublished report for Echo Bay Minerals Company, 145 p.

Schwartz, G.M., 1951, Classification and definitions of ore textures and mineral structures in ores: Economic Geology, v. 46, p. 578-591.

Scott, S.D., and Barnes, H.L., 1971, Sphalerite geothermometry and geobarometry: Economic Geology, v. 66, p. 653-669.

Seedorff, E., 1991, Magmatism, extension, and ore deposits of Eocene to Holocene age in the Great Basin – mutual effects and preliminary proposed genetic relationships, *in* Raines, G.L., Lisle, R.E., Schafer, R.W., and Wilkinson, W.H., eds., Geology and ore deposits of the Great Basin, April 1-5, 1990: Reno, Nevada, Geological Society of Nevada Symposium Proceedings, p. 133-178.

Shallow, L.J., and Thompson, T.B., Structure, alteration, and geochemistry from the Rain mine, Elko County, Nevada, *in* Ralph J. Roberts Center for Research in Economic Geology Annual Meeting Program and Reports, January 7-8, 1999, University of Nevada, Reno, 67 p.

Shepherd, T.J., Rankin, A.H., and Alderton, D.H.M., 1985, A practical guide to fluid inclusion studies: Glascow, Scotland, Blackie & Son Ltd., 239 p.

Sheppard, S.M.F., and Gilg, H.A., 1996, Stable isotope geochemistry of clay minerals: Clay Minerals, v. 31, p. 1-24.

Silberling, N.J., and Roberts, R.J., 1962, Pre-Tertiary stratigraphy and structure of northwestern Nevada: Geological Society of America Special Paper 72, 53 p.

Sillitoe, R.H., 1983, Styles of low-grade gold mineralization in volcano-plutonic arcs: Nevada Bureau of Mines and Geology Report 36, p. 52-68.

Sillitoe, R.H., and Bonham, H.F., 1990, Sediment-hosted gold deposits: Distal products of magmatic-hydrothermal systems: Geology, v. 18, p. 157-161.

Simon, G., Kesler, S.E., and Chryssoulis, S., 1999, Geochemistry and textures of gold-bearing arsenian pyrite, Twin Creeks, Nevada: Implications for deposition of gold in Carlin-type deposits: Economic Geology, v. 94, no. 3, p. 405-422.

Spurr, J.E., 1907, A theory of ore deposition: Economic Geology, v. 2, p. 781-795.

Stager, H.K., 1977, Part II: Mineral Deposits, *in* Geology and mineral deposits of Lander County, Nevada: Nevada Bureau of Mines and Geology Bulletin 88, p. 86-87.

Staudacher, T.H., Jessberger, E.K., Dorflinger, D., and Kiko, J., 1978, A refined ultrahigh-vacuum furnace for rare gas analyses: Journal of Physics, E: Scientific Instruments, v. 11, p. 781-784.

Steven, T.A., Mehnert, H.H., and Obradovich, J.D., 1967, Age of volcanic activity in the San Juan Mountains, Colorado: United States Geological Survey Professional Paper 575-D, p. 47-55.

Stewart, J.H., and McKee, E.D., 1977, Part I: Geology, *in* Geology and mineral deposits of Lander County, Nevada: Nevada Bureau of Mines and Geology Bulletin 88, p. 1-59.

Streiff, R.E., 1994, Geology and mineralization of the Panther Canyon Clastic Member at the Cove Mine, Nevada: unpublished report for Echo Bay Minerals Company, 20 p.

Takahashi, M., Aramaki, S., and Ishihara, S., 1980, Magnetite-series/ilmenite-series vs. I type/S-type granitoids: Mining Geology Special Issue, no. 8, p. 13-28

Theodore, T.G., and Jones, G.M., 1990, Geochemistry and geology of gold in jasperoid, Elephant Head area, Lander County, Nevada: United States Geological Survey Open File Report 90-13, p. 13-14.

Theodore, T.G., 1998a, Pluton-related gold in the Battle Mountain mining district – an overview, *in* Tosdal, R.M., ed., Contributions to the Gold Metallogeny of Northern Nevada: United States Geological Survey Open-File Report 98-338, p. 251-252.

Theodore, T.G., 1998b, Large distal-disseminated precious metal deposits, Battle Mountain mining district, Nevada, *in* Tosdal, R.M., ed., Contributions to the Gold Metallogeny of Northern Nevada: United States Geological Survey Open-File Report 98-338, p. 253-258.

Thode, H.G., Monster, J., and Dunford, H.B., 1961, Sulphur isotope geochemistry: Geochimica et Cosmochimica Acta, v. 25, no. 3, p. 159-174.

Thorman, C.H., Nutt, C.J., and Brooks, W.E., 1994, Middle Eocene volcanism and pre middle Eocene attenuation faulting in the eastern Great Basin and their relation to gold mineralization, *in* Williams, C., ed., Structural Geology and Mineral Deposits in Northeastern Nevada: Elko, Nevada, Geological Society of Nevada Symposium Volume, 12 p.

Thorman, C.H., Brooks, W.E., Snee, L.W., Hofstra, A.H., Christensen, O.D., and Wilton, D.T., 1996, Eocene-Oligocene model for Carlin-type deposits in northern Nevada, *in* Coyner, A.R., and Fahey, P.L., eds., Geology and Ore Deposits of the American Cordillera, April, 1995: Reno/Sparks, Nevada, Geological Society of Nevada Symposium Proceedings, p. 75.

Titley, S.R., 1982, The style and progress of mineralization and alteration in porphyry copper systems, *in* Titley, S.R., ed., Advances in the Geology of the Porphyry Copper Deposits, Southwestern North America: Tucson, Arizona, University of Arizona Press, p. 93-116.

Titley, S.R., 1993, Characteristics of porphyry copper occurrences in the American southwest, *in* Kirkham, R.V., Sinclair, W.D., Thorpe, R.I., and Duke, J.M., eds., Mineral Deposit Modeling: Geological Association of Canada Special Paper 40, p. 433-464.

Titley, S.E., and Marozas, D.C., 1995, Processes and products of supergene copper enrichment, *in* Pierce, F.W., and Bolm, J.G., eds., Porphyry copper deposits of the American Cordillera: Tuscon, Arizona, Arizona Geological Society Digest, v. 20, p. 156-168.

Tretbar, D.R., 2000, Controls on gold deposition in the 194 orebody, a collapse breccia in the Getchell mine, Humboldt County, Nevada *in* Ralph J. Roberts Center for Research in Economic Geology Annual Meeting Program and Reports, January 6-7, 2000, University of Nevada, Reno, 51 p.

Tretbar, D., 2001, The distribution, chemistry, and dating of galkhaite, an uncommon but important accessory mineral in Carlin-type gold deposits: Geological Society of Nevada Membership Directory 2001-2002, p. 95-96

Tunnell, G., 1930, The oxidation of disseminated copper ores in altered porphyry: Cambridge, Massachusetts, Harvard University, Ph.D. dissertation, 106 p.

Tunnell, G., and Posnjak, E., 1931, Aportion of the system, ferric oxide-cupric oxide-sulfur trioxide-water: Journal of Physical Chemistry, v. 35, p. 929-946.

Turneaure, F.S., 1960, A comparitive study of major ore deposits of central Bolivia: Economic Geology, v. 55, p. 217-254, 574-606.

Turneaure, F.S., 1971, The Bolivian tin-silver province: Economic Geology, v. 66, p. 215-225.

Vanderburg, W.O., 1939, Reconnaissance of mining districts in Lander County, Nevada: United States Bureau of Mines Information Circulation 7043, p. 64-65.

Vandervoort, D.S., and Schmitt, J.G., 1990, Cretaceous to early Tertiary paleogeography in the hinterland of the Sevier thrust belt, east-central Nevada: Geology, v. 18, p. 567-570.

Vaughan, D.J., and Craig, J.R., 1997, Sulfide ore mineral stabilities, morphologies, and intergrowth textures, *in* Barnes, H.L., ed., Geochemistry of Hydrothermal Ore Deposits, 3rd edition: New York, New York, John Wiley & Sons, Inc., p. 367-434.

Volk, J.A., Lauha, E., Leonardson, R.W., and Rahn, J.E., 1996, Structural geology of the Betze-Post and Meikle deposits, Elko and Eureka Counties, *in* Green, S.M., and Struhsaker, E., eds., Road log for Trip B; Structural Geology of the Carlin Trend: Geology and Ore Deposits of the American Cordillera Field Trip Guidebook Compendium: Reno, Nevada, Geological Society of Nevada, p. 180-194.

Weaver, K.D., and Cline, J.S., 1999, Geochemistry of ore-stage and non-ore pyrite and marcasite from the Getchell Carlin-type gold deposit, Nevada: Geological Society of America Cordilleran Section Abstracts with Programs, v. 31, no. 6, p. A106.

Weiss, S.I., Percival, T.J., Noble, D.C., and Ressel, M.W., 2000, The "Carlin-Type" – "Carlin-like" dichotomy revisited: The general association of sedimentary rock-hosted gold deposits with magmatic activity, *in* Cluer, J.K., Price, J.G., Struhsacker, E.M., Hardyman, R.F., and Morris, C.L., eds., Geology and Ore Deposits 2000: The Great Basin and Beyond, May 15-18, 2000: Reno, Nevada, Geological Society of Nevada, Symposium Proceedings, p. A4.

Wendt, I., and Carl, C., 1991, The statistical distribution of the mean squared weighted deviation: Chemical Geology, v. 86, p. 275-285.

Williams, C.J., Thompson, T.B., Powell, J.L., and Dunbar, W.W., 1999, The Rain mine gold-bearing breccia system: Part I: Field relationships, *in* Ralph J. Roberts Center for Research in Economic Geology Annual Meeting Program and Reports, January 7-8, 1999, University of Nevada, Reno, 59 p.

Wilson, P.N., and Parry, W.T., 1995, Characterization and dating of argillic alteration in the Mercur gold district, Utah: Economic Geology, v. 90, p. 1197-1216.

Young-Mitchell, M., and Titley, S.R., 2000, Gold enrichments and paleoenvironments of Ordovician siliciclastic host rocks for gold deposits, Great Basin, U.S.A., *in* Cluer, J.K., Price, J.G., Struhsacker, E.M., Hardyman, R.F., and Morris, C.L., eds., Geology and Ore Deposits 2000: The Great Basin and Beyond, May 15-18, 2000: Reno, Nevada, Geological Society of Nevada, Symposium Proceedings, p. B4.

APPENDIX I

Structural Data for the Cove Deposit

NUMBER	BENCH	ORIENTATION	MINERALIZED?
1	4145E	N31E,66NW	
2	4145E	N54E,79NW	
3	4145E	N46W,49SW	X
4	4145E	N46E,80NW	
5	4145E	N69W,47NE	X
6	4145E	N54E,81NW	
7	4145E	N35W,34NE	X
8	4145E	N50W,47NE	X
9	4145E	N9E,67SE	
10	4145E	N52W,70NE	
11	4145E	N52W,78SW	?
12	4145E	N31W,77SW	
13	4145E	N64E,76SE	
14	4145E	N61E,49NW	
15	4205E	N64W,60SW	
16	4205E	N50W,49SW	
17	4205E	N54W,49SW?	X
18	4205E	N82W,41SW?	X
19	4205E	N49W,60NE	
20	4205E	N50W,51NE	
21	4205E	N49W,40NE	
22	4205E	N31W,79NE	
23	4205E	N54W,39NE	X
24	4205E	N42W,70NE	X
25	4205E	N44W,76NE	
26	4205E	N59E,61NW	
27	4205E	N76E,54SE	
28	4205E	N11E,56NW	
29	4205E	N32W,59SW	
30	4245E	N16W,56SW	
31	4245E	N19W,45SW	X
32	4245E	N49E,89SE	
33	4245E	N57W,40SW	X
34	4245E	N49W,40NE	X
35	4245E	N42E,67NW	
36	4245E	N44W,43NE	
37	4245E	N48W,46NE	X
38	4245E	N56W,77NE	
39	4285E	N88W,45SW	X
40	4285E	N51E,70NW	X
41	4285E	N10W,51NW	
42	4285E	N59E,74NW	
43	4285E	N31E,64NW	
44	4285E	N53E,49NW	
45	4285E	N60E,81NW	
46	4325E	N46E,60NW	X
47	4325E	N42E,61NW	
48	4325E	N31W,60SW	
49	4325E	N82E,66NW	
50	4365E	N52E,73NW	
51	4365E	N47E,26SE	
52	4365E	N75E,67NW	
53	4365E	N11W,42NE	
54	4465E	N34E,vertical	

Appendix I-A: Pervasive joint set attitudes for the Cove deposit

NUMBER	BENCH	ORIENTATION	MINERALIZED?
55	4465E	N67E,86NW	
56	4465E	N61E,53NW	
57	4525E	N49E,62NW	
58	AR-DW-5	N50E,62NW	
59	AR4655E	N54E,59NW	
60	AR4655E	N40E,26NW	

Appendix I-A: Pervasive joint set attitudes for the Cove deposit

NUMBER	BENCH	ATTITUDE
1	4145E	N16W,28NE
2	4145E	N30W,24NE
3	4145E	N32W,34NE
4	4145E	N6E,14SE
5	4145E	N2W,22NE
6	4145E	N16W,12NE
7	4145E	N47E,17SE
8	4145E	N20W,22NE
9	4145E	N82E,22NW
10	4145E	N4W,36SW
11	4145E	N1W,5SW
12	4145E	N14W,9SW
13	4145E	N84W,13SW
14	4145E	N45W,14SW
15	4145E	N52W,15SW
16	4145E	N49W,27SW
17	4145E	N81E,21SE
18	4145E	N77W,24SW
19	4145E	N79W,18SW
20	4145E	N76E,15SE
21	4145E	N81W,18SW
22	4145E	N64E,20SE
23	4145E	N44W,13SW
24	4145E	N79W,9SW
25	4145E	N79E,21SE
26	4145E	N61E,26SE
27	4145E	N81E,25SE
28	4145E	N76E,25SE
29	4145E	N13E,30SE
30	4145E	N54E,40SE
31	4145E	N52E,22SE
32	4145E	N26E,24SE
33	4205E	N17W,25NE
34	4205E	N4W,29NE
35	4205E	N18W,18NE
36	4205E	N69W,19NE
37	4205E	N30W,14SW
38	4205E	N79E,23SE
39	4205E	N65E,16SE
40	4205E	N85E,14SE
41	4205E	N84W,18SW
42	4205E	N88E,18S
43	4205E	N79E,19SE
44	4205E	N62W,29SW
45	4205E	N70E,17SE
46	4205E	N81E,20SE
47	4205E	N76E,34SE
48	4205E	N66E,26SE
49	4205E	N62E,29SE
50	4205E	N63E,29SE
51	4205E	N28W,41NE
52	4205E	N23W,49NE
53	4205E	N30W,62NE
54	4245E	N9W,28NE

Appendix I-B: Bedding attitudes for the Cove deposit

NUMBER	BENCH	ATTITUDE
55	4245E	N6W,39NE
56	4245E	N17W,41NE
57	4245E	N26W,51NE
58	4245E	N19W,42NE
59	4245E	N14W,40NE
60	4245E	N8W,46NE
61	4245E	N16W,45NE
62	4245E	N76E,35SE
63	4245E	N54E,46SE
64	4245E	N79E,18SE
65	4245E	N56E,28SE
66	4245E	N72E,31SE
67	4245E	N67E,39SE
68	4245E	N42E,41SE
69	4245E	N86E,20SE
70	4245E	N27W,23NE
71	4245E	N8E,21SE
72	4245E	N72E,23SE
73	4245E	N41E,19SE
74	4245E	N46E,15SE
75	4285E	N36W,32NE
76	4285E	N16W,29NE
77	4285E	N19W,20NE
78	4285E	N20W,62NE
79	4285E	N11W,48NE
80	4285E	N16W,32NE
81	4285E	N8W,40NE
82	4285E	N13W,51NE
83	4285E	N53E,30SE
84	4285E	N64E,20SE
85	4285E	N79W,22NE? np
86	4285E	N81E,20SE
87	4285E	N68W,16SW? np
88	4285E	N64E,24SE
89	4285E	N67W,32SW
90	4285E	N79W,42SW
91	4285E	N82W,18SW
92	4285E	N76W,34SW
93	4285E	N86W,27SW
94	4325E	N54E,23SE
95	4325E	N16W,40NE
96	4325E	N11E,33SE
97	4325E	N3E,36SE
98	4325E	N4E,26SE
99	4325E	N11W,55NE
100	4325E	N33W,44NE
101	4325E	N78W,38N
102	4325E	N41W,28NE
103	4325E-A	N22W,28NE
104	4365E	N5W,30E
105	4365E	N18W,37NE
106	4365E	N6E,38E
107	4365E	N23E,31SE
108	4365E	N34E,29SE

Appendix I-B: Bedding attitudes for the Cove deposit

NUMBER	BENCH	ATTITUDE
109	4365E	N1W,38E
110	4365E	N47E,26SE
111	4365E	N5W,22E
112	4365E	N24W,32NE
113	4365E	N37W,40NE
114	4365E	N46W,29NE
115	4365E	N41W,34NE
116	4365E	N31W,40NE
117	4365E	N21W,53NE
118	4365E	N39W,53NE
119	4365E	N23W,43NE
120	4365E	N16W,44NE
121	4365E	N20W,45NE
122	4365E	N11W,42NE
123	4365E	N1W,45E
124	4365E	N16E,53SE
125	4365E	N3E,24SE
126	4365E	N44E,33SE
127	4365E	N63E,31SE
128	4365E	N63E,30SE
129	4365E	N76E,26SE
130	4365E	N80E,30SE
131	4365E	N73E,14SE
132	4365E	N86W,30S
133	4365E	N87E,27S
134	4365E	N68W,39S
135	4365E	N63E,43SE
136	4365E	N6E,25SE
137	4365E	N76W,14S
138	4365E	N82W,28S
139	4405E	N37W,19NE
140	4405E	N86E,9N np
141	4405E	N74W,20N np
142	4465E	N84W,35SW
143	4465E	N78E,32S
144	4465E	N54W,27SW
145	4465E	N86W,34S
146	4465E	N59E,33SE
147	4465E	N10W,22W
148	4465E	N68E,34SE
149	4465E	N19W,9NE
150	4465E	N35W,13SW
151	4465E	N89E,15S
152	4465E	N58E,29SE
153	4465E	N27E,31SE
154	4465E	N22W,32NE
155	4465E	N8W,26NE
156	4465E	N52W,27NE
157	4465E	N61W,30NE
158	4465E	N9W,26NE
159	4465E	N45W,44NE
160	4465E	N10W,17E
161	4465E	N27E,36SE
162	4465E	N24E,22SE

Appendix I-B: Bedding attitudes for the Cove deposit

NUMBER	BENCH	ATTITUDE
163	4465E	N26E,35SE
164	4465E	N1W,38E
165	4465E	N34W,40NE
166	4465E	N7W,45E
167	4465E	N26W,28NE
168	4465E	N4W,24NE
169	4465E	N9W,38NE
170	4465E	N2E,42NE
171	4465E	N12W,32NE
172	4465E	N31W,50NE
173	4465E	N16W,21NE
174	4465E	N18W,29NE
175	4465E	N18W,30NE
176	4465E	N27W,40NE
177	4465E	N5E,38E
178	4465E	N21W,42NE
179	4465E	N19W,40NE
180	4465E	N8W,38NE
181	4465E	N11W,46NE
182	4465E	N5W,34NE
183	4465E	N23W,33NE
184	4465E	N13E,21E
185	4465E	N86W,24S
186	4465E	N76E,14S
187	4465E	N61E,36SE
188	4465E	N46E,30SE
189	4465E	N88W,25S
190	4465E	N89W,23S
191	4465E	N83E,29S
192	4465E	N43E,35SE
193	4465E	N79E,24S
194	4465E	N79W,23S
195	4465E	N55W,23NE np
196	4465E	N89W,35S
197	4465E	N57W,30NE np
198	4465E	N66E,22SE
199	4465E	N84E,32S
200	4465E	N85W,34S
201	4525E	N74W,19S
202	4525E	N89W,24S
203	4525E	N53W,19NE
204	4525E	N57E,22SE
205	4525E	N71E,36SE
206	4525E	N90E,23S
207	4525E	N86W,26S
208	4525E	N89W,19S
209	4525E	N81E,18S
210	4525E	N90E,27S
211	4525E	N72E,26S
212	4525E	N88W,17S
213	4525E	N82E,26S
214	4525E	N82E,26S
215	4525E	N83W,12S
216	4525E	N67E,27S

Appendix I-B: Bedding attitudes for the Cove deposit

NUMBER	BENCH	ATTITUDE
217	4525E	N73E,24S
218	4525E	N79E,27S
219	4525E	N59E,26SE
220	4525E	N49E,24SE
221	4525E	N56E,44SE
222	4525E	N47E,39SE
223	4525E	N48E,17SE
224	4525E	N46E,24SE
225	4525E	N46E,24SE
226	4525E	N12W,24E
227	4525E	N19W,36E
228	4725E	N5W,47E
229	4725E	N11W,42E
230	4725E	N19W,33NE
231	4725E	N12W,52E
232	4725E	N12W,39E
233	4725E	N13W,43NE
234	AR-DW-5	N37E,36SE
235	AR-DW-5	N54E,39SE
236	AR-DW-5	N64E,49SE
237	AR-DW-5	N45E,36SE
238	AR-DW-5	N84W,26S
239	AR-DW-5	N74E,35S
240	AR-DW-5	N57E,32SE
241	AR-DW-5	N61E,54SE
242	AR-DW-5	N67E,49SE
243	AR-DW-5	N70E,46SE
244	AR-DW-5	N68E,51SE
245	AR-DW-5	N65E,48SE
246	AR-DW-5	N80E,36S
247	AR-DW-5	N72E,43S
248	AR-DW-5	N83E,54S
249	AR-DW-5	N85E,34S
250	AR-DW-5	N89E,25S
251	AR-DW-5	N46W,25SW
252	AR-DW-5	N46E,33NW
253	AR-DW-5	N60W,16SW
254	AR-DW-5	N69W,27S
255	AR-DW-5	N69W,31S
256	AR-DW-5	N71W,30S
257	AR-DW-5	N81W,18S
258	AR-DW-5	N79W,19S
259	AR-DW-5	N74W,20S
260	AR-DW-5	N56W,24SW
261	4750-4775E	N33W,29SW
262	4750-4775E	N56W,26SW
263	4750-4775E	N39W,30SW
264	4750-4775E	N37W,29SW
265	4750-4775E	N22W,26SW
266	4750-4775E	N36W,30SW
267	4750-4775E	N8W,36W
268	4750-4775E	N51W,34SW
269	4750-4775E	N71E,26S
270	4750-4775E	N42W,13SW

Appendix I-B: Bedding attitudes for the Cove deposit

NUMBER	BENCH	ATTITUDE
271	4750-4775E	N61W,12SW
272	4750-4775E	N66W,26SW
273	4750-4775E	N61W,26SW
274	4750-4775E	N53W,20SW
275	4750-4775E	N62W,31SW
276	4750-4775E	N88E,34S
277	4750-4775E	N58W,41SW
278	4750-4775E	N75W,30SW
279	4825-4850E	N46E,36SE
280	4825-4850E	N47E,46SE
281	4825-4850E	N35E,25SE
282	4825-4850E	N86W,39S
283	4825-4850E	N63E,32SE
284	4825-4850E	N66E,37SE
285	4825-4850E	N66E,37SE
286	4825-4850E	N69E,45SE
287	4825-4850E	N78E,19SE
288	4825-4850E	N84E,30SE
289	AR-4655E	N7W,29E
290	AR-4655E	N63W,35NE
291	AR-4655E	N12W,40E
292	AR-4655E	N26W,46NE
293	AR-4655E	N19W,41NE
294	AR-4655E	N2W,36E
295	AR-4655E	N4W,34E
296	AR-4655E	N3E,40E
297	AR-4655E	N12E,34E
298	AR-4655E	N12W,49E
299	AR-4655E	N11E,44E
300	AR-4655E	N9E,49E
301	4655E	N83W,23S
302	4655E	N67W,19S
303	4655E	N81W,26S
304	4655E	N89E,24S
305	4655E	N29W,43SW
306	4655E	N79E,15S
307	4655E	N52W,19SW
308	4655E	N59W,24SW
309	4655E	N70W,33SW
310	4655E	N68W,32SW
311	4655E	N71W,30SW
312	4655E	N70E,21SE
313	4655E	N73E,25S
314	4655E	N74W,28S
315	4655E	N83W,21S
316	4655E	N68W,25S
317	4595E	N47W,33SW
318	4595E	N39W,12SW
319	pb10/10	N54W,12NE
320	pb10/10	N5E,17E
321	pb10/10	N78E,14S
322	pb10/10	N72E,17S
323	pb10/10	N65W,31S
324	pb10/10	N54W,33S

Appendix I-B: Bedding attitudes for the Cove deposit

NUMBER	BENCH	ATTITUDE
325	pb10/10	N46E,26S
326	pb10/10	N70E,18S
327	pb10/10	N62W,46S
328	4005	N5W,29NE
329	4005	N26E,27SE
330	4005	N56W,24NE
331	4005	N58W,34NE
332	4005	N43W,14NE
333	4005	N66W,31NE
334	4005	N32W,22NE
335	4005	N21W,44NE
336	4005A	N76W,24S
337	4005A	N63W,29SW
338	4005A	N78W,10S
339	4005A	N58W,22SW
340	4005A	N89W,18S
341	4005A	N75W,16S
342	4005A	N74W,33S
343	4005A	N42E,29SE
344	4005A	N27E,20SE
345	4005A	N17W,12SW
346	4005A	N47W,6NE
347	4005A	N70E,18SE
348	4005A	N12W,32NE
349	ARPB	N31E,30SE
350	ARPB	N83E,34S
351	ARPB	N6E,9E
352	ARPB	N28W,27NE
353	ARPB	N46W,27NE
354	ARPB	N81W,27N
355	ARPB	N72W,28N
356	ARPB	N35W,22NE
357	ARPB	N4W,16E
358	ARPB	N7W,29E
359	ARPB	N23W,24NE
360	ARPB	N13W,18NE
361	ARPB	N54W,35NE
362	ARPB	N31W,21NE
363	3965	N77W,32NE
364	3965	N13W,19NE
365	3965	N28W,33NE
366	3965	N16W,22NE
367	AR4955&4955	N72E,22S
368	AR4955&4955	N72E,27SE
369	AR4955&4955	N59E,32SE
370	AR4955&4955	N73E,26SE
371	AR4955&4955	N55E,31SE
372	AR4955&4955	N46E,23SE
373	AR4955&4955	N35E,29SE
374	AR4955&4955	N56W,44NE
375	AR4955&4955	N47W,43NE
376	AR4955&4955	N17W,45NE
377	AR4955&4955	N4W,32E
378	AR4955&4955	N12W,39NE

Appendix I-B: Bedding attitudes for the Cove deposit

NUMBER	BENCH	ATTITUDE
379	AR4955&4955	N3W,42NE
380	AR4955&4955	N16W,44NE
381	AR4835	N62E,18SE
382	4895	N22E,32SE
383	5075	N30E,38SE
384	5015	N64E,31SE
385	5015	N20E,31SE
386	5015	N83E,32SE
387	5015	N36E,20SE
388	5015	N83E,16SE
389	5015	N34E,36SE
390	5015	N47E,75SE
391	5015	N10E,16SE
392	5015	N55E,32SE
393	5015	N51E,24SE

Appendix I-B: Bedding attitudes for the Cove deposit

FAULT #	FAULT NAME	BENCH	OFFSET	ORIENTATION	COMMENTS
1		4145E		N23E,37NW	thin
2	Lighthouse sympathetic	4145E		N30W,88NE	
3		4145E	"large"	N51E,73NW	large structural feature
4		4145E		N58E,72NW	related to Bay; sympathetic?
5	Lighthouse	4145E	"large"	N22W,76NE	
6	Bay sympathetic I	4145E		N46E,71NW	
7		4145E	6'	N34E,70SE	conjugate
8	Song's/Blasthole sympathetic	4145E		N65E,64NW	conjugate
9	Song's/Blasthole	4145E	large?	N46E,44NW	
10		4145E		N43W,variable dip	highly irregular shear; corrugated
11		4205E		N41E,87SE	
12		4205E		N13W,89NE	does not offset Bay
13		4205E		N49E,58NW	
14		4205E	"small"	N56E,60NW	
15		4205E	"small?"	N70E,50NW	
16		4205E		N37W,81SW	conjugate, thin
17		4205E		N55E,80SE	conjugate
18		4205E		N30W,vertical dip	thin
19		4205E		N29W,76SW	relatively large
20		4205E		N35W,86NE	
21		4205E		N46E,66NW	large
22		4205E		N36W,75NE	thin
23		4205E	"small"	N38E,71NW	
24		4205E		N31W,76SW	thin
25		4205E		N9E,22SE	shallow dipping fault!
26		4205E		N46E,87SE	
27		4205E		N48E,36NW	
28		4205E		N20W,51NE	calcite vein
29		4245E		N35E,76NW	
30		4245E		N29W,51NE	truncated
31	SE Intrusive offsetter	4245E	at least 20'	N85W,39N	
32		4245E		N28W,50NE	6' wide
33		4245E		N27W,75NE	
34		4245E	2'	N34W,vertical dip	
35		4245E	8'	N76W,vertical	offsets shallow dipping fault
36		4245E	"very little"	N3W,82SW	
37		4245E		N26W,74NE	irregular conjugate
38		4245E		N61W,83SW	irregular conjugate
39		4245E	"small"	N7W,35NE	
40		4245E		N33W,44NE	5' wide
41		4245E	6'	N41E,72SE	offsets #40
42	Lighthouse sympathetic?	4245E		N35W,73NE	thin
43		4245E	4'	N16W,89NE	
44	Bay sympathetic	4245E		N54E,73NW	
45		4245E		N49E,62NW	thin
46		4245E	1'	N51E,49NW	conjugate
47		4245E		N56E,59SE	conjugate, thin

Appendix I-C: Measured fault orientations for the Cove deposit

FAULT #	FAULT NAME	BENCH	OFFSET	ORIENTATION	COMMENTS
48		4245E	6'	N15W,79SW	
49		4245E	<1'	N4E,69E	
50		4245E	2'	N64E,59NW	
51		4245E	12'	N35W,88SW	
52		4245E	0.5'	N14W,70SW	thin
53		4285E		N71E,56NW	large conspicuous shear
54		4285E		N37E,52NW	thin
55		4285E		N20W,66SW	
56		4285E		N38W,35NE	concordant
57		4285E	10+'(?)	N24E,53NW	
58		4285E		N6E,32NW	
59		4285E		N56E,66NW	
60		4285E		N71E,66NW	irregular
61		4285E		N8W,75SW	
62		4285E		N17W,78NE	conjugate, thin
63		4285E		N44W,67SW	thin
64		4285E		N72W,71NE	thin
65		4285E	>10'	N40W,81SW	
66	Lighthouse splay	4285E		N18E,64NW	
67		4285E	1'	N14E,80SE	
68		4285E	1'	N8E,81E	
69		4285E	6'	N49W,86SW	conjugate
70		4285E	6'	N31E,73NW	conjugate
71		4285E	1'	N7E,66NW	
72		4285E	10'	N5E,vertical dip	
73		4285E	<1'	N41W,81SW	
74		4285E	"large"	N39W,81NE	
75	Cay offsetter	4285E	20'	N0E,61W	continuation of Cay offsetter
76	Cay offsetter II	4285E		N42W,86NE	
77		4285E	14'	N2W,64W	
78		4285E	3'	N45W,74SW	
79		4285E		N25W,78NE	
80	Bay sympathetic II	4285E		N6E,72NW	
81	Bay sympathetic	4285E		N36E,63NW	
82		4285E		N35W,variable dip	irregular, highly mineralized
83		4325E		N3E,62W	
84		4325E		N49E,56NW	
85		4325E		N82E,86N	thin
86		4325E		N52W,20NE	thin, truncates in #85
87		4325E		N55E,64NW	
88		4325E		N1W,59E	offsets #89
89		4325E		N48E,42NW	
90		4325E		N26E,78NW	
91		4325E		N71E,62N	
92		4325E		N36E,49NW	4' wide
93		4325E		N19W,57NE	thin
94		4325E		N61E,76NW	thin

Appendix I-C: Measured fault orientations for the Cove deposit

FAULT #	FAULT NAME	BENCH	OFFSET	ORIENTATION	COMMENTS
95		4325E		N51E,62NW	
96		4325E		N53E,86NW	
97		4325E		N49W,85SW	
98		4325E		N62E,79NW	
99	Bay splay	4325E		N67E,75NW	
100		4325E		N12E,43NW	thin
101		4325E		N71E,57NW	thin
102		4325E		N11E,33SE	
103		4325E		N49E,76NW	thin
104		4325E		N41W,29NE	concordant
105		4325E		N51E,76NW	
106		4325E		N49W,34NE	concordant
107		4365E		N0E,70W	
108		4365E		N53W,59NE	
109		4365E		N72E,50N	thin
110		4365E		N11W,45NE	
111		4365E		N76E,75N	thin
112		4365E		N18W,74SW	
113		4365E		N67E,66NW	truncates a concordant fault
114		4365E		N26E,58NW	
115		4365E		N53W,61SW	
116	Blasthole?	4365E		N66E,49NW	
117		4365E		N1W,vertical dip	
118		4365E		N7W,86NE	
119		4365E		N53W,78NE	irregular
120		4365E		N29E,75SE	thin
121		4365E		N4W,70E	thin, filled with spar and gouge
122	Lighthouse dike A	4365E		N20W,81NE	intensely clay altered
123	Lighthouse dike B	4365E		N26E,85SE	intensely clay altered
124	Lighthouse	4365E	"large"	N13E,63SE	
125		4365E	"large"	N10E,82E	
126		4405E		N4W,82W	
127		4405E		N65E,74NW	
128		4405E		N65E,74NW	
129		4405E		N11E,70NW	
130		4405E		N8W,65W	
131		4405E		N81E,72N	
132	L2?	4405E		N32W,44NE	
133	Bay	4465E	"large"	N47E,64NW	
134		4465E		N66W,74NE	thin
135		4465E		N66W,79NE	thin
136	Northwester	4465E	"large?"	N72W,69NE	mineralized
137	Northwester	4465E	"large?"	N26W,88NE	mineralized
138		4465E		N66W,68NE	
139		4465E		N16E,50NW	
140		4465E		N37W,65SW	thin
141		4465E		N12W,66SW	thin

Appendix I-C: Measured fault orientations for the Cove deposit

FAULT #	FAULT NAME	BENCH	OFFSET	ORIENTATION	COMMENTS
142		4465E		N79E,67N	
143		4465E		N66W,34NE	concordant
144		4465E		N31E,50NW	
145		4465E		N55E,76NW	
146		4465E		N74E,70N	
147		4465E		N41W,51SW	
148		4465E		N58E,83NW	
149		4465E		N14W,44SW	
150		4465E		N55E,67NW	splay from #149?
151		4465E		N67E,85NW	thin
152		4465E		N89E,69N	truncates #151
153		4465E		N72E,68NW	
154		4465E		N80E,62N	thin, truncates #154
155		4465E		N44E,46SE	thin
156		4465E		N19W,79NE	
157		4465E	1'	N50W,84SW	
158		4465E		N51W,75SW	thin
159		4465E	2"	N14W,68W	
160		4465E		N18E,78E	lined with calcite vein
161		4465E	"large"	N49W,72NE	
162		4465E		N36E,72SE	
163		4465E		N36W,78NE	
164		4465E		N38E,55NW	
165		4465E		N60E,61NW	
166	Lighthouse splay II	4465E		N1W,82E	
167		4465E		N18W,54E	thin
168		4465E		N18W,60SW	thin
169		4465E		N54W,77NE	thin
170		4465E		N86W,76S	
171		4725E		N52E,40SE	
172		4725E		N43E,33NW	
173	Blasthole?	4725E		N59E,52NW	
174		AR-DW-5		N13W,66SW	thin
175		AR-DW-5		N8W,76NE	
176		AR-DW-5		N23W,68SW	
177		AR-DW-5		N13W,70SW	
178		AR-DW-5		N14W,60E	
179		AR-DW-5		N58E,58NW	
180		AR-DW-5		N52E,58NW	5' wide shear zone
181		4750-4775		N41E,61NW	
182		4750-4775		N32E,88SE	
183		4750-4775		N48E,84NW	thin
184		4750-4775	"large"	N38E,67SE	
185		4750-4775		N7W,72W	
186		4750-4775		N49E,54NW	whin
187		4750-4775		N40E,50NW	
188		4750-4775		N64E,67NW	8' wide shear zone

Appendix I-C: Measured fault orientations for the Cove deposit

FAULT #	FAULT NAME	BENCH	OFFSET	ORIENTATION	COMMENTS
189		4825-4850		N37W,76SW	
190		4825-4850		N46W,79NE	
191		4825-4850		N61W,72SW	filled with dike
192		4825-4850		N52W,75SW	
193		AR4655E		N61W,78NE	irregular
194		AR4655E		N69E,50NW	
195		AR4655E		N42E,69NW	shear zone
196		AR4655E		N62E,61NW	
197		4715E		N34E,73NW	
198		4655E		N66W,85SW	shear with dike
199		4655E		N78W,85S	
200		4655E		N59E,vertical dip	
201		4655E		N50E,80NW	
202		4655E		N18E,80NW	
203		4655E		N33E,84NW	
204	110?	4655E		N36E,62NW	
205		4025E		N11E,80W	
206		4025E		N47W,89SW	
207		4025E		N11W,77W	irregular
208		4025E		N28E,vertical dip	
209		4025E		N78W,86S	
210		4025E		N51E,74NW	
211		4025E		N62W,74SW	
212		4025E	6"	N23W,87NE	
213		4025E	10'+	N36E,53NW	
214		4025E	2'	N35E,vertical dip	
215		4025E	10'+	N43E,45NW	
216		4025E		N53E,48NW	
217		4025E	"small"	N10E,69W	
218		4025E		N34E,68NW	very thin
219	Lighthouse splay	4005E		N41W,73NE	
220		4005E		N3W,85E	
221		4005E		N36W,vertical dip	
222		4005E		N43W,vertical dip	
223		4005E		N22W,vertical dip	
224		4005E		N56E,62NW	
225		4005E		N23W,vertical dip	
226	Lighthouse reverser splay	4005E		N35E,73NW	
227		4005E		N29W,82NE	
228		4005E		N13W,83NE	
229		4005E		N21W,68NE	
230	Blasthole splay	4005E		N63E,66NW	
231	Blasthole	4005E		N15E,68NW	
232		4005E		N22W,vertical dip	
233		4005E		N27E,80NW	
234		4005E		N13W,73W	
235		4005E		N20W,80SW	

Appendix I-C: Measured fault orientations for the Cove deposit

FAULT #	FAULT NAME	BENCH	OFFSET	ORIENTATION	COMMENTS
236		4005E		N2E,81E	
237		4005E		N25E,75NW	
238		4005E		N27E,62NW	filled with BMVT vein
239		4005E		N80E,65N	filled with BMVT vein
240		4005E		N12W,86SW	filled with 5" wide BMVT vein
241		4005E		N33E,55SE	filled with BMVT vein
242		4005E		N50E,62NW	filled with BMVT vein
243		4005E		N86W,66N	cuts the Cay fault/dike
244	Lighthouse lesser splay	4005E		N24E,59NW	veined
245		4005E		N42W,75SW	
246	Lighthouse splay	4005E		N13W,74NE	
247		ARPB		N24E,81NW	
248		ARPB		N45E,76NW	
249		ARPB		N42E,62NW	
250		ARPB		N67E,60NW	large, filled with BMVT vein
251		ARPB		N31E,78NW	filled with BMVT vein
252		ARPB		N21E,83SE	filled with BMVT vein
253		ARPB		N39E,68NW	filled with BMVT vein
254		ARPB		N32E,72NW	
255		ARPB		N54E,80NW	no veins
256		ARPB		N58E,60NW	no veins
257		ARPB		N5W,67E	thin
258		ARPB		N28W,87SW	
259	Lighthouse splay	ARPB		N32W,80NE	
260	Lighthouse splay	ARPB		N28W,70NE	
261		ARPB		N52W,48SW	1' wide prominent structure
262		3965E		N56E,77NW	thin
263	Lighthouse splay sympathetic	3965E		N25W,59NE	
264		3965E		N46E,74NW	
265		AR4955		N4E,81W	
266	Lighthouse fault array	ARPB		N21W,83NE	
267	Lighthouse fault array	ARPB		N4E,56E	
268	Lighthouse fault array	ARPB		N7W,66NE	
269		ARPB		N46E,62NW	
270	Lighthouse	ARPB		N7E,75E	
271	Lighthouse splay	Bottom		N41W,81NE	
272	Lighthouse splay	Bottom		N7W,76NE	
273	Lighthouse splay	Bottom		N2E,56E	
274		4005E		N5W,72NE	1' wide
275		4005E		N53E,59NW	6" wide
276	SE intrusive	4005E		N63E,63NW	
277		4005E		N80W,80N	
278		4955E	40-50'	N10W,61W	
279		4955E		N12E,67W	
280		4955E		N80E,78N	
281		4955E		N28E,29SE	bottom of Caetano
282		AR4835		N28W,78SW	

Appendix I-C: Measured fault orientations for the Cove deposit

FAULT #	FAULT NAME	BENCH	OFFSET	ORIENTATION	COMMENTS
283		AR4835		N22E,78NW	
284		5075		N74E,54NW	cuts intrusive
285		5075		N15E,61NW	fault bounding intrusive
286		5015		N59W,83SW	shear zone
287		5015		N10E,16SE	concordant fault with jasperoid

Appendix I-C: Measured fault orientations for the Cove deposit

APPENDIX II

Sample Descriptions

NO.	SAMPLE	BENCH	DATE ACQUIRED	FIELD NOTES/DESCRIPTION
1	CV-1-1 series	pit bottom*	2/9/98	samples from bms veins in Cove Anticline axis, pit bottom on 2/9/98
2	CP4145E-1	4145E	5/20/98	chert pebble cong, silica cement, sulfides in fractures
3	CP4145E-2	4145E	5/20/98	cong
4	CP4145E-3	4145E	5/20/98	cong
5	CP4145E-4	4145E	5/20/98	from alt zone in cong
6	CP4145E-5	4145E	5/20/98	purple ss pod, diss & fracture mineralization
7	CP4145E-6	4145E	5/20/98	na
8	CP4145E-7	4145E	5/20/98	vfg ss layer
9	CP4145E-8	4145E	5/20/98	cong lens, porous w/ sulfides in vugs
10	CP4145E-8B	4145E	5/20/98	ss below porous cong, fracture lined w/ sulfides
11	CP4145E-9	4145E	5/20/98	sulfides & vuggy cong
12	CP4145E-10	4145E	5/20/98	blue clay & sulfides from thin fractures (shears)
13	CP4145E-11	4145E	5/20/98	qtzite, massive
14	CP4145E-12	4145E	5/20/98	2 cm thick discordant bms vein
15	CP4145E-13	4145E	5/20/98	qtzite lens w/ dk olive gray sand & chert/qtzite pebbles
16	CP4145E-14	4145E	5/20/98	dk olive gray (clay) from (Lighthouse) fault margin
17	CP4145E-15	4145E	5/20/98	bms vein w/ clay alt
18	CP4145E-16	4145E	5/20/98	from qtzite - "CHECK FOR ALT & MIN PETROLOGICALLY"
19	CP4145E-17A	4145E	5/20/98	ss in footwall of Lighthouse sympathetic
20	CP4145E-17B	4145E	5/20/98	blue clay, mineralized, from Lighthouse sympathetic (?)
21	CP4145E-17C	4145E	5/20/98	intrusive in hanging wall of Lighthouse sympathetic
22	CP4145E-18	4145E	5/21/98	from mineralized shear zone
23	CP4145E-19	4145E	5/21/98	Bay porph dike
24	CP4145E-20	4145E	5/21/98	pod of dk olive gray coarser seds below Bay dike, slightly coarser bms
25	CP4145E-21	4145E	5/21/98	from rubble, bms vein cutting dike
26	CP4145E-22	4145E	5/21/98	vfg qtzite w/ vein/veinlets
27	CP4145E-23	4145E	5/21/98	vfg qtzite just above contact w/ dol (Panther Canyon or Home Station)
28	CP4145E-24	4145E	5/21/98	vuggy dol (top of P.C. submember or Home Station), good marker bed
29	CP4145E-25	4145E	5/21/98	intersecting bms veins w/ calcite, from rubble
30	CP4145E-25*	4145E	5/27/98	minerlized fault gouge
31	CP4145E-26	4145E	5/27/98	bms pod, friable, sooty
32	CP4145E-27	4145E	5/27/98	bms pod, friable, sooty
33	CP4145E-28	4145E	5/27/98	dol in footwall of CR4145E-27, sanded?
34	CP4145E-29	4145E	5/27/98	from blasted ore above /in 4125, directly across 1000' marker
35	CP4145E-30	4145E	5/27/98	major normal fault
36	CP4145E-31	4145E	5/27/98	unmineralized dol
37	4145E-32	4145E	5/27/98	from clastics just above dol contact
38	4145E-33	4145E	5/27/98	from fault - "CHECK FOR MINERALIZATION"
39	4145E-34	4145E	5/28/98	slstone - "COMPARE TO SLTSTN ON OTHER SIDE OF LIGHTHOUSE"
40	4145E-35	4145E	5/28/98	clay from fault zone
41	4145E-36	4145E	5/28/98	boulder from float - "USE FOR VEIN PARAGENESIS"
42	4145E-37	4145E	5/28/98	below dol marker unit in Panther Canyon clastics
43	4145E-38	4145E	5/28/98	in dol marker unit in Panther Canyon clastics
44	4145E-39	4145E	5/28/98	above dol marker unit in Panther Canyon clastics
45	4145E-40	4145E	5/28/98	clay alt sltstn from near border w/ Cay
46	4145E-41	4145E	5/28/98	clay alt sltstn from further away from Cay
47	4145E-42	4145E	5/28/98	clay alt sltstn from even further away from Cay

Appendix II-A: Rock samples collected from the Cove open pit

NO.	SAMPLE	BENCH	DATE ACQUIRED	FIELD NOTES/DESCRIPTION
48	4145E-43	4145E	5/28/98	Cay porph dike
49	4145E-44	4145E	5/28/98	more resistant Cay dike
50	4145E-45	4145E	5/28/98	sltstn w/ sparse diss % veinlet sulfides
51	4145E-46	4145E	5/29/98	Lighthouse footwall sltstn
52	4145E-47	4145E	5/29/98	Lighthouse footwall sltstn
53	4145E-48	4145E	5/29/98	Lighthouse footwall sltstn
54	4145E-49	4145E	5/29/98	Lighthouse footwall sltstn
55	4145E-50	4145E	5/29/98	vein (sulfides, sooty) in Lighthouse footwall sltstn
56	4145E-51	4145E	5/29/98	Lighthouse fault core
57	4145E-52	4145E	5/29/98	calcite vein from float, pink tint, no (?) sulfides, metallic rhombic mineral
58	4145E-53	4145E	5/29/98	random carbonaceous ls from float
59	4145E-54	4145E	5/29/98	"INTERESTING SAMPLE GRABBED FROM FLOAT"
60	4145E-55	4145E	5/29/98	sample from bedding
61	4145E-56	4145E	5/29/98	thin calcite veining w/ sulfides, from carbonaceous ls
62	4145E-57	4145E	5/29/98	bleached carbonaceous ls near SE Int
63	4145E-58	4145E	5/29/98	SE Int - blue stain & sulfides in fractures
64	4145E-59	4145E	5/29/98	SE Int - fresh piece - "USE FOR SCOPE & DATES (?)"
65	4145E-60	4145E	5/29/98	SE Int - fresh piece w/ slicks & calcite on one side
66	4145E-61	4145E	5/29/98	SE Int - gouge from bottom lft contact, w/ blue stained clay (?)
67	4205E-1	4205E	5/31/98	very friable alt cong from lens in sltstn
68	4205E-2	4205E	5/31/98	resistant sltstn around cong lens
69	4205E-3	4205E	5/31/98	clay alt cong from bleached zone in shear zone
70	4205E-4	4205E	5/31/98	cong in footwall of Bay dike/fault, alt
71	4205E-5	4205E	5/31/98	porph from Bay dike/fault
72	4205E-6	4205E	5/31/98	intensely alt cong from Bay dike/fault
73	4205E-7	4205E	5/31/98	intensely alt porph from Bay dike/fault
74	4205E-8	4205E	6/1/98	mineralized heavy blue clay from Lighthouse
75	4205E-9	4205E	6/1/98	from shear zone - sltstn block w/in ?
76	4205E-10	4205E	6/1/98	just above Bay dike - extremely dense bms network in hangingwall
77	4205E-11	4205E	6/1/98	sltstn in Bay dike footwall, veinlet py
78	4205E-12	4205E	6/1/98	sltstn from float w/ calcite veins cutting sulfide veinlets
79	4205E-13	4205E	6/1/98	sltstn w/ abundant small diss py + calcite cement
80	4205E-14	4205E	6/2/98	irregular pod of clay w/ sparse small diss py
81	4205E-15	4205E	6/2/98	1 cm thick concordant calcite & bms veins
82	4205E-16	4205E	6/2/98	1 cm thick calcite vein from joint adjacent to Song's/Blasthole fault
83	4205E-17	4205E	6/3/98	larger diss py cubes from sltstn in float
84	4205E-18	4205E	6/3/98	ochre fracture stain - "ACTIVELY PPTing JAROSITE ?"
85	4205E-19	4205E	6/3/98	Cay dike porph - 'WHAT IS GREEN MINERAL ?"
86	4205E-20	4205E	6/3/98	from white clay in Lighthouse - "SEVERELY ALT PORPH ?"
87	4205E-21	4205E	6/3/98	clay from shear, very low sulfide content
88	4205E-22	4205E	6/9/98	SE Int bottom sill - glassy matrix w/ bio, plag, diss sulfides
89	4205E-23	4205E	6/9/98	SE Int core - phenos more abundant & larger
90	4205E-24	4205E	6/9/98	3 cm wide calcite vein w/ no (?) sulfides
91	4245E-1	4245E	6/9/98	clay alt ls pod above dol/clastics contact
92	4245E-2	4245E	6/9/98	conjugate shear w/ clay & calcite veins
93	4245E-3	4245E	6/10/98	intensely alt ls xenolith in SE Int
94	4245E-4	4245E	6/10/98	?vein

Appendix II-A: Rock samples collected from the Cove open pit

NO.	SAMPLE	BENCH	DATE ACQUIRED	FIELD NOTES/DESCRIPTION
95	4245E-5	4245E	6/10/98	sample from float - "USE FOR VEIN PARAGENESIS"
96	4245E-6	4245E	6/11/98	clay in Lighthouse splay
97	4245E-7	4245E	6/11/98	Panther Canyon: 1 cong & 1 sltstn from Lighthouse footwall
98	4245E-8	4245E	6/11/98	cong/sltstn contact showing both
99	4245E-9	4245E	6/11/98	dk olive gray clay alt pod
100	4245E-10	4245E	6/11/98	clay alt cong between 2 shears
101	4245E-11	4245E	6/15/98	15 cm wide clay filled shear breccia, somewhat mineralized
102	4245E-12	4245E	6/15/98	random Panther Canyon clastics
103	4245E-13	4245E	6/15/98	.5-2 cm thick discordant bms vein
104	4245E-14	4245E	6/15/98	severely alt cong: chert to clay, cement to sulfides, from float
105	4245E-15	4245E	6/15/98	bms cemented breccia from float
106	4245E-16	4245E	6/15/98	zone of clay cemented breccia frags - cong, bms, etc.
107	4245E-17	4245E	6/15/98	bms vein from float
108	4245E-18	4245E	6/15/98	sltstn from footwall below Bay sympathetic
109	4245E-19	4245E	6/15/98	concordant bms/clay vein
110	4285E-1	4285E	6/16/98	clay from Bay fault - "OBLITERATED PORPH DIKE ?"
111	4285E-2	4285E	6/16/98	random Smelser Pass ls w/ no clay/oxide
112	4285E-3	4285E	6/16/98	3-10 cm thick concordant calcite veins
113	4285E-4	4285E	6/16/98	clay/oxide alt Smelser Pass ls
114	4285E-5	4285E	6/16/98	layered clay alt
115	4285E-6	4285E	6/16/98	vein - bms in clay w/ calcite
116	4285E-7	4285E	6/16/98	vein from float - bms in clay w/ calcite
117	4285E-8	4285E	6/17/98	Smelser Pass boulders from bench w/ calcite AND qtz veins !!
118	4285E-9	4285E	6/17/98	cong clasts in clay matrix + mineralized cong from Lighthouse fault zone
119	4285E-10	4285E	6/18/98	Cay dike - plag, bio, qtz
120	4285E-11	4285E	6/18/98	Cay sill - fresh plag, bio, qtz, no (?) sulfides
121	4285E-12	4285E	6/19/98	from clay in Song's/Blasthole fault - "COMPARE TO BELOW !"
122	4285E-13	4285E	6/19/98	cong lens - more mineralization (?), clay alt, friable, sulfides present
123	4285E-14	4285E	6/19/98	sltstn just below contact w/ cong lens - "COMPARE TO CONG LENS"
124	4285E-15	4285E	6/19/98	Bay dike cut by bms veins
125	4285E-16	4285E	6/19/98	argillized Bay dike from float
126	4285E-17	4285E	6/19/98	bms oddballs from slide float
127	4285E-18	4285E	6/19/98	highly mineralized shear
128	4285E-19	4285E	6/19/98	odd clay cemented breccia "vein"
129	4325E-1	4325E	6/25/98	from float from clay/oxide above: darker calcite, pyrolusite
130	4325E-2	4325E	6/25/98	from float from clay/oxide above: stalactitic cc in vug - "DIAGENETIC?"
131	4325E-3	4325E	6/25/98	wall rocks & calcite vein: Smelser Pass, 1 has rextallized mollusc (?)
132	4325E-4	4325E	6/25/98	calcite vein from fault #238
133	REALGAR A	4325E	6/25/98	realgar w/ stibnite & calcite
134	REALGAR B	4325E	6/25/98	realgar w/ calcite in clay
135	REALGAR C	4325E	6/25/98	general realgar samples
136	4325E-5	4325E	6/26/98	siderite from float (from above)
137	4325E-6	4325E	6/26/98	from float: large rextallized mollusc/ammonite (?)
138	4325E-7	4325E	6/26/98	in situ realgar w/ clay
139	4325E-8	4325E	6/26/98	from float: realgar w/ later (?) calcite vein !
140	4325E-9	4325E	6/26/98	from float: boxwork textured (?) sample from above
141	4325E-10	4325E	6/26/98	from float: jasperoids (first appearance)

Appendix II-A: Rock samples collected from the Cove open pit

NO.	SAMPLE	BENCH	DATE ACQUIRED	FIELD NOTES/DESCRIPTION
142	4325E-11	4325E	6/26/98	clay alt Bay porph dike w/ diss py
143	4325E-12	4325E	6/26/98	Bay dike, clay alt, small diss py
144	BOTTOMA	pit bottom (4105')	7/9/98	sulfides w/ qtz
145	BOTTOMB	pit bottom (4105')	7/9/98	sulfides w/ qtz
146	4325E-A1	4325E-A	7/9/98	from float: Mn clay/oxide + dark calcite vein w/ clay/oxide in ls
147	4365E-1	4365E	7/10/98	sulfide veins in ls w/ bluish tint
148	4365E-1A	4365E	7/10/98	sulfide veins in ls w/ bluish tint
149	4365E-2	4365E	7/10/98	clay from "L2" fault zone
150	4365E-4	4365E	7/10/98	random Smelser Pass from non-clay/oxide zone
151	4365E-5	4365E	7/10/98	from float: pyrolusite w/ calcite
152	4365E-6	4365E	7/10/98	interbedded calcareous sh w/ ls - contains small diss py
153	4365E-7	4365E	7/11/98	from float: calcite & sulfides (py & blue?)
154	4365E-8	4365E	7/11/98	from float: pyrolusite (?) on clay/oxide alt ls
155	4365E-9	4365E	7/13/98	from float: dogtooth calcite - "SUPERGENE ?"
156	4365E-10	4365E	7/13/98	from float: clay/oxide alt ls w/ goethite
157	4365E-11	4365E	7/13/98	concordant calcite vein
158	4365E-12	4365E	7/13/98	intense primary clay alt Smelser Pass
159	4365E-13	4365E	7/13/98	from float: pervasive oxidation of Panther Canyon siltstone
160	4405E-1	4405E	7/13/98	argillized dike
161	4405E-2	4405E	7/13/98	from float: sill/dike porph from above
162	4465E-1	4465E	7/14/98	mineralized clay from "NEW ONE A" shear
163	4465E-2	4465E	7/14/98	minerlized clay & breccia from "NEW ONE A"
164	4465E-3	4465E	7/14/98	dogtooth calcite in clay alt ls from slide
165	4465E-4	4465E	7/14/98	strange clay alt ls from slide
166	4465E-5	4465E	7/16/98	from float: orange-brown, fairly massive calcite in clay/oxide ls
167	4465E-6	4465E	7/16/98	from float: travertine w/ polished foreign clasts on margin
168	4465E-7	4465E	7/16/98	travertine
169	4465E-8	4465E	7/17/98	random Smelser Pass - "CAN'T SEE ANY PY W/ HANDLENS"
170	4465E-9	4465E	7/18/98	SE Int porph: A = slightly oxidized, B = intensely oxidized
171	4465E-10	4465E	7/18/98	Smelser Pass w/ primary clay alt - "HOW MUCH ALT ?"
172	4465E-11	4465E	7/18/98	from float: propylitized SE Int w/ unk green mineral
173	4465E-12	4465E	7/19/98	from float: ellipsoidal vug w/ boxwork calcite & unknown Ag(?)/Mn(?) mineral
174	4465E-13	4465E	7/19/98	from float: large dogtooth calcite xtals from vein
175	4465E-14	4465E	7/19/98	from float: oxide alt Panther Canyon cong
176	4525E-1	4525E	7/23/98	slightly oxide alt Panther Canyon cong
177	4525E-2	4525E	7/23/98	sltstn/vfg ss w/ possible bioclasts -"CHECK FOR TRANSITIONAL FOSSILS"
178	4525E-3	4525E	7/23/98	Smelser Pass from just above basal contact
179	4525E-4	4525E	7/24/98	from float: hem/goeth(?) from intense oxide (limonite ?) zone in fault footwall
180	4525E-5	4525E	7/25/98	bleached Smelser Pass - significant primary clay alt ?; from no clay/oxide zone
181	7/26/98-1	4145E	7/26/98	float vein samples for polished sections
182	7/26/98-2	4145E	7/26/98	vuggy dol w/ qtz & sulfides from contact on N wall
183	DW-12-1	AR-DW-12	8/5/98	Mn jasperoid from xenolith in SE Int
184	DW-12-2	AR-DW-12	8/5/98	Mn clay from xenolith in SE Int
185	4725E-1	4725E	8/5/98	Mn jasperoid
186	4725E-2	4725E	8/5/98	intensely alt Smelser Pass associated w/ Mn jasperoid
187	4725E-3	4725E	8/5/98	from float: high Mn content jasperoid
188	4725E-4	4725E	8/6/98	from slide: porph sill w/ bio & feldspar, no qtz - "DIFF FROM OTHERS?"

Appendix II-A: Rock samples collected from the Cove open pit

NO.	SAMPLE	BENCH	DATE ACQUIRED	FIELD NOTES/DESCRIPTION
189	AR-1	AR-DW-5	8/6/98	strange silicic alt (jasperoid) from fault
190	AR-2	AR-DW-5	8/7/98	porph clasts from karst fill (?)
191	AR-5	AR-DW-5	8/7/98	porph clasts from karst fill (?)
192	AR-6	AR-DW-5	8/7/98	from float: large int dike
193	AR-7	AR-DW-5	8/7/98	from float: jasperoid/ls
194	AR-8	AR-DW-5	8/7/98	from float: Lighthouse int porph - "DIFF FROM OTHER INT - COMPARE!"
195	25-50-1	4825-4850E	8/8/98	no oxide alt int porph - "ARGILLIC OR PHYLLIC ALT?"
196	25-50-2	4825-4850E	8/8/98	100% oxide alt int porph
197	25-50-3	4825-4850E	8/8/98	50% oxide alt int porph - "APATITE ALT TO GREEN PHOSPHATE MIN?"
198	25-50-4	4825-4850E	8/8/98	intensely bleached Smelser Pass - "COMPARE TO OTHER S.P. SAMPLES"
199	AR4655E-1	AR-4655E	8/9/98	from float: porph similar to SE Int
200	AR4655E-2	AR-4655E	8/9/98	from float: random Smelser Pass - "COMPARE TO OTHER S.P. SAMPLES"
201	4655E-1	4655E	8/9/98	from slide: Caetano tuff - "LOOKS IDENTICAL TO AR-2 & AR-5 KARST FILL"
202	PB 10/10-1	pit bottom	10/10/98	large vein in mineralized shear #2
203	PB 10/10-2	pit bottom	10/10/98	from veins & bms pod near base of shear
204	PB 10/10-3	pit bottom	10/10/98	Blasthole fault; heavily mineralized with veins & bms pod
205	PB 10/10-4	pit bottom	10/10/98	cm+ wide bms veins w/ brecciated fragments
206	4005E-1	4005E	6/11/99	vuggy Home Station, don't see hypogene linings
207	4005E-2	(4045E)	6/11/99	py + calcite vein
208	4005E-3	(4045E)	6/11/99	sooty bms pod, 1' diam - "WHAT IS GANGUE - Mn?"
209	4005E-4	(4045E)	6/11/99	calcite only veins, compare isotopically?
210	4005E-5	4005E	6/11/99	from float, vein from bot 567' structure filled w/ 2" wide calcite w/ bms vein
211	4005E-6	4005E	6/12/99	from float, earlier bms vein cut by later calcite vein
212	4005E-7	4005E	6/12/99	5" wide bms vein from fault
213	4005E-8	4005E	6/12/99	cross-cutting veins w/ 1 calcite vein cut by bms vein!!!
214	ARPB-1	ARPB	6/12/99	very vuggy bms vein w/ calcite & qtz
215	ARPB-2	ARPB	6/12/99	extremely coarse bms pod (left sample w/ Don for assay)
216	ARPB-3	ARPB	6/12/99	calcite vein cutting ARPB-2 - "CHECK ISOTOPICALLY?"
217	4005E-A-1	4005A	6/13/99	random Home Station
218	ARPB-4	ARPB	6/13/99	random Home Station
219	AR4955E-1	AR4955	6/14/99	intrusive, similar to others, large apatite, fresh bio, very friable
220	AR4955E-2	AR4955	6/14/99	ditto for AR4955E-1 - "USE FOR AGES, PETROLOGY - DIFFERENT?"
221	AR4955E-3	AR4955	6/14/99	dk olive gray clay from intrusive, smells like sulfides present
222	PB-1	pit bottom	6/15/99	from float, probably from above = veined Panther Canyon cong!
223	4955E-1	4955	6/16/99	from float, clasts of Panther Canyon from clastic dike - "MINERALIZED?"
224	4955E-2	4955	6/16/99	coherent welded Caetano
225	4955E-3	4955	6/16/99	less coherent, slightly oxidized Caetano
226	4955E-4	4955	6/16/99	unwelded, much less dense Caetano
227	AR4835E-1	AR4835	6/17/99	sooty silicified Smelser Pass pod
228	AR4835E-2	AR4835	6/17/99	intrusive, fresh bio, similar to others, no visible py
229	4835E-1	4835	6/17/99	dissolution/collapse breccia Smelser Pass related to jasperoid pod
230	4835E-2	4835	6/17/99	float Mn jasperoid related to 4835E-1
231	4835E-3	4835	6/17/99	oxidized intrusive
232	4835E-4	4835	6/17/99	Mn jasperoid
233	4835E-4*	4835	6/17/99	unaltered ls related to 4835E-1&2
234	4835E-5	4835	6/17/99	incipient alteration of ls related to 4835E-1,2,&3
235	5015-1	5015	6/19/99	from float, Smelser Pass w/ dessication cracks - subaerial???

Appendix II-A: Rock samples collected from the Cove open pit

NO.	SAMPLE	BENCH	DATE ACQUIRED	FIELD NOTES/DESCRIPTION
236	5015-2	5015	6/19/99	foliated yellow jasperoid (?) from concordant fault
237	5015-3	5015	6/19/99	Smelser Pass transition to jasp (=multiple jasp types; see p. 67 in f.n. #3)
238				
239	HS-1			
240	HS-2			
241	HS-3			
242	HS-4			
243	HS-5			
244	HS-6			
245	UK-1			bms vein
246	UK-2			
247	UK-3			tabular calcite xtals on qtz, abundant small diss sulfides
248	UK-4			calcite & bms vein, calcite has pink tint
249	UK-5			dogtooth calcite from '99 summer large display
250	UK-6			prismatic calcite associated with supergene & rhodochrosite
251	UK-7			summer '98 large dogtooth calcite vein
252	UK-8			same loc as ARPB-1, intergrown cc & sulfides, calcite white to dk gray
253	sup unk			supergene unknown
254	AUK-1			

Appendix II-A: Rock samples collected from the Cove open pit

NO.	SAMPLE	DATE ACQUIRED	FIELD NOTES/DESCRIPTION
1	TC4 MID +66'	na	from Don Ryan - underground sample w/ abundant qtz - "FLUID INCLUSIONS"
2	TC6 FS 65'	na	high-grade underground vein, W rib - (Don has assay samp)
3	TC6A-117'	7/27/99	actually CE6FS + 117', vein bms from NW rib
4	CSD-1	7/27/99	Cove South Deep, half way between CV248 & CV248 FS; 18" above realgar vein
5	CSD-2	7/27/99	Cove South Deep, half way between CV248 & CV248 FS; 12" above realgar vein
6	CSD-3	7/27/99	Cove South Deep, half way between CV248 & CV248 FS; 6" above realgar vein
7	CSD-4	7/27/99	Cove South Deep, half way between CV248 & CV248 FS; in realgar vein
8	CSD-5	7/27/99	Cove South Deep, half way between CV248 & CV248 FS; 6" below realgar vein
9	CSD-6	7/27/99	Cove South Deep, half way between CV248 & CV248 FS; 12" below realgar vein
10	CSD-7	7/27/99	Cove South Deep, half way between CV248 & CV248 FS; 18" below realgar vein
11	248-A	7/27/99	Collected by Dave Emmons, same locality as CSD series
12	248-B	7/27/99	Collected by Dave Emmons, same locality as CSD series
13	248-C	7/27/99	Collected by Dave Emmons, same locality as CSD series
14	CSD-A1	7/27/99	5' from CV248, realgar vein
15	TC8-A1	7/27/99	TC8FS + 170', cong crustiform sulfide veinlets above sill
16	TC8-A2	7/27/99	TC8FS + 170', high density of flat sulfide veinlets from within sill
17	TC8FS + 150'	7/27/99	2" wide bms vein
18	CV291FSN +100'	8/17/99	from Don Ryan - realgar with orpiment or native S
19	CU-0'	3/13/00	transect across bms manto-like ore zone, 50' marker = CE-17
20	CU-10'	3/13/00	transect across bms manto-like ore zone, 50' marker = CE-17
21	CU-20'	3/13/00	transect across bms manto-like ore zone, 50' marker = CE-17
22	CU-25'	3/13/00	transect across bms manto-like ore zone, 50' marker = CE-17
23	CU-30'	3/13/00	transect across bms manto-like ore zone, 50' marker = CE-17
24	CU-40'	3/13/00	transect across bms manto-like ore zone, 50' marker = CE-17
25	CU-45'	3/13/00	transect across bms manto-like ore zone, 50' marker = CE-17
26	CU-46'	3/13/00	transect across bms manto-like ore zone, 50' marker = CE-17
27	CU-47'	3/13/00	transect across bms manto-like ore zone, 50' marker = CE-17
28	CU-48'	3/13/00	transect across bms manto-like ore zone, 50' marker = CE-17
29	CU-49'	3/13/00	transect across bms manto-like ore zone, 50' marker = CE-17
30	CU-50'	3/13/00	transect across bms manto-like ore zone, 50' marker = CE-17
31	CU-51'	3/13/00	transect across bms manto-like ore zone, 50' marker = CE-17
32	CU-52'	3/13/00	transect across bms manto-like ore zone, 50' marker = CE-17
33	CU-53'	3/13/00	transect across bms manto-like ore zone, 50' marker = CE-17
34	CU-54'	3/13/00	transect across bms manto-like ore zone, 50' marker = CE-17
35	CU-55'	3/13/00	transect across bms manto-like ore zone, 50' marker = CE-17
36	CU-59'	3/13/00	transect across bms manto-like ore zone, 50' marker = CE-17, unkwn acicular min
37	CU-60'	3/13/00	transect across bms manto-like ore zone, 50' marker = CE-17
38	CU-70'	3/13/00	transect across bms manto-like ore zone, 50' marker = CE-17
39	CU-80'	3/13/00	transect across bms manto-like ore zone, 50' marker = CE-17
40	CU-90'	3/13/00	transect across bms manto-like ore zone, 50' marker = CE-17
41	CU-95'	3/13/00	transect across bms manto-like ore zone, 50' marker = CE-17
42	CU-100'	3/13/00	transect across bms manto-like ore zone, 50' marker = CE-17
43	CU-105'	3/13/00	transect across bms manto-like ore zone, 50' marker = CE-17
44	CU-110'	3/13/00	transect across bms manto-like ore zone, 50' marker = CE-17
45	CU-115'	3/13/00	transect across bms manto-like ore zone, 50' marker = CE-17
46	CU-120'	3/13/00	transect across bms manto-like ore zone, 50' marker = CE-17
47	CUBM-59'	3/13/00	same location as CU-59', bms with late unknown acicular metallic mineral
48	3980-INT	3/13/00	south rib, bms with pinkish carbonate - rhodochrosite?
49	STOPE 5	na	from Don Ryan, stope 5 qtz + bms vein

Appendix II-B: Rock samples collected from the Cove underground

NO.	SAMPLE	DATE ACQUIRED	FIELD NOTES/DESCRIPTION
1	CVC-218-675.5	6/18/99	Sampling CVC-218 core across Carlin-style ore zone in H.S., depth in feet
2	CVC-218-684	6/18/99	Sampling CVC-218 core across Carlin-style ore zone in H.S., depth in feet
3	CVC-218-715.6	6/18/99	Sampling CVC-218 core across Carlin-style ore zone in H.S., depth in feet
4	CVC-218-808	6/18/99	Sampling CVC-218 core across Carlin-style ore zone in H.S., depth in feet
5	CVC-218-813.5	6/18/99	Sampling CVC-218 core across Carlin-style ore zone in H.S., depth in feet
6	CVC-218-831.9	6/18/99	Sampling CVC-218 core across Carlin-style ore zone in H.S., depth in feet
7	CVC-218-857.5	6/18/99	Sampling CVC-218 core across Carlin-style ore zone in H.S., depth in feet
8	CVC-218-870.2	6/18/99	Sampling CVC-218 core across Carlin-style ore zone in H.S., depth in feet
9	CVC-218-877	6/18/99	Sampling CVC-218 core across Carlin-style ore zone in H.S., depth in feet
10	oxide Au	8/17/99	borrowed from Keith Jones - native Au/electrum in cong from oxide ore zone
11	CVC4-1793'	na	core from Dave Emmons, oddball alteration & mineralization
12	CVC205A-1019.5'	na	core from Dave Emmons, Home Station Member
13	CVC2?5A-10??.5'	na	core from Dave Emmons, Home Station Member

Appendix II-C: Rock samples collected from Cove drill core

NO.	SAMPLE	DATE ACQUIRED	FIELD NOTES/DESCRIPTION
1	MC-1-1	2/9/98	pyrrhotite (?) from skarn on NM side of Brown stock
2	MC-1-3	2/9/98	Cane Spring ls
3	MC-1-4	2/9/98	Augusta Mountain Fm (=Smelser Pass Member)
4	na	2/9/98	Cane Spring ls, more regularly bedded than Smelser Pass
5	BROWN STOCK SE TOP	na	Brown Stock @ McCoy - "DIFFERENT FROM COVE INTRUSIVES ?"

Appendix II-D: Rock samples collected from the McCoy open pit

APPENDIX III

X-Ray Diffraction Data for Samples from Cove

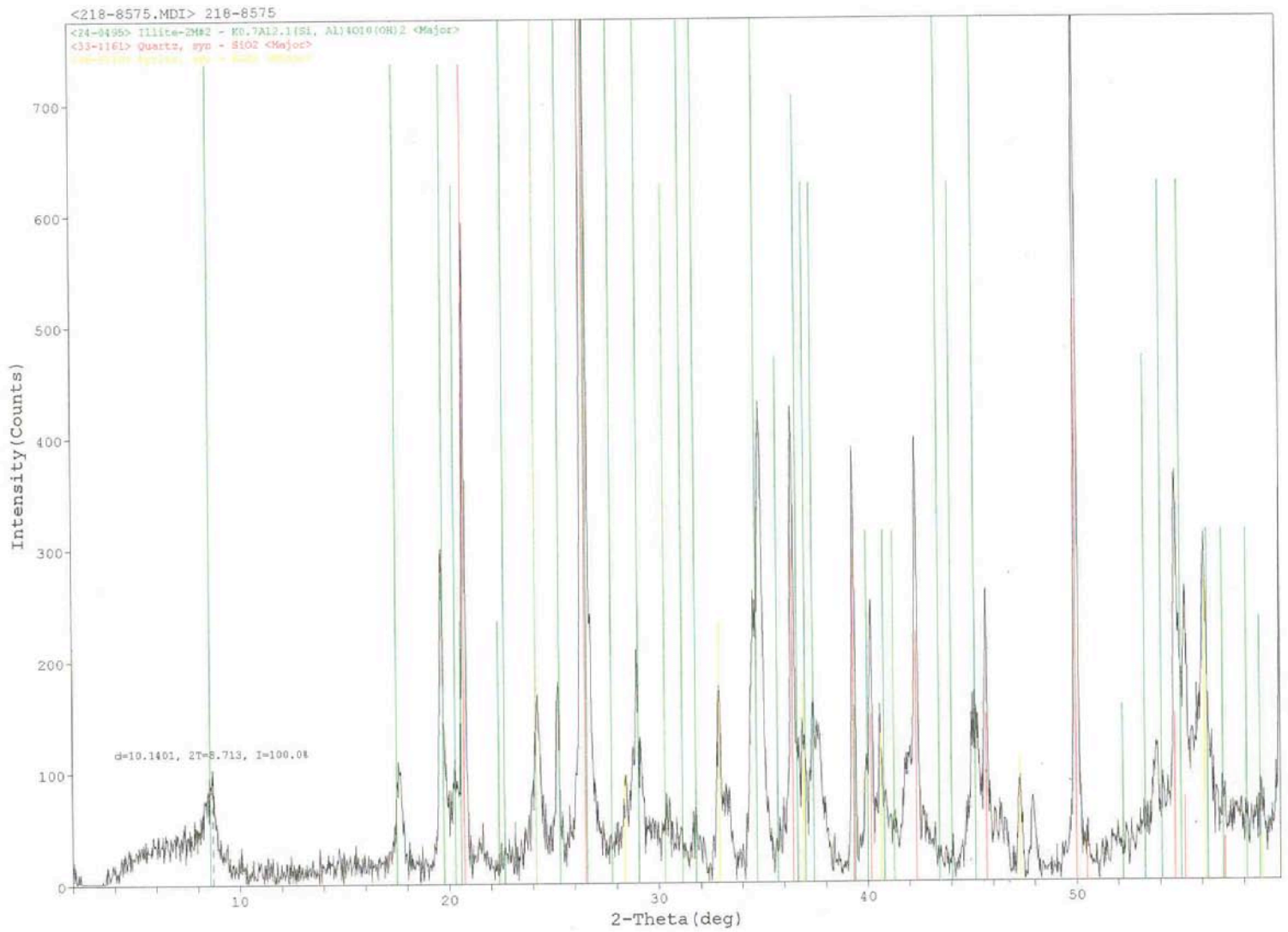
<218-8575.MDI> 218-8575
<24-0495> Illite-2M#2 - K0.7Al2.1(Si, Al)4O10(OH)2 <Major>
<33-1161> Quartz, syn - SiO2 <Major>
d=10.1401, 2T=8.713, I=100.0%
Intensity(Counts)
2-Theta(deg)
0
100
200
300
400
500
600
700
10
20
30
40
50

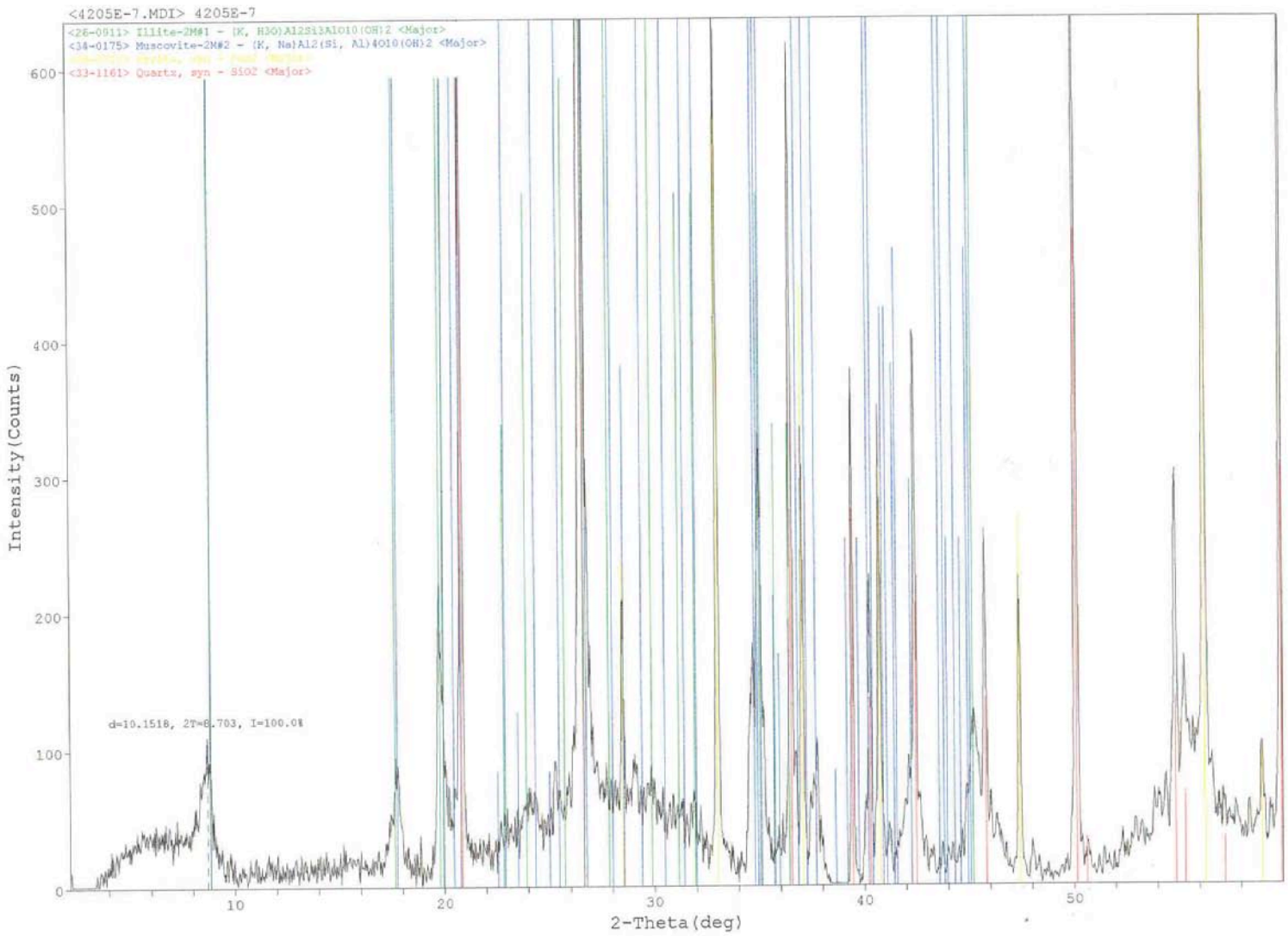
<4205E-7.MDI> 4205E-7
<26-0911> Illite-2M#1 - (K, H3O)Al2Si3AlO10(OH)2 <Major>
<34-0175> Muscovite-2M#2 - (K, Na)Al2(Si, Al)4O10(OH)2 <Major>
<33-1161> Quartz, syn - SiO2 <Major>
d=10.1518, 2T=8.703, I=100.0%
Intensity(Counts)
2-Theta(deg)
0
100
200
300
400
500
600
10
20
30
40
50

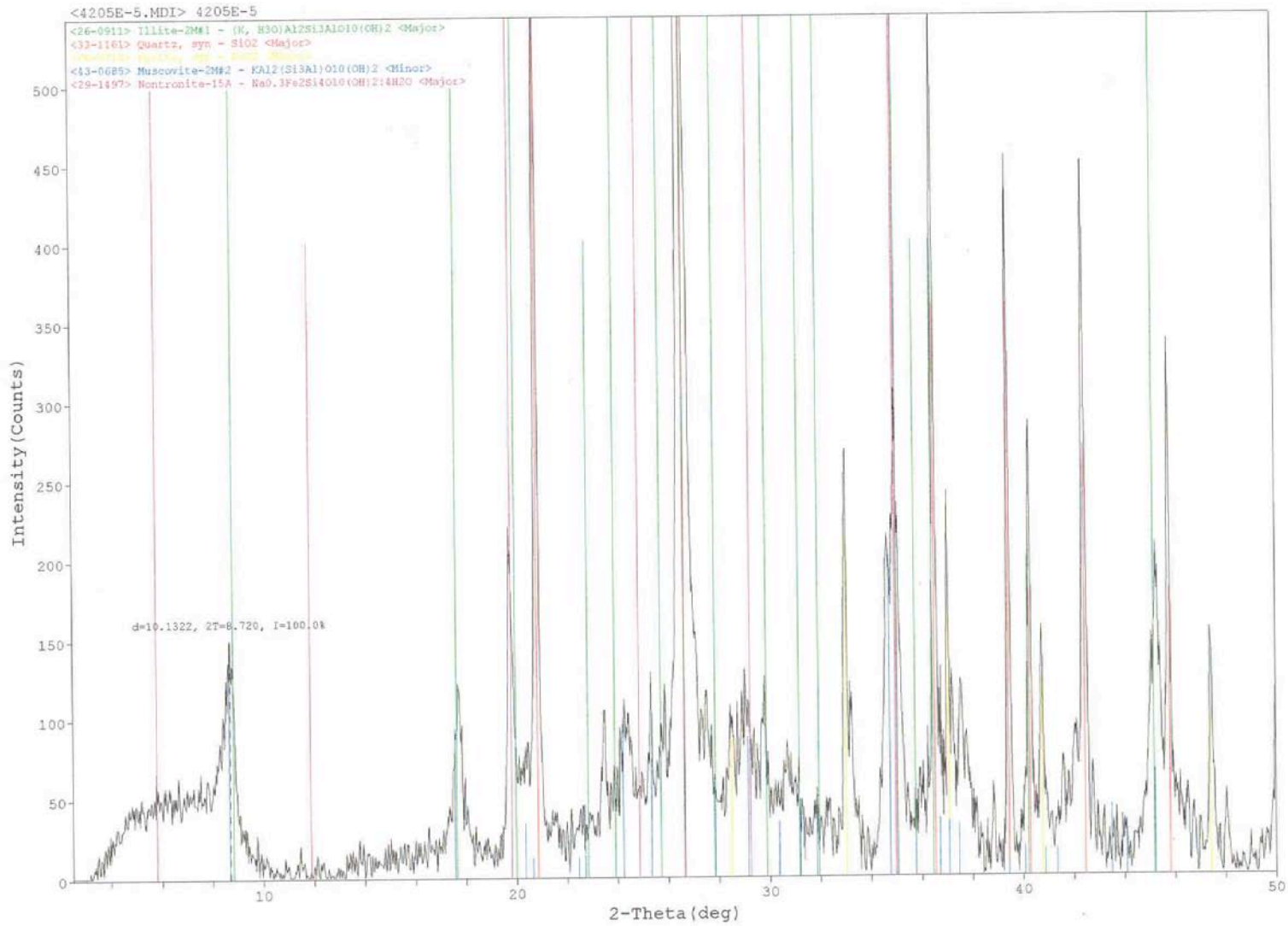
<4205E-5.MDI> 4205E-5
<26-0911> Illite-2M#1 - (K, H3O)Al2Si3AlO10(OH)2 <Major>
<33-1161> Quartz, syn - SiO2 <Major>
<43-0685> Muscovite-2M#2 - KAl2(Si3Al)O10(OH)2 <Minor>
<29-1497> Montronite-15A - Na0.3Fe2Si4O10(OH)2·4H2O <Major>
d=10.1322, 2T=8.720, I=100.0%
Intensity(Counts)
2-Theta(deg)
0
50
100
150
200
250
300
350
400
450
500
10
20
30
40
50

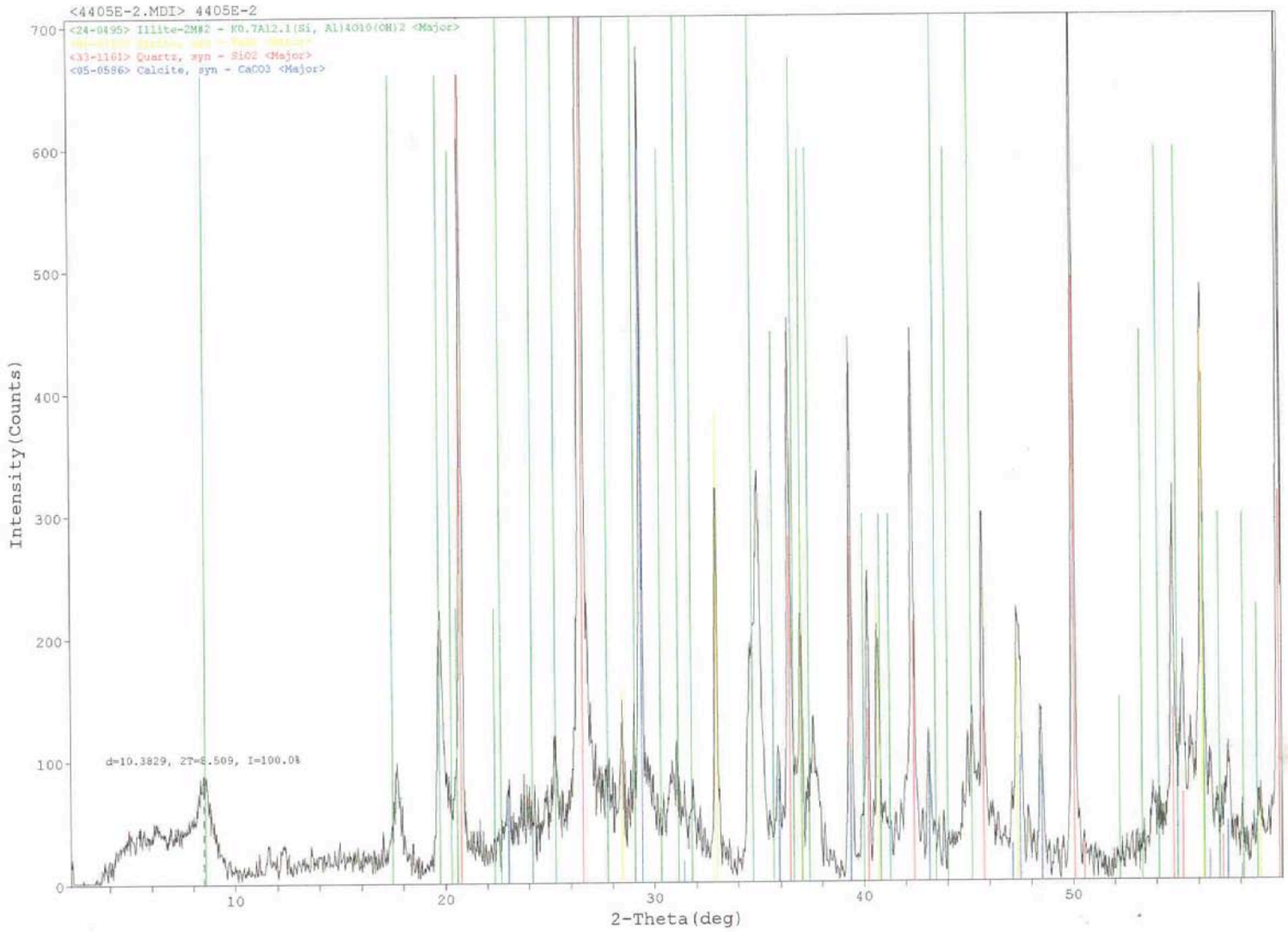
<4405E-2.MDI> 4405E-2
<24-0495> Illite-2M#2 - K0.7Al2.1(Si, Al)4O10(OH)2 <Major>
<83-1161> Quartz, syn - SiO2 <Major>
<05-0586> Calcite, syn - CaCO3 <Major>
d=10.3829, 2T=8.509, I=100.0%
Intensity(Counts)
2-Theta(deg)
0
100
200
300
400
500
600
700
10
20
30
40
50

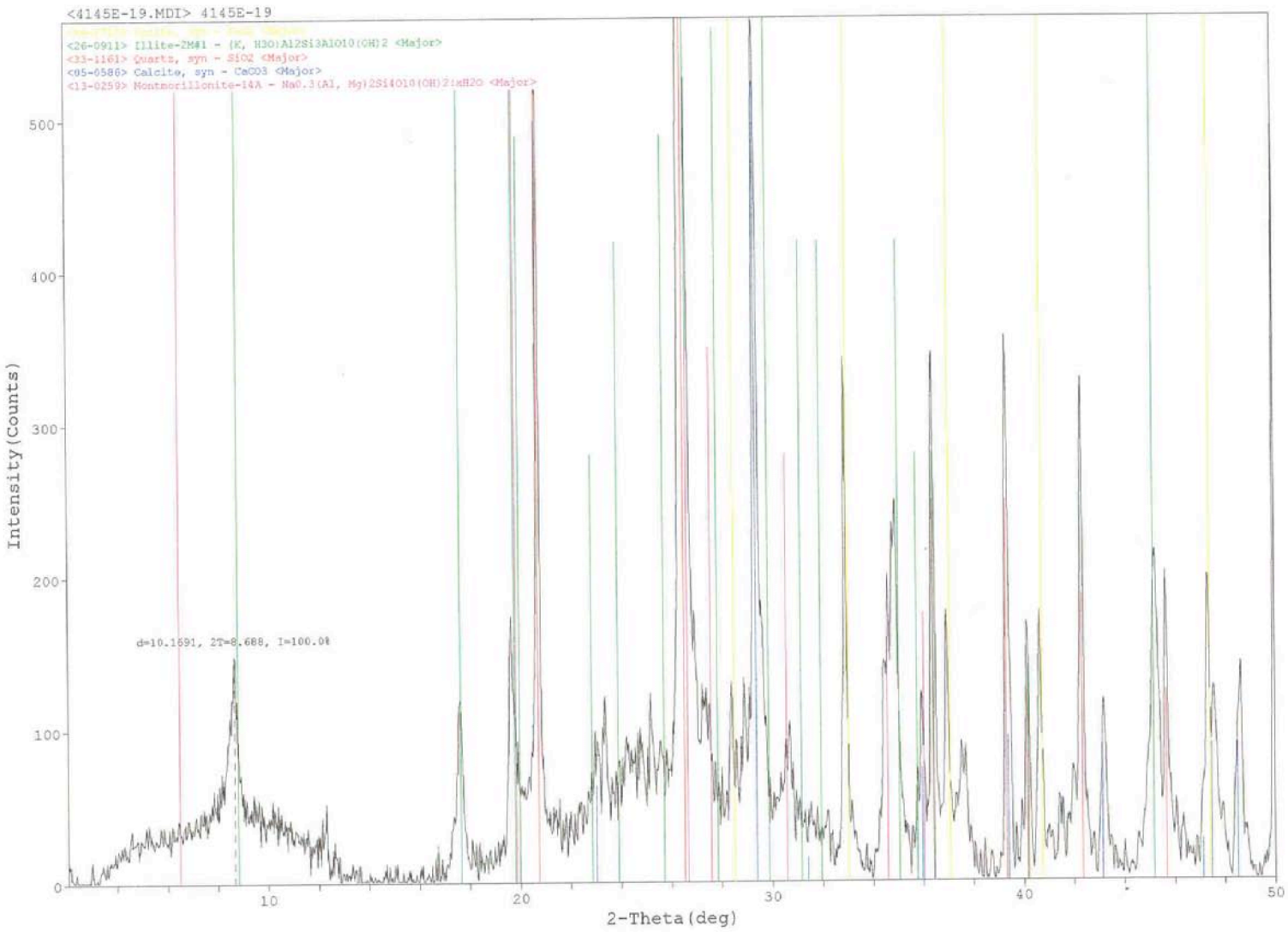
<4145E-19.MDI> 4145E-19
<26-0911> Illite-2M#1 - (K, H3O)Al2Si3AlO10(OH)2 <Major>
<33-1161> Quartz, syn - SiO2 <Major>
<05-0586> Calcite, syn - CaCO3 <Major>
<13-0259> Montmorillonite-14A - Na0.3(Al, Mg)2Si4O10(OH)2:xH2O <Major>
d=10.1691, 2T=8.688, I=100.0%
Intensity(Counts)
0
100
200
300
400
500
10
20
30
40
50
2-Theta(deg)

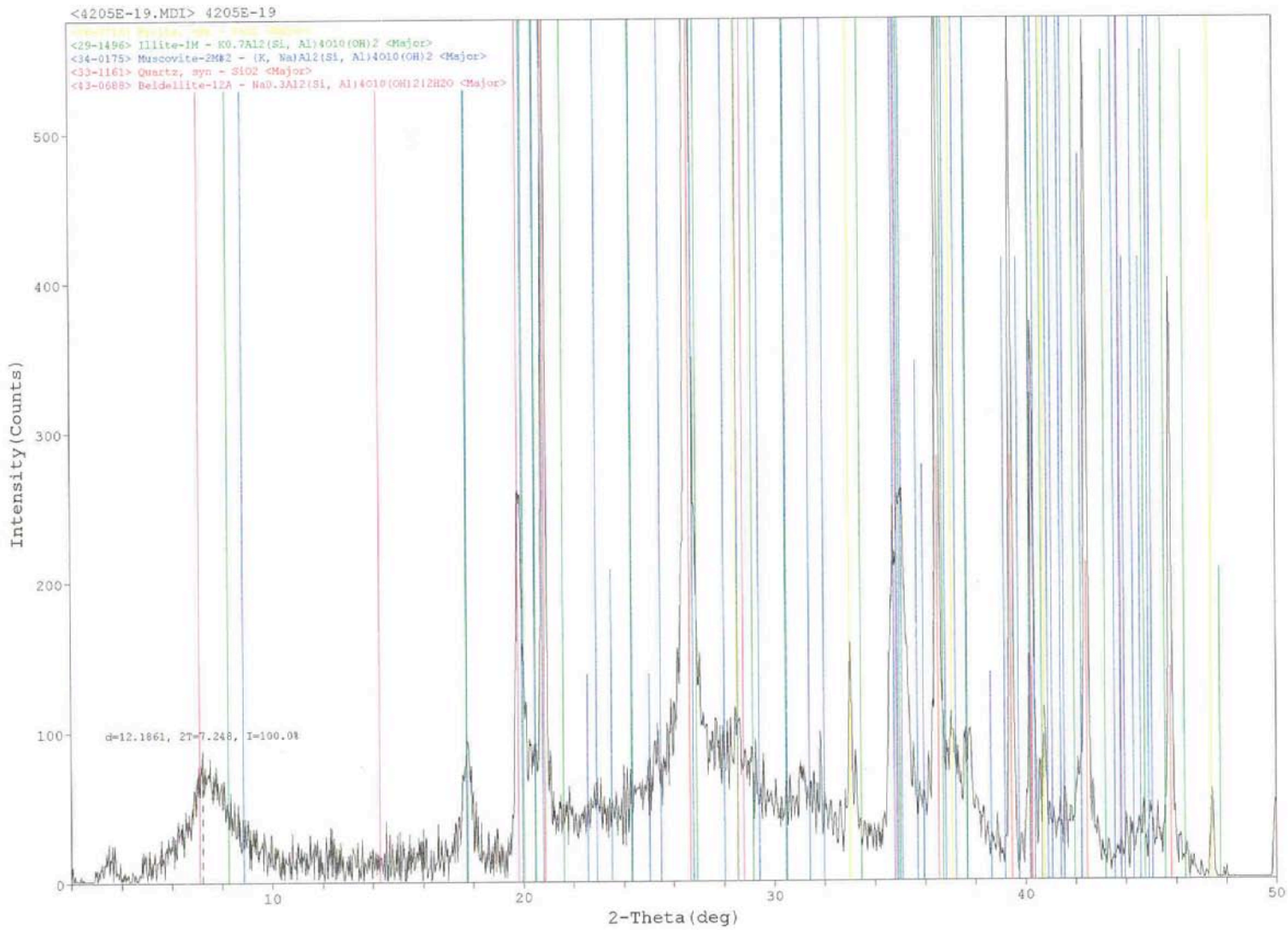
<4205E-19.MDI> 4205E-19
<29-1496> Illite-1M - K0.7Al2(Si, Al)4O10(OH)2 <Major>
<34-0175> Muscovite-2M#2 - (K, Na)Al2(Si, Al)4O10(OH)2 <Major>
<33-1161> Quartz, syn - SiO2 <Major>
<43-0688> Beidellite-12A - Na0.3Al2(Si, Al)4O10(OH)212H2O <Major>
d=12.1861, 2T=7.248, I=100.0%
Intensity(Counts)
2-Theta(deg)
0
100
200
300
400
500
10
20
30
40
50

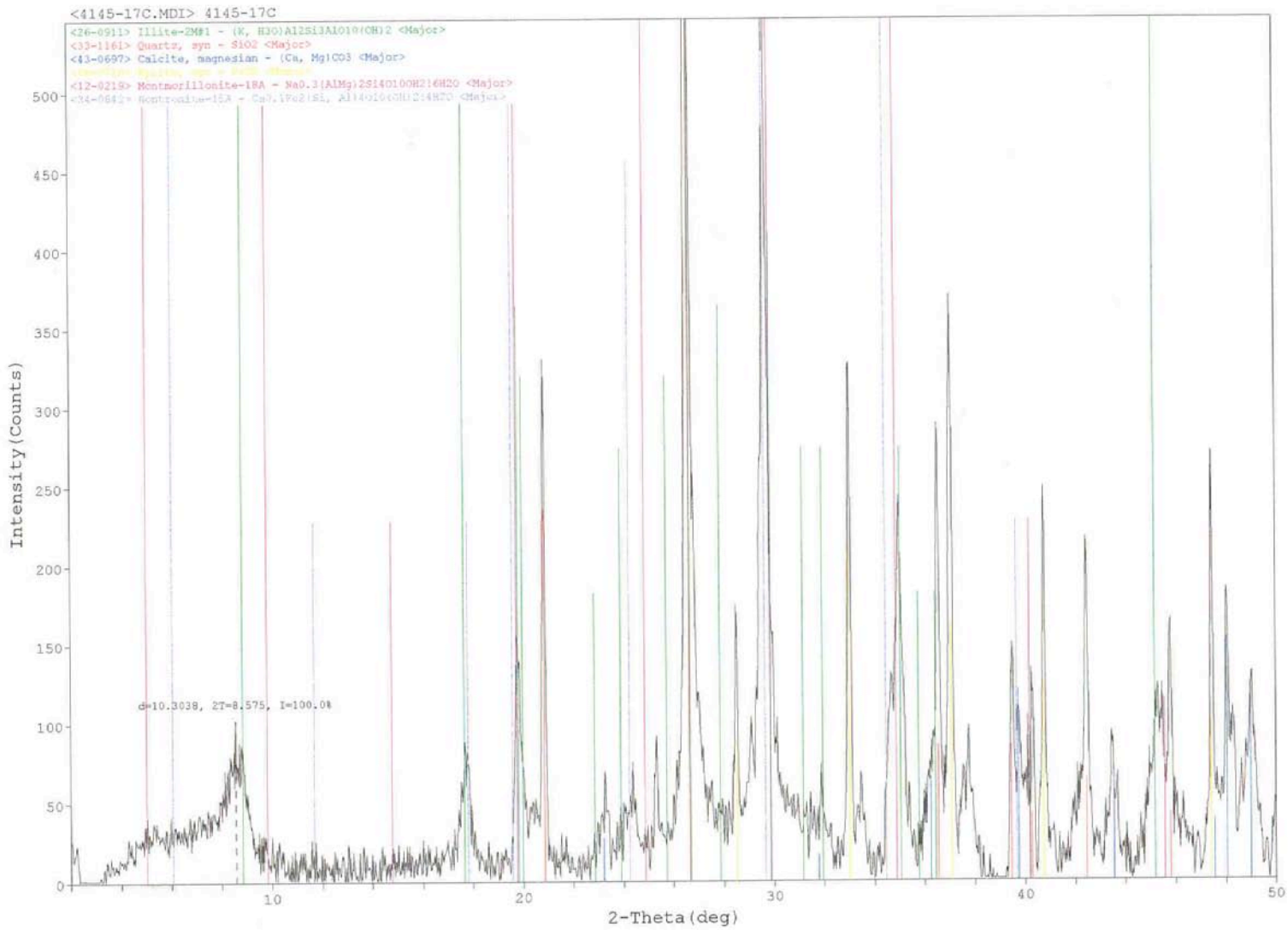
<4145-17C.MDI> 4145-17C
<26-0911> Illite-2M#1 - (K, H3O)Al2Si3AlO10(OH)2 <Major>
<33-1161> Quartz, syn - SiO2 <Major>
<43-0697> Calcite, magnesian - (Ca, Mg)CO3 <Major>
<12-0219> Montmorillonite-18A - Na0.3(AlMg)2Si4O10OH2?6H2O <Major>
d=10.3038, 2T=8.575, I=100.0%
Intensity(Counts)
2-Theta(deg)
0
50
100
150
200
250
300
350
400
450
500
10
20
30
40
50

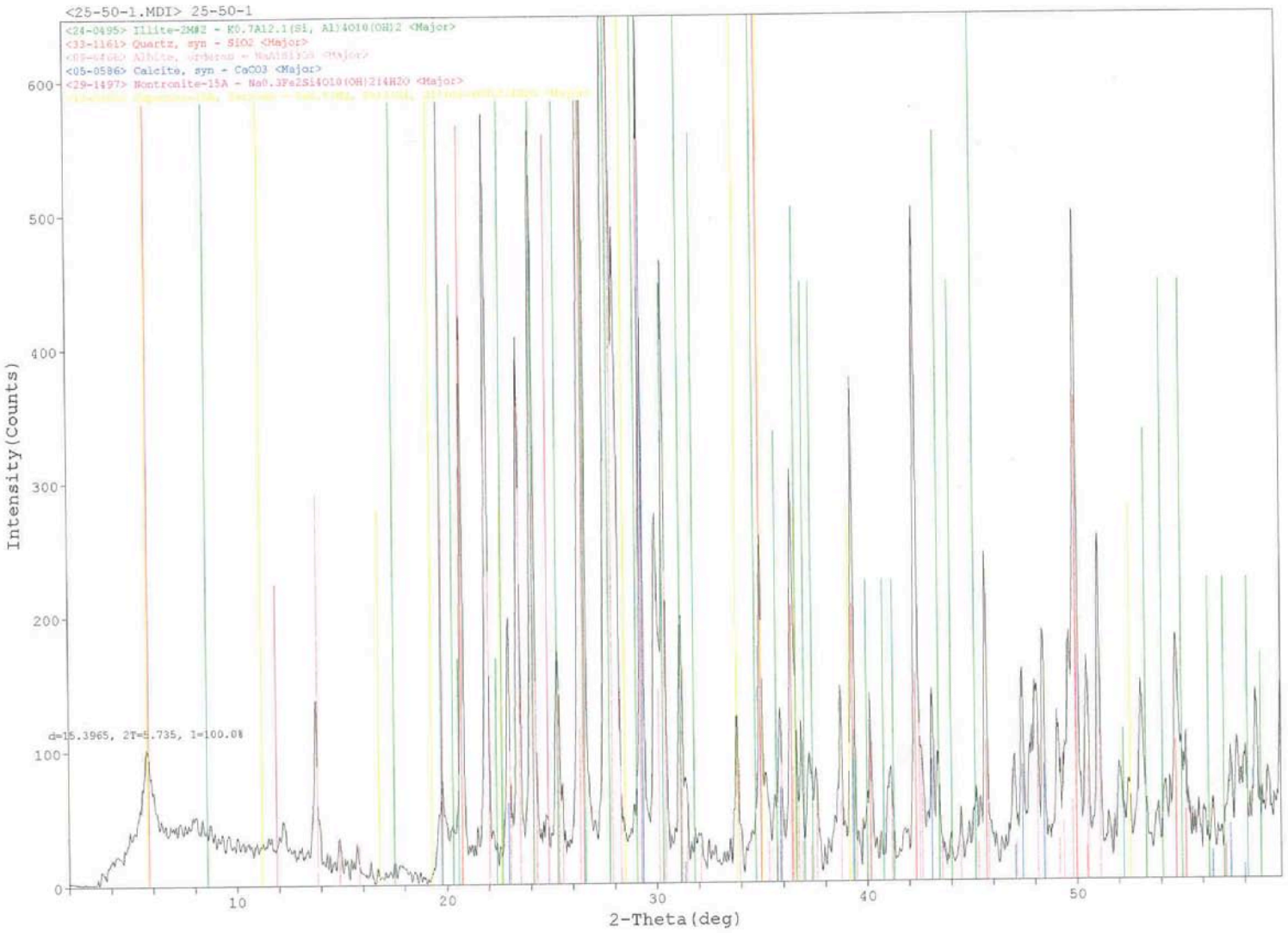
<25-50-1.MDI> 25-50-1
<24-0495> Illite-2M#2 - K0.7Al2.1(Si, Al)4O10(OH)2 <Major>
<33-1161> Quartz, syn - SiO2 <Major>
<05-0586> Calcite, syn - CaCO3 <Major>
<29-1497> Montronite-15A - Na0.3Fe2Si4O10(OH)2.14H2O <Major>
d=15.3965, 2T=5.735, I=100.00
Intensity(Counts)
2-Theta(deg)
0
100
200
300
400
500
600
10
20
30
40
50

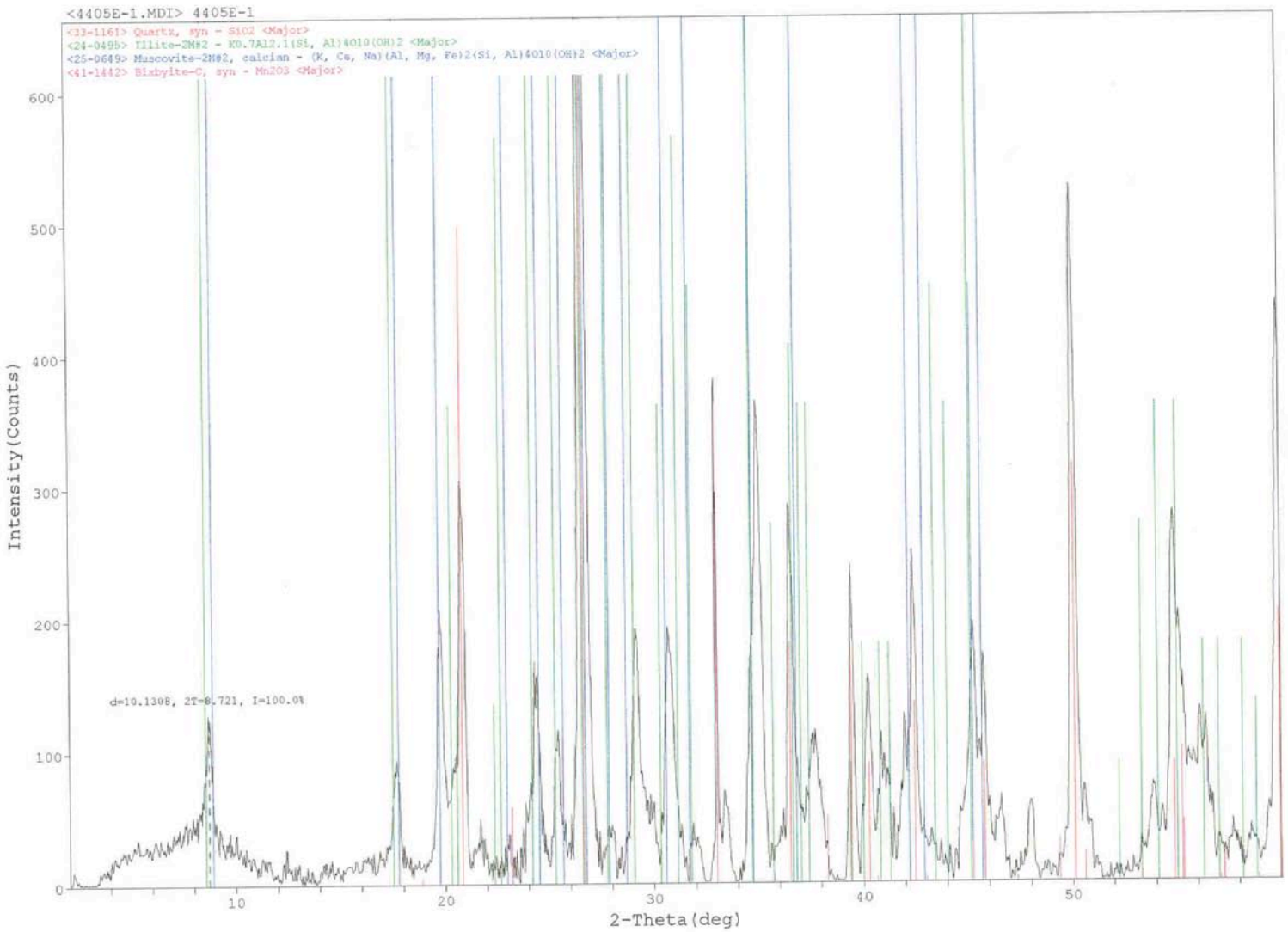
<4405E-1.MDI> 4405E-1
<33-1161> Quartz, syn - SiO2 <Major>
<24-0495> Illite-2M#2 - K0.7Al2.1(Si, Al)4O10(OH)2 <Major>
<25-0649> Muscovite-2M#2, calcian - (K, Ca, Na)(Al, Mg, Fe)2(Si, Al)4O10(OH)2 <Major>
<41-1442> Bixbyite-C, syn - Mn2O3 <Major>
d=10.1308, 2T=8.721, I=100.0%
Intensity(Counts)
2-Theta(deg)
0
100
200
300
400
500
600
10
20
30
40
50

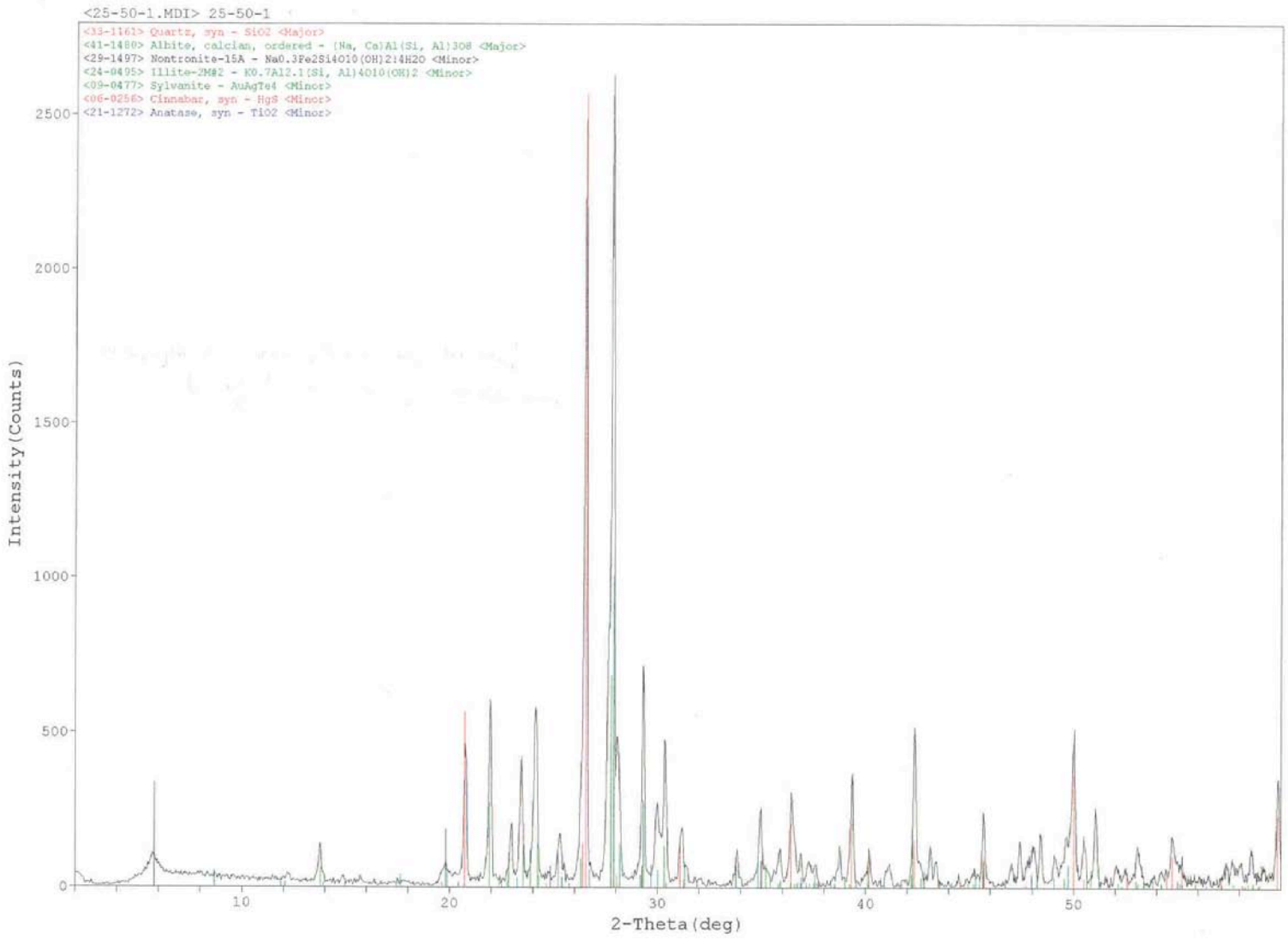
<25-50-1.MDI> 25-50-1
<33-1161> Quartz, syn - SiO2 <Major>
<41-1480> Albite, calcian, ordered - (Na, Ca)Al(Si, Al)3O8 <Major>
<29-1497> Montronite-15A - Na0.3Fe2Si4O10(OH)2·4H2O <Minor>
<24-0495> Illite-2M#2 - K0.7Al2.1(Si, Al)4O10(OH)2 <Minor>
<09-0477> Sylvanite - AuAgTe4 <Minor>
<06-0256> Cinnabar, syn - HgS <Minor>
<21-1272> Anatase, syn - TiO2 <Minor>
Intensity(Counts)
2500
2000
1500
1000
500
0
10
20
30
40
50
2-Theta(deg)

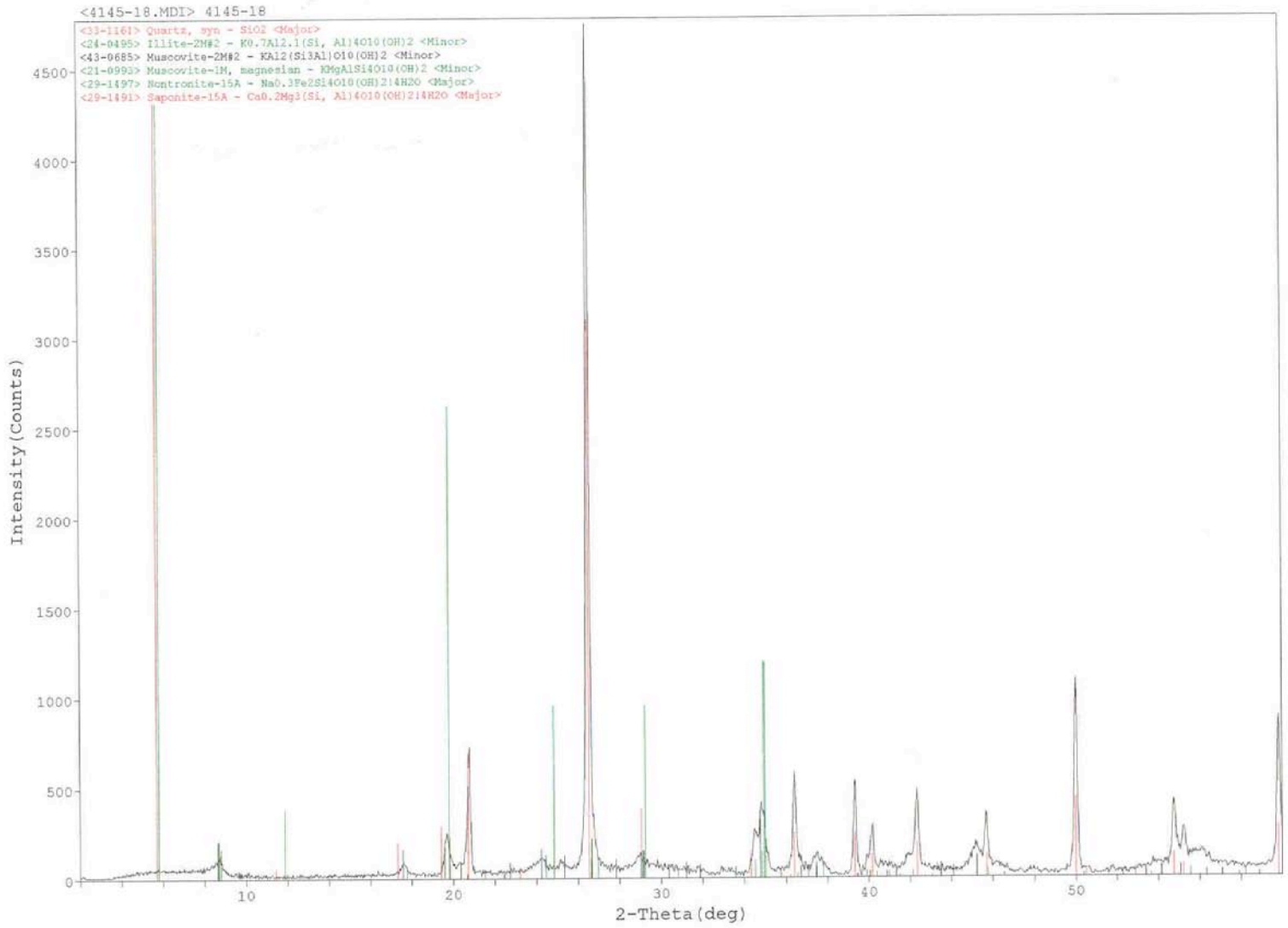
<4145-18.MDI> 4145-18
<33-1161> Quartz, syn - SiO2 <Major>
<24-0495> Illite-2M#2 - K0.7Al2.1(Si, Al)4O10(OH)2 <Minor>
<43-0685> Muscovite-2M#2 - KAl2(Si3Al)O10(OH)2 <Minor>
<21-0993> Muscovite-1M, magnesian - KMgAlSi4O10(OH)2 <Minor>
<29-1497> Montronite-15A - Na0.3Fe2Si4O10(OH)2·4H2O <Major>
<29-1491> Saponite-15A - Ca0.2Mg3(Si, Al)4O10(OH)2·4H2O <Major>
Intensity(Counts)
0
500
1000
1500
2000
2500
3000
3500
4000
4500
10
20
30
40
50
2-Theta(deg)

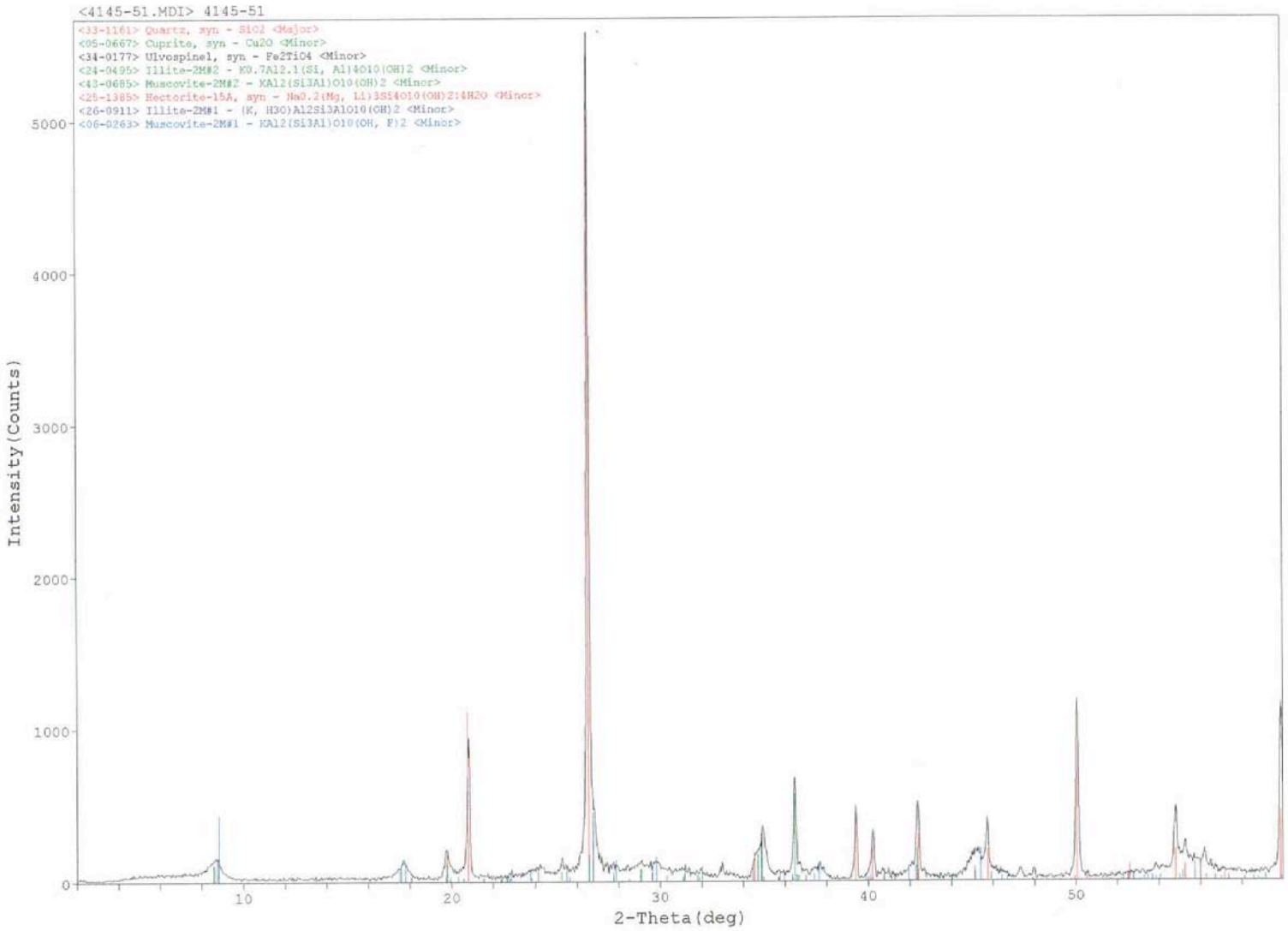
<4145-51.MDI> 4145-51
<33-1161> Quartz, syn - SiO2 <Major>
<05-0667> Cuprite, syn - Cu2O <Minor>
<34-0177> Ulvospinel, syn - Fe2TiO4 <Minor>
<24-0495> Illite-2M#2 - K0.7Al2.1(Si, Al)4O10(OH)2 <Minor>
<43-0685> Muscovite-2M#2 - KAl2(Si3Al)O10(OH)2 <Minor>
<25-1385> Hectorite-15A, syn - Na0.2(Mg, Li)3Si4O10(OH)2:4H2O <Minor>
<26-0911> Illite-2M#1 - (K, H3O)Al2Si3AlO10(OH)2 <Minor>
<06-0263> Muscovite-2M#1 - KAl2(Si3Al)O10(OH, F)2 <Minor>
Intensity(Counts)
5000
4000
3000
2000
1000
0
10
20
30
40
50
2-Theta(deg)

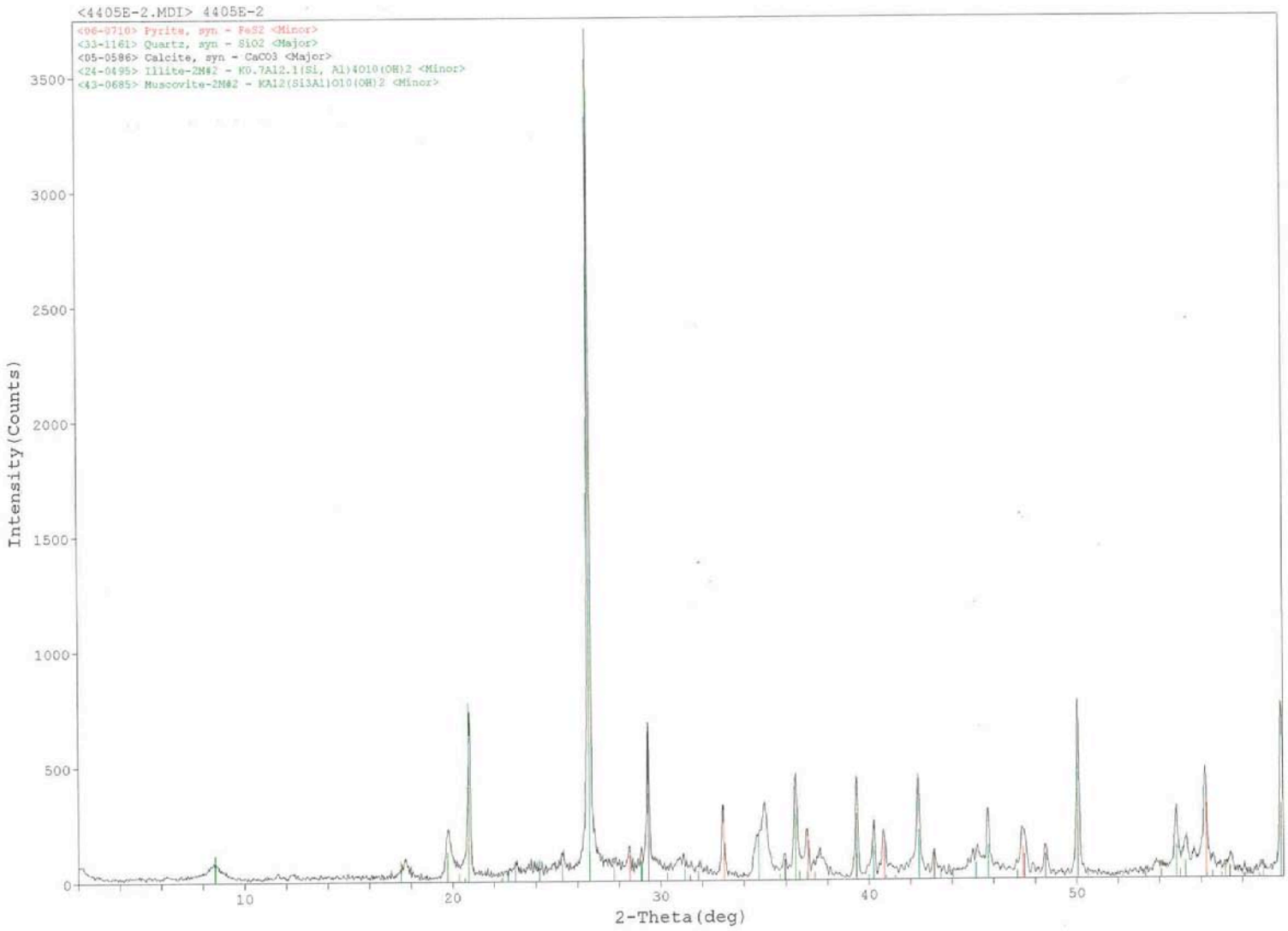
<4405E-2.MDI> 4405E-2
<06-0710> Pyrite, syn - FeS2 <Minor>
<33-1161> Quartz, syn - SiO2 <Major>
<05-0586> Calcite, syn - CaCO3 <Major>
<24-0495> Illite-2M#2 - K0.7Al2.1(Si, Al)4O10(OH)2 <Minor>
<43-0685> Muscovite-2M#2 - KAl2(Si3Al1)O10(OH)2 <Minor>
Intensity(Counts)
0
500
1000
1500
2000
2500
3000
3500
10
20
30
40
50
2-Theta(deg)

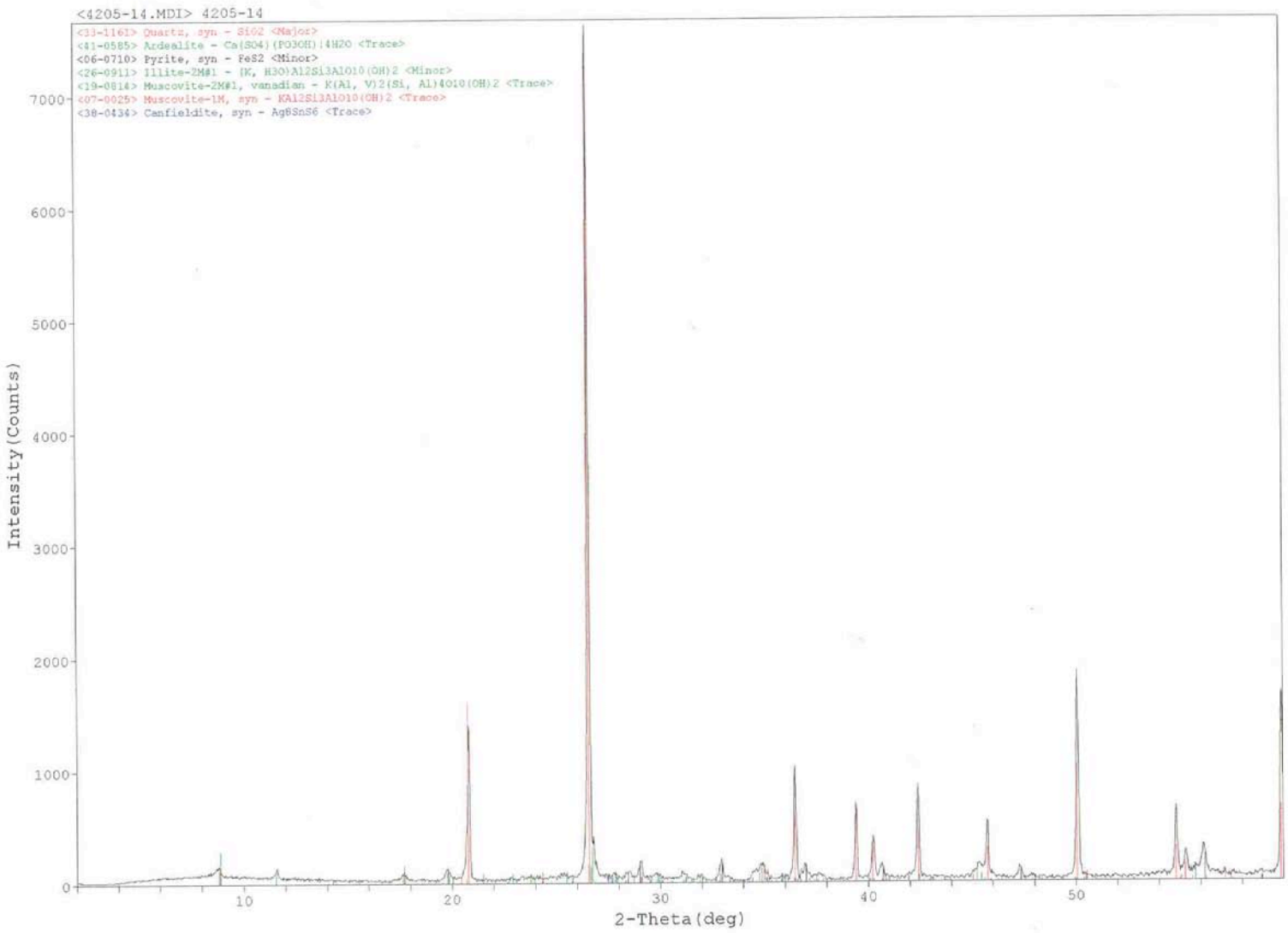
<4205-14.MDI> 4205-14
<33-1161> Quartz, syn - SiO2 <Major>
<41-0585> Ardealite - Ca(SO4)(PO3OH)|4H2O <Trace>
<06-0710> Pyrite, syn - FeS2 <Minor>
<26-0911> Illite-2M#1 - (K, H3O)Al2Si3AlO10(OH)2 <Minor>
<19-0814> Muscovite-2M#1, vanadian - K(Al, V)2(Si, Al)4O10(OH)2 <Trace>
<07-0025> Muscovite-1M, syn - KAl2Si3AlO10(OH)2 <Trace>
<38-0434> Canfieldite, syn - Ag8SnS6 <Trace>
Intensity(Counts)
7000
6000
5000
4000
3000
2000
1000
0
10
20
30
40
50
2-Theta(deg)

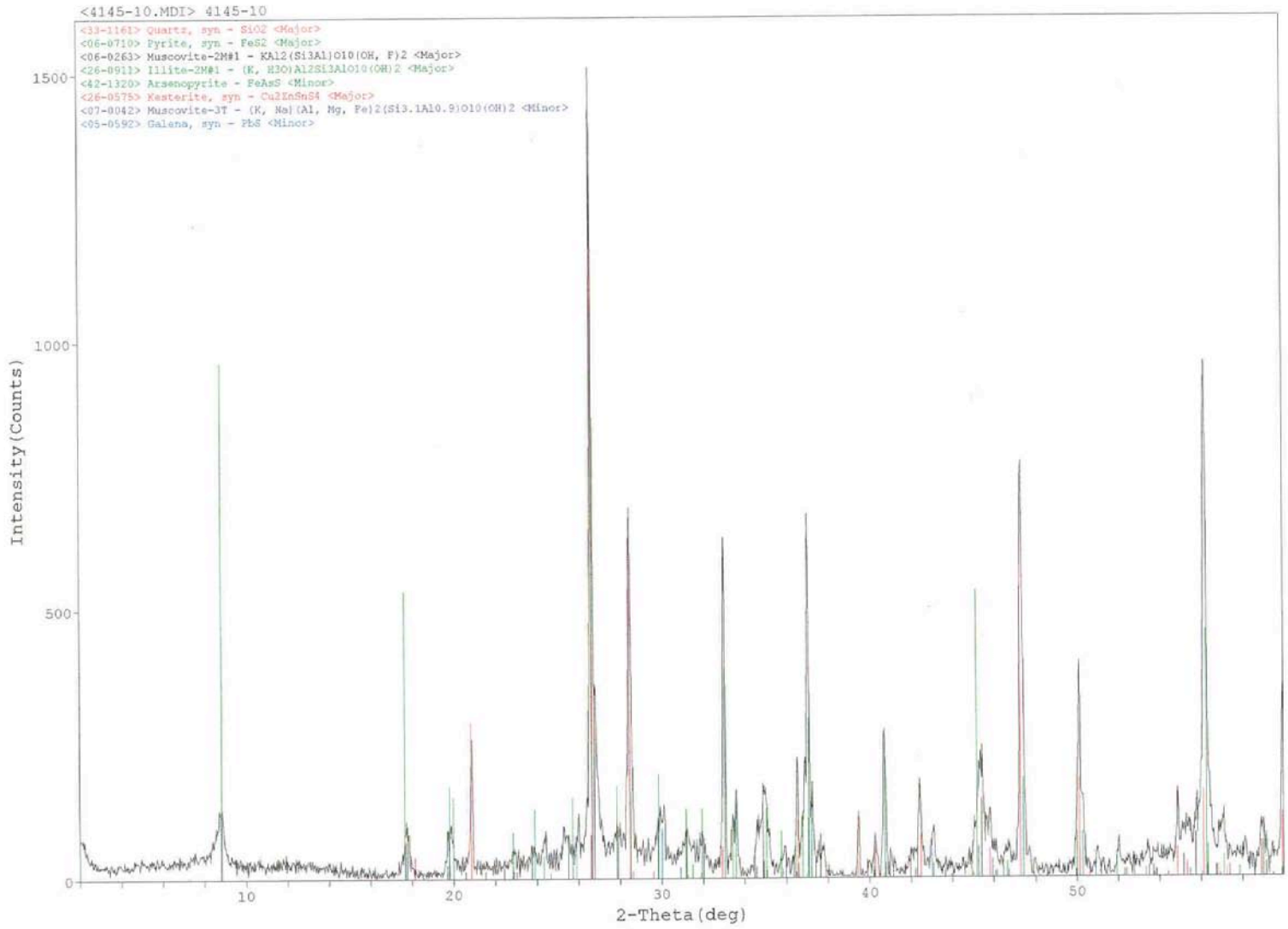
<4145-10.MDI> 4145-10
<33-1161> Quartz, syn - SiO2 <Major>
<06-0710> Pyrite, syn - FeS2 <Major>
<06-0263> Muscovite-2M#1 - KAl2(Si3Al)O10(OH, F)2 <Major>
<26-0911> Illite-2M#1 - (K, H3O)Al2Si3AlO10(OH)2 <Major>
<42-1320> Arsenopyrite - FeAsS <Minor>
<26-0575> Kesterite, syn - Cu2ZnSnS4 <Major>
<07-0042> Muscovite-3T - (K, Na)(Al, Mg, Fe)2(Si3.1Al0.9)O10(OH)2 <Minor>
<05-0592> Galena, syn - PbS <Minor>
Intensity(Counts)
1500
1000
500
0
10
20
30
40
50
2-Theta(deg)

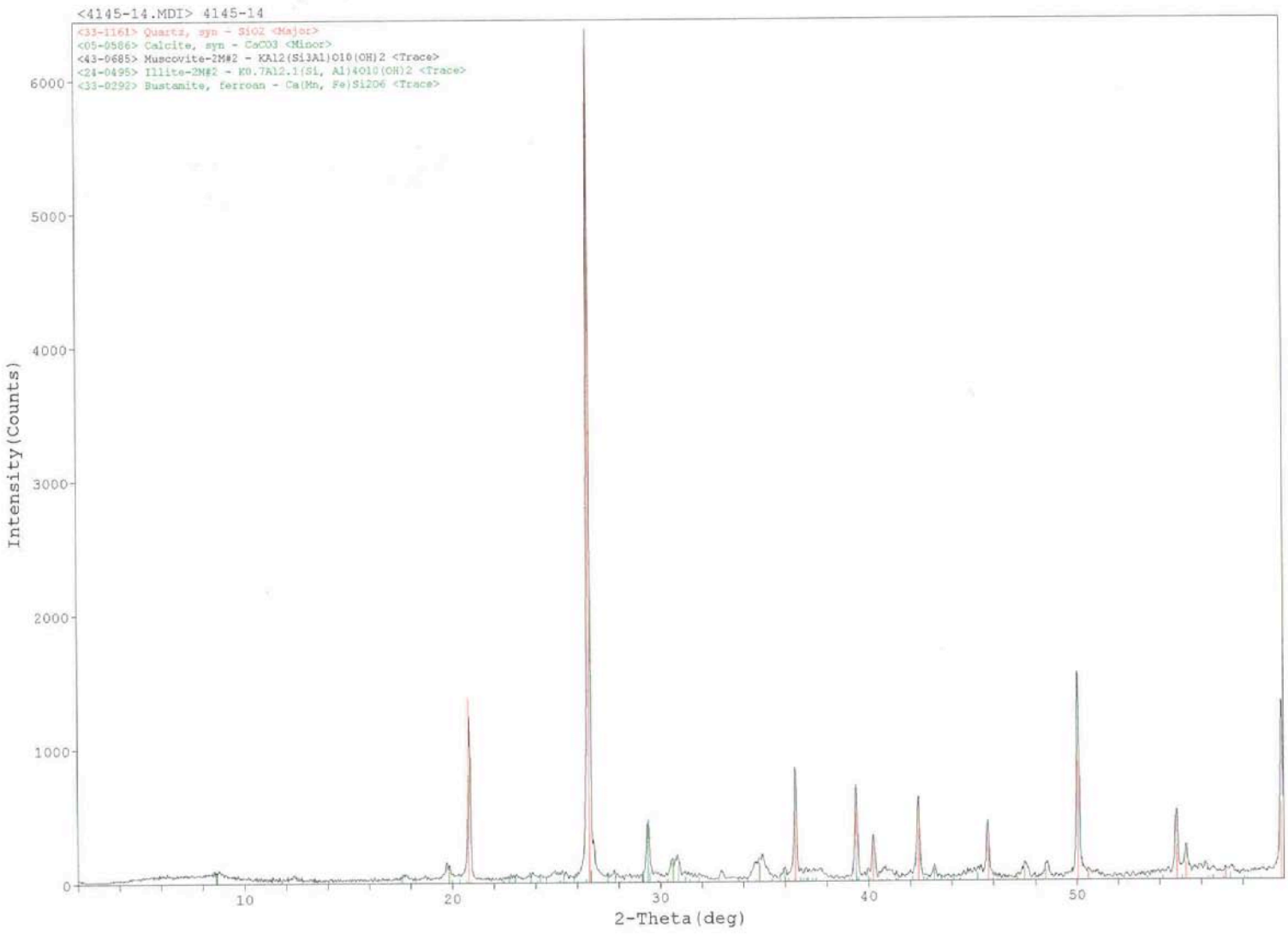
<4145-14.MDI> 4145-14
<33-1161> Quartz, syn - SiO2 <Major>
<05-0586> Calcite, syn - CaCO3 <Minor>
<43-0685> Muscovite-2M#2 - KAl2(SiJAl)O10(OH)2 <Trace>
<24-0495> Illite-2M#2 - K0.7Al2.1(Si, Al)4O10(OH)2 <Trace>
<33-0292> Bustamite, ferroan - Ca(Mn, Fe)Si2O6 <Trace>
Intensity(Counts)
6000
5000
4000
3000
2000
1000
0
10
20
30
40
50
2-Theta(deg)

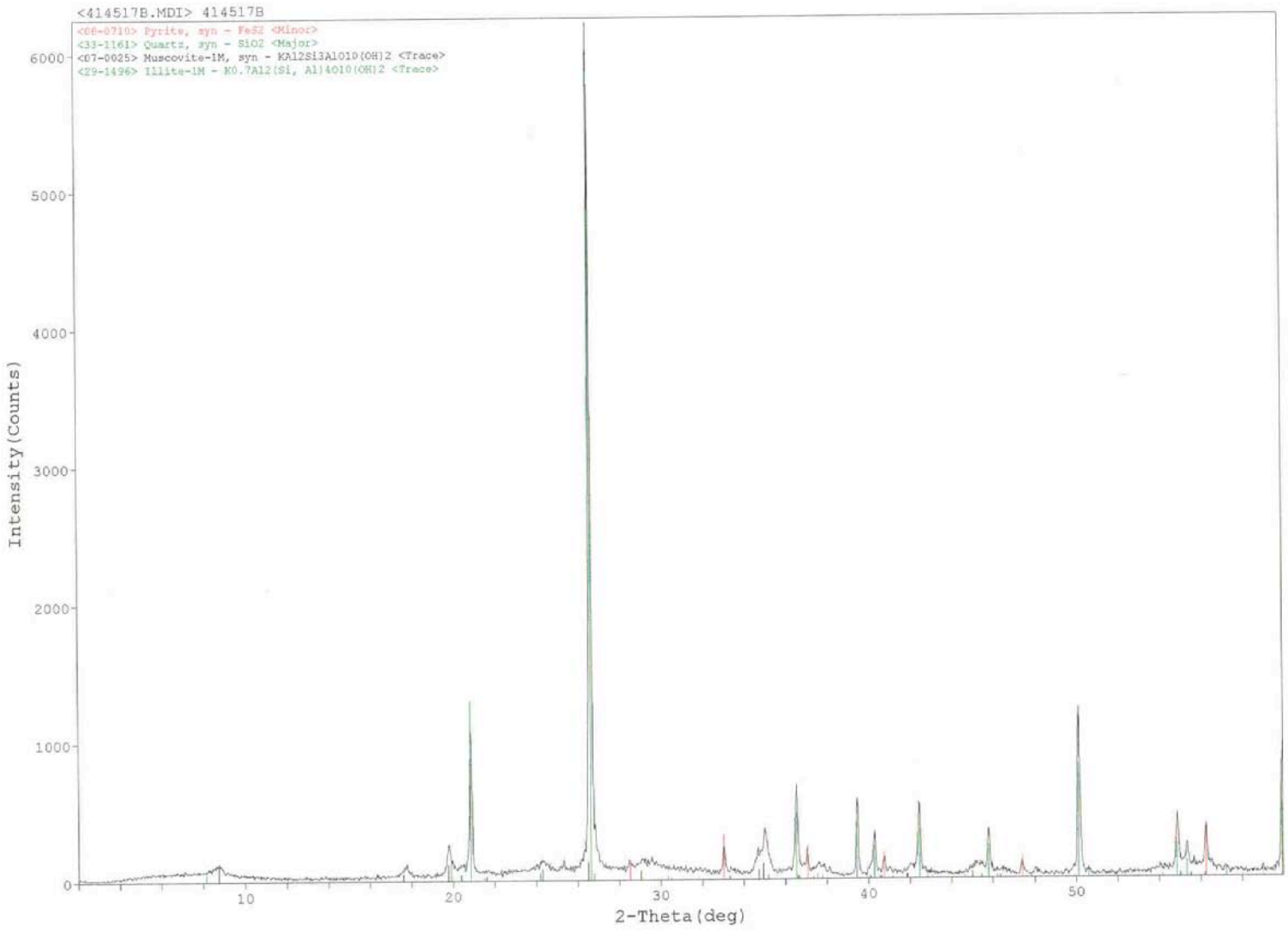
<414517B.MDI> 414517B
<06-0710> Pyrite, syn - FeS2 <Minor>
<33-1161> Quartz, syn - SiO2 <Major>
<07-0025> Muscovite-1M, syn - KAl2Si3Al010(OH)2 <Trace>
<29-1496> Illite-1M - K0.7Al2(Si, Al)4O10(OH)2 <Trace>
Intensity(Counts)
6000
5000
4000
3000
2000
1000
0
10
20
30
40
50
2-Theta(deg)

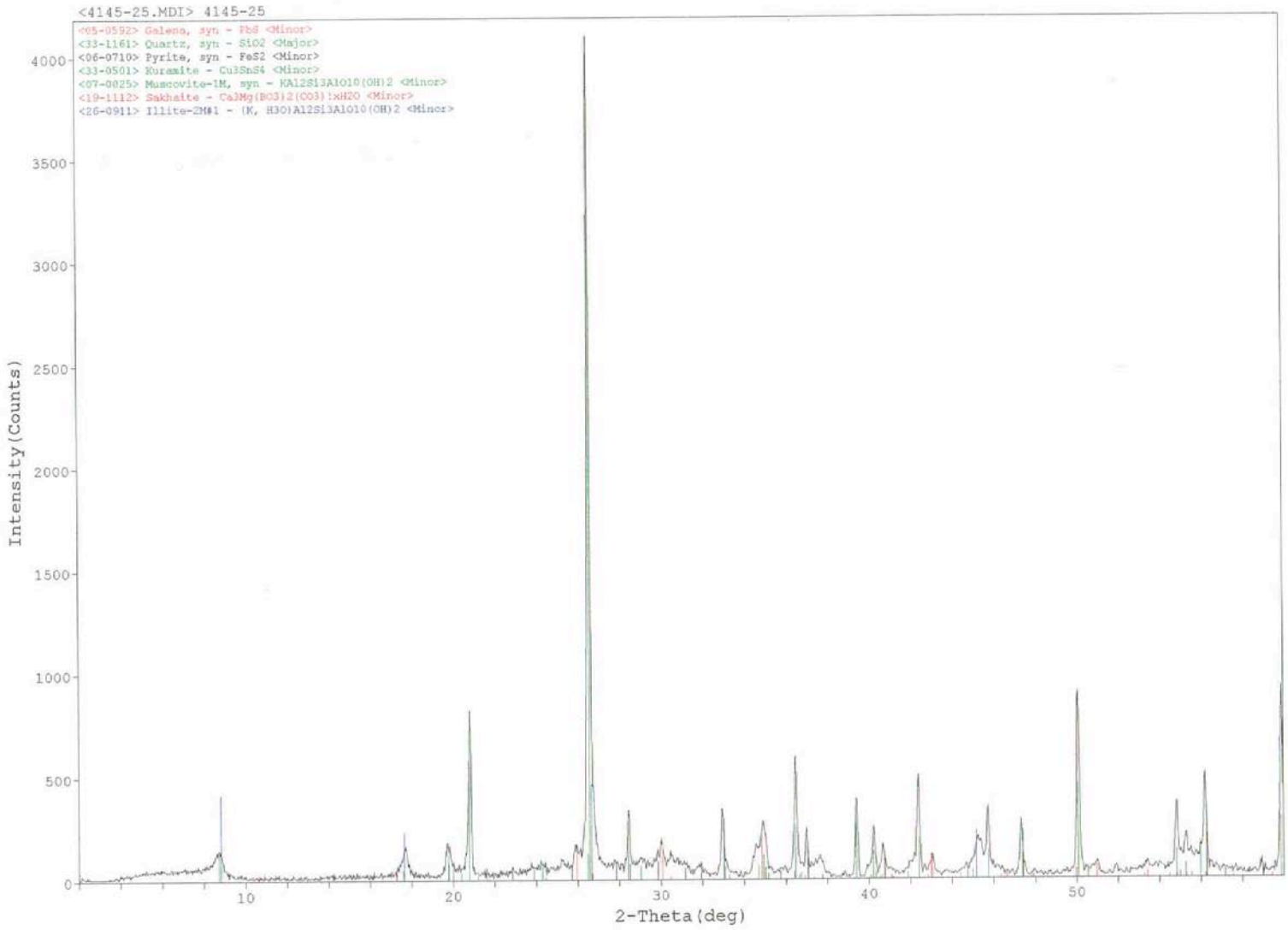
<4145-25.MDI> 4145-25
<05-0592> Galena, syn - PbS <Minor>
<33-1161> Quartz, syn - SiO2 <Major>
<06-0710> Pyrite, syn - FeS2 <Minor>
<33-0501> Kuramite - Cu3SnS4 <Minor>
<07-0025> Muscovite-1M, syn - KAl2Si3AlO10(OH)2 <Minor>
<19-1112> Sakhaite - CaMg(BO3)2(CO3)!xH2O <Minor>
<26-0911> Illite-2M#1 - (K, H3O)Al2Si3AlO10(OH)2 <Minor>
Intensity(Counts)
0
500
1000
1500
2000
2500
3000
3500
4000
10
20
30
40
50
2-Theta(deg)

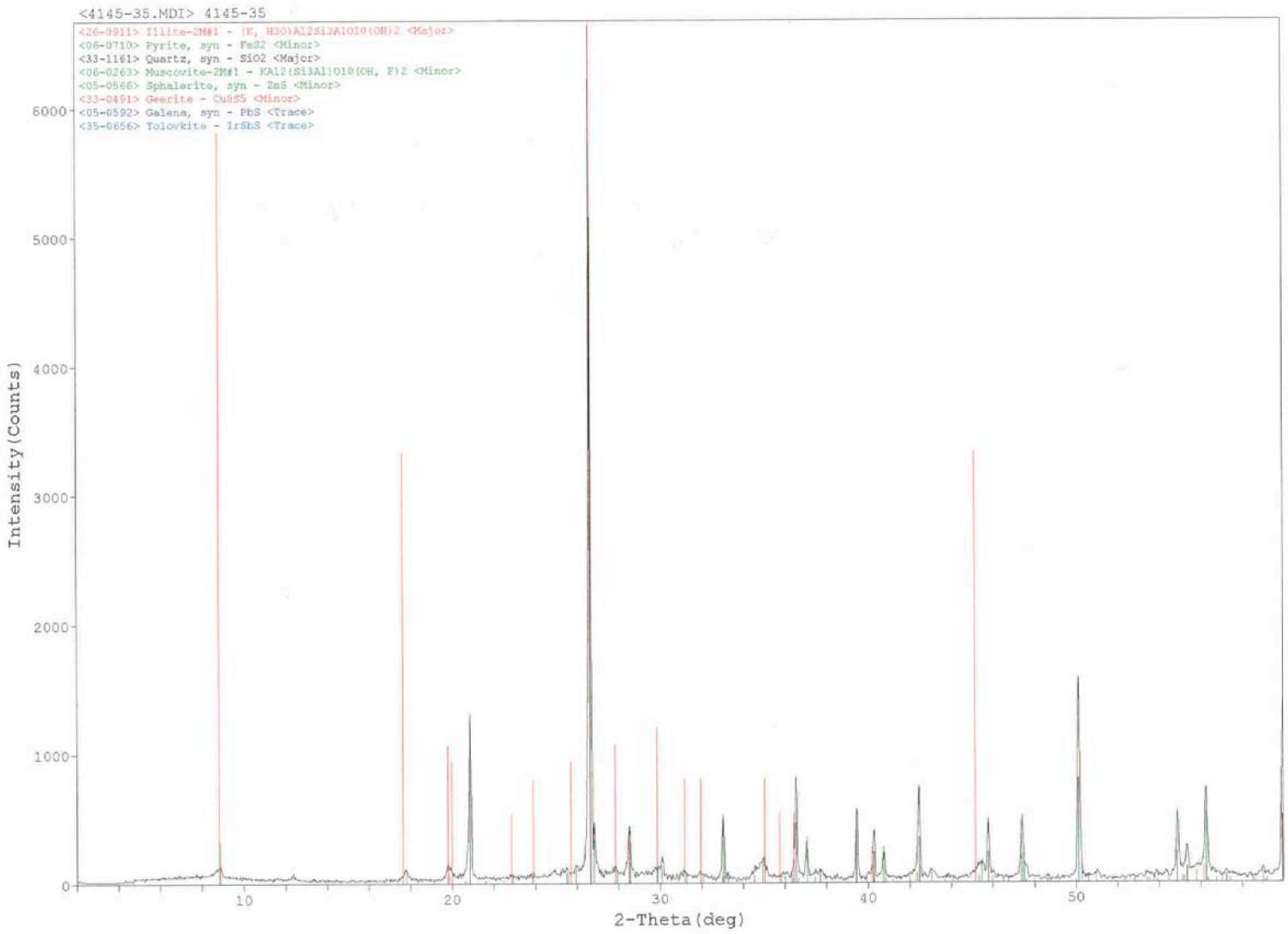
<4145-35.MDI> 4145-35
<26-0911> Illite-2M#1 - (K, H3O)Al2Si3AlO10(OH)2 <Major>
<06-0710> Pyrite, syn - FeS2 <Minor>
<33-1161> Quartz, syn - SiO2 <Major>
<06-0263> Muscovite-2M#1 - KAl2(Si3Al)O10(OH, F)2 <Minor>
<05-0566> Sphalerite, syn - ZnS <Minor>
<33-0491> Geerite - Cu8S5 <Minor>
<05-0592> Galena, syn - PbS <Trace>
<35-0656> Tolovkite - IrSbS <Trace>
Intensity(Counts)
6000
5000
4000
3000
2000
1000
0
10
20
30
40
50
2-Theta(deg)

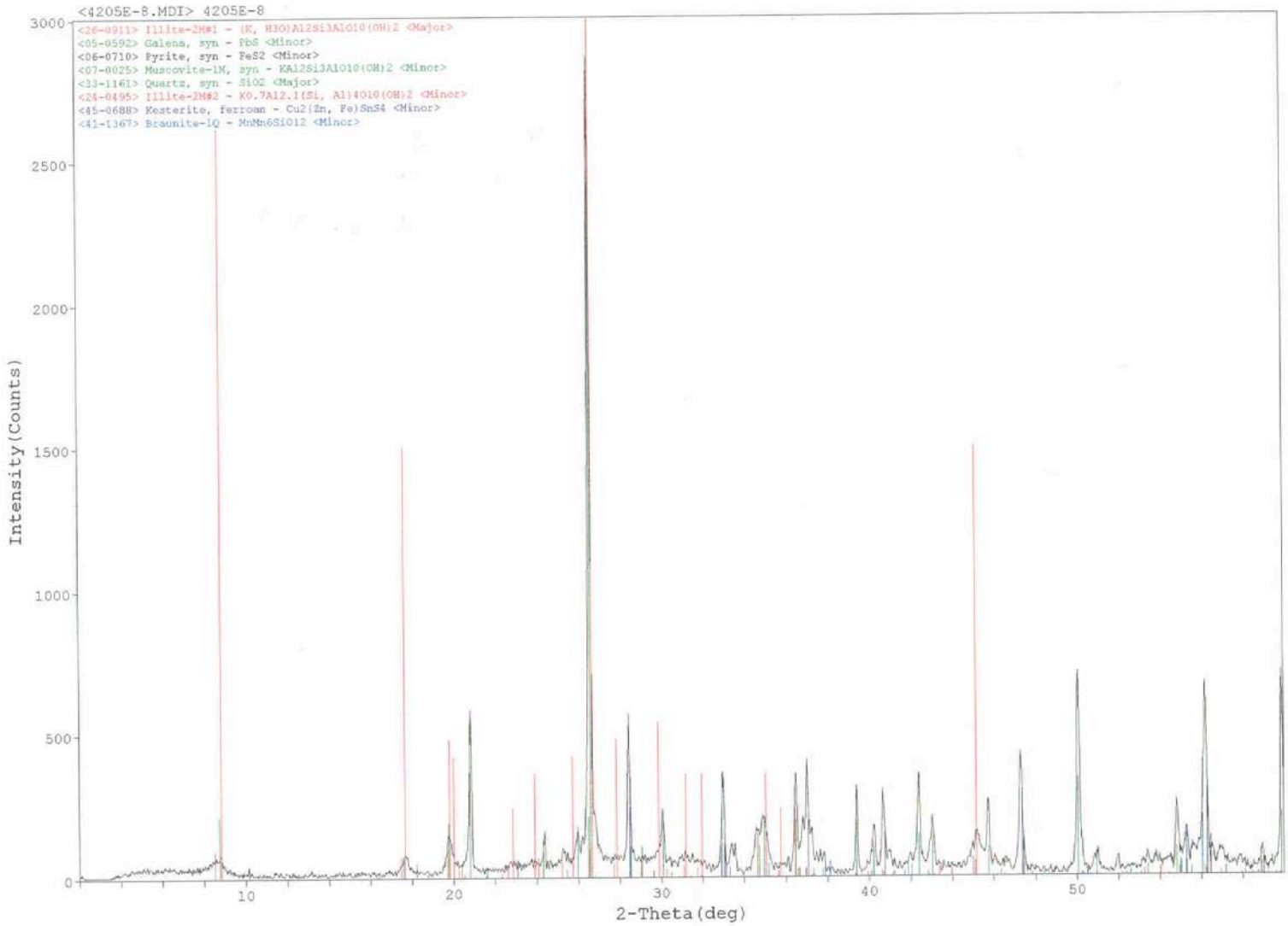
<4205E-8.MDI> 4205E-8
<26-0911> Illite-2M#1 - (K, H3O)Al2Si3AlO10(OH)2 <Major>
<05-0592> Galena, syn - PbS <Minor>
<06-0710> Pyrite, syn - FeS2 <Minor>
<07-0025> Muscovite-1M, syn - KAl2Si3AlO10(OH)2 <Minor>
<33-1161> Quartz, syn - SiO2 <Major>
<24-0495> Illite-2M#2 - K0.7Al2.1(Si, Al)4O10(OH)2 <Minor>
<45-0688> Kesterite, ferroan - Cu2(Zn, Fe)SnS4 <Minor>
<41-1367> Braunite-1Q - MnMn6SiO12 <Minor>
Intensity(Counts)
3000
2500
2000
1500
1000
500
0
10
20
30
40
50
2-Theta(deg)

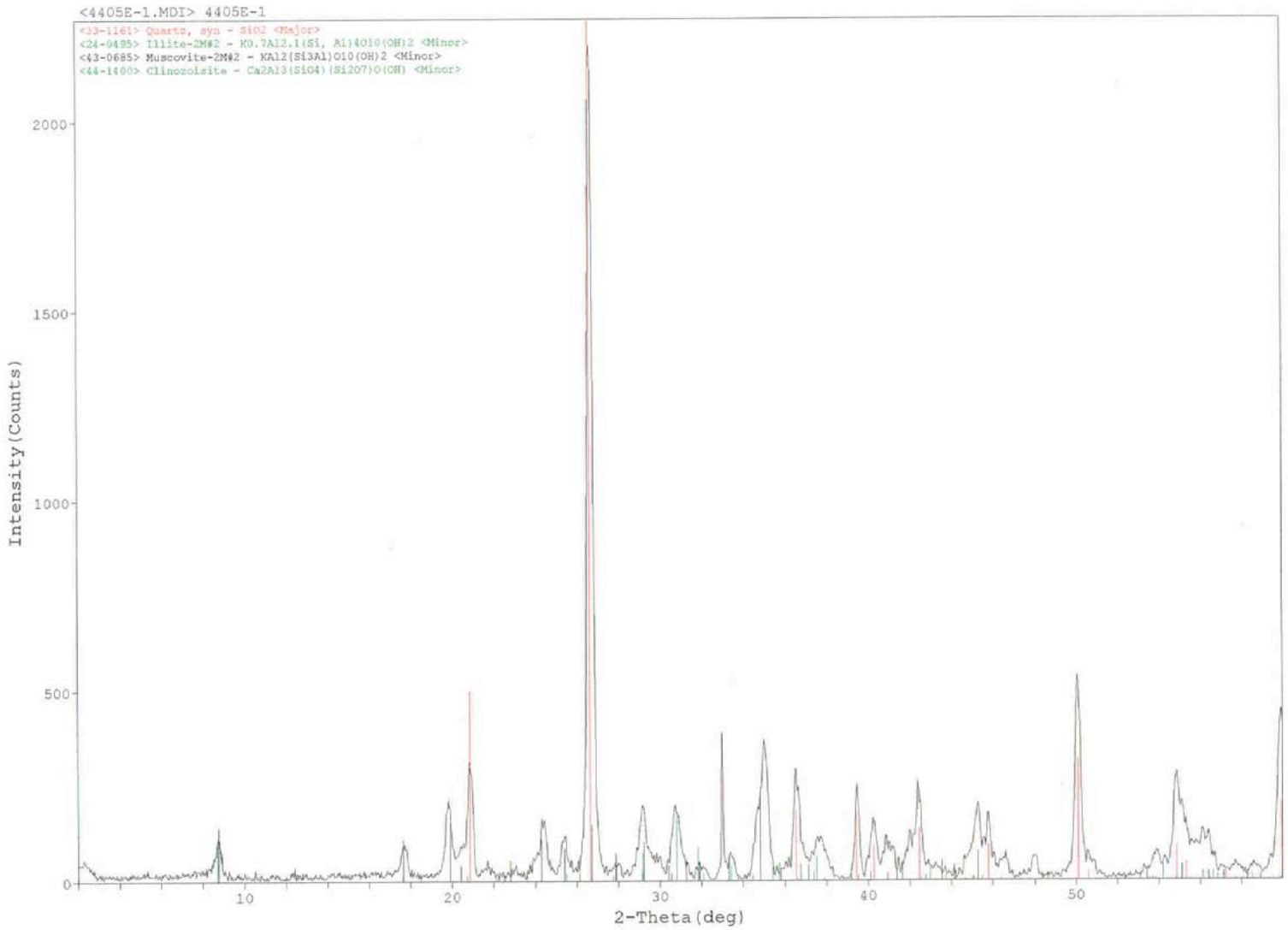
<4405E-1.MDI> 4405E-1
<33-1161> Quartz, syn - SiO2 <Major>
<24-0495> Illite-2M#2 - K0.7Al2.1(Si, Al)4O10(OH)2 <Minor>
<43-0685> Muscovite-2M#2 - KAl2(Si3Al)O10(OH)2 <Minor>
<44-1400> Clinozoisite - Ca2Al3(SiO4)(Si2O7)O(OH) <Minor>
Intensity(Counts)
2000
1500
1000
500
0
10
20
30
40
50
2-Theta(deg)

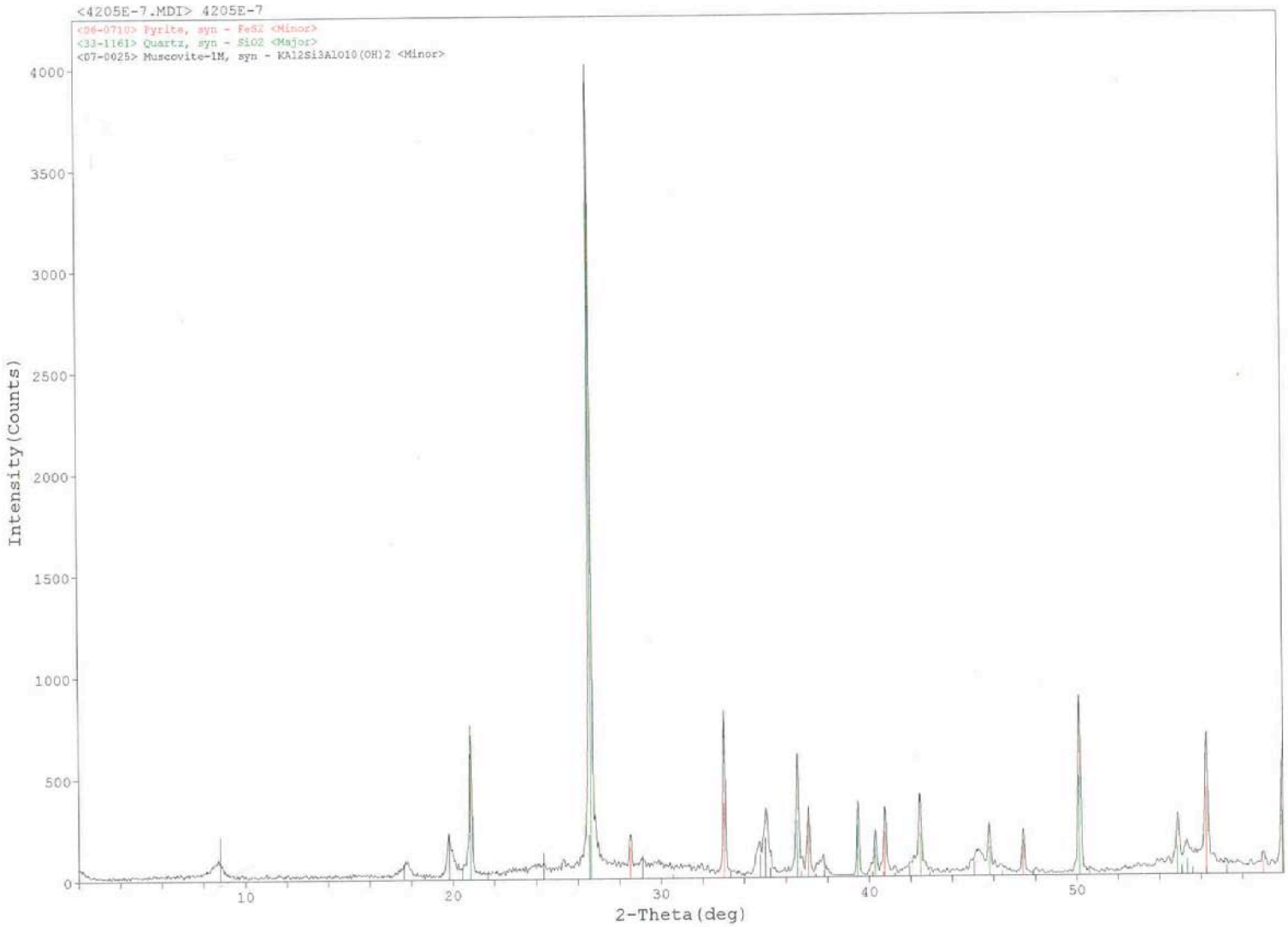
<4205E-7.MDI> 4205E-7
<26-0710> Pyrite, syn - FeS2 <Minor>
<33-1161> Quartz, syn - SiO2 <Major>
<07-0025> Muscovite-1M, syn - KAl2Si3AlO10(OH)2 <Minor>
Intensity(Counts)
4000
3500
3000
2500
2000
1500
1000
500
0
10
20
30
40
50
2-Theta(deg)

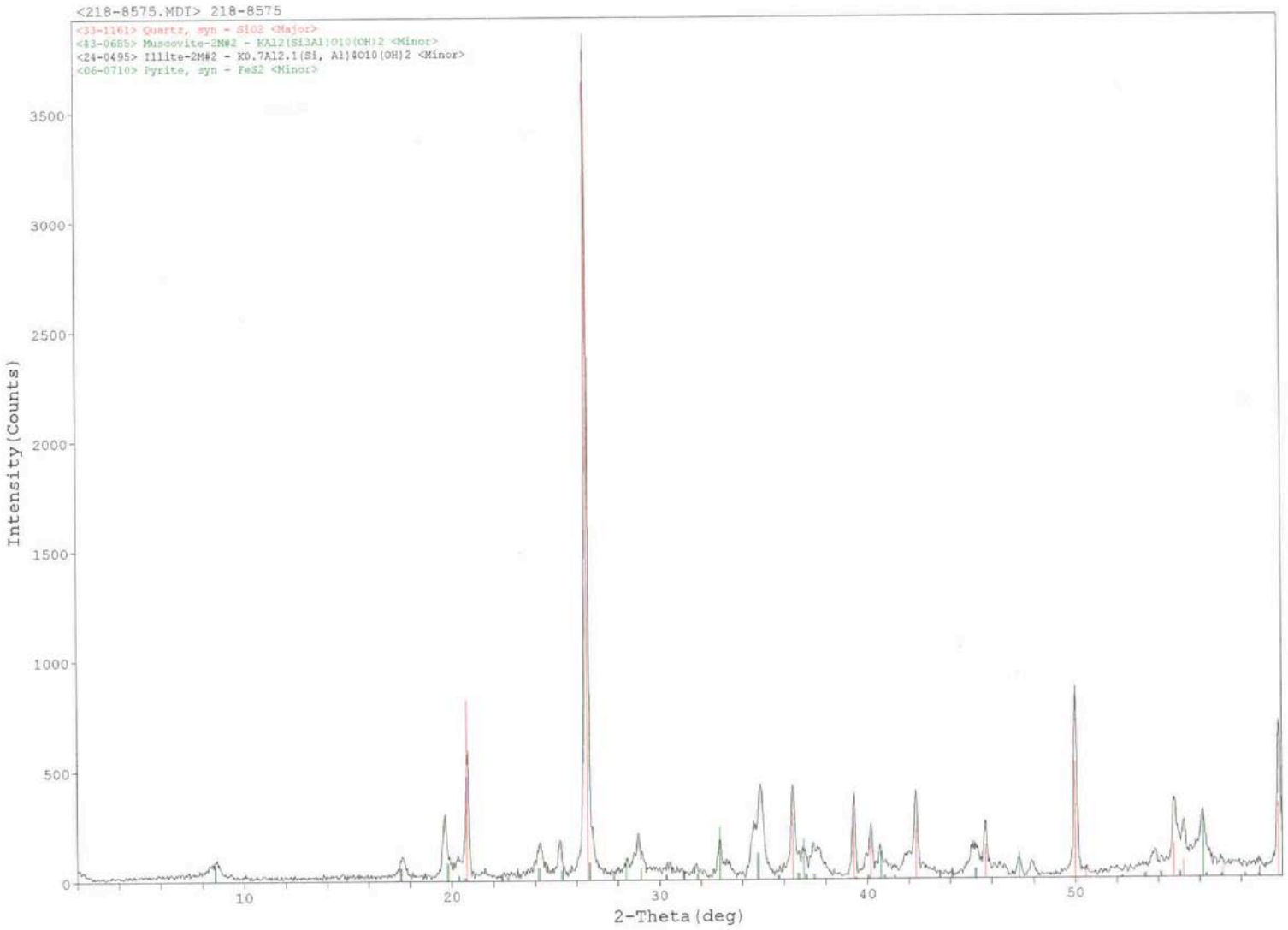
<218-8575.MDI> 218-8575
<33-1161> Quartz, syn - SiO2 <Major>
<43-0685> Muscovite-2M#2 - KAl2(Si3Al)O10(OH)2 <Minor>
<24-0495> Illite-2M#2 - K0.7Al2.1(Si, Al)4O10(OH)2 <Minor>
<06-0710> Pyrite, syn - FeS2 <Minor>
Intensity(Counts)
0
500
1000
1500
2000
2500
3000
3500
10
20
30
40
50
2-Theta(deg)

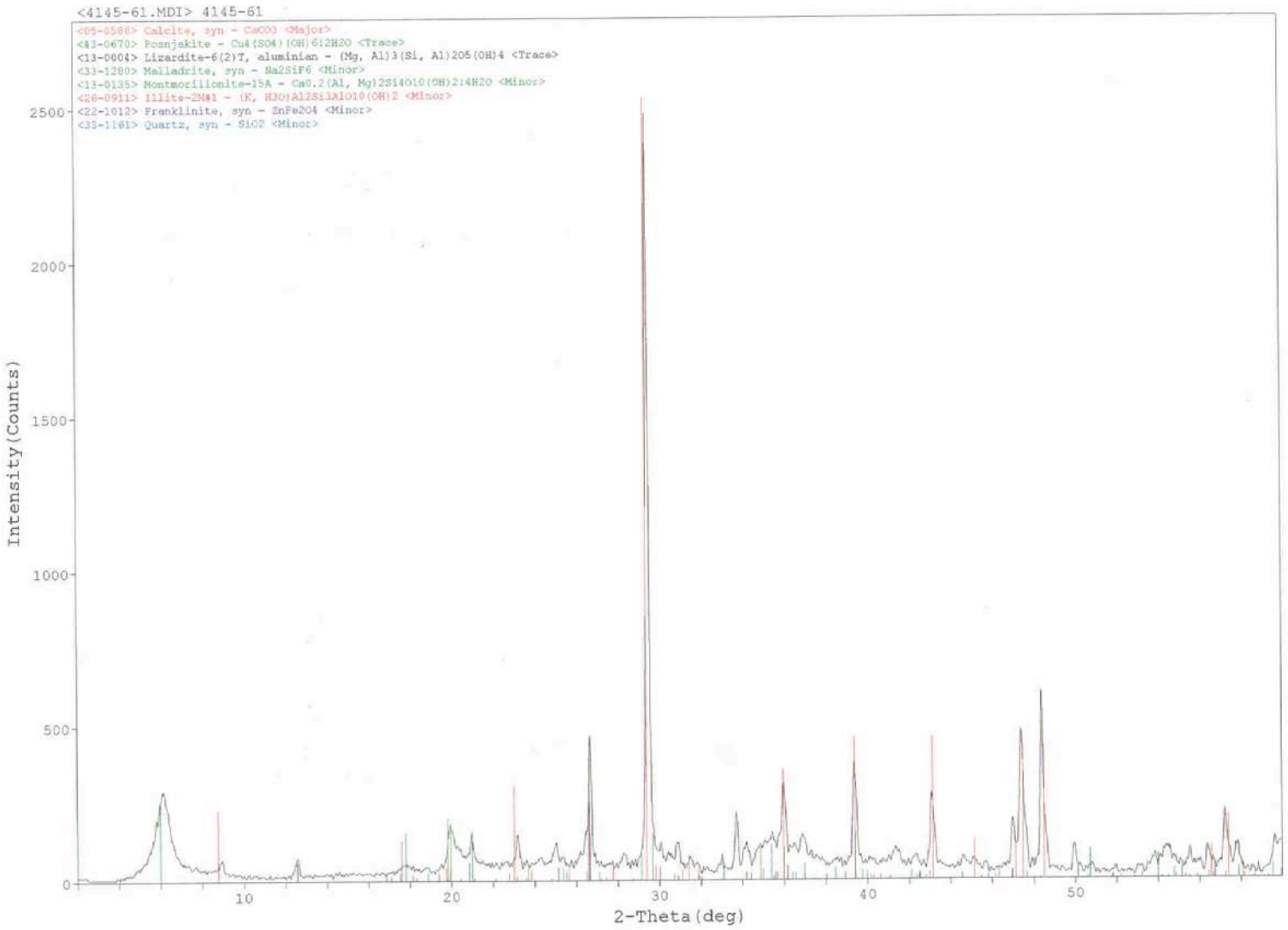
<4145-61.MDI> 4145-61
<05-0586> Calcite, syn - CaCO3 <Major>
<43-0670> Posnjakite - Cu4(SO4)(OH)612H2O <Trace>
<13-0004> Lizardite-6(2)T, aluminian - (Mg, Al)3(Si, Al)2O5(OH)4 <Trace>
<33-1280> Malladrite, syn - Na2SiF6 <Minor>
<13-0135> Montmorillonite-15A - Ca0.2(Al, Mg)2Si4O10(OH)2.4H2O <Minor>
<26-0911> Illite-2M$1 - (K, H3O)Al2Si3AlO10(OH)2 <Minor>
<22-1012> Franklinite, syn - ZnFe2O4 <Minor>
<33-1161> Quartz, syn - SiO2 <Minor>
Intensity(Counts)
2500
2000
1500
1000
500
0
10
20
30
40
50
2-Theta(deg)

APPENDIX IV

Electron Microprobe Data for BMVT Sphalerite from Cove

SAMPLE/GRAIN #	Zn	S	Fe	Cd	Se	Ga	As	Ag	Au	Cu	TOTAL
4245-17 ZnS 2	44.17	46.28	9.07	0.18	0.00	0.21	0.09	0.00	0.00	0.00	100.00
4245-17 ZnS 2	44.48	46.37	8.76	0.17	0.00	0.00	0.07	0.00	0.00	0.15	100.00
4245-17 ZnS 2	45.17	45.78	8.20	0.18	0.00	0.49	0.11	0.00	0.00	0.06	99.99
4245-17 ZnS 2	44.06	45.64	9.59	0.19	0.00	0.23	0.22	0.00	0.00	0.06	99.99
4245-17 ZnS 2	44.13	45.76	9.56	0.24	0.00	0.22	0.07	0.01	0.00	0.00	99.99
4245-17 ZnS 2	44.98	45.47	9.24	0.20	0.00	0.01	0.10	0.00	0.00	0.00	100.00
4245-17 ZnS 2	44.13	45.71	9.67	0.17	0.00	0.14	0.11	0.00	0.00	0.07	100.00
4245-17 ZnS 2	44.66	45.25	9.67	0.19	0.00	0.00	0.20	0.00	0.02	0.01	100.00
4245-17 ZnS 2	44.50	45.43	9.16	0.20	0.00	0.49	0.18	0.00	0.00	0.04	100.00
4245-17 ZnS 2	44.27	45.42	8.94	0.18	0.00	0.28	0.31	0.00	0.00	0.61	100.01
4245-17 ZnS 2	44.85	45.22	9.06	0.17	0.00	0.26	0.35	0.00	0.02	0.07	100.00
4245-17 ZnS 2	44.94	45.82	8.90	0.23	0.00	0.10	0.01	0.00	0.00	0.00	100.00
4245-17 ZnS 2	46.99	44.72	5.70	0.16	0.00	0.59	0.08	0.00	0.00	1.76	100.00
4245-17 ZnS 2	45.16	45.54	8.82	0.17	0.00	0.13	0.08	0.00	0.00	0.10	100.00
4245-17 ZnS 2	44.01	46.17	9.27	0.16	0.00	0.05	0.27	0.00	0.00	0.07	100.00
4245-17 ZnS 2	44.88	46.05	8.46	0.17	0.00	0.37	0.00	0.00	0.00	0.06	99.99
4245-17 ZnS 2	45.33	44.93	9.20	0.17	0.00	0.20	0.10	0.00	0.00	0.06	99.99
4245-17 ZnS 2	45.93	44.59	6.03	0.14	0.00	0.10	0.21	0.00	0.00	3.00	100.00
4245-17 ZnS 2	44.94	44.31	5.68	0.18	0.00	0.28	0.06	0.00	0.00	4.56	100.01
4245-17 ZnS 2	46.37	45.01	4.88	0.18	0.02	0.29	0.26	0.00	0.00	2.99	100.00
4245-17 ZnS 2	45.43	45.54	6.16	0.14	0.04	0.39	0.02	0.00	0.00	2.29	100.01
4245-17 ZnS 2	45.20	45.33	8.76	0.18	0.00	0.38	0.02	0.00	0.01	0.12	100.00
4245-17 ZnS 3	44.43	45.17	9.71	0.20	0.00	0.07	0.22	na	na	0.20	100.00
4245-17 ZnS 3	44.72	44.88	9.73	0.21	0.00	0.11	0.23	na	na	0.13	100.01
4245-17 ZnS 3	45.40	45.63	8.25	0.22	0.00	0.14	0.17	na	na	0.19	100.00
4245-17 ZnS 3	44.38	45.92	8.28	0.18	0.00	0.00	0.12	na	na	1.12	100.00
4245-17 ZnS 3	45.69	44.81	8.47	0.21	0.00	0.09	0.27	na	na	0.45	99.99
4245-17 ZnS 3	45.94	43.80	6.32	0.21	0.00	0.00	0.11	na	na	3.63	100.01
4245-17 ZnS 3	44.98	44.96	9.70	0.18	0.01	0.00	0.11	na	na	0.07	100.01
4245-17 ZnS 3	46.53	45.40	7.58	0.22	0.00	0.13	0.06	na	na	0.09	100.01
4245-17 ZnS 3	45.02	45.69	8.81	0.22	0.00	0.00	0.18	na	na	0.08	100.00
4245-17 ZnS 3	45.72	45.60	7.66	0.20	0.00	0.29	0.22	na	na	0.32	100.01
4245-17 ZnS 4	45.92	44.59	9.07	0.22	0.00	0.00	0.19	na	na	0.01	100.00
4245-17 ZnS 4	45.88	44.07	9.65	0.17	0.06	0.00	0.09	na	na	0.08	100.00
4245-17 ZnS 4	46.14	45.10	7.87	0.19	0.00	0.00	0.29	na	na	0.42	100.01
4245-17 ZnS 4	44.93	45.13	5.69	0.17	0.00	0.00	0.02	na	na	4.06	100.00
4205-10 ZnS 1	45.54	44.42	9.59	0.19	0.00	0.11	0.06	na	na	0.08	99.99
4205-10 ZnS 1	44.88	44.01	10.19	0.15	0.15	0.00	0.56	na	na	0.06	100.00
4205-10 ZnS 1	44.50	45.46	7.17	0.10	0.30	0.22	0.29	na	na	1.96	100.00
4205-10 ZnS 1	45.36	44.11	9.56	0.16	0.36	0.03	0.42	na	na	0.00	100.00
4205-10 ZnS 1	42.45	47.24	9.04	0.19	0.39	0.00	0.69	na	na	0.01	100.01
4205-10 ZnS 1	44.34	45.04	9.53	0.17	0.25	0.09	0.47	na	na	0.11	100.00
4205-10 ZnS 1	45.20	44.01	9.53	0.15	0.24	0.34	0.53	na	na	0.00	100.00
4205-10 ZnS 2	46.59	44.21	8.42	0.18	0.03	0.45	0.03	na	na	0.08	99.99
4205-10 ZnS 2	45.37	45.54	8.13	0.20	0.18	0.32	0.19	na	na	0.08	100.01
4205-10 ZnS 2	46.58	44.40	8.29	0.17	0.05	0.26	0.10	na	na	0.14	99.99
4205-10 ZnS 2	45.27	44.56	9.06	0.19	0.25	0.60	0.00	na	na	0.08	100.01
4205-10 ZnS 3	44.43	44.99	8.18	0.19	0.00	0.19	0.03	na	na	1.99	100.00

Appendix IV: Cove BMVT sphalerite EMP analyses results (na = not analyzed)

SAMPLE/GRAIN #	Zn	S	Fe	Cd	Se	Ga	As	Ag	Au	Cu	TOTAL
4205-10 ZnS 3	44.47	45.45	9.33	0.19	0.02	0.00	0.52	na	na	0.01	99.99
4205-10 ZnS 3	44.46	45.07	9.65	0.15	0.00	0.18	0.40	na	na	0.09	100.00
4205-10 ZnS 3	45.66	45.87	8.20	0.15	0.00	0.10	0.00	na	na	0.02	100.00
4205-10 ZnS 3	46.12	45.72	7.71	0.17	0.00	0.00	0.08	na	na	0.20	100.00
4145-21 ZnS 1	45.00	44.50	9.97	0.13	0.00	0.29	0.00	na	na	0.11	100.00
4145-21 ZnS 1	45.76	44.24	9.47	0.15	0.00	0.33	0.00	na	na	0.05	100.00
4145-21 ZnS 1	45.24	44.13	10.03	0.15	0.00	0.43	0.00	na	na	0.02	100.00
4145-21 ZnS 1	45.70	43.51	10.54	0.16	0.00	0.00	0.10	na	na	0.00	100.01
4145-21 ZnS 1	44.63	45.02	10.20	0.15	0.00	0.00	0.00	na	na	0.00	100.00
4145-21 ZnS 1	45.52	43.99	10.08	0.18	0.00	0.16	0.07	na	na	0.00	100.00
4145-21 ZnS 1	47.35	44.35	8.12	0.12	0.01	0.01	0.00	na	na	0.05	100.01
4145-21 ZnS 2	44.96	44.67	9.79	0.18	0.13	0.25	0.00	na	na	0.01	99.99
4145-21 ZnS 2	45.35	44.12	9.88	0.15	0.17	0.00	0.19	na	na	0.14	100.00
4145-21 ZnS 2	44.90	43.92	10.26	0.17	0.15	0.19	0.34	na	na	0.08	100.01
4145-21 ZnS 2	44.84	43.79	10.03	0.23	0.18	0.16	0.38	na	na	0.40	100.01
4145-21 ZnS 2	44.62	45.13	9.72	0.16	0.12	0.00	0.23	na	na	0.02	100.00
4145-21 ZnS 2	45.44	44.41	9.83	0.17	0.13	0.00	0.00	na	na	0.03	100.01
4145-21 ZnS 2	45.28	44.86	9.27	0.16	0.18	0.02	0.18	na	na	0.05	100.00
4145-21 ZnS 3	43.91	43.79	9.70	0.20	0.88	0.60	0.84	na	na	0.08	100.00
4145-21 ZnS 3	42.84	43.91	9.93	0.21	0.90	1.17	0.88	na	na	0.17	100.01
4145-21 ZnS 3	43.97	43.55	9.59	0.22	0.75	0.83	1.02	na	na	0.07	100.00
4145-21 ZnS 3	43.29	43.84	9.77	0.18	0.90	0.79	1.05	na	na	0.18	100.00
4145-21 ZnS 3	44.09	43.31	9.55	0.23	0.79	0.84	1.02	na	na	0.17	100.00
4145-21 ZnS 3	44.48	42.51	9.25	0.26	0.83	0.78	1.05	na	na	0.84	100.00
7/26/98-2B ZnS 1	43.39	47.40	8.66	0.24	0.09	0.00	0.10	na	na	0.12	100.00
7/26/98-2B ZnS 1	43.39	46.71	9.32	0.19	0.13	0.05	0.09	na	na	0.11	99.99
7/26/98-2B ZnS 1	43.72	47.01	8.91	0.19	0.05	0.01	0.06	na	na	0.05	100.00
7/26/98-2B ZnS 1	43.16	46.98	9.09	0.23	0.12	0.19	0.14	na	na	0.09	100.00
7/26/98-2B ZnS 1	43.35	46.90	9.17	0.19	0.12	0.00	0.15	na	na	0.11	99.99
7/26/98-2B ZnS 1	43.38	46.83	9.19	0.21	0.16	0.14	0.08	na	na	0.01	100.00
7/26/98-2B ZnS 1	43.60	47.56	8.33	0.23	0.12	0.00	0.07	na	na	0.08	99.99
7/26/98-2B ZnS 1	44.23	46.43	8.66	0.20	0.05	0.20	0.12	na	na	0.10	99.99
7/26/98-2B ZnS 1	44.02	46.25	8.98	0.18	0.15	0.00	0.30	na	na	0.11	99.99
7/26/98-2B ZnS 2	45.38	47.78	5.71	0.22	0.11	0.44	0.22	na	na	0.15	100.01
7/26/98-2B ZnS 2	46.49	47.56	5.00	0.19	0.29	0.04	0.29	na	na	0.14	100.00
7/26/98-2B ZnS 2	44.54	46.40	6.34	0.19	0.21	0.07	0.17	na	na	2.08	100.00
7/26/98-2B ZnS 2	45.32	48.32	5.35	0.18	0.14	0.06	0.09	na	na	0.54	100.00
7/26/98-2B ZnS 3	43.33	46.83	9.24	0.21	0.16	0.16	0.04	na	na	0.04	100.01
7/26/98-2B ZnS 3	42.50	47.54	9.23	0.20	0.25	0.15	0.09	na	na	0.05	100.01
7/26/98-2B ZnS 3	43.05	47.12	9.18	0.21	0.17	0.12	0.10	na	na	0.05	100.00
7/26/98-2B ZnS 3	43.26	47.38	9.10	0.21	0.01	0.00	0.03	na	na	0.01	100.00
7/26/98-2B ZnS 4	44.19	47.54	7.63	0.23	0.15	0.10	0.05	na	na	0.12	100.01
7/26/98-2B ZnS 4	44.81	47.31	7.38	0.19	0.15	0.05	0.03	na	na	0.08	100.00
7/26/98-2B ZnS 4	46.08	47.43	4.97	0.20	0.21	0.20	0.09	na	na	0.81	99.99
7/26/98-2B ZnS 4	44.82	48.38	5.60	0.20	0.17	0.24	0.18	na	na	0.41	100.00
7/26/98-2B ZnS 4	44.18	46.86	7.58	0.20	0.31	0.33	0.38	na	na	0.15	99.99
7/26/98-2B ZnS 5	43.76	47.27	7.55	0.19	0.55	0.00	0.44	na	na	0.24	100.00
7/26/98-2B ZnS 5	44.26	46.42	7.58	0.20	0.62	0.12	0.57	na	na	0.22	99.99

Appendix IV: Cove BMVT sphalerite EMP analyses results (na = not analyzed)

SAMPLE/GRAIN #	Zn	S	Fe	Cd	Se	Ga	As	Ag	Au	Cu	TOTAL
7/26/98-2B ZnS 5	43.82	46.49	7.71	0.20	0.57	0.21	0.37	na	na	0.64	100.01
7/26/98-2B ZnS 5	44.48	46.65	7.60	0.19	0.48	0.09	0.39	na	na	0.12	100.00
4245E-14 ZnS 1	42.35	50.36	6.85	0.21	0.00	0.00	0.01	na	na	0.22	100.00
4245E-14 ZnS 1	42.96	49.92	6.54	0.19	0.00	0.00	0.28	na	na	0.11	100.00
4245E-14 ZnS 1	42.45	49.62	7.42	0.20	0.00	0.00	0.00	na	na	0.31	100.00
4245E-14 ZnS 1	42.63	50.92	6.25	0.19	0.00	0.00	0.00	na	na	0.01	100.00
4245E-14 ZnS 1	42.51	50.03	6.92	0.17	0.00	0.13	0.15	na	na	0.09	100.00
4245E-14 ZnS 1	42.53	49.19	7.52	0.19	0.00	0.00	0.16	na	na	0.42	100.01
4245E-14 ZnS 1	41.58	51.97	6.00	0.21	0.00	0.02	0.16	na	na	0.06	100.00
4245E-14 ZnS 2	43.62	48.42	7.35	0.17	0.06	0.02	0.14	na	na	0.21	99.99
4245E-14 ZnS 2	44.05	48.64	6.19	0.20	0.13	0.02	0.21	na	na	0.57	100.01
4245E-14 ZnS 2	43.33	49.27	6.83	0.16	0.04	0.36	0.02	na	na	0.00	100.01
4245E-14 ZnS 2	43.53	49.10	6.78	0.19	0.21	0.00	0.18	na	na	0.00	99.99
4245E-14 ZnS 2	41.88	50.73	6.71	0.20	0.08	0.26	0.13	na	na	0.01	100.00
4245E-14 ZnS 5	42.53	48.28	7.42	0.20	0.00	0.81	0.00	na	na	0.76	100.00
4245E-14 ZnS 5	43.73	46.02	8.66	0.18	0.00	1.40	0.01	na	na	0.00	100.00
4245E-14 ZnS 5	42.29	47.04	10.14	0.11	0.00	0.41	0.00	na	na	0.02	100.01
4245E-14 ZnS 5	43.27	47.38	8.25	0.16	0.13	0.64	0.03	na	na	0.13	99.99
4245E-14 ZnS 5	44.63	46.00	8.37	0.16	0.00	0.74	0.11	na	na	0.00	100.01

Appendix IV: Cove BMVT sphalerite EMP analyses results (na = not analyzed)

APPENDIX V

Multi-Element Geochemical Data for Samples from Cove

Sample	Rock Type	Company	B. D. (g/cc)	Al %	As ppm	Sb ppm	Ba ppm	Be ppm
4145-40	P.C. trans	Chemex	2.07	5.40	356	11.4	240	0.95
4145-41	P.C. trans	Chemex	2.16	5.52	52	13.0	250	0.95
4145-42	P.C. trans	Chemex	2.29	4.73	59	6.0	260	0.95
4145-46	P.C. trans	Chemex	1.97	6.73	110	8.9	700	1.40
4145-47	P.C. trans	Chemex	2.41	1.30	245	8.3	100	0.45
4145-48	P.C. trans	Chemex	2.15	3.96	245	18.4	290	1.10
4145-49	P.C. trans	Chemex	2.18	7.05	133	12.1	480	1.90
4245-7A	P.C. trans	Chemex	2.47	1.76	101	9.8	470	0.20
4245-7B	P.C. trans	Chemex	2.65	5.49	61	5.7	660	1.05
HS-1	H.S.	Chemex	2.74	0.32	46	3.2	10	0.20
HS-2	H.S.	Chemex	2.70	0.26	11	1.0	10	0.15
HS-3	H.S.	Chemex	2.54	1.87	2360	600.0	15	<0.50
HS-4	bms pod	Chemex	4.57	0.34	4140	405.0	25	<0.50
HS-5	sooty bms	Chemex	3.16	3.52	2110	432.0	80	<0.50
HS-6	intrusion	Chemex	2.04	8.44	85	21.3	350	1.30
4725-4	intrusion	Chemex	2.51	8.53	6	0.7	900	1.55
4205-23	intrusion	Chemex	2.43	7.92	17	2.4	1140	1.50
4285-11	intrusion	Chemex	2.37	7.56	4	3.8	1140	1.55
AR-8	intrusion	Chemex	2.46	8.68	4	0.4	890	1.70
4205-5	intrusion	Chemex	2.42	8.12	191	11.4	1120	1.10
4205-7	intrusion	Chemex	2.33	8.85	117	12.9	560	2.15
4405-2	intrusion	Chemex	2.48	8.46	26	3.0	950	1.55
CU-0	P.C. dol?	Chemex	na	0.50	26	6.1	60	0.10
CU-10	P.C. dol?	Chemex	na	0.52	17	7.5	40	<0.05
CU-20	P.C. dol?	Chemex	na	0.44	69	11.1	70	0.05
CU-25	P.C. dol?	Chemex	na	0.63	257	20.6	70	0.20
CU-30	P.C. dol?	Chemex	na	0.54	293	7.5	110	0.10
CU-35	P.C. dol?	Chemex	na	0.65	210	15.5	50	0.15
CU-40	P.C. dol?	Chemex	na	0.52	89	56.3	100	0.20
CU-45	P.C. dol?	Chemex	na	0.61	119	9.0	90	0.30
CU-46	P.C. dol?	Chemex	na	0.86	201	10.2	170	0.25
CU-47	P.C. dol?	Chemex	na	1.67	564	17.2	90	0.45
CU-48	P.C. dol?	Chemex	na	2.07	510	29.8	60	0.30
CU-49	P.C. dol?	Chemex	na	1.36	491	12.2	60	0.15
CU-50	P.C. dol?	Chemex	na	3.25	3670	155.0	70	<0.05
CU-51	P.C. dol?	Chemex	na	2.45	2120	126.0	70	<0.05
CU-52	P.C. dol?	Chemex	na	1.18	508	40.9	80	0.30
CU-53	P.C. dol?	Chemex	na	1.77	915	122.0	60	0.35
CU-54	P.C. dol?	Chemex	na	1.95	1785	353.0	60	<0.05
CU-55	P.C. dol?	Chemex	na	3.19	2730	177.0	60	<0.05
CU-60	P.C. dol?	Chemex	na	3.45	6910	1460.0	50	<0.05
CU-70	P.C. dol?	Chemex	na	1.03	716	41.3	70	0.35
CU-80	P.C. dol?	Chemex	na	1.98	62100	2870.0	10	<0.05
CU-90	P.C. dol?	Chemex	na	4.83	1780	85.2	50	0.65
CU-95	P.C. dol?	Chemex	na	2.35	39200	745.0	20	<0.05
CU-100	P.C. dol?	Chemex	na	0.26	165	12.1	30	0.20
CU-105	P.C. dol?	Chemex	na	0.54	157	18.4	30	0.25
CU-110	P.C. dol?	Chemex	na	0.46	1210	130.5	20	0.05

Appendix V: Cove deposit multi-element geochemical data (B.D. = bulk density; na = not analyzed)

Sample	Rock Type	Company	B. D. (g/cc)	Al %	As ppm	Sb ppm	Ba ppm	Be ppm
CU-115	P.C. dol?	Chemex	na	2.82	1670	109.0	60	0.40
CU-120	P.C. dol?	Chemex	na	1.29	342	33.4	30	0.35
CVC218 800.3-810	H.S.	Cone?	na	0.06	4306	1211.0	6	<1
CVC218 810-811.7	H.S.	Cone?	na	0.05	4808	1456.0	38	<1
CVC218 815-820	H.S.	Cone?	na	0.12	3220	559.0	22	<1
CVC218 830-835	H.S.	Cone?	na	0.05	1098	380.0	9	<1
CVC218 835-836.2	H.S.	Cone?	na	0.10	5639	281.0	19	<1
CVC218 840-845	H.S.	Cone?	na	0.16	2433	179.0	52	<1
CVC218 855-859.5	H.S.	Cone?	na	0.14	4932	42.0	40	<1
248-A	H.S.?	Cone	na	na	7892	166.0	51	<1
248-B	realgar vein	Cone	na	na	>10%	>1%	4	<1
248-C	P.C. dol?	Cone	na	na	751	94.0	10	<1
86921	H.S.	Cone	na	na	87	<2	14	<1
86922	H.S.	Cone	na	na	2106	436	9	<1
86923	H.S.	Cone	na	na	3235	436	10	<1
CVC-15 1000-1010	P.C. trans	Chemex, Monitor ave. *	na	0.45	125	5	100	<0.5
CVC-15 1010-1020	P.C. trans	Chemex, Monitor ave. *	na	0.32	180	25	60	<0.5
CVC-15 1020-1030	P.C. trans	Chemex, Monitor ave. *	na	0.49	305	35	100	<0.5
CVC-15 1030-1040	P.C. trans	Chemex, Monitor ave. *	na	0.39	445	60	60	<0.5
CVC-15 1040-1050	P.C. trans	Chemex, Monitor ave. *	na	0.38	290	60	60	<0.5
CVC-15 1050-1060	P.C. trans	Chemex, Monitor ave. *	na	0.50	290	25	180	<0.5
CVC-15 1060-1070	P.C. trans	Chemex, Monitor ave. *	na	0.66	425	20	150	<0.5
CVC-15 1070-1080	P.C. trans	Chemex, Monitor ave. *	na	0.71	685	10	100	<0.5
CVC-15 1080-1090	P.C. trans	Chemex, Monitor ave. *	na	0.55	2940	35	50	<0.5
CVC-15 1090-1100	P.C. trans	Chemex, Monitor ave. *	na	1.11	4040	30	110	<0.5
CVC-15 1100-1110	P.C. trans	Chemex, Monitor ave. *	na	0.71	430	10	80	<0.5
CVC-15 1110-1120	P.C. trans	Chemex, Monitor ave. *	na	0.48	710	20	90	<0.5
CVC-15 1120-1130	P.C. trans	Chemex, Monitor ave. *	na	0.37	3190	30	90	<0.5
CVC-15 1130-1140	P.C. trans	Chemex, Monitor ave. *	na	0.37	3200	35	80	<0.5
CVC-15 1140-1150	P.C. trans	Chemex, Monitor ave. *	na	0.61	1470	10	140	<0.5
CVC-15 1150-1160	P.C. trans	Chemex, Monitor ave. *	na	0.60	950	15	110	<0.5
CVC-15 1160-1170	P.C. trans	Chemex, Monitor ave. *	na	0.69	630	20	90	<0.5
CVC-15 1170-1180	P.C. trans	Chemex, Monitor ave. *	na	0.60	475	35	90	<0.5
CVC-15 1180-1190	P.C. trans	Chemex, Monitor ave. *	na	1.53	165	15	170	0.5
CVC-15 1190-1200	P.C. trans	Chemex, Monitor ave. *	na	1.31	300	20	80	<0.5
CVC-15 1200-1210	P.C. trans	Chemex, Monitor ave. *	na	1.11	230	10	90	<0.5
CVC-15 1210-1220	P.C. trans	Chemex, Monitor ave. *	na	0.87	285	10	110	<0.5
CVC-15 1220-1230	P.C. trans	Chemex, Monitor ave. *	na	0.77	315	15	90	<0.5
CVC-15 1230-1240	P.C. trans	Chemex, Monitor ave. *	na	0.75	450	10	90	<0.5
CVC-15 1240-1250	P.C. trans	Chemex, Monitor ave. *	na	0.87	205	5	80	<0.5
CVC-15 1250-1260	P.C. trans	Chemex, Monitor ave. *	na	1.17	265	15	140	<0.5
CVC-15 1260-1270	P.C. trans	Chemex, Monitor ave. *	na	1.02	135	10	150	<0.5
CVC-15 1270-1280	P.C. trans	Chemex, Monitor ave. *	na	0.88	210	15	60	<0.5
CVC-15 1280-1290	P.C. trans	Chemex, Monitor ave. *	na	0.73	215	15	220	<0.5
CVC-15 1290-1300	P.C. trans	Chemex, Monitor ave. *	na	0.69	95	10	90	<0.5
CVC-15 1300-1310	P.C. trans	Chemex, Monitor ave. *	na	0.51	35	10	70	<0.5
CVC-15 1310-1320	P.C. trans	Chemex, Monitor ave. *	na	0.81	45	20	380	<0.5
CVC-15 1320-1330	P.C. trans	Chemex, Monitor ave. *	na	0.61	105	10	90	<0.5

Appendix V: Cove deposit multi-element geochemical data (B.D. = bulk density; na = not analyzed)

Sample	Rock Type	Company	B. D. (g/cc)	Al %	As ppm	Sb ppm	Ba ppm	Be ppm
CVC-15 1330-1340	P.C. trans	Chemex, Monitor ave. *	na	0.31	565	45	70	<0.5
CVC-15 1340-1350	P.C. trans	Chemex, Monitor ave. *	na	0.55	225	20	170	<0.5
CVC-15 1350-1360	P.C. trans	Chemex, Monitor ave. *	na	0.51	20	5	80	<0.5
CVC-15 1360-1370	P.C. trans	Chemex, Monitor ave. *	na	0.55	35	30	<10	<0.5
CVC-15 1370-1380	P.C. trans	Chemex, Monitor ave. *	na	0.82	50	85	<10	<0.5
CVC-15 1380-1390	P.C. trans	Chemex, Monitor ave. *	na	0.62	70	70	10	<0.5
CVC-15 1390-1400	P.C. dol	Chemex, Monitor ave. *	na	0.29	50	10	40	<0.5
CVC-15 1400-1410	P.C. dol	Chemex, Monitor ave. *	na	0.25	20	5	50	<0.5
CVC-15 1410-1420	P.C. dol	Chemex, Monitor ave. *	na	0.49	40	5	40	<0.5
CVC-15 1420-1430	P.C. dol	Chemex, Monitor ave. *	na	0.54	70	5	40	<0.5
CVC-15 1430-1440	P.C. dol	Chemex, Monitor ave. *	na	0.80	70	10	90	<0.5
CVC-15 1440-1450	P.C. dol	Chemex, Monitor ave. *	na	0.65	250	40	210	<0.5
CVC-15 1450-1460	P.C. dol	Chemex, Monitor ave. *	na	0.27	360	10	280	<0.5
CVC-15 1460-1470	P.C. dol	Chemex, Monitor ave. *	na	0.29	125	5	560	<0.5
CVC-15 1470-1480	P.C. dol	Chemex, Monitor ave. *	na	0.44	10	5	290	<0.5
CVC-15 1480-1490	P.C. dol	Chemex, Monitor ave. *	na	0.69	165	10	220	<0.5
CVC-15 1490-1500	P.C. dol	Chemex, Monitor ave. *	na	0.67	60	10	40	<0.5
CVC-10 0920-0930	P.C. trans?	Chemex, Monitor ave. *	na	0.62	510	75	40	<0.5
CVC-10 0930-0940	P.C. trans?	Chemex, Monitor ave. *	na	0.64	915	195	20	<0.5
CVC-10 0940-0950	P.C. trans?	Chemex, Monitor ave. *	na	0.86	360	50	40	<0.5
CVC-10 0950-0960	P.C. trans?	Chemex, Monitor ave. *	na	0.58	370	30	20	<0.5
CVC-10 0960-0970	P.C. trans?	Chemex, Monitor ave. *	na	0.60	265	5	40	<0.5
CVC-10 0970-0980	P.C. trans?	Chemex, Monitor ave. *	na	0.53	350	10	30	<0.5
CVC-10 0980-0990	P.C. trans?	Chemex, Monitor ave. *	na	0.54	205	10	40	<0.5
CVC-10 0990-1000	P.C. trans?	Chemex, Monitor ave. *	na	0.62	480	85	50	1.0
CVC-10 1000-1010	P.C. trans?	Chemex, Monitor ave. *	na	0.64	285	110	40	0.5
CVC-10 1010-1020	P.C. dol?	Chemex, Monitor ave. *	na	0.65	345	75	60	<0.5
CVC-10 1020-1030	P.C. dol?	Chemex, Monitor ave. *	na	0.53	1410	540	30	1.0
CVC-10 1030-1040	P.C. dol?	Chemex, Monitor ave. *	na	0.78	65	10	190	<0.5
CVC-10 1040-1050	P.C. dol?	Chemex, Monitor ave. *	na	0.46	110	20	160	0.5
CVC-10 1050-1060	P.C. dol?	Chemex, Monitor ave. *	na	0.25	355	90	40	<0.5
CVC-10 1060-1070	P.C. dol?	Chemex, Monitor ave. *	na	0.31	125	20	110	<0.5
CVC-10 1070-1080	H.S.	Chemex, Monitor ave. *	na	0.67	945	265	10	0.5
CVC-10 1080-1090	H.S.	Chemex, Monitor ave. *	na	0.13	45	<5	<10	<0.5
CVC-10 1090-1099.5	H.S.	Chemex, Monitor ave. *	na	0.39	125	20	60	<0.5
CVC-10 1099.5-1110	H.S.	Chemex, Monitor ave. *	na	0.53	605	205	10	0.5
CVC-10 1110-1120	H.S.	Chemex, Monitor ave. *	na	0.39	415	140	30	<0.5
CVC-10 1120-1130	H.S.	Chemex, Monitor ave. *	na	0.79	1025	280	10	<0.5
CVC-10 1130-1140	H.S.	Chemex, Monitor ave. *	na	0.57	840	155	10	<0.5
CVC-10 1140-1150	H.S.	Chemex, Monitor ave. *	na	0.86	900	135	30	1.5
CVC-10 1150-1160	H.S.	Chemex, Monitor ave. *	na	0.46	135	70	30	<0.5
CVC-10 1160-1170	H.S.	Chemex, Monitor ave. *	na	0.59	325	140	40	<0.5
CVC-10 1170-1180	H.S.	Chemex, Monitor ave. *	na	0.79	95	20	20	0.5
CVC-10 1180-1190	H.S.	Chemex, Monitor ave. *	na	0.39	130	30	10	<0.5
CVC-10 1190-1200	H.S.	Chemex, Monitor ave. *	na	0.30	315	160	10	<0.5
CVC-10 1200-1210	H.S.	Chemex, Monitor ave. *	na	0.40	295	65	20	<0.5
CVC-10 1210-1220	H.S.	Chemex, Monitor ave. *	na	0.50	390	80	20	1
CVC-10 1220-1230	H.S.	Chemex, Monitor ave. *	na	0.55	165	15	40	<0.5

Appendix V: Cove deposit multi-element geochemical data (B.D. = bulk density; na = not analyzed)

Sample	Rock Type	Company	B. D. (g/cc)	Al %	As ppm	Sb ppm	Ba ppm	Be ppm
CVC-10 1230-1240	H.S.	Chemex, Monitor ave. *	na	0.36	80	75	40	<0.5
CVC-10 1240-1250	H.S.	Chemex, Monitor ave. *	na	0.39	135	65	100	0.5
CVC-10 1250-1260	H.S.	Chemex, Monitor ave. *	na	0.33	665	140	20	1.5
CVC-10 1260-1270	H.S.	Chemex, Monitor ave. *	na	0.71	440	70	40	<0.5
CVC-10 1270-1280	H.S.	Chemex, Monitor ave. *	na	0.55	390	115	30	<0.5
CVC-10 1280-1290	H.S.	Chemex, Monitor ave. *	na	0.55	250	125	40	<0.5
CVC-10 1290-1300	H.S.	Chemex, Monitor ave. *	na	0.77	225	110	60	<0.5
CVC-10 1300-1310	H.S.	Chemex, Monitor ave. *	na	0.92	335	130	70	<0.5
CVC-10 1310-1320	H.S.	Chemex, Monitor ave. *	na	0.57	165	110	40	<0.5
CVC-10 1320-1330	H.S.	Chemex, Monitor ave. *	na	0.77	85	35	40	<0.5
CVC-10 1330-1340	H.S.	Chemex, Monitor ave. *	na	0.75	85	10	30	<0.5
CVC-10 1340-1350	H.S.	Chemex, Monitor ave. *	na	0.64	240	50	30	<0.5
CVC-10 1350-1360	H.S.	Chemex, Monitor ave. *	na	0.79	120	15	20	<0.5
CVC-10 1360-1370	H.S.	Chemex, Monitor ave. *	na	0.50	135	25	20	<0.5
CVC-10 1370-1380	H.S.	Chemex, Monitor ave. *	na	0.57	160	10	20	<0.5
CVC-10 1380-1390	H.S.	Chemex, Monitor ave. *	na	0.61	125	30	20	<0.5
CVC-10 1390-1400	H.S.	Chemex, Monitor ave. *	na	0.51	130	25	20	<0.5
CVC-11 1000-1010	P.C. trans	Chemex, Monitor ave. *	na	0.46	210	30	40	<0.5
CVC-11 1010-1020	P.C. trans	Chemex, Monitor ave. *	na	0.81	85	15	100	<0.5
CVC-11 1020-1030	P.C. trans	Chemex, Monitor ave. *	na	1.27	35	5	90	0.5
CVC-11 1030-1040	P.C. trans	Chemex, Monitor ave. *	na	1.45	390	25	70	<0.5
CVC-11 1040-1050	P.C. dol	Chemex, Monitor ave. *	na	0.28	110	10	10	<0.5
CVC-11 1050-1060	P.C. dol	Chemex, Monitor ave. *	na	0.35	85	15	10	<0.5
CVC-11 1060-1070	P.C. dol	Chemex, Monitor ave. *	na	0.10	65	5	<10	<0.5
CVC-11 1070-1080	P.C. dol	Chemex, Monitor ave. *	na	0.09	75	5	10	<0.5
CVC-11 1080-1090	P.C. dol	Chemex, Monitor ave. *	na	0.11	170	5	<10	<0.5
CVC-11 1090-1100	H.S.	Chemex, Monitor ave. *	na	0.48	260	30	10	<0.5
CVC-11 1100-1110	H.S.	Chemex, Monitor ave. *	na	0.84	225	40	10	<0.5
CVC-11 1110-1120	H.S.	Chemex, Monitor ave. *	na	0.51	125	10	10	<0.5
CVC-11 1120-1130	H.S.	Chemex, Monitor ave. *	na	1.09	1030	45	10	<0.5
CVC-11 1130-1140	H.S.	Chemex, Monitor ave. *	na	1.14	280	20	150	<0.5
CVC-11 1140-1150	H.S.	Chemex, Monitor ave. *	na	0.83	625	80	10	<0.5
CVC-11 1150-1160	H.S.	Chemex, Monitor ave. *	na	0.57	295	45	20	<0.5
CVC-11 1160-1170	H.S.	Chemex, Monitor ave. *	na	0.40	325	55	50	<0.5
CVC-11 1170-1180	H.S.	Chemex, Monitor ave. *	na	0.34	210	110	10	<0.5
CVC-11 1180-1190	H.S.	Chemex, Monitor ave. *	na	0.50	240	100	30	<0.5
CVC-11 1190-1200	H.S.	Chemex, Monitor ave. *	na	0.53	165	30	40	<0.5
CVC-11 1200-1210	H.S.	Chemex, Monitor ave. *	na	0.45	125	20	10	<0.5
CVC-11 1210-1220	H.S.	Chemex, Monitor ave. *	na	0.28	80	20	20	<0.5
CVC-11 1220-1230	H.S.	Chemex, Monitor ave. *	na	0.32	60	20	80	<0.5
CVC-11 1230-1240	H.S.	Chemex, Monitor ave. *	na	0.52	485	15	50	<0.5
CVC-11 1240-1250	H.S.	Chemex, Monitor ave. *	na	0.25	360	65	50	<0.5
CVC-11 1250-1260	H.S.	Chemex, Monitor ave. *	na	0.18	85	25	50	<0.5
CVC-11 1260-1270	H.S.	Chemex, Monitor ave. *	na	0.31	265	40	50	<0.5
CVC-11 1270-1280	H.S.	Chemex, Monitor ave. *	na	0.33	90	25	30	<0.5
CVC-11 1280-1290	H.S.	Chemex, Monitor ave. *	na	0.55	100	10	30	<0.5
CVC-11 1290-1300	H.S.	Chemex, Monitor ave. *	na	0.42	70	15	40	<0.5
CVC-11 1300-1310	H.S.	Chemex, Monitor ave. *	na	0.65	175	25	40	<0.5

Appendix V: Cove deposit multi-element geochemical data (B.D. = bulk density; na = not analyzed)

Sample	Rock Type	Company	B. D. (g/cc)	Al %	As ppm	Sb ppm	Ba ppm	Be ppm
CVC-11 1310-1320	H.S.	Chemex, Monitor ave. *	na	0.89	360	60	80	<0.5
CVC-11 1320-1330	H.S.	Chemex, Monitor ave. *	na	0.45	330	90	80	<0.5
CVC-11 1330-1340	H.S.	Chemex, Monitor ave. *	na	0.51	945	200	40	<0.5
CVC-11 1340-1350	H.S.	Chemex, Monitor ave. *	na	0.47	3240	395	110	<0.5
CVC-11 1350-1360	H.S.	Chemex, Monitor ave. *	na	0.43	170	195	570	<0.5
CVC-11 1360-1370	H.S.	Chemex, Monitor ave. *	na	0.74	185	30	550	<0.5
CVC-11 1370-1380	H.S.	Chemex, Monitor ave. *	na	0.45	145	25	310	<0.5
CVC-11 1380-1390	H.S.	Chemex, Monitor ave. *	na	0.95	325	45	370	<0.5
CVC-11 1390-1400	H.S.	Chemex, Monitor ave. *	na	0.85	165	40	220	<0.5

Appendix V: Cove deposit multi-element geochemical data (B.D. = bulk density; na = not analyzed)

Sample	Bi ppm	B ppm	Cd ppm	Ca %	Ce ppm	Cs ppm	Cr ppm	Co ppm	Cu ppm
4145-40	0.46	na	0.2	0.38	42.7	9.60	93	8.4	8
4145-41	0.66	na	0.3	0.28	50.7	14.20	98	9.2	6
4145-42	0.06	na	0.3	1.90	47.6	8.10	98	8.6	4
4145-46	0.16	na	0.1	0.33	50.6	11.85	129	4.4	4
4145-47	0.02	na	0.3	15.30	15.45	2.60	31	10.2	<1
4145-48	0.08	na	0.1	9.09	30.9	8.05	80	7.6	10
4145-49	0.10	na	0.4	0.37	63.4	15.90	120	7.6	2
4245-7A	0.08	na	0.1	0.06	29.0	2.70	342	6.8	22
4245-7B	0.08	na	0.4	0.12	54.0	12.05	111	3.4	4
HS-1	<0.02	na	<0.1	17.70	47.1	0.55	11	0.6	<1
HS-2	<0.02	na	<0.1	19.45	21.5	0.10	7	0.6	<1
HS-3	0.40	na	355.0	10.22	17.0	3.50	63	2.5	1385
HS-4	8.25	na	275.0	0.06	1.5	2.00	106	2.0	1398
HS-5	1.55	na	920.0	1.54	25.5	9.50	175	1.0	2805
HS-6	0.04	na	1.2	0.22	69.9	12.90	62	4.6	3
4725-4	0.04	na	0.5	2.39	62.0	2.25	33	5.4	1
4205-23	0.04	na	0.2	2.06	48.3	2.00	60	4.6	3
4285-11	0.06	na	0.1	3.39	52.6	4.20	32	5.0	4
AR-8	<0.02	na	0.2	3.39	59.9	2.95	11	7.4	1
4205-5	0.14	na	1.7	0.25	51.1	7.15	152	14.6	10
4205-7	0.04	na	0.1	0.28	81.7	8.85	163	15.4	1
4405-2	0.02	na	0.3	2.79	54.1	6.50	51	8.0	5
CU-0	0.04	na	0.06	19.05	3.81	0.85	17	1.0	<1
CU-10	<0.01	na	0.02	18.05	4.48	0.70	11	1.0	<1
CU-20	<0.01	na	0.16	19.35	4.44	0.70	9	1.0	<1
CU-25	<0.01	na	0.06	18.20	6.14	1.05	12	1.0	<1
CU-30	<0.01	na	0.02	19.10	5.13	1.10	14	1.0	<1
CU-35	0.01	na	1.04	18.35	5.7	1.45	10	1.0	3
CU-40	0.01	na	0.24	19.55	6.38	1.20	12	1.0	19
CU-45	0.01	na	0.04	18.50	7.58	2.00	14	1.0	<1
CU-46	0.01	na	0.12	18.25	9.13	2.40	10	1.0	<1
CU-47	0.01	na	0.22	14.85	18.9	0.60	21	1.0	<1
CU-48	0.02	na	0.94	14.25	21.1	0.50	23	1.0	5
CU-49	0.02	na	0.32	15.15	14.2	1.65	22	0.8	4
CU-50	<0.01	na	1.5	12.05	25.5	5.50	42	4.0	38
CU-51	<0.01	na	0.5	13.20	22.7	3.50	32	3.0	20
CU-52	<0.01	na	0.44	17.75	13.1	0.70	17	1.0	5
CU-53	0.03	na	7.78	14.45	15.2	1.50	29	1.0	74
CU-54	<0.01	na	16	12.35	17	2.50	35	3.0	142
CU-55	<0.01	na	7	13.30	20.2	2.50	21	4.0	102
CU-60	0.1	na	97	9.45	23.7	4.00	73	8.0	526
CU-70	0.01	na	0.54	15.35	8.22	1.10	22	0.8	1
CU-80	1.8	na	359	3.25	9.21	2.00	57	11.0	2770
CU-90	0.04	na	1.24	9.19	28.5	1.10	51	2.0	28
CU-95	1	na	16.5	2.19	16.1	2.50	128	10.0	624
CU-100	<0.01	na	1.5	19.60	3.32	0.50	7	0.8	6
CU-105	<0.01	na	0.44	18.15	3.03	1.85	10	0.8	1
CU-110	0.01	na	0.24	18.05	3.55	2.15	9	1.0	27

Appendix V: Cove deposit multi-element geochemical data (B.D. = bulk density; na = not analyzed)

Sample	Bi ppm	B ppm	Cd ppm	Ca %	Ce ppm	Cs ppm	Cr ppm	Co ppm	Cu ppm
CU-115	0.02	na	2.28	12.55	12.15	0.80	37	1.2	23
CU-120	<0.01	na	2.08	15.65	7.34	1.80	17	1.0	11
CVC218 800.3-810	<20	<1	6.9	16.15	na	na	na	2.0	51
CVC218 810-811.7	<20	<1	9	16.04	na	na	na	1.0	100
CVC218 815-820	<20	2	4.9	8.60	na	na	na	2.0	25
CVC218 830-835	<20	<1	2.1	8.57	na	na	na	4.0	16
CVC218 835-836.2	<20	<1	6.9	9.34	na	na	na	3.0	19
CVC218 840-845	<20	2	3	1.24	na	na	na	31.0	29
CVC218 855-859.5	<20	4	5.7	1.89	na	na	na	34.0	24
248-A	<20	<1	13.9	na	na	na	na	8.0	25
248-B	345	<1	459	na	na	na	na	3.0	83
248-C	<20	<1	1.3	na	na	na	na	<1	6
86921	<20	<1	<5	na	na	na	na	2	3
86922	<20	<1	309.7	na	na	na	na	8	1570
86923	28	<1	337.1	na	na	na	na	10	2605
CVC-15 1000-1010	<2	na	2.0	0.08	na	na	194	3	31
CVC-15 1010-1020	<2	na	10.5	0.11	na	na	211	4	84
CVC-15 1020-1030	<2	na	24.5	0.12	na	na	182	3	184
CVC-15 1030-1040	<2	na	99.0	0.08	na	na	191	5	492
CVC-15 1040-1050	<2	na	71.5	0.09	na	na	191	3	473
CVC-15 1050-1060	<2	na	26.0	0.09	na	na	123	10	112
CVC-15 1060-1070	<2	na	8.0	0.12	na	na	33	7	96
CVC-15 1070-1080	<2	na	8.5	0.22	na	na	24	8	53
CVC-15 1080-1090	<2	na	17.0	0.13	na	na	82	11	127
CVC-15 1090-1100	<2	na	46.5	0.23	na	na	98	17	227
CVC-15 1100-1110	<2	na	5.5	0.12	na	na	34	8	32
CVC-15 1110-1120	<2	na	6.0	0.15	na	na	80	5	62
CVC-15 1120-1130	<2	na	22.5	0.14	na	na	159	8	127
CVC-15 1130-1140	<2	na	36.5	0.10	na	na	94	7	167
CVC-15 1140-1150	<2	na	8.5	0.19	na	na	68	7	30
CVC-15 1150-1160	<2	na	10.0	0.15	na	na	138	4	54
CVC-15 1160-1170	<2	na	18.0	0.16	na	na	111	6	96
CVC-15 1170-1180	<2	na	5.0	0.13	na	na	125	5	144
CVC-15 1180-1190	<2	na	6.0	3.09	na	na	57	5	33
CVC-15 1190-1200	<2	na	6.5	5.60	na	na	41	5	138
CVC-15 1200-1210	<2	na	1.0	1.83	na	na	31	5	1
CVC-15 1210-1220	<2	na	1.0	1.73	na	na	15	6	68
CVC-15 1220-1230	<2	na	10.5	2.59	na	na	18	5	23
CVC-15 1230-1240	<2	na	6.0	1.28	na	na	20	6	41
CVC-15 1240-1250	<2	na	<0.5	3.67	na	na	21	6	<1
CVC-15 1250-1260	<2	na	10.0	3.30	na	na	31	5	48
CVC-15 1260-1270	<2	na	1.5	5.25	na	na	22	6	11
CVC-15 1270-1280	<2	na	0.5	6.52	na	na	18	5	24
CVC-15 1280-1290	<2	na	1.0	8.10	na	na	12	4	13
CVC-15 1290-1300	<2	na	<0.5	9.69	na	na	10	2	8
CVC-15 1300-1310	<2	na	<0.5	9.24	na	na	8	1	5
CVC-15 1310-1320	<2	na	1.0	5.00	na	na	20	8	26
CVC-15 1320-1330	<2	na	0.5	8.14	na	na	18	3	9

Appendix V: Cove deposit multi-element geochemical data (B.D. = bulk density; na = not analyzed)

Sample	Bi ppm	B ppm	Cd ppm	Ca %	Ce ppm	Cs ppm	Cr ppm	Co ppm	Cu ppm
CVC-15 1330-1340	<2	na	6.5	10.25	na	na	10	1	59
CVC-15 1340-1350	<2	na	1.0	8.26	na	na	20	2	31
CVC-15 1350-1360	<2	na	<0.5	14.80	na	na	15	<1	<1
CVC-15 1360-1370	<2	na	0.5	13.10	na	na	22	<1	4
CVC-15 1370-1380	<2	na	1.0	11.25	na	na	26	1	20
CVC-15 1380-1390	<2	na	1.0	10.95	na	na	21	3	12
CVC-15 1390-1400	<2	na	<0.5	>15.00	na	na	3	3	<1
CVC-15 1400-1410	<2	na	<0.5	>15.00	na	na	5	4	4
CVC-15 1410-1420	<2	na	<0.5	>15.00	na	na	10	4	6
CVC-15 1420-1430	<2	na	<0.5	7.88	na	na	12	4	9
CVC-15 1430-1440	<2	na	<0.5	11.30	na	na	23	5	10
CVC-15 1440-1450	<2	na	1.5	>15.00	na	na	22	4	17
CVC-15 1450-1460	4	na	2.5	>15.00	na	na	8	4	23
CVC-15 1460-1470	4	na	0.5	>15.00	na	na	9	4	6
CVC-15 1470-1480	2	na	<0.5	>15.00	na	na	11	5	7
CVC-15 1480-1490	2	na	0.5	>15.00	na	na	20	6	16
CVC-15 1490-1500	2	na	<0.5	>15.00	na	na	23	6	19
CVC-10 0920-0930	<2	na	>100.0	0.99	na	na	82	5	773
CVC-10 0930-0940	<2	na	>100.0	2.81	na	na	68	11	1595
CVC-10 0940-0950	<2	na	80.5	1.52	na	na	65	9	443
CVC-10 0950-0960	2	na	39.5	5.01	na	na	50	9	282
CVC-10 0960-0970	<2	na	3.0	7.23	na	na	50	5	47
CVC-10 0970-0980	2	na	11.5	10.15	na	na	38	8	105
CVC-10 0980-0990	8	na	0.5	6.33	na	na	51	9	56
CVC-10 0990-1000	18	na	>100.0	12.55	na	na	61	11	718
CVC-10 1000-1010	6	na	81.0	>15.00	na	na	43	6	705
CVC-10 1010-1020	12	na	>100.0	6.07	na	na	66	9	626
CVC-10 1020-1030	38	na	>100.0	9.79	na	na	31	12	3940
CVC-10 1030-1040	10	na	9.0	14.10	na	na	39	6	72
CVC-10 1040-1050	10	na	25.5	>15.00	na	na	26	6	118
CVC-10 1050-1060	<2	na	>100.0	>15.00	na	na	41	<1	1060
CVC-10 1060-1070	<2	na	17.5	>15.00	na	na	18	<1	138
CVC-10 1070-1080	8	na	>100.0	>15.00	na	na	39	6	1665
CVC-10 1080-1090	<2	na	<0.5	>15.00	na	na	12	<1	15
CVC-10 1090-1099.5	<2	na	59.0	>15.00	na	na	21	<1	180
CVC-10 1099.5-1110	<2	na	>100.0	>15.00	na	na	37	6	1475
CVC-10 1110-1120	<2	na	>100.0	>15.00	na	na	22	4	964
CVC-10 1120-1130	<2	na	>100.0	14.30	na	na	45	6	1635
CVC-10 1130-1140	<2	na	>100.0	>15.00	na	na	62	4	630
CVC-10 1140-1150	6	na	>100.0	7.29	na	na	87	5	1000
CVC-10 1150-1160	<2	na	28.5	>15.00	na	na	46	7	185
CVC-10 1160-1170	<2	na	97.0	12.70	na	na	104	4	731
CVC-10 1170-1180	2	na	19.5	>15.00	na	na	48	3	141
CVC-10 1180-1190	<2	na	28.5	>15.00	na	na	36	6	172
CVC-10 1190-1200	<2	na	87.0	14.85	na	na	65	6	557
CVC-10 1200-1210	<2	na	64.0	>15.00	na	na	64	5	343
CVC-10 1210-1220	<2	na	>100.0	5.05	na	na	119	3	462
CVC-10 1220-1230	<2	na	24.0	12.90	na	na	53	4	113

Appendix V: Cove deposit multi-element geochemical data (B.D. = bulk density; na = not analyzed)

Sample	Bi ppm	B ppm	Cd ppm	Ca %	Ce ppm	Cs ppm	Cr ppm	Co ppm	Cu ppm
CVC-10 1230-1240	<2	na	12.0	>15.00	na	na	33	5	180
CVC-10 1240-1250	<2	na	26.5	>15.00	na	na	24	4	214
CVC-10 1250-1260	8	na	>100.0	8.89	na	na	60	2	718
CVC-10 1260-1270	<2	na	88.5	1.08	na	na	112	5	390
CVC-10 1270-1280	<2	na	>100.0	0.66	na	na	89	6	565
CVC-10 1280-1290	<2	na	85.5	2.01	na	na	44	6	483
CVC-10 1290-1300	<2	na	76.0	2.40	na	na	58	6	408
CVC-10 1300-1310	<2	na	93.5	2.16	na	na	73	8	590
CVC-10 1310-1320	2	na	24.0	1.38	na	na	57	8	315
CVC-10 1320-1330	<2	na	12.0	1.55	na	na	55	6	120
CVC-10 1330-1340	<2	na	5.5	1.25	na	na	42	7	52
CVC-10 1340-1350	2	na	34.5	1.78	na	na	42	5	242
CVC-10 1350-1360	<2	na	5.5	2.35	na	na	41	6	40
CVC-10 1360-1370	<2	na	4.5	5.49	na	na	36	7	96
CVC-10 1370-1380	2	na	2.5	0.93	na	na	41	6	29
CVC-10 1380-1390	<2	na	2.5	8.66	na	na	39	5	53
CVC-10 1390-1400	<2	na	6.0	7.02	na	na	35	6	53
CVC-11 1000-1010	<2	na	82.0	9.53	na	na	33	2	345
CVC-11 1010-1020	<2	na	27.0	14.45	na	na	28	1	139
CVC-11 1020-1030	<2	na	3.5	4.98	na	na	29	5	22
CVC-11 1030-1040	<2	na	56.0	12.75	na	na	39	5	166
CVC-11 1040-1050	<2	na	14.5	>15.00	na	na	23	<1	29
CVC-11 1050-1060	<2	na	3.5	>15.00	na	na	15	<1	44
CVC-11 1060-1070	<2	na	0.5	>15.00	na	na	9	<1	6
CVC-11 1070-1080	<2	na	1.5	>15.00	na	na	10	<1	4
CVC-11 1080-1090	<2	na	<0.5	>15.00	na	na	12	<1	7
CVC-11 1090-1100	<2	na	36.0	>15.00	na	na	27	<1	202
CVC-11 1100-1110	<2	na	23.0	>15.00	na	na	26	1	210
CVC-11 1110-1120	<2	na	6.0	>15.00	na	na	24	1	18
CVC-11 1120-1130	<2	na	62.0	>15.00	na	na	48	3	151
CVC-11 1130-1140	<2	na	2.5	>15.00	na	na	30	3	35
CVC-11 1140-1150	<2	na	59.5	>15.00	na	na	55	3	251
CVC-11 1150-1160	<2	na	48.5	>15.00	na	na	33	2	185
CVC-11 1160-1170	<2	na	58.0	>15.00	na	na	21	3	201
CVC-11 1170-1180	<2	na	15.5	>15.00	na	na	36	3	253
CVC-11 1180-1190	2	na	45.5	12.75	na	na	51	3	345
CVC-11 1190-1200	<2	na	31.5	>15.00	na	na	33	3	186
CVC-11 1200-1210	<2	na	9.5	4.72	na	na	51	2	92
CVC-11 1210-1220	<2	na	10.5	>15.00	na	na	29	2	100
CVC-11 1220-1230	<2	na	6.5	>15.00	na	na	32	2	90
CVC-11 1230-1240	<2	na	19.5	>15.00	na	na	34	3	113
CVC-11 1240-1250	<2	na	39.0	>15.00	na	na	38	2	329
CVC-11 1250-1260	<2	na	19.0	>15.00	na	na	18	2	139
CVC-11 1260-1270	<2	na	39.0	14.80	na	na	32	3	254
CVC-11 1270-1280	<2	na	8.5	>15.00	na	na	24	2	78
CVC-11 1280-1290	<2	na	10.5	8.80	na	na	59	3	99
CVC-11 1290-1300	<2	na	7.0	10.00	na	na	53	3	98
CVC-11 1300-1310	<2	na	9.5	8.56	na	na	51	5	82

Appendix V: Cove deposit multi-element geochemical data (B.D. = bulk density; na = not analyzed)

Sample	Bi ppm	B ppm	Cd ppm	Ca %	Ce ppm	Cs ppm	Cr ppm	Co ppm	Cu ppm
CVC-11 1310-1320	<2	na	25.5	4.39	na	na	74	6	200
CVC-11 1320-1330	<2	na	16.5	7.45	na	na	52	4	201
CVC-11 1330-1340	<2	na	>100.0	5.50	na	na	44	4	991
CVC-11 1340-1350	<2	na	>100.0	5.88	na	na	42	4	1280
CVC-11 1350-1360	<2	na	24.0	>15.00	na	na	40	5	394
CVC-11 1360-1370	<2	na	6.0	>15.00	na	na	32	7	66
CVC-11 1370-1380	<2	na	3.0	>15.00	na	na	35	7	52
CVC-11 1380-1390	<2	na	3.0	5.58	na	na	67	6	79
CVC-11 1390-1400	<2	na	6.0	5.29	na	na	42	7	79

Appendix V: Cove deposit multi-element geochemical data (B.D. = bulk density; na = not analyzed)

Sample	F ppm	Ga ppm	Ge ppm	Au ppb	Au opt	Fe %	La ppm	Pb ppm	Li ppm
4145-40	1040	13.0	1.5	89.1	0.0026	1.81	22.0	22.0	17.6
4145-41	1200	13.0	1.4	174.9	0.0051	1.91	26.5	21.5	8.0
4145-42	960	10.0	1.3	6.9	0.0002	1.98	28.0	10.5	13.2
4145-46	1220	16.8	1.8	54.9	0.0016	2.58	27.0	12.5	10.8
4145-47	220	2.8	<0.1	198.9	0.0058	1.20	8.5	23.0	2.0
4145-48	700	8.9	0.6	51.4	0.0015	1.49	17.0	13.5	5.4
4145-49	1220	19.5	1.6	92.6	0.0027	1.95	34.0	21.0	5.4
4245-7A	200	4.2	1.5	322.3	0.0094	1.84	16.5	4.5	2.0
4245-7B	750	13.1	1.4	48	0.0014	1.87	28.0	28.5	3.6
HS-1	220	0.9	<0.1	205.7	0.0060	0.14	3.0	7.0	2.4
HS-2	170	0.5	<0.1	305.1	0.0089	0.13	1.5	5.0	1.6
HS-3	1650	11.0	1.0	5081.1	0.1482	5.10	10.0	45800	12.0
HS-4	70	4.0	3.0	3840.0	0.1120	35.20	<5.0	73700	<2.0
HS-5	1650	29.0	1.0	4241.1	0.1237	20.20	10.0	48800	2.0
HS-6	670	18.9	1.2	1148.6	0.0335	1.93	34.5	111.0	24.2
4725-4	460	19.0	1.2	44.6	0.0013	2.86	33.5	53.5	18.8
4205-23	360	16.9	0.7	44.6	0.0013	1.75	26.5	38.0	17.8
4285-11	410	16.9	0.7	202.3	0.0059	1.84	29.5	33.0	21.6
AR-8	410	18.9	3.7	61.7	0.0018	2.26	32.0	22.5	43.0
4205-5	520	19.2	1.2	517.7	0.0151	3.24	26.5	45.0	5.0
4205-7	680	19.6	1.0	257.1	0.0075	5.37	44.0	19.0	5.0
4405-2	480	20.0	1.0	34.3	0.0010	2.48	28.0	24.0	7.0
CU-0	170	1.1	<0.1	45.0	na	0.18	2.0	13.5	3.8
CU-10	140	1.2	<0.1	130.0	na	0.16	2.5	13.5	3.8
CU-20	150	1.1	<0.1	270.0	na	0.18	2.5	39.5	2.4
CU-25	220	1.7	<0.1	965.0	na	0.25	3.5	11.0	3.8
CU-30	190	1.2	<0.1	620.0	na	0.2	3.0	5.0	2.6
CU-35	210	1.4	<0.1	230.0	na	0.23	3.0	117.5	3.4
CU-40	290	1.5	<0.1	195.0	na	0.17	4.0	149.0	3.0
CU-45	300	1.8	<0.1	360.0	na	0.21	4.0	28.0	2.4
CU-46	450	2.3	<0.1	575.0	na	0.23	5.5	23.5	4.0
CU-47	770	3.8	<0.1	230.0	na	0.36	10.5	65.0	12.8
CU-48	940	4.0	0.1	310.0	na	0.48	11.5	221.0	14.6
CU-49	800	3.3	0.1	570.0	na	0.42	7.5	93.5	7.8
CU-50	1600	11.0	<0.1	6340.0	na	1.68	15.0	1190.0	14.0
CU-51	1250	7.0	<0.1	4460.0	na	1.04	10.0	244.0	12.0
CU-52	440	2.7	<0.1	1750.0	na	0.32	7.5	117.5	12.4
CU-53	670	4.5	0.2	2220.0	na	0.66	8.5	800.0	13.8
CU-54	830	6.0	<0.1	2850.0	na	1.24	10.0	1395.0	12.0
CU-55	1170	9.0	<0.1	3700.0	na	1.89	10.0	836.0	14.0
CU-60	1350	12.0	<0.1	13165.0	0.3840	5.43	10.0	18100.0	22.0
CU-70	300	3.1	0.1	1005.0	na	0.65	4.5	329.0	11.2
CU-80	500	9.0	<0.1	10011.0	0.2920	19.1	<0.5	91400.0	4.0
CU-90	1280	12.1	0.4	530.0	na	1.66	13.5	365.0	29.0
CU-95	1180	8.0	<0.1	2890.0	na	28.3	10.0	51500.0	4.0
CU-100	180	0.8	<0.1	210.0	na	0.21	2.0	254.0	1.6
CU-105	150	1.8	<0.1	500.0	na	0.27	1.5	96.0	2.8
CU-110	130	1.5	<0.1	9090.0	na	0.91	2.0	162.5	2.6

Appendix V: Cove deposit multi-element geochemical data (B.D. = bulk density; na = not analyzed)

Sample	F ppm	Ga ppm	Ge ppm	Au ppb	Au opt	Fe %	La ppm	Pb ppm	Li ppm
CU-115	630	5.6	0.2	2870.0	na	1.15	5.5	998.0	17.8
CU-120	300	3.2	0.3	1020.0	na	0.44	3.5	247.0	11.6
CVC218 800.3-810	na	na	na	1851.4	0.0540	0.6607	na	1263.0	2.0
CVC218 810-811.7	na	na	na	1954.3	0.0570	0.7329	na	1589.0	2.0
CVC218 815-820	na	na	na	13200	0.3850	0.7587	na	508.0	1.0
CVC218 830-835	na	na	na	10114.3	0.2950	0.9569	na	253.0	1.0
CVC218 835-836.2	na	na	na	81291.4	2.3710	0.9979	na	189.0	1.0
CVC218 840-845	na	na	na	26057.1	0.7600	3.638	na	18.0	<1
CVC218 855-859.5	na	na	na	9497.1	0.2770	4.3397	na	21.0	<1
248-A	na	na	na	5348.6	0.1560	na	na	68.0	<1
248-B	na	na	na	186068.4	5.4270	na	na	126.0	<1
248-C	na	na	na	3840.0	0.1120	na	na	59.0	<1
86921	na	na	na	171.4	0.005	na	na	31	5
86922	na	na	na	4148.6	0.121	na	na	43845	5
86923	na	na	na	3051.4	0.089	na	na	25540	3
CVC-15 1000-1010	na	<10	na	531.4	0.0155	2.20	20	480	na
CVC-15 1010-1020	na	<10	na	1885.7	0.0550	3.57	10	2140	na
CVC-15 1020-1030	na	<10	na	1937.1	0.0565	4.11	10	3560	na
CVC-15 1030-1040	na	<10	na	1011.4	0.0295	3.65	10	7690	na
CVC-15 1040-1050	na	<10	na	462.9	0.0135	3.84	10	6680	na
CVC-15 1050-1060	na	<10	na	2091.4	0.0610	3.24	10	3150	na
CVC-15 1060-1070	na	<10	na	908.6	0.0265	2.65	10	946	na
CVC-15 1070-1080	na	<10	na	805.7	0.0235	2.90	10	736	na
CVC-15 1080-1090	na	<10	na	2468.6	0.0720	3.37	20	1800	na
CVC-15 1090-1100	na	<10	na	788.6	0.0230	6.25	40	2980	na
CVC-15 1100-1110	na	<10	na	428.6	0.0125	2.43	20	684	na
CVC-15 1110-1120	na	<10	na	960	0.0280	1.98	20	684	na
CVC-15 1120-1130	na	<10	na	1697.1	0.0495	1.84	10	2120	na
CVC-15 1130-1140	na	<10	na	1457.1	0.0425	2.34	10	4660	na
CVC-15 1140-1150	na	<10	na	2160	0.0630	2.66	20	860	na
CVC-15 1150-1160	na	<10	na	1045.7	0.0305	2.08	10	1240	na
CVC-15 1160-1170	na	<10	na	1080	0.0315	2.34	10	2480	na
CVC-15 1170-1180	na	<10	na	822.9	0.0240	1.62	10	1165	na
CVC-15 1180-1190	na	<10	na	205.7	0.0060	2.21	<10	774	na
CVC-15 1190-1200	na	<10	na	445.7	0.0130	1.85	<10	988	na
CVC-15 1200-1210	na	<10	na	68.6	0.0020	1.66	20	70	na
CVC-15 1210-1220	na	<10	na	257.1	0.0075	1.72	10	314	na
CVC-15 1220-1230	na	<10	na	514.3	0.0150	1.46	<10	554	na
CVC-15 1230-1240	na	<10	na	480	0.0140	1.98	20	870	na
CVC-15 1240-1250	na	<10	na	257.1	0.0075	2.41	<10	24	na
CVC-15 1250-1260	na	<10	na	325.7	0.0095	1.63	<10	324	na
CVC-15 1260-1270	na	<10	na	34.3	0.0010	1.66	<10	78	na
CVC-15 1270-1280	na	<10	na	0	0.0000	1.64	<10	30	na
CVC-15 1280-1290	na	<10	na	68.6	0.0020	1.56	<10	184	na
CVC-15 1290-1300	na	<10	na	102.9	0.0030	1.49	<10	<2	na
CVC-15 1300-1310	na	<10	na	120	0.0035	1.20	<10	2	na
CVC-15 1310-1320	na	<10	na	34.3	0.0010	1.75	<10	28	na
CVC-15 1320-1330	na	<10	na	34.3	0.0010	1.35	<10	82	na

Appendix V: Cove deposit multi-element geochemical data (B.D. = bulk density; na = not analyzed)

Sample	F ppm	Ga ppm	Ge ppm	Au ppb	Au opt	Fe %	La ppm	Pb ppm	Li ppm
CVC-15 1330-1340	na	<10	na	2588.6	0.0755	1.31	<10	654	na
CVC-15 1340-1350	na	<10	na	240	0.0070	1.64	<10	152	na
CVC-15 1350-1360	na	<10	na	0	0.0000	0.43	<10	10	na
CVC-15 1360-1370	na	<10	na	240	0.0070	0.56	<10	66	na
CVC-15 1370-1380	na	<10	na	171.4	0.0050	0.55	<10	328	na
CVC-15 1380-1390	na	<10	na	342.9	0.0100	0.77	<10	324	na
CVC-15 1390-1400	na	<10	na	274.3	0.0080	0.32	<10	38	na
CVC-15 1400-1410	na	<10	na	68.6	0.0020	0.42	<10	12	na
CVC-15 1410-1420	na	<10	na	291.4	0.0085	0.73	<10	14	na
CVC-15 1420-1430	na	<10	na	462.9	0.0135	0.90	<10	16	na
CVC-15 1430-1440	na	<10	na	874.3	0.0255	0.88	<10	8	na
CVC-15 1440-1450	na	<10	na	1765.7	0.0515	0.73	<10	364	na
CVC-15 1450-1460	na	<10	na	445.7	0.0130	0.32	<10	276	na
CVC-15 1460-1470	na	<10	na	0	0.0000	0.27	<10	38	na
CVC-15 1470-1480	na	<10	na	0	0.0000	0.45	<10	2	na
CVC-15 1480-1490	na	<10	na	0	0.0000	0.81	<10	66	na
CVC-15 1490-1500	na	<10	na	34.3	0.0010	0.93	<10	14	na
CVC-10 0920-0930	na	10	na	411.4	0.0120	6.50	10	>10000	na
CVC-10 0930-0940	na	10	na	925.7	0.0270	10.40	<10	>10000	na
CVC-10 0940-0950	na	10	na	445.7	0.0130	5.40	<10	>10000	na
CVC-10 0950-0960	na	10	na	342.9	0.0100	4.37	<10	6990	na
CVC-10 0960-0970	na	<10	na	325.7	0.0095	1.89	<10	478	na
CVC-10 0970-0980	na	<10	na	308.6	0.0090	2.18	<10	1450	na
CVC-10 0980-0990	na	<10	na	360	0.0105	2.03	<10	692	na
CVC-10 0990-1000	na	<10	na	497.1	0.0145	6.57	<10	>10000	na
CVC-10 1000-1010	na	<10	na	188.6	0.0055	3.62	<10	>10000	na
CVC-10 1010-1020	na	10	na	634.3	0.0185	5.26	<10	>10000	na
CVC-10 1020-1030	na	50	na	2125.7	0.0620	13.60	<10	>10000	na
CVC-10 1030-1040	na	<10	na	154.3	0.0045	1.51	<10	1645	na
CVC-10 1040-1050	na	<10	na	257.1	0.0075	1.80	<10	4780	na
CVC-10 1050-1060	na	<10	na	205.7	0.0060	4.68	<10	>10000	na
CVC-10 1060-1070	na	<10	na	120	0.0035	1.14	<10	2800	na
CVC-10 1070-1080	na	<10	na	2736	0.0798	11.55	<10	>10000	na
CVC-10 1080-1090	na	<10	na	51.4	0.0015	0.31	<10	152	na
CVC-10 1090-1099.5	na	<10	na	222.9	0.0065	1.55	<10	3900	na
CVC-10 1099.5-1110	na	<10	na	538.3	0.0157	9.35	<10	>10000	na
CVC-10 1110-1120	na	<10	na	1114.3	0.0325	6.90	<10	>10000	na
CVC-10 1120-1130	na	<10	na	1320	0.0385	10.85	<10	>10000	na
CVC-10 1130-1140	na	<10	na	874.3	0.0255	8.17	<10	>10000	na
CVC-10 1140-1150	na	<10	na	1268.6	0.0370	8.94	<10	>10000	na
CVC-10 1150-1160	na	<10	na	188.6	0.0055	1.60	<10	4260	na
CVC-10 1160-1170	na	<10	na	308.6	0.0090	3.82	<10	8970	na
CVC-10 1170-1180	na	<10	na	171.4	0.0050	1.56	<10	2080	na
CVC-10 1180-1190	na	<10	na	222.9	0.0065	1.89	<10	3130	na
CVC-10 1190-1200	na	<10	na	565.7	0.0165	3.20	<10	>10000	na
CVC-10 1200-1210	na	<10	na	497.1	0.0145	2.73	<10	6150	na
CVC-10 1210-1220	na	<10	na	514.3	0.0150	6.33	<10	>10000	na
CVC-10 1220-1230	na	<10	na	222.9	0.0065	1.87	<10	2050	na

Appendix V: Cove deposit multi-element geochemical data (B.D. = bulk density; na = not analyzed)

Sample	F ppm	Ga ppm	Ge ppm	Au ppb	Au opt	Fe %	La ppm	Pb ppm	Li ppm
CVC-10 1230-1240	na	<10	na	308.6	0.0090	1.27	<10	3120	na
CVC-10 1240-1250	na	<10	na	137.1	0.0040	1.53	<10	2780	na
CVC-10 1250-1260	na	<10	na	788.6	0.0230	11.15	<10	>10000	na
CVC-10 1260-1270	na	10	na	737.1	0.0215	6.31	10	>10000	na
CVC-10 1270-1280	na	10	na	1320	0.0385	7.15	10	>10000	na
CVC-10 1280-1290	na	10	na	497.1	0.0145	4.16	20	>10000	na
CVC-10 1290-1300	na	10	na	531.4	0.0155	2.94	20	6680	na
CVC-10 1300-1310	na	10	na	514.3	0.0150	4.61	20	9740	na
CVC-10 1310-1320	na	10	na	274.3	0.0080	2.81	30	2030	na
CVC-10 1320-1330	na	<10	na	291.4	0.0085	1.65	20	1075	na
CVC-10 1330-1340	na	<10	na	205.7	0.0060	1.75	30	884	na
CVC-10 1340-1350	na	<10	na	240	0.0070	2.40	20	4370	na
CVC-10 1350-1360	na	10	na	325.7	0.0095	1.59	20	708	na
CVC-10 1360-1370	na	<10	na	377.1	0.0110	1.82	<10	812	na
CVC-10 1370-1380	na	<10	na	514.3	0.0150	1.88	20	378	na
CVC-10 1380-1390	na	<10	na	565.7	0.0165	1.42	<10	306	na
CVC-10 1390-1400	na	<10	na	360	0.0105	1.56	<10	624	na
CVC-11 1000-1010	na	<10	na	171.4	0.0050	3.49	<10	6350	na
CVC-11 1010-1020	na	<10	na	154.3	0.0045	1.70	<10	2550	na
CVC-11 1020-1030	na	<10	na	0	0.0000	1.69	<10	354	na
CVC-11 1030-1040	na	<10	na	394.3	0.0115	2.89	<10	5280	na
CVC-11 1040-1050	na	<10	na	274.3	0.0080	1.02	<10	1550	na
CVC-11 1050-1060	na	<10	na	291.4	0.0085	0.65	<10	498	na
CVC-11 1060-1070	na	<10	na	514.3	0.0150	0.29	<10	84	na
CVC-11 1070-1080	na	<10	na	462.9	0.0135	0.49	<10	150	na
CVC-11 1080-1090	na	<10	na	394.3	0.0115	0.45	<10	118	na
CVC-11 1090-1100	na	<10	na	360	0.0105	1.62	<10	4220	na
CVC-11 1100-1110	na	<10	na	222.9	0.0065	1.41	<10	3300	na
CVC-11 1110-1120	na	<10	na	154.3	0.0045	0.93	<10	726	na
CVC-11 1120-1130	na	<10	na	1320	0.0385	2.91	<10	7370	na
CVC-11 1130-1140	na	<10	na	240	0.0070	0.83	<10	658	na
CVC-11 1140-1150	na	<10	na	428.6	0.0125	3.56	<10	>10000	na
CVC-11 1150-1160	na	<10	na	548.6	0.0160	1.69	<10	4900	na
CVC-11 1160-1170	na	<10	na	497.1	0.0145	1.89	<10	8020	na
CVC-11 1170-1180	na	<10	na	702.9	0.0205	1.13	<10	2450	na
CVC-11 1180-1190	na	<10	na	514.3	0.0150	2.01	<10	8110	na
CVC-11 1190-1200	na	<10	na	325.7	0.0095	1.35	<10	2830	na
CVC-11 1200-1210	na	<10	na	325.7	0.0095	1.31	<10	2070	na
CVC-11 1210-1220	na	<10	na	120	0.0035	0.72	<10	1160	na
CVC-11 1220-1230	na	<10	na	51.4	0.0015	0.79	<10	1220	na
CVC-11 1230-1240	na	<10	na	274.3	0.0080	1.36	<10	1370	na
CVC-11 1240-1250	na	<10	na	702.9	0.0205	1.83	<10	4350	na
CVC-11 1250-1260	na	<10	na	342.9	0.0100	0.92	<10	1690	na
CVC-11 1260-1270	na	<10	na	977.1	0.0285	2.00	<10	4330	na
CVC-11 1270-1280	na	<10	na	171.4	0.0050	1.15	<10	1265	na
CVC-11 1280-1290	na	<10	na	171.4	0.0050	1.49	<10	1240	na
CVC-11 1290-1300	na	<10	na	325.7	0.0095	1.24	<10	986	na
CVC-11 1300-1310	na	<10	na	360	0.0105	1.79	<10	1310	na

Appendix V: Cove deposit multi-element geochemical data (B.D. = bulk density; na = not analyzed)

Sample	F ppm	Ga ppm	Ge ppm	Au ppb	Au opt	Fe %	La ppm	Pb ppm	Li ppm
CVC-11 1310-1320	na	<10	na	1302.9	0.0380	2.40	<10	2260	na
CVC-11 1320-1330	na	<10	na	5674.3	0.1655	1.66	<10	1330	na
CVC-11 1330-1340	na	<10	na	2280	0.0665	7.03	<10	>10000	na
CVC-11 1340-1350	na	<10	na	3377.1	0.0985	9.18	<10	>10000	na
CVC-11 1350-1360	na	<10	na	497.1	0.0145	1.64	<10	3470	na
CVC-11 1360-1370	na	<10	na	548.6	0.0160	1.67	<10	906	na
CVC-11 1370-1380	na	<10	na	480	0.0140	1.46	<10	316	na
CVC-11 1380-1390	na	<10	na	1491.4	0.0435	1.78	<10	430	na
CVC-11 1390-1400	na	<10	na	480	0.0140	1.59	<10	348	na

Appendix V: Cove deposit multi-element geochemical data (B.D. = bulk density; na = not analyzed)

Sample	Mg %	Mn ppm	Hg ppb	Mo ppm	Ni ppm	Nb ppm	P ppm	K %	Rb ppm
4145-40	0.29	20	70	<1	25.2	10.2	1050	1.29	58.2
4145-41	0.47	20	1920	<1	27.0	10.0	900	2.04	115.5
4145-42	1.12	410	90	<1	21.0	7.8	890	1.57	65.6
4145-46	0.55	65	390	<1	18.4	9.6	1150	2.98	141.0
4145-47	9.60	1850	2210	<1	19.6	1.6	310	0.56	23.0
4145-48	5.83	1390	1160	<1	22.8	5.4	740	1.89	71.8
4145-49	0.53	45	600	<1	28.4	11.0	1470	3.06	153.0
4245-7A	0.09	45	2420	<1	17.4	2.4	350	0.66	30.2
4245-7B	0.30	60	660	<1	20.8	10.0	470	2.32	115.0
HS-1	12.30	715	730	2	6.4	0.2	810	0.12	6.2
HS-2	12.70	960	110	1	2.0	<0.2	220	0.13	2.8
HS-3	5.89	1100	28200	2	13.0	<2.0	7655	0.52	28.0
HS-4	0.04	435	12460	<1	4.5	<2.0	85	0.09	4.0
HS-5	0.34	1165	16150	6	14.5	2.0	6895	0.94	60.0
HS-6	0.30	35	23900	<1	10.6	6.4	640	1.94	87.6
4725-4	0.82	290	70	<1	1.0	12.2	900	2.12	73.8
4205-23	1.20	385	210	<1	7.4	7.0	520	2.35	78.4
4285-11	0.92	1150	30	<1	9.8	6.4	560	2.61	87.0
AR-8	1.03	315	50	<1	1.6	9.6	960	2.05	72.6
4205-5	0.37	130	1290	<1	25.0	8.0	720	3.69	168.0
4205-7	0.33	50	300	<1	74.8	13.6	850	3.19	158.5
4405-2	0.35	215	520	<1	2.8	9.2	990	2.60	135.5
CU-0	11.80	1495	1000	1.6	6.6	0.2	630	0.18	9.0
CU-10	11.15	1450	2980	1.6	7.6	0.2	710	0.16	8.2
CU-20	11.85	4670	1630	1.2	7.6	<0.2	1120	0.18	8.6
CU-25	10.75	6250	7090	1.6	8.2	0.2	1580	0.25	12.8
CU-30	11.65	3090	2690	1.4	7.6	0.2	1530	0.19	9.4
CU-35	11.30	2010	3500	1.4	7.8	0.2	1250	0.25	12.2
CU-40	11.85	3130	1120	1.6	8.6	0.2	2010	0.20	9.8
CU-45	11.20	3600	1200	1.6	9.8	0.2	2140	0.24	13.4
CU-46	10.45	4990	2260	1.8	8.8	0.2	3030	0.28	14.6
CU-47	7.78	3450	3370	2.4	9.4	1.2	5320	0.04	2.2
CU-48	7.46	3590	6080	2.4	9.0	1.4	6950	0.03	1.6
CU-49	8.33	3380	1920	1.4	7.8	1.2	3530	0.32	16.2
CU-50	5.54	14900	1960	<1.0	6.0	6.0	6820	0.48	30.0
CU-51	6.09	19000	43300	2	7.0	4.0	5990	0.27	16.0
CU-52	9.33	6410	5860	1.6	8.6	1.0	3080	0.05	3.0
CU-53	7.31	6870	2770	2.2	7.8	1.6	3400	0.17	9.6
CU-54	5.83	17100	4820	<1.0	4.0	2.0	3610	0.34	20.0
CU-55	5.19	33900	5600	<1.0	4.0	4.0	6190	0.51	26.0
CU-60	3.21	20300	4840	1	10.0	4.0	6560	0.43	26.0
CU-70	7.78	8430	1900	2	6.2	0.4	980	0.15	8.6
CU-80	1.42	3400	22800	<1.0	4.0	2.0	2180	0.04	4.0
CU-90	4.28	3910	15270	8.4	16.0	6.2	5070	0.03	2.0
CU-95	0.45	1180	15250	6	9.0	2.0	5940	0.06	4.0
CU-100	12.50	1665	1190	1.4	9.4	0.2	930	0.08	4.0
CU-105	11.30	6420	2380	1.6	8.6	0.2	480	0.20	11.0
CU-110	11.40	4050	280000	1.8	8.0	0.2	540	0.15	8.6

Appendix V: Cove deposit multi-element geochemical data (B.D. = bulk density; na = not analyzed)

Sample	Mg %	Mn ppm	Hg ppb	Mo ppm	Ni ppm	Nb ppm	P ppm	K %	Rb ppm
CU-115	7.16	4490	38600	7.8	14.2	2.4	3180	0.04	2.0
CU-120	9.42	6760	13550	2.6	8.6	0.4	1280	0.20	13.4
CVC218 800.3-810	3.13	31343	3000	3	3.0	na	1233	na	na
CVC218 810-811.7	17.63	17627	1000	1	3.0	na	1397	na	na
CVC218 815-820	2.58	2578	3000	4	9.0	na	>1%	na	na
CVC218 830-835	2.72	2724	12000	4	12.0	na	2535	na	na
CVC218 835-836.2	2.78	2784	1000	3	8.0	na	3890	na	na
CVC218 840-845	0.54	540	3000	2	70.0	na	1850	na	na
CVC218 855-859.5	1.12	1171	4000	2	79.0	na	1444	na	na
248-A	na	141	3000	8	24.0	na	1173	na	na
248-B	na	14	263000	4	6.0	na	826	na	na
248-C	na	292	13000	5	<1	na	690	na	na
86921	na	na	2 ppm	3	8	na	>1%	na	na
86922	na	na	15 ppm	9	20	na	7812	na	na
86923	na	na	19 ppm	3	5	na	2161	na	na
CVC-15 1000-1010	0.02	35	<1 ppm	2	17	na	290	0.20	na
CVC-15 1010-1020	0.01	95	<1 ppm	2	16	na	380	0.14	na
CVC-15 1020-1030	0.03	150	<1 ppm	<1	19	na	370	0.21	na
CVC-15 1030-1040	0.02	335	<1 ppm	<1	47	na	370	0.17	na
CVC-15 1040-1050	0.02	250	<1 ppm	<1	11	na	340	0.17	na
CVC-15 1050-1060	0.04	125	<1 ppm	<1	21	na	240	0.25	na
CVC-15 1060-1070	0.08	60	1 ppm	<1	25	na	270	0.37	na
CVC-15 1070-1080	0.06	90	2 ppm	<1	26	na	480	0.42	na
CVC-15 1080-1090	0.02	65	3 ppm	1	26	na	370	0.28	na
CVC-15 1090-1100	0.08	185	3 ppm	<1	49	na	730	0.56	na
CVC-15 1100-1110	0.04	45	<1 ppm	1	27	na	370	0.44	na
CVC-15 1110-1120	0.01	40	<1 ppm	1	17	na	550	0.30	na
CVC-15 1120-1130	<0.01	105	<1 ppm	<1	18	na	540	0.21	na
CVC-15 1130-1140	<0.01	135	2 ppm	1	16	na	360	0.22	na
CVC-15 1140-1150	0.03	45	3 ppm	<1	24	na	750	0.34	na
CVC-15 1150-1160	0.04	210	<1 ppm	1	17	na	510	0.36	na
CVC-15 1160-1170	0.08	185	<1 ppm	<1	21	na	550	0.36	na
CVC-15 1170-1180	0.03	35	<1 ppm	<1	18	na	470	0.37	na
CVC-15 1180-1190	1.14	615	1 ppm	<1	21	na	700	0.55	na
CVC-15 1190-1200	1.99	1550	<1 ppm	<1	17	na	690	0.28	na
CVC-15 1200-1210	0.65	350	1 ppm	<1	17	na	920	0.48	na
CVC-15 1210-1220	0.48	250	1 ppm	<1	19	na	890	0.44	na
CVC-15 1220-1230	0.51	360	<1 ppm	<1	12	na	880	0.38	na
CVC-15 1230-1240	0.23	150	<1 ppm	<1	19	na	960	0.40	na
CVC-15 1240-1250	0.29	285	<1 ppm	<1	25	na	970	0.43	na
CVC-15 1250-1260	1.06	890	<1 ppm	<1	14	na	1080	0.30	na
CVC-15 1260-1270	2.29	975	1 ppm	<1	17	na	1130	0.36	na
CVC-15 1270-1280	3.80	870	<1 ppm	<1	20	na	1090	0.53	na
CVC-15 1280-1290	4.37	780	<1 ppm	<1	18	na	870	0.45	na
CVC-15 1290-1300	5.31	695	2 ppm	<1	17	na	790	0.45	na
CVC-15 1300-1310	5.33	1085	<1 ppm	<1	14	na	960	0.33	na
CVC-15 1310-1320	2.61	455	4 ppm	<1	25	na	1090	0.49	na
CVC-15 1320-1330	4.16	1450	4 ppm	<1	14	na	1890	0.29	na

Appendix V: Cove deposit multi-element geochemical data (B.D. = bulk density; na = not analyzed)

Sample	Mg %	Mn ppm	Hg ppb	Mo ppm	Ni ppm	Nb ppm	P ppm	K %	Rb ppm
CVC-15 1330-1340	5.96	1720	4 ppm	1	15	na	1290	0.17	na
CVC-15 1340-1350	5.18	885	3 ppm	2	19	na	960	0.29	na
CVC-15 1350-1360	7.75	4590	2 ppm	3	10	na	5710	0.26	na
CVC-15 1360-1370	6.41	5910	2 ppm	2	8	na	4290	0.22	na
CVC-15 1370-1380	4.25	7900	3 ppm	1	6	na	4310	0.17	na
CVC-15 1380-1390	2.70	6980	7 ppm	1	11	na	7690	0.16	na
CVC-15 1390-1400	0.20	885	<1 ppm	<1	3	na	1440	0.16	na
CVC-15 1400-1410	0.72	495	<1 ppm	<1	2	na	1110	0.11	na
CVC-15 1410-1420	1.44	860	1 ppm	<1	5	na	2950	0.22	na
CVC-15 1420-1430	0.57	435	<1 ppm	<1	8	na	2320	0.28	na
CVC-15 1430-1440	0.45	505	<1 ppm	<1	11	na	3280	0.42	na
CVC-15 1440-1450	0.21	2320	3 ppm	1	14	na	6250	0.34	na
CVC-15 1450-1460	0.40	1395	<1 ppm	<1	6	na	2610	0.14	na
CVC-15 1460-1470	0.86	380	<1 ppm	<1	6	na	2700	0.14	na
CVC-15 1470-1480	0.89	325	<1 ppm	1	8	na	2110	0.23	na
CVC-15 1480-1490	0.85	505	<1 ppm	3	21	na	3800	0.38	na
CVC-15 1490-1500	0.86	545	<1 ppm	1	15	na	2740	0.37	na
CVC-10 0920-0930	0.43	570	<1 ppm	<1	17	na	990	0.26	na
CVC-10 0930-0940	1.49	1175	<1 ppm	<1	30	na	930	0.26	na
CVC-10 0940-0950	0.56	780	2 ppm	<1	29	na	1100	0.37	na
CVC-10 0950-0960	1.07	1510	<1 ppm	<1	26	na	1010	0.24	na
CVC-10 0960-0970	2.64	1740	<1 ppm	<1	16	na	1130	0.29	na
CVC-10 0970-0980	2.19	2850	<1 ppm	<1	19	na	960	0.26	na
CVC-10 0980-0990	1.45	1045	<1 ppm	<1	22	na	1930	0.25	na
CVC-10 0990-1000	1.83	3630	2 ppm	<1	22	na	1520	0.20	na
CVC-10 1000-1010	5.35	4480	<1 ppm	4	17	na	740	0.26	na
CVC-10 1010-1020	2.08	2380	<1 ppm	3	28	na	1260	0.29	na
CVC-10 1020-1030	2.48	3360	<1 ppm	13	13	na	700	0.17	na
CVC-10 1030-1040	2.62	2180	<1 ppm	1	12	na	1260	0.24	na
CVC-10 1040-1050	3.15	3120	1 ppm	15	10	na	790	0.21	na
CVC-10 1050-1060	8.36	4020	1 ppm	1	3	na	830	<0.01	na
CVC-10 1060-1070	7.96	5410	<1 ppm	1	2	na	720	0.01	na
CVC-10 1070-1080	7.01	4710	4 ppm	3	7	na	7960	<0.01	na
CVC-10 1080-1090	10.50	2720	<1 ppm	2	2	na	1220	<0.01	na
CVC-10 1090-1099.5	6.07	7240	<1 ppm	1	3	na	2500	<0.01	na
CVC-10 1099.5-1110	2.16	>10000	5 ppm	1	6	na	2340	0.04	na
CVC-10 1110-1120	2.24	>10000	<1 ppm	1	3	na	930	<0.01	na
CVC-10 1120-1130	3.65	>10000	7 ppm	3	9	na	5470	0.02	na
CVC-10 1130-1140	4.66	>10000	1 ppm	<1	12	na	3060	<0.01	na
CVC-10 1140-1150	2.12	7280	5 ppm	1	8	na	6960	0.13	na
CVC-10 1150-1160	1.35	>10000	2 ppm	3	6	na	4540	0.08	na
CVC-10 1160-1170	1.04	8790	3 ppm	1	6	na	3510	0.12	na
CVC-10 1170-1180	1.53	5150	1 ppm	2	6	na	3730	0.24	na
CVC-10 1180-1190	1.25	>10000	4 ppm	2	7	na	3760	0.05	na
CVC-10 1190-1200	0.28	>10000	6 ppm	2	6	na	2700	0.12	na
CVC-10 1200-1210	0.32	>10000	2 ppm	1	7	na	4550	0.17	na
CVC-10 1210-1220	0.17	6350	6 ppm	2	7	na	2820	0.23	na
CVC-10 1220-1230	0.30	5560	4 ppm	<1	6	na	1760	0.27	na

Appendix V: Cove deposit multi-element geochemical data (B.D. = bulk density; na = not analyzed)

Sample	Mg %	Mn ppm	Hg ppb	Mo ppm	Ni ppm	Nb ppm	P ppm	K %	Rb ppm
CVC-10 1230-1240	0.13	7740	2 ppm	<1	5	na	1670	0.19	na
CVC-10 1240-1250	0.12	7990	1 ppm	<1	4	na	1110	0.21	na
CVC-10 1250-1260	0.05	5170	2 ppm	1	4	na	1620	0.12	na
CVC-10 1260-1270	0.06	1195	6 ppm	3	14	na	2430	0.32	na
CVC-10 1270-1280	0.09	1110	5 ppm	3	16	na	1710	0.27	na
CVC-10 1280-1290	0.07	1300	2 ppm	3	22	na	5560	0.27	na
CVC-10 1290-1300	0.09	1090	4 ppm	4	25	na	8050	0.38	na
CVC-10 1300-1310	0.12	480	2 ppm	12	43	na	9200	0.43	na
CVC-10 1310-1320	0.08	130	4 ppm	3	41	na	5970	0.27	na
CVC-10 1320-1330	0.10	90	1 ppm	2	23	na	6480	0.37	na
CVC-10 1330-1340	0.10	65	<1 ppm	1	26	na	5190	0.37	na
CVC-10 1340-1350	0.09	205	<1 ppm	4	21	na	7850	0.34	na
CVC-10 1350-1360	0.16	525	2 ppm	2	17	na	7400	0.44	na
CVC-10 1360-1370	0.12	940	1 ppm	1	18	na	3990	0.32	na
CVC-10 1370-1380	0.08	90	1 ppm	2	23	na	3960	0.33	na
CVC-10 1380-1390	0.16	1980	1 ppm	<1	16	na	4900	0.37	na
CVC-10 1390-1400	0.15	2070	2 ppm	2	19	na	4670	0.31	na
CVC-11 1000-1010	5.28	1780	1 ppm	6	17	na	950	0.08	na
CVC-11 1010-1020	4.45	2080	<1 ppm	8	14	na	1230	0.06	na
CVC-11 1020-1030	1.42	995	2 ppm	3	9	na	770	0.24	na
CVC-11 1030-1040	2.86	1900	1 ppm	26	13	na	860	0.20	na
CVC-11 1040-1050	9.40	1135	2 ppm	3	5	na	610	0.01	na
CVC-11 1050-1060	7.55	1675	3 ppm	1	5	na	1700	0.01	na
CVC-11 1060-1070	10.90	910	<1 ppm	1	7	na	2860	0.03	na
CVC-11 1070-1080	10.90	970	2 ppm	1	3	na	700	0.02	na
CVC-11 1080-1090	9.94	895	2 ppm	2	5	na	1060	0.03	na
CVC-11 1090-1100	7.38	1310	2 ppm	2	6	na	3490	0.01	na
CVC-11 1100-1110	4.60	2520	4 ppm	2	6	na	2620	<0.01	na
CVC-11 1110-1120	4.58	4220	2 ppm	1	7	na	1720	<0.01	na
CVC-11 1120-1130	2.86	4440	6 ppm	1	11	na	7030	0.04	na
CVC-11 1130-1140	1.61	2950	6 ppm	3	10	na	>10000	<0.01	na
CVC-11 1140-1150	1.69	2740	5 ppm	7	9	na	6920	0.01	na
CVC-11 1150-1160	3.29	3240	4 ppm	4	12	na	6890	0.06	na
CVC-11 1160-1170	0.43	2140	6 ppm	3	7	na	6550	0.11	na
CVC-11 1170-1180	0.32	2280	4 ppm	1	7	na	3470	0.13	na
CVC-11 1180-1190	0.79	1605	3 ppm	2	9	na	4890	0.12	na
CVC-11 1190-1200	1.18	1925	4 ppm	1	10	na	6370	0.04	na
CVC-11 1200-1210	0.59	750	2 ppm	3	6	na	4350	0.05	na
CVC-11 1210-1220	0.39	1045	2 ppm	<1	6	na	4590	0.05	na
CVC-11 1220-1230	0.65	1060	2 ppm	<1	2	na	2180	0.08	na
CVC-11 1230-1240	0.94	1070	2 ppm	<1	4	na	2180	0.16	na
CVC-11 1240-1250	0.15	750	2 ppm	<1	4	na	1400	0.13	na
CVC-11 1250-1260	0.15	1425	7 ppm	<1	3	na	960	0.10	na
CVC-11 1260-1270	0.13	1375	8 ppm	<1	2	na	1290	0.18	na
CVC-11 1270-1280	0.16	1395	3 ppm	<1	5	na	3200	0.17	na
CVC-11 1280-1290	0.44	1375	5 ppm	<1	9	na	2060	0.26	na
CVC-11 1290-1300	0.22	950	6 ppm	<1	8	na	1420	0.23	na
CVC-11 1300-1310	0.27	785	5 ppm	<1	13	na	2090	0.32	na

Appendix V: Cove deposit multi-element geochemical data (B.D. = bulk density; na = not analyzed)

Sample	Mg %	Mn ppm	Hg ppb	Mo ppm	Ni ppm	Nb ppm	P ppm	K %	Rb ppm
CVC-11 1310-1320	0.16	990	8 ppm	2	19	na	4520	0.40	na
CVC-11 1320-1330	0.16	2390	7 ppm	3	14	na	3250	0.20	na
CVC-11 1330-1340	0.11	3670	6 ppm	2	22	na	7040	0.23	na
CVC-11 1340-1350	0.11	2540	6 ppm	9	20	na	7720	0.19	na
CVC-11 1350-1360	0.22	4670	4 ppm	1	19	na	4280	0.20	na
CVC-11 1360-1370	0.23	6380	5 ppm	12	35	na	7960	0.34	na
CVC-11 1370-1380	0.20	4840	4 ppm	3	21	na	3540	0.21	na
CVC-11 1380-1390	0.17	1625	4 ppm	2	21	na	6710	0.39	na
CVC-11 1390-1400	0.16	2580	3 ppm	2	21	na	6020	0.34	na

Appendix V: Cove deposit multi-element geochemical data (B.D. = bulk density; na = not analyzed)

Sample	Sc ppm	Se ppm	Ag ppm	Ag opt	Na %	Sr ppm	S %	Ta ppm	Te ppm
4145-40	na	na	1.10	<0.01	0.09	32.0	na	0.6	<0.05
4145-41	na	na	1.00	<0.01	0.08	30.2	na	0.6	<0.05
4145-42	na	na	0.65	<0.01	0.06	24.0	na	0.4	<0.05
4145-46	na	na	3.65	0.08	0.12	21.2	na	0.6	<0.05
4145-47	na	na	10.40	0.29	<0.01	92.4	na	<0.2	<0.05
4145-48	na	na	11.55	0.33	0.02	66.0	na	0.2	<0.05
4145-49	na	na	4.50	0.11	0.14	52.0	na	0.6	0.05
4245-7A	na	na	6.80	0.17	0.04	151.0	na	<0.2	<0.05
4245-7B	na	na	4.75	0.11	0.10	98.1	na	0.6	<0.05
HS-1	na	na	1.00	0.01	0.05	75.6	na	<0.2	<0.05
HS-2	na	na	3.75	0.13	0.19	38.6	na	<0.2	<0.05
HS-3	na	na	168	4.90	0.70	157.5	na	<0.50	<0.50
HS-4	na	na	387.43	11.30	0.01	4.0	na	<0.50	1.00
HS-5	na	na	325.71	9.50	0.04	63.5	na	<0.50	<0.20
HS-6	na	na	1.50	0.04	0.15	21.2	na	0.2	<0.05
4725-4	na	na	1.50	0.02	2.03	471	na	0.8	<0.05
4205-23	na	na	1.30	0.01	1.53	412	na	0.4	<0.05
4285-11	na	na	1.60	0.06	0.70	323	na	0.2	<0.05
AR-8	na	na	0.70	0.01	0.99	143.0	na	0.6	<0.05
4205-5	na	na	7.90	0.21	0.15	55.3	na	0.6	<0.05
4205-7	na	na	5.45	0.14	0.19	32.4	na	1.0	<0.05
4405-2	na	na	0.90	0.01	0.34	244	na	0.4	<0.05
CU-0	na	na	0.60	na	0.04	57.6	na	<0.05	<0.05
CU-10	na	na	1.70	na	0.02	64.2	na	<0.05	<0.05
CU-20	na	na	1.80	na	0.03	63.6	na	<0.05	<0.05
CU-25	na	na	1.10	na	0.03	70.2	na	<0.05	0.05
CU-30	na	na	0.65	na	0.01	67.4	na	<0.05	<0.05
CU-35	na	na	2.80	na	0.02	66.1	na	<0.05	<0.05
CU-40	na	na	23.90	na	0.03	81.8	na	<0.05	<0.05
CU-45	na	na	1.50	na	0.01	80.6	na	<0.05	<0.05
CU-46	na	na	1.95	na	0.02	79.1	na	<0.05	<0.05
CU-47	na	na	1.90	na	0.03	67.5	na	<0.05	<0.05
CU-48	na	na	3.65	na	0.04	60	na	<0.05	<0.05
CU-49	na	na	3.35	na	0.02	70.1	na	<0.05	<0.05
CU-50	na	na	21.20	na	0.03	71	na	<0.05	<0.05
CU-51	na	na	12.60	na	0.03	79	na	<0.05	<0.05
CU-52	na	na	7.40	na	0.03	75	na	<0.05	<0.05
CU-53	na	na	29.90	na	0.01	69.8	na	<0.05	<0.05
CU-54	na	na	53.60	na	0.01	60	na	<0.05	<0.05
CU-55	na	na	52.60	na	0.01	71	na	<0.05	<0.05
CU-60	na	na	579.43	16.90	0.06	58	na	<0.05	<0.05
CU-70	na	na	4.30	na	0.02	73.2	na	<0.05	0.05
CU-80	na	na	1179.43	34.40	0.02	21	na	<0.05	0.05
CU-90	na	na	16.05	na	0.03	64.2	na	0.05	<0.05
CU-95	na	na	456.00	13.30	0.01	35	na	<0.05	0.05
CU-100	na	na	5.15	na	0.03	79	na	<0.05	<0.05
CU-105	na	na	3.90	na	0.01	55.3	na	<0.05	<0.05
CU-110	na	na	70.40	na	0.02	54.5	na	<0.05	<0.05

Appendix V: Cove deposit multi-element geochemical data (B.D. = bulk density; na = not analyzed)

Sample	Sc ppm	Se ppm	Ag ppm	Ag opt	Na %	Sr ppm	S %	Ta ppm	Te ppm
CU-115	na	na	32.50	na	0.02	60.9	na	0.05	<0.05
CU-120	na	na	11.80	na	0.02	58.9	na	<0.05	<0.05
CVC218 800.3-810	na	11.0	230.40	na	0.011	60	0.5505	na	<20
CVC218 810-811.7	na	15.0	292.10	na	0.0115	71	0.6435	na	<20
CVC218 815-820	na	<10	107.60	na	0.0133	82	0.6749	na	<20
CVC218 830-835	na	<10	56.80	na	0.009	44	0.979	na	<20
CVC218 835-836.2	na	<10	61.20	na	0.0117	70	0.7707	na	<20
CVC218 840-845	na	<10	18.30	na	0.0065	41	3.4138	na	<20
CVC218 855-859.5	na	<10	9.70	na	0.006	44	4.0444	na	<20
248-A	na	<10	21.10	0.76	na	36	2.52	na	<20
248-B	na	55.0	342.80	10.05	na	11	17.69	na	<20
248-C	na	<10	12.10	0.75	na	61	0.39	na	<20
86921	na	<10	1.0	0.09	na	99	0.44	na	<20
86922	na	27	309.1	8.25	na	43	11.04	na	<20
86923	na	<10	270.5	8.95	na	10	18.68	na	<20
CVC-15 1000-1010	1	na	33.0	1.025	0.01	11	na	na	na
CVC-15 1010-1020	<1	na	141.5	4.025	0.01	9	na	na	na
CVC-15 1020-1030	1	na	189.0	4.975	0.01	12	na	na	na
CVC-15 1030-1040	<1	na	187.5	5.200	0.01	8	na	na	na
CVC-15 1040-1050	<1	na	147.5	2.875	0.01	7	na	na	na
CVC-15 1050-1060	1	na	58.4	1.525	0.01	9	na	na	na
CVC-15 1060-1070	3	na	30.4	0.875	0.01	10	na	na	na
CVC-15 1070-1080	4	na	16.4	0.550	0.01	14	na	na	na
CVC-15 1080-1090	2	na	40.2	1.075	0.01	23	na	na	na
CVC-15 1090-1100	4	na	40.6	0.675	0.01	56	na	na	na
CVC-15 1100-1110	3	na	14.2	0.500	0.01	20	na	na	na
CVC-15 1110-1120	2	na	28.4	0.925	0.01	19	na	na	na
CVC-15 1120-1130	1	na	41.2	1.250	0.01	38	na	na	na
CVC-15 1130-1140	1	na	50.6	1.625	0.01	35	na	na	na
CVC-15 1140-1150	3	na	15.6	0.525	0.01	47	na	na	na
CVC-15 1150-1160	2	na	13.6	0.350	0.01	15	na	na	na
CVC-15 1160-1170	2	na	23.6	0.625	0.01	45	na	na	na
CVC-15 1170-1180	2	na	35.0	0.925	0.01	16	na	na	na
CVC-15 1180-1190	4	na	9.0	0.175	0.01	61	na	na	na
CVC-15 1190-1200	4	na	20.0	0.575	0.01	89	na	na	na
CVC-15 1200-1210	4	na	1.6	0.050	0.01	29	na	na	na
CVC-15 1210-1220	3	na	7.8	0.225	0.01	30	na	na	na
CVC-15 1220-1230	3	na	6.0	0.175	0.01	29	na	na	na
CVC-15 1230-1240	3	na	11.4	0.325	0.01	26	na	na	na
CVC-15 1240-1250	3	na	1.6	0.100	0.01	39	na	na	na
CVC-15 1250-1260	3	na	15.0	0.425	0.01	29	na	na	na
CVC-15 1260-1270	5	na	3.4	0.100	0.01	39	na	na	na
CVC-15 1270-1280	4	na	10.6	0.275	0.01	42	na	na	na
CVC-15 1280-1290	4	na	21.2	0.600	0.01	45	na	na	na
CVC-15 1290-1300	4	na	1.2	0.050	0.01	57	na	na	na
CVC-15 1300-1310	3	na	5.0	0.125	0.01	46	na	na	na
CVC-15 1310-1320	4	na	14.4	0.475	0.01	37	na	na	na
CVC-15 1320-1330	3	na	8.2	0.225	0.01	43	na	na	na

Appendix V: Cove deposit multi-element geochemical data (B.D. = bulk density; na = not analyzed)

Sample	Sc ppm	Se ppm	Ag ppm	Ag opt	Na %	Sr ppm	S %	Ta ppm	Te ppm
CVC-15 1330-1340	3	na	39.8	0.850	0.02	49	na	na	na
CVC-15 1340-1350	3	na	12.0	0.300	0.01	48	na	na	na
CVC-15 1350-1360	2	na	4.4	0.125	0.01	74	na	na	na
CVC-15 1360-1370	3	na	20.0	0.525	0.01	71	na	na	na
CVC-15 1370-1380	3	na	67.0	2.100	0.01	62	na	na	na
CVC-15 1380-1390	3	na	49.8	1.625	0.01	72	na	na	na
CVC-15 1390-1400	2	na	5.6	0.150	0.01	163	na	na	na
CVC-15 1400-1410	2	na	<0.2	0.000	0.01	249	na	na	na
CVC-15 1410-1420	2	na	1.0	0.050	0.01	187	na	na	na
CVC-15 1420-1430	2	na	2.8	0.150	0.01	126	na	na	na
CVC-15 1430-1440	3	na	3.0	0.150	0.01	192	na	na	na
CVC-15 1440-1450	4	na	19.8	0.575	0.01	259	na	na	na
CVC-15 1450-1460	1	na	5.2	0.125	0.01	642	na	na	na
CVC-15 1460-1470	1	na	0.4	0.000	0.01	731	na	na	na
CVC-15 1470-1480	2	na	<0.2	0.100	0.01	640	na	na	na
CVC-15 1480-1490	3	na	2.0	0.075	0.01	537	na	na	na
CVC-15 1490-1500	4	na	1.2	0.100	0.01	476	na	na	na
CVC-10 0920-0930	2	na	84.0	2.300	0.01	20	na	na	na
CVC-10 0930-0940	3	na	174.0	4.900	0.01	19	na	na	na
CVC-10 0940-0950	3	na	60.0	3.375	0.01	12	na	na	na
CVC-10 0950-0960	3	na	40.0	0.600	0.01	22	na	na	na
CVC-10 0960-0970	3	na	7.0	0.025	0.01	30	na	na	na
CVC-10 0970-0980	3	na	11.8	0.125	0.01	42	na	na	na
CVC-10 0980-0990	2	na	8.0	0.150	0.01	31	na	na	na
CVC-10 0990-1000	3	na	84.0	2.650	0.01	49	na	na	na
CVC-10 1000-1010	3	na	56.0	1.575	0.01	63	na	na	na
CVC-10 1010-1020	3	na	64.0	1.900	0.01	37	na	na	na
CVC-10 1020-1030	4	na	>200	10.840	0.01	48	na	na	na
CVC-10 1030-1040	3	na	8.4	0.150	0.01	81	na	na	na
CVC-10 1040-1050	3	na	21.6	0.525	0.01	89	na	na	na
CVC-10 1050-1060	2	na	90.0	2.550	0.02	79	na	na	na
CVC-10 1060-1070	3	na	15.8	0.125	0.01	94	na	na	na
CVC-10 1070-1080	4	na	>200	10.105	0.02	152	na	na	na
CVC-10 1080-1090	1	na	0.4	0.000	0.01	66	na	na	na
CVC-10 1090-1099.5	2	na	27.2	0.425	0.01	94	na	na	na
CVC-10 1099.5-1110	3	na	>200	3.855	0.01	69	na	na	na
CVC-10 1110-1120	3	na	160.0	3.825	0.01	66	na	na	na
CVC-10 1120-1130	4	na	>200	7.475	0.01	69	na	na	na
CVC-10 1130-1140	4	na	180.0	4.125	0.01	74	na	na	na
CVC-10 1140-1150	2	na	166.0	4.075	0.01	48	na	na	na
CVC-10 1150-1160	3	na	78.0	1.950	0.01	69	na	na	na
CVC-10 1160-1170	2	na	122.0	2.975	0.01	70	na	na	na
CVC-10 1170-1180	3	na	16.0	0.250	0.01	82	na	na	na
CVC-10 1180-1190	3	na	37.0	0.900	0.01	94	na	na	na
CVC-10 1190-1200	2	na	>200	5.925	0.01	51	na	na	na
CVC-10 1200-1210	2	na	80.0	1.975	0.01	87	na	na	na
CVC-10 1210-1220	1	na	122.0	2.475	0.01	28	na	na	na
CVC-10 1220-1230	3	na	22.4	0.400	0.01	91	na	na	na

Appendix V: Cove deposit multi-element geochemical data (B.D. = bulk density; na = not analyzed)

Sample	Sc ppm	Se ppm	Ag ppm	Ag opt	Na %	Sr ppm	S %	Ta ppm	Te ppm
CVC-10 1230-1240	2	na	76.0	2.100	0.01	134	na	na	na
CVC-10 1240-1250	3	na	74.0	1.925	0.01	190	na	na	na
CVC-10 1250-1260	2	na	>200	5.125	0.01	67	na	na	na
CVC-10 1260-1270	1	na	100.0	2.300	0.01	27	na	na	na
CVC-10 1270-1280	1	na	160.0	4.050	0.01	19	na	na	na
CVC-10 1280-1290	1	na	136.0	3.425	0.01	67	na	na	na
CVC-10 1290-1300	1	na	120.0	2.950	0.01	101	na	na	na
CVC-10 1300-1310	2	na	152.0	3.825	0.01	97	na	na	na
CVC-10 1310-1320	1	na	90.0	2.200	0.01	78	na	na	na
CVC-10 1320-1330	1	na	36.4	0.950	0.01	97	na	na	na
CVC-10 1330-1340	1	na	12.2	0.175	0.01	74	na	na	na
CVC-10 1340-1350	2	na	43.8	1.150	0.01	111	na	na	na
CVC-10 1350-1360	2	na	9.0	0.225	0.01	124	na	na	na
CVC-10 1360-1370	3	na	16.0	0.475	0.01	141	na	na	na
CVC-10 1370-1380	1	na	9.0	0.175	0.01	52	na	na	na
CVC-10 1380-1390	3	na	28.4	0.625	0.01	211	na	na	na
CVC-10 1390-1400	3	na	19.4	0.525	0.01	167	na	na	na
CVC-11 1000-1010	2	na	37.2	1.275	0.01	58	na	na	na
CVC-11 1010-1020	2	na	18.6	0.725	0.01	137	na	na	na
CVC-11 1020-1030	2	na	1.6	0.275	0.01	151	na	na	na
CVC-11 1030-1040	3	na	31.6	1.075	0.01	94	na	na	na
CVC-11 1040-1050	2	na	9.6	0.500	0.01	65	na	na	na
CVC-11 1050-1060	1	na	5.2	0.425	0.01	79	na	na	na
CVC-11 1060-1070	1	na	<0.2	0.175	0.01	86	na	na	na
CVC-11 1070-1080	1	na	0.6	0.275	0.01	59	na	na	na
CVC-11 1080-1090	1	na	<0.2	0.150	0.01	72	na	na	na
CVC-11 1090-1100	2	na	27.4	0.750	0.01	74	na	na	na
CVC-11 1100-1110	2	na	21.0	0.650	0.01	82	na	na	na
CVC-11 1110-1120	2	na	4.4	0.100	0.01	89	na	na	na
CVC-11 1120-1130	4	na	39.6	1.025	0.01	78	na	na	na
CVC-11 1130-1140	4	na	19.6	0.125	0.01	117	na	na	na
CVC-11 1140-1150	3	na	69.4	2.225	0.01	69	na	na	na
CVC-11 1150-1160	3	na	37.6	0.875	0.01	76	na	na	na
CVC-11 1160-1170	2	na	52.4	1.675	0.01	141	na	na	na
CVC-11 1170-1180	2	na	46.2	1.450	0.01	139	na	na	na
CVC-11 1180-1190	2	na	70.0	1.875	0.01	84	na	na	na
CVC-11 1190-1200	3	na	19.6	0.425	0.01	121	na	na	na
CVC-11 1200-1210	1	na	16.0	0.400	0.01	38	na	na	na
CVC-11 1210-1220	1	na	10.8	0.150	<0.01	220	na	na	na
CVC-11 1220-1230	1	na	11.0	0.200	<0.01	155	na	na	na
CVC-11 1230-1240	2	na	10.0	0.175	0.01	171	na	na	na
CVC-11 1240-1250	2	na	37.6	0.925	<0.01	277	na	na	na
CVC-11 1250-1260	2	na	20.0	0.375	<0.01	290	na	na	na
CVC-11 1260-1270	1	na	40.0	0.925	0.01	203	na	na	na
CVC-11 1270-1280	2	na	20.0	0.425	<0.01	202	na	na	na
CVC-11 1280-1290	2	na	8.2	0.100	0.01	93	na	na	na
CVC-11 1290-1300	2	na	7.4	0.175	<0.01	133	na	na	na
CVC-11 1300-1310	2	na	14.0	0.250	0.01	119	na	na	na

Appendix V: Cove deposit multi-element geochemical data (B.D. = bulk density; na = not analyzed)

Sample	Sc ppm	Se ppm	Ag ppm	Ag opt	Na %	Sr ppm	S %	Ta ppm	Te ppm
CVC-11 1310-1320	2	na	47.8	1.325	0.01	91	na	na	na
CVC-11 1320-1330	1	na	76.6	2.425	0.01	143	na	na	na
CVC-11 1330-1340	1	na	193.5	3.900	0.01	94	na	na	na
CVC-11 1340-1350	1	na	>200	1.650	0.01	114	na	na	na
CVC-11 1350-1360	2	na	165.0	4.425	0.01	316	na	na	na
CVC-11 1360-1370	4	na	23.0	0.725	0.01	262	na	na	na
CVC-11 1370-1380	4	na	20.6	0.525	0.01	317	na	na	na
CVC-11 1380-1390	2	na	36.4	1.075	0.01	185	na	na	na
CVC-11 1390-1400	2	na	36.8	1.150	0.01	103	na	na	na

Appendix V: Cove deposit multi-element geochemical data (B.D. = bulk density; na = not analyzed)

Sample	Tl ppm	Th ppm	Sn ppm	Ti %	W ppm	U ppm	V ppm	Y ppm	Zn ppm
4145-40	1.65	8.6	<2	0.32	1.6	2.2	64	17.6	88
4145-41	1.55	8.2	<2	0.31	1.6	1.8	64	22.0	54
4145-42	0.60	6.8	<2	0.26	2.2	1.8	64	22.8	52
4145-46	0.75	9.0	3.0	0.31	3.8	3.4	112	17.1	40
4145-47	1.55	1.2	<2	0.07	0.4	1.4	42	9.4	62
4145-48	0.70	4.8	<2	0.19	1.4	2.6	85	13.8	46
4145-49	1.25	10.4	<2	0.34	3.4	4	150	23.8	74
4245-7A	2.95	2.0	<2	0.08	0.6	1.4	89	10.9	34
4245-7B	0.90	9.2	4.0	0.32	2.2	1.8	104	12.8	58
HS-1	0.95	0.4	<2	0.01	0.2	1.4	15	4.3	14
HS-2	0.05	<0.2	<2	<0.01	0.2	0.6	5	2.3	14
HS-3	8.50	<0.20	14.0	0.04	7.5	6.0	46	11.0	41300
HS-4	25.00	<0.20	67.0	0.01	15.0	<2.0	4	<1.0	33000
HS-5	18.50	2.0	37.0	0.11	13.0	6.0	52	12.0	97700
HS-6	12.10	11.2	<2	0.21	2.4	4.2	60	10.7	238
4725-4	0.70	9.2	<2	0.36	0.8	1.8	93	15.1	130
4205-23	0.55	8.4	<2	0.22	1.8	2.8	44	9.0	84
4285-11	0.70	9.8	<2	0.21	2.6	3.8	48	10.8	78
AR-8	1.60	9.0	<2	0.33	0.6	3.8	83	17.5	104
4205-5	6.60	8.2	<2	0.32	2.0	4.4	104	11.5	350
4205-7	2.85	13.4	<2	0.43	1.6	5.6	101	18.2	270
4405-2	1.15	6.2	<2	0.39	1.0	1.4	101	14.6	90
CU-0	0.64	0.6	<2	<0.01	0.2	1.6	<1	3.4	28
CU-10	0.92	0.6	<2	0.01	0.3	1.6	2	4.2	4
CU-20	0.74	0.4	<2	<0.01	0.2	1.4	4	4.0	14
CU-25	4.76	0.6	<2	0.01	0.5	1.6	10	5.0	10
CU-30	1.56	0.6	<2	0.01	0.3	1.4	9	4.4	2
CU-35	1.36	0.6	<2	0.01	0.3	1.2	3	4.6	140
CU-40	0.70	0.6	<2	0.01	0.3	1.6	6	4.9	18
CU-45	0.88	0.8	<2	0.01	0.3	2	10	5.7	6
CU-46	1.28	1.0	<2	0.01	0.8	2.4	17	7.3	14
CU-47	0.94	2.0	<2	0.05	3.0	5	26	14.4	34
CU-48	2.50	2.4	2.0	0.06	3.3	4.4	37	15.9	142
CU-49	0.86	1.4	<2	0.05	1.3	3.8	24	10.5	48
CU-50	0.60	4.0	15.0	0.12	5.0	6	41	18.0	226
CU-51	8.20	2.0	7.0	0.09	4.0	4	44	16.0	94
CU-52	1.96	1.6	<2	0.03	1.7	2.4	20	9.4	60
CU-53	0.34	2.0	16.0	0.07	1.9	3.8	26	11.2	1010
CU-54	1.80	2.0	39.0	0.09	2.0	4	27	12.0	2030
CU-55	1.40	4.0	20.0	0.13	4.0	4	37	15.0	926
CU-60	2.40	4.0	48.0	0.1	6.0	6	52	16.0	8180
CU-70	0.28	0.8	<2	0.04	1.7	4.2	42	6.0	80
CU-80	5.20	4.0	98.0	0.06	4.0	4	36	6.0	37000
CU-90	2.64	6.8	9.0	0.19	13.3	15.8	122	15.8	180
CU-95	3.40	2.0	69.0	0.08	8.0	12	61	10.0	1615
CU-100	0.28	0.2	<2	0.01	0.4	2.2	7	3.2	184
CU-105	1.62	0.6	<2	0.01	0.5	1.8	5	3.3	50
CU-110	173.50	0.6	<2	<0.01	0.3	1.6	4	3.2	22

Appendix V: Cove deposit multi-element geochemical data (B.D. = bulk density; na = not analyzed)

Sample	Tl ppm	Th ppm	Sn ppm	Ti %	W ppm	U ppm	V ppm	Y ppm	Zn ppm
CU-115	24.40	3.4	6.0	0.11	10.6	5.2	52	9.3	360
CU-120	8.74	1.4	<2	0.01	1.3	2.2	19	6.0	238
CVC218 800.3-810	<50	na	<50	<.01	<5	na	15	na	774
CVC218 810-811.7	<50	na	61.0	<.01	<5	na	14	na	1450
CVC218 815-820	<50	na	<50	<.01	<5	na	13	na	534
CVC218 830-835	<50	na	<50	<.01	<5	na	14	na	388
CVC218 835-836.2	<50	na	<50	<.01	<5	na	16	na	311
CVC218 840-845	<50	na	<50	<.01	<5	na	12	na	86
CVC218 855-859.5	<50	na	<50	<.01	<5	na	12	na	70
248-A	<50	na	<50	5	13.0	na	9	na	627
248-B	492.00	na	<50	2	18.0	na	3	na	578
248-C	<50	na	<50	4	<5	na	10	na	154
86921	<50	na	<50	8 ppm	<5	na	34	na	23
86922	<50	na	274	7 ppm	<5	na	12	na	35619
86923	<50	na	124	4 ppm	<5	na	3	na	35869
CVC-15 1000-1010	<10	na	14	<0.01	<10	<10	14	na	386
CVC-15 1010-1020	<10	na	38	<0.01	10	<10	11	na	1725
CVC-15 1020-1030	<10	na	70	<0.01	10	<10	13	na	3560
CVC-15 1030-1040	<10	na	110	<0.01	30	<10	13	na	>10000
CVC-15 1040-1050	<10	na	100	<0.01	10	<10	13	na	9280
CVC-15 1050-1060	<10	na	36	<0.01	10	<10	12	na	3600
CVC-15 1060-1070	<10	na	18	<0.01	<10	<10	10	na	1095
CVC-15 1070-1080	<10	na	10	<0.01	<10	<10	4	na	1315
CVC-15 1080-1090	<10	na	18	<0.01	<10	<10	3	na	1550
CVC-15 1090-1100	<10	na	15	<0.01	<10	<10	8	na	5350
CVC-15 1100-1110	<10	na	7	<0.01	<10	<10	5	na	658
CVC-15 1110-1120	<10	na	11	<0.01	<10	<10	3	na	786
CVC-15 1120-1130	<10	na	15	<0.01	<10	<10	6	na	3200
CVC-15 1130-1140	<10	na	31	<0.01	<10	<10	4	na	4760
CVC-15 1140-1150	<10	na	10	<0.01	<10	<10	6	na	888
CVC-15 1150-1160	<10	na	10	<0.01	<10	<10	8	na	1260
CVC-15 1160-1170	<10	na	7	<0.01	<10	<10	12	na	2500
CVC-15 1170-1180	<10	na	16	<0.01	<10	<10	9	na	668
CVC-15 1180-1190	<10	na	7	<0.01	<10	<10	20	na	834
CVC-15 1190-1200	<10	na	12	<0.01	<10	<10	13	na	724
CVC-15 1200-1210	<10	na	<2	<0.01	<10	<10	12	na	140
CVC-15 1210-1220	<10	na	2	<0.01	<10	<10	9	na	194
CVC-15 1220-1230	<10	na	3	<0.01	<10	<10	9	na	1290
CVC-15 1230-1240	<10	na	6	<0.01	<10	<10	12	na	676
CVC-15 1240-1250	<10	na	<2	<0.01	<10	<10	11	na	48
CVC-15 1250-1260	<10	na	16	<0.01	<10	<10	13	na	1405
CVC-15 1260-1270	<10	na	4	<0.01	<10	<10	16	na	268
CVC-15 1270-1280	<10	na	<2	<0.01	<10	<10	12	na	84
CVC-15 1280-1290	<10	na	<2	<0.01	<10	<10	19	na	244
CVC-15 1290-1300	<10	na	<2	<0.01	<10	<10	11	na	50
CVC-15 1300-1310	<10	na	<2	<0.01	<10	<10	7	na	40
CVC-15 1310-1320	<10	na	<2	<0.01	<10	<10	13	na	318
CVC-15 1320-1330	<10	na	<2	<0.01	<10	<10	5	na	160

Appendix V: Cove deposit multi-element geochemical data (B.D. = bulk density; na = not analyzed)

Sample	Tl ppm	Th ppm	Sn ppm	Ti %	W ppm	U ppm	V ppm	Y ppm	Zn ppm
CVC-15 1330-1340	<10	na	2	<0.01	10	<10	4	na	742
CVC-15 1340-1350	<10	na	2	<0.01	<10	<10	10	na	258
CVC-15 1350-1360	<10	na	<2	<0.01	<10	<10	14	na	10
CVC-15 1360-1370	<10	na	2	<0.01	<10	<10	8	na	158
CVC-15 1370-1380	<10	na	8	<0.01	<10	<10	9	na	296
CVC-15 1380-1390	<10	na	7	<0.01	<10	<10	5	na	172
CVC-15 1390-1400	<10	na	<2	<0.01	<10	<10	<1	na	40
CVC-15 1400-1410	<10	na	<2	<0.01	<10	<10	4	na	20
CVC-15 1410-1420	<10	na	<2	<0.01	<10	<10	8	na	56
CVC-15 1420-1430	<10	na	<2	<0.01	<10	<10	9	na	36
CVC-15 1430-1440	<10	na	<2	<0.01	<10	<10	12	na	60
CVC-15 1440-1450	<10	na	2	<0.01	<10	<10	12	na	260
CVC-15 1450-1460	<10	na	3	<0.01	<10	<10	5	na	398
CVC-15 1460-1470	<10	na	<2	<0.01	<10	<10	5	na	60
CVC-15 1470-1480	<10	na	<2	<0.01	<10	<10	8	na	22
CVC-15 1480-1490	<10	na	<2	<0.01	<10	<10	16	na	68
CVC-15 1490-1500	<10	na	<2	<0.01	<10	<10	17	na	58
CVC-10 0920-0930	<10	na	45	<0.01	10	<10	18	na	>10000
CVC-10 0930-0940	<10	na	80	<0.01	10	<10	20	na	>10000
CVC-10 0940-0950	<10	na	31	<0.01	10	<10	25	na	8440
CVC-10 0950-0960	<10	na	31	<0.01	<10	<10	21	na	4180
CVC-10 0960-0970	<10	na	13	<0.01	<10	<10	18	na	468
CVC-10 0970-0980	<10	na	12	<0.01	<10	<10	17	na	1340
CVC-10 0980-0990	<10	na	10	<0.01	<10	<10	16	na	220
CVC-10 0990-1000	<10	na	24	<0.01	50	<10	23	na	>10000
CVC-10 1000-1010	<10	na	23	<0.01	30	<10	20	na	7480
CVC-10 1010-1020	<10	na	30	<0.01	30	<10	24	na	>10000
CVC-10 1020-1030	<10	na	57	<0.01	100	40	19	na	>10000
CVC-10 1030-1040	<10	na	9	<0.01	<10	<10	17	na	868
CVC-10 1040-1050	<10	na	8	<0.01	10	<10	12	na	2390
CVC-10 1050-1060	<10	na	19	<0.01	70	<10	12	na	>10000
CVC-10 1060-1070	<10	na	8	<0.01	<10	<10	12	na	1775
CVC-10 1070-1080	<10	na	30	<0.01	100	<10	39	na	>10000
CVC-10 1080-1090	<10	na	2	<0.01	<10	<10	10	na	162
CVC-10 1090-1099.5	<10	na	7	<0.01	<10	<10	15	na	5680
CVC-10 1099.5-1110	<10	na	28	<0.01	30	<10	25	na	>10000
CVC-10 1110-1120	<10	na	19	<0.01	20	<10	8	na	>10000
CVC-10 1120-1130	<10	na	38	<0.01	50	<10	24	na	>10000
CVC-10 1130-1140	<10	na	36	<0.01	<10	<10	22	na	>10000
CVC-10 1140-1150	<10	na	21	<0.01	30	<10	20	na	>10000
CVC-10 1150-1160	<10	na	18	<0.01	<10	<10	17	na	2750
CVC-10 1160-1170	<10	na	25	<0.01	20	<10	9	na	9540
CVC-10 1170-1180	<10	na	12	<0.01	<10	<10	12	na	2200
CVC-10 1180-1190	<10	na	13	<0.01	<10	<10	8	na	2870
CVC-10 1190-1200	<10	na	28	<0.01	<10	<10	3	na	8770
CVC-10 1200-1210	<10	na	16	<0.01	10	<10	2	na	6590
CVC-10 1210-1220	<10	na	15	<0.01	20	<10	2	na	>10000
CVC-10 1220-1230	<10	na	16	<0.01	<10	<10	4	na	2710

Appendix V: Cove deposit multi-element geochemical data (B.D. = bulk density; na = not analyzed)

Sample	Tl ppm	Th ppm	Sn ppm	Ti %	W ppm	U ppm	V ppm	Y ppm	Zn ppm
CVC-10 1230-1240	<10	na	8	<0.01	<10	<10	1	na	1260
CVC-10 1240-1250	<10	na	9	<0.01	<10	<10	<1	na	2740
CVC-10 1250-1260	<10	na	33	<0.01	40	<10	1	na	>10000
CVC-10 1260-1270	<10	na	40	<0.01	<10	<10	7	na	9170
CVC-10 1270-1280	<10	na	33	<0.01	10	<10	5	na	>10000
CVC-10 1280-1290	<10	na	22	<0.01	10	<10	10	na	7960
CVC-10 1290-1300	<10	na	11	<0.01	<10	<10	12	na	6920
CVC-10 1300-1310	<10	na	17	<0.01	10	<10	23	na	8580
CVC-10 1310-1320	<10	na	8	<0.01	<10	<10	23	na	2120
CVC-10 1320-1330	<10	na	6	<0.01	<10	<10	15	na	1205
CVC-10 1330-1340	<10	na	4	<0.01	<10	<10	17	na	3598
CVC-10 1340-1350	<10	na	8	<0.01	<10	<10	16	na	3070
CVC-10 1350-1360	<10	na	5	<0.01	<10	<10	22	na	600
CVC-10 1360-1370	<10	na	5	<0.01	<10	<10	18	na	488
CVC-10 1370-1380	<10	na	3	<0.01	<10	<10	16	na	308
CVC-10 1380-1390	<10	na	3	<0.01	<10	<10	18	na	226
CVC-10 1390-1400	<10	na	3	<0.01	<10	<10	16	na	596
CVC-11 1000-1010	<10	na	43	<0.01	<10	<10	14	na	8400
CVC-11 1010-1020	<10	na	12	<0.01	<10	<10	14	na	2910
CVC-11 1020-1030	<10	na	2	<0.01	<10	<10	11	na	488
CVC-11 1030-1040	<10	na	19	<0.01	<10	<10	15	na	6140
CVC-11 1040-1050	<10	na	7	<0.01	<10	<10	7	na	1740
CVC-11 1050-1060	<10	na	3	<0.01	<10	<10	12	na	416
CVC-11 1060-1070	<10	na	<2	<0.01	<10	<10	14	na	108
CVC-11 1070-1080	<10	na	2	<0.01	<10	<10	7	na	186
CVC-11 1080-1090	<10	na	<2	<0.01	<10	<10	7	na	78
CVC-11 1090-1100	<10	na	9	<0.01	<10	<10	16	na	3610
CVC-11 1100-1110	<10	na	10	<0.01	<10	<10	31	na	2330
CVC-11 1110-1120	<10	na	5	<0.01	<10	<10	9	na	758
CVC-11 1120-1130	<10	na	17	<0.01	<10	<10	27	na	6640
CVC-11 1130-1140	<10	na	6	<0.01	<10	<10	24	na	354
CVC-11 1140-1150	<10	na	38	<0.01	<10	<10	31	na	6090
CVC-11 1150-1160	<10	na	25	<0.01	<10	<10	21	na	4800
CVC-11 1160-1170	<10	na	12	<0.01	<10	<10	11	na	6500
CVC-11 1170-1180	<10	na	7	<0.01	<10	<10	8	na	1490
CVC-11 1180-1190	<10	na	12	<0.01	<10	<10	11	na	4140
CVC-11 1190-1200	<10	na	9	<0.01	<10	<10	20	na	2950
CVC-11 1200-1210	<10	na	18	<0.01	<10	<10	11	na	1045
CVC-11 1210-1220	<10	na	5	<0.01	<10	<10	7	na	1100
CVC-11 1220-1230	<10	na	5	<0.01	<10	<10	6	na	676
CVC-11 1230-1240	<10	na	5	<0.01	<10	<10	8	na	1950
CVC-11 1240-1250	<10	na	8	<0.01	<10	<10	5	na	3670
CVC-11 1250-1260	<10	na	3	<0.01	<10	<10	3	na	1835
CVC-11 1260-1270	<10	na	7	<0.01	<10	<10	3	na	3960
CVC-11 1270-1280	<10	na	2	<0.01	<10	<10	6	na	876
CVC-11 1280-1290	<10	na	3	<0.01	<10	<10	7	na	1065
CVC-11 1290-1300	<10	na	2	<0.01	<10	<10	8	na	706
CVC-11 1300-1310	<10	na	4	<0.01	<10	<10	9	na	1135

Appendix V: Cove deposit multi-element geochemical data (B.D. = bulk density; na = not analyzed)

Sample	Tl ppm	Th ppm	Sn ppm	Ti %	W ppm	U ppm	V ppm	Y ppm	Zn ppm
CVC-11 1310-1320	<10	na	5	<0.01	<10	<10	12	na	2410
CVC-11 1320-1330	<10	na	4	<0.01	<10	<10	7	na	1585
CVC-11 1330-1340	<10	na	14	<0.01	<10	<10	5	na	>10000
CVC-11 1340-1350	<10	na	12	<0.01	<10	<10	4	na	>10000
CVC-11 1350-1360	<10	na	5	<0.01	<10	<10	8	na	2280
CVC-11 1360-1370	<10	na	<2	<0.01	<10	<10	15	na	694
CVC-11 1370-1380	<10	na	2	<0.01	<10	<10	13	na	350
CVC-11 1380-1390	<10	na	2	<0.01	<10	<10	17	na	366
CVC-11 1390-1400	<10	na	<2	<0.01	<10	<10	15	na	628

Appendix V: Cove deposit multi-element geochemical data (B.D. = bulk density; na = not analyzed)

APPENDIX VI

Unreliable Age Data for ^{40}Ar-^{39}Ar Analyses of Altered Intrusive Rocks from Cove

The following descriptions of unreliable results for three samples analyzed for ^{40}Ar-^{39}Ar ages are summarized from descriptions produced by the Nevada Isotope Geochronology Laboratory (NIGL) at the University of Nevada, Las Vegas.

Sample CVC-218-857.5

Sample CVC-218-857.5 was collected from drill core CVC-218, which penetrated the Cove South Deep (CSD) orebody (see Fig. 77 for location). The sample consists of QSP-altered Omega dike, which is a principal control on the distribution of Au and Ag in the CSD orebody. CVC-218-857.5 is a whole rock sample that produced a discordant age spectrum characterized by apparent ages that increase from ~88 to ~138 Ma, then decrease with the final gas released (Fig. A1). The spectrum defines neither an age plateau nor an isochron, probably due to excess Ar.

Sample 4405E-1

This sample was collected from an exposure in the northwest highwall of the Cove open pit (see Plate 1 for the location). The sample was collected from a thin, QSP-altered dike that occupied an unnamed northwest-striking fault (see Plate 1), and was submitted to the NIGL for whole-rock analysis. The analysis produced a discordant age spectrum characterized by ages ranging from ~81 Ma in the lowest temperature fraction to ~145 Ma in the highest temperature fraction (Fig. A2). There is no plateau and no isochron, probably due to excess Ar.

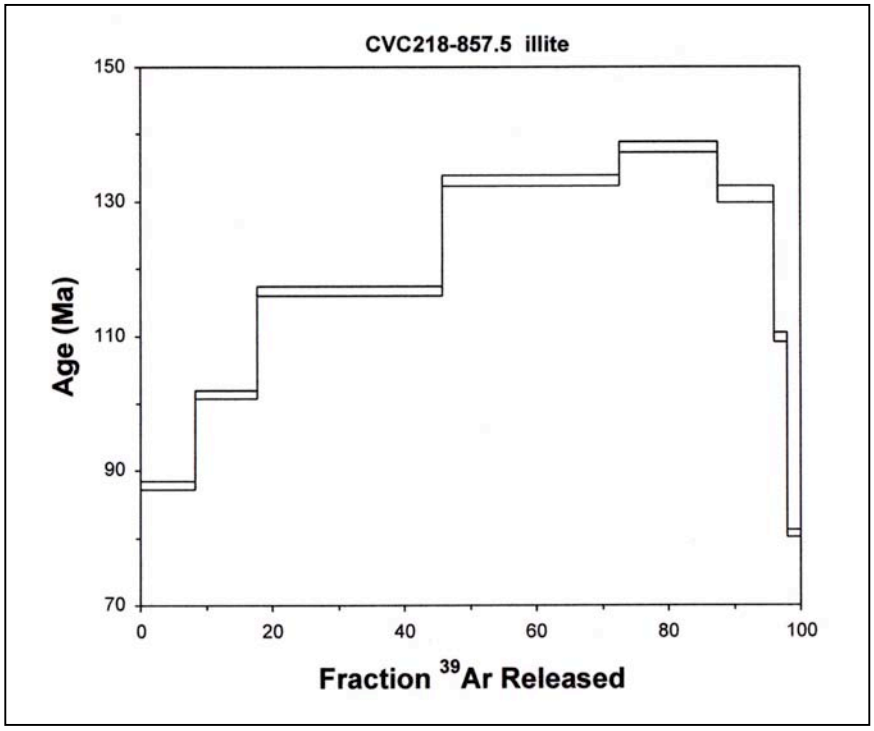

FIG. A1. Incremental heating ^{40}Ar-^{39}Ar age spectrum for sample CVC-218-857.5.

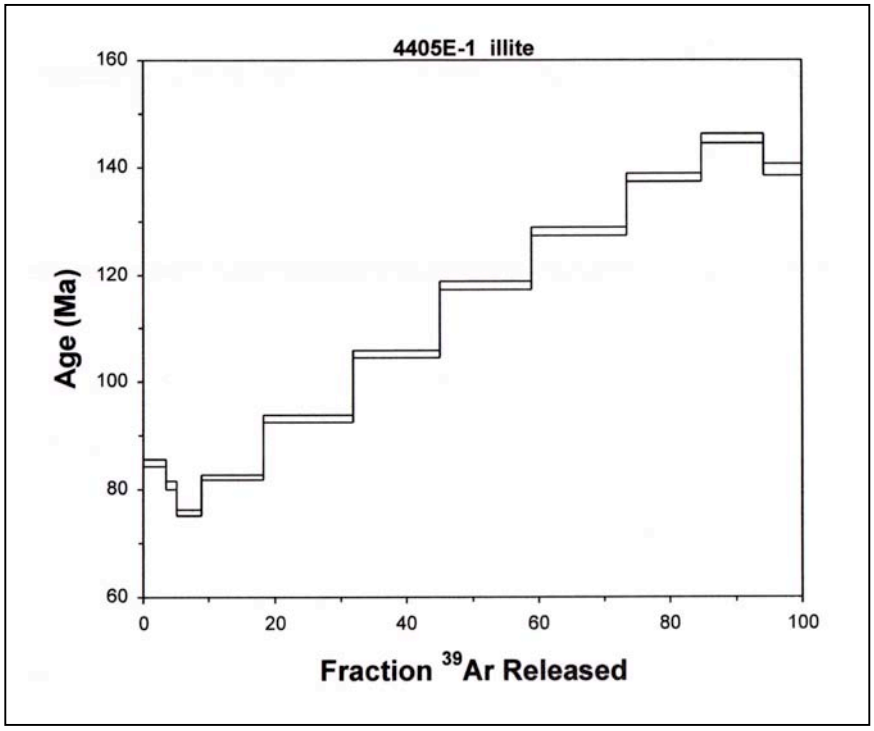

FIG. A2. Incremental heating ^{40}Ar-^{39}Ar age spectrum for sample 4405E-1.

Sample 4145E-29

This sample consists of a composite illite-sulfide selvage collected from the margins of a BMVT vein in the dolostone submember of the Panther Canyon Member. The age spectrum from sample 4145E-29 is nearly flat for steps 2 through 7, defining an apparent plateau age of ~73 Ma (Fig. A3A). Steps 4 through 7 also define a valid isochron age of ~78 Ma (Fig. A3B). Neither of these ages can be associated with the mineralizing event that produced the BMVT vein; the vein is part of a series of BMVT veins that cuts, and is therefore younger than, the Bay dike. As shown in Table 3, the Bay dike is late Eocene (around 40 Ma) in age.

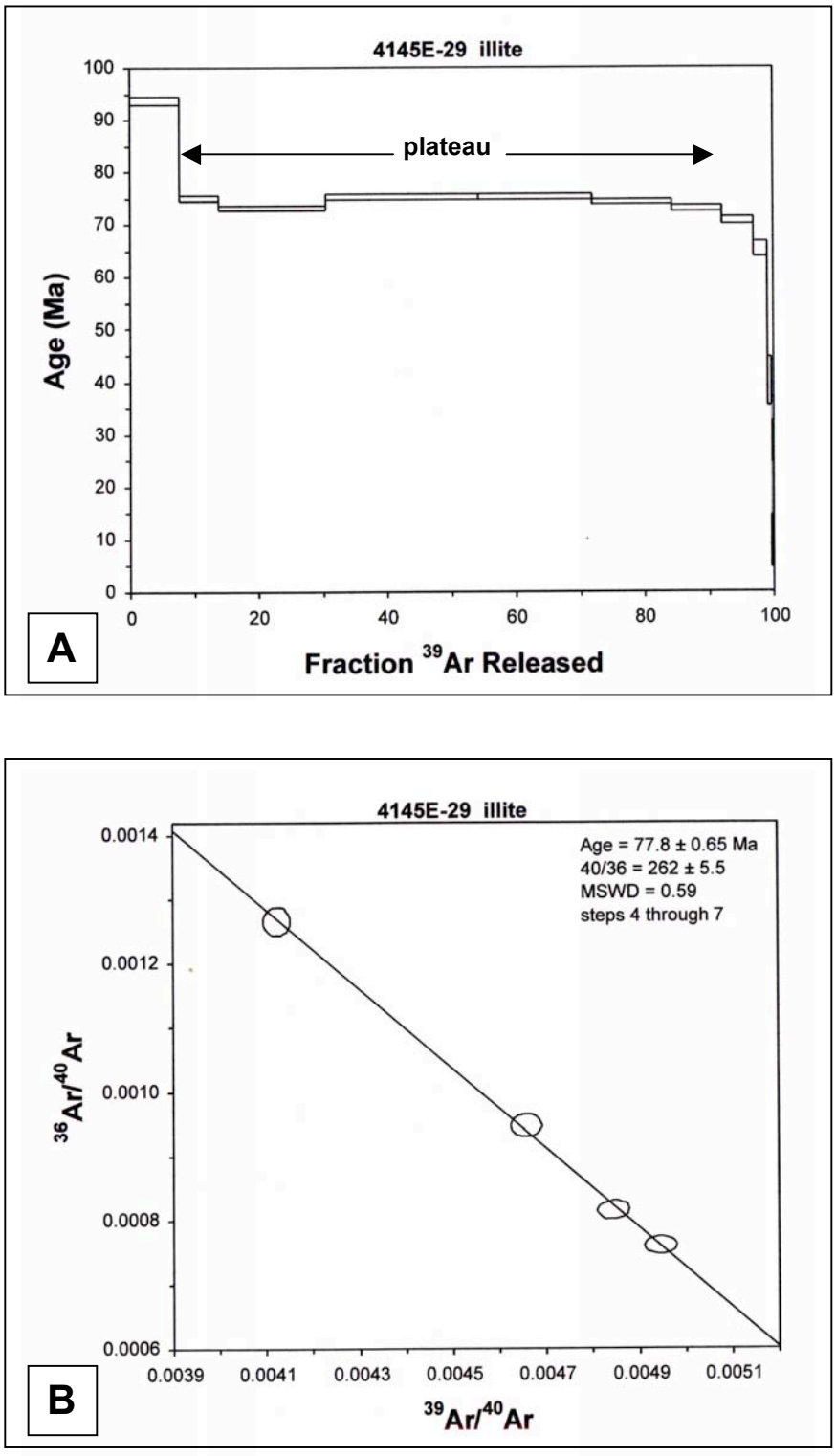

FIG. A3. Age data for sample 4145E-29. A. Incremental heating ^{40}Ar-^{39}Ar age spectrum. B. Isochron plot for sample 4145E-29.

APPENDIX VII

Concentrations of Au and Ag in Pyrite from Carlin-Style Ore at Cove

Microcrystalline pyrite			Fine-grained pyrite			Coarse-grained pyrite			Arsenopyrite	
test #	Au, ppm	Ag, ppm	test #	Au, ppm	Ag, ppm	test #	Au, ppm	Ag, ppm	test #	Au, ppm
C21	116.47	804.61	C21	18.42	165.96	C21	0.23	2.49	C21	43.25
C21	144.27	986.92	C21	12.97	167.53	C21	0.70	26.43	C21	70.32
C21	152.22	666.56	C21	51.15	34.28	C21	4.69	85.28	C21	106.54
C21	153.67	765.64	C21	41.44	318.89	C21	1.37	10.69	C21	37.92
C21	106.66	563.85	C21	6.32	140.48	C21	6.94	149.29	C21	91.51
C21	46.55	254.16	C21	13.94	216.16	C21	8.24	26.63	C21	59.60
C21	127.01	728.55	C21	6.05	67.10	C21	0.83	15.95	C21	136.07
C21	15.00	-	C21	7.36	122.79	C21	1.14	20.27	C21	16.33
C21	39.78	-	C21	9.72	136.30	C21	3.76	35.30	C21	9.21
C21	7.12	-	C21	56.26	471.63	C21	0.16	1.83	C21	0.75
C21	4.13	-	C21	23.07	445.97	C21	4.03	-	C21	741.71
C21	17.56	-	C21	26.57	4755.41	C21	4.20	-	C21	167.46
C84	367.57	281.20	C21	82.98	-	C21	0.87	-	C21	190.97
C84	289.68	230.34	C21	40.15	-	128	0.77	7.01	C21	127.92
C84	41.13	136.33	C21	6.08	-	128	0.46	2.34	C21	98.67
C84	11.97	-	C21	12.48	-	128	1.10	9.53	C21	275.32
C84	8.19	-	C21	6.84	-	128	0.44	8.08	128	179.77
C84	8.32	-	C21	11.33	-	128	0.30	2.02	128	115.77
C84	62.76	-	C21	0.40	-	128	0.61	2.35	128	59.50
C84	45.90	-	C21	14.80	-	128	0.94	11.77	128	100.10
C84	4.55	-	C21	23.52	-	128	2.57	49.13	128	96.93
C84	8.88	-	C21	7.05	-	128	4.42	44.20	128	211.30
C84	18.75	-	128	8.57	51.40	128	0.37	7.02	128	67.67
C84	35.12	-	128	6.74	97.32	128	1.12	5.39	128	153.01
129	227.28	147.11	128	10.00	80.90	128	1.59	12.23	128	240.05
C108	59.89	219.88	128	5.71	93.60	128	0.36	2.46	128	90.26
C108	29.67	125.02	128	11.04	15.86	128	2.56	21.43	128	42.42
C108	52.20	142.64	128	6.79	100.63	128	2.67	36.21	128	157.79
C108	45.62	83.82	128	13.01	59.07	128	2.23	3.22	128	154.52
C108	62.00	227.07	128	5.48	54.27	128	0.21	2.30	128	50.97
C108	66.90	232.28	128	9.09	136.59	128	3.19	4.00	128	39.90
125	-	461.92	128	4.46	96.08	128	0.14	0.33	128	58.87
125	144.93	476.75	128	4.58	55.03	128	0.39	6.80	128	123.01
125	133.12	-	128	4.75	62.03	128	2.57	26.72	128	47.09
			128	9.75	72.66	128	0.60	18.79	128	72.95
			128	10.32	140.90	128	1.66	32.63	128	135.51
			128	6.81	104.00	128	0.39	4.74	128	104.99
			128	3.75	15.93	88	0.39	13.55	128	10.80
			128	-	127.53	88	1.04	24.57	128	192.81
			88	7.52	37.59	88	-	24.03	C84	82.73
			88	7.76	170.89	88	3.25	34.24	C84	31.32
			88	1.87	20.56	88	0.63	9.77	C84	73.89
			88	0.82	14.11	C84	0.93	18.82	C84	240.82
			C84	5.48	118.92	C84	4.12	29.93	129	25.62
			C84	7.78	139.45	C84	0.23	2.16	129	243.52
			C84	3.16	26.62	C84	1.59	31.49	129	24.80
			C84	6.23	60.92	C84	1.43	17.41	129	30.77
			C84	20.78	74.75	C84	0.30	9.78	129	221.44
			C84	6.78	95.87	C84	0.31	12.72	129	524.71
			C84	8.34	81.32	C84	0.10	0.74	129	106.55
			C84	4.98	47.47	C84	0.37	7.96	129	59.04
			C84	11.08	98.09	C84	0.23	5.16	129	43.31
			C84	9.87	103.78	C84	1.02	29.48	129	69.61
			C84	10.47	90.08	C84	1.02	22.63	129	54.75
			C84	8.39	128.46	C84	0.16	2.22	129	25.67
			C84	2.15	21.20	C84	0.56	12.19	129	60.13
			129	4.36	22.47	C84	1.54	21.29	129	7.99
			129	7.59	89.54	C84	0.24	25.96	129	79.97
			129	2.80	10.47	C84	5.43	85.09	129	82.27
			129	13.74	250.25	129	0.43	20.00	129	139.12
			129	8.91	37.90	129	0.14	13.41	129	129.92
			129	2.59	51.97	129	1.16	6.44	129	62.69
			129	1.49	28.36	129	1.44	26.64	129	10.48
			129	7.89	37.82	129	1.62	4.06	129	86.84
			129	2.04	24.61	129	0.67	7.99	129	35.96
			129	22.35	108.36	129	0.11	1.51	129	105.23

Appendix VII: Au and Ag concentrations in pyrite and arsenopyrite from Carlin-style ore at Cove (all data from Chryssoulis et al., 1997)

Microcrystalline pyrite			Fine-grained pyrite			Coarse-grained pyrite			Arsenopyrite	
test #	Au, ppm	Ag, ppm	test #	Au, ppm	Ag, ppm	test #	Au, ppm	Ag, ppm	test #	Au, ppm
			129	10.18	70.90	129	4.06	6.82	129	74.98
			129	4.79	139.48	129	0.44	18.28	129	186.67
			129	7.92	16.94	129	4.62	8.48	129	151.18
			129	14.26	335.07	129	0.14	2.29	129	43.55
			129	8.36	104.70	129	0.24	1.87	129	1411.97
			C108	11.11	153.91	129	2.00	30.62	129	39.98
			C108	3.46	129.68	129	1.04	14.60	129	15.77
			C108	12.57	74.77	C108	0.11	1.03	129	39.68
			C108	9.54	174.35	C108	0.63	42.61	129	170.48
			C108	6.54	124.92	C108	1.14	24.19	C108	208.81
			C108	15.64	185.04	C108	10.88	57.24	C108	111.02
			C108	6.59	80.33	C108	2.52	9.35	C108	263.26
			C108	7.74	154.04	C108	2.13	40.66	125	26.12
			C108	8.05	109.69	C108	1.39	49.63	125	9.59
			C108	6.61	95.41	C108	0.72	26.08	125	1.40
			C108	6.33	76.99	C108	0.63	17.97	125	3.84
			C108	8.05	136.74	C108	0.57	29.23	125	760.42
			C108	10.64	152.78	C108	0.29	9.94	125	2.67
			125	16.93	25.33	C108	0.30	9.21	125	52.99
			125	14.84	77.36	C108	1.00	11.75	125	66.27
			125	14.67	104.27	C108	0.99	29.17	125	2.65
			125	4.09	29.62	C108	1.50	9.45	125	27.09
			125	0.60	25.98	C108	0.76	24.16	125	46.41
			125	12.53	162.82	125	3.46	42.79	125	6.37
			125	2.75	95.25	125	0.14	2.05	125	6.95
			92	3.66	71.82	125	0.72	12.91	125	4.87
			92	5.99	36.91	125	0.89	16.25	125	169.12
			92	5.09	27.53	125	1.23	4.32	125	26.32
			92	6.44	13.13	125	0.70	11.48	125	61.85
			C81	1.24	55.94	125	1.03	10.53	125	15.23
			C81	16.26	278.23	125	0.46	11.85	125	0.61
			C81	3.45	24.85	125	0.53	14.75	125	41.52
			C81	4.62	18.08	125	0.41	7.56	125	3.62
			C81	-	83.02	125	1.19	53.72	125	84.69
			C81	13.38	46.22	125	0.10	1.21	125	67.42
			C81	6.64	50.84	125	0.80	9.29	C81	21.30
			C81	8.67	114.24	125	0.60	17.99	C81	138.21
			C81	4.82	27.61	125	0.34	17.84	C81	21.30
			C81	8.81	101.88	125	0.29	7.81	C81	16.45
			C81	17.92	227.92	92	2.13	25.05	C81	49.04
			C81	5.46	112.75	92	2.04	40.26	C81	69.91
			C81	9.15	187.75	92	2.55	19.98	C81	17.02
			C81	14.27	457.54	92	0.73	14.01	C81	43.65
			C81	9.47	277.57	92	5.12	25.81		
			C81	1.49	52.64	92	1.52	58.16		
			C81	5.51	6.91	92	3.09	8.29		
			C168	13.46	76.50	92	1.13	11.27		
						92	3.36	23.96		
						C81	2.15	14.71		
						C81	0.53	13.31		
						C81	1.94	74.82		
						C81	0.90	7.16		
						C81	0.29	5.74		
						C81	0.99	13.03		
						C81	0.57	10.38		
						C81	0.86	17.55		
						C168	1.42	16.51		
						C168	3.78	13.65		
						C168	4.00	-		
						C168	3.16	32.47		
						C168	2.55	50.75		
						C168	1.30	9.93		

Appendix VII: Au and Ag concentrations in pyrite and arsenopyrite from Carlin-style ore at Cove (all data from Chryssoulis et al., 1997)